The shoshonite-associated Endeavour 26 North porphyry Cu–Au deposit, Goonumbla, New South Wales

Paul Sinclair Heithersay

A thesis submitted for the degree of Doctor of Philosophy, Australian National University

July 1991

Declaration

The observations and interpretations presented in this Thesis are entirely my own unless duly acknowledged.

Paul Heithersay

CONTENTS

PART 1

Appendices

PART 2

Plans

PLATES

FIGURES

TABLES

ACKNOWLEDGMENTS

It is my pleasure to acknowledge the many individuals and organizations that have helped this study. First thanks must go to Brian Williams and Ross Large for setting up the project. Geopeko generously supported the study. The many geologists at Geopeko's exploration base at Parkes including Wayne O'Neill, Pete Dunn, Michael Love, Paul Balind, Ren Shuang Kui, and Bill Platts for discussions on many aspects of the geology of the deposit and the region. Dr John Walshe is thanked for his supervision, patience and guidance through the too lengthy PhD process. Dr Scott Halley for assistance particularly with respect to fluid inclusion research. Chris Foudoulis for assistance with XRD work and Nick Ware for assistance on the microprobe. Dr. Bruce Chappell for assistance with whole rock analyses and discussions about the tectonics of the Lachlan Fold Belt. Professor Ken Campbell provided access to the facilities at the Geology Department of the ANU. Dr. Lawrie Sherwin of the Department of Minerals and Energy, New South Wales for information on the regional geology and palaeontological age determinations. Dr. Caroline Perkins for her involvement with the dating of the Goonumbla deposits. Dr Graham Carr, Dr David Whitford and Judith Dean, CSIRO Division of Exploration Geoscience, for assistance with lead, strontium, neodymium and samarium isotope determinations. Mike Power, University of Tasmania, and Central Science Laboratory for supervising sulphur isotope determinations. Brian Harrold for assistance with things computing and for assistance in generating phase diagrams. Harley Jones and the Geopeko cartography section in Parkes supervised the generation of maps and diagrams.

Jacque Hibburt and Jamie Williams of PIRSA helped to push this thesis across the line and their help is gratefully acknowledged.

Finally I especially acknowledge the support and encouragement from my wife, Celine and our four children Sam, Sophie, Jack and Karmen.

ABSTRACT

The Endeavour 26 North porphyry Cu–Au deposit is the largest of a group of porphyry deposits which occur within the Goonumbla Volcanic Complex, near Parkes, central New South Wales. The Goonumbla Volcanic Complex is interpreted to have been a high-K calc-alkaline to shoshonitic stratovolcanoe of Late Ordovician age that developed on a marine substrate and subsequently emerged above sea level, developing a caldera that subsequently breached. Geochemically the complex is characterised by initial ratios of $^{86}Sr/^{88}Sr$ which range between 0.70404 and 0.70464, and ratios of $^{207}Pb/^{204}Pb$ ranging between 15.47 and 15.58. Two samples returned εNd values of 6 and 6.2. These data indicate that the magmas were derived from primitive source rocks that had been geochemically enriched at some time. The lack of crustal contamination weighs against contemporaneous subduction in a sedimentary environment that is dominated by quartz-rich greywacke. A possible scenario is Cambrian arc material being recycled to provide an enriched source material during incipient rifting or strike slip readjustment along long lived structures during the Late Ordovician.

The Endeavour deposits are confined to a circular structure within the Goonumbla Volcanic Complex. On the basis of geophysical and geological information this feature is interpreted to mark the limit of the summit caldera. Intrusions that are co-magmatic with the volcanism appear to have lost their volatiles, and evolved at moderate to high pressure along an essentially anhydrous olivine fractionation path. Intrusions associated with mineralisation have contained their volatiles, and evolved at a higher level along a hydrous fractionation path of plagioclase–biotite fractionation to form a geochemical path that will be useful as an exploration vector.

The porphyry Cu–Au deposits at Endeavour 22, 26 North and 27 are unusual in that they have extreme pipelike geometries and occur as satellites around the parent Endeavour 31 stock, which is itself weakly mineralised. Hydrothermal fluids generated from the larger parent below Endeavour 31 were focused towards its contact and channelled up conduits along with residual melt. The mineralised body is built up of successive generations of monzonite to quartz monzonite porphyries accompanying a progressive paragenesis of hydrothermal fluids following the same conduits.

At Endeavour 26 North the earliest alteration assemblage associated with the first local intrusive porphyry (QMP1) is a biotite, magnetite anhydrite assemblage with minor chalcopyrite (Stage 3), which records fluid inclusion temperatures between 500 and 600 °C and salinities around 70 wt% NaCl equivalent. Redox conditions determined by fluid–mineral equilibria suggest that early secondary biotite formation was no more than 1 or 2

log units below the hematite magnetite buffer, and generally consistent with the condition of $f_{H2S}=f_{SO2}$ as indicated by S isotope studies as well as the sphene–rutile–quartz–anhydrite buffer. Peak hydrothermal conditions were in Stage 4 of the paragenesis with vapour homogenisation temperatures between 470 and 1090 °C, and peaks at 580 and 760 °C. Salinities ranged between 50 and 80% NaCl equivalent, and coexisting vapour-rich inclusions suggest phase separation at this stage. At these temperatures and redox states, magnetite is the stable iron oxide. As it is not observed, Cu and S abundances in the fluid must be sufficient to maintain bornite saturation only at this stage. These constraints suggest an increase in the Cu and S content of the fluids from Stage 3 to 4 as the system heats up. This increase in temperature is sufficient to account for the dissolution of the secondary biotite formed at Stage 3. Stage 5 represents the main mineralising event at Endeavour 26 North leading to the development of the main stockwork zone. The mineralogy at this stage is quartz, bornite, anhydrite and sericite, with minor chalcopyrite, digenite, hematite and rutile. Fluid temperatures by this stage had declined to around 400 to 600 °C, and fluid inclusions show evidence of boiling. The gradual decrease in overall salinity can be explained by phase separation at a constant pressure in the vicinity of 300 to 500 b.

The waning hydrothermal system was reactivated post Stage 5 by the emplacement of a second mineralising porphyry, QMP2, which partly digested previously formed mineralisation. This prograde event may have prevented the influx of significant meteoric waters, leading to only weakly developed quartz–sericite alteration in contrast to most other porphyry systems. A consequence of this lack of feldspar-destructive alteration is that the features indicative of fluid melt separation, such as crenulate quartz layers, brain rock and vein dykes, are preserved in the core of the orebody. These magmatic hydrothermal features form Stage 6, and exhibit fluid homogenisation temperatures ranging from 440 to 980 °C, with a peak around 700 °C, some 200 degrees higher than Stage 5. This is consistent with a new magmatic hydrothermal event.

QMP2 generated its own paragenetic sequence that shows an overall decrease in temperature without a major change in salinity. This paragenetic cycle is less mineralised than the cycle related to QMP1.

Chapter 1
INTRODUCTION

1.1 BACKGROUND

Porphyry Cu–Au mineralisation was discovered in 1977 at Goonumbla, near Parkes, in New South Wales (Fig. 1.1) by Geopeko, the mineral exploration arm of Peko Wallsend. Since then, 11 centres of mineralisation have been delineated in the Northparkes area, within a Late Ordovician shoshonitic volcanic complex, herein called the Goonumbla Volcanic Complex. They are the first porphyry-style deposits discovered in Australia with grades high enough to support a large mining operation. The reserves for the three main deposits — Endeavour 22, 26 North and 27 — are given in Table 1.1.

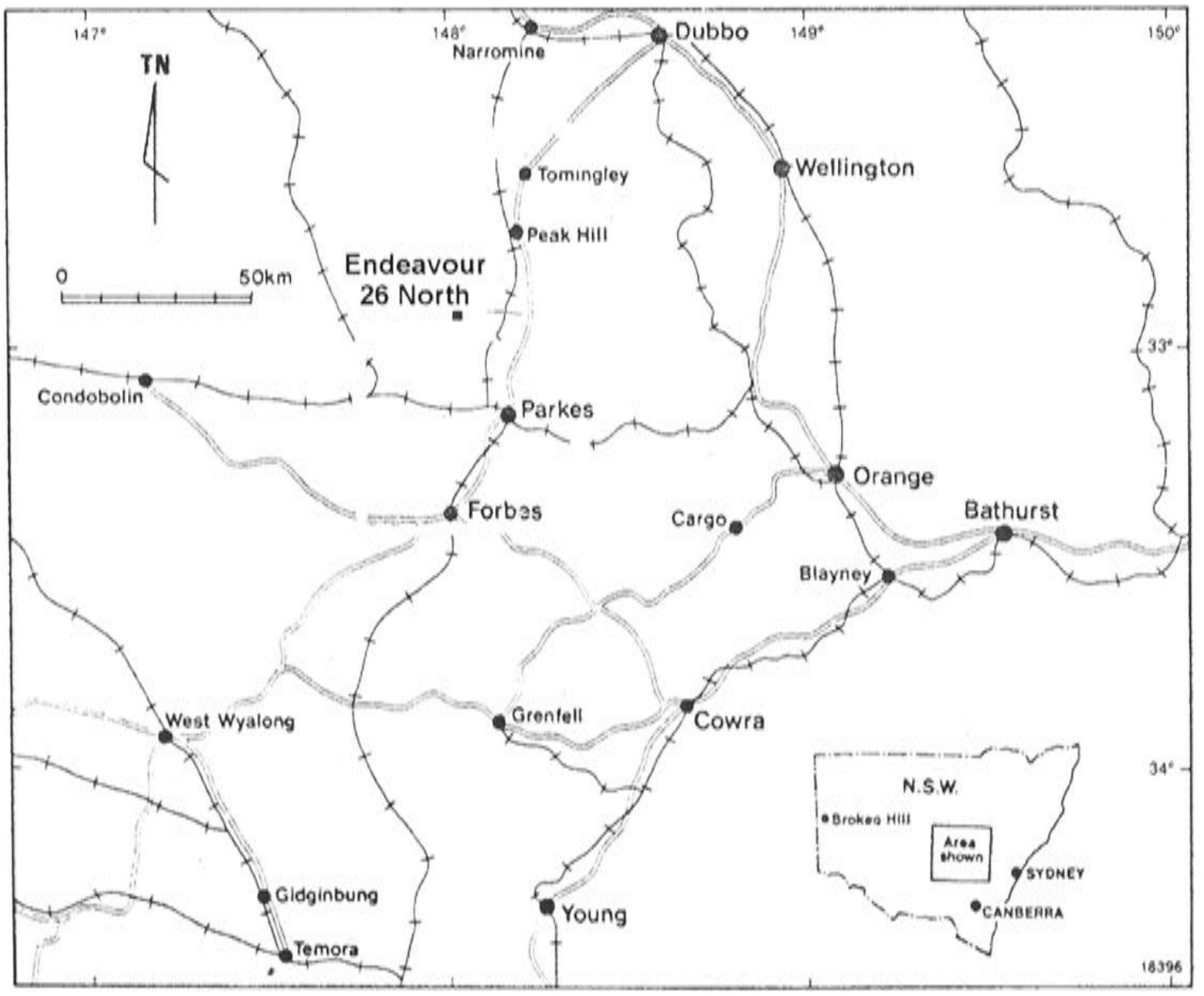

Figure 1.1 Location map for the study area.

Table 1.1 Pre-production Cu–Au reserves for Endeavour 22, 26 North and 27*.

	'000 t	Cu (%)	Au (g/t)
Oxide Au — in-pit resource (+1.0 g/t)			
E22	370		2.02
E27	996		2.27
Total	**1366**		**2.20**
Oxide Cu–Au — in-pit resource (+1.5 g/t)			
E22	380	1.19	1.15
E27	1 280	1.09	1.41
Total	**1 660**	**1.11**	**1.35**
Sulphide Cu–Au — in-pit resource (+0.6% eCu)			
E22	11 693	0.72	0.59
E27	11 073	0.71	0.73
E26	10 020	1.31	0.17
Total	**32 786**	**1.31**	**0.17**
Sulphide Cu–Au — underground (inferred and indicated)			
E26	29 573	1.79	0.61
Total	**29 573**	**1.79**	**0.61**

* Figures submitted for use in the 1989/90 North Broken Hill Peko Annual Report.

eCu = Cu equivalent

The Endeavour 26 North deposit is the largest of the deposits and is the focus of mining operations. The discovery is a credit to Supervising Geologist Gary Jones whose persistence with the technique of reconnaissance bedrock drilling, in a region with deep soil cover and limited outcrop, led to the initial discovery of the mineralisation leading to the rapid discovery of subsequent deposits described in this thesis.

On a world scale, porphyry-style deposits are the dominant suppliers of Cu and Mo and very significant suppliers of Au and Ag. Most are within Mesozoic or younger fold belts, clearly related to calc-alkaline volcanism in convergent margin settings. In contrast, the Goonumbla deposits occur in a much older (Palaeozoic) sequence for which the tectonic setting is controversial. In addition, the host rocks are of the high-K calc-alkaline to shoshonite association — highly potassic rocks, which are only a relatively minor component of most island- and continental-arcs.

The Endeavour 26 North deposit thus provides an opportunity to study porphyry Cu–Au mineralisation in a relatively old volcanic sequence of unusual geochemical affinity for which the tectonic setting may not be simple. The understanding of the deposit has important implications for the discovery of similar

deposits in the Goonumbla region and elsewhere in the highly prospective Lachlan Fold Belt.

1.2 PREVIOUS WORK

Unpublished in-house Geopeko reports by Senior Geologist Gary Arnold provided the first comprehensive study of the Goonumbla deposits, particularly the geology and alteration of Endeavour 22, 26 North and 27. Jones (1985) described the regional geology and the three main porphyry deposits based on Geopeko's early work in the area. Heithersay (1986) gave a detailed description of the Endeavour 26 North deposit with emphasis on alteration studies using the early results of the present study. The Geological Survey of New South Wales completed a regional review of the geological setting of the Cu and Au deposits in the Parkes region (Krynen et al., 1990), including a revision of the regional stratigraphy, geophysical work, details of the Au deposits and geochemistry of the volcanic rocks. The most complete description of the region and the three main deposits is given by Heithersay et al. (1990), and includes an account of Geopeko's exploration history in the region. This draws on work completed by Geopeko geologists in a number of in-house reports, with key authors including Wayne O'Neill, Michael Love, Gary Jones, Gary Arnold, Paul Harbon, Peter Van der Helder and Paul Balind. The author contributed to research using the Ar–Ar technique to date the alteration at the deposits with Dr C. Perkins of the Australian National University. Preliminary details of this work were given in Perkins et al. (1990).

1.3 AIMS OF THE STUDY

The discovery of the Northparkes Endeavour deposits at Goonumbla gives a unique opportunity to investigate and describe a new porphyry Cu–Au deposit.

In doing so the aim of the thesis is to place the deposit in its correct tectonic setting, both from a review of the literature of the Lachlan Fold Belt and analogous tectonic settings overseas, but also through the regional geology and geophysics of this mineral deposit setting together with the clues given by the petrology.

At a detailed level the study aims to describe the Endeavour 26 North deposit in three dimensions and compare and contrast with other porphyry Cu–Au systems. Ultimately the explorationists will wish to know why the deposit is where it is, and what techniques and approaches will help to find more.

1.4 METHODOLOGY

Field work for this thesis was completed when the author was stationed in Parkes as a senior and later supervising geologist. Outcrop is very poor in the field area so mine-camp-scale geology was constructed using hundreds of end-of-hole chip samples from a systematic grid across the Goonumbla Volcanic Complex, coupled with available diamond drillhole information and outcrop mapping. These data are combined with detailed magnetics made available for the study by Geopeko.

The prime method of geological investigation was detailed logging and sampling of >8000 m of diamond core drilled during the pre-feasibility study of Endeavour 26 North. Over 400 samples were collected from various parts of the Endeavour 26 North deposit and ~200 were selected for polished and thin sections. Samples for closer examination, in fluid inclusion studies, were selected on the basis of paragenetic sequence.

This work provided data on alteration styles and paragenetic relationships, facilitating careful selection of samples for radiometric dating ($^{40}Ar/^{39}Ar$ method), S, Pb, Sr and Nd–Sm isotope analysis, fluid inclusion analysis, and electron microprobe analysis of silicates and sulphides.

1.5 THE PRESENT STUDY

The early chapters of the thesis provide background information, which is used as a framework upon which to build the detailed description of the deposit. Chapter 2 is a review of the geology of the Lachlan Fold Belt and summarises the previous tectonic models for the Ordovician period. Chapter 3 describes the regional geological setting and geology of the Goonumbla Volcanic Complex. A review of the shoshonite association in Chapter 4 looks at the distribution of shoshonites in New South Wales and, using examples from around the world, summarises the geological setting, petrography, geochemistry, petrogenesis, tectonic setting and associated mineralisation for this association. Chapter 5 examines the petrogenesis of the Goonumbla Volcanic Complex — including the petrography, geochemistry, and Pb, Sr, Nd and Sm isotopes — with a view to constraining the tectonic setting of the region and relating the genesis of the deposits to the genesis of the Goonumbla Volcanic Complex.

The second half of the thesis documents the magmatic-hydrothermal evolution of the Endeavour 26 North deposit. Chapter 6 describes the deposit and the local geological framework. The detailed paragenesis of the deposit, documented in Chapter 7, permits an analysis of the temporal and spatial evolution of the hydrothermal system that formed the Endeavour 26 North Cu–Au deposits.

Chapter 8 reports the results of a sulphur isotope study of sulphides and sulphates to show the temporal and spatial variation in ratios, and to determine the temperature and redox conditions of sulphide formation. Chapter 9 details the types of inclusions found in quartz at each paragenetic stage. Interest centres on defining fluid paths in P–T–X space. Finally, Chapter 10 provides a summary discussion of the salient conclusions about the tectonic setting, the significance of the shoshonite association and the mechanisms that control the formation of these unusual magmatic hydrothermal deposits.

Chapter 2

REVIEW OF LACHLAN FOLD BELT GEOLOGY

2.1 INTRODUCTION

The aim of this chapter is to present an overview of the geological history of the Lachlan Fold Belt and a review of Ordovician tectonic models. This will provide a framework for describing the geological setting for Goonumbla porphyry Cu–Au deposits. Equally it will highlight the gaps in knowledge of the Lachlan Fold Belt, to which this study may be able to contribute.

2.2 THE GEOLOGICAL HISTORY OF THE LACHLAN FOLD BELT

The Lachlan Fold Belt is an important part of the Tasman Fold Belt System (Scheibner, 1978), a dominantly Palaeozoic to early Mesozoic mountain belt which makes up the eastern third of the Australian continent (Fig. 2.1).

The orogenic belt stretches 4000 km, from Tasmania in the south to Cape York in northern Queensland. When it formed it was part of a gigantic orogenic system (Fig. 2.2) that extended along the Pacific margin of Gondwanaland, from the northern Andes of South America through the Pacific margin of Antarctica and into eastern Australia (Coney et al., 1990).

The Tasman Fold Belt System comprises five orogenic belts and a foredeep basin (Scheibner, 1985b). The fold belts become progressively younger from west to east. They are the Kanmantoo, Thomson, Lachlan, Hodgkinson – Broken River and New England Fold Belts. The New England Fold Belt in the east is separated from the older fold belts by the Bowen–Sydney Basin (Fig. 2.1).

The Lachlan Fold Belt or Lachlan Terrane (Coney, 1990) as exposed, varies in width from 800 km in Victoria to 400 km in central New South Wales. Magnetic and gravity data show that it underlies the Murray Basin and the southern end of the Great Artesian Basin.

Figure 2.1 Schematic structural map of eastern Australia (from Scheibner, 1978).

In a review of the regional tectonics of the Tasman Orogenic System, Coney (1990) breaks the Lachlan Terrane into major lithotectonic associations, which range from Cambrian to Late Devonian – Early Carboniferous in age. The first association is the Cambrian greenstones, which are restricted to Victoria. The second is the widespread, mainly Ordovician to Lower Silurian, greywackes or flysch sediments. The third is a complex, mostly Silurian to Devonian, volcanic–sedimentary package associated with a wide belt of meridionally linear granites of Siluro-Devonian age. This empirical approach differs from that of Cas (1983) and Powell (1984 a, b) whom review tectonic and palaeogeographic models, through the history of the Lachlan Fold Belt.

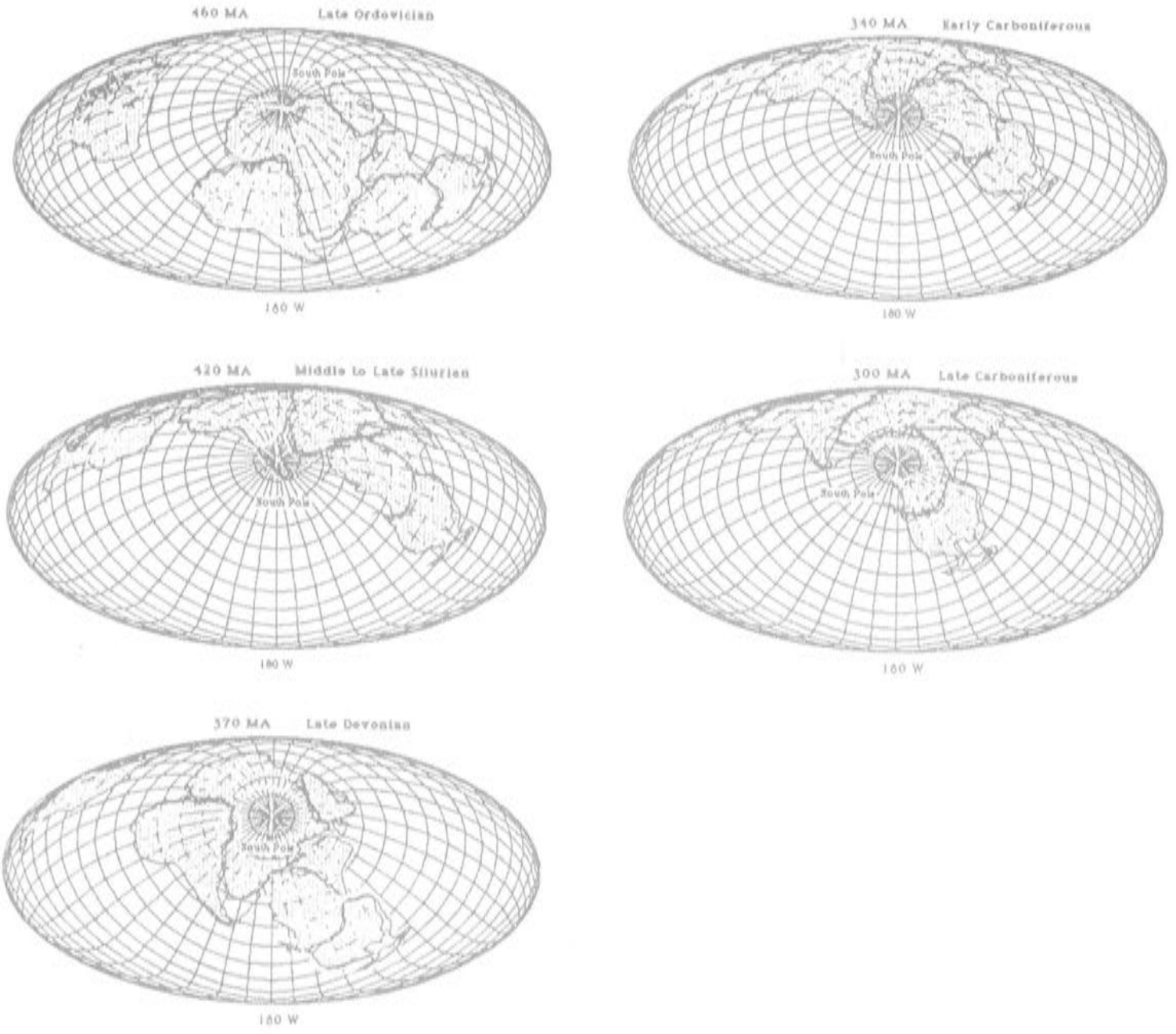

Figure 2.2 Palaeozoic reconstructions of Gondwanaland and the proto-Pacific Ocean.

2.2.1 The basement to the Lachlan Fold Belt

The Tasman Orogenic System lies east of the Archean and lower to middle Proterozoic cratonic basement of Australia. No exposures of Archean to Proterozoic rocks occur east of the so called 'Tasman Line' which marks the western edge of the Tasman Orogenic System (Hill, 1951; Scheibner, 1974; Murray et al., 1989). The nature of the basement beyond the Tasman Line remains controversial. Rutland (1976) suggests that the orogenic zone is floored by old continental basement, while Scheibner (1974, 1987) provides a model based on Proterozoic microcontinents and early Palaeozoic ensimatic basement. In contrast, Crook (1980) provides for an exclusively Palaeozoic oceanic crust as basement in his tectonic model.

Evidence for the nature of the basement comes primarily from B.W. Chappell and A.J.R. White and coworkers. White et al. (1975) initially proposed that the I–S line was a major tectonic feature, dividing granitoids derived from only igneous rocks to the east from granitoids derived from both metasedimentary and igneous rocks to the west. This change in granitoid chemistry, coupled with a transition from a structural regime dominated by wrench faulting in the west to thrust faulting in the east, provided White et al. (1976) with evidence to suggest that the I–S line marks the eastern boundary of crystalline basement of possible Precambrian age.

Further evidence for a Precambrian basement includes:

1. The major element geochemistry of many of the S-type granites, indicates that they are too rich in Ca, Na, Pb and Sr to have been derived from the Ordovician quartzose clastics they intrude (Wyborn and Chappell, 1979).Compston and Chappell (1979) showed that I-type granites of the Lachlan Fold Belt have a wide range of initial $^{87}Sr/^{86}Sr$ isotopic ratios (0.704 to 0.712), which they ascribed to varying ages of mantle derivation from I-type source rocks over a long period beginning ~1.1 Ga ago. This argues against relatively new oceanic crust as a source.

2. McCulloch and Chappell (1982) showed that I-type granites in the Berridale and Kosciusko Batholiths exhibited initial Sr and Nd compositions which ranged covariantly, consistent with either mixing of two isotopically different components (mantle and crust) or derivation from the mantle over a long period of time. The latter conclusion is consistent with the work of Compston and Chappell (1979). McCulloch and Chappell (1982) also demonstrated that S-type granites from the Berridale and Kosciusko Batholiths had a restricted range in εNd (-6 to +9.8), but a large range in εSr (+70 to +200). The data imply that S-type components were extracted from the mantle over a restricted period of time. Later weathering of this material gave rocks of varying Rb/Sr ratios which, with time, developed a variety of $^{87}Sr/^{86}Sr$ ratios. McCulloch and Chappell (1982) concluded that S-type granites were derived from a 1.4 Ga sedimentary or metasedimentary source.

3. Recent work has recorded Proterozoic and older isotopic ages from U–Pb dating of zircons from Palaeozoic granites (Williams et al., 1983). Zircons taken from Ordovician sediments have similar ages, albeit with different frequency distributions. If the compositional requirements of the Lachlan Fold Belt granites are ignored, then these results could be consistent with a sedimentary source composed of subducted Ordovician sediments.

2.2.2 Cambrian

Outcrops of Cambrian rocks are restricted to northwestern New South Wales, western Victoria and western Tasmania. In the northwest of New South Wales the volcanics and associated shallow-water sediments are called the Mount Wright Volcanic Arc (Fig. 2.3) by Scheibner (1972). On the gravity map (Fig. 2.4) they form a ridge (Murray et al., 1989) which is probably continuous with the Padthaway Ridge (Parker, 1986).

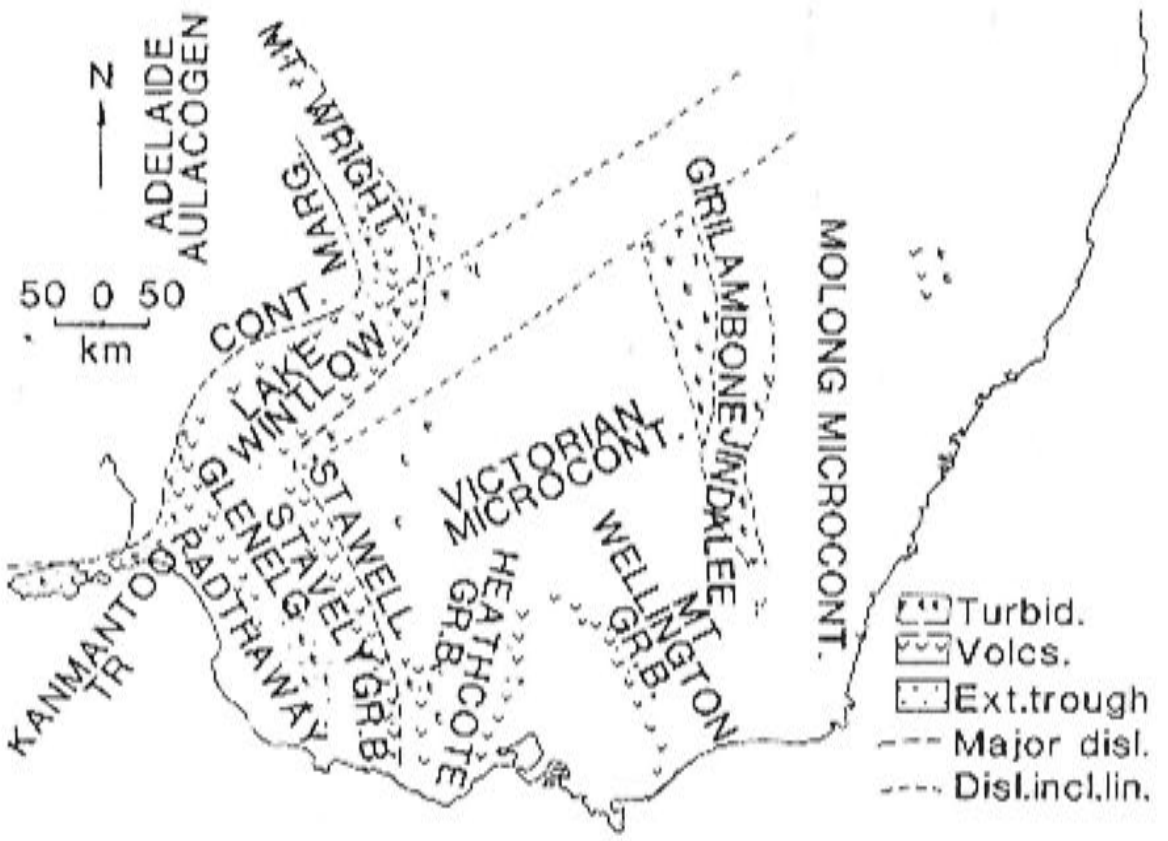

Figure 2.3 Schematic palaeogeographic map for the Early Cambrian (after Scheibner 1989b)

The Mount Stavely Greenstone Belt in western Victoria also presents a strong gravity and magnetic ridge. It consists of andesitic to dacitic volcanics together with serpentinites and represents remnants of a calc-alkaline volcanic arc (Crawford, 1983). This volcanic belt may join up with the Mount Wright volcanics; however outcrop is very poor and drilling information too sparse to confirm this. The Heathcote and Mount Wellington Greenstone Belts in eastern Victoria have been interpreted as representing fore-arc boninites overlain by MORB rocks related to back-arc basin development (Crawford and Cameron, 1985). Medium-K and high-K andesites also occur in the Wellington Belt. Low Ti, together with enrichments in Sr, Ba and LREE, give these rocks a distinctive continental or island-arc signature. Low-Ti andesites together with boninites indicate a volcanic arc related setting. Coney (1990) points out that no associated trench assemblage has been recognised (a problem shared by Ordovician arc-type rocks). The boninite lava – MORB association is known only from modern west Pacific-type subduction related settings (Crawford et al., 1981), hence it is

reasonable to conclude that the Cambrian greenstone belts represent a subduction-related, island-arc – back-arc setting.

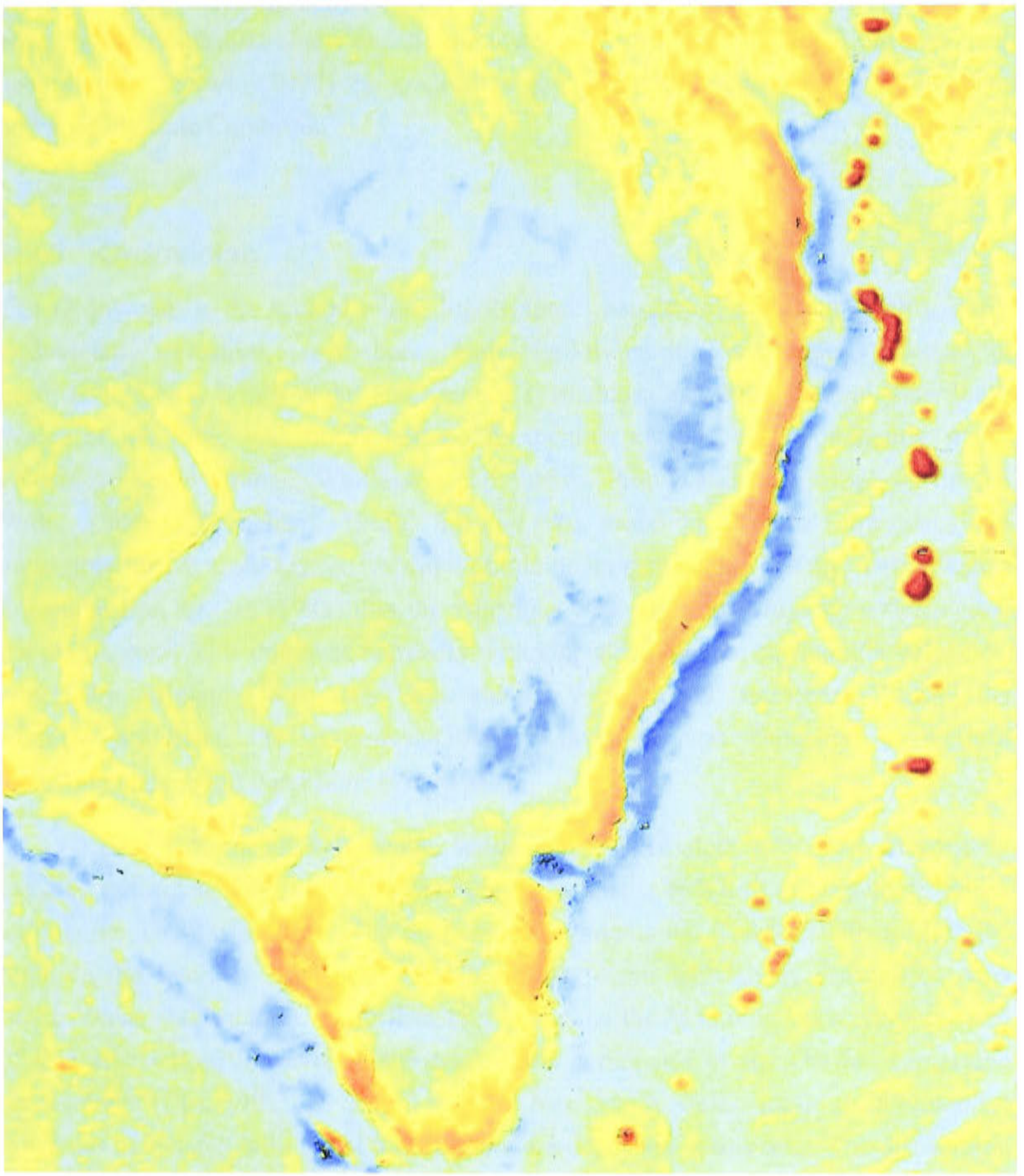

Figure 2.4 Bouguer gravity map of eastern Australia (data from BMR).

The Mount Read Volcanics in western Tasmania are of Early to Middle Cambrian age. Geochemically, three distinct volcanic suites can be recognised on the basis of major and trace elements; two high-K calc-alkaline suites and an unusual shoshonitic association. The volcanic rocks appear to have been erupted in a series of extensional basins following an arc–continent collision. In central New South Wales there are no outcrops of unequivocally Cambrian age. The Jindalee Beds are correlated with the Cambro-Ordovician Girilambone Group (Fig. 2.3) on mainly lithological and

structural grounds; however further work is required to confirm this (Basden, 1982). In the Parkes area there is a gravity and magnetic ridge extending from Narromine through Parkes to West Wyalong (Fig. 2.4), which is comparable to the Mount Wright Ridge. Near Parkes graptolitic cherts overlie the lower part of the Nelungaloo Volcanics, and according to Sherwin (1979) the graptolites give a minimum age of Early Ordovician and possibly Late Cambrian.

2.2.3 Ordovician

The Ordovician is the second major lithotectonic association of Coney (1990). Early Ordovician terrestrial, near-shore and shallow-marine successions occur in northwestern New South Wales and western Tasmania (Cas, 1983). Central New South Wales at this time was dominated be terrigenous clastics with dominantly mafic volcanics around Orange, Wellington and Parkes. Pillow basalts are reported in the Walli Andesite (Packham, 1969), but are not found at Parkes. Limestones are noticeably absent from Lower to Middle Ordovician sequences (Webby, 1976), hence the suggestion by Cas (1983) that the volcanics were laid down in deep water, below the photic zone. This contrasts markedly with Upper Ordovician shoshonitic volcanics, which are intimately associated with shallow-water reefal limestones. During the Middle Ordovician the extensive Gordon Limestone was deposited in western Tasmania under shelf conditions (Cas, 1983).

Late Ordovician deep-water sedimentary successions are most extensively exposed in the Lachlan Fold Belt. They consist of quartz-rich turbidites, pelagic pelites and cherts. The uniformity of the deep-water sediments led Coney (1990) to describe them as the Lachlan 'mud-pile'. The sediments occur extensively throughout New South Wales and Victoria. In northeastern Tasmania the Mathinna Beds represent part of this association; however in the west, shelf carbonates of the Gordon Limestone predominate (Cas, 1983). In central western New South Wales, mafic to intermediate volcanics associated with reefal limestones were deposited at this time. The distribution of the sequences is shown in Figure 2.5 and a time–space plot is given in Figure 2.6.

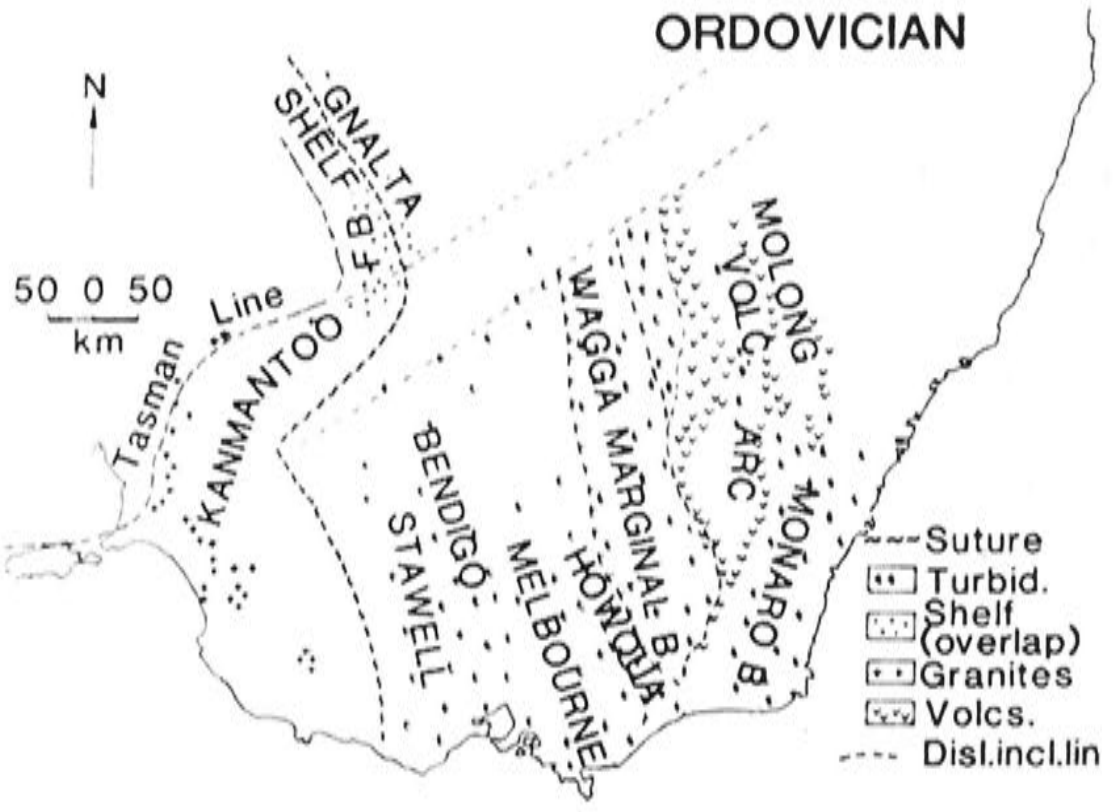

Figure 2.5 Ordovician palaeogeography (after Scheibner, 1989b).

A palaeogeographic model for the Ordovician proposed by Cas (1983), shown in Figure 2.7, contains the following elements:

1. the Tasmanian carbonate shelf
2. continental shoreline along the western margin of the Lachlan Fold Belt
3. the widespread quiet-water domain (below wave base) dominated by quartz-rich turbidites, pelagic pelites and cherts
4. mafic to intermediate volcanic centres with fringing limestone reefs.

The significance of the volcanic successions is the most contentious part of the model. Cas et al. (1980) provided a scale perspective for any palaeogeographic reconstructions by comparing the Ordovician facies pattern with the Quaternary pattern in the Andaman–Nicobar island arc and basin region of the northeast Indian Ocean (Fig. 2.8). This provides an attractive analogue as it allows for a sedimentary environment proximal to a major terrigenous source, the Bengal fan delta. The comparison also suggests that individual Ordovician volcanic centres were too small to be considered volcanic arcs in their own right, and Cas (1983) argues that there was originally a single, northwest-trending magmatic arc extending from Mount Dijou in the northwest through Bathurst and south to Kiandra. This interpretation has been questioned by Scheibner (1989b), who points out that the Mount Dijou Volcanics appear to be alkaline and of oceanic-island affinity, and mafic volcanics around Louth are probably of Early Devonian age.

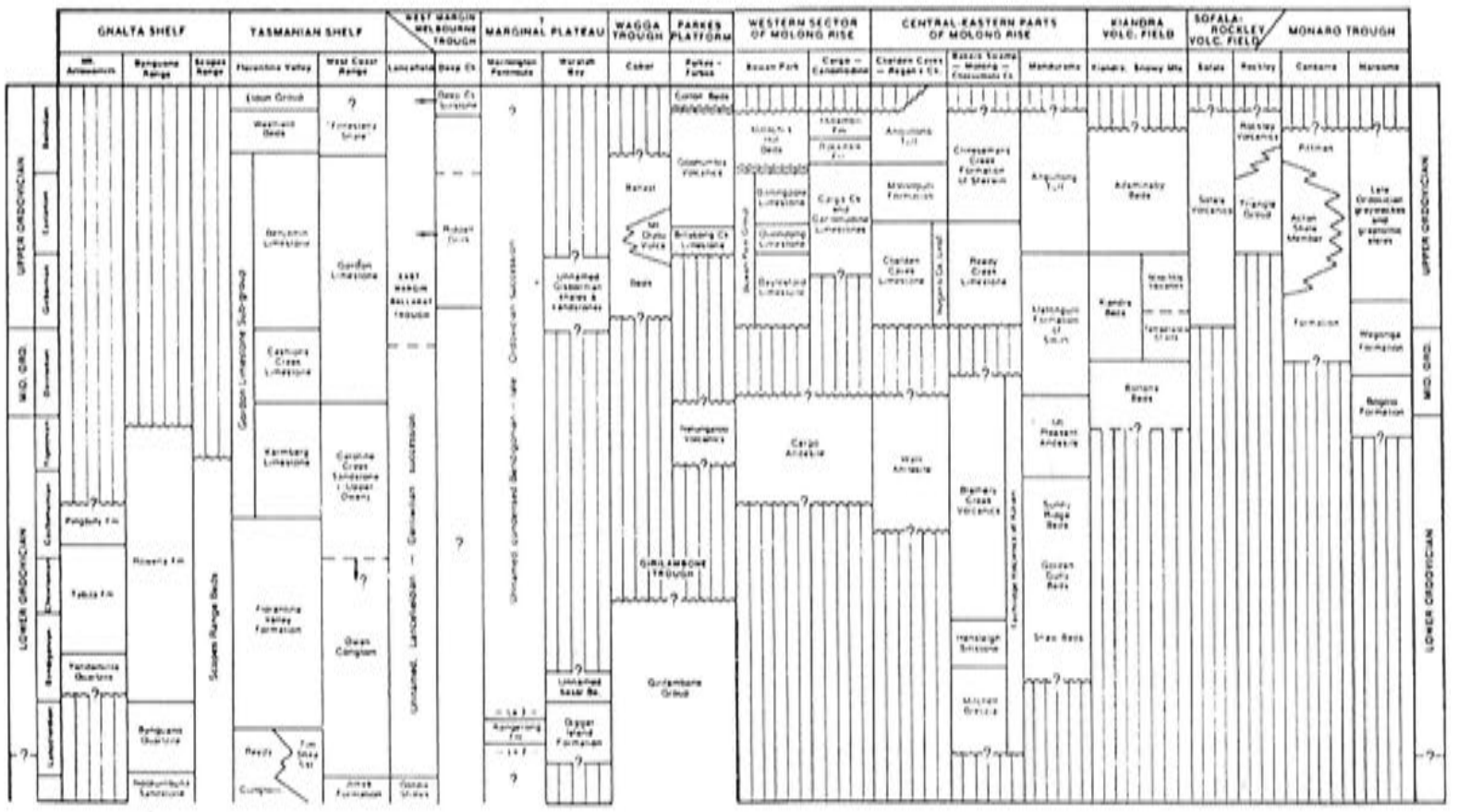

Figure 2.6 Time–space plot for the Ordovician successions of southeast Australia (after Webby, 1976).

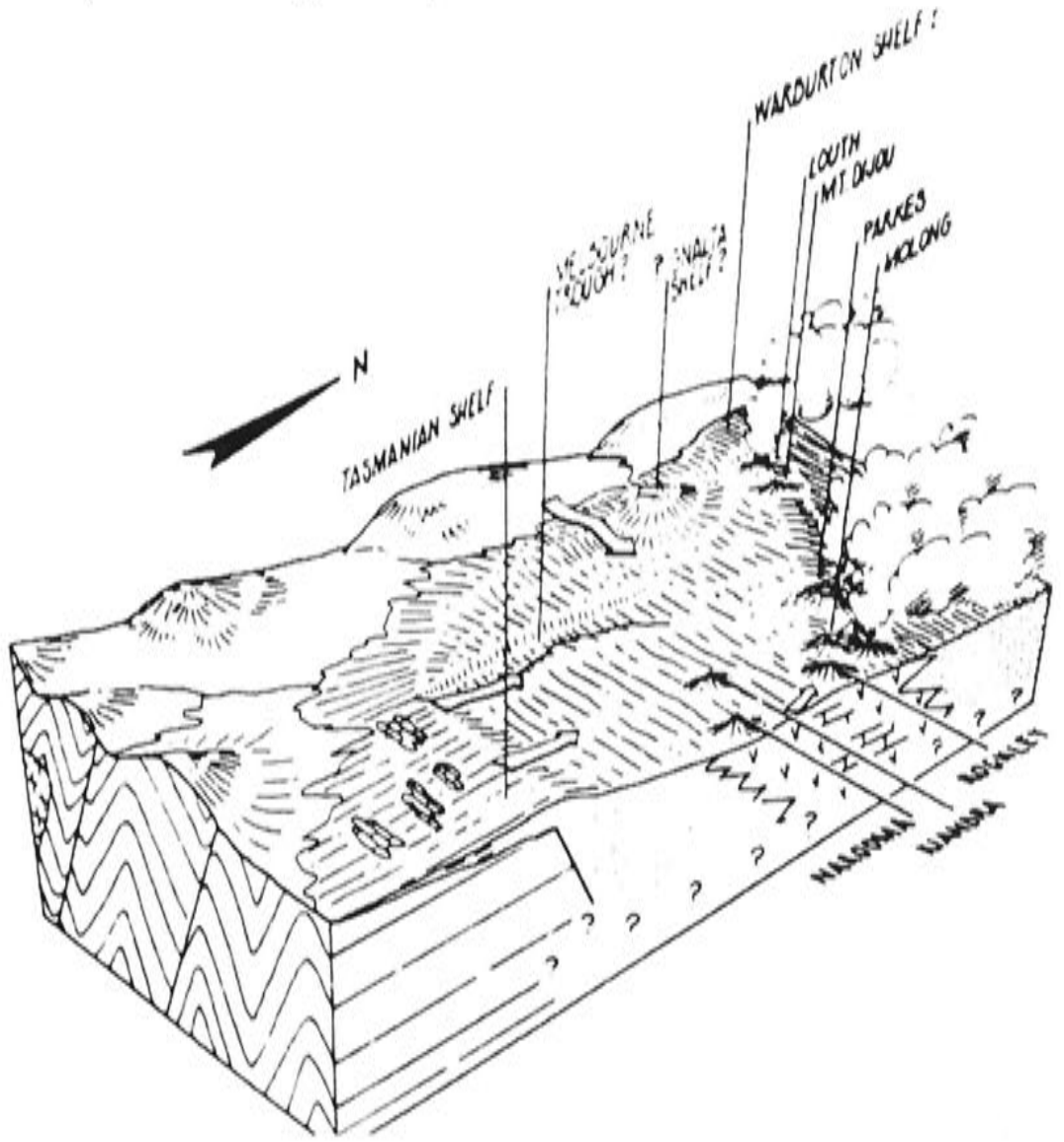

Figure 2.7 Schematic block diagram of Late Ordovician palaeogeography, southeastern Australia (after Powell 1984b).

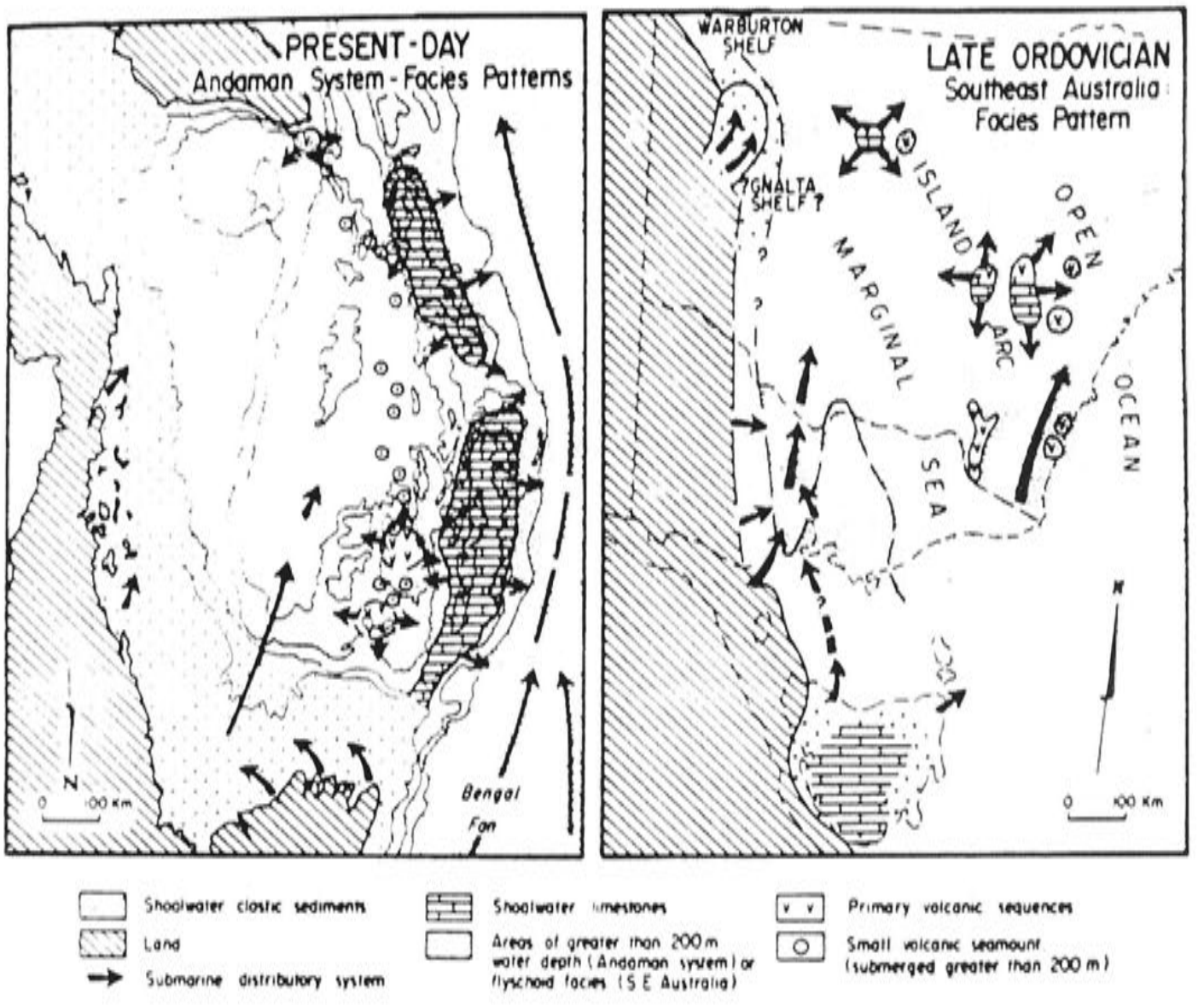

Figure 2.8 Schematic map comparing the facies distribution of the Andaman Basin region with southeastern Australia (after Cas et al., 1980).

2.2.4 Early to Middle Silurian

The Early to Middle Silurian rocks are mainly deep-water successions with minor shallow-marine sequences. The complete lack of Silurian successions in western New South Wales indicates that the area was essentially emergent after the Benambran Orogeny at the end of the Late Ordovician. The alternative explanation, that any sequences deposited were subsequently completely eroded, seems unlikely. The Benambran deformational event involved intense folding and high temperature – low pressure style metamorphism of the western belt of rocks to form the Wagga Metamorphic Belt. S-type granites were intruded into this belt soon after. It is noteworthy that the main effects of the Benambran Orogeny appear to be confined to the area west of a line now marked by the Gilmore Suture (Fig. 2.9).

According to Powell (1984b), the Early Silurian palaeography included a Benambran Landmass on the western side of the fold belt, a shallow-marine shelf and a deep-marine basin receiving flysch (Figs 2.10, 2.11).

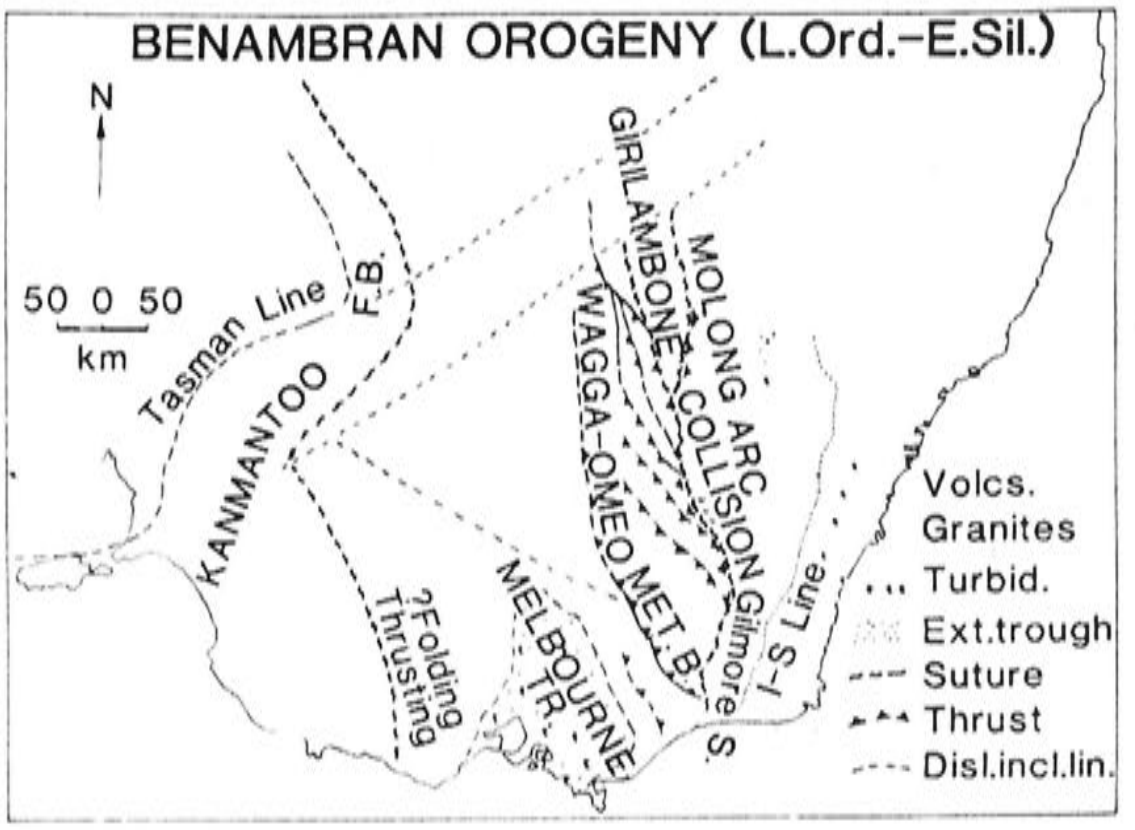

Figure 2.9 Palaeogeography at Benambran time (after Scheibner, 1989b).

2.2.5 Middle Silurian to Early Devonian

During the Middle Silurian, in the area east of the Wagga Metamorphic Belt there was local uplift and erosion of older sequences (the Quidongan Orogeny of Crook et al., 1973). Powell (1984a) however, regards the Quidongan Orogeny more as local movements on the eastern edge of the rising Benambran Landmass.

The first widespread silicic volcanism occurred in the Middle Silurian together with intrusion of coeval granitic complexes. The volcanic sequences are closely associated with either shallow-marine carbonates and epiclastics or deep-water epiclastics (Cas, 1983).

Meridional horsts and grabens began to form in the eastern Lachlan Fold Belt during the Middle Silurian and were well established by the Late Silurian. Graben initiation was heralded by the widespread eruption of rhyolitic to rhyodacitic volcanics. Figure 2.12 shows a schematic diagram of the palaeogeography of the Late Silurian and Early Devonian.

Scheibner (1974) argued that extension occurred in a back-arc setting with a frontal volcanic arc positioned outboard of New England and oblique subduction causing transtension. Powell (1984b) suggests an alternative model in which a dextral transform plate margin developed and the resulting transtensional regime persisted from the mid Silurian to the mid Devonian. The North American Basin and Range Province is used as an analogy. A third model, proposed by Packham (1987), suggests that the Silurian troughs were related to major sinistral strike-slip displacement of individual segments of the Ordovician arc.

Figure 2.10 Early Silurian palaeogeography (after Powell, 1984b).

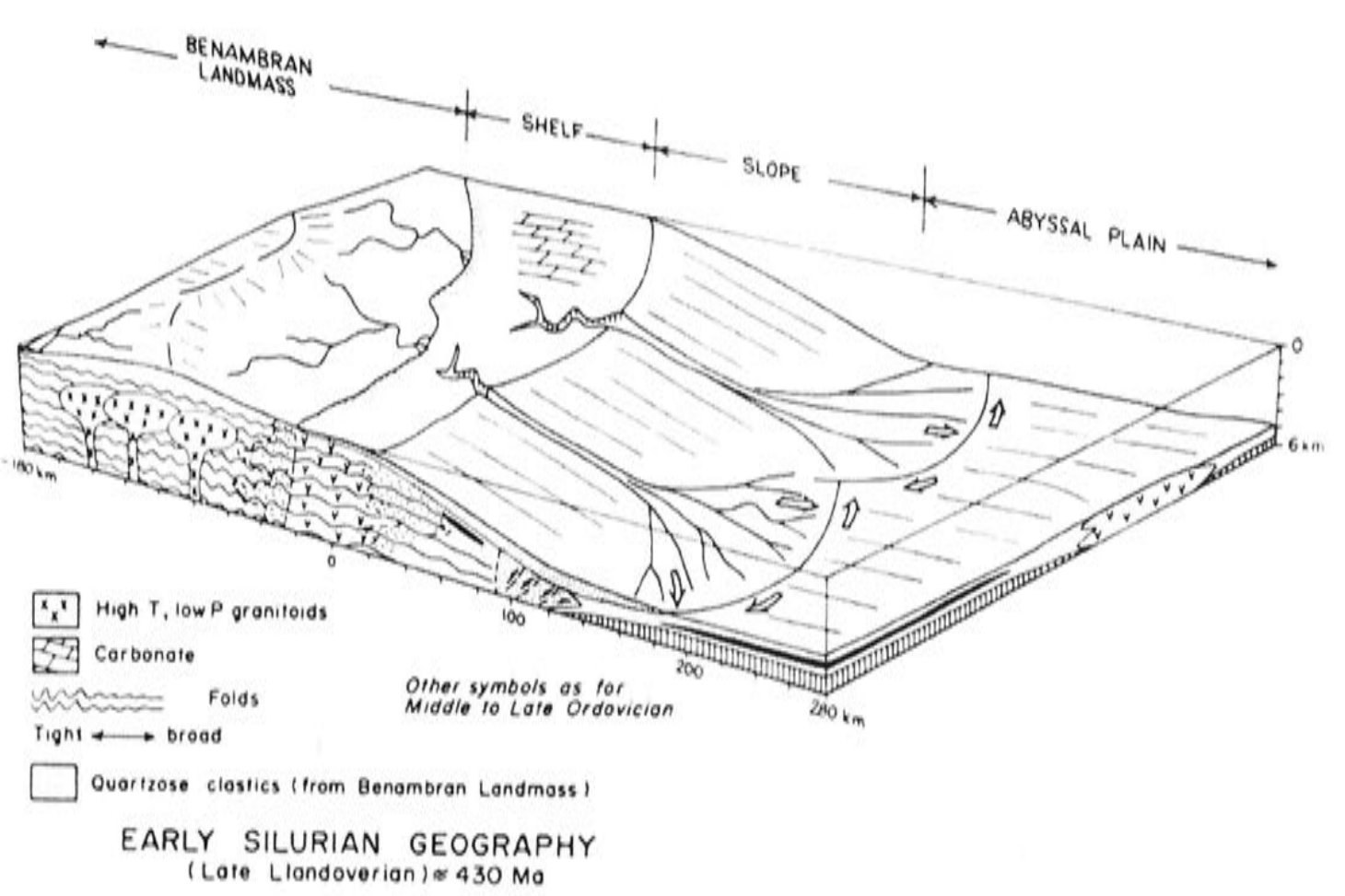

Figure 2.11 Schematic block diagram of Early Silurian palaeogeography (after Powell, 1984b).

During the latest Silurian to earliest Devonian time the Bowning–Bindi thermal event affected a zone between the Gilmore Suture and the so-called Coolac–Narromine Suture. These structures flank the Parkes Terrace which is the stratotectonic unit containing the Goonumbla porphyry complexes. This event coincided with the intrusion of numerous granites across the Lachlan Fold Belt. This massive melting event was short lived, but volumetrically it was the most important igneous event in the Lachlan Fold Belt.

2.2.6 Middle Devonian to Early Carboniferous

The Early to Middle Devonian interval is considered to represent a period of transition from the preceding mixed marine and terrestrial geography to a dominantly terrestrial setting in the Late Devonian to Early Carboniferous (Fig. 2.13). During the Late Devonian and Early Carboniferous, the eastern and southern areas of the Lachlan Fold Belt resembled modern continental, bimodal volcanic rift terrains such as the East African Rift, and the Basin and Range Province (Cas, 1983). The Kanimblan Orogeny affected the Lachlan Fold Belt during the Carboniferous.

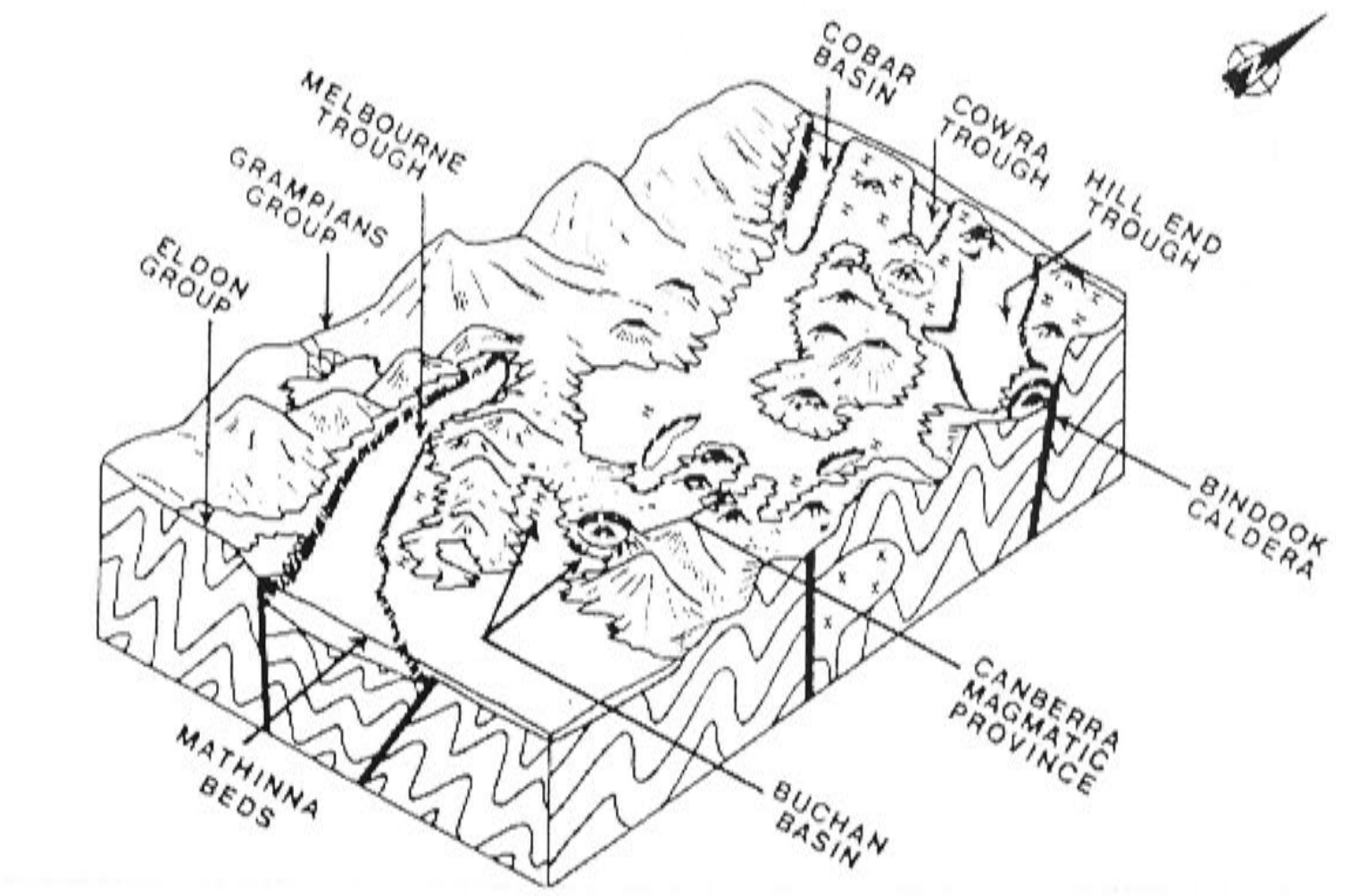

Figure 2.12 Schematic block diagram of Late Silurian and Early Devonian palaeogeography (after Powell 1984b).

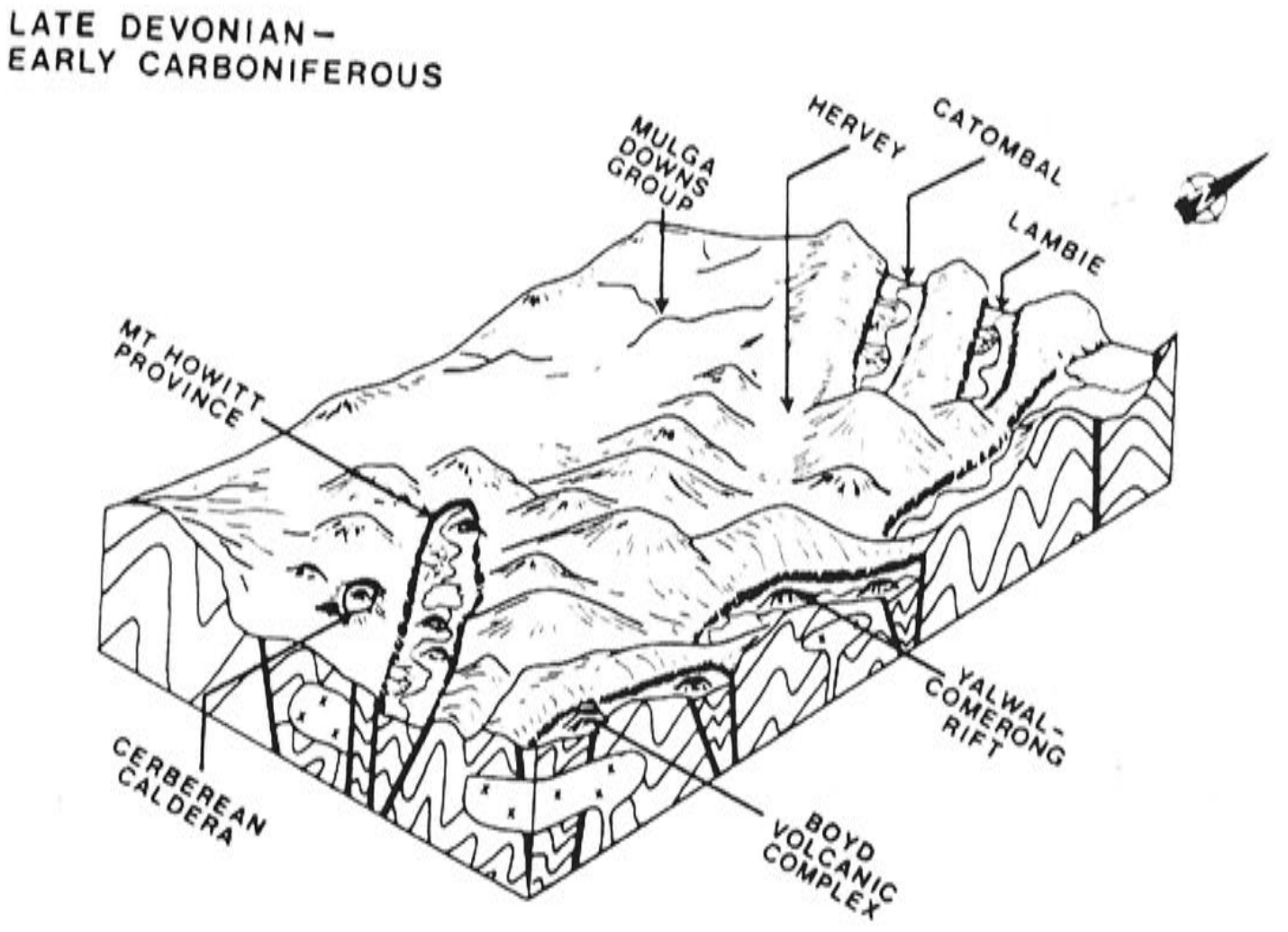

Figure 2.13 Schematic block diagram of Late Devonian to Early Carboniferous palaeogeography (after Powell 1984b).

2.3 REVIEW OF ORDOVICIAN TECTONIC MODELS

The Ordovician stratotectonic units not only comprise a significant part of the Lachlan Fold Belt, but they also have important metallogenic associations (Fig. 2.14). Because of these features a number of tectonic reconstructions have been made for the Ordovician (Oversby, 1971; Solomon and Griffiths, 1972; Packham, 1973; Scheibner, 1973; Griffiths, 1977; Crook, 1980; Powell, 1984b). In the review of some of these tectonic models presented below, note the critical role of the mafic to intermediate volcanics.

Scheibner (1973) was one of the first to provide an exhaustive account of the Lachlan Fold Belt using the paradigm of modern plate tectonics. He considered that the Parkes volcanic belt, Molong volcanic belt and the Sofala Volcanics formed a contiguous belt in the Middle Ordovician, at the leading edge of the Parkes Terrace (a microcontinent made up of Cambro-Ordovician Girilambone Beds (Fig. 2.15)). A marginal sea (Wagga Marginal Basin) separated the microcontinent – arc complex from the western edge of the craton.

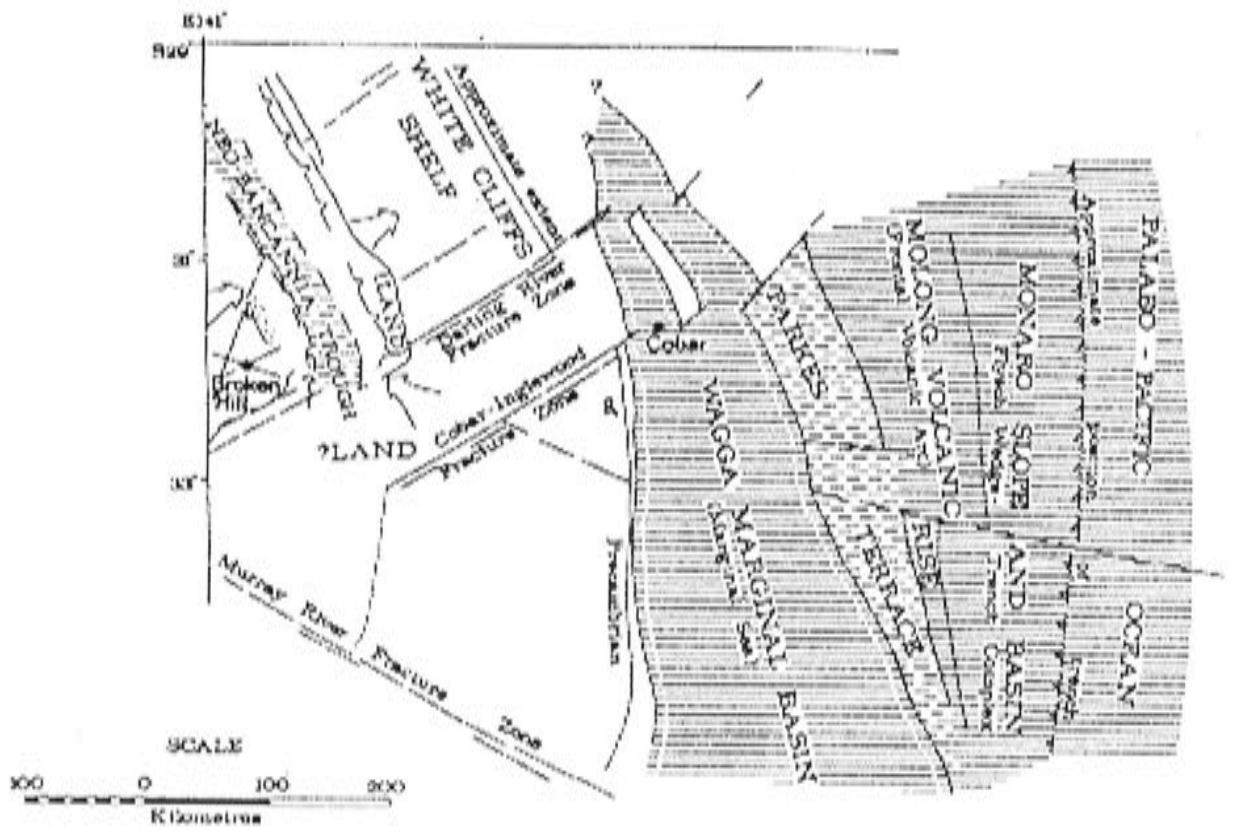

Figure 2.14 Palinspastic map of New South Wales during the Middle Ordovician (Scheibner 1989b).

Scheibner called the volcanic arc the Molong Volcanic Rise, and stated that it had 'typical orogenic island-arc volcanism' meaning calc-alkaline volcanics. Subsequent studies have shown that only a minor part of the Molong Volcanic Rise is of calc-alkaline character, and that it is dominated by rocks of the shoshonite association (Owen and Wyborn, 1979; Clarke, 1990; Heithersay et al., 1990). Chapter 5 of this study reviews shoshonitic tectonic settings, and concludes that shoshonites can form in a variety of tectonic environments which may not necessarily be associated with contemporaneous subduction. Trace elements in the Ordovician rocks do however have a typical arc signature, characterised by low Ti and Nb. The dominance of shoshonites in the Late Ordovician volcanic piles does not invalidate Scheibner's thesis; however chemical grounds alone are insufficient to prove the existence of an island or continental arc.

Using the interarc rifting model of Karig (1971), Scheibner (1973) went on to suggest that the arc split to form the initial Cowra Trough with the active part of the arc displaced eastwards. Accretion of the flysch wedge further east in the Monaro Slope and Basin continued (Fig. 2.16). The trench complex needed to be even further east and Powell(1983) argued that it is represented by the deformed Wagonga Formation on the south coast of New South Wales. The Benambran Orogeny in the Late Ordovician closed this Ordovician stage.

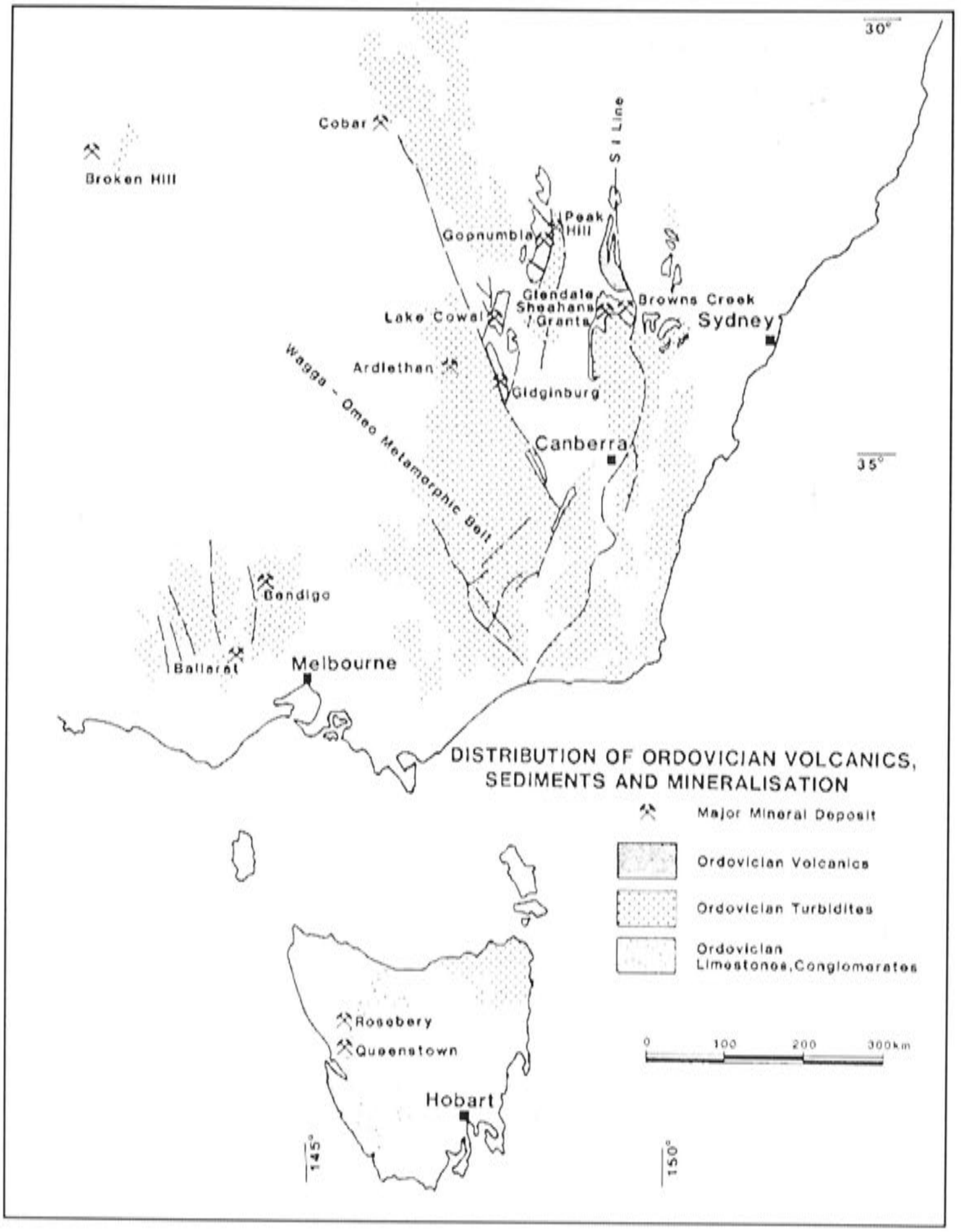

Figure 2.15 Ordovician geology and mineralisation.

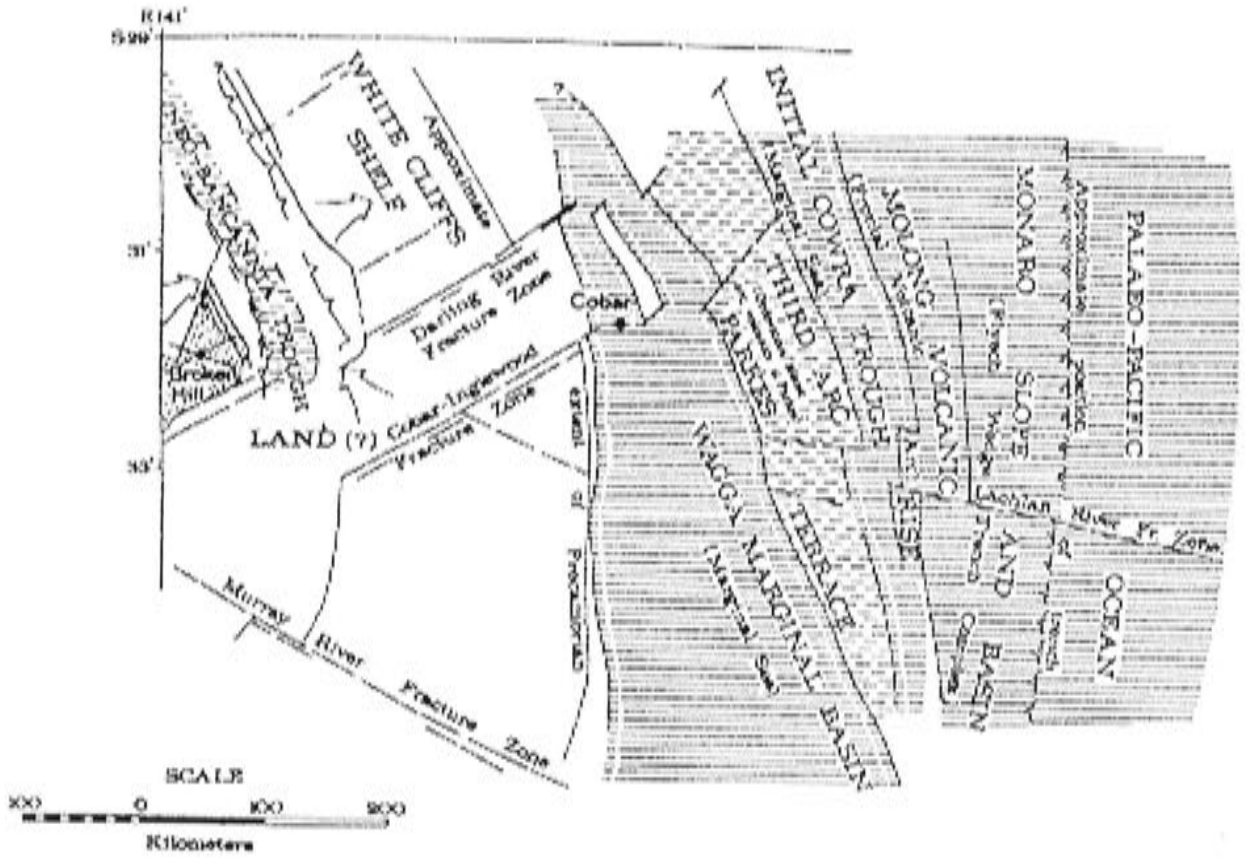

Figure 2.16 Palinspastic map of New South Wales for the Late Ordovician (Scheibner 1989b).

In a recent review of the tectonics of New South Wales, Scheibner (1989b) presents a modified model which accommodates new data, while retaining the basic notion of arc–subduction complexes. He argues that because the oldest volcanics in the Molong Arc occur in the westernmost Parkes segment (Nelungaloo Volcanics; Sherwin, 1979) and the arc youngs eastwards, the arc may have progressively moved eastwards during westerly dipping subduction. The model envisages west-facing, Mariana-type subduction developing east of the Molong Microcontinent. The Molong Arc developed on the Molong Microcontinent, further east was the Monaro Slope and Basin, and still further east, the accretionary prism (Wagonga Beds). During the Late Ordovician the Mariana-type boundary changed from west dipping to an east dipping Chilean-type convergent margin due to an incoming hypothetical Proterozoic intraoceanic volcanic arc. Scheibner is not clear on this latter part, but presumably means the Kosciusko Terrane of Chappell et al. (1988). This microplate possibly reactivated the arc from the eastern side causing subduction to 'flip' and dip to the west. Finally the Ordovician arc, together with its Proterozoic microplate, collided with the Wagga Marginal Basin in the Late Ordovician – Early Silurian Benambran Orogeny. The collision line is now marked in part by the Gilmore Suture. This model of continental margin splitting with arcs built on an older substrate, coupled with marginal sea formation, encompasses the models of Oversby (1971), Packham (1973), Solomon and Griffiths (1972), Cas et al. (1980) and Powell (1983).

A second model, proposed by Crook (1980), centres on the nature of the basement to the Lachlan Fold Belt. He acknowledges the evidence of granitoid geochemistry (Chappell and White, 1974), possible granite source ages (Compston and Chappell, 1979) and the geochemistry of possible protoliths for S-type granitoids (Wyborn, 1977) which suggest a Proterozoic sialic basement. However, he points out the paradox of widespread deep-water sediments, mafic volcanics in the older parts of the succession and the presence of ophiolites and boninites (Crawford and Cameron, 1985), which suggest an ensimatic origin for the Palaeozoic sediments and volcanics and therefore an oceanic substrate. He postulates a new model in which vertical and lateral growth of continental crust and its eventual stabilisation is a consequence of extended evolution of the fore-arc regions of magmatic arcs. The Palaeozoic of southeastern Australia grew through fore-arc evolution of 10 east-facing arc terrains, similar to the Marianas Arc Complex today which is built on oceanic crust. Of the 10 arc terrains only two were active at any one time. Continental accretion resulted from subduction of the marginal sea between the two arcs, with the landward arc being accreted on the continent during the resulting collision. A new arc develops on the seaward side and the cycle continues. After collision, the defunct landward arc is buried under 'post-arc sediments'.

A third model, proposed by Crawford (1983), was derived from the perspective of the geological relationship of the Cambrian 'greenstones' to the overlying Ordovician succession. He contends that geochemically, the boninite–MORB association proves that the Cambrian formed as part of a Marianas-type, island-arc – back-arc style setting. The continued subduction of oceanic crust in this setting led to the return of a microcontinent which had rifted from the Australian craton in the late Precambrian. The microcontintent eventually collided with the island-arc – back-arc setting in the Late Ordovician, which is recorded as the Benambran Orogeny. Further convergence was accommodated by the microcontinent passively thrusting over the main continental block at a low angle for several hundred kilometres, to become effectively a mega allochthonous terrane. The author draws an analogy with the Appalachian Fold Belt. A problem with this model is that there are no known thrusts in the overriding plate, a feature which is documented in younger fold belts where arc–continent collisions have occurred (Powell, 1984b). This model is important however, as it was one of the first to consider that large-scale terrane movements may have occurred in the development of the Lachlan Fold Belt.

The application of concepts of terrane analysis to eastern Australia has drawn attention to the possibility of large-scale movement of stratotectonic blocks (Leitch and Scheibner, 1987). A fourth model which emerged from the realisation of these concepts was presented by Packham (1985), who was one of the first authors to use the plate tectonics paradigm in New South Wales. He suggests that the remnant Ordovician

volcanic centres were originally part of a single arc, some 1700 km long. Oblique subduction in the Late Ordovician would have allowed a spreading centre – transform junction to be subducted, with the result of a triple point moving south along the trench with sinistral motion north of it and subduction of young crust to the south. By the Early Silurian the arc – marginal sea complex had become a zone of strike-slip tectonics, with uplift and deformation of the Wagga belt commencing with transform movement along the Gilmore Fault. The net effect of this transform movement was to place the linear outcrops of Ordovician volcanics in their current configuration with the development of Silurian basins in between (Figs 2.17 and 2.18).

Owen and Wyborn (1979) and Wyborn (1988) consider the tectonic setting from a petrological viewpoint. Their data, together with that of Clarke (1990) and Heithersay et al. (1990), suggest that most of the Ordovician volcanism falls within the shoshonitic association, with minor tholeiitic basalts in the southern part of the arc near Kiandra. At Parkes, high-K calc-alkaline intrusives have been noted, but the succession is dominantly shoshonitic. Owen and Wyborn (1979) express doubts about using the shoshonitic character of the volcanics to prove a subduction model for the Molong Arc.

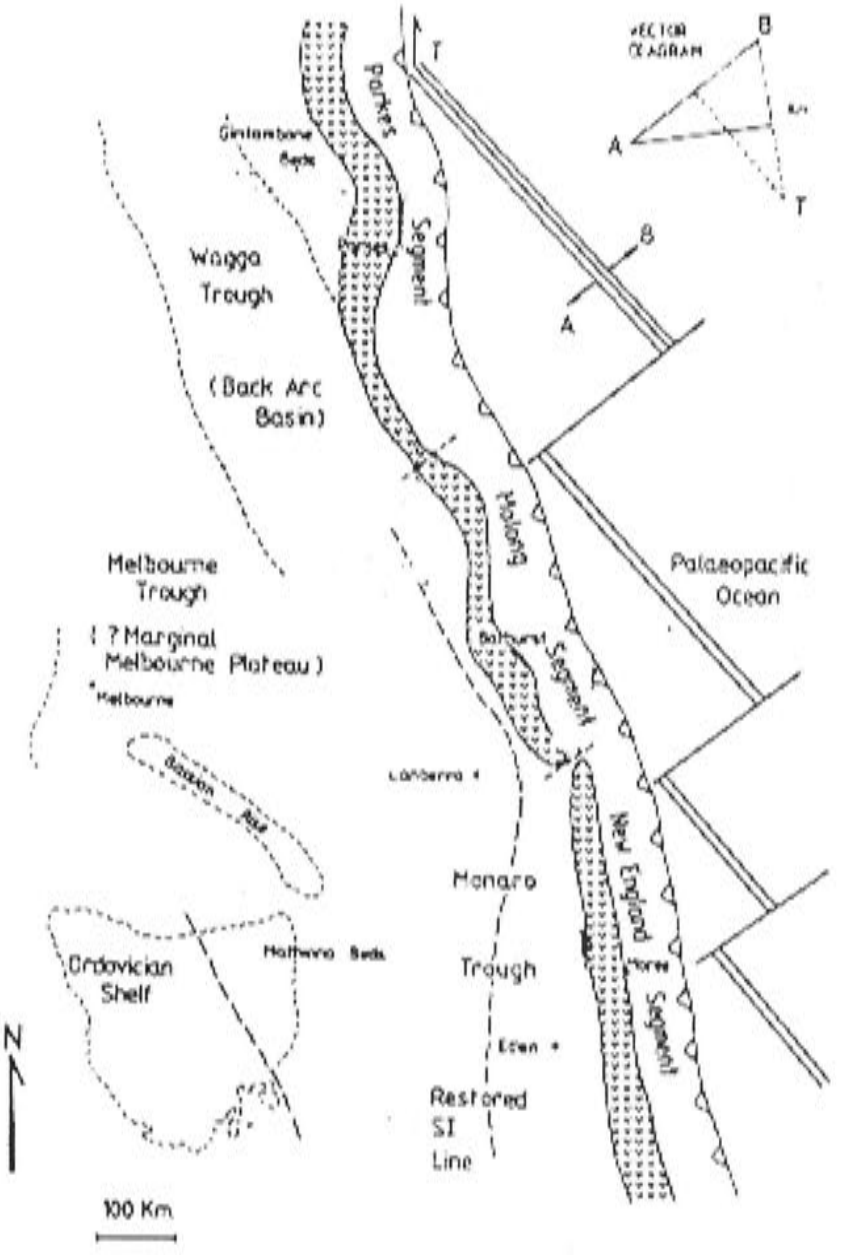

Figure 2.17 Palaeogeography at the end of the Ordovician (Packham,1985).

Wyborn (1988) suggested that the Ordovician volcanics formed by partial melting of subcontinental upper mantle, after delamination of cold and dense subcontinental lithosphere had caused the crust to founder. Wyborn (1988) notes that the rocks are enriched in a suite of elements, K, Ba, Sr and P, which is commonly attributed to subduction-related devolatisation of subducted lithosphere (Pearce, 1983). The low Th, U and LREE in the rocks — elements which are not normally depleted in arc magmas — led him to suggest that processes other than subduction applied.

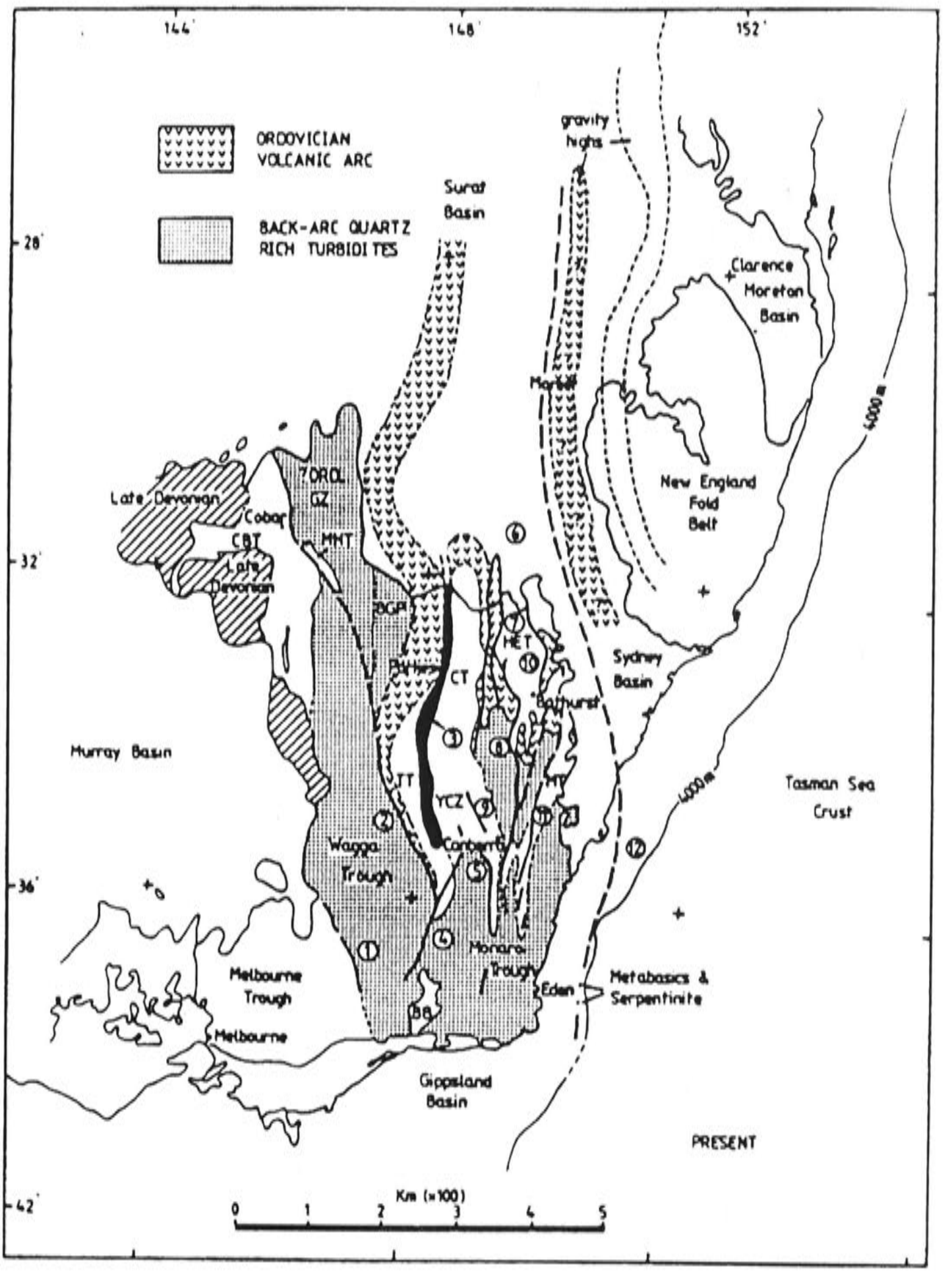

Figure 2.18 Present day configuration (after Packham, 1985).

2.4 SUMMARY

In the early seventies Scheibner and Crook applied the modern plate tectonics paradigm to the Lachlan Fold Belt, proposing models of multiple subduction zones, accretion and extension leading to the present configuration of volcanics and intrusions. In the same period Chappell and White (1974), challenged this approach based on geochemical and isotopic analysis of the widespread granites in the Lachlan Fold Belt. Their central thesis was that granite chemistry directly reflected, and indeed mapped, the source regions and therefore basement to the LFB, which they concluded was largely Proterozoic crust. In a series of papers in the late eighties they invoked alternate largely intraplate styles of tectonic development for the Lachlan Fold Belt.

The data outlined in subsequent chapters in this thesis lends weight to an oceanic substrate overlain by arc-derived volcanics and intrusions, albeit of an uncommon type (shoshonitic). Isotopic data reported here points to a mantle source for all the metals, with little evidence for crustal contamination. The chemistry of the Ordovician volcanics near Parkes unequivocally represent arc volcanics. Taken together, these data point to an ocean-island setting for the Parkes segment of the Ordovician volcanic belt.

Chapter 3

THE GOONUMBLA VOLCANIC COMPLEX: REGIONAL SETTING AND GEOLOGY

3.1 INTRODUCTION

This chapter presents the regional geological setting and the geology of the Goonumbla Volcanic Complex. The complex is part of a coherent geophysical and geological block which extends form Narromine through Parkes to West Wyalong (Fig. 3.2) and includes parts of two major structural subdivisions of the Lachlan Fold Belt; the Girilambone Anticlinorial Zone and the Tumut Synclinorial Zone (Scheibner, 1985a). Outcrop in the region is generally very poor, and an understanding of the regional geology has been achieved only after considering gravity and magnetic data in conjunction with outcrop and float mapping, and the results of regional drilling.

The general physiography of the Central West of New South Wales is of slopes and plains. Around Parkes the Ordovician and Silurian sequences occur in the floors of broad, flat valleys and are usually covered by a veneer of Cainozoic alluvial gravels and clays. Pastures and wheatfields commonly cover these areas. The valleys are flanked to the east and west by low ridges and hills of Devonian sandstones and volcanics. Poorly consolidated Mesozoic gravels, representing palaeo-river channels, cover bedrock in some areas west of Parkes.

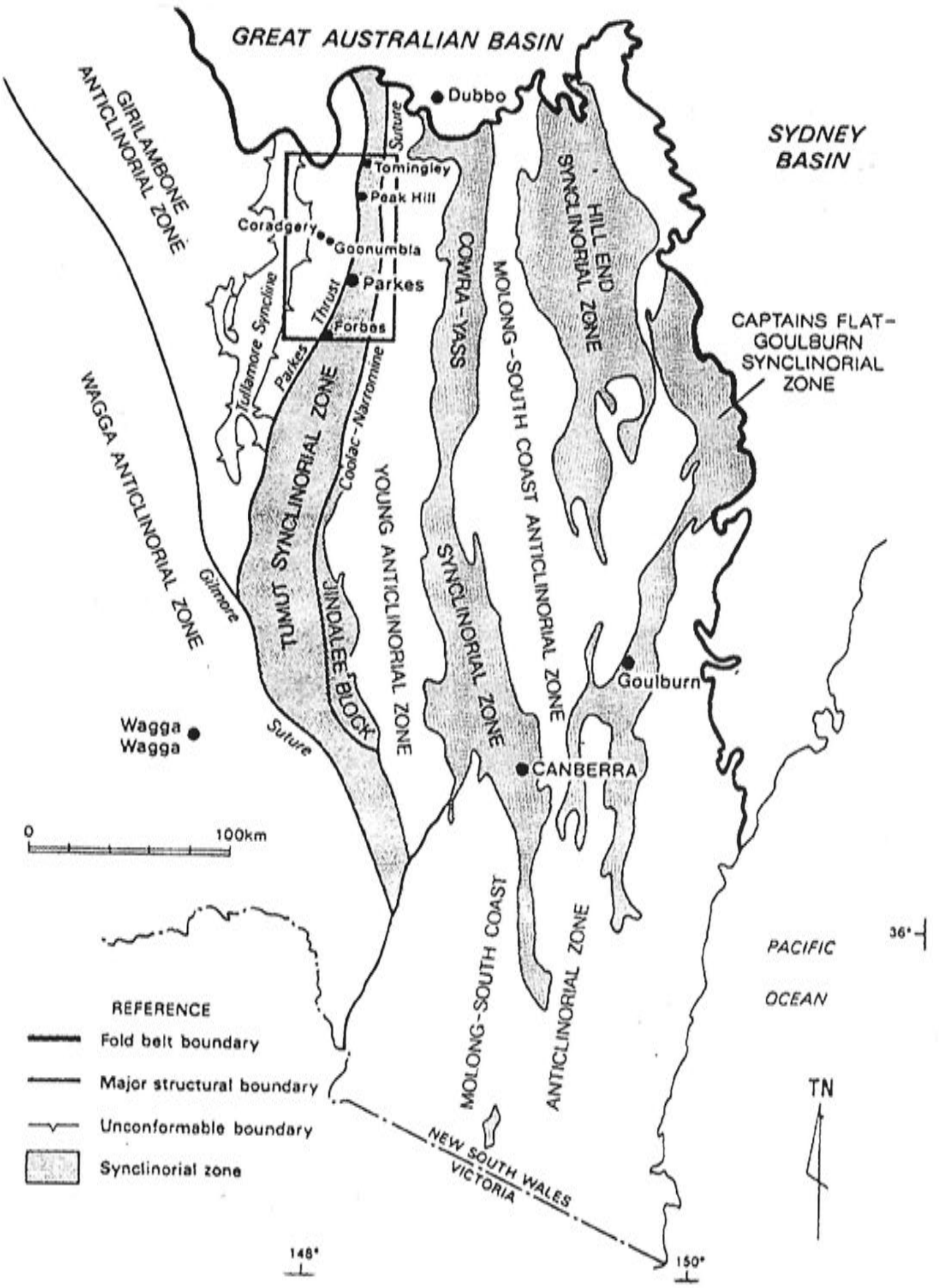

Figure 3.1 Structural subdivision of the Lachlan Fold Belt (after Scheibner, 1985b).

3.2 NARROMINE–PARKES – WEST WYALONG BLOCK

3.2.1 Gravity data

A prominent ridge in the gravity image of eastern Australia (Fig. 2.4) has been called the Parkes Gravity Ridge (Tenison Woods, 1990). The gross geometry and dimensions of the ridge are very similar to the Cambrian Mount Wright – Stavely Volcanic Arc in western New South Wales, which hints at similar sources for the gravity configurations.

It is noteworthy that the sinusoidal grain of the Proterozoic in the west seems to persist across to the Parkes Gravity Ridge, suggesting that if the basement of the Lachlan Fold Belt is indeed Proterozoic crust then cover structures may be expected to reflect underlying older structure.

In detail, the Parkes Gravity Ridge (Fig. 3.2a) contains a central gravity low caused by sediments of the Tullamore Syncline (c.f. Figs 3.2, 3.3, 3.5). The extent of Late Ordovician volcanics is also shown in Figure 3.2 and it is clear that the main volcanic complexes have a close spatial relationship with the gravity ridge. It is noteworthy that the western side of the gravity ridge is over rocks of the Girilambone Anticlinorial Zone, which are deformed metasediments with low-specific gravity.

Tenison Woods (1990) did modelling of the Parkes Gravity Ridge along an east–west profile using a two-dimensional forward modelling program with average densities assigned to known rock units. The results (Fig. 3.3) suggest that the gravity ridge reflects a combination of near-surface intermediate volcanics and pre-Ordovician, moderate- to high-specific gravity basement at a depth of around 9 km. The bulk of the Ordovician sequence was interpreted to be pelagic sediments. It is noteworthy that the depth to the proposed pre-Ordovician basement is reflected in the broad pattern of the anomaly. The density contrast of the pre-Ordovician basement at 0.15 is the same as that of the intermediate volcanics at the surface, suggesting that intermediate volcanics may form part of the pre-Ordovician basement.

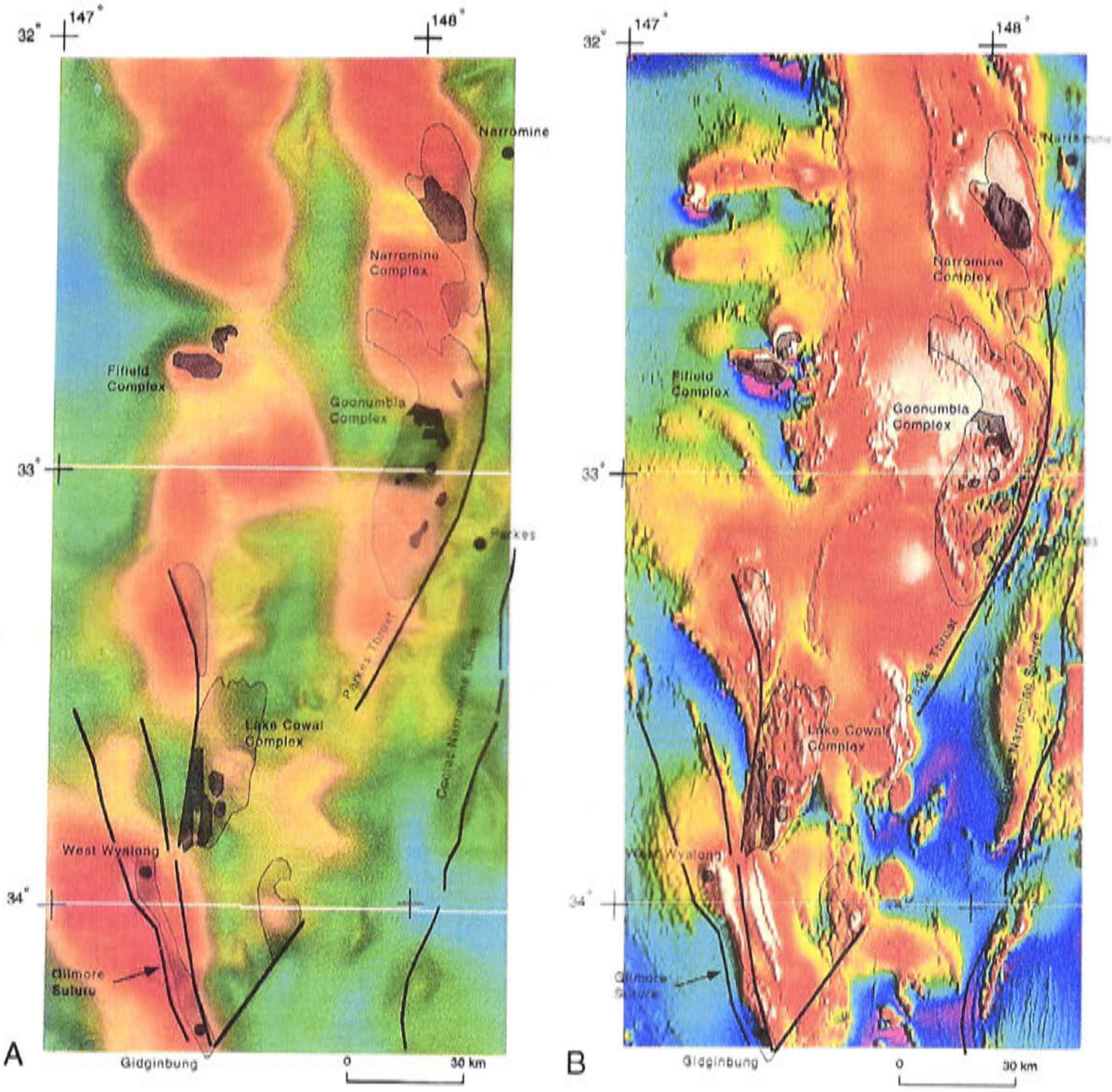

Figure 3.2 Gravity **(a)** and aeromagnetic features **(b)** of the Parkes – Narromine Volcanic Belt. Acquisition of gravity data was completed by the Bureau of Mineral Resources in 1973 using a grid cell of 11 km; the gravity image is an image enhanced view of these data. The aeromagnetic image is also derived from the Bureau of Mineral Resources data acquired in 1973. The Ordovician volcanic centres of Gidginbung – West Wyalong, Lake Cowal, Goonumbla and Narromine are annotated.

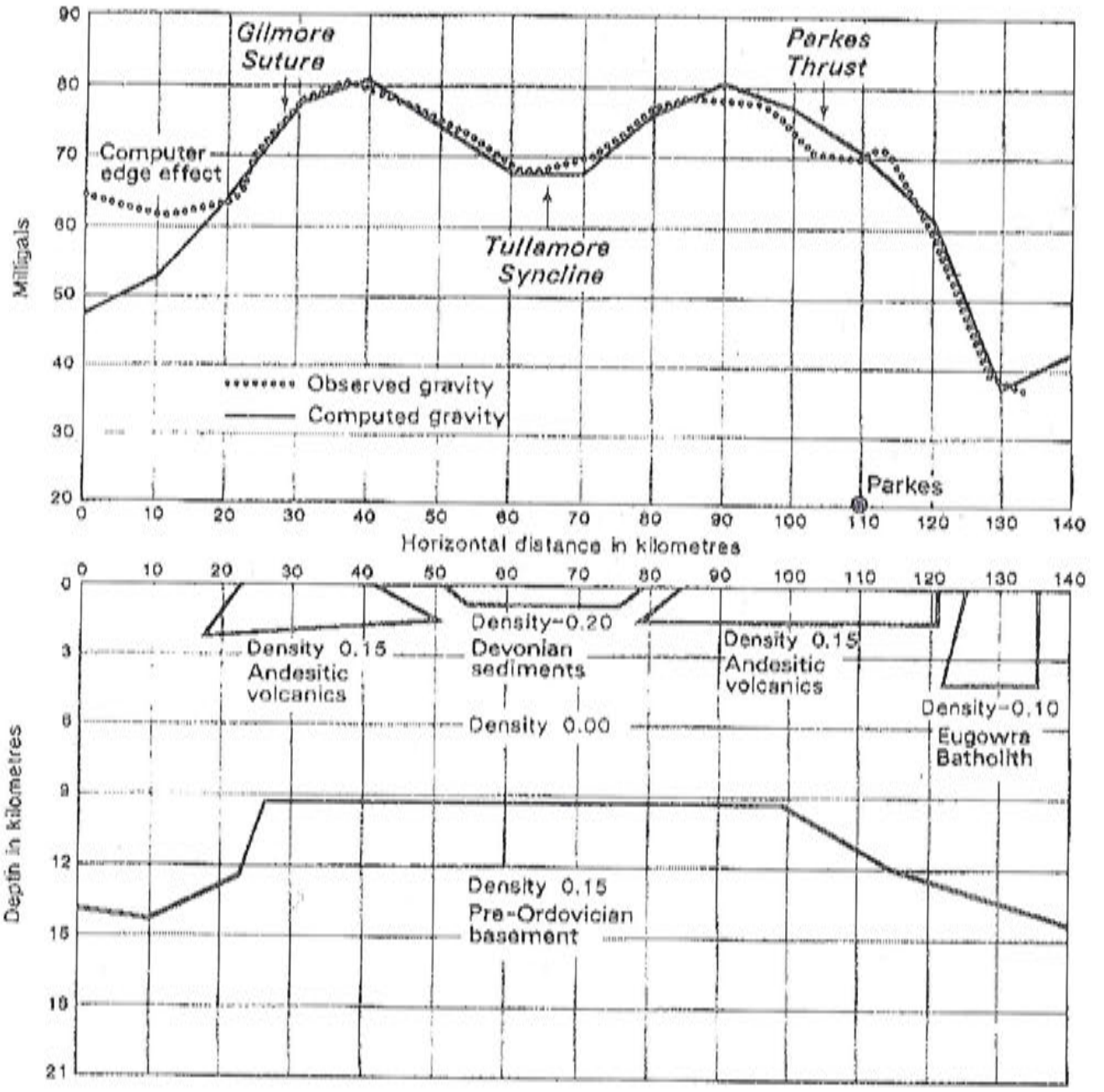

Figure 3.3 Observed and computed gravity profiles along an east – west traverse across the Forbes 1:250 000 sheet at approximately 33°08'S.

3.2.2 Magnetic data

The extent of Ordovician volcanic rocks can be readily seen in the aeromagnetic data (Figs 3.2b, 3.4). Five major complexes of mafic to intermediate volcanics, all mapped by Geopeko, are delineated in the magnetics: the Narromine, Goonumbla, Lake Cowal, Temora and Quandialla Complexes. To date the Goonumbla, Lake Cowal and Temora Complexes have shown themselves to be hosts to significant mineral deposits; most notably the Endeavour 22, 26 North, 27 and 44 deposits in the Goonumbla Complex, Endeavour 42 in the Lake Cowal Complex and the Gidginbung deposit in the Temora Complex. Other areas of complex magnetics can be related to Silurian or Devonian volcanic rocks.

A feature of Figure 3.2b is the northerly trending linear band of intense magnetic highs, 70 km northwest of Parkes. These highs reflect the platinum-bearing ultrabasic intrusive rocks of the Fifield Platinum Province (Barron et al., 1991); an area that has been the target of intense exploration in recent years. These rocks have been classified as Alaskan- or Ural-type gabbro–peridotite intrusions (Barron et al., 1990), and two schools of thought have emerged as to the genesis and significance of these

intrusions. Barron et al. (1991) envisage crustal thinning of a failed, back-arc setting with geosutures marked by thin bodies of Alpine peridotite. Raised geotherms facilitated development of high-temperature felsic magma with shoshonitic or tholeiitic affinities. These magmas invaded the extended region and produced volcanic and intrusive complexes. Zoned alkali ultramafic complexes resulted due to assimilation of Alpine peridotite by felsic magma at depths of 12 to 18 km. The authors imply that the failed back arc was an Ordovician feature related to subduction, with later crustal thinning occurring during the Devonian along this locus of weakness. Wyborn and Cameron (1990) regard these ultramafic bodies as cumulates related to Ordovician magma chambers, which ultimately gave rise to shoshonitic volcanism. They contend that the bodies have classical cumulate textures with olivine and clinopyroxene dominating initially to produce dunites and wehrlites, followed by hornblende clinopyroxenites and monzogabbros. This question will be examined more fully in Chapter 5, but note that Sherwin (1973) has mapped mafic and ultramafic cobbles in the base of the Early Devonian Derriwong Group which lends weight to Wyborn and Cameron's argument that the Fifield complexes are Ordovician in age.

The Gilmore Suture is well defined south and north of West Wyalong by north- to north-northwest-trending linear features in the aeromagnetics. The suture, which marks an important break between structural blocks, was activated during the Late Ordovician Benambran Orogeny and has been reactivated many times since. To the north of West Wyalong it splinters into a fan-like array of structures so that the magnetic volcanic sequences are repeated in a series of fault slices. The suture separates the magnetically subdued rocks of the Wagga–Omeo Metamorphic Belt (Girilambone Group in Fig. 3.5) from the volcanic and plutonic rocks to the east, which have stronger and more complex magnetic patterns (Fig. 3.4).

Two sub-parallel north-northeasterly trending structures are shown on the eastern side of Figure 3.2b, which are important regional structural boundaries. The first in part defines the eastern margin of the Goonumbla Complex, and is mapped as the Parkes Thrust near Forbes and Parkes (Sherwin, 1973). It can be inferred from the magnetics that this feature extends north to Narromine and south towards West Wyalong and the Gilmore Suture. Scheibner (1985b) uses this feature to separate the Tumut Synclinorial Zone from the Girilambone Anticlinorial Zone. The second structure is a fault called the Coolac–Narromine Suture by Scheibner (1989a.), which is the boundary between the Tumut Synclinorial Zone and the Young Anticlinorial Zone.

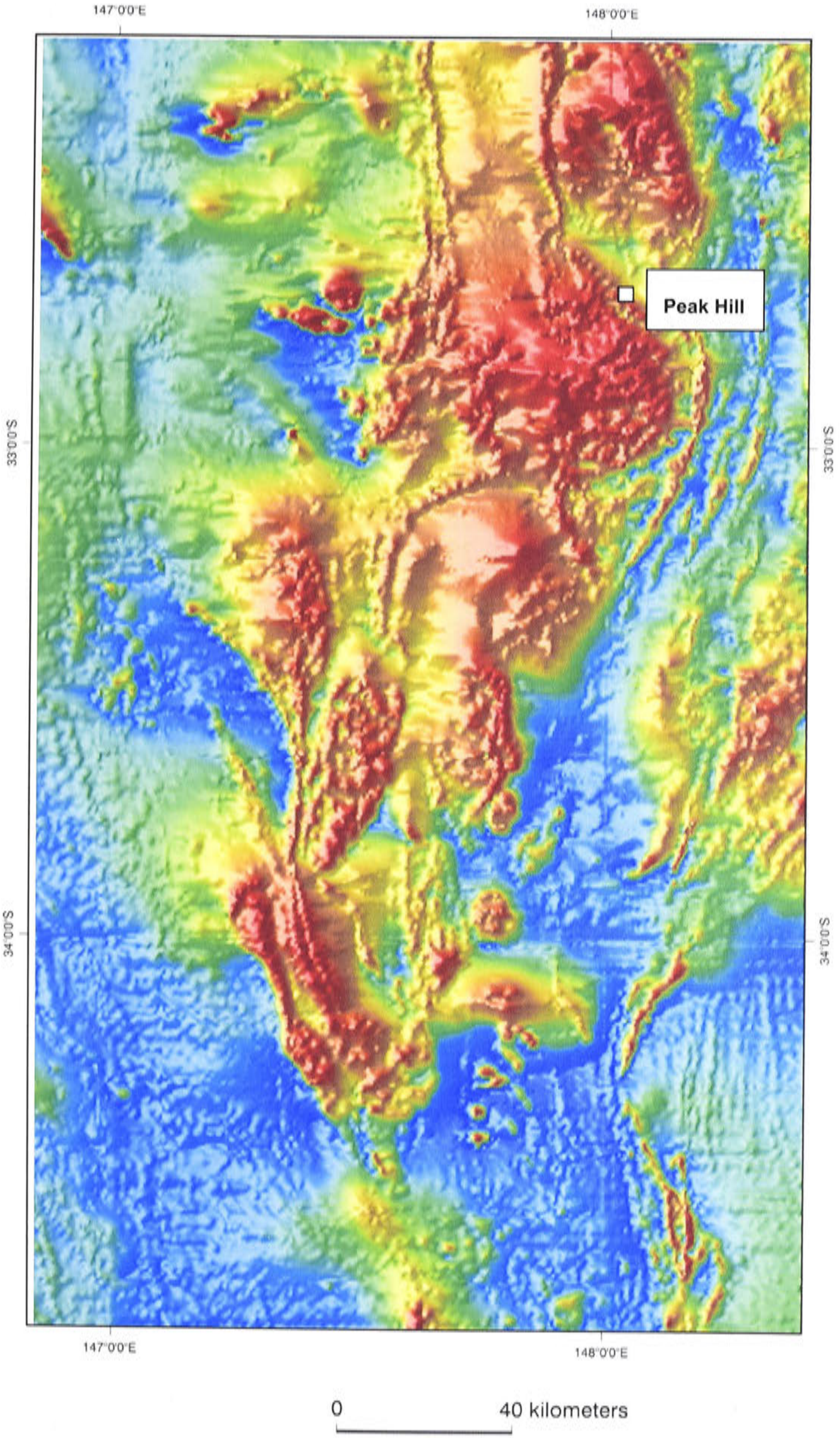

Figure 3.4 Aeromagnetic image of the Parkes region, based on Bureau of Mineral Resources 1973 data

Of major importance in the understanding of the Goonumbla Porphyry Cu–Au district is the pronounced circular feature in the magnetics northwest of Parkes. Jones (1985) interpreted the circular feature within the Goonumbla Volcanic Complex to be a collapsed caldera. The magnetic ring feature is partly defined by magnetite-bearing monzonites and diorites that form a ring dyke on the margin of the interpreted caldera. Other circular features, possibly representing collapsed calderas, occur through the Ordovician belt (Fig. 3.2b).

3.2.3 Cambro-Ordovician

The oldest rocks exposed in the region are rocks of the Cambro-Ordovician Girilambone Group, which occur in the west of the Parkes region and, as noted, are in part bounded by the Gilmore Suture. The group is composed of turbidite, chert and slate with minor marl, conglomerate, quartz–magnetite rock and greenstone, which have been multiply deformed and metamorphosed. The rocks appear to form the basement for the western part of the Molong Volcanic Arc (Suppel and Scheibner, 1990). The Kirribilli Beds which lie east of the Goonumbla Volcanic Complex can be correlated with the Girilambone Group because they are also complexly folded phyllites with evidence of refolded folds, at least three cleavage fabrics and strong rodding. Contacts between the Kirribilli Beds and surrounding rocks are always faulted and abundant quartz veining is a feature. Evidence of intense, multiple deformations are not noted in younger rocks. The absolute date of the Girilambone Group is poorly constrained, but Cambrian to Early Ordovician is the general view (Scheibner, 1976).

The cross-section through the Parkes area in Figure 3.6 shows a doming of the Early Ordovician into the Forbes Anticline, whereas the Kirribilli Beds are inferred to have been thrust into their present position. This interpretation explains the juxtaposition of highly deformed phyllites against variably but less-deformed Ordovician sediments. This implies that the Girilambone Group forms the basement to the Ordovician volcanic succession.

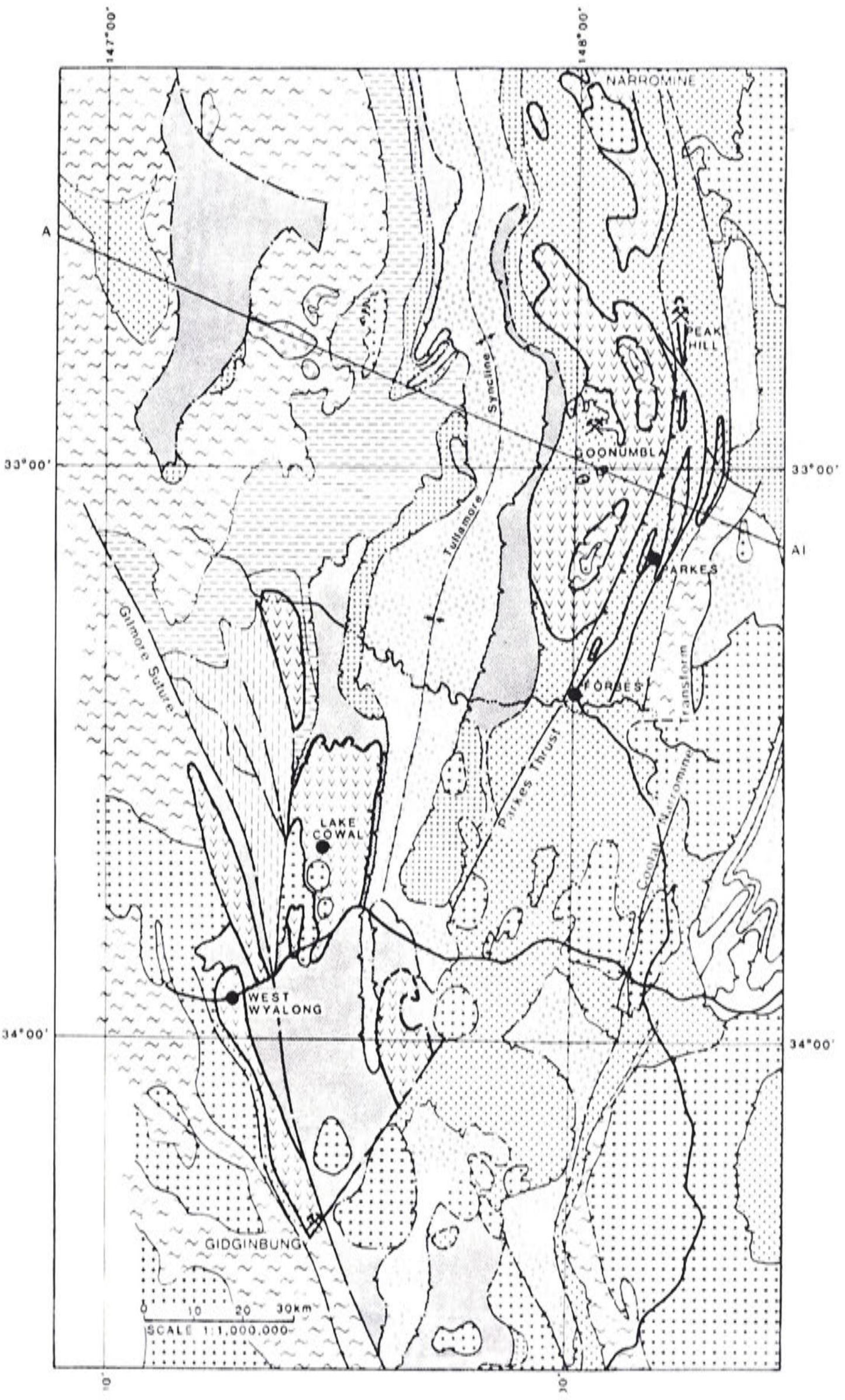

Figure 3.5 Interpretive geological map of the Parkes region based on existing New South Wales Geological Survey data and mapping by Geopeko with interpretation based on aeromagnetic data. See Figure 3.6 for legend.

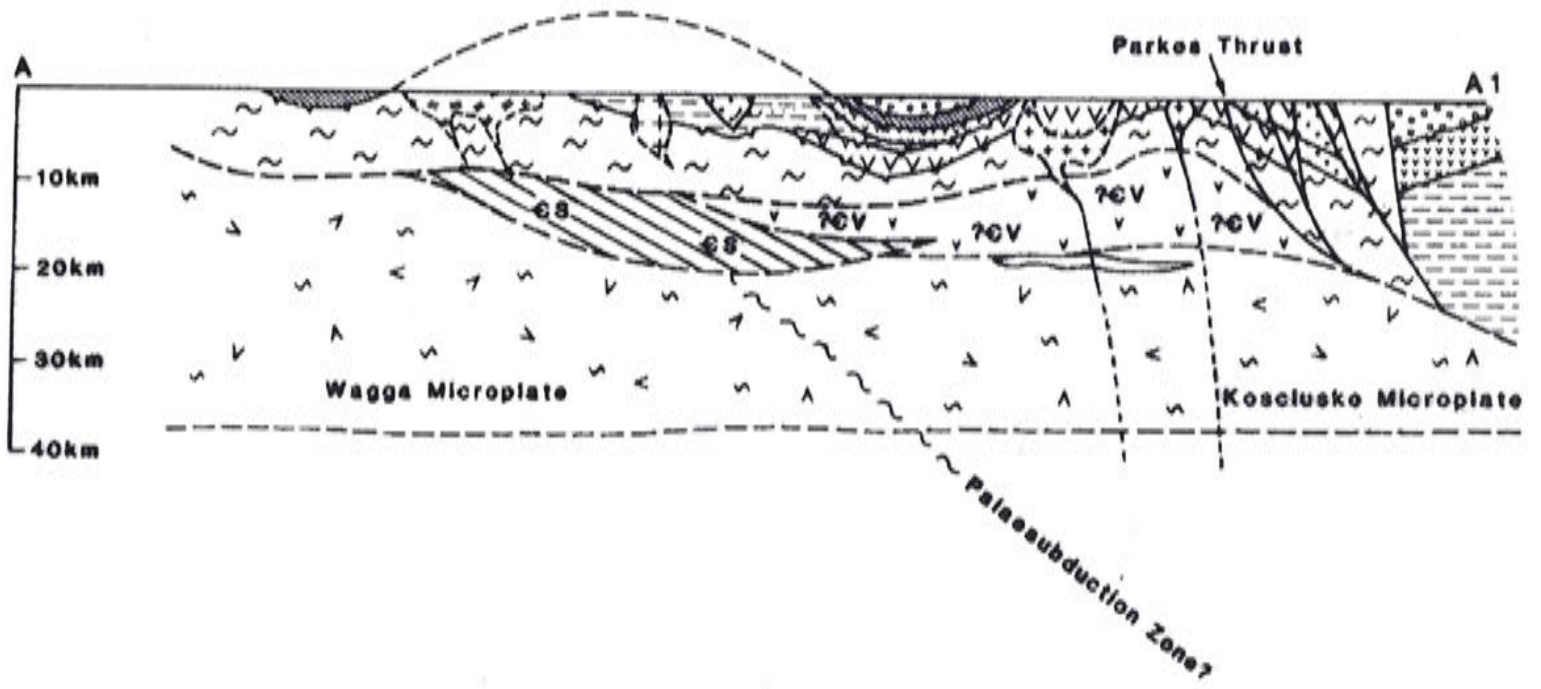

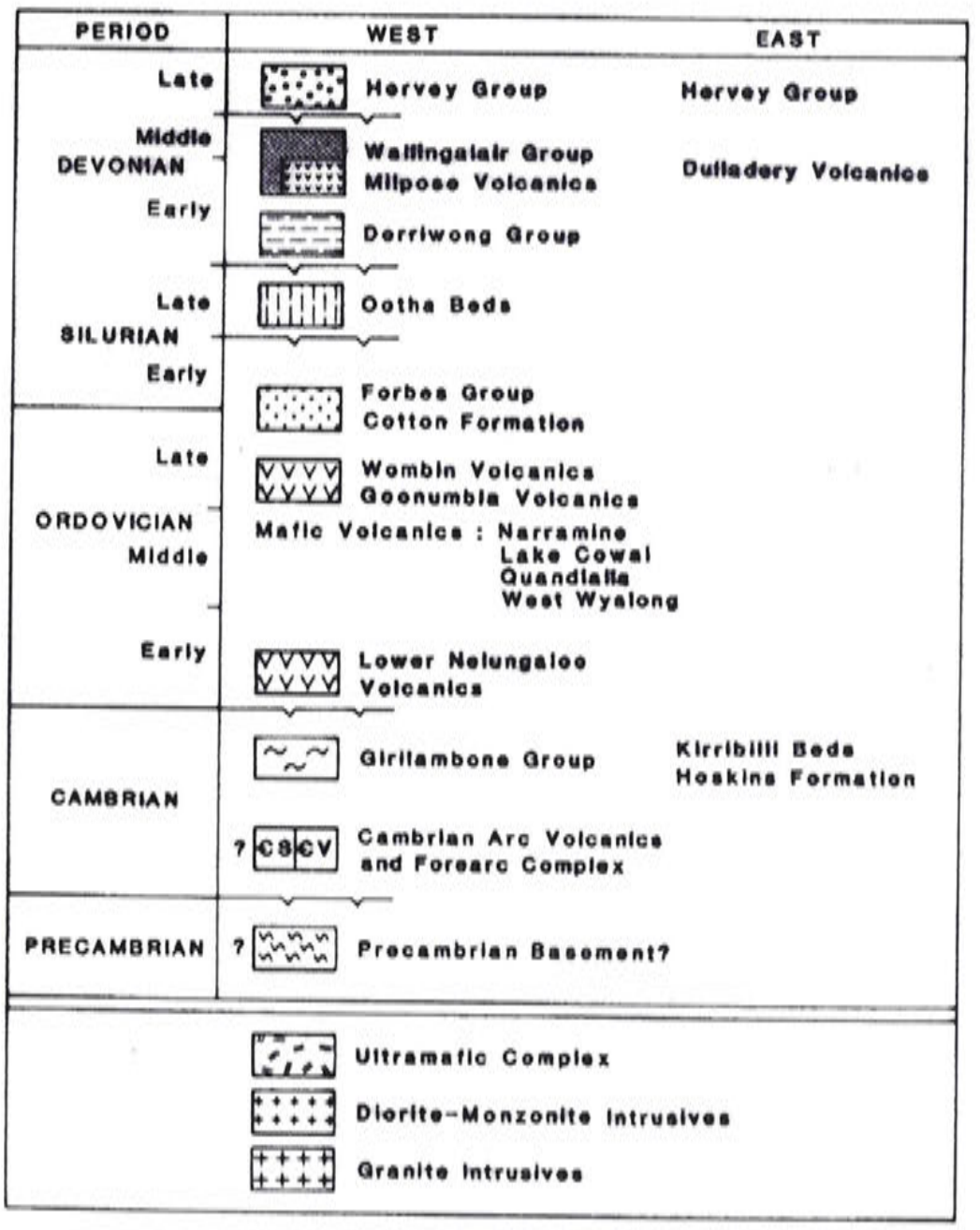

Figure 3.6 Interpretive cross-section A–A' through the Parkes region. Line of section is located in Figure 3.5.

3.2.4 Ordovician – Early Silurian

The Ordovician sequence is made up of two distinct successions separated by the Parkes Thrust. The rocks of the western succession are dominantly volcanic with minor sediments, whereas those of the eastern succession are dominantly deformed sedimentary rocks with some volcanic rocks (Figs 3.5, 3.6). The volcanic complexes in the western succession range from lavas through volcaniclastics to reworked epiclastics and are characterised by high-level, coeval intrusives. The composition of the volcanics is dominantly shoshonitic, however the Lake Cowal Complex appears to be more high-K calc-alkaline. Fossils from the sedimentary units give mainly Late Ordovician ages, but the overall range is from Early Ordovician to the late part of the Early Silurian (Sherwin, 1973, 1974, 1983).

The eastern succession around Parkes is made up of dominantly mudstone with lesser chert, siliceous mudstone and lava. The few fossil ages that have been obtained are all Late Ordovician. Clarke (1990) argues from chemical considerations, that the volcanic units represent separate volcanic centres. The contacts of many volcanic units with surrounding sediments are faulted however, so it is possible that the volcanics were emplaced by faulting from an underlying sequence. Most sedimentary rocks in the eastern succession have a prominent north–south cleavage that is in contrast to the western succession where there is no structural fabric at all. The intensity of deformation in the eastern succession is variable and changes rapidly normal to strike. Narrow high-strain zones can be mapped, often with vertical rodding, suggesting thrust movement. This interpretation is depicted in the cross-section in Figure 3.5.

3.2.5 Middle to Late Silurian

Unconformably overlying the Ordovician – Early Silurian rocks are shallow- to deep-water sediments of the Forbes Group. Near Parkes the unit has a basal conglomerate which contains pebbles of volcanics, chert, quartzite and monzonite, up to 100 mm in diameter, in a limey matrix. The source of most of these pebbles is likely to have been the eroding Goonumbla Volcanic Complex. The rest of the Forbes Group is dominated by silty mudstone and minor sandstone. The unit represents a marine transgression developing finally into a deep-water setting. Fossil evidence indicates a Middle to Late Silurian age (Sherwin, 1975).

3.2.6 Early Devonian

Unconformably overlying the older sequences are Early Devonian shallow-marine sediments containing lenses of terrestrial volcanics. Lithologies include quartz sandstone and conglomerate at the base of the unit, overlain by interbedded shale, impure limestone, sandstone and rhyolitic volcanic rocks.

3.2.7 Late Devonian

The Late Devonian Hervey Group, composed of dominantly sandstone and conglomerate, unconformably overlies the Early Devonian rocks. Taken together, the Devonian sequences define the low ridges and hills that flank Parkes.

3.2.8 Mesozoic

Remnants of an ancient drainage system, comprising poorly cemented coarse conglomerate, occur along the western side of the area. Poorly preserved plant fossils suggest a Jurassic age (Pickett, 1985).

3.3 GEOLOGY OF THE GOONUMBLA VOLCANIC COMPLEX

The Goonumbla Volcanic Complex is part of the western succession of Ordovician units described above. The stratigraphic units are shown in a time–space plot in Figure 3.7 and will be described briefly below. The structure and stratigraphy of the complex can be determined in some detail from the shadow image of low-level aeromagnetics (Plate 3.1). Figure 3.8 shows the geology of Ordovician rocks west of the Parkes Thrust based on mapping by Geopeko. An important structural feature of the area is the broad, open Forbes Anticline which gently domes the volcanic sequence.

3.3.1 Basement sequence

The oldest part of the succession is an unnamed sedimentary sequence which occupies the core of the Forbes Anticline. It shows as the magnetically quiet area in the northeast part of the aeromagnetic image (Plate 3.1), and forms a dome in the southern part of the Forbes Anticline. The sequence is very poorly exposed and has been intersected in only a few drillholes. It consists of siltstone usually with a bleached orange-white appearance; however it is almost black when exposed in drill core below the base of oxidation. Small-scale folds of bedding are common in the rocks and bedding is generally steeply dipping. This is in contrast to the overlying Goonumbla Volcanics

which do not have small-scale folds and are gently dipping, which suggests that there may be an unconformity between the two units.

In the northern area, an exposure of the sequence in a gravel scrape on a low hill (G.R. 055692) has provided some important information on the lithology and age of the unit. The scrape consists of thinly bedded sandy siltstone which is very similar in appearance to the sediments of the Late Ordovician – Early Silurian Cotton Formation. Bedding is folded with fold axes plunging steeply to the southeast. Cross-cutting the siltstone are thin, 50 to 10m mm wide dykes of feldspar porphyry, composed of prominent phenocrysts of plagioclase set in a fine-grained matrix. The dykes are identical to the Nelungaloo Volcanics, which are described below. This timing relationship suggests that the sedimentary sequence either predates or overlaps the Nelungaloo Volcanics. Recently the graptolite *Tetragraptus approximatus* has been found in the quarry (L. Sherwin, pers. comm., 1991), which gives an age of Lancefieldian 3 for the sequence. Similar graptolites have been found in the Yarrimbah Chert Member which overlies the Nelungaloo Volcanics in the south of the area (see next section).

Overall, the geological relationships suggest that the Nelungaloo Volcanics and Yarrimbah Chert are broadly contemporaneous, and locally discordant, with the basement sedimentary sequence. The difference in the styles of deformation remains a problem and perhaps the very tight folding may have occurred only locally in the otherwise broad Forbes Anticline. Nevertheless it is clear that the Early Ordovician volcanism occurred in a sedimentary environment forming below wave base.

3.3.2 Nelungaloo Volcanics

The Nelungaloo Volcanics are the oldest volcanic rocks in the area. The sequence has poor exposure in the core of the Forbes Anticline west of Parkes, and again in the inferred extension of the Forbes Anticline west of Alectown. Where exposed the rock type ranges from a black, phyric vesicular lava to a porphyritic pink-red lava with coarse stubby crystals of plagioclase. There is no bedding in the Nelungaloo Volcanics, however sediments that immediately overlie the sequence are flat lying. In the type area at Yarrimbah porphyritic lava is overlain by sediments of the Yarrimbah Chert Member, the source of graptolites for Sherwin's (1979) study which provided an Early Ordovician (Lancefieldian 3) age for the volcanics.

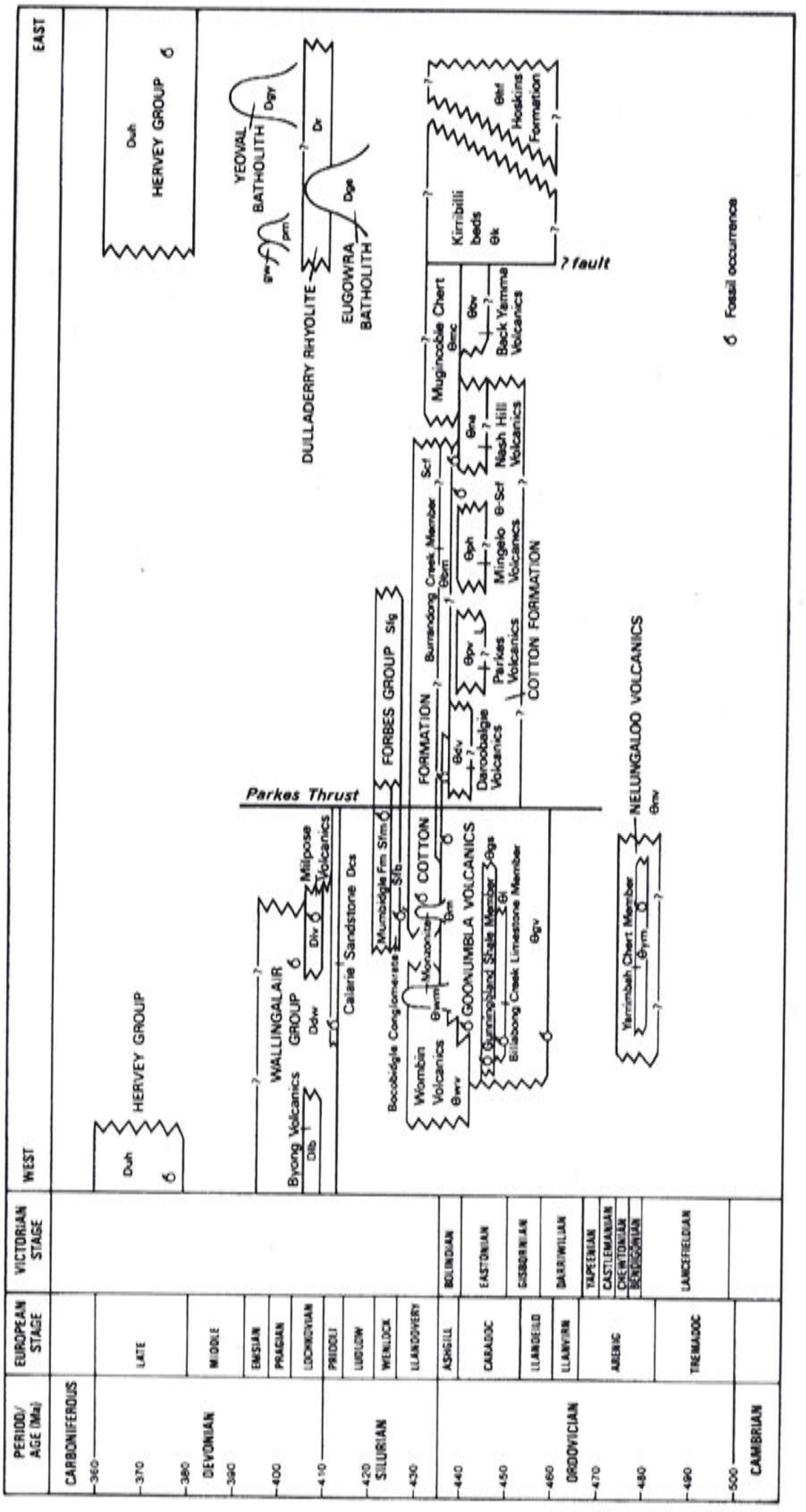

Figure 3.7 Time–space plot for units in the Goonumbla Volcanic Complex.

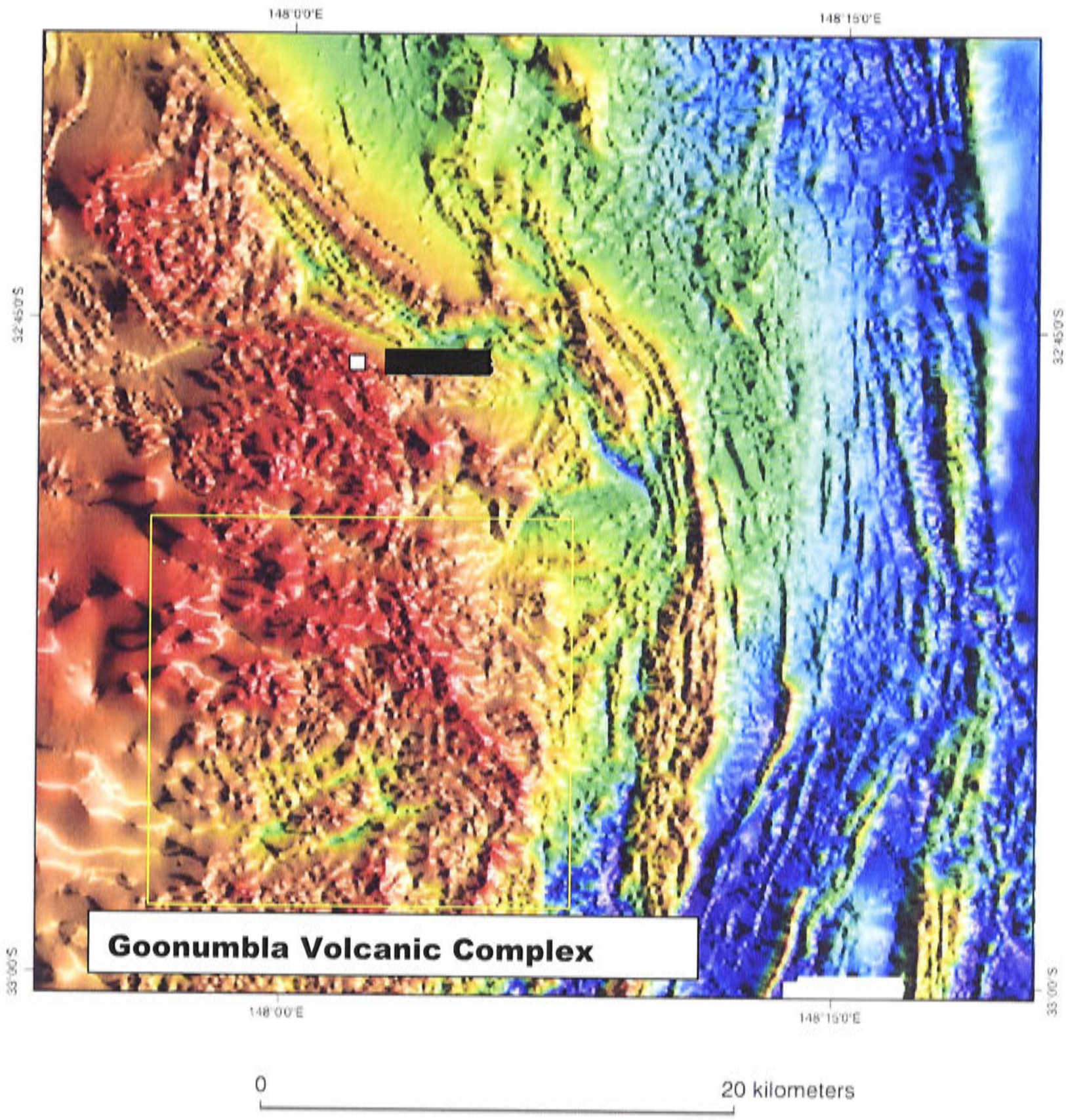

Plate 3.1 Shadow image of aeromagnetic data of the Goonumbla Volcanic Complex (flown by Austirex for Geopeko).

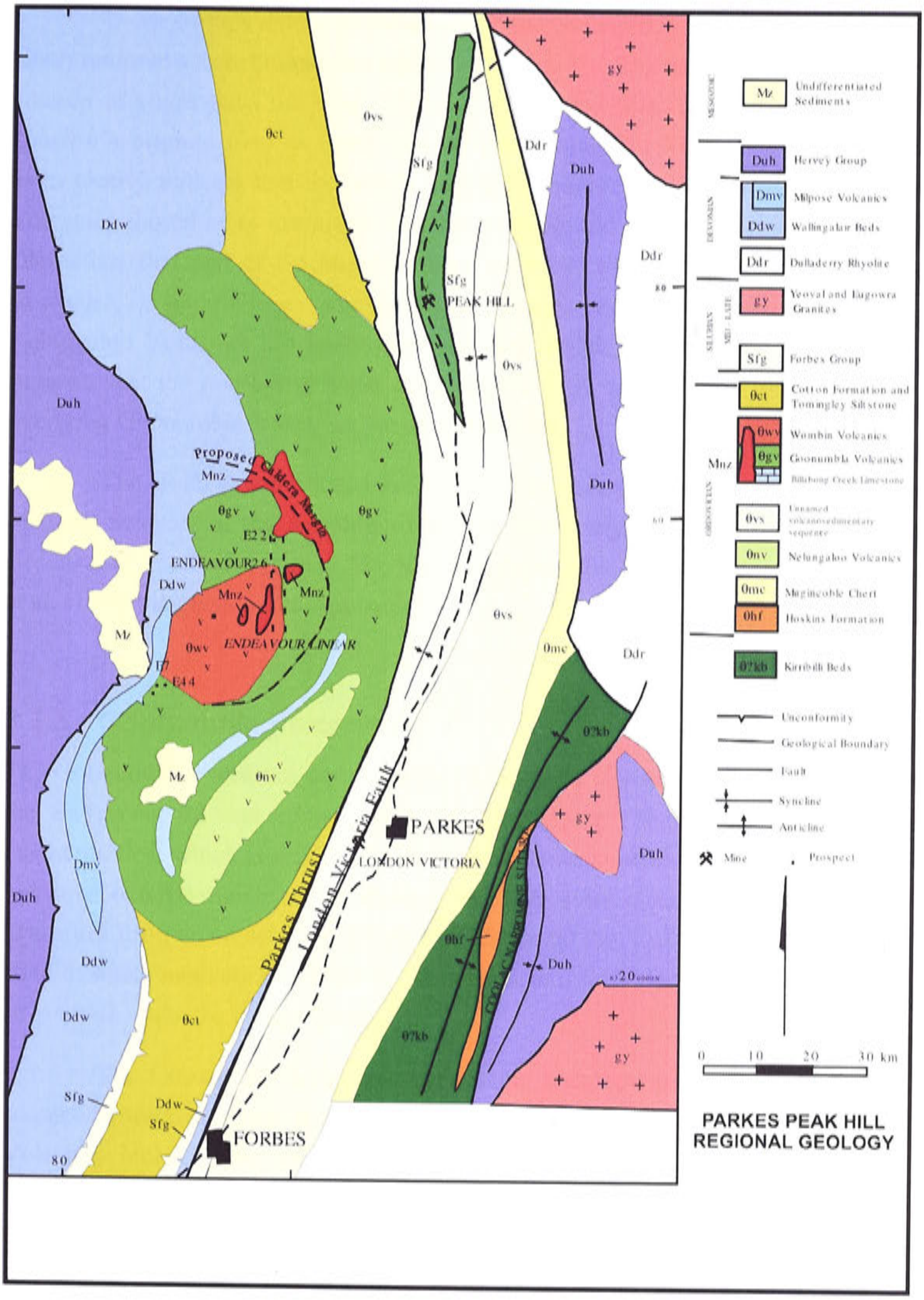

Figure 3.8 Geology of the Goonumbla Volcanic Complex (compiled from Geopeko reports and Krynen et al. (1990b)).

U–Pb isotope dating of zircons from the Nelungaloo Volcanics (Perkins et al., 1990) returned a Late Ordovician age of 438.5±3.6 Ma. The dated sample came from an outcrop of phyric lava near the 'Timaroo' homestead (Fig. 3.8), which is marked on Sherwin's original map as being part of the Nelungaloo Volcanics. The conflicting dates clearly indicate that the poorly exposed sequence nominated as the Nelungaloo Volcanics should be re-examined, and that younger and older units probably exist. The alternative, that part of the sequence may belong to the Late Ordovician Goonumbla Volcanics, is unlikely for compositional reasons. Although most samples of the Nelungaloo Volcanics are heavily altered, one sample was analysed in this study. It suggests that the porphyritic lavas are at best high-K calc-alkaline rocks, whereas the overlying Goonumbla Volcanics are all shoshonitic.

The U–Pb dating utilised the SHRIMP ion micro-probe at the Research School of Earth Sciences at the Australian National University. Of interest were some relict zircons that returned an age of 511 Ma. The paper which details this work (Heithersay et al. (1990)) is given in the Appendixes.

3.3.3 Goonumbla Volcanics

The Goonumbla Volcanics dominate the Goonumbla Volcanic Complex and they host the Endeavour 22 and 27 porphyry Cu–Au deposits (Fig. 3.2a). They tend to be magnetite rich, which is reflected in their noisy aeromagnetic character (Plate 3.1). The volcanics outcrop mainly on the limbs of the Forbes Anticline. On the western limb the exposures form an arcuate belt which extends for 60 km, and makes up the bulk of the zone of noisy magnetics in Plate 3.1. In the eastern limb the volcanics form a narrow strip which abuts the Parkes Thrust.

The Goonumbla Volcanics overlie the Nelungaloo Volcanics, although the contact between the two is never exposed. The basal sequence of the Goonumbla Volcanics includes thin sedimentary units, including the Billabong Creek Limestone Member and the Gunningbland Shale Member (Krynen et al., 1990a). The Billabong Creek Limestone Member varies from marl to oolitic limestone, and the base is rich in corals and gastropods. The age from brachiopods, conodonts and stromatoporoids is Late Ordovician, from early to mid Eastonian (Webby, 1980; Pickett, 1984). The limestone overlies a carbonate-cemented conglomerate, with clasts made up dominantly of Goonumbla Volcanics. Taken together, these units suggest an environment with boulder detritus and limestone reefs flanking an emergent volcano. The Gunningbland Shale Member is a thin shale and sandstone unit which is best exposed near 'New Durran' (G.R. 873307). It contains graptolites, trilobites and brachiopods which also provide an Eastonian age (Sherwin, 1973).

The Goonumbla Volcanics are dominantly K-rich trachyandesites, and consist of interlayered lavas and epiclastics with minor pyroclastics. Lavas range in thickness from metres to tens of metres. Pyroclastics range from coarse agglomerates to fine ash tuffs. Lavas and volcanic breccias are predominant near the centre of the Goonumbla Complex and also north of Wombin Gossan. Elsewhere epiclastic and bedded volcanic sandstones predominate.

Outcrop within the circular feature is poor, and the district is characterised by extensive soil cover which varies up to 80 m thick (average 30 m). The rocks that do outcrop tend to be relatively potassic trachyandesitic lavas, and in some cases subvolcanic intrusives. Rapid facies changes mean that detailed correlation between units is only rarely achievable. This is to be expected in a rapidly evolving volcanic pile.

A broad open syncline, the Milpose Syncline, has been discerned to the east of the Forbes Anticline (Fig. 3.8). It has been defined using an extensive set of measurements, of the dip of contacts between units, taken from oriented drill core and is supported by limited field evidence.

The volcanics are typically dark-grey to greenish grey, crystal-rich rocks and have the appearance of andesites. Plagioclase phenocrysts, 2 to 6 mm in length, make up 20–30% of the rocks. Subordinate hornblende and augite are also present. The matrix consists of fine plagioclase laths and interstitial anhedral potassium feldspar. Based on silica content, the volcanics range from basaltic andesites to andesites. Using the nomenclature of Peccerillo and Taylor (1976) for potassic rocks (Fig. 3.9), the Goonumbla Volcanics range from absarokites, through shoshonites to banakites or latites. Most are shoshonites or banakites.

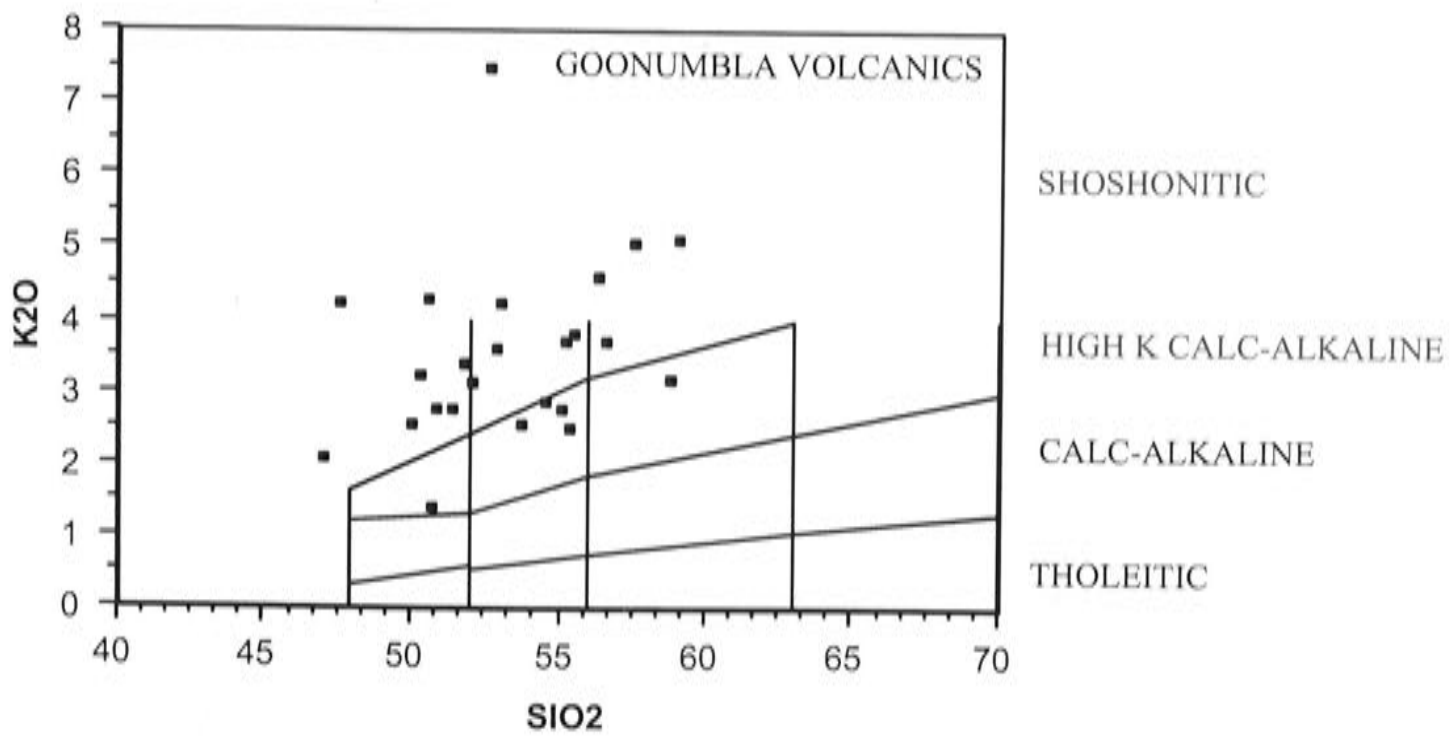

Figure 3.9 K_2O vs SiO_2 plot showing Goonumbla Volcanics. Fields after Peccerillo and Taylor (1976).

The narrow volcanic lenses east of the Parkes Thrust are also shoshonitic (Clarke, 1990). As mentioned above, it is possible that they represent upfaulted slices of underlying Goonumbla Volcanic equivalents.

3.3.4 Wombin Volcanics

The Wombin Volcanics are generally more felsic than the underlying Goonumbla Volcanics and they host the Endeavour 26 North porphyry Cu–Au deposit (Fig. 3.7). The unit was originally defined by Bowman et al. (1982), but its extent was never clearly defined. In accordance with Heithersay et al. (1990), it is suggested that the Wombin Volcanics be restricted to a sequence of porphyritic latitic to trachytic lavas, epiclastics and hyaloclastites, which conformably overlie the Goonumbla Volcanics. The bulk of the Wombin Volcanics is preserved in the centre of the Milpose Syncline, and appear to be truncated in the south by a major east-trending fault. The Wombin Volcanics outcrop poorly, however a good section occurs near Nash's Hill immediately overlying the Goonumbla Volcanics. The potassium-rich trachytes are characteristically brownish red in colour and distinctive from the dark trachyandesites. The sequence is dominated by lavas and hyaloclastites with subordinate ash tuffs. Lavas are usually massive and structureless in outcrop, but occasionally show flow banding. They contain scattered euhedral plagioclase laths up to 2 mm long in a sanidine-rich, trachytic groundmass. Some features within the sequence, including large mass-flow and slump deposits containing trachytic boulders up to 1 m in diameter, may be attributable to a rapidly developing volcanic pile.

3.3.5 Intrusions

Intrusions of gabbros, diorites, monzodiorites and monzonites cut all the major volcanic units described above. The diorites to monzonites are medium- to fine-grained rocks suggestive of subvolcanic emplacement. Indeed some of the monzonites are very similar to the volcanics they intrude.

A series of stocks, ranging from diorite to monzodiorite, are exposed in the core of the Forbes Anticline and are spatially related to the Nelungaloo Volcanics. The ages of the stocks are unconstrained by crosscutting relationships, other than being younger than the Nelungaloo Volcanics.

In contrast, monzonite and subordinate diorite intrusions cut both the Goonumbla and Wombin volcanic successions. In turn, quartz monzonite porphyries related to porphyry mineralisation clearly crosscut the dioritic to monzonitic stocks and

dykes. The absolute date of these intrusions is constrained by an overprinting of quartz–sericite alteration which has been dated by $^{40}Ar/^{39}Ar$ methods (Perkins et al., 1990). Dating of sericite separates gave an age of 439.2±1.2 Ma, which is effectively indistinguishable from U–Pb dates gained from the oldest volcanic unit in the succession. It is clear therefore that these intrusions are contemporaneous with the volcanics they intrude, and that the Goonumbla Volcanic Complex and associated mineralised porphyries developed over only a few million years.

The intrusive history within the proposed caldera is complex. Including the northern ring dyke, ~20% of the rocks exposed within the caldera are of intrusive origin. Detailed work has identified multistage intrusive activity within each stock complex. Breccia pipes and pebble dykes are common, hence a subvolcanic environment is indicated. The oldest intrusions are dioritic to monzodioritic in composition. These mafic intrusions are always crosscut by more felsic intrusions. They are composed of euhedral, zoned andesine (50–60%), hornblende (5–10%), clinopyroxene (5–10%) and interstitial cloudy perthitic potassium feldspar (15%). Biotite commonly encloses plagioclase, hornblende and pyroxene. Magnetite and apatite are common accessories. The volumetrically dominant type of intrusion is a medium-grained monzonite to monzonite porphyry. It commonly has a brick-red colour, resulting from fine-grained hematite dusting the feldspar. The rocks are holocrystalline, consisting of subhedral oligoclase to andesine crystals (20–30%) set in a hypidiomorphic granular groundmass of stumpy feldspars. Biotite (5–10%) and hornblende (5–10%) are the common mafic phases, and interstitial quartz ranges from 3 to 10%. Accessory minerals include apatite, sphene and magnetite.

The porphyry Cu–Au mineralisation is invariably associated with small subvertical, pipe-like intrusive bodies of quartz monzonite porphyry that form as satellites to the larger monzonite bodies (see Ch. 6). Their diameters seldom exceed 100 m, but they may have vertical continuity of over 900 m. A typical quartz monzonite porphyry has a strong pink to pinkish orange colour and is mostly coarsely porphyritic, containing 20 to 40% plagioclase phenocrysts which commonly reach 4 mm in maximum dimension. Quartz phenocrysts, seldom exceeding 1 mm, may comprise 10 to 20% of the rock, and the matrix is of fine-grained potassium feldspar and quartz. Biotite and hornblende are minor phases, and magnetite, sphene and apatite are accessories.

Evidence for multistage intrusive activity is quite common in the quartz monzonite porphyries; however contacts between phases are generally poorly defined. This suggests that the timing of the intrusive events may have been very close, and possibly overlapping. Individual phases are identifiable by slight textural and compositional variations (see discussion in Ch. 6).

Post-mineralisation intrusions, known locally as Zero Porphyries, are common and include porphyritic dykes of monzonitic to syenitic composition. They are always devoid of mineralisation and are thought to represent the waning stages of the magmatic cycle.

3.3.6 Regional alteration, geochemistry and structure in the Goonumbla Volcanic Complex

Figure 3.10a shows the simplified geology within the Goonumbla circular feature, highlighting the Wombin Volcanics in the south and the Goonumbla Volcanics in the north wrapping around the nose of the Milpose Syncline. Figure 3.8b shows the main areas of elevated Cu and Au geochemistry, and the cluster of porphyry deposits that are located within it. Exploration drilling was undertaken using rotary air blade methods to sample bedrock through a weathered or transported cover. The entire circular feature has been systematically drilled and two main clusters of Cu–Au geochemistry have been found. Figure 3.8c shows the regional extent of hydrothermal alteration. The grey areas represent strong to intense quartz–sericite alteration, while the black areas represent potassic alteration. A broad linear corridor, the Endeavour Linear, contains the majority of the alteration and, with the exception of the Endeavour 37 prospect, the bulk of the porphyry centres. Figure 3.8d outlines the main linear features which are drawn largely from aeromagnetics, including the Endeavour Linear.

3.3.7 Other mineralisation in the area

In order to complete the picture a brief reference to other styles of mineralisation is warranted. Epithermal style veining is present in a few prospects which occur marginal to the Goonumbla circular feature, and these are shown in Figure 3.10. One of the more promising prospects occurs at Endeavour 29, where Au-bearing, colloform-banded silica was mined early this century. Another style of mineralisation occurs at the Endeavour 6, 7, and 44 prospects in the southwestern corner of circular feature. Here Pb–Zn skarns grade along strike into Au-bearing skarns, and a possible minable Au resource exists at Endeavour 44.

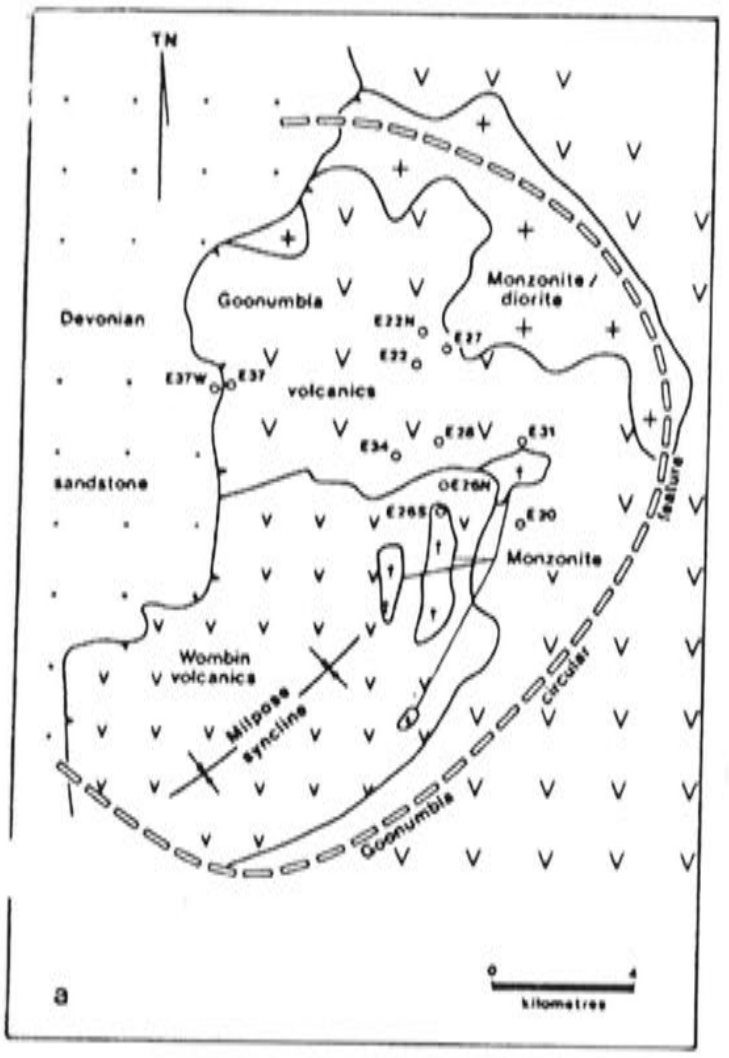

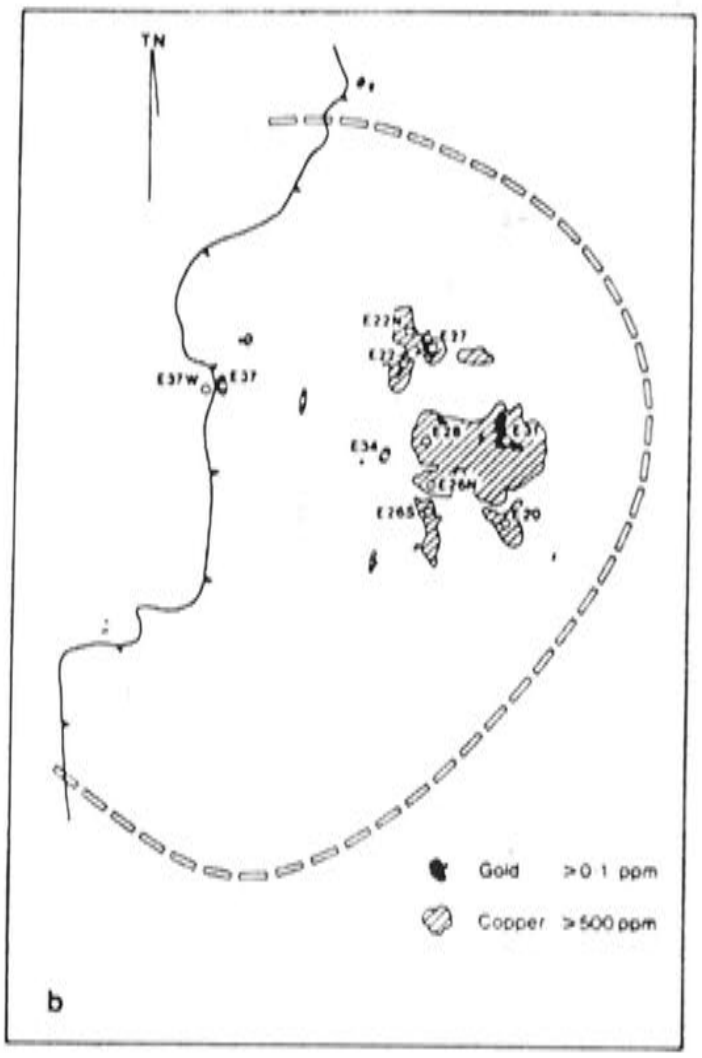

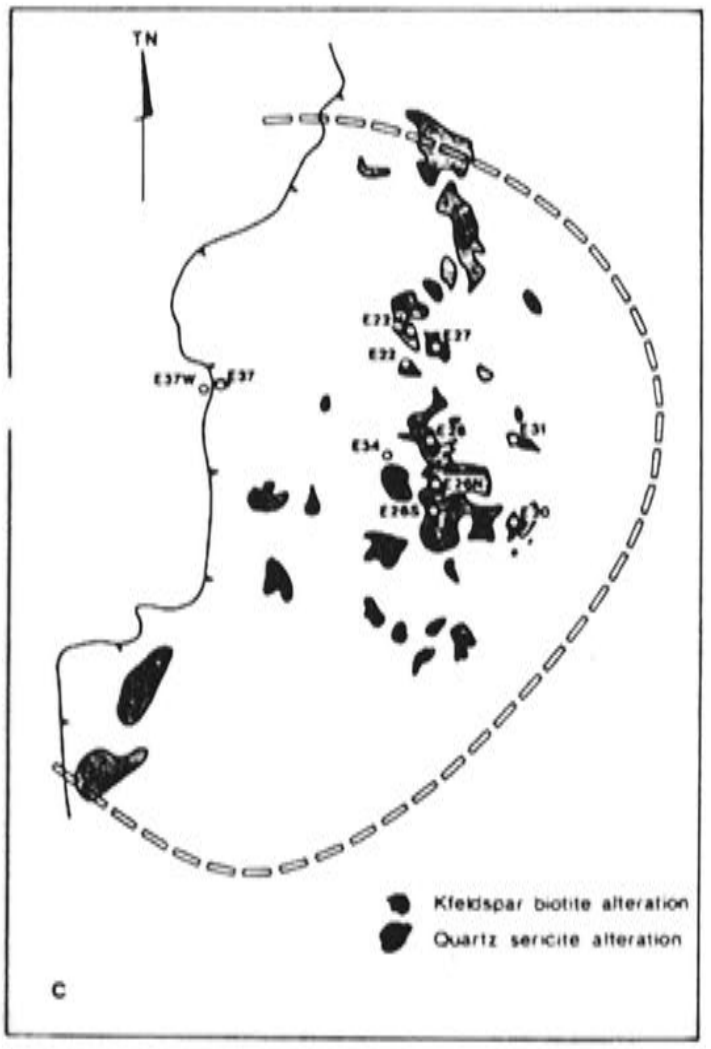

Figure 3.10 Plans showing the **(a)** geology, **(b)** geochemistry, **(c)** alteration and **(d)** lineaments of the central Goonumbla area.

Chapter 4

A REVIEW OF THE SHOSHONITE ASSOCIATION

4.1 INTRODUCTION

This chapter is a short sidestep from the detailed description of the Goonumbla deposits. The fact that the intrusions and the volcanics that host these important Cu–Au deposits are shoshonitic is a relationship which is shared by a number of important Au-bearing systems, including the giant Lihir Island and Mount Hagen deposits in New Guinea (Wyborn, 1988), the Emperor Au–Te deposit in Fiji (Gill and Whelan, 1989), and the Bajo de la Alumbera porphyry system in Bolivia (Sillitoe, 1990). Is this relationship critical or incidental to the genesis of the Au deposits? The origin of shoshonitic magmatism remains controversial, and the relative importance of factors such as the source composition, conditions of partial melting and fractionation during emplacement in the genesis of the magmas are yet to be resolved. Do these processes control the eventual production of porphyry Cu–Au deposits?

A second, but related, consideration is the tectonic setting of the Lachlan Fold Belt. The review of tectonic models in Chapter 2 showed that the Ordovician volcanic sequences play a pivotal role in the discussions of this controversial question. Most of the models, which involve either a continental or island arc above a subduction zone, are predicated on the assumption that the Ordovician volcanics are largely calc-alkaline andesites and are therefore subduction related. This thesis will examine both this hypothesis as it relates to the Parkes area, and the ability to predict tectonic settings from the recognition of the shoshonitic association.

Reviews of the shoshonite association include those of Joplin (1964, 1965), Jakes and White (1972) and Morrison (1980). Since 1980, new data on recently recognised areas of shoshonitic volcanism has been published (Stern et al., 1988), as well as additional data on well-known areas of shoshonitic volcanism (principally on REE and isotopic compositions). This chapter builds on those earlier reviews and summarises the field and tectonic settings, as well as the mineralogical, petrographical and geochemical data that define this association. The purpose is to provide a set of criteria with which to assess the significance of the shoshonitic rocks at Goonumbla in respect to tectonic setting and the origins of the mineralisation. Appendix 1 provides a detailed summary of the material presented in this chapter.

4.1.1 Ordovician shoshonites in New South Wales

The distribution of Ordovician shoshonitic volcanic sequences in New South Wales is shown in Figure 4.1. The Ordovician volcanic rocks in the Lachlan Fold Belt are poorly described in the literature and the main published descriptions are of the Nine Mile Volcanics near Kiandra, south of Tumut (Owen and Wyborn (1979); the Sofala Volcanics northeast of Bathurst (Barron, 1976); and the Walli Andesite at Cliefden, west of the Sheahan–Grants Gold Mine (Smith and Smith, 1976).

Owen and Wyborn (1979) showed that many of the Ordovician volcanics in the Lachlan Fold Belt are of a particular basaltic type, characterised by high K, Sr, Ba, P and low Ti, Zr, Y and Nb; an element pattern typical of the shoshonite association. Geopeko recognised the unusually potassic nature of the Goonumbla and Wombin Volcanics in the late seventies, and used it as a criterion to test the prospectivity of other volcanic belts in the Lachlan Fold Belt for porphyry Cu mineralisation. The potassic nature of the volcanics could be determined rapidly by acid etching and staining with sodium cobaltinitrate. In 1985, after discussions with D. Wyborn, the author realised that the volcanics in the Parkes district were also shoshonitic in character, and this was written up in internal company reports. The Geological Survey of New South Wales began a review of the Parkes region at this time, with full access to Geopeko data, and the first publication to outline the shoshonitic character of the volcanics near Parkes was that of Clarke (1987).

4.2 DEFINITION

Rocks of the shoshonite association are commonly identified on the basis of their whole-rock geochemistry, principally K_2O vs SiO_2, using fields such as those defined by Peccerillo and Taylor (1976) or MacKenzie and Chappell (1972). This is insufficient, however, as it does not distinguish between the shoshonitic and alkali-olivine basalt associations. The all encompassing term 'alkaline' often binds these two associations together in the literature. Low TiO_2 is a feature that shoshonites share with calc-alkaline arc rocks, but distinguishes them from truly 'alkaline' rocks. This discussion of the shoshonite association will be confined to rocks whose silica content ranges from 40 to 70% and K_2O values which exceed from 1 to 3% over the same silica range, following the Peccerillo and Taylor (1976) definition. The other important criterion is that TiO_2 contents remain below 1.5%.

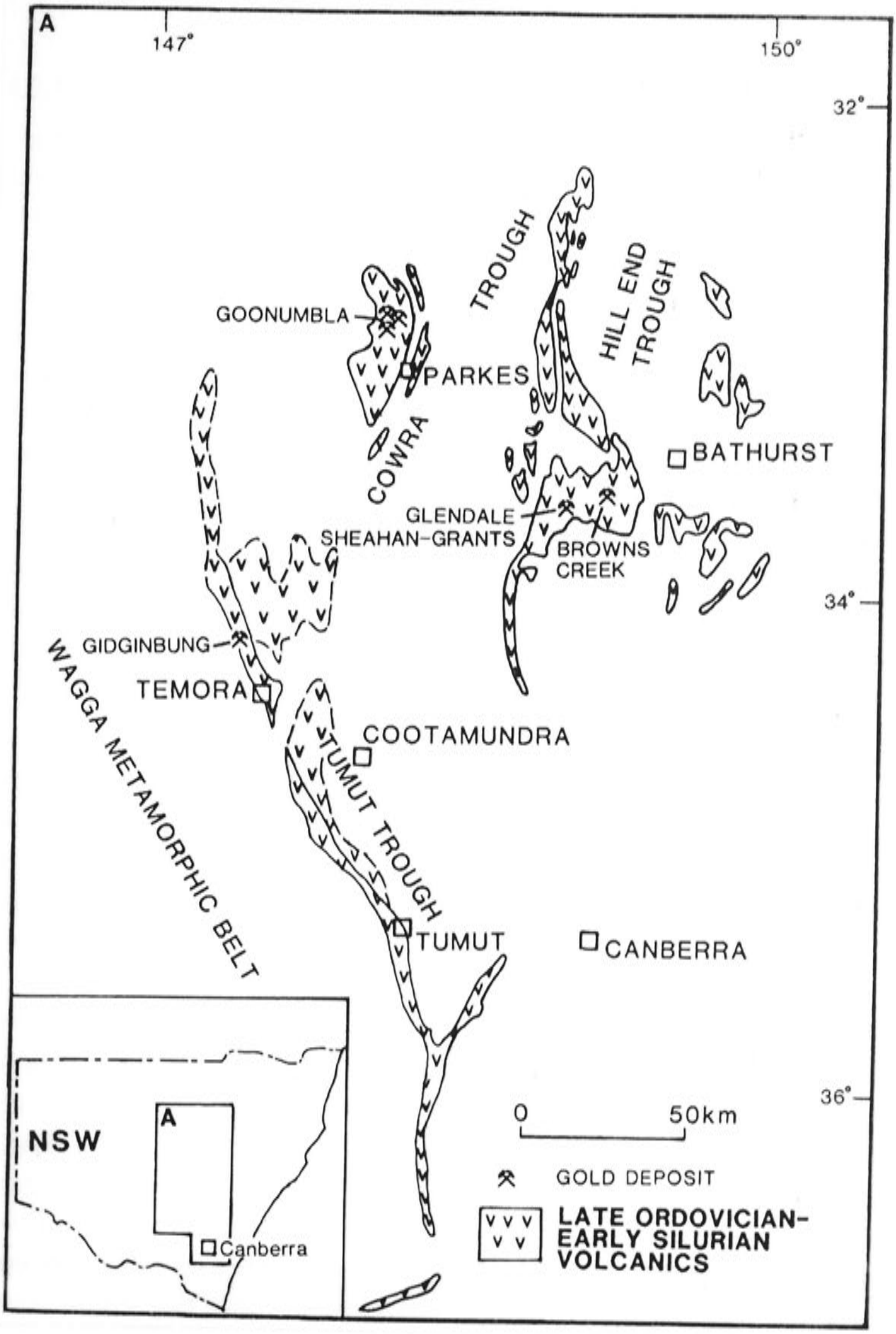

Figure 4.1 Distribution of Ordovician shoshonitic volcanics and associated mineralisation in the New South Wales potion of the Lachlan Fold Belt.

4.3 FIELD SETTINGS, MINERALOGICAL AND PETROGRAPHIC FEATURES

4.3.1 The Absaroka volcanic field

The type area of the shoshonite association is the Eocene Absaroka volcanic field in the Absaroka Mountains of Wyoming and Montana. The field covers an area of some 24 000 km^2 and is made up of 90% calc-alkaline andesites and dacites, and around 10% shoshonite suite rocks. In the type area (Iddings, 1895), absarokites have a groundmass containing pyroxene, calcic plagioclase and sanidine, with phenocrysts of olivine and pyroxene but not plagioclase. Augite is the dominant pyroxene and zoning is evident on the outer edge of many phenocrysts. Resorption textures are evident locally on olivine and augite. Based on silica content alone, absarokites fall within the basalt field. In contrast, shoshonites (which span the basaltic andesite to andesite field on silica content), contain phenocrysts of calcic plagioclase, commonly in aggregates up to 15 mm long, in addition to lesser phenocrysts of olivine and pyroxene. The shoshonite groundmass is made up of pyroxene, calcic plagioclase and sanidine. Plagioclase phenocrysts may show resorption textures and are commonly rimmed by sanidine (Gest and McBirney, 1979). Meen and Eggler (1987) report glomerocrysts of augite and hypersthene mantled by titaniferous biotite.

The Crandall ring-dyke complex is representative of subvolcanic feeders to the Absaroka field (Kudo and Broxton, 1985). It consists of a gabbroic to dioritic core which has been cut by a shoshonitic ring dyke, which is in turn cut by quartz monzonite dykes. The mineralogy of the central intrusion is plagioclase, two pyroxenes, biotite and ilmenite. Texturally early plagioclase is commonly mantled by pyroxene.

4.3.2 Shoshonites in the highlands of Papua New Guinea

In the highlands of Papua New Guinea there are many large, well-studied, strato-volcanoes composed of both shoshonitic and calc-alkaline rocks (Mackenzie and Chappell, 1972; Smith, 1972). They grade from high-K andesite and high-K, high-Al basalt through shoshonite to absarokite, and this variation may occur both within provinces and in individual centres. The volcanoes form clusters rather than linear belts and commonly have composite calderas. Volcanic successions consist of lavas, agglomerates, tuffs and lahar deposits. The shoshonitic volcanoes are underlain by Mesozoic and Cainozoic sedimentary rocks in some areas, and by Palaeozoic basement granites and metamorphic rocks in others. The volcanism occurred in the Middle Pleistocene following uplift, orogenesis and major fault movement in the Late Miocene and Pliocene. There is no seismic evidence for a contemporaneous subduction zone. Indeed the volcanism, with its mixture of calc-alkaline and shoshonitic rocks, together

with the clustering of volcanic centres, shows no zonation in time and space indicative of contemporaneous subduction.

The shoshonites consist of phenocrysts of plagioclase (andesine to labradorite), augite and olivine in a groundmass of plagioclase, augite, magnetite, apatite and interstitial sanidine. Plagioclase crystals show resorption textures and are commonly rimmed by sanidine. Some of the shoshonites contain amphibole which is commonly rimmed by magnetite, pyroxene and plagioclase, perhaps indicating disequilibrium with conditions at the surface (MacKenzie and Chappell, 1972).

Smith (1972) recorded two 'shoshonitic' intrusive trends in rocks from southeastern Papua New Guinea: a near-saturated group ranging from gabbros to syenites, and a nepheline-normative undersaturated group. These high-K intrusions were implaced in the Middle Miocene during regional block faulting and vertical movements. This tectonic activity was the beginning of a period of Late Cainozoic uplift, perhaps due to mantle instability prior to an orogenic episode. The high-K rocks intrude in excess of 3 km of tholeiitic basalts.

The near-saturated rocks include small stocks of gabbro, monzonite, diorite and syenite. Biotite pyroxenite is associated with near-saturated gabbro of the Watuti River stock. The near-saturated group show regular variations in mineralogy. Gabbros consist of labradorite, clinopyroxene and biotite, and minor olivine, accessory apatite and interstitial K-feldspar. Biotite is usually moulded around early formed minerals. Monzonites and diorites consist of K-feldspar and andesine, with clinopyroxene, biotite, accessory apatite, sphene and rarely quartz. K-feldspar in monzonites commonly contains exsolved albite lamellae, and may occur as large tablets enclosing earlier formed minerals, particularly plagioclase. Syenites consist of minor mafic minerals surrounded by perthitic K-feldspar. The undersaturated group forms gabbros, trachybasalts, sanidine porphyries and porphyritic monzonites. Pyroxenites are found as inclusions in some of the undersaturated rocks. Biotite, clinopyroxene and opaques occur in a sanidine groundmass.

The documentation of the two suites in this shoshonitic volcanic belt is not an isolated occurrence and the subdivision between undersaturated (leucite bearing) and near-saturated rocks was outlined in a review by Joplin (1965). Morrison (1980) discounted Joplin's undersaturated subdivision and appeared to reclassify these rocks into the alkali-basalt association. This important point will be taken up again later.

4.3.3 The Italian alkaline province and Aeolian arc

Perhaps the most complicated and well-studied area of potassic volcanism is the Italian alkaline province, or the 'Roman Comagmatic Province', described by Washington

(1906). A variety of high-K rocks occur in this tectonically complex area, ranging from true shoshonitic members through to ultra-potassic rocks. A study by Civetta et al. (1981) looked in detail at potassic volcanics from the Ernici Mountains in Southern Latium. Twenty small edifices occur in a corridor 20 km long. The rocks are dominantly pyroclastics with minor flows, and were erupted after regional distension caused subsidence. K-rich volcanics were erupted first, followed by a less K-rich suite. The authors divided the rocks from this volcanic area into a K series (KS) and a high-K series (HKS). Apart from the high K_2O contents, both suites have TiO_2 below 1% which distinguishes them from alkali basalts. HKS rocks are dominantly silica-undersaturated tephritic leucitites, which contain phenocrysts of clinopyroxene and minor olivine with a groundmass of leucite, salitic pyroxene and opaques. Pyroxenes are zoned with compositions ranging from diopside to salite. KS rocks range from leucite-alkali basalts (low TiO_2) to trachybasalts and are slightly silica undersaturated. Phenocrysts include diopsidic to salitic pyroxene with minor olivine and rare plagioclase.

Rocks from the Aeolian arc span a greater range, from trachybasalt to alkali rhyolite (Keller, 1974). Trachybasalts contain phenocrysts of olivine and augite ± plagioclase. The groundmass consists of intergrown plagioclase and K-feldspar, which is diagnostic of the shoshonite association (Nicholls and Carmichael, 1969). Alkali rhyolites are qualitatively composed of the same minerals as the trachybasalts, with the addition of quartz in the microgranophyric groundmass. Olivine persists as partially resorbed grains.

4.3.4 Shoshonites in Fiji

Another well-documented shoshonitic occurrence is in Fiji (Gill and Whelan, 1989). Using the definition of Peccerillo and Taylor (1976), Gill and Whelan recognise absarokites, shoshonites and banakites which are spatially associated with calc-alkaline and tholeiitic basalts. The shoshonites are associated with the early rifting stage of tectonic development. Volcanic centres are structurally controlled in an east-northeast alignment (Viti Levu and Vatulele-Beqa Lineaments), and a north-northwest alignment (Lomaiviti Lineament). Plagioclase-phyric shoshonites and monzonites intruded primarily during the caldera formation, and banakites (trachyandesites) occur as domes in the caldera. Calc-alkaline magmas erupted at the same time from adjacent volcanoes. Overall the shoshonitic and calc-alkaline rocks form a continuum with increasing alkali enrichment. The absarokites have phenocrysts of olivine, augite, ± plagioclase and magnetite. Shoshonites have plagioclase, augite, minor olivine and magnetite as phenocrysts. Banakites have phenocrysts of plagioclase, augite, magnetite and biotite.

The groundmass for all phases is K-feldspar, biotite and rare nepheline. Plagioclase is not mentioned as a groundmass phase.

4.3.5 Shoshonites in the Andes

The Central Andes in northern Chile and Argentina contain one of the more complete records of igneous activity for western South America where oceanic and continental lithosphere interact in a convergent margin setting. Volcanism took place in a series of cycles, which erupted in partially superimposed longitudinal belts (Dostal et al., 1977). Most of the volcanism is calc-alkaline, but the zone farthest (~500 km) from the axis of the trench is shoshonitic. Geochemically Rb, Ba Sr and Zr increase away from the trench. The authors concluded that the distribution of major and trace elements is consistent with a model in which magmas were derived by anatexis of an upper-mantle source already enriched in large ion lithophile elements, and located above a descending slab of oceanic crust. This locality gives empirical support to the idea that there could be a relationship between variations in magma chemistry and the depth to the Benioff Zone

4.3.6 Shoshonites in the northern Mariana arc

The Mariana volcanic arc is characterised by two rock series; one subalkalic and the other alkalic (Bloomer et al., 1989). The subalkaline series occurs in the central and northern part of the arc and includes low-K and medium-K rocks, ranging from basalts to andesites and dacites. The alkalic series occurs farther north in the Mariana arc and shows enrichments in K, K/Na, Rb, Ba and Sr relative to the other volcanic series. Element ratios and isotopic evidence require distinct magma sources for the parental magmas. The authors suggest that although the characteristics of the shoshonite source (low Ba/La, high Ba/Zr) may be the consequence of the subduction of large intraplate ridges, they favour a model in which a less-depleted mantle source is uncovered by the propagation of the Mariana Trough spreading centre into the Volcano arc.

4.3.7 Shoshonites of Central British Columbia

The belt of Upper Triassic volcanic sequences of central British Columbia has long been recognized to contain a mixture of alkaline potassic, alkaline sodic, as well as calc-alkaline sequences. They are especially significant in this work as well known porphyry deposits including Galore Creek occur in them. The shoshonitic character of the alkaline suites was recognized by Meade (1977) for the Takla Group. At Galore

Creek, in the Stuhini Group, Allen et al (1976) compared the unusual leucitic phonolites and syenites to the Mediterranean and western Alaskan assemblages.

All suites, except the Galore Creek Upper unit (Stuhini), belong to the near saturated group as defined by Joplin. All suites are composed of shoshonites sensu stricto and some absorokites. Sub alkaline rocks associated with the shoshonite4s belong to medium K to high K cal-alkaline and high Al basaltic suites.

Shoshonitic volcanism in British Columbia is important in unraveling the tectonic history of British Columbia. Upper Triassic shoshonites occurred during a period of 'docking' of the Stikinia , Cache Creek, Quesnellia, and Eastern Terrains and their accretion to North America. Spence (1984) argues that the occurrence in a narrow belt of contemporaneous medium K and high K requires a steeply dipping subduction zone during Upper Triassic and Lower Jurassic times.

Spence (1984) suggests that a Philippines model may be appropriate where the Upper Triassic subduction zone, after being disturbed by the collision of the allochthonous terranes and having generated the calc-alkaline-shoshonitic Nicola-Takla-Stuhini arc as it became subvertical, was eventually reversed during accretion to North America.

4.3.8 A summary of field relationships, mineralogy and petrography

Several themes about shoshonites emerge from the discussion above and the review table in Appendix 1. Shoshonitic volcanoes range from stratovolcanoes to small cones in terrestrial and marine environments. Shoshonitic provinces can contain numerous centres with caldera complexes, dyke swarms, ring dykes and breccia pipes. They may group in clusters (Papua New Guinea) or in linear belts (Andes). Shoshonitic volcanics are not abundant in the stratigraphic column, but they are often associated with substantial calc-alkaline (Absaroka Mountains) or tholeiitic volcanism (Fiji). They are usually the youngest rocks in a volcanic sequence.

The petrographic descriptions in the review indicate that phenocrysts include olivine, clinopyroxene, plagioclase, biotite, hornblende and rarely orthopyroxene. Accessories include magnetite and apatite. Olivine appears as a persistent mineral spanning basic to intermediate melts. Plagioclase, when present, will often form cumulophyric clots with pyroxene, ± olivine and magnetite. This textural observation provides some evidence of crystal fractionation (Mackenzie and Chappell, 1972). K-feldspar is always late in the paragenesis, commonly mantling plagioclase, and in some rocks poikilitically enclosing pyroxene. Biotite also crystallises late and will often poikilitically enclose early-formed minerals.

A summary of the mineralogical and petrographic features of extrusive and intrusive rocks in the shoshonite suite is presented below. A first order subdivision is made following Joplin (1964), based on the presence or absence of leucite which distinguishes between silica-saturated or near-saturated types and silica undersaturated types.

1. Saturated and near-saturated rocks:

Extrusive rocks

Absarokites (potassic trachybasalt)

Phenocrysts: olivine, clinopyroxene (augite to salite) and titanomagnetite.

Groundmass: pyroxene, olivine, titanomagnetite, plagioclase microlites (calcic) and ubiquitous interstitial K-feldspar. Biotite is common in Absarokites from Fiji.

Shoshonites (potassic basaltic andesite)

Phenocrysts: calcic plagioclase, clinopyroxene, olivine and titanomagnetite.

Groundmass: clinopyroxene, calcic plagioclase and K-feldspar (sanidine).

K-feldspar commonly mantles plagioclase phenocrysts which commonly show evidence of resorption. When biotite is present it mantles earlier formed phenocrysts.

Banakite (latite, trachyandesite)

Phenocrysts: calcic to sodic plagioclase, augite, hornblende, biotite, ± olivine and titanomagnetite.

Groundmass: subtrachytic groundmass consisting of plagioclase microlites, hornblende, magnetite and sphene.

Trachyte (Toscanite)

Phenocrysts: sodic plagioclase, pyroxene, hornblende, ± biotite and quartz, and rare olivine and magnetite.

Groundmass: trachytic intergrowth of plagioclase and K-feldspar.

Intrusive rocks

Gabbro

Calcic plagioclase, clinopyroxene, biotite, olivine and apatite with interstitial K-feldspar. Biotite is typically moulded around earlier formed minerals.

Monzonite, diorite

K-feldspar, plagioclase (andesine), and subordinate clinopyroxene, biotite, magnetite, apatite and sphene. Goonumbla monzonites commonly have hornblende. Some monzonites can contain in excess of 10% quartz and are correctly termed quartz monzonites. K-feldspar phenocrysts commonly enclose earlier formed minerals.

2. Undersaturated rocks:

Extrusive rocks

Leucite basanite

Phenocrysts: olivine, clinopyroxene and leucite. Microphenocrysts of pyroxene, leucite, plagioclase and magnetite.

Leucite tephrite

Phenocrysts: calcic plagioclase, clinopyroxene and minor olivine.
Groundmass: leucite, salitic pyroxene and opaques.

Leucite trachyte

Trachytic intergrowth of leucite and K-feldspar.

Intrusive rocks

Gabbro

Clinopyroxene, biotite, calcic plagioclase and K-feldspar. Commonly the matrix will be made up of large poikilitic K-feldspar crystals.

4.4 WHOLE ROCK GEOCHEMISTRY

Extensive reviews of the major element characteristics of volcanic and intrusive rocks from young orogenic belts undertaken during the seventies (Jakes and White, 1972; Jakes and Gill, 1970; Mackenzie and Chappell, 1972), led to the evolution of a non-genetic classification of rock associations based on major element geochemistry. A review paper by Morrison (1980) compared available chemical data for shoshonitic rocks with the chemical characteristics of island-arc tholeiites, calc-alkaline suites and alkali-olivine basalt suites. He showed that the shoshonite association has similarities with the calc-alkaline and alkali-basalt suites, but cannot be unambiguously classified with either. Standard geochemical plots show a number of important points.

4.4.1 The $Na_2O + K_2O$ vs SiO_2 plot

The total alkalis versus silica plot shows the alkaline nature of the shoshonite association, and Le Bas et al. (1976) used it as a discriminant diagram. Data from several areas of shoshonitic volcanism (Fig. 4.2) show a variation from basalts and basaltic andesites through potassic trachybasalts, shoshonites, latites to trachytes. The trend supports the conclusion of Meen (1990), who shows from experimental work, that shoshonites can be derived from basaltic andesites. The shoshonite series should not necessarily be thought of as a parallel and independent trend to the calc-alkaline series.

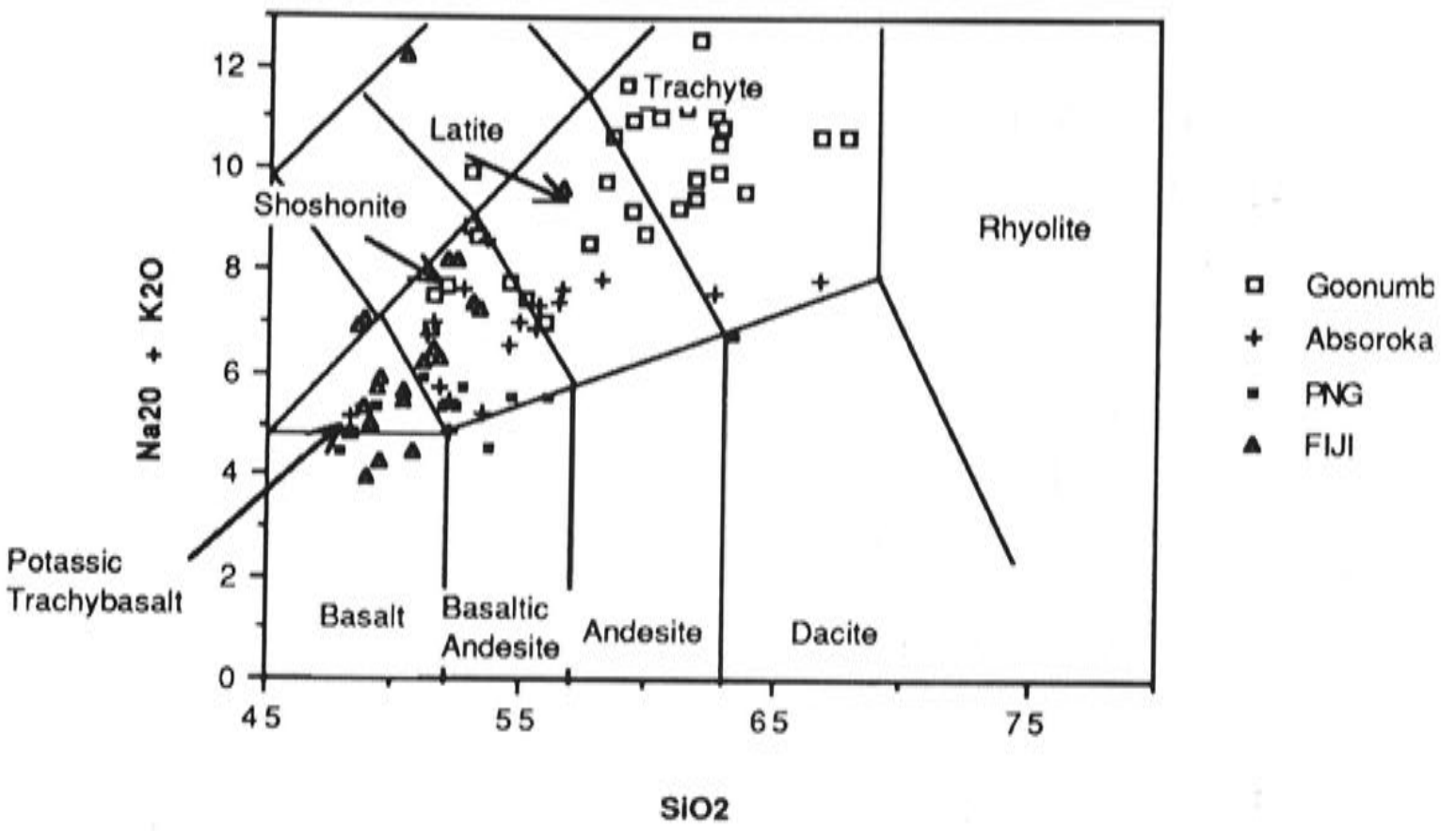

Figure 4.2 Total alkalis vs SiO_2 showing shoshonite association.

4.4.2 The K_2O vs SiO_2 plot

The K_2O versus SiO_2 plot is the main diagram for discriminating the shoshonite association, particularly with respect to the calc-alkaline and tholeiitic associations. The fields designated by Peccerillo and Taylor (1976) are shown in Figure 4.3a. Shoshonitic rocks scatter widely (Fig. 4.3.b) in contrast to the relatively confined field for calc-alkaline rocks. This hints that further fine detail may be determined from this plot, particularly if individual magmatic suites are taken into account.

K_2O versus SiO_2 plots for a range of shoshonitic centres (Fig. 4.4) reveal distinct compositional differences between individual volcanic centres. The northern Mariana arc data separate into three fields (Fig. 4.4.b), corresponding to individual volcanic centres (Bloomer et al., 1989). In the plot of a number of Fijian volcanoes (Fig. 4.4.d; Gill and Whelan, 1989) the Tavua centre forms a distinct, highly potassic trend. The Tavua Volcano on Viti Levu hosts the Emperor Au–Te mine. Similarly for the Aeolian Islands of Italy (Fig. 4.4.e) there are distinct fields for the older and younger volcanic series at the Stromboli volcanic centre, as well as the older and younger series at the Volcano centre (Ellam et al., 1989). Southeastern Papua New Guinea (Fig. 4.4.f) provides an extreme example where potassic intrusions form near-saturated and undersaturated trends (Smith, 1972). Two different centres in the Absaroka Mountains (Gest and McBirney, 1979; Meen and Eggler, 1987) also plot as two different fields (Fig. 4.4.c).

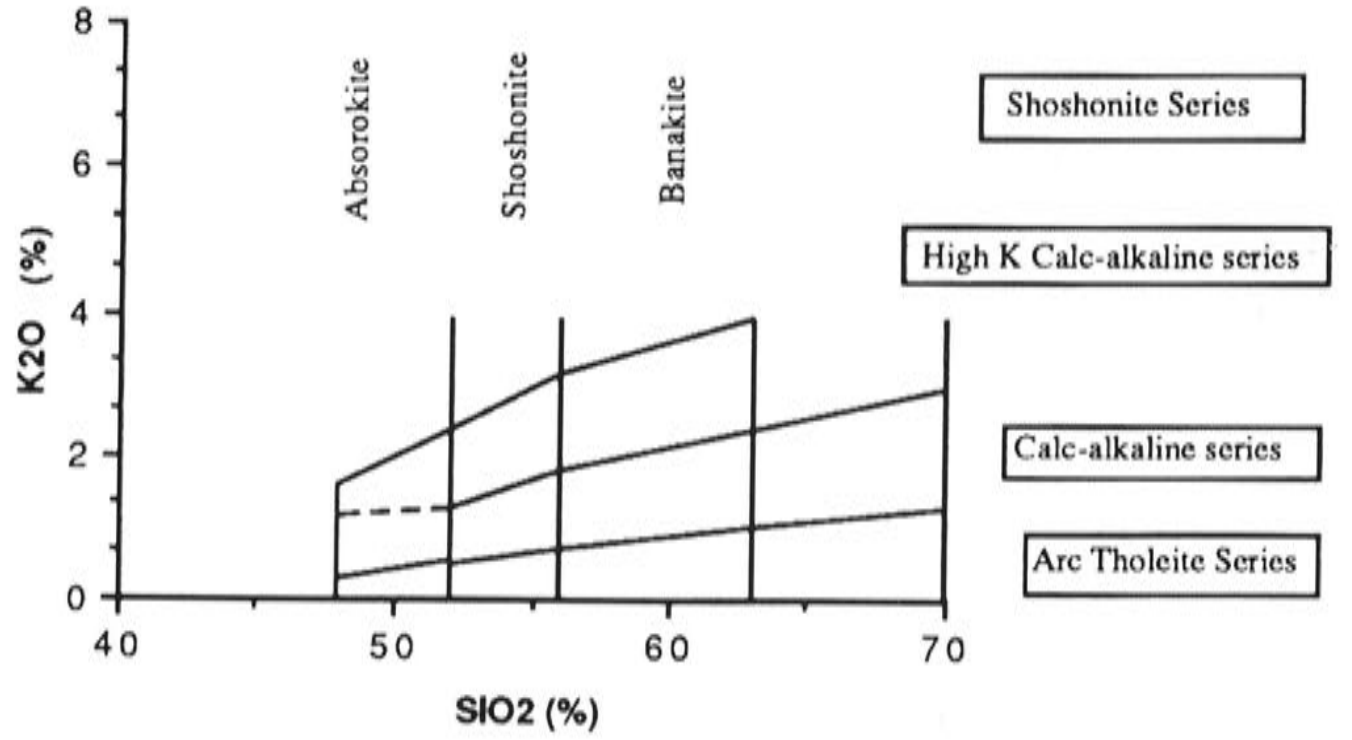

Figure 4.3a Shoshonite classification (after Peccerillo and Taylor (1976)).

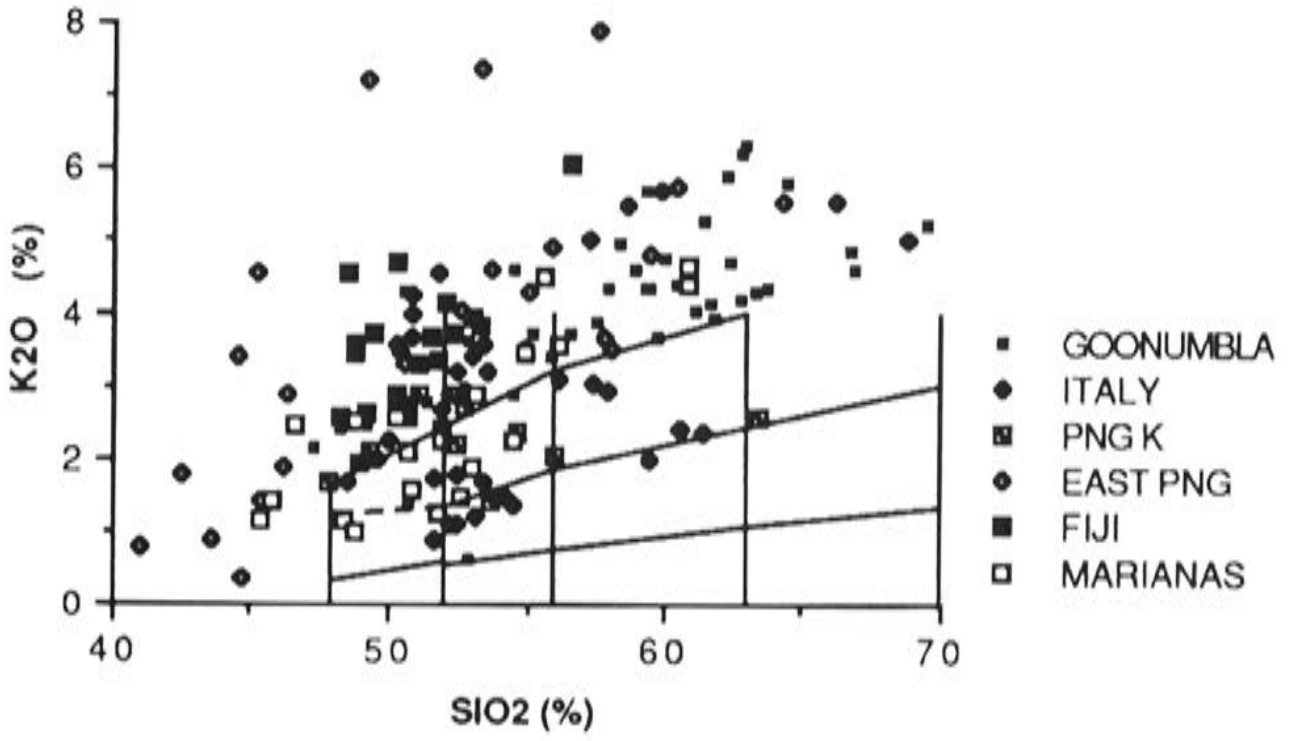

Figure 4.3b K_2O vs SiO_2 plot with fields (after Peccerillo and Taylor (1976)).

In the Goonumbla Volcanic Complex two subtle but clear trends are also revealed in the K_2O versus SiO_2 plot of volcanics and intrusions (Fig. 4.4.a). One trend straddles the shoshonite – high-K calc-alkaline boundary, while the other defines a trend with higher K_2O levels. It is noteworthy that the lower, more silicic trend corresponds to the suite of intrusions related to mineralisation, whereas the upper more potassic trend is related to barren intrusions and the bulk of the volcanics.

Taken as a whole, it is clear that individual magmatic suites can form sub-linear trends, which span a large field in K_2O versus SiO_2 space. A single volcanic centre is capable of generating a range of magmatic suites that commonly vary from initially moderately potassic to later highly potassic compositions. In Figure 4.5, data from the Mount Hagen, Ladolum (Lihir), Marian and Emperor deposits show that both

the moderately and highly potassic trends may be associated with significant mineral deposits.

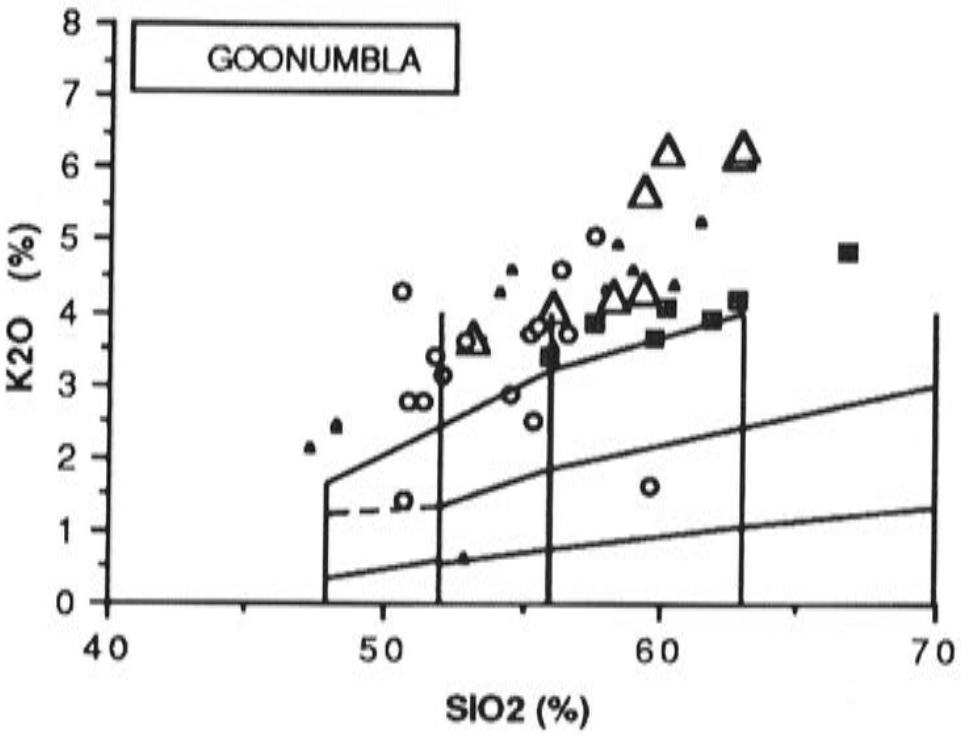

Figure 4.4a K_2O vs SiO_2 plot, Goonumbla.

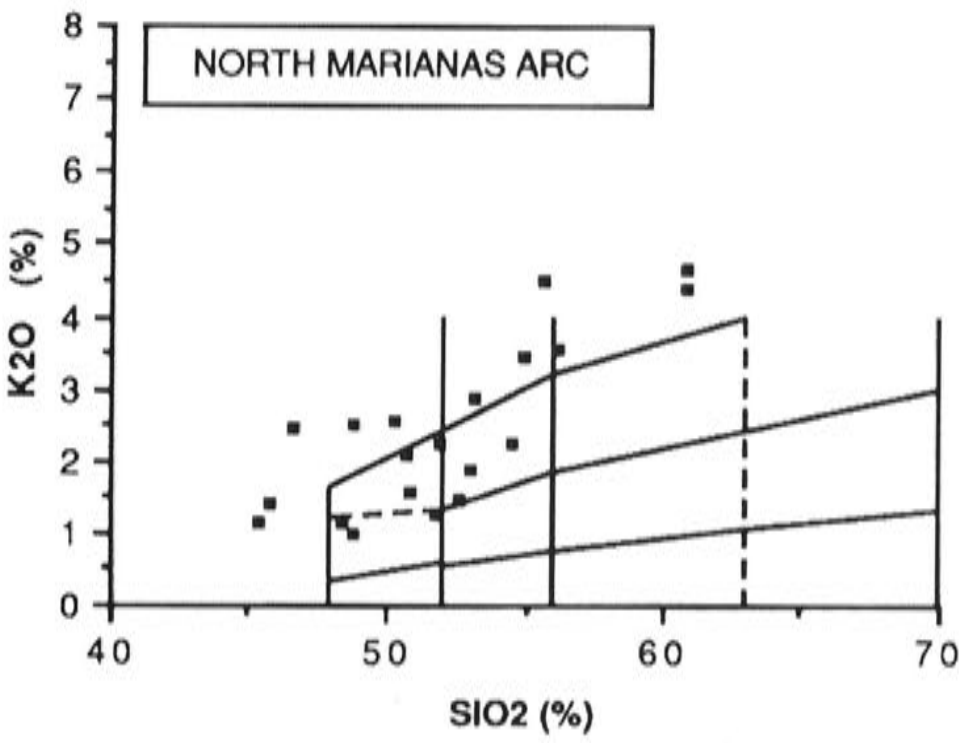

Figure 4.4b K_2O vs SiO_2 plot, North Marianas Arc.

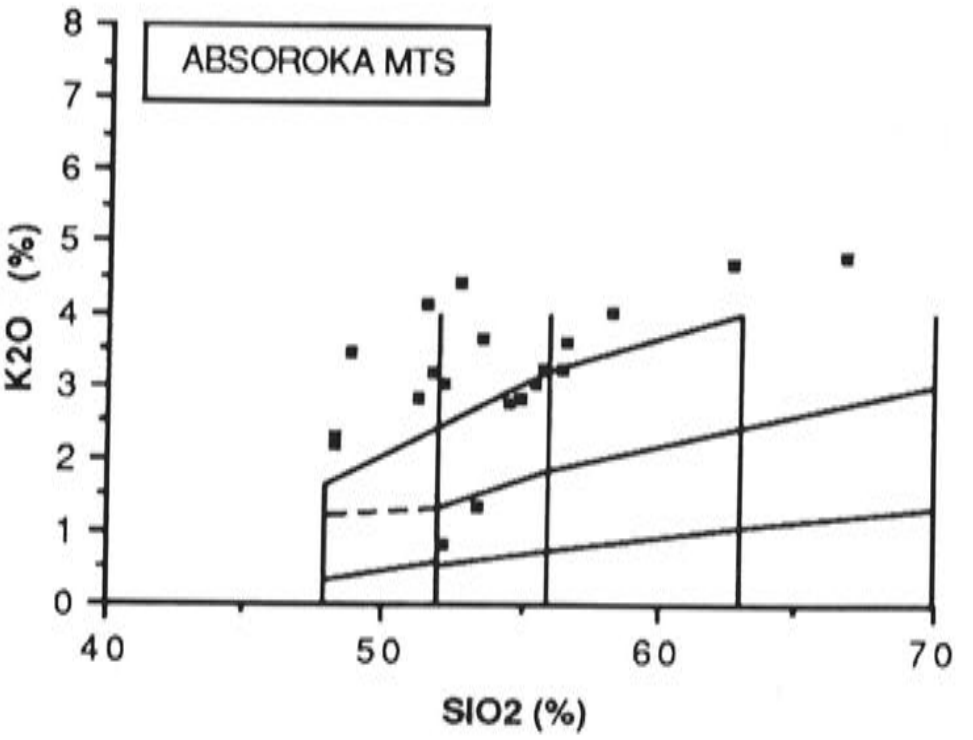

Figure 4.4c K_2O vs SiO_2 plot, Absaroka Mountains.

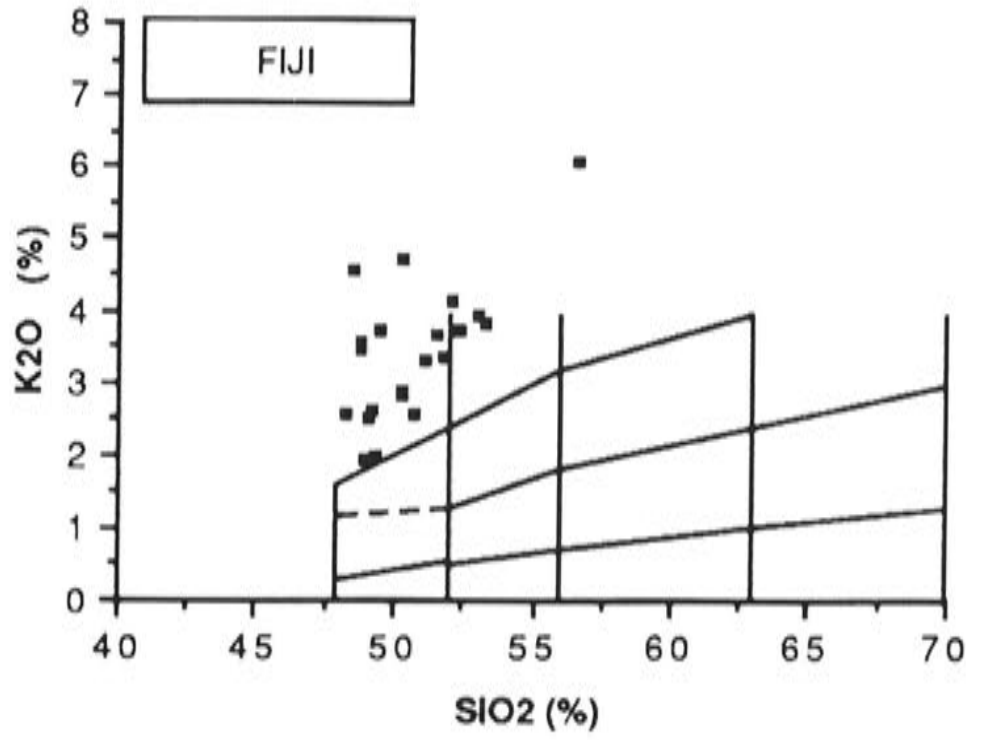

Figure 4.4d K_2O vs SiO_2 plot, Fiji.

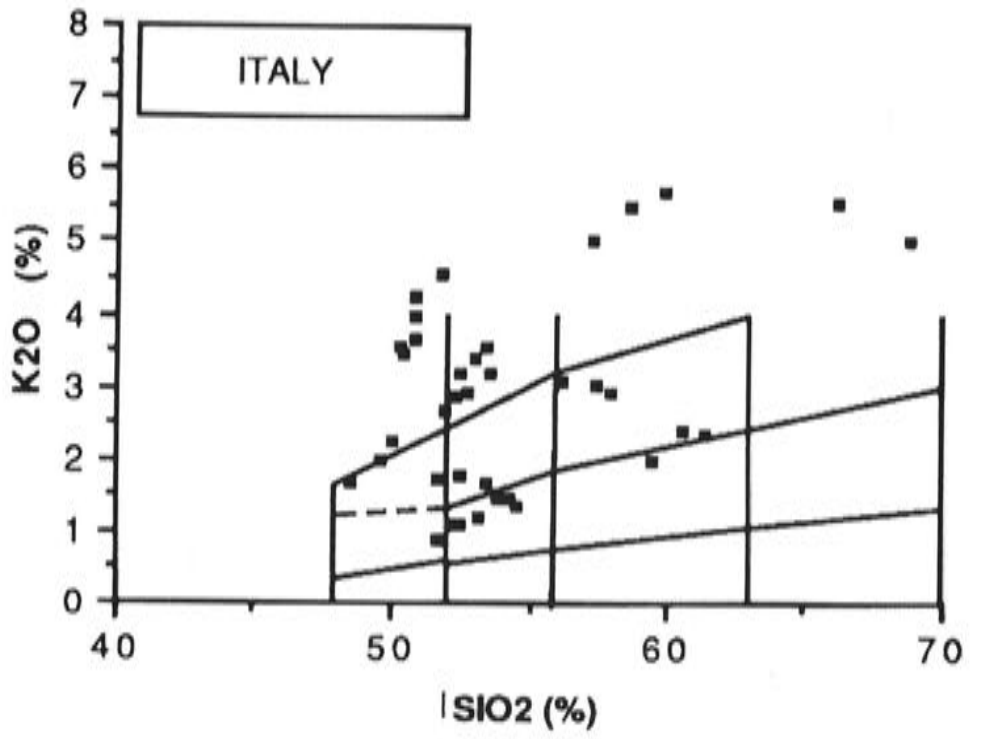

Figure 4.4e K_2O vs SiO_2 plot, Italy.

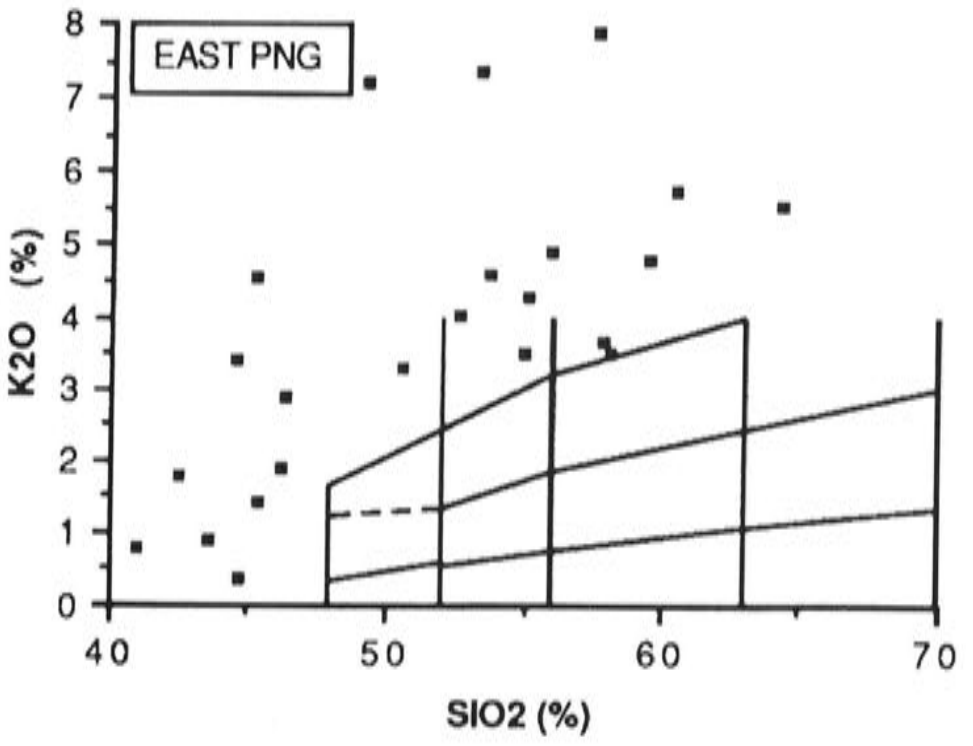

Figure 4.4f K_2O vs SiO_2 plot, east Papua New Guinea.

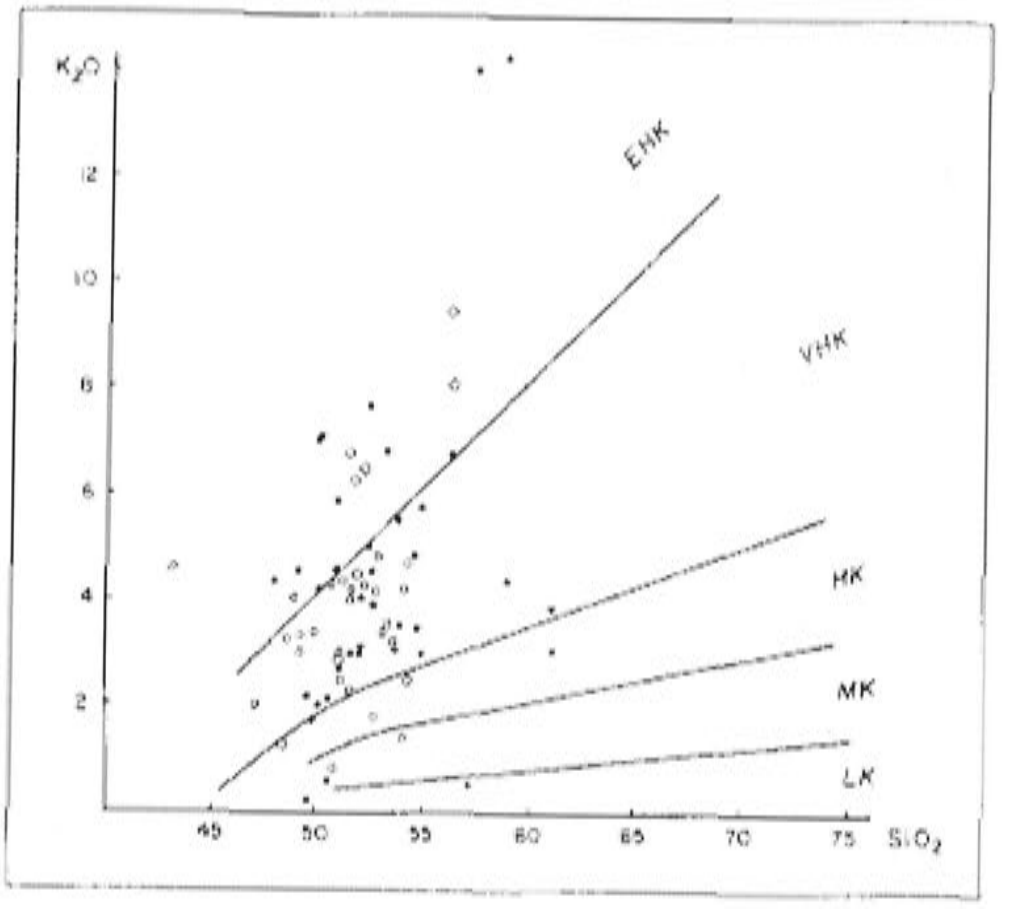

Figure 4.4g K_2O vs SiO_2 plot, British Columbia (after Spence 1985)

4.4.3 AFM diagram

The lack of a strong Fe-enrichment trend for the shoshonite association on an AFM plot (Fig. 4.6), led Morrison (1980) to suggest that it has a calc-alkaline affinity. He did note, however, that the association could not be unambiguously assigned to either the alkaline or calc-alkaline classes on the diagram, and therefore was best treated as a separate association.

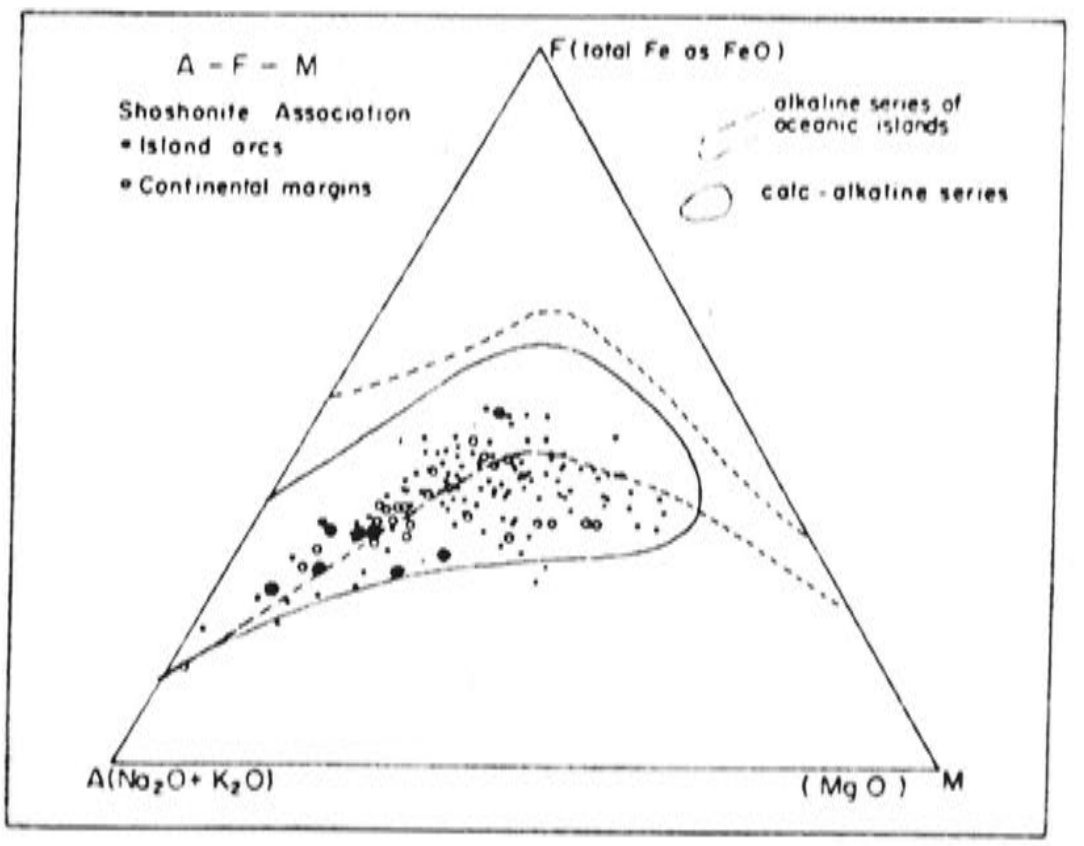

Figure 4.5 AFM diagram (after Morrison, 1980).

4.4.4 Major element characteristics of the shoshonite association

The major element content of various important rock associations are summarised in Table 4.1 from Morrison (1980). The shoshonite association differs from the other associations as follows:

1. From the tholeiite association — higher Fe_2O_3/FeO, $Na_2O + K_2O$, K_2O, P, Rb, Sr, Ba, Pb and LREE.
2. From the calc-alkaline association — higher $Na_2O + K_2O$, K_2O/Na_2O, P, Rb, Sr, Ba, Pb and K_2O/SiO_2.
3. From the alkali-basalt association — a greater range in silica content; higher average SiO_2, Fe_2O_3/FeO, $Na_2O + K_2O$, P, Rb, Sr, Ba and Pb; lower Fe-enrichment and lower TiO_2.

The SiO_2 content of shoshonitic rocks can vary over a wide range, from 40 to 70%, and in this respect the shoshonitic association is significantly different from the other rock associations. Nevertheless it should be noted that, the great majority of rocks in the shoshonite association fall in the basalt to basaltic andesite range.

	1	2	3	4	5
SiO_2	51.57	50.59	50.62	48.5	47.0
TiO_2	0.80	1.05	0.83	2.2	2.5
Al_2O_3	15.91	16.29	16.01	16.3	15.8
Fe_2O_3	2.74	3.66	4.11	3.1	3.3
FeO	7.04	5.08	4.55	8.0	7.9
MnO	0.17	0.17	0.17	0.17	0.16
MgO	6.73	8.96	6.24	6.6	7.1
CaO	11.74	9.50	9.26	9.9	10.1
Na_2O	2.41	2.89	2.93	3.0	3.2
K_2O	0.44	1.07	2.74	1.0	1.4
P_2O_5	0.11	0.21	0.44	0.36	0.50
H_2O	0.45	0.81	1.62	0.9	1.0
$K_2O + Na_2O$	2.85	3.96	5.67	4.0	4.6
K_2O/Na_2O	0.18	0.37	0.94	0.33	0.44
FeO^T	9.50	8.37	8.25	10.79	10.87
Fe_2O_3/FeO	0.39	0.72	0.91	0.39	0.42

Table 4.1 Major element contents of basalts from various associations (from Morrison, 1980).

TiO_2 abundance is an important discriminant between rock associations. TiO_2 levels in the shoshonite association rarely exceed 1.2%, and are commonly below 1%. This is a characteristic shoshonites share with island-arc tholeiites and calc-alkaline rocks (and indeed with the continental-arc equivalents). As will be discussed later, however, shoshonites are not unique to island- or continental-arc environments. This

fact has not stopped workers from invoking a convergent margin setting for most shoshonitic occurrences: based partly on the TiO_2 content, and partly on the relationship between potassium content and depth to Benioff Zone (first outlined by Dickinson (1975)).

Al_2O_3 is uniformly high (11–20%) in shoshonites as are Fe_2O_3/FeO ratios. This high-oxidation state has important consequences for metal transport in the porphyry environment, and will be discussed more fully in a later section.

$Na_2O + K_2O$ is higher in the shoshonite association than in the tholeiitic, calc-alkaline or alkaline associations. In addition the Na_2O/K_2O ratio is an important discriminant. The ratio is around one in the shoshonite association, whereas in all other associations it is greater than one.

4.4.5 Trace element and REE characteristics

The variation in trace element and REE abundances is best displayed on spidergrams. Figure 4.6 compares shoshonitic basalts from Fiji and Goonumbla with an alkali basalt from Hawaii. The plots are normalised against the composition of a typical MORB (Pearce, 1983). The Fijian sample shows enrichment in large ion lithophile elements (LILE) such as (K, Rb, Ba, Sr) and the LREE. High-field strength elements (HFSE), P, Ti and Zr are low. In contrast, the Hawaiian alkali basalt shows a weaker enrichment in LILE and, of importance, the HFSE are not depleted. The critical point of this diagram is the spiked nature of the shoshonitic samples compared to the alkali-basalt sample. This feature is typical of arc-related basalts. The elements Ta and Nb are particularly depleted, as well as Zr and Ti. This pattern of depletion and enrichment is part of the argument that shoshonites form in an island- or continental-arc setting.

Foley and Wheller (1990) discuss the role of residual titanites in establishing the characteristic Ti, Nb, and Ta depletion in island-arc volcanics in continental ultrapotassic rocks. They suggest that potassic magma in the Sunda arc was derived from at least two mantle sources, both of which contain residual titanites during partial melting. Titanite saturation in basic melts is promoted by a combination of the effects of high pressure; low temperature assisted by high H_2O content; high f_{O_2}; and high amounts of incompatible elements. Continental ultrapotassic rocks show a gradation of HFSE abundances which overlap with island-arc potassic rocks. They conclude that zones of enriched continental mantle may be analogous to K-rich components beneath island arcs. In both cases, comparably low-heat-flow regimes would allow low degrees of melting of hydrous mantle material. It is therefore clear that although Ti, Nb and Ta depletion is a feature of arc magmatism, it is not unique.

4.4.6 Isotope geochemistry

Meen and Eggler (1987) reported low values of $^{87}Sr/^{86}Sr$ and $^{143}Nd/^{144}Nd$, that is, they fall to the left of the mantle array. Pb isotopes of their shoshonitic series (HATS) define linear arrays in $^{207}Pb/^{204}Pb$ – $^{206}Pb/^{204}Pb$, but not in $^{208}Pb/^{204}Pb$ – $^{206}Pb/^{204}Pb$ space. They conclude that a granulite is a possible source (LREE enriched) to explain the Sr–Nd–Sm pattern; however a very large crustal contaminant would be required and this is deemed unlikely in these basic rocks. Mixing of a subcontinental mantle with a component from a subducted slab is another option, however compositional evidence argues against this possibility. Meen and Eggler (1987) conclude that the isotopic evidence is consistent with an ancient enriched mantle source.

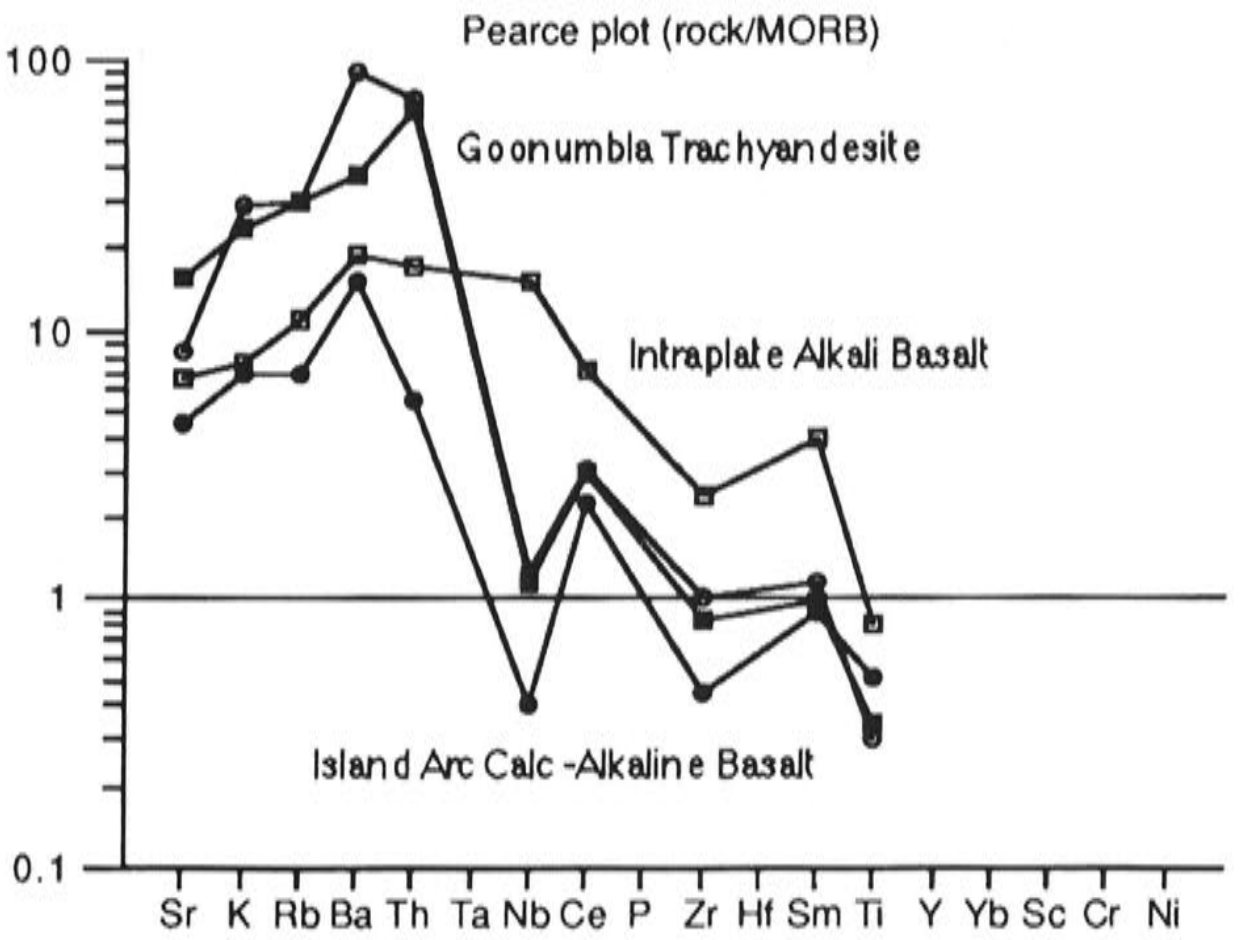

Figure 4.6 Spidergram comparing basalt types. Normalisation factors after Thompson (1982).

4.4.6 Isotope geochemistry

Meen and Eggler (1987) reported low values of $^{87}Sr/^{86}Sr$ and $^{143}Nd/^{144}Nd$, that is, they fall to the left of the mantle array. Pb isotopes of their shoshonitic series (HATS) define linear arrays in $^{207}Pb/^{204}Pb$ – $^{206}Pb/^{204}Pb$, but not in $^{208}Pb/^{204}Pb$ – $^{206}Pb/^{204}Pb$ space. They conclude that a granulite is a possible source (LREE enriched) to explain the Sr–Nd–Sm pattern; however a very large crustal contaminant would be required and this is deemed unlikely in these basic rocks. Mixing of a subcontinental mantle with a component from a subducted slab is another option, however compositional evidence

argues against this possibility. Meen and Eggler (1987) conclude that the isotopic evidence is consistent with an ancient enriched mantle source.

4.5 EXPERIMENTAL WORK AND FRACTIONATION MECHANISM

Meen (1990) has conducted experimental work on rocks from the Independence volcano located in the Absaroka volcanic field, from which absarokite, shoshonite and banakite were originally defined. One magmatic trend described by Meen varies from high-alumina tholeiitic basalt through shoshonite to high-K dacite (HATS series), and can be modelled by fractional crystallisation of observed phenocryst phases (plagioclase, hypersthene, augite, magnetite). Trace elements and Sr and Nd isotopic compositions are consistent with this model. The compositions of partial melts from experiments on a basaltic andesite, shoshonite and two intermediate compositions, at 1 atm and 10 kb, were studied in order to test whether the HATS trend could be reproduced experimentally at these conditions. Results showed that the rock compositions represent a nearly anhydrous liquid line of descent at pressures closer to 10 kb, than 1 atm. The line of descent involves crystallisation of orthopyroxene, not olivine, which results in strong enrichment in K_2O with little increase in SiO_2. Either increasing water content, or decreasing the crystallisation pressure, results in enrichment in both K_2O and SiO_2. On a K_2O versus SiO_2 plot the high-pressure crystallisation data plot on a steeper trend, whereas low-pressure data plot on a flatter, more calc-alkaline trend. The implication of this study is that, high-pressure fractional crystallisation of basaltic magma occurring at the base of thick crust can result in enrichment in potassium, with minor increase in silica. Low-pressure fractionation of the same melt will produce a more silicic melt.

4.6 TECTONIC SETTINGS

Gest and McBirney (1979) conclude that shoshonitic lavas in the Absaroka Mountains formed in an extensional tectonic environment dominated by block faulting. Similarly, Meen and Eggler (1987) conclude that, although the Independence volcano has trace element characteristics that are similar to typical orogenic volcanics, the rocks have Ba/Th and La/Th ratios which are far higher than the typical ratios reported by Gill (1981) for orogenic volcanics. They conclude that the shoshonites are sourced from an ancient enriched subcontinental mantle, but are not clear on the tectonic regime.

Dostal et al. (1977) observe that shoshonitic rocks in northern Chile and Argentina occur in longitudinal belts parallel to a subduction-related orogen. The authors deduce from the evidence of increasing Rb, Ba, Sr and Zr away from the

inferred trench, together with increasing enrichment in LREE and fractionated HREE, that the volcanics are sourced from enriched mantle above a subduction zone.

The shoshonites in Italy provide several different tectonic settings. Keller (1974) describes the Aeolian arc, where shoshonites occur with calc-alkaline rocks in an island-arc environment. The shoshonitic rocks are generally the youngest and only shoshonitic activity is still going on. The Aeolian arc is in the final stages of arc evolution as there is no more oceanic crust to subduct. Present seismicity is sourced from depths of from 200 to 350 km. Keller (1974) concludes that the seismic gap from 50 to 200 km, and lack of present day calc-alkaline activity, is explained by a model involving a detached slab sinking into the mantle. Varecamp and Kalamarides (1989) describe a suite of highly potassic undersaturated rocks (HKS) and a lower K series (LKS) which have erupted from the Vulsini centre. The volcanics occur in a post-collisional tectonic setting in a Pliocene graben structure. The authors envisage an extensional phase postdating subduction, which had moved further south by this time. Sloman (1989) describes shoshonitic volcanics in the Dolomites of northern Italy, which are associated with a change from continental to marine conditions at the onset of block faulting. There is no evidence of contemporaneous subduction, and Sloman concludes that the tectonic regime is one of strike-slip faulting in a transcurrent or transtensional regime. He resolves the dilemma of the characteristic island-arc signature by proposing that the suite inherited the signature from a Permo-Carboniferous subduction event prior to the Hercynian Orogeny.

The Papua New Guinea highlands provide another example of shoshonitic volcanism without any contemporaneous subduction (Mackenzie and Chappell, 1972). Shoshonitic rocks occur in close association with calc-alkaline rocks, but they occur in clusters rather than linear belts, which argues against a zonation in time and space due to subduction. Similarly there is no seismic evidence for a subduction zone. They suggest that these volcanics appeared in a period of uplift, orogeny and major fault movement. Smith (1972) invokes a similar tectonic regime for the potassic intrusions he describes in southeastern Papua New Guinea. Mackenzie and Chappell (1972) invoke a model, similar to that of Keller (1974), in which magma generation is due to detached and sinking eclogite, with zone refining of small partial melts during the passage of the melt through the mantle.

Fiji provides a complex tectonic environment in which tholeiitic, calc-alkaline and shoshonitic rocks are clearly spatially associated, and exhibit trace element patterns that suggest a genetic link. Gill and Whelan (1989) conclude that it was the inception of rifting at 5.5 Ma that was responsible for shoshonites . They appeal to small degrees of partial melting to explain enrichment in LILE, and a role for titanites to explain depletion of HFSE, giving the characteristic arc signature.

The most recent discovery of shoshonites comes from investigations in the north Mariana arc. Here shoshonites are associated with tholeiites in essentially a back-arc extensional environment. The shoshonitic rocks come from the northern end of the rift at the 'unzippering' end of the basin. Bloomer et al. (1989) suggest that mantle upwelling in the leading edge of the magmatic front exposes deeper parts of the mantle which have not been previously melted.

Spence (1984) suggests that a Philippines model may be appropriate for British Columbia where the Upper Triassic subduction zone, after being disturbed by the collision of the allochthonous terranes and having generated the calc-alkaline-shoshonitic Nicola-Takla-Stuhini arc as it became subvertical, was eventually reversed during accretion to North America.

4.7 SIGNIFICANCE FOR MINERALISATION

The rationale behind this thesis is the belief that porphyry mineralisation is the result of characteristics of the magma source, the path from source to emplacement, and the transition from magmatic to hydrothermal conditions. In the context of examining shoshonitic porphyry Cu–Au mineralisation, it is important to examine the metal content of the source, establish the potential volatile content of the melt and review the behaviour of S in shoshonitic melts.

Rock and Groves (1988a, b) suggested that shoshonitic lamprophyre magmas might have acquired anomalous Au contents from deep mantle plume sources. Wyborn (1988) and Wyborn and Cameron (1990) have established that Ordovician shoshonitic volcanics of the Lachlan Fold Belt reveal ~10-fold enrichments in Au, Pd and Pt (Pt + Pd typically 20–40 ppb), whereas S contents are low (<200 ppm). The Goonumbla rocks, by comparison, have from 50 to 500 ppm S in rocks well away from mineralisation. Wyborn and Cameron (1990) suggest that shoshonites may be a second-stage melt of K-metasomatised, S-depleted (<50 ppm), subcontinental lithospheric mantle. In these circumstances Au, Pd and Pt will behave incompatibly during partial melting. They will be partitioned into the silicate melt phase in the absence of a separate sulphide-liquid fraction that would normally be retained in the upper mantle (Hamlyn et al., 1985). Fractionation of the Au-enriched shoshonite parent can lead to further Au enrichment, provided the magma does not become sulphide saturated. Wyborn (1988) suggests that such melts are the sources for the low-S, porphyry Cu–Au systems at Goonumbla. A problem with this model is that it does not take into account the large amount of sulphate, in the form of anhydrite, that occurs in the Goonumbla systems. These systems are more correctly called low-sulphide systems.

Tatsumi and Koyaguchi (1989) regard amphibole- or phlogopite-bearing metasomatised peridotites as a likely source of primitive shoshonitic magmas. Mantle enrichment processes that lead to amphibole formation can also result in up to 25 times enrichment in Au over normal mantle abundance (Lorand et al., 1989). In oxidised mantle material, such as occurs in subduction-related environments (Ballhaus et al., 1990), sulphides will be unstable, thereby releasing Au to behave incompatibly during partial melting.

Taken together, these are plausible models of source and source processes which point to primitive shoshonitic magmas containing order of magnitude Au enrichments.

Volatile content and behaviour in shoshonitic magmas is an important ingredient in considering shoshonitic-hosted mineralisation. Tatsumi and Koyaguchi (1989) report on an absarokite from the Katamata volcano in southwest Japan. The absarokite studied is primitive, that is it contains 9.2% MgO (Mg Number = 0.7) and high concentrations of Ni, Cr and Co. The sample contains 3.29 wt% water, which is manifest by the presence of hornblende and phlogopite. Phlogopite forms early in the paragenesis. Shoshonitic rocks however, do not commonly have hydrous phases in the mafic end members. The water content of the shoshonite group is variable.

Juvenile S abundance in shoshonitic rocks is difficult to estimate due to either the effects of alteration, which may not be obvious, or degassing. The average S content in primitive shoshonitic lamprophyres, taken from the University of Western Australia database, is 320 ppm with a range from 100 to 700 ppm. This compares with Cosgrove (1972), who gives an average of 158 ppm with a range of 35 to 673 ppm.

Cu and Au are chalcophile elements that will strongly partition into the aqueous phase that will develop when water-bearing magmas exsolve through retrograde boiling. Similarly, S also partitions into the magmatic aqueous phase and is present in the fluid as H_2S and SO_2. Burnham and Ohmoto (1980) suggest that S exists in hydrous melts, principally as HS-, but exists in the aqueous phase as both H_2S and SO_2. The partition coefficient is sensitive to f_{H_2O} and f_{O_2}, and an increase in oxidation will favour partitioning into SO_2, which resolves readily into the magmatic hydrothermal fluid. Carrol and Rutherford (1985) studied S solubility in hydrous dacite melts and found that it increased with increasing f_{O_2} (at constant p_{H_2O}, T and %FeO). This implies that relatively oxidised shoshonitic magmas can transport more S and other chalcophile elements from their source region.

4.8 CONCLUSIONS

Shoshonite volcanism is a minor, but important part of the rock record. A number of important Au deposits are associated with shoshonitic rocks, including the Northparkes or Goonumbla porphyry Cu–Au deposits. The shoshonite association is distinguished by low-Fe enrichment, high K_2O, high total alkalis, high LILE, high Fe_2O_3/FeO ratios, and low TiO_2 and Nb. Magmatic series plotted on K_2O versus SiO_2 span a large field which, in several instances, can be resolved into a number of discrete trends. In some cases the variation can be seen in magmatic products from the same volcano. Meen (1990) established a process to account for this variation based on the pressure of partial melting. Moderate to high pressures at the point of partial melting can suppress olivine from the liquidus, thereby promoting pyroxene crystal fractionation. This has the effect of raising K_2O, with minor increases in SiO_2. Trace element and REE data show distinctive patterns typical of island or continental arcs; however the characteristic Ti, Nb and Ta completion is known in intraplate settings.

Rocks of the shoshonite association come from a variety of tectonic settings. Above active subduction zones they are only a minor part of the total product of magmatism. In these settings, they occur above the deepest parts of the subduction zone and late in the succession. Shoshonites appear more commonly during and after continental collision following the closing of ocean basins. The potassic magmatism may follow the geosuture geographically, and may appear either soon after the collision or after a delay. Meen and Eggler (1987) demonstrated that the enrichment process in the source for the shoshonites of the Absaroka Mountains could have occurred in the Archean. Therefore, enriched mantle is capable of persisting for a considerable period of time under thick crust. Some shoshonitic rocks have been reported grading to ultrapotassic rocks in intraplate settings (Foley and Wheller, 1990).

Clearly the shoshonitic association can occur in a variety of tectonic settings, ranging from true continental- or island-arc settings to the beginning, or end, of rifting events which may or may not be related to subduction. The characteristic island-arc trace element signature does not necessarily prove contemporaneous subduction, but does indicate subduction processes were involved in some point in the magmatic history. The only study to date that evaluates this suggestion is Meen and Eggler (1987), who discount enrichment via crustal processes. They provide evidence of ancient enrichment of the mantle beneath the Absaroka Mountains. It is clear, however, that shoshonitic rocks cannot uniquely prove an arc setting. The oxidised nature of the shoshonitic melts and their metal carrying capacity makes them an attractive source for Au and Cu.

Chapter 5

PETROGENESIS OF THE GOONUMBLA VOLCANIC COMPLEX

5.1 INTRODUCTION

The general aim of this part of the study is to investigate the petrogenesis of the Goonumbla Volcanic Complex and, if possible, constrain its tectonic setting and relationship to other Ordovician volcanic complexes in the region. A more specific aim is to investigate the geochemical relationships between the intrusive rocks of the complex and the volcanic rocks that they intrude, and attempt to establish criteria which may serve to identify intrusions related to mineralisation.

The focus is on the igneous rocks west of the Parkes Thrust and, in particular, those rocks with some spatial association with mineralisation. Over 50 samples were collected for whole-rock and trace-element analysis. Most samples have been affected to some degree by a prehnite-pumpellyite-grade metamorphic overprint. All samples have been described petrographically, and only those samples with the least alteration have been included in the data set that forms the basis of this part of the thesis. The petrology of the igneous rocks of the Parkes area was addressed in a recent study on the geological setting of Au and Cu deposits in the Parkes area by Clarke (1990). Nineteen samples from that study have been included in the present data set.

5.2 FIELD NOMENCLATURE

Field identification of extrusive rocks in the Parkes area has relied mainly on estimating the quartz, plagioclase and K-feldspar content, and using the classification of Streckeisen (1973). Similarly, for intrusive rocks the QAPF system is used. Estimations of K-feldspar content, particularly in the groundmass, were routinely checked by etching with hydrofluoric acid and staining with sodium cobaltinitrate. A subdivision into two broad compositional categories, trachytes and trachyandesites, is used in field identifications and textural qualifiers are added to complete the rock name. Features of the two categories are presented below.

5.2.1 Trachytes

Trachytes are composed dominantly of a very fine-grained, aphanitic to microgranular K-feldspar groundmass. K-feldspar comprises 65–90% of total feldspar. The plagioclase present commonly occurs as lenticular phenocrysts, typically about 2 mm long (but up to 5 mm). Biotite, pyroxene and rarely olivine are minor constituents. Magnetite and apatite are common accessories. In outcrop trachytes have a brown to pale-pink colour, due primarily to fine hematite dusting of the K-feldspar. Trachytic lavas are commonly sparsely porphyritic to totally aphanitic. Trachytic volcaniclastics range in grain size from fine ash tuffs through coarse ash tuffs to lapilli tuffs and agglomerates. Reworked volcaniclastics or epiclastics also occur in the succession.

5.2.2 Trachyandesites

The term 'trachyandesite' has been used to cover the fields which encompass latite through latite-andesite or latite-basalt (basaltic andesite). In outcrop, the rocks vary in colour from reddish brown through maroon-grey to dark grey, and are always porphyritic. Pale-grey plagioclase phenocrysts and dark-grey mafic phenocrysts impart a porphyritic texture to the rock. Pink-red K-feldspar may be evident as interstitial material, but it is usually necessary to resort to staining to reveal the true K-feldspar content. By definition, from 10 to 35% of the total feldspar is K-feldspar (or albite) and this is dominantly in the groundmass. Approximately 65% of phenocrysts are plagioclase, which are commonly 2–5 mm in length. The remainder of the phenocryst fraction includes clinopyroxene, with lesser hornblende, biotite and olivine. Magnetite is ubiquitous, and forms fine granules through the groundmass and commonly larger grains approaching 1 mm in diameter. Trachyandesites occur as lavas and volcaniclastics spanning the range from fine ash tuff to agglomerate.

5.3 DETAILED PETROGRAPHY AND GEOCHEMISTRY

A more rigorous classification of the rocks from the Parkes area is achieved using the templates on the total alkalis versus silica diagram of Le Bas et al. (1986), and the K_2O versus SiO_2 diagram of Peccerillo and Taylor (1976). Figures 5.1 and 5.2 show that the Goonumbla Suite (encompassing both the Goonumbla Volcanics and the Wombin Volcanics) spans the high-K alkaline or shoshonite field. Compositions range from absarokite to trachyte. The Goonumbla Suite is unusual because it exhibits a wide range of silica values compared to other shoshonitic centres (Fig. 4.4). A re-examination of the samples, in the light of this classification, allows a more detailed description of this important suite.

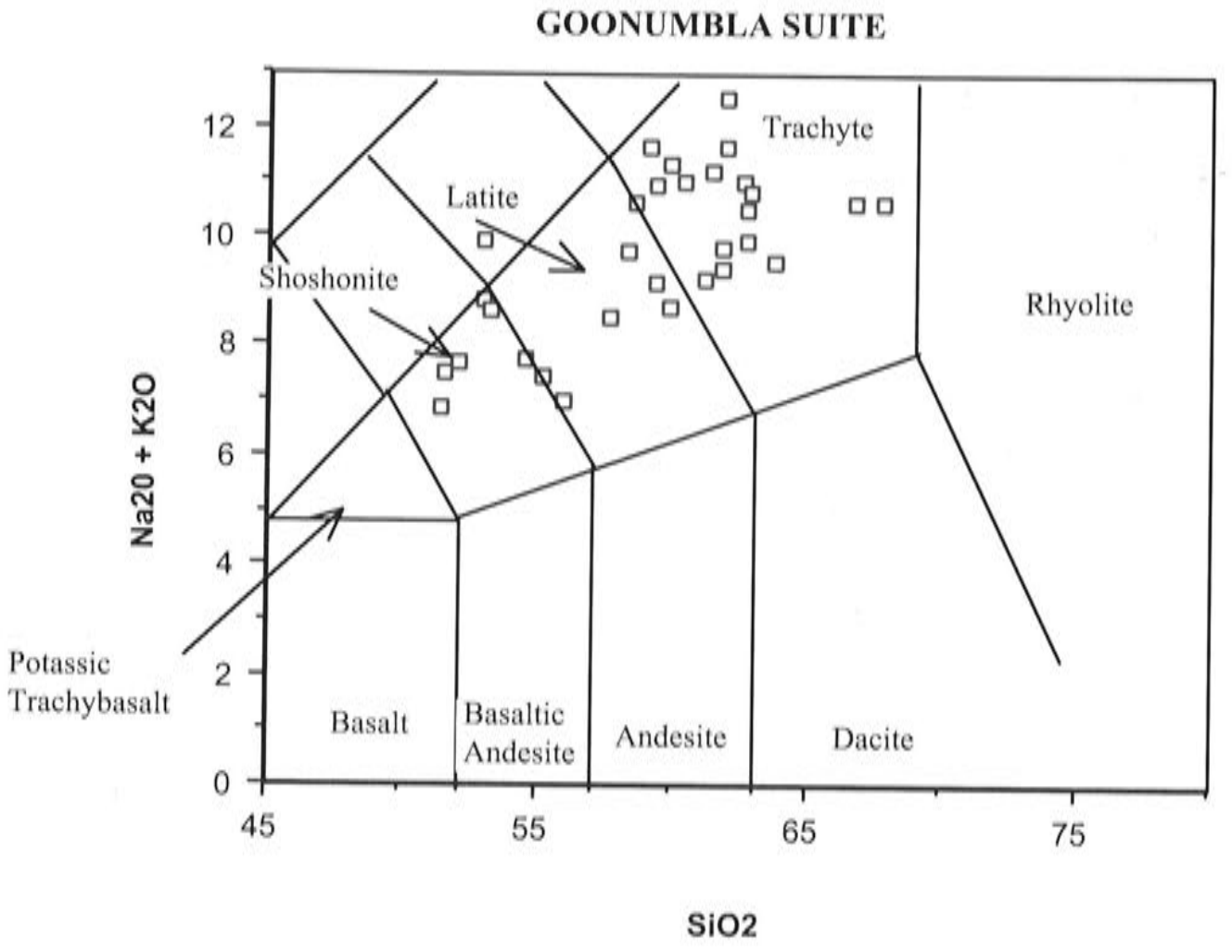

Figure 5.1 $Na_2O + K_2O$ vs SiO_2 plot of Goonumbla and Wombin Volcanics, with fields after Le Bas et al. (1986).

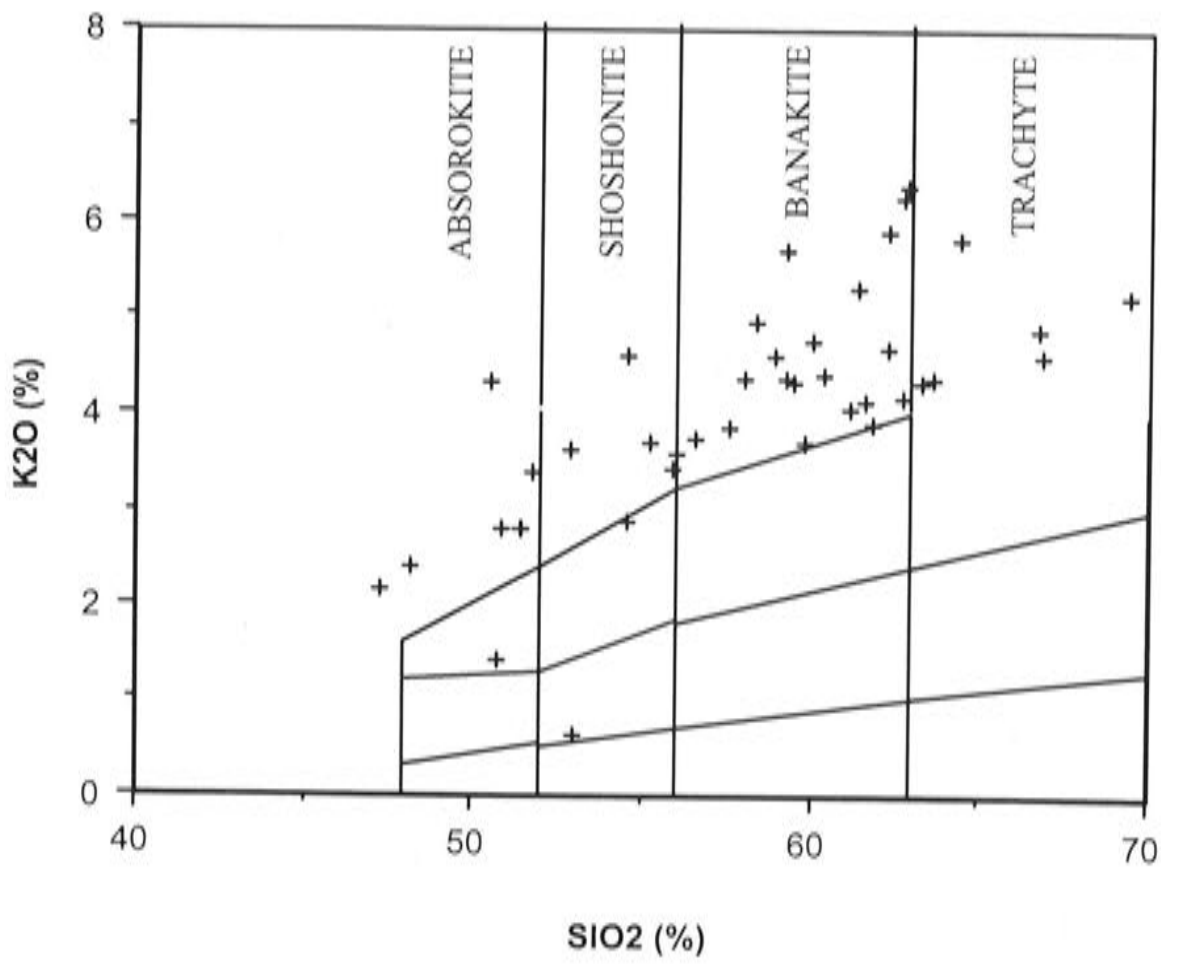

Figure 5.2 K_2O vs SiO_2 plot of Goonumbla and Wombin Volcanics, with fields after Peccerillo and Taylor (1976).

5.3.1 Volcanics

Absarokite: phenocrysts of plagioclase, pyroxene and olivine, in a groundmass of microphenocrysts consisting of plagioclase, K-feldspar and magnetite. Plagioclase forms a bimodal phenocryst distribution. Olivine and pyroxene occur as individual phenocrysts or in clusters of both minerals.

Shoshonite: typical shoshonitic lavas consist of phenocrysts of plagioclase (An_{30-53}) and euhedral to subhedral clinopyroxene which can form quite coarse crystals. Shoshonites at Goonumbla are very crystal rich in contrast to glassy lavas noted in other shoshonitic fields. Flow alignment of phenocrysts is a common feature, and vesicles filled with zeolites and carbonate occur in some localities. Plagioclase phenocrysts commonly form skeletal forms indicating rapid quenching. The matrix typically is a microgranular mosaic of plagioclase, K-feldspar, pyroxene and abundant magnetite. Apatite is common as small, isolated subhedral crystals. Prehnite and pumpellyite are common secondary minerals and impart a greenish tinge to many of the rocks. Other secondary minerals include actinolite, calcite, quartz, chlorite and zeolites.

Banakite (latite) – trachyte: rocks which have been called trachytes in the field range chemically from banakites (or latites) to trachytes. Good examples of 'trachytic' lava from Nash's Hill straddle the boundary between latites and trachytes on the Le Bas et al. (1986) total alkalis versus silica diagram. The rocks are usually porphyritic with lenticular crystals of twinned plagioclase, in a felsitic groundmass of K-feldspar and plagioclase. Isolated phenocrysts of biotite and/or pyroxene, and rarely olivine, occur as well. Small crystals of apatite are commonplace, and magnetite occurs dispersed through the groundmass.

5.3.2 Intrusive rocks

The intrusive rocks, spanning the same compositional range as the volcanic rocks, are diorite, monzodiorite, monzonite and quartz monzonite.

Diorite: euhedral crystals of plagioclase, with well-defined twinning, and generally mantled by large K-feldspar crystals. Smaller crystals of plagioclase occur totally enclosed by K-feldspar. There are sparse crystals of pyroxene and they are mantled by biotite. Biotite is interstitial to earlier minerals. The sequence of crystallisation was from early plagioclase and pyroxene to later K-feldspar and biotite.

Monzodiorite: holocrystalline, medium-grained rocks consisting of euhedral, zoned andesine (50–60%), hornblende (5–10%) and clinopyroxene (5–10%), with interstitial cloudy perthitic K-feldspar (15%). Biotite poikilitically encloses plagioclase, hornblende and clinopyroxene. Magnetite and apatite are common accessories.

Plate 5.1 Shoshonite: autobrecciated lavas from the Goonumbla Quarry.

Plate 5.2 Flow-banded trachyte.

Monzonite: holocrystalline rock consisting of subhedral oligoclase to andesine crystals (20–35%), commonly as cumulophyric aggregates, set in a holocrystalline, hypidiomorphic granular groundmass of stumpy K-feldspar crystals. These groundmass grains are always red-brown to pink-red due to a dusting of iron oxide. K-feldspar commonly forms rims to plagioclase crystals and, in rare cases, large tablets of orthoclase poikilitically enclose earlier formed phenocrysts of plagioclase, hornblende and clinopyroxene. Magnetite and apatite are common accessories.

Quartz monzonite – quartz monzonite porphyry: the porphyry representatives are conspicuously porphyritic with grey, evenly distributed laths of albite to oligoclase (20–30%), set in a pink, fine-grained groundmass of K-feldspar and quartz. Hornblende and minor biotite are sparsely distributed and may make up to 10% by volume. Rare tablet-shaped megacrysts of perthitic orthoclase poikilitically enclose plagioclase crystals. Quartz is interstitial and its abundance varies up to about 13 %. These porphyries are the main intrusive phase related to mineralisation.

5.3.3 Major elements

On the K_2O versus SiO_2 diagram (Fig. 5.3) the entire Goonumbla data set, including both volcanic and intrusive rocks, plots as a broad spread which diverges towards higher silica values. The plot emphasises the wide range of silica values in these rocks, which is atypical for shoshonite suites. The intrusive rocks in the Forbes Anticline plot in the high-K calc-alkaline field. The suite of intrusives related to mineralisation (shown as open circles) varies in silica content from 56 to 70%, and clearly defines a trend which is parallel to the boundary between the shoshonite and high-K calc-alkaline fields. In contrast, the unmineralised intrusive rocks and the Wombin and Goonumbla Volcanics define an upward curving trend to higher K_2O levels. This suggests that there may be two magmatic evolutionary trends separating mineralised from non-mineralised intrusive systems. It is interesting to note that there appear to be no extrusive equivalents to the mineralised suite.

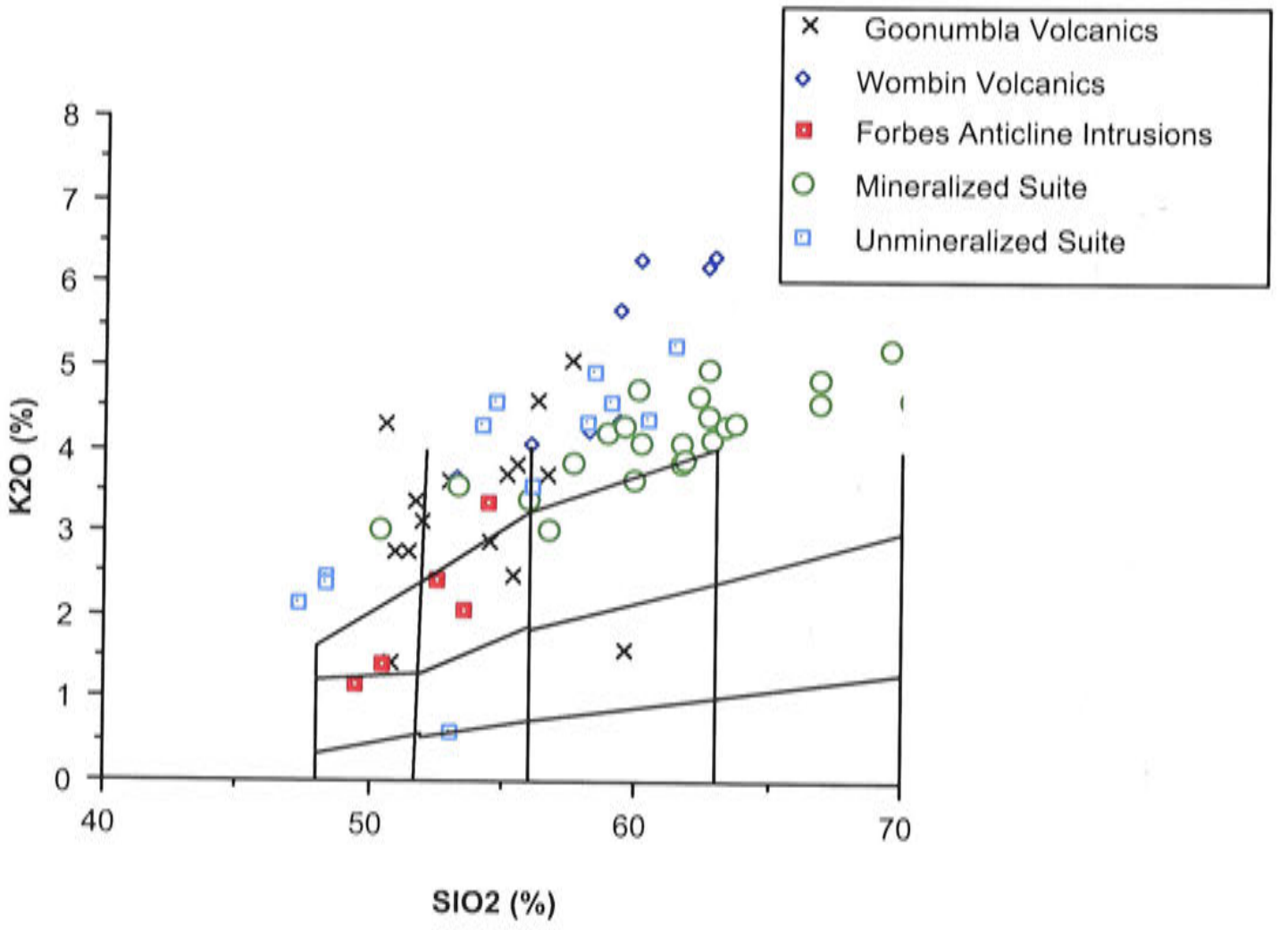

Figure 5.3 K_2O vs SiO_2 plot of Goonumbla and Wombin Volcanics and intrusions.

Harker diagrams for various elements are given in Figure 5.4a–h. The plots for P_2O_5, CaO, TiO_2, Fe_2O_3, MnO and MgO all show good correlations for all samples, although the intrusive rocks in the Forbes Anticline tend to cluster separately on the P_2O_5 plot. These patterns suggest that the Wombin and Goonumbla Volcanics, and the intrusive bodies that cut them, are genetically related.

The fact that the major element patterns for the volcanics and the intrusives (with the exception of those in the Forbes Anticline) show evidence for both distinct and common evolutionary trends requires elaboration. It was noted in Chapter 4 that distinct evolutionary trends are a common feature of the shoshonite association, and can usually be attributed to spatial and temporal differences. In the present case, however, the rocks are from a single volcanic centre and radiometric dating (Perkins et al., 1990) shows that they are all of the same age. Assuming that the Goonumbla magma was mantle derived, then the maximum MgO value of 6 % in the samples, suggests that the primitive magma had undergone significant crystal fractionation of ferromagnesian phases at depth. Furthermore, in the Endeavour 31 stock described below, there is a mineralogical gradation from diorite to quartz monzonite, which is reflected in the flat trend of the mineralised suite on the K_2O versus SiO_2 plot. The variation in major elements therefore reflects crystal fractionation in both deep-seated and high-level, low-pressure environments.

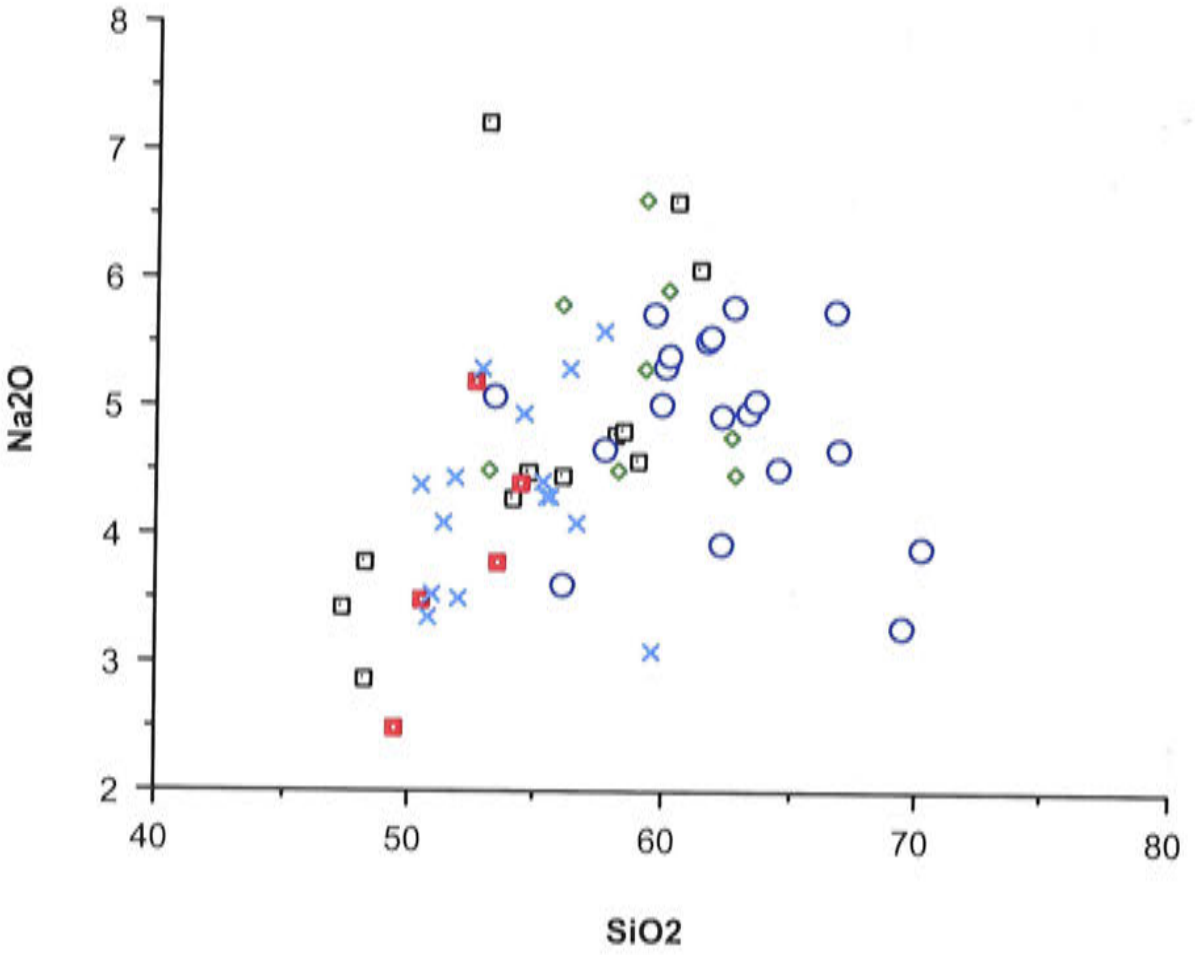

Figure 5.4a Na_2O vs SiO_2 plot of Goonumbla and Wombin Volcanics and intrusions. See Figure 5.4d for legend.

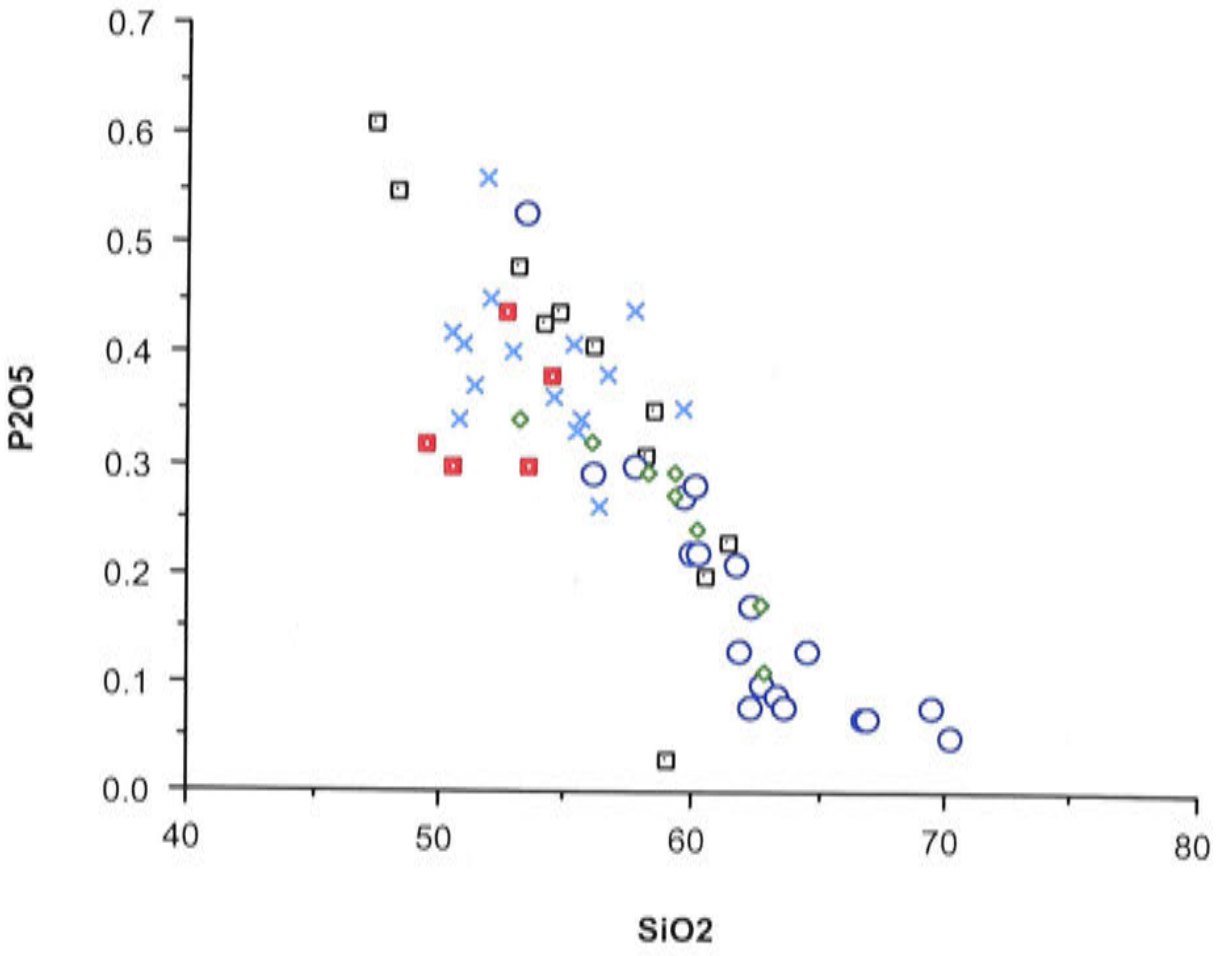

Figure 5.4b P_2O_5 vs SiO_2 plot of Goonumbla and Wombin Volcanics and intrusions. See Figure 5.4d for legend.

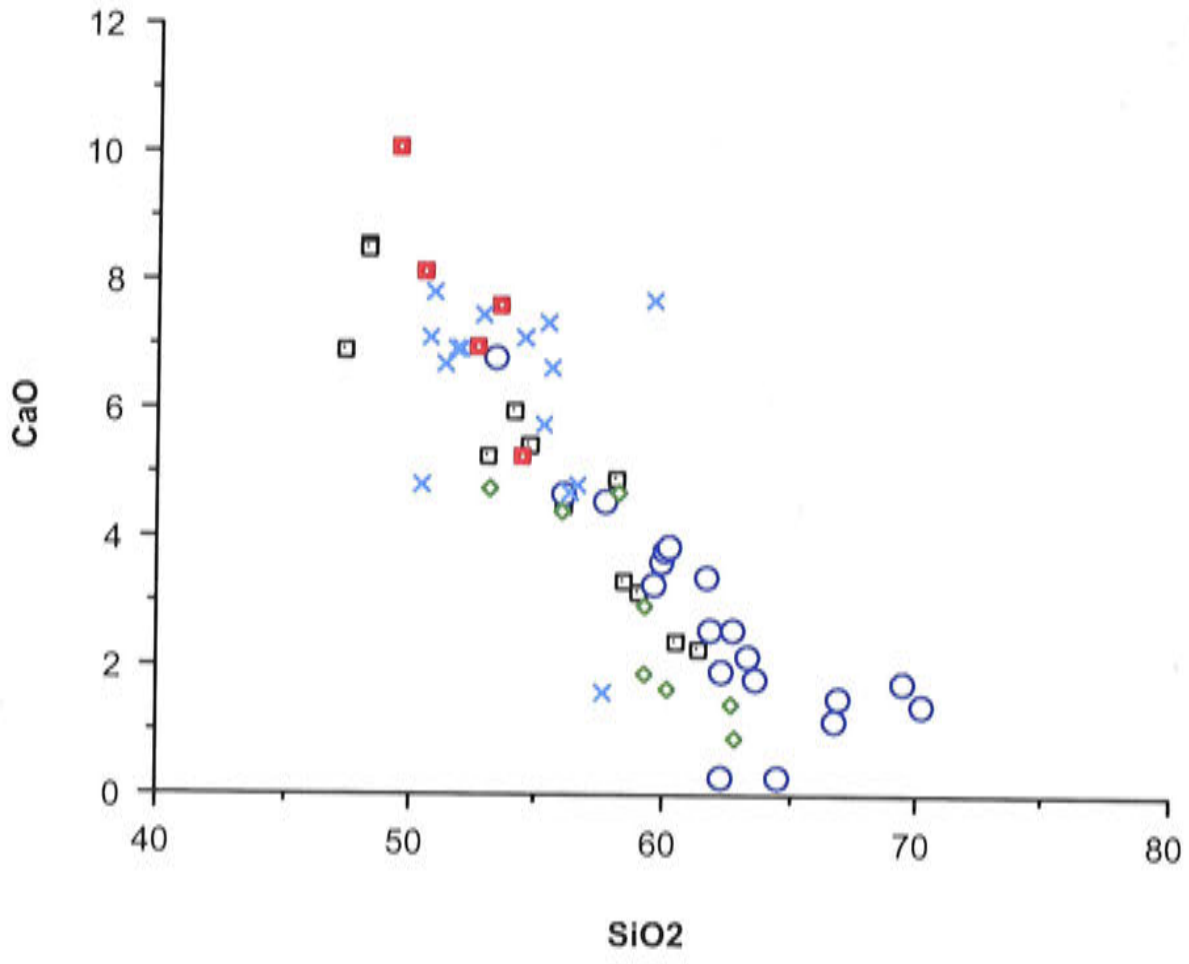

Figure 5.4c CaO vs SiO_2 plot of Goonumbla and Wombin Volcanics and intrusions. See Figure 5.4d for legend.

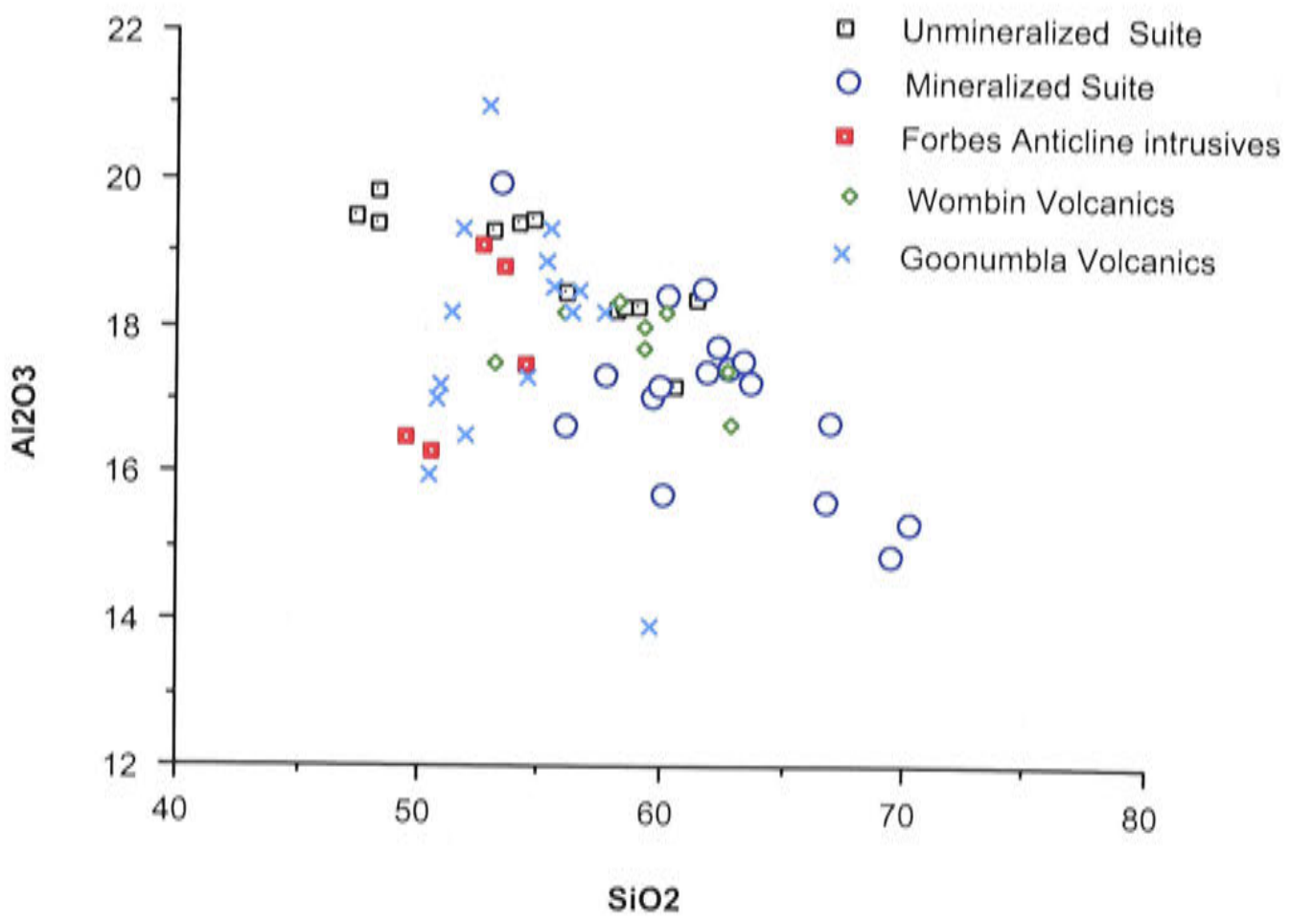

Figure 5.4d Al_2O_3 vs SiO_2 plot of Goonumbla and Wombin Volcanics and intrusions.

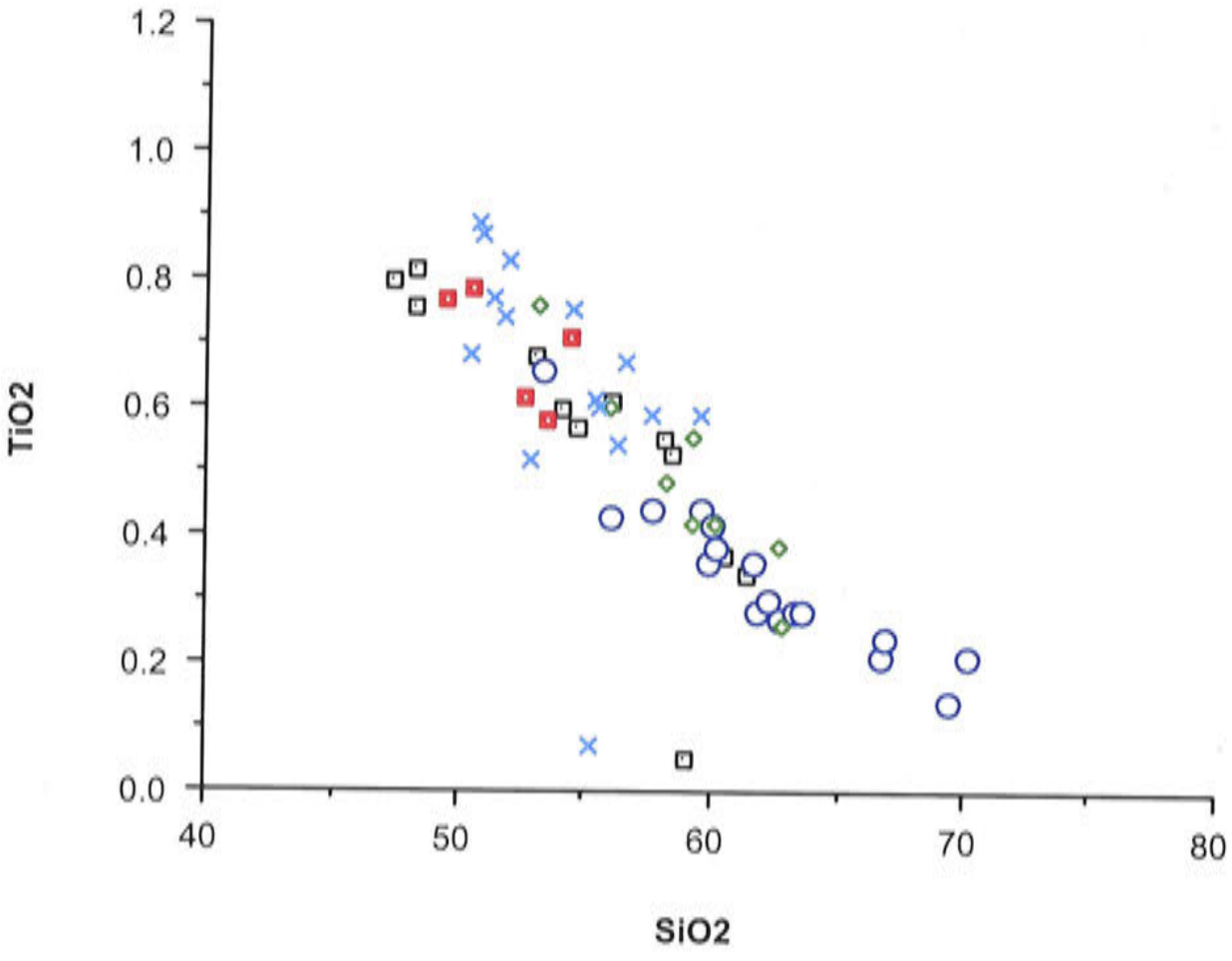

Figure 5.4e TiO_2 vs SiO_2 plot of Goonumbla and Wombin Volcanics and intrusions. See Figure 5.4d for legend.

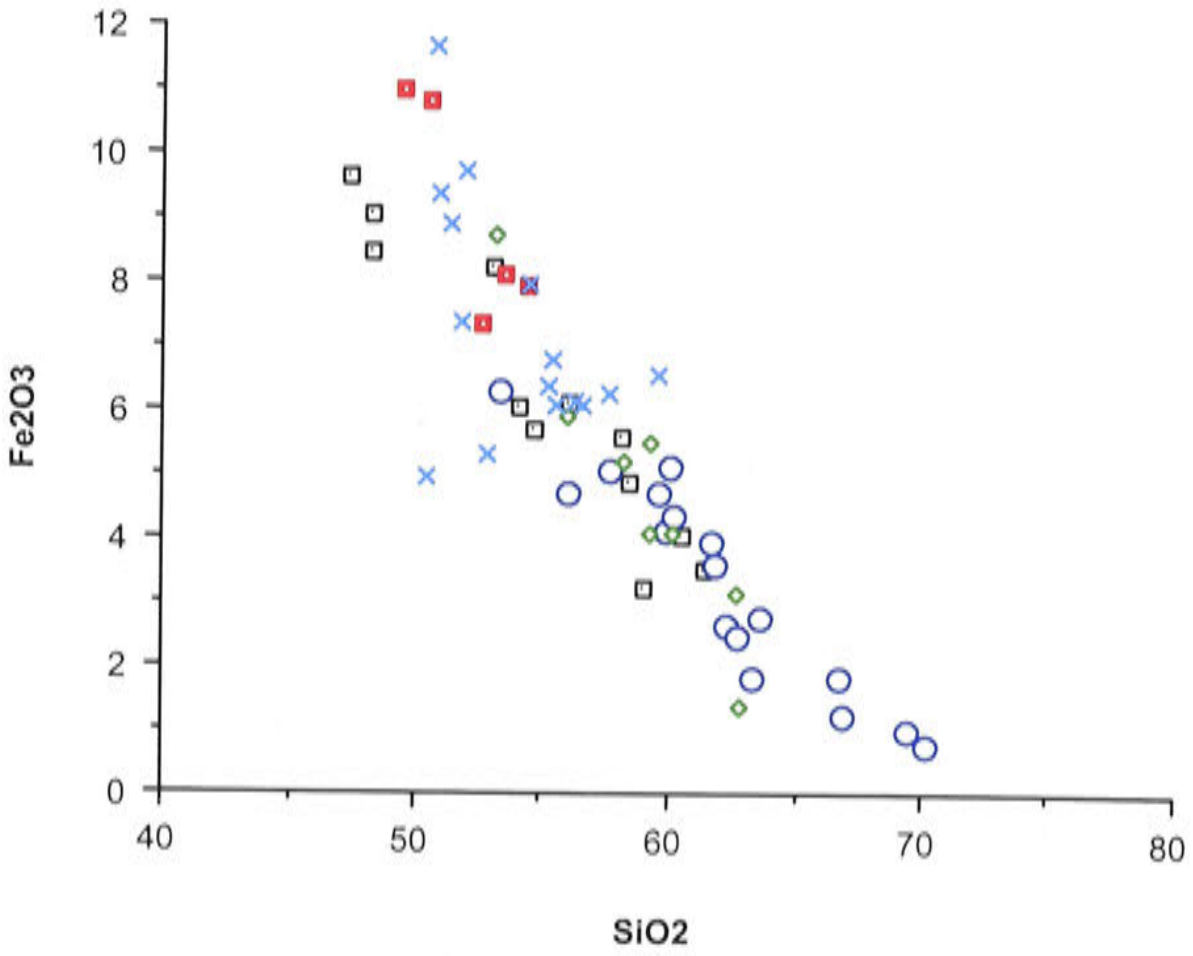

Figure 5.4f Fe_2O_3 (total iron) vs SiO_2 plot of Goonumbla and Wombin Volcanics and intrusions. See Figure 5.4d for legend.

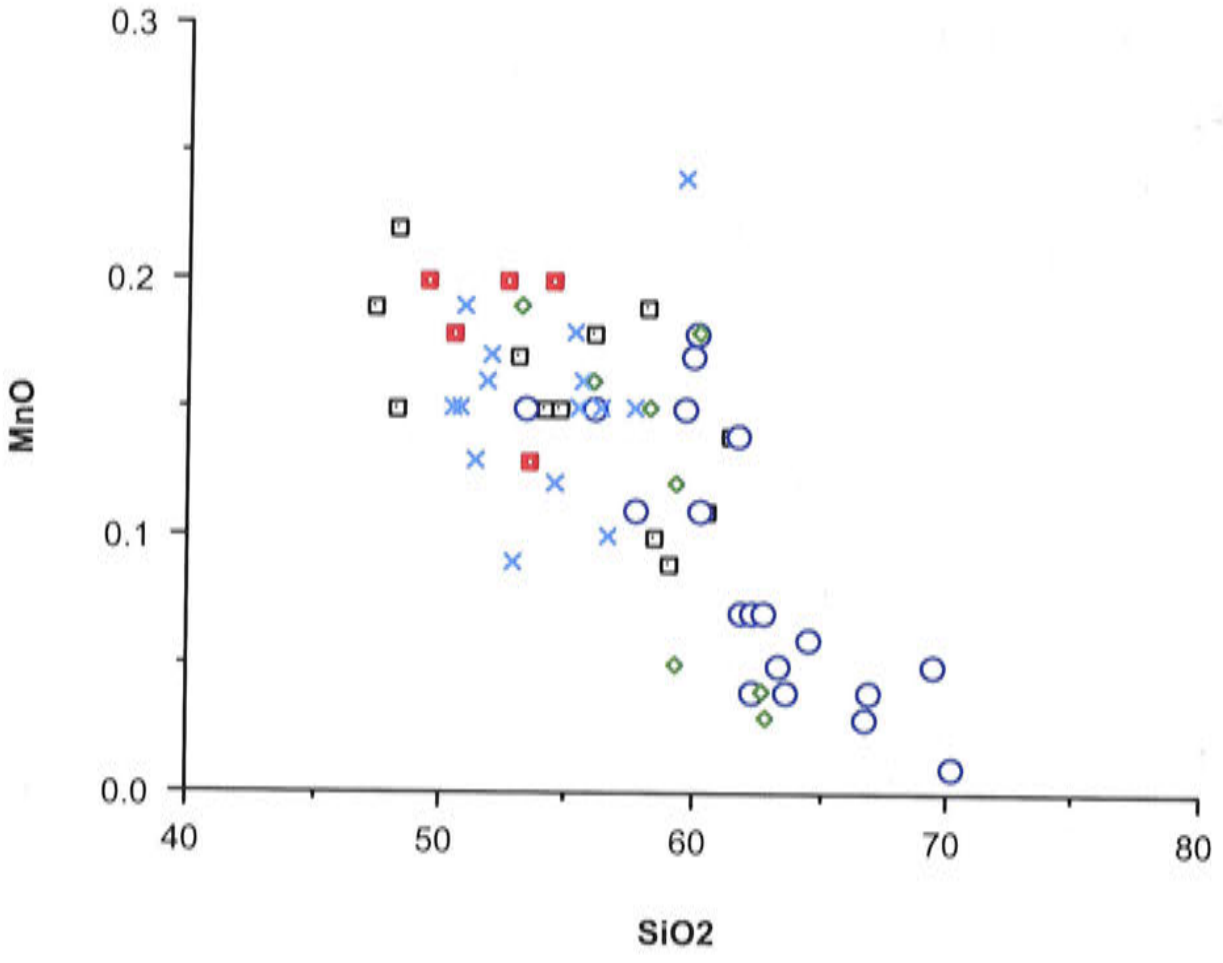

Figure 5.4g MnO vs SiO_2 plot of Goonumbla and Wombin Volcanics and intrusions. See Figure 5.4d for legend.

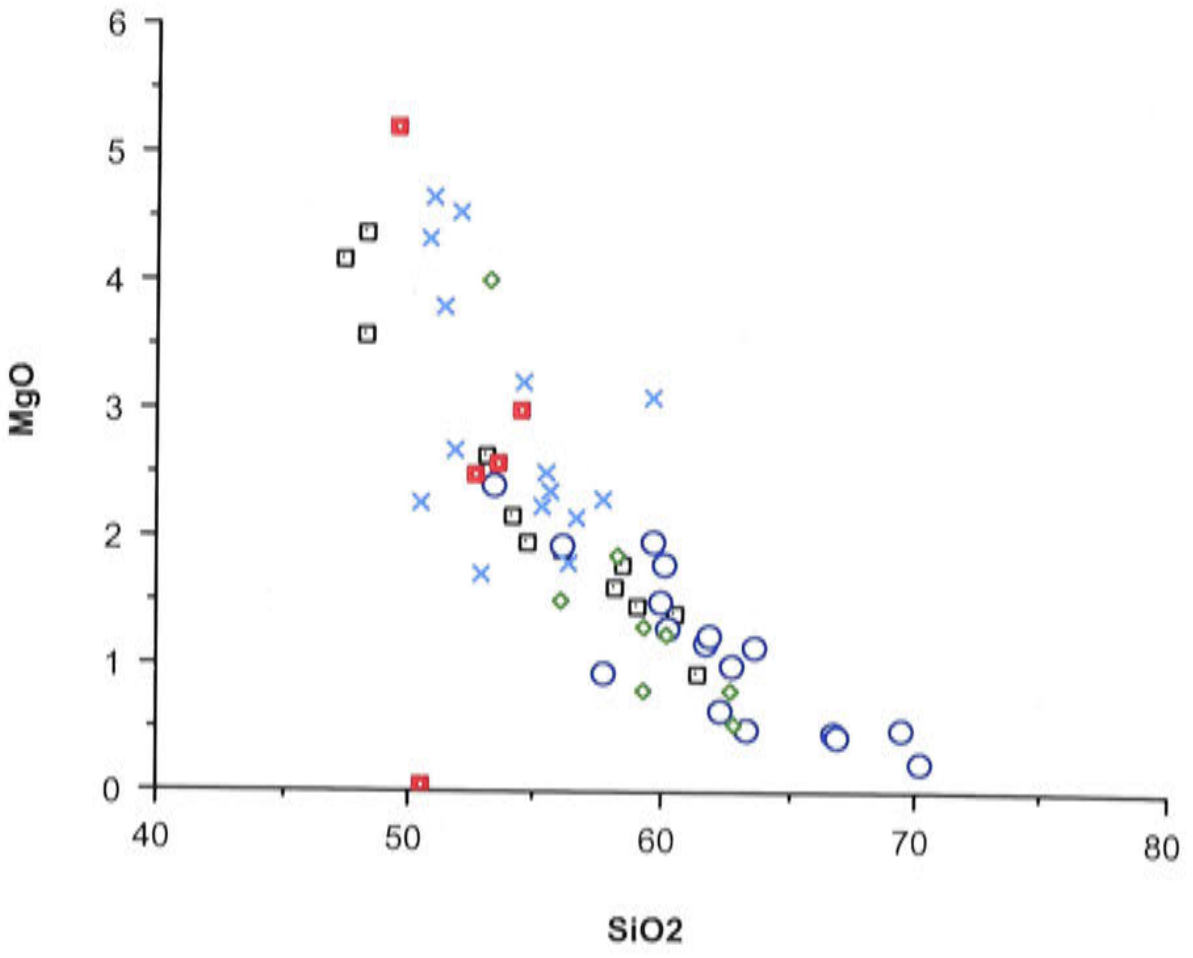

Figure 5.4h MgO vs SiO_2 plot of Goonumbla and Wombin Volcanics and intrusions. See Figure 5.4d for legend.

5.3.4 Trace elements

Variation diagrams for trace elements provide some indication of the main fractionating phases in the Goonumbla Suite. Ba (Fig. 5.5a) shows a positive correlation, albeit with some scatter. Interestingly, the Forbes Anticline intrusions cluster at low Ba levels. Samples from the mineralised suite show a flat trend which mimics their trend on the K_2O versus SiO_2 plot. This is expected as Ba substitutes for K in K-feldspar. Similarly, Rb (Fig. 5.5b) mimics the flat trend of the mineralised suite. Sr (Fig. 5.5c) shows a broadly negative trend, reflecting the role of plagioclase fractionation. Ce also shows a broad negative correlation with SiO_2 (Fig. 5.5d).

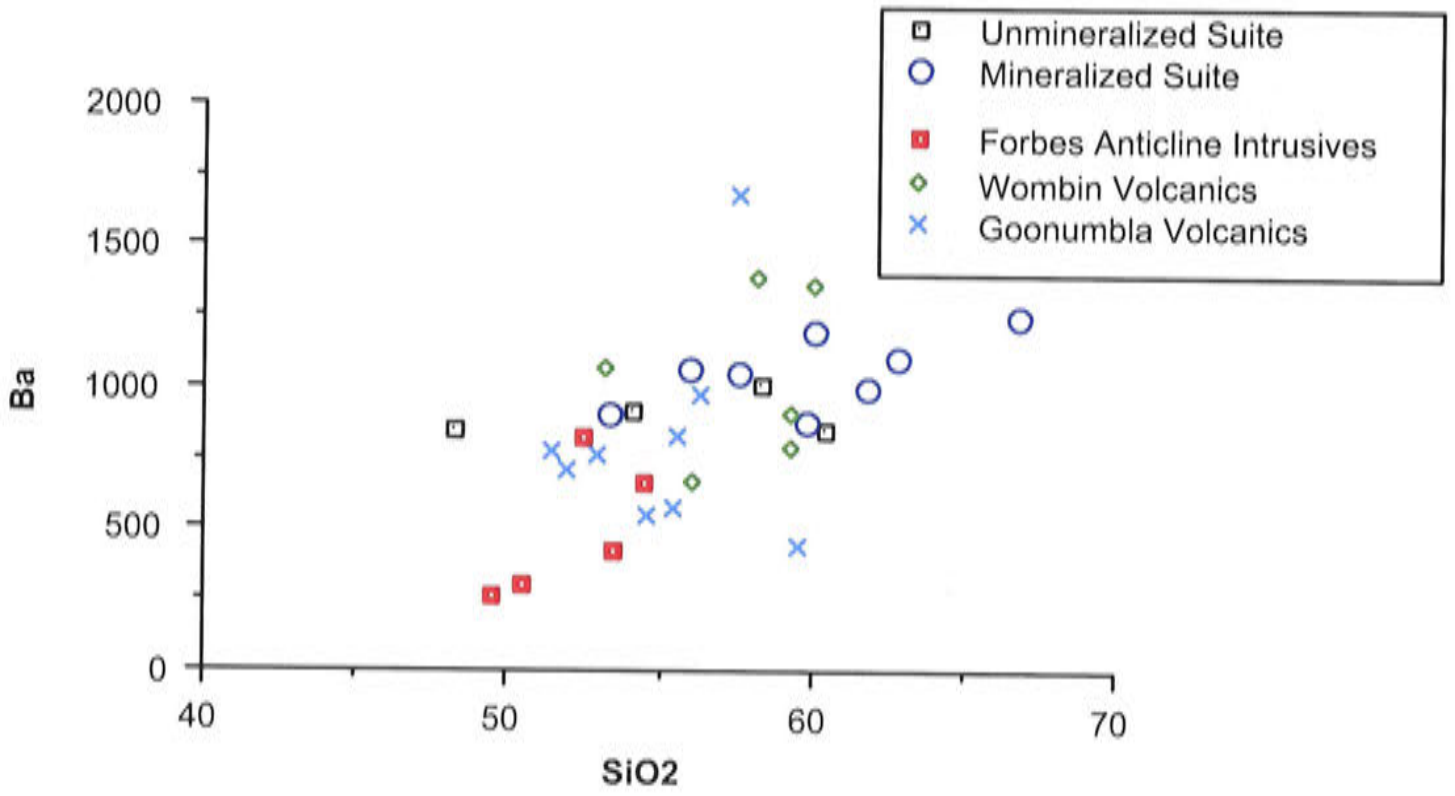

Figure 5.5a Ba vs SiO_2 plot of Goonumbla and Wombin Volcanics and intrusions.

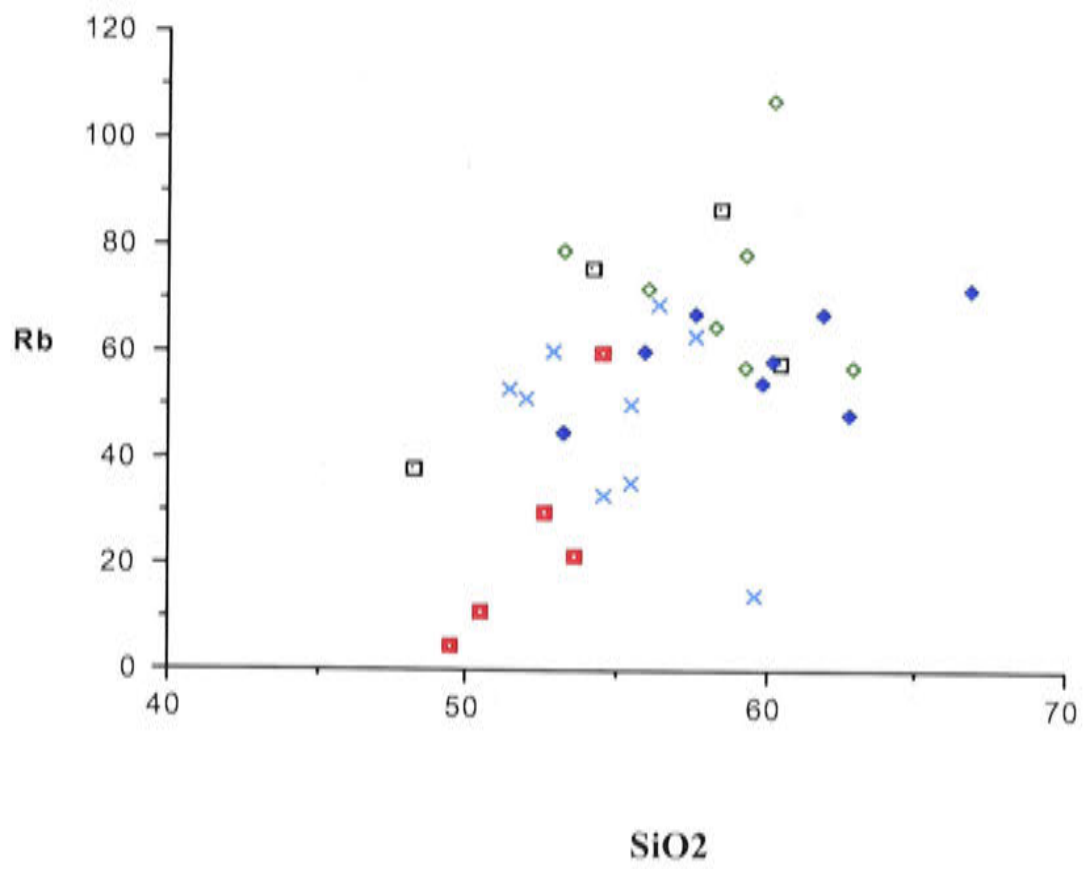

Figure 5.5b Rb vs SiO_2 plot of Goonumbla and Wombin Volcanics and intrusions. See Figure 5.5a for legend.

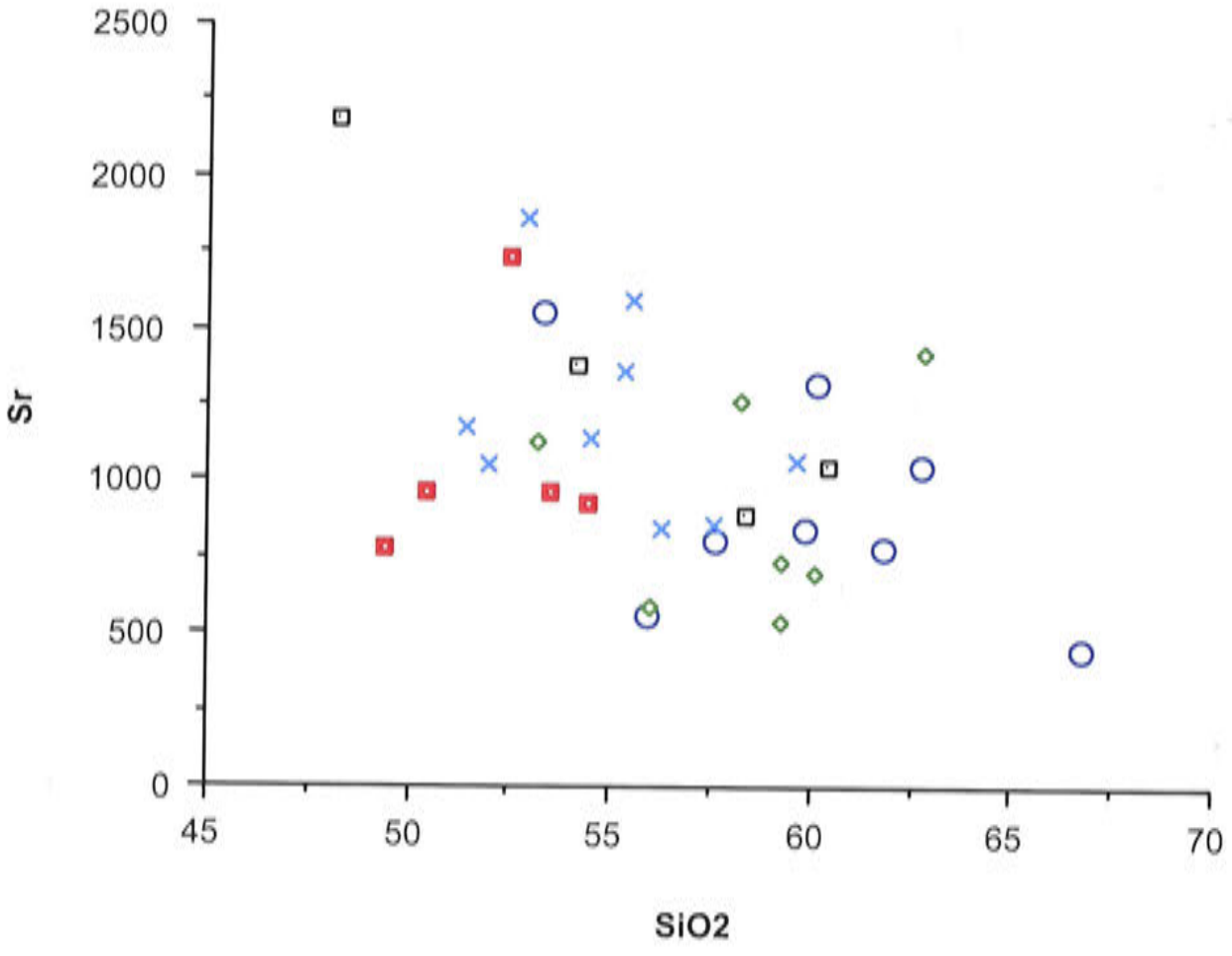

Figure 5.5c Sr vs SiO_2 plot of Goonumbla and Wombin Volcanics and intrusions. See Figure 5.5a for legend.

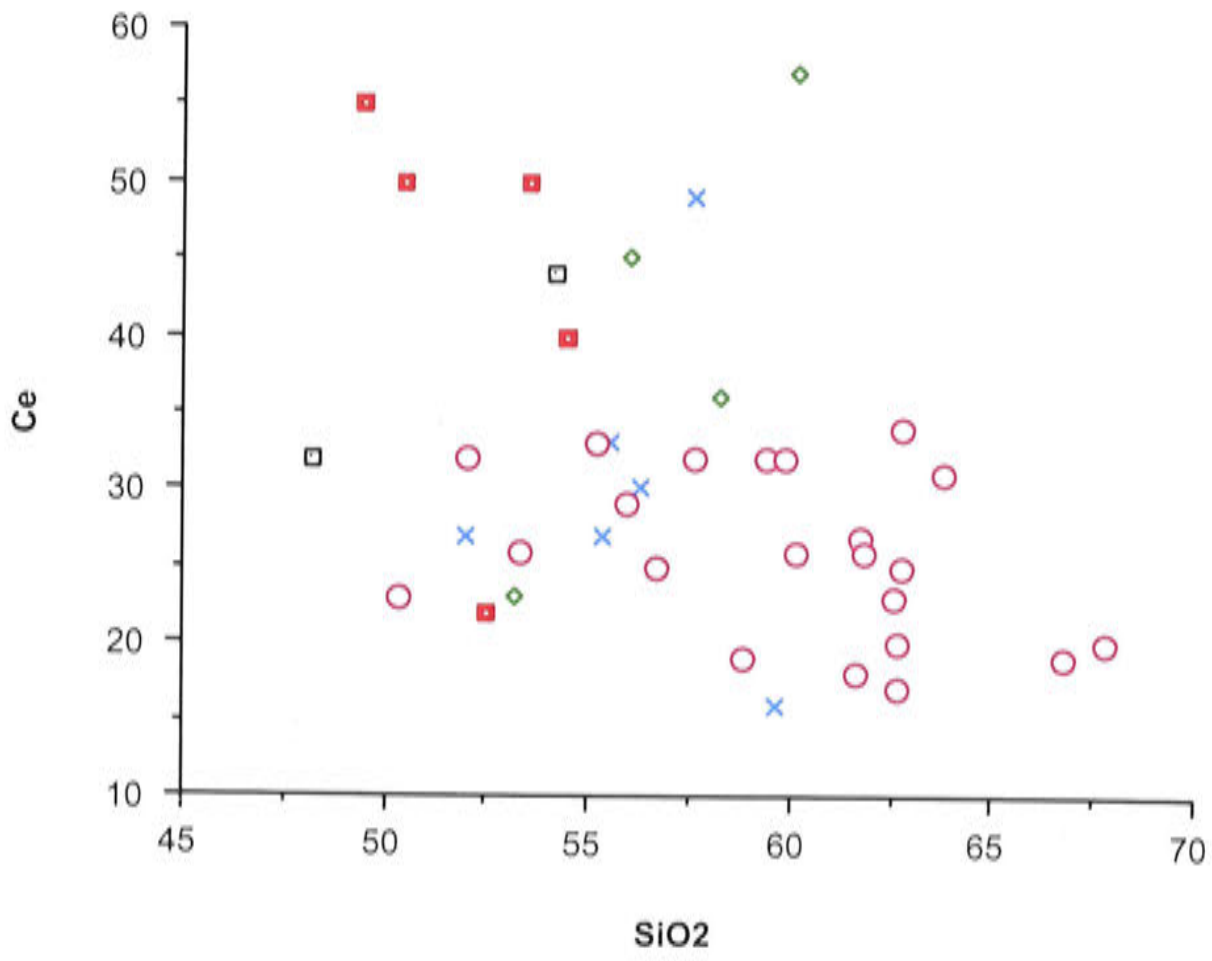

Figure 5.5d Ce vs SiO_2 plot of Goonumbla and Wombin Volcanics and intrusions. See Figure 5.5a for legend.

Variation diagrams, which plot elements against Zr, are instructive for the Goonumbla Suite. Zr versus SiO_2 (Fig. 5.6a) shows a broadly positive correlation for the volcanics and non-mineralised intrusives. The mineralised suite, however, defines a distinctly flatter trend with respect to Zr, which implies that Zr was not behaving incompatibly during crystallisation of the mineralised suite. Zr will substitute for Ti in biotite, and primary biotite in the suite often contains fine grains of zircon. This suggests that biotite has played a role in the development of the mineralised diorite to quartz monzonite suite.

Nb is characteristically low in the Goonumbla rocks, and its positive correlation with Zr (Fig. 5.6b) again highlights the comagmatic relationship between intrusives and volcanics. Ce (Fig. 5.6c) also exhibits a broad positive correlation with Zr for all samples except the intrusions in the Forbes Anticline. The mineralised suite has the lowest Zr and Ce values. Within this suite the most differentiated samples, on the basis of SiO_2 content, have the least Ce. Apatite is a common accessory in the more mafic rocks, and fractionation of apatite would certainly deplete the melt in the LREE such as Ce.

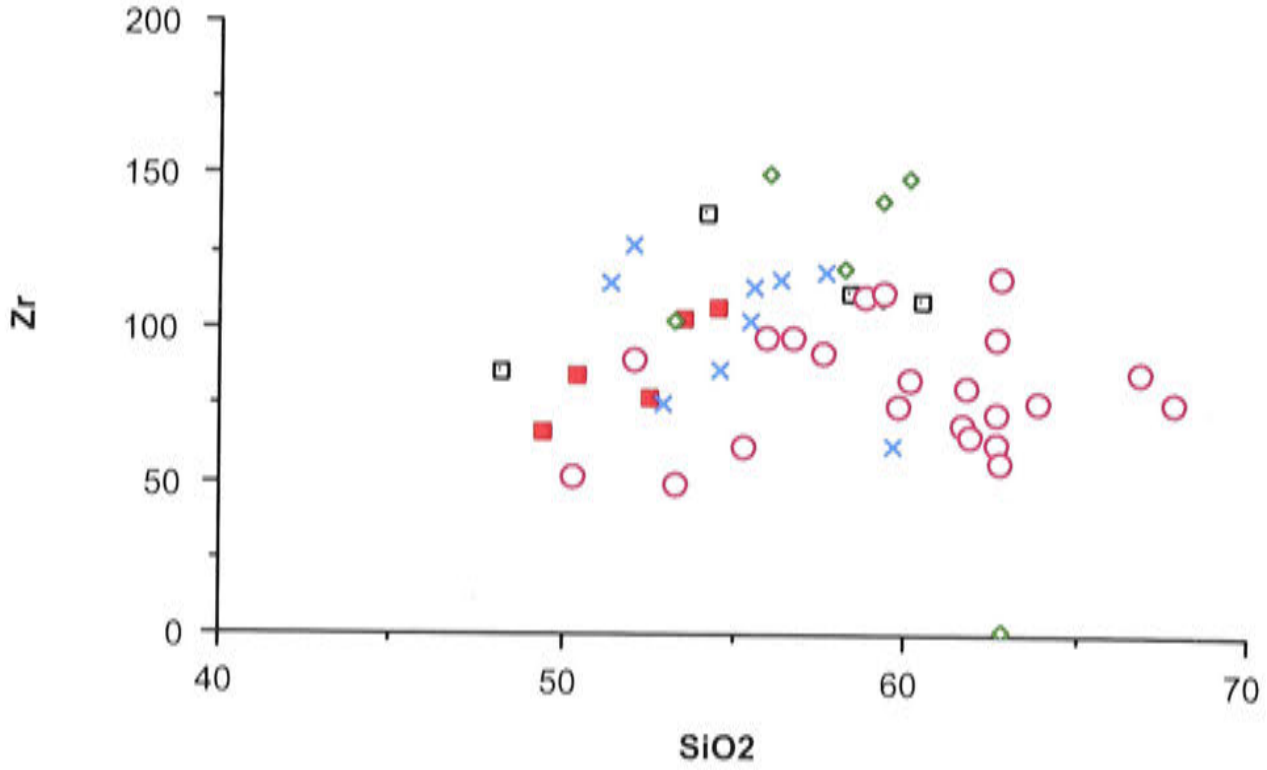

Figure 5.6a Zr vs SiO_2 plot of Goonumbla and Wombin Volcanics and intrusions. See Figure 5.6c for legend.

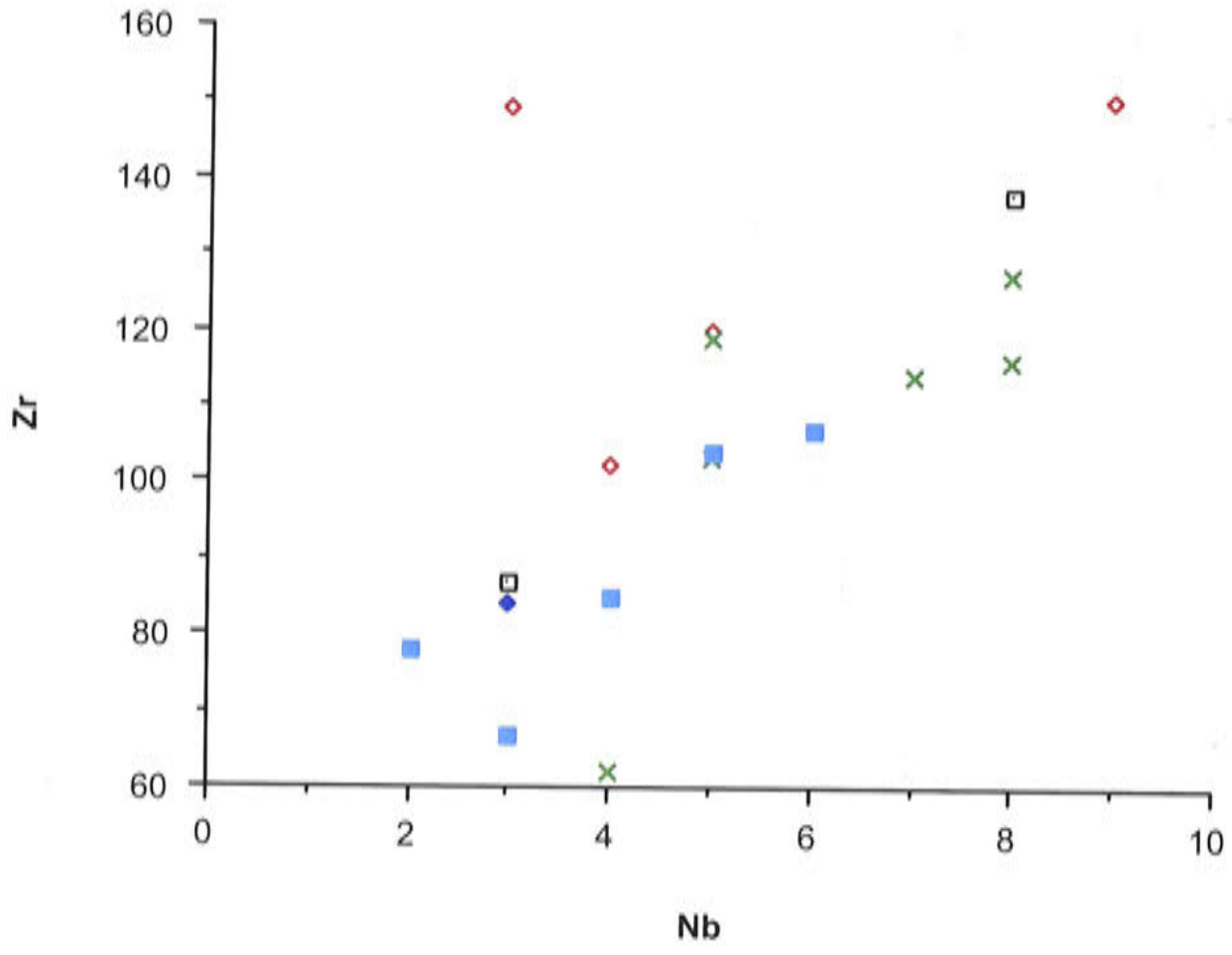

Figure 5.6b Zr vs Nb SiO_2 plot of Goonumbla and Wombin Volcanics and intrusions. See Figure 5.6c for legend.

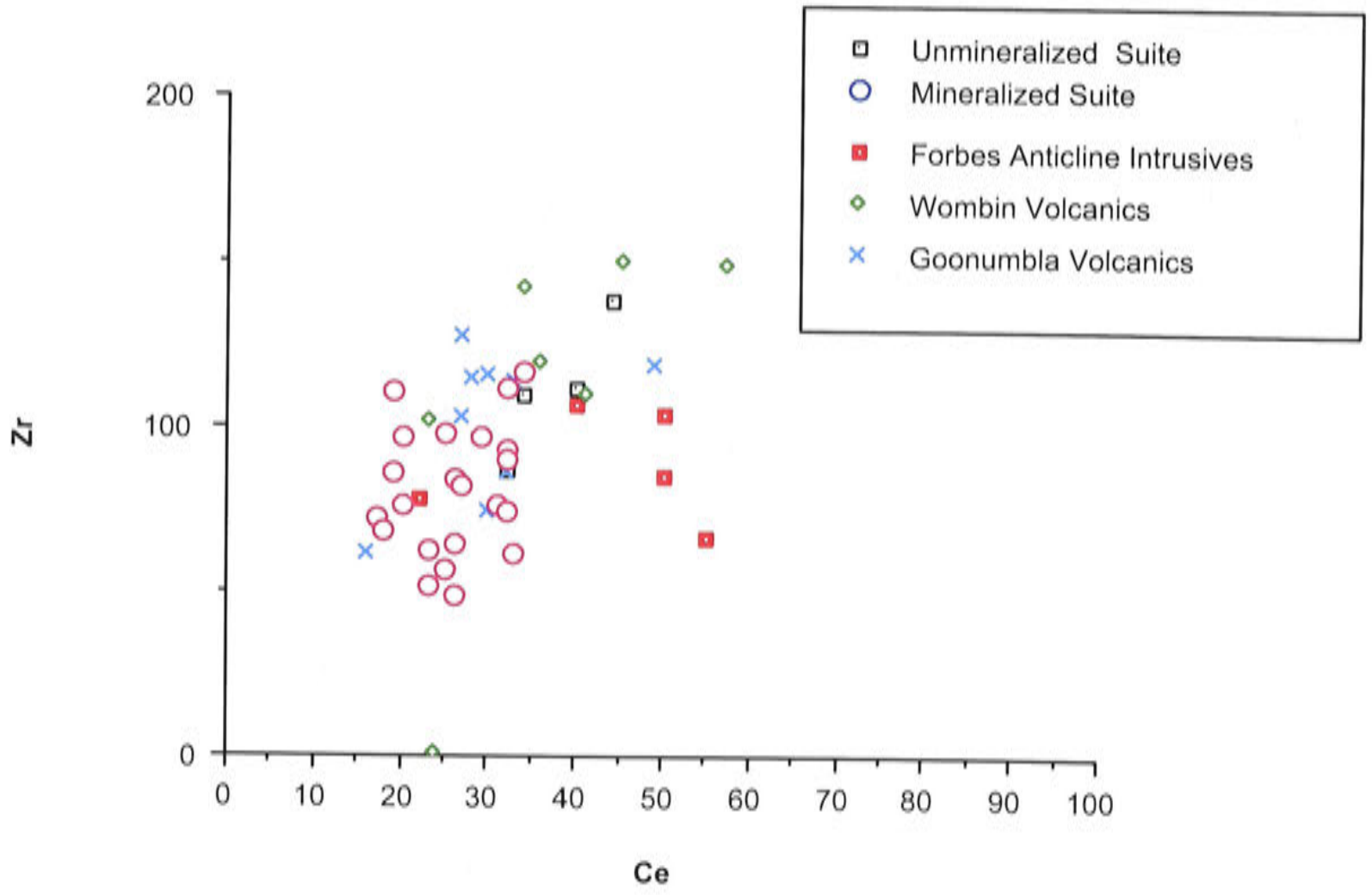

Figure 5.6c Zr vs Ce SiO_2 plot of Goonumbla and Wombin Volcanics and intrusions.

The use of spidergrams is an increasingly common way of presenting trace element data. Figure 5.7a is a spidergram for Goonumbla rocks constructed using the method of Wood et al. (1979), in which a range of incompatible elements are normalised against hypothetical primordial mantle. The elements are arranged in order of increasing incompatibility, from right to left. The Goonumbla 'curves' show an overall negative slope, which is consistent with incompatible elemental abundances increasing during fractionation. In detail some elements, notably Ti, Ce, Nb, Th and U, develop negative anomalies. The depletion of Ti is consistent with crystallisation of Ti-bearing magnetite. Similarly the depletion in Ce, U and Th is consistent with removal of apatite and zircon. A range of samples from the mineralised suite is plotted in Figure 5.7b, including a diorite (M33/162), monzodiorite (M33/169), monzonite (M33/167) and the quartz monzonites which are central to the mineralisation (M33/166/168/159). It appears that the more evolved, quartz-bearing samples are lowest in Y, Ti, Nd, Sr and Ce, and are relatively enriched in the LILE, particularly Rb, Ba, Th, U, K and Nb.

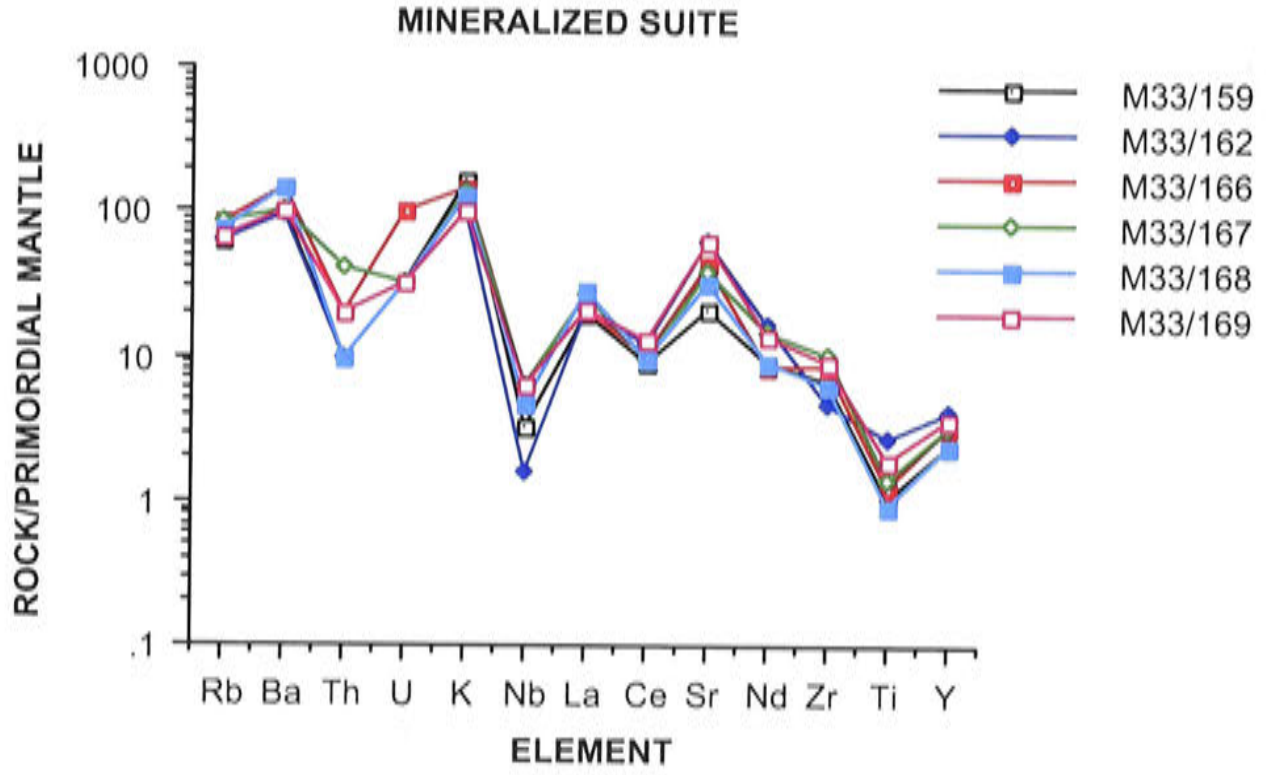

Figure 5.7a Spidergram of mafic to felsic intrusions related to mineralisation, Goonumbla rocks. Normalisation factors after Wood et al. (1979).

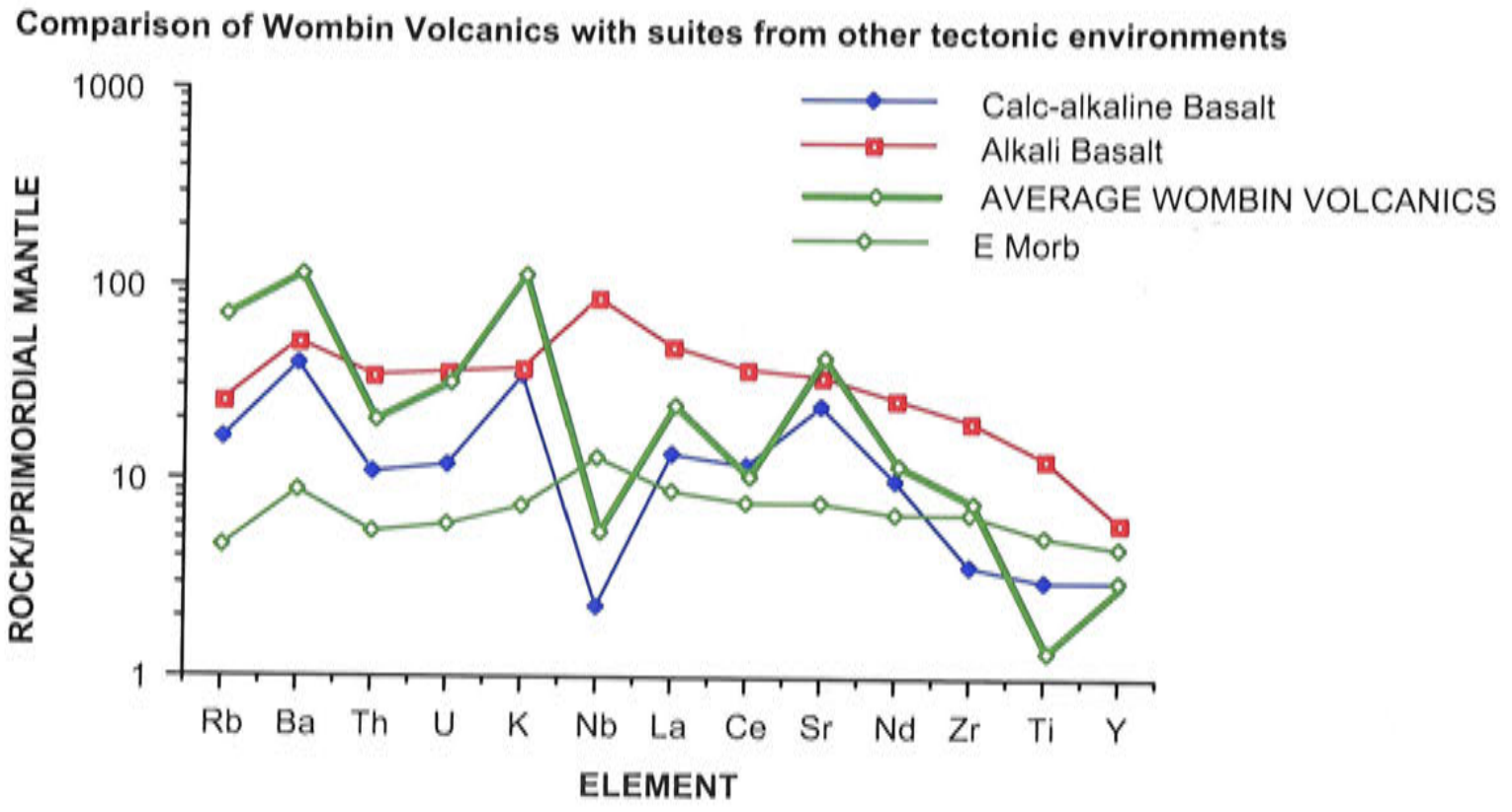

Figure 5.7b Spidergram of average Wombin Volcanics composition, E MORB, alkali basalt and calc-alkali basalt. Normalisation factors after Wood et al. (1979).

In Figure 5.7b the spidergram for the average Wombin Volcanics composition is compared to an average E MORB, alkali basalt and calc-alkaline basalt. It is clear that the overall pattern of the shoshonitic rocks is the same as that of typical island-arc basalts. This is the so called 'island-arc signature' which is characteristic of shoshonites. The signature is a spiked pattern with the persistent depletion in Nb, Ta and Ti, and relative depletion in Zr. It is clear that the Goonumbla rocks share this arc signature, however as was discussed in chapter 4, this trace element pattern is not sufficient in itself to prove an arc setting.

5.4 HIGH- AND LOW-PRESSURE FRACTIONATION OF THE GOONUMBLA SUITE

The data indicate that the main evolutionary trend that occurs at Goonumbla, is defined by the Goonumbla Volcanics, Wombin Volcanics, the Forbes Anticline intrusions and unmineralised intrusive suite. These data define an initially steep set of points on the K_2O versus SiO_2 plot, which flattens out around 53 Wt % to a flatter curve (Fig. 5.3). A second-order fractionation path, due to the local evolution of the mineralised suite, is superimposed on the main trend, and gives a flatter trend which parallels the boundary between calc-alkaline and shoshonitic fields.

Meen (1990) suggests that the variation of K_2O versus SiO_2 typical of shoshonitic rocks is largely a function of the depth of fractionation, because anhydrous basaltic melts ponding at the base of the continental crust may develop very potassic liquids without significant silica enrichment. He argues that moderate to high pressures (>15 kb) tend to suppress olivine crystallisation, and enhance the stability of plagioclase and augite. For a given temperature interval more pyroxene than olivine crystallises at 10–15 kb than at low pressures. The relatively high SiO_2 content of pyroxene compared to olivine produces a silica-poor melt, and one consequence is that the Mg number will decrease less at moderate pressures than at low pressures. Similarly, for a given range of enrichment in K_2O in the melt, the associated increase in SiO_2 will be much less at 15 kb (crystallisation of plagioclase and augite) than at low pressures (crystallisation of olivine). In Figure 5.8 data from Meen (1990) is shows the trends resulting from high-and low-pressure fractionation.

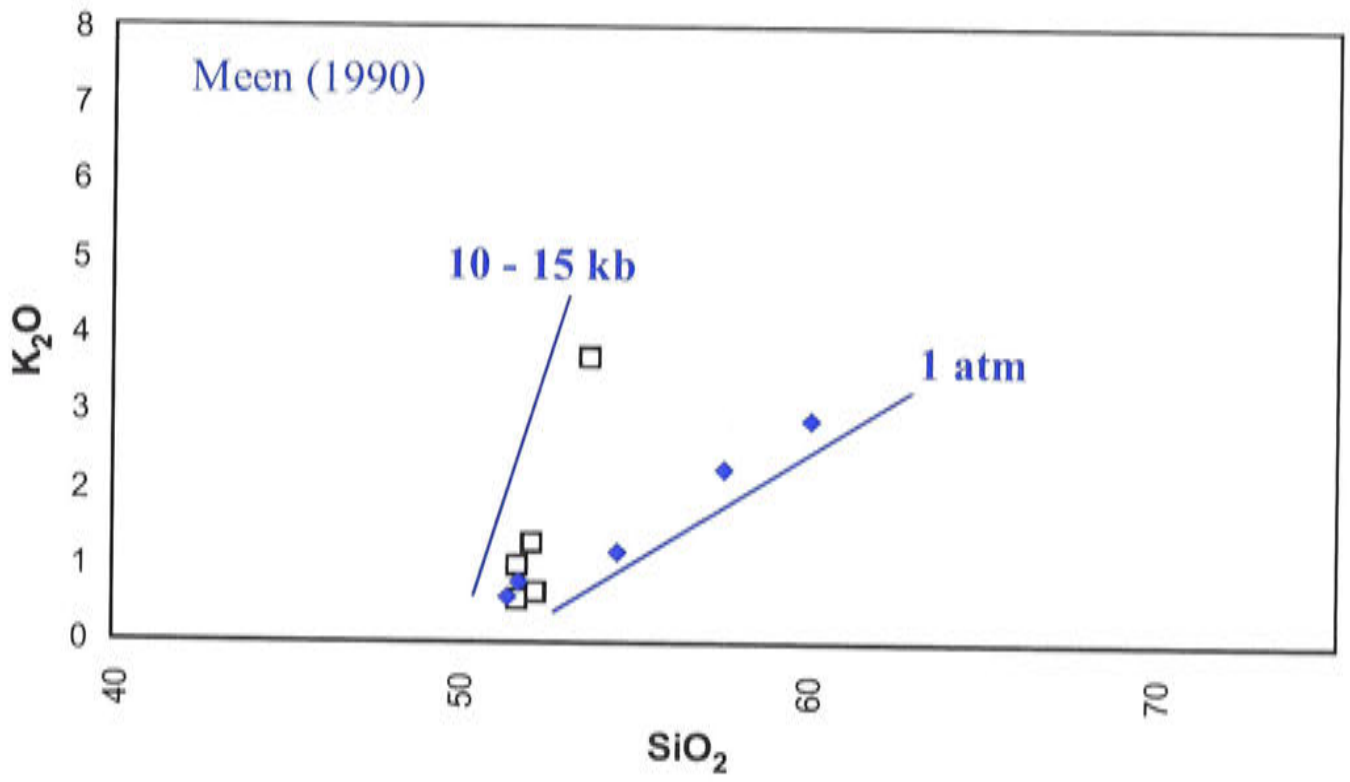

Figure 5.8 Experimental points from Meen (1990).

In Figure 5.9 these curves are superimposed on the Goonumbla data set, and it can be seen that the high-pressure trend mirrors the steep trend at low silica values, suggesting that pyroxene fractionation at high pressure is important. The flatter trend which occurs beyond 53% SiO_2 parallels the low-pressure trend of Meen (1990).

It is clear, however, that these trends do not explain the flatter distribution of the mineralised suite. Observation indicates that biotite and plagioclase are phases that may have fractionated. By subtracting these phases, it is possible to drive the resulting liquid in the direction of the mineralised suite. Figure 5.10 geometrically illustrates the proposed mechanism. The parent liquid is taken to contain 53% SiO_2.

As described in Sections 5.3.1 and 5.3.2 a coeval range of intrusives ranging from diorites containing > 60 % plagioclase and interstitial biotite as well as biotite enclosing plagioclase. This trend continues with the monzodiorite that make up the bulk of the intrusive complex both within the Endeavour 31 intrusion and in the intrusives which are located the ring structure. Here the rocks contain 50 – 60 % zoned andesine, interstitial biotite and biotite enclosing plagioclase, hornblende and clinproxene. Following the fractionation trend further see the appearance of monzonites and quartz monzonites with andesine crystals making up 20 – 35% of the cumulophyric aggregates. Biotite is present but uncommon as Kfeldspar takes over as the main potassic mineral. Taken together these observations are entirely consistent with fractionation by plagioclase and biotite.

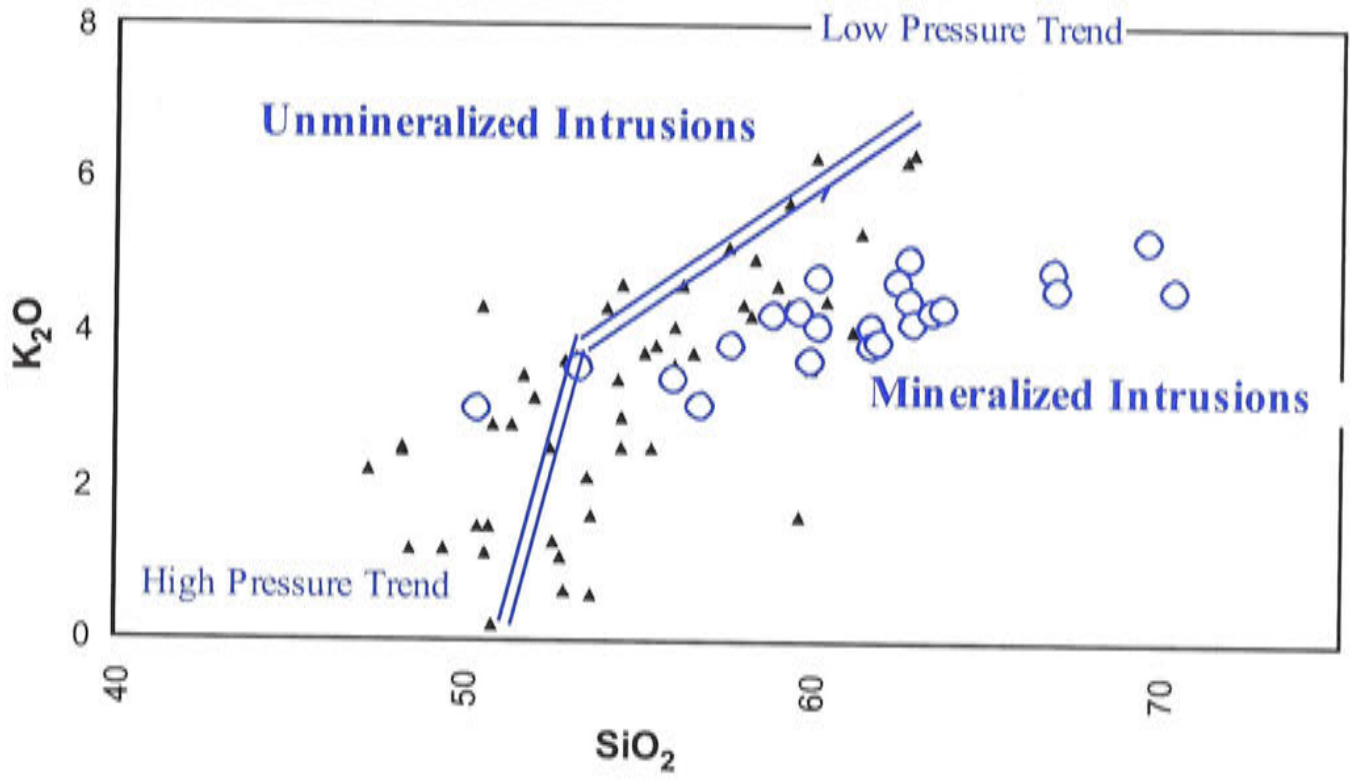

Figure 5.9 Experimental trends from Meen (1990) superimposed on the Goonumbla data set.

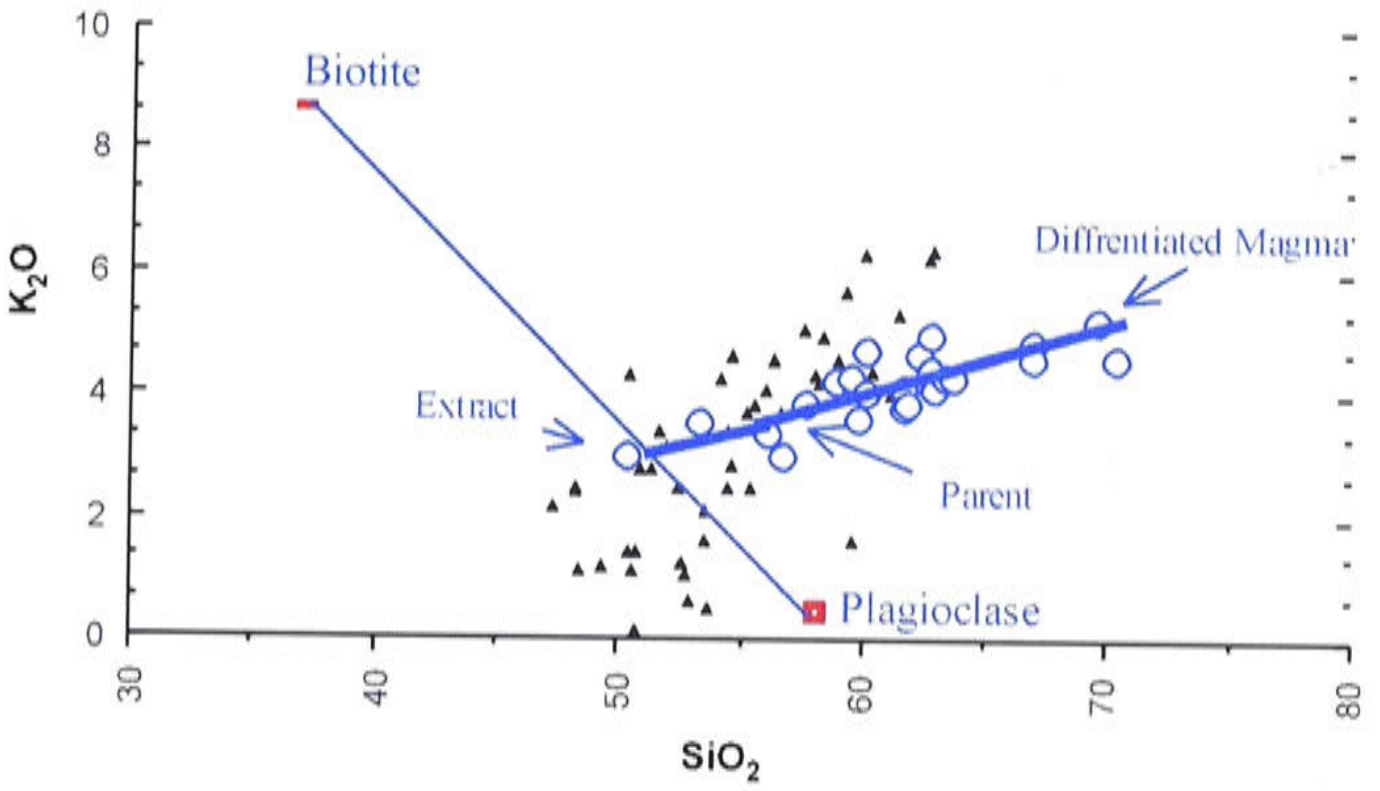

Figure 5.10 Proposed mechanism of crystal fractionation.

5.5 Pb ISOTOPES

A Pb isotope study of the Endeavour 26 North deposit was conducted in conjunction with Dr Graham Carr and Judy Dean from CSIRO, North Ryde, Sydney. Pb isotopes have been used extensively in recent years in studies on the provenances of igneous rocks and ore deposits (Cooper and Richards, 1966; Oversby and Gast, 1970; Oversby and Ewart, 1972; Doe and Zartman 1980; Doe and Stacey 1974). The major applications in ore genesis studies are in defining the source material for the Pb in ores or alteration minerals such as K-feldspar, and in determining the age of mineralisation. Pb isotopes have found considerable success in distinguishing between Pb associated with major base-metal ore deposits and Pb from minor unrelated occurrences, because mineral deposits can exhibit a 'finger print' which is unique to that deposit. The present study compares the isotopic composition of the ore zone (and alteration halo) at the Endeavour 26 North with unmineralised host rocks.

5.5.1 Background

The variation in Pb isotopic composition is the result of radioactive decay. ^{238}U and ^{235}U decay to the radiogenic isotopes ^{206}Pb and ^{207}Pb respectively, while ^{232}Th decays to ^{208}Pb. The stable Pb isotope, ^{204}Pb, has no long-lived radioactive parent. Isotopic fractionation due to physiochemical changes are negligible in Pb isotopes in contrast to stable isotopes. They are therefore important 'tracers', as they are not affected by hypogene or supergene alteration processes.

The standard way of representing Pb isotope compositions is through ratios of the radiogenic Pb isotopes to the non-radiogenic isotope, whose abundance does not change with time ($^{206}Pb/^{204}Pb$, $^{207}Pb/^{204}Pb$, $^{208}Pb/^{204}Pb$). A present day Pb isotope ratio has evolved from an initial Pb isotope ratio plus radiogenic addition. The detailed theory of the evolution of Pb isotopes by radioactive decay has been well documented and will not be discussed further. The reader is referred to Doe and Stacey (1974), Stacey and Kramers (1975), and Cumming and Richards (1975).

5.5.2 Samples

A list of samples with locations and brief descriptions is presented in Table 5.1. Twenty-three samples were analysed and were broadly separated into two groups; ore zone samples and unmineralised host rocks. The ore zone samples were taken from within the early Mosaic Porphyry (referred to as QMP1), the later Square Porphyry (QMP2) and the host trachytic sequence. High Pb samples were taken from the propylitic–phyllic halo, where rare veinlets containing galena and sphalerite can be detected.

Table 5.1 Pb isotope samples, Endeavour 26 North ore deposit.

Number	Type	Drillhole, *depth (m)*	Description
Endeavour 26 ore zone samples			
B710	Monzonite	DDH26–44, *232.6*	Early biot. alt.; qtz–kfs–bor veins
B711	QMP2	DDH26–26, *198.2*	Weak mineralisation; qtz–bor veinlets
B712	Trachytic fragmental	DDH26–31, *207.8*	Intense K alt.; stockwork qtz–bor vein
B713	QMP1	DDH26–38, *252.5*	Intense K-alt.; stockwork qtz–bor veins
B714	Trachyte	DDH26–21, *85–87*	Intense K-alt.; disseminated and vein bor
B715	QMP1	DDH26–76, *669.2*	Intense K-alt.; veinlet bor + qtz–bor veins
B716	QMP2	DDH226–76, *692.6*	Bor blebs + qtz–bor veinlets
B717	Monzonite	DDH26–76, *667.4*	Stockwork qtz–bor veins
B718	QMP1	DDH26–39, *538.3*	Intense K-alt.+ veinlet bor + qtz–bor–anhydrite veins
B719	QMP2	DDH26–39, *568*	Qtz–cpy–bor veins
B720	Porphyritic trachyte	DDH26–39, *651*	K-alt.; disseminated and vein bor
B721	QMP1	DDH26–42, *635.7*	Intense K-alt.; qtz–kfs +qtz–bor veins.
B722	Monzonite	DDH26–66, *1054*	Biot veins + qtz–bor veins
B723	Monzonite	DDH26–46, *885*	Anhydrite–cpy vein
Unmineralised host rocks			
C375	Monzonite	DDH26S–80, *515*	Prehnite–carbonate alt
C376	Monzonite	Goonumbla Hill o/c	
C377	Trachyte	Nash's Hill o/c	
C378	Trachy-andesite	ACH967–100 *39*	
C379	Trachyandesite	Goonumbla Hill o/c	

alt. = alteration; biot. = biotite; bor = bornite; cpy = chalcopyrite; kfs = K-feldspar; qtz = quartz

Table 5.2 Pb isotope ratios and Pb and U contents of Endeavour 26 North ore zone.

Sample	$^{208}Pb/^{206}Pb$	$^{207}Pb/^{206}Pb$	$^{206}Pb/^{204}Pb$	$^{207}Pb/^{204}Pb$	$^{208}Pb/^{204}Pb$	**Pb** (ppm)	**U** (ppm)
QMP1							
1 B713fl	2.0551	0.8327	18.624	15.509	38.274	2	0.1
2 B713sul	2.07	0.843	18.416	15.525	38.122	35	0.2
3 B713sul R1	2.0691	0.8427	18.404	15.509	38.079	35	0.2
4 B713sul R2	2.0714	0.8431	18.39	15.505	38.093	36	0.2
5 B715wr	2.072	0.8408	18.444	15.507	38.216	4	0.2
6 B718sul	2.0729	0.8449	18.342	15.497	38.02	14	0.1
7 B721sul	2.0706	0.8461	18.303	15.486	17.898		
Strong K alteration							
8 B712bor	2.0712	0.8465	18.291	15.483	37.884	44	0.1
9 B714bor	2.0711	0.8427	18.472	15.567	38.257	16	0.2
QMP2							
10 B711feld	2.0768	0.8531	18.169	15.5	37.733		
11 B711sul	2.069	0.8482	18.32	15.539	37.903	126	0.5
12 B716bor	2.079	0.8487	18.249	15.487	37.939	58	0.1
13 B719sul	2.0734	0.8486	18.235	15.474	37.808	414	0.2
Other samples							
14 B710mag	1.9472	0.7829	19.921	15.595	38.789	3	0.8
15 B710mag R	1.9455	0.7831	19.89	15.575	38.695	3	0.8
16 B710mag R	1.9457	0.7834	19.886	15.579	38.691		
17 B717bor	2.0817	0.8481	18.28	15.504	38.503	42	0
18 B720sul	2.0771	0.8476	18.376	15.575	38.168	10	0.1
19 B722sul	2.0832	0.8518	18.206	15.508	37.927	142	0.2
20 B723sul	2.0716	0.8479	18.29	15.508	37.891	40	0.5

bor = bornite; feld -feldspar concentrate; fl = silicate/carbonate component (float in heavy media); mag = magnetite; R,R1 etc = repeat analyses; sul = mixed sulfide concentrate with minor silicate component; wr = whole rock powder.

Sample number prefixes refer to points plotted on figures.

Table 5.3 Pb isotope results from unaltered host rocks.

Sample	$^{208}Pb/^{206}Pb$	$^{207}Pb/^{206}Pb$	$^{206}Pb/^{204}Pb$	$^{207}Pb/^{204}Pb$	$^{208}Pb/^{204}Pb$	**Pb** (ppm)	**U** (ppm)
20 C375wr	2.0475	0.8337	18.608	15.514	38.101	8	0.4
21 C376wr	2.0309	0.8207	18.945	15.549	38.476	3	0.3
22 C377wr	2.0381	0.8297	18.725	15.536	38.164	6	0.5
23 C378wr	1.9878	0.7993	19.471	15.563	38.705	2	0.3
24 C379wr	1.852	0.7236	21.671	15.68	40.134	1	0.3

5.5.3 Methods

Samples of quarter diamond drill core were crushed and sulphides (where present) were separated, either by hand picking, or techniques involving heavy-media separation and froth flotation. This was undertaken in order to get subsamples representative of mineralisation and the highest possible Pb contents. Where samples contained insufficient sulphides for separation, the whole rock was crushed and pulverised.

A single galena sample, C369, was dissolved in concentrated nitric acid and Pb was electroplated onto Pt electrodes. The other samples were digested in a 7N nitric and 7N hydrochloric solution prior to ion exchange and electroplating as above. An acid attack such as this totally dissolves sulphides and magnetite, but only partially leaches Pb from silicate rock. Samples were analysed on an ISOMASS S4E solid source thermal ionisation mass spectrometer, in fully automated mode. Precision estimates, representing two standard deviations about the mean of over 700 analyses of standards, are shown in the top left hand corner of the figures presented below.

5.5.4 Results

The results for the Endeavour 26 North ore zone are presented in Table 5.2, and plotted as conventional $^{206}Pb/^{204}Pb$ versus $^{207}Pb/^{204}Pb$ and $^{208}Pb/^{204}Pb$ versus $^{207}Pb/^{204}Pb$ diagrams in Figures 5.11 and 5.12. For reference, the average crustal growth curve of Cumming and Richards (1975) is shown on the diagrams.

Endeavour 26 North ore samples

The Endeavour 26 North ore zone data (Table 5.2, Figs 5.11, 5.12) generally plot over a restricted range but, significantly, well below the average crustal growth curve. The $^{206}Pb/^{204}Pb$ ratios vary between 18.17 to 18.47 (excluding the low-Pb samples B710 and B713f1), and $^{207}Pb/^{204}Pb$ varies between 15.47 to 15.58. Unlike sulphur isotopes (Ch. 8), there is no systematic spatial variation within the orebody. There may, however, be a difference between the QMP1 (the early stage mineralising porphyry) and QMP2 (the later stage mineralising porphyry), based on $^{206}Pb/^{204}Pb$ ratios (Fig. 5.12). This could be a function of different initial ratios (i.e. isotopic composition at the time of formation of the ores), but this seems unlikely given that QMP1 and QMP2 are both derived from the Endeavour 31 stock. Alternatively, since these samples contain low levels of Pb, it could result from addition of radiogenic Pb to QMP1 since the time of deposition.

The very low Pb samples from the unaltered host rocks have considerably higher $^{206}Pb/^{204}Pb$ ratios, which is due to addition of radiogenic ^{206}Pb since the formation of the deposit.

Endeavour 26 North host rocks

The isotopic composition of the host rocks (Table 5.3, Figs 5.11, 5.12) form a linear arrays on both diagrams. The linear array on the $^{207}Pb/^{204}Pb$ versus $^{206}Pb/^{204}Pb$ diagram projects through the cluster of data for the ore samples, suggesting that their initial ratios would have been similar except for the addition of radiogenic Pb.

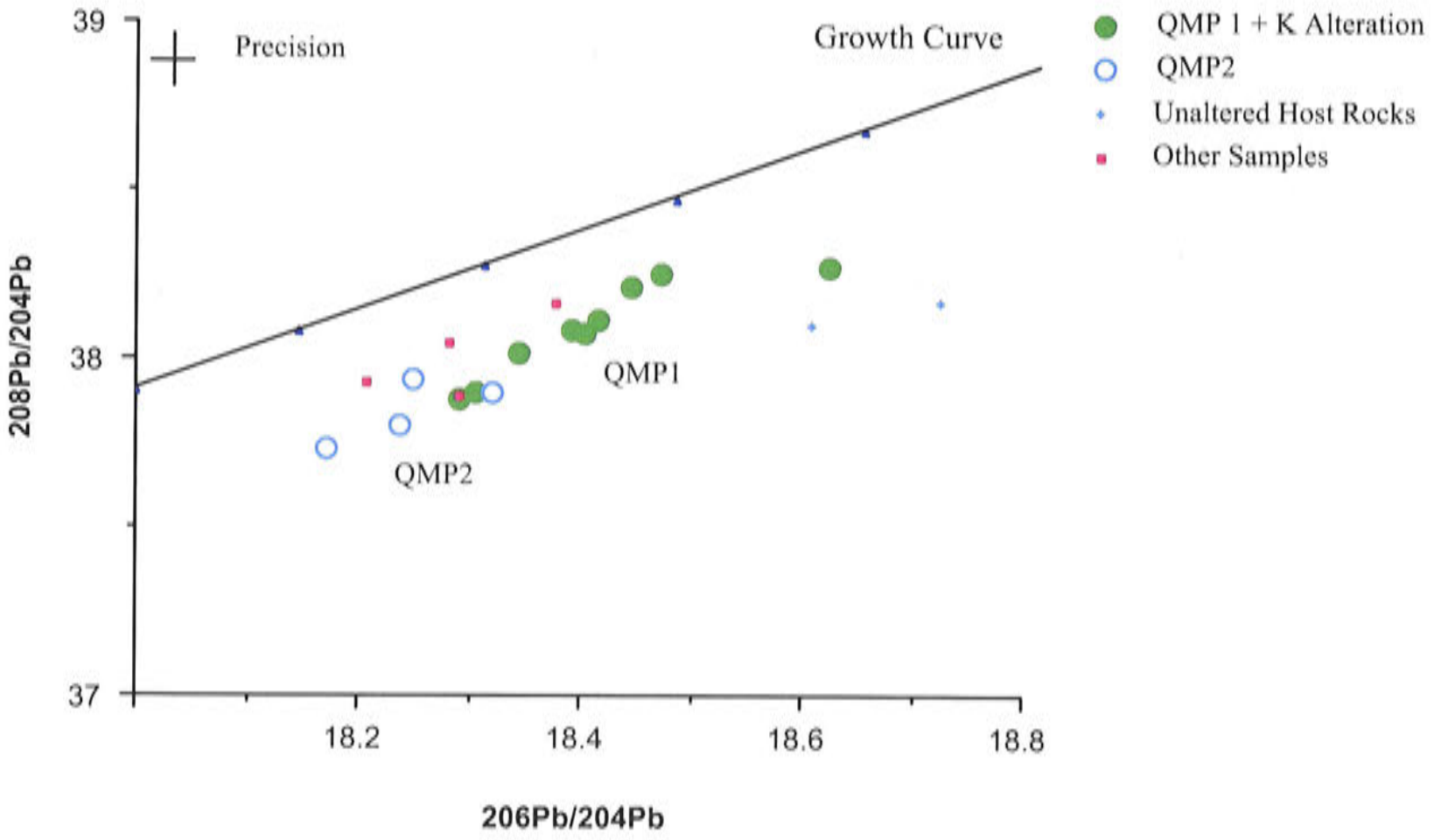

Figure 5.11 Plot of $^{208}Pb/^{204}Pb$ vs $^{206}Pb/^{204}Pb$, Endeavour 26 North ore zone.

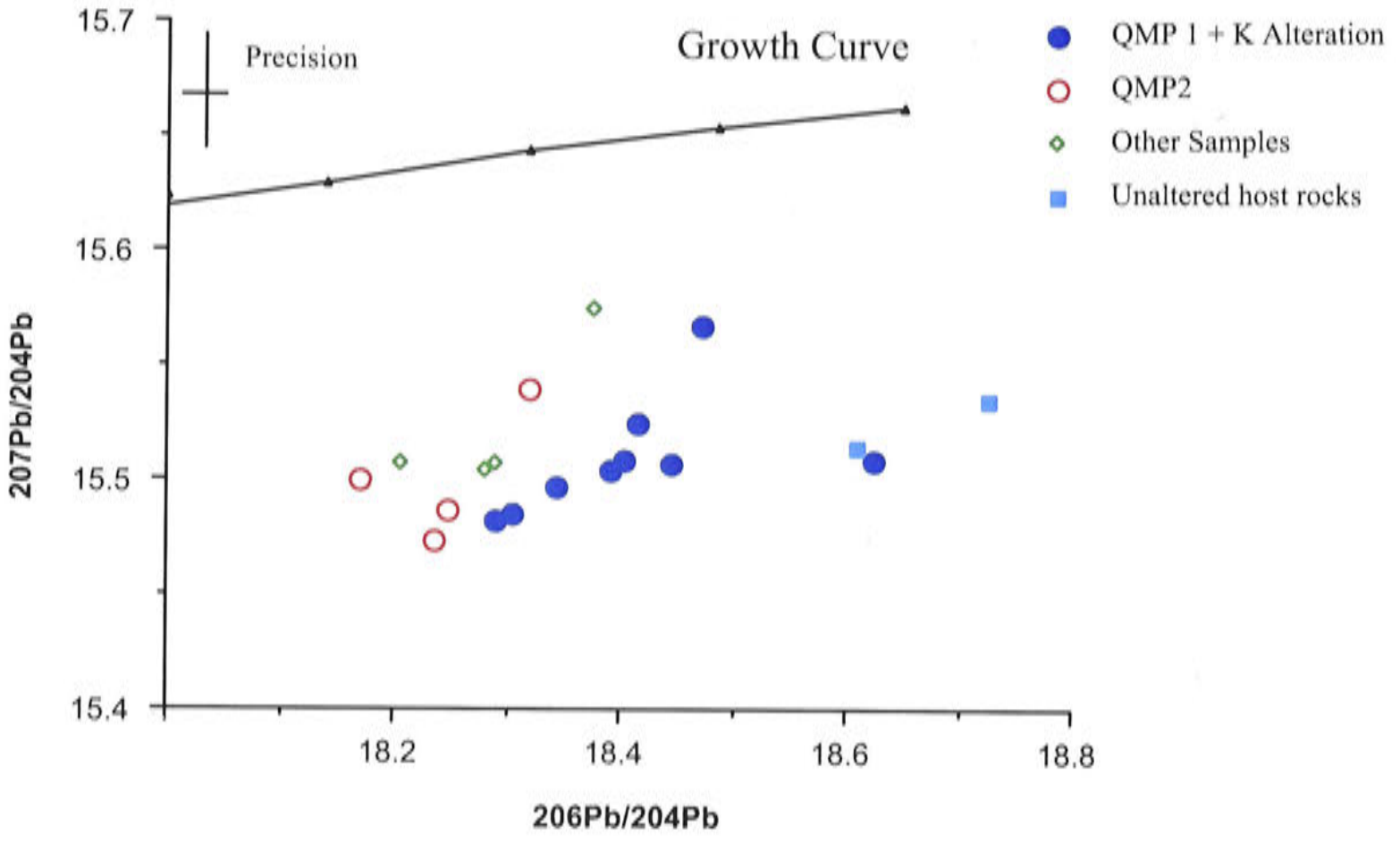

Figure 5.12 Plot of $^{207}Pb/^{204}Pb$ vs $^{206}Pb/^{204}Pb$, Endeavour 26 North ore zone.

5.5.5 Discussion

The Pb isotope data suggest that there is no substantial isotopic difference between Pb from the high-grade mineralisation and background host rocks. This implies that the Pb in the deposit and the trace amounts of Pb in the volcanic pile share a common ancestry, and that hydrothermal activity associated with the formation of the mineralisation has not extracted Pb from any source other than this package of volcanic rocks. The Pb isotope signature therefore provides a signature for the Goonumbla Volcanic Complex, but not a unique signature for mineralisation at Endeavour 26 North.

The combined data set is plotted in Figure 5.13, with the crustal growth curve of Cumming and Richards (1975) and the 'Northern Hemisphere Reference Line' of Hart (1984). The very low $^{207}Pb/^{204}Pb$ ratio of the Goonumbla data is indicative of a source with a low U to Pb ratio. This could be the mantle or lower crust. The lower crust and mantle are depleted in U relative to Pb, and plot on a curve below that of the crust. In contrast, deposits containing Pb derived from the upper crust plot on, or near to, the crustal growth curve. Massive sulphide deposits, such as Elura from the Lachlan Fold Belt, plot on or near the curve as shown in Figure 5.13.

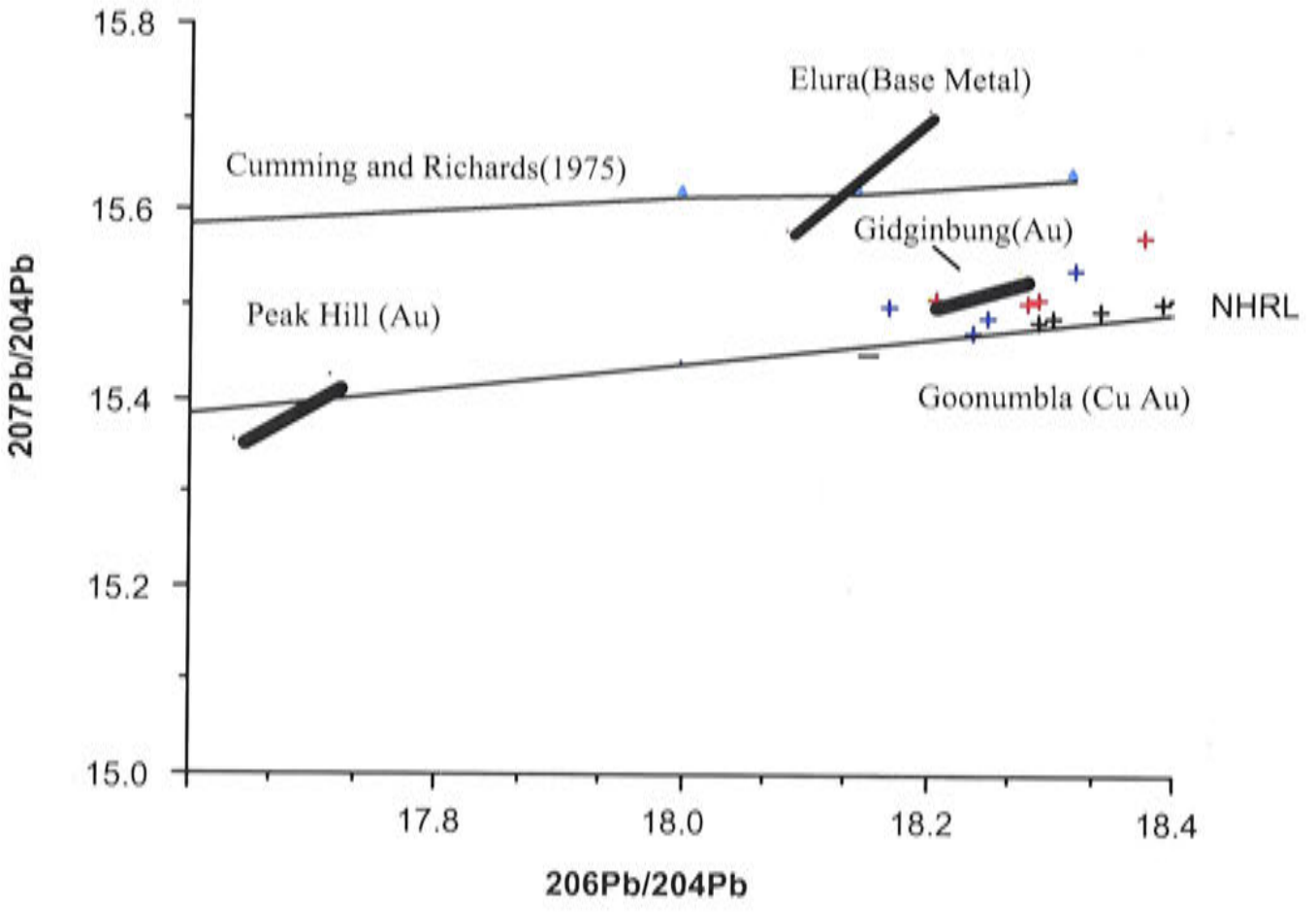

Figure 5.13 Combined $^{207}Pb/^{204}Pb$ vs $^{207}Pb/^{204}Pb$ plot, Endeavour 26 North ore deposit

The spread in the $^{206}Pb/^{204}Pb$ data in Figure 5.13 requires some explanation. The $^{206}Pb/^{204}Pb$ initial ratios plot near the mantle curve, and thus are equal to or greater than that of present day mantle Pb. This spread could be explained by mixing of Pb which has been derived from two sources. The Goonumbla data have been included in a Pb isotope study of mineral deposits in New South Wales by the CSIRO in conjunction with the Geological Survey of New South Wales. From the information gathered so far, it has become apparent that the initial ratios for mineral deposits associated with Ordovician volcanic complexes — such as Peak Hill (Au), Gidginbung (Au) and Goonumbla (Cu–Au) — plot in linear arrays well below the crustal growth curve, indicating the Pb was extracted from source rocks with a long geological history of low U/Pb (μ) and Th/Pb ratios. Carr et al (1991) suggest the arrays represent mixing of source reservoirs with two distinctive Pb isotopic compositions which are similar to depleted mantle MORB (DMM) and PRIMA (Zindler and Hart, 1986), although the Ordovician equivalents of these modern mantle signatures would have obviously contained less radiogenic Pb. It is therefore unlikely that there was any significant contribution to the Ordovician mantle signatures of upper crustal Pb; either due to the incorporation of pelagic sediments in subducted oceanic crust, or contamination of mantle-derived magma by sialic crust. Carr and Dean (1991) also note that the linear array on the $^{207}Pb/^{204}Pb$ versus $^{206}Pb/^{204}Pb$ diagram has a MSWD of 0.6, and if it is

considered an isochron, then it gives a t_1 of ~2.2 Ga assuming a t_2 of 440 Ma. This is similar to source ages for modern mantle derived volcanics (MORB, OIB; Hart, 1984). It is noteworthy that inherited zircons in mid-Palaeozoic granites of the Lachlan Fold Belt exhibit ages which fall into three groups; 650–450 Ma, 1075–800 Ma, and another less well defined group which includes up to 3350 Ma.(Williams et al., 1983). It is therefore possible that ancient enriched mantle is part of the source for Ordovician volcanism.

5.6 Sr, Nd, Sm ISOTOPES

In order to further investigate the primitive nature of the Ordovician magmatism, seven Sr isotope measurements were made, and two Sm and Nd isotopes following on from this.

5.6.1 Samples

Seven samples were selected and the results are listed below.

Table 5.4 Rb and Sr results.

Sample	Location	Lithology	Rb (ppm)[1]	Sr (ppm)[1]	$^{87}Rb/^{86}Sr$	$^{87}Sr/^{86}Sr$[2]	$(^{87}Sr/^{86}Sr)i$[3]
68603	H967/106m	Monzonite	75	711	0.305	0.70606±5	0.70415
68604	H1504/2/50m	Diorite	8	1040	0.0222	0.70418±5	0.70404
68605	H26/36/377m	QMP2	53	938	0.163	0.70518±6	0.70416
68606	H1959/2/10m	Porp. trachyte	86	758	0.328	0.70614±5	0.70409
68607	GR004556	Monzonite	66	1200	0.159	0.70509±5	0.70409
68608	GR057442	Trachyand. lava	51	1530	0.0964	0.70486±5	0.70426
68609	GR000400	Lava	21	349	0.174	0.70572±6	0.70464

1 Determined by XRF on pressed powders, using method of Norrish and Chappell (1967).

2 $^{87}Sr/^{86}Sr$ ratios have been normalised to $^{86}Sr/^{88}Sr = 0.1194$ NBS 987 $^{87}Sr/^{86}Sr = 0.710289\pm50$ n=41. This external precision sets a lower limit of the precision of individual samples. Samples have been analysed on a VG354 thermal ionisation mass spectrometer run in single collector mode.

3 Initial ratios have been calculated assuming an age of 439 Ma (Perkins et al, 1990).

Table 5.5 Sm, Nd results.

Sample number	Grid reference	Lithology	Sm (ppm)	Nd (ppm)	$^{147}Sm/^{144}Nd$	$^{143}Nd/^{144}Nd$	εNd
68607	GR057442	Trachyand. lava	1.83	8.79	0.1272	0.1512756±9	6
68608	GR000400	Trachyand. lava	3.79	16.4	0.1392	0.512807±7	6.2

5.6.2 Discussion of Results

The initial ratios of $^{86}/Sr/^{88}Sr$ are low and close to bulk earth ratio. Most range from 0.70404 to 0.70426 with another value at 0.70464. The main group of values are all from shoshonitic rocks. The higher value is from a sample of Nelungaloo Volcanics which is also a high K calc-alkaline rock. It may suggest some crustal contamination in these volcanics. The two epsilon Nd values are similar at 6.2 and 6. These positive values indicate initial $^{143}Nd/^{144}Nd$ ratios which are greater than the bulk earth value. The data are plotted on an epsilon Nd vs $^{86}/Sr/^{88}Sr$ graph in Figure 5.14. The points fall close to the mantle array as defined by MORBs and OIBs. The results reinforce the conclusions drawn from the sulphur isotope study that the source rocks for the potassic volcanics are primitive and indicate an absence of a crustal signature.

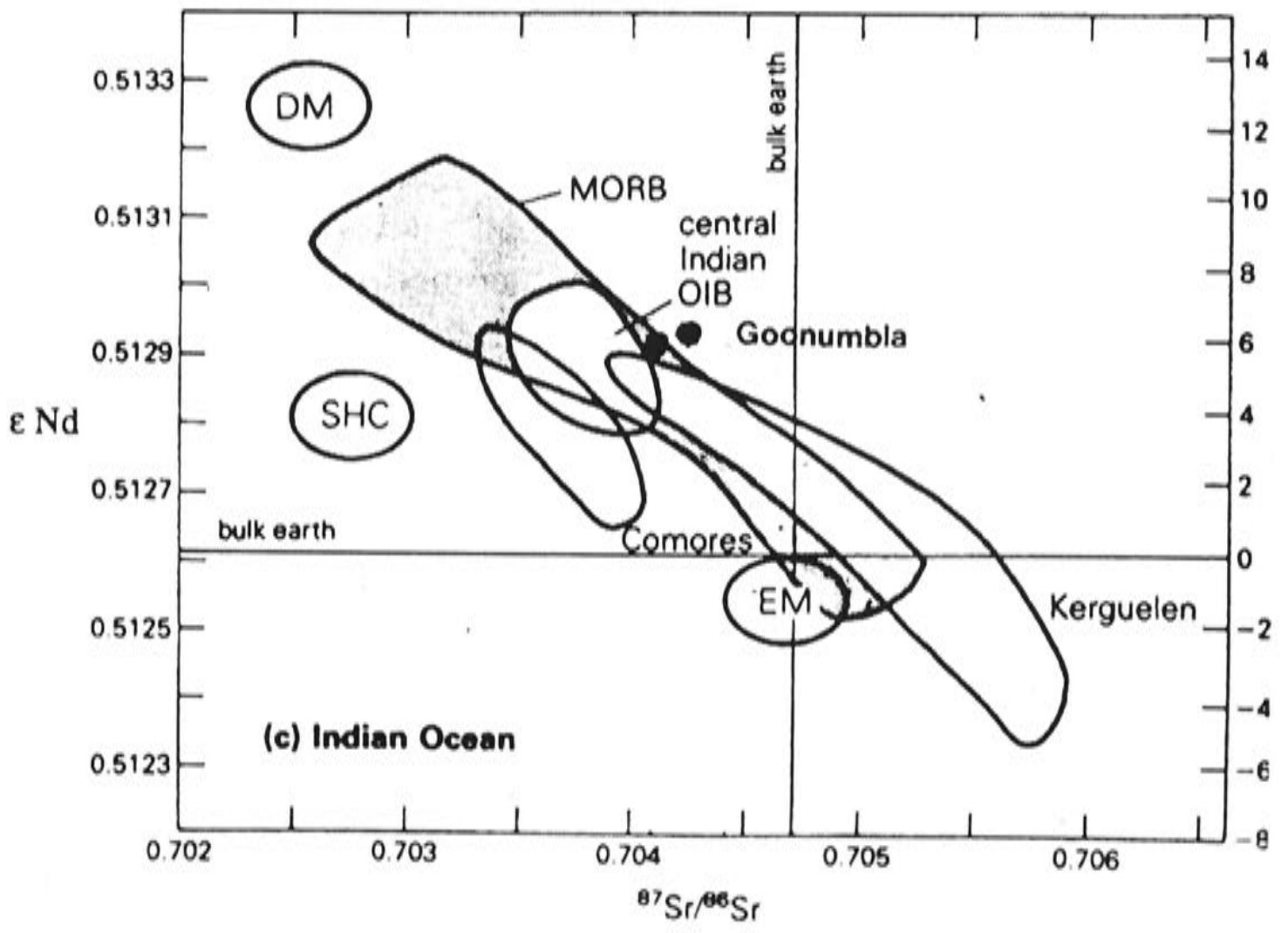

Figure 5.14 Epsilon Nd vs $^{86}Sr/^{88}Sr$.

5.7 SUMMARY DISCUSSION: MAGMATISM, TECTONISM AND MINERALIZATION

5.7.1 Origins of the shoshonitic magmatism

As noted in chapter 2 substantial disagreement exists on the question of the tectonic evolution of the Lachlan Fold Belt (LFB). The essential point of contention is the nature of the basement. Is it oceanic or continental crust? In this context the petrogenesis of the Ordovician shoshonitic magmatism is a pivotal issue.

The review of shoshonitic magmatism indicated that the magmatism cannot be related to a particular tectonic setting. A general picture emerges of deep-seated melting and high pressure fractionation of basaltic liquids at pressures of greater than 10Kb, commonly followed by low pressure fractionation. The source rocks must be at least water-enriched and oxidised mantle that upon melting could produce residual titanites that control the fractionation of the HFSR. This mechanism remains conjectural. An alternative explanation is that the HFSE signature is inherited from the enriched source which could for example be the product of subduction of island-arc material. The timing of the enrichment is poorly constrained. The proposed source for the Absoraka Mountain volcanics is Archean in age but equally shoshonitic magmatism in arcs could reflect an immediate response to enrichment of the mantle by the descending slab.

The geochemical character of the Goonumbla Volcanic Complex mirrors much of the character of other documented shoshonitic complexes. Noteably the complex contains a wide range of rock types from absorakites to banakites but the basaltic members are poorly represented indicating the extensive fractionation that has occurred to produce the complex. This is also reflected in the low Mg-numbers of these rocks. The pattern HFSE depletions is typical of shoshonites and related rocks.

The initial ratios of $^{86}Sr/^{88}Sr$ and $^{143}Nd/^{144}Nd$ as well as the lead isotope ratios all indicate primitive source rocks for the magmas. Most importantly there is no evidence of crustal contamination, which has been recognized in the lead isotope ratios of some base metal deposits in the LFB. Equally the data suggest that the source rocks may be some combination of depleted mantle (DM) and some other enriched source. There is some speculation from the lead isotope data that the age of the source rocks may be Lower Proterozoic. Also of significance to this discussion is the recent work on dating zircons from the Goonumbla Volcanic Complex using the ion microprobe (Perkins et al., 1991). This work has identified inherited cores that are Cambrian in age (510 Ma) The sulphur isotope data documented in chapter 8 indicate that the sulphur isotopic composition of the magmas was -2 per mil i.e. close the primitive value of zero per mil. Whilst these data do not uniquely resolve the question of the nature of the source rocks that produced the shoshonitic magmatism at Goonumbla, they do provide some useful constraints, The lack of a crustal signature suggests that this magmatism is unlikely to

be the product of Ordovician subduction, As noted in Chapter 2, a characteristic feature of the LFB is the widespread development of thick quartz rich turbidite sequences, It would be difficult, but not impossible, to avoid a sedimentary component in any material subducted in the Ordovician.

An alternative explanation is that the enriched material reflects a subducted or buried and delaminated Cambrian volcanic arc. This proposal is attractive on two accounts. Firstly, the source material would have the characteristic HFSE array that is common to shoshonites and island arcs. Secondly, it would neatly account for the 510 Ma inheritance age in zircons from the Goonumbla Volcanic Complex. A second alternative is that the shoshonites are sourced in some more ancient and enriched subcrustal or mantle material. There is hint of this possibility in the lead isotope data. In this instance melting could be initiated from a rising mantle plume.

5.7.2 Tectonic setting

The preferred option at this stage is to derive the high- K calc-alkaline to shoshonitic magmas from recycled Cambrian arc-material and enriched mantle, The possiblity of mantle-plume initiated melting of an ancient enriched source in the sublithospheric mantle cannot be dismissed. The components of a Cambrian arc-system: boninites, calc-alkaline basalts and arc tholeiites, are present in Victoria along major thrust boundmies and they are inferred to occur extensively beneath these thrusts. A similar situation is not inconceivable further to the north. A Cambrian arc-system could be an element of the basement terrane model proposed by Chappell et al. (1988) who envisages a number of Proterozoic to Cambrian microplates which remain unsutured until the Late Cambrian, Hence a plausible scenario for the Cambrian in the northern LFB is that the terrane now represented by the Wagga Metamorphic Belt in the west and the Kosciusko Terrane in the east was separated by an ocean basin and island arc. Collision in the late Cambrian as envisaged by Fergussan and Coney (1991) would have closed subduction with some probable thrusting leading to fault slivers of ophiolites (e.g. the Coolac Serpentinite Belt). Relaxation, post collision, would have led to remelting of an enriched mantle wedge and the accreted Cambrian Volcanics. At early stages of rifting, postcollision shoshonites are known to occur (Chapter 3). An extensional, basin-forming stage would allow the thick accumulation of turbiditic sediments. This extensional phase may be broadly a back arc setting or possibly a passive mmgin. Ponding at the base of the thickened crust may have generated the varying potassic trends of Ordovician shoshonitic activity.

5.7.3 Development of the Goonumbla Volcanic Complex

The oldest volcanics of the Goonumbla Volcanic Complex, the Nelungaloo Volcanics, were deposited on a quartz-rich turbidite basement, probably unconformably. Fossil evidence documented in Chapter 3 indicates an age of around 480 Ma, The earliest volcanic products were high-K calc-alkaline lavas which unlike the succeeding lavas, show some evidence of crustal contamination., A poorly understood hiatus occurs until around 440Ma when development of the Goonumbla Volcanic Complex began. It is built unconformably on a substrate of early Ordovician sediments and volcanics which are possibly the equivalent to the Giralambone Beds. The volcanic edifice was initially submarine, gradually building up to be subaerial in its later stages, It was fringed by shallow marine limestones, The circular feature in the magnetics is taken to represent the outer limits of a central caldera which would have been about 20 km in diameter. Monzonite-monzodiorite intrusions in the northern part of the complex were emplaced along the caldera rim, These sub-volcanic intrusions are co-magmatic with the volcanics and appear to have been the volcanic feeders., Subsequent to their emplacement the caldera collapsed as the chamber was emptied. The trachytic Wombin volcanics were deposited within the caldera.

The composition of the volcanics and subvolcanic intrusions that built the edifice lie along the low-pressure olivine fractionation trend. This trend is interpreted as an 'anhydrous' fractionation trend resulting from the continued loss of volatiles during volcanism, It is clearly unlikely that intrusions related to their coeval volcanics are capable of generating magmatic hydrothermal systems.

5.7.4 The Mineralising Trend

The main low-pressure fractionation trend is defined by the Goonumbla Volcanics, the Wombin Volcanics and co-magmatic intrusions and the Forbes Anticline intrusions. A second low-pressure fractionation trend is defined by intrusions related to mineralization. It is marked by a greater enrichment of silica and is best explained by fractionation of plagioclase and biotite. This hints at a build up in the volatile in these magmas and suggests that the key element in the sequence of events required to produce a porphyry deposit is the containment and controlled release of the volatiles. This critical part of porphyry copper development is best illustrated by the Endeavour 31 stock and its attendant satellites of mineralised porphyries. The second half of the thesis will be directed to exploring this theme via a detailed study of one of those satellite porphyries, the Endeavour 26 North deposit.

Chapter 6

THE GEOLOGY OF THE ENDEAVOUR 26 NORTH CU–AU DEPOSIT

6.1 INTRODUCTION

The Endeavour 26 North porphyry Cu–Au deposit is the largest Cu resource found in the Goonumbla region to date. Nine deposits have been discovered by Geopeko and these are described by Jones (1985). Individual centres of mineralisation in the Goonumbla project area are named 'Endeavour', with the suffix number running in sequence of discovery date. In early 1989, a final feasibility study was completed on the open-cut potential of Endeavour 22, 26 North and 27. A mining lease application covering the three main prospects was applied for in late 1990.

6.2 ENDEAVOUR 31 INTRUSIVE COMPLEX

The Endeavour 26 North deposit is a stockwork quartz, sulphide system developed on the margins and apices of two quartz monzonite porphyry intrusions. The other Endeavour deposits are, generally, the same and differ only in detail, such as Au/Cu ratio and degree of hydrothermal alteration. Endeavour 26, 28, 31 North, 31 South and 20 encircle a monzonite to monzodiorite stock, known locally as the Endeavour 31 stock (Figs 6.1, 6.2). Quartz monzonite porphyries related to Endeavour 31 North and 26 North crosscut the phases within the Endeavour 31 stock. In addition, the western contact of the stock forms the floor to the Endeavour 26 North deposit (see below). Hence the mineralised porphyries have a close spatial relationship to the Endeavour 31 stock. A close geochemical link, which is discussed in Chapter 3, binds the mineralised porphyries with the Endeavour 31 stock. The geology of the Endeavour 31 complex will be described in order to set the geological framework of the Endeavour 26 North deposit.

6.2.1 Field relationships

The Endeavour 31 stock, together with its satellite quartz monzonite porphyries, is located in the northeast quadrant of the Goonumbla ring complex (Figs 3.8, 3.10). The stock is 1.5 x 1 km in size, with the long dimension trending in a northwesterly direction. The shape and trend of the stock is due, in part, to post-intrusive faulting. Where the intrusion–volcanic contact is not faulted, it may be sharp with associated minor microsyenite dykelets or brecciation, as is the case on the northwestern edge of the stock. Here, fine- to medium-grained, trachyandesitic, crystal-rich lapilli tuffs have been brecciated by emplacement of microsyenite to monzonite intrusions. In detail, a web of thin quartz, K-feldspar veinlets can be traced into fine- to medium-grained monzonitic dykelets which surround volcanic breccia fragments. The monzonitic dykelets range up from millimetres in width, and textures vary from sparsely porphyritic to crowded. The monzonitic dykelets display a thin chilled margin, usually 1–2 mm in thickness. In outcrop, over 30 m, the contact varies from a fine network of quartz, K-feldspar veinlets, through an intrusive breccia zone to uniform monzonite with xenoliths of biotite altered volcanics.

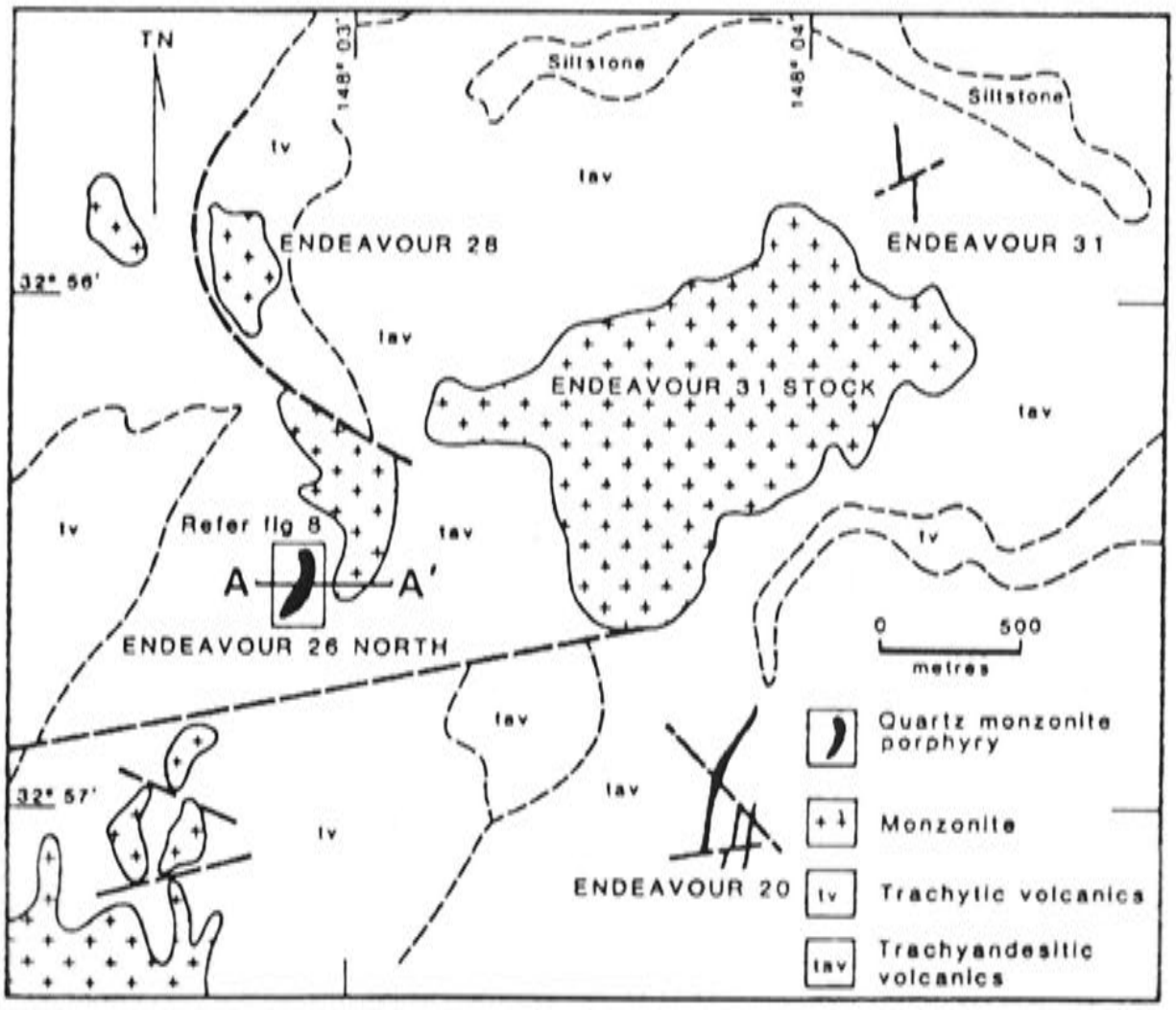

Figure 6.1 Geology of the Endeavour 31 complex.

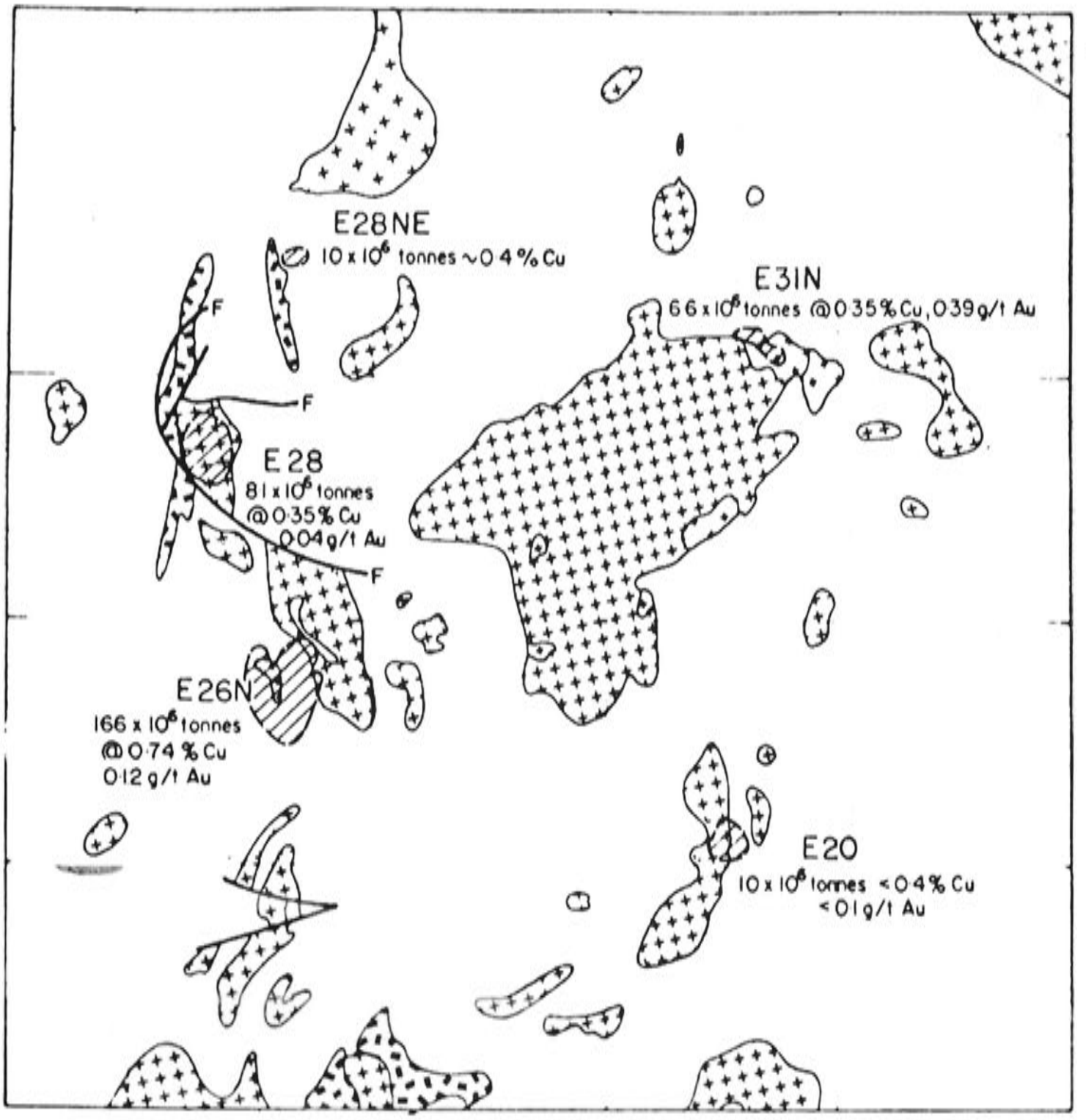

Figure 6.2 Intrusions and mineralisation around the Endeavour 31 stock.

These observations suggest that the Endeavour 31 stock intruded the volcanic pile by first fracturing the rock by release of overpressured fluids. Subsequently, monzonitic magma intruded along the fractures. This pattern is repeated with most of the intrusions associated with the Endeavour 31 stock, and suggests that fracturing and stoping of the host volcanics was the prime method of intrusion. However, the process may not be entirely general as diorites intruding the Nelungaloo Volcanics to the south appear to have domed the volcanics.

The rocks of the Endeavour 31 stock are characterised by subhedral oligoclase to andesine crystals (20–35%), which commonly form cumulophyric aggregates set in a

holocrystalline, hypidiomorphic, granular groundmass of stumpy, K-feldspar crystals. The feldspar is always red-brown to pink-red due to iron-oxide crystals dusted through the crystals. It commonly rims plagioclase and, rarely, tablets of orthoclase poikilitically enclose earlier formed crystals of plagioclase. Biotite (5–10%) and hornblende (5–10%) are the common mafic minerals. Interstitial quartz ranges between 3 and 10%, and accessories include magnetite, apatite, sphene and rutile.

Despite the broad uniformity in lithology, important variations do occur on the margins of the stock. This information is provided by DDH46 — a 1.8 km long diamond-drillhole which penetrates through 1 km of the Endeavour 31 stock in plan, and tests the southwestern contact of the intrusive complex. As such, the drill penetrates rock some 700 m below the main locus of drilling at Endeavour 26 North, and so provides information about the roots of the system. DDH46 intersects monzonite, with minor variations from 20 to 1281 m. Rock types vary from mafic monzodiorites through monzonite porphyries to syenites from 1281 to 1800 m. The zone approximates the outer 350 m of the stock. Through this outer zone there is a gradational change from the brick-red coloured monzonite to a black monzodiorite. Texturally, this gradational change is reflected in a gradational decrease in interstitial K-feldspar and concomitant crowding of plagioclase. Equally, hornblende and clinopyroxene gradually increase in abundance. The resulting monzodiorite is a holocrystalline medium-grained rock, consisting of euhedral zoned andesine (50–60%), hornblende (5–10%) and clinopyroxene (5–10%) with interstitial cloudy perthitic potassium feldspar (15%). Biotite poikilitically encloses plagioclase, hornblende and clinopyroxene. Magnetite and apatite are common accessories.

Taken together these observations are consistent with the more mafic members of the Endeavour 31 stock being cumulates or accumulates, which have crystallised early on the margins of the Endeavour 31 stock. Crosscutting this marginal zone are a series of monzonite porphyry dykes ranging in thickness from 10 to 30 m. It is noteworthy that this marginal 350 m appears to have received much more intrusive activity than the central part of the Endeavour 31 stock. The monzonite porphyries are a distinctive pink-red colour in contrast to the dark-red colour of the host monzonite. They consist of a porphyritic aggregate of plagioclase phenocrysts set in a granular mosaic of quartz and K-feldspar. Biotite is the main mafic mineral; however it only accounts for ~5% of the rock.

Dunn and O'Neill (1984; unpublished Geopeko report) noted this distinctive rock type and named it Mosaic Porphyry. They noted that low-grade mineralisation was clearly associated with these porphyries and, hence, may be associated with the porphyries in the mineralised zones at Endeavour 26 North. (1984; unpublished Geopeko report) further proposed that the Mosaic Porphyry formed the mineralised shell to the weakly mineralised core of the Endeavour 31 stock.

It is clear that the marginal 350 m of the Endeavour 31 stock has been the focus of considerable intrusive activity, in contrast to the central part of the stock.

6.2.2 Bedrock geochemistry

Bedrock sampling has proven to be the best exploration tool in the region. Sampling is undertaken with a rotary air blast (RAB) drill, which may be required to penetrate in excess of 30 m to reach bedrock. Due to the prospectivity of the area, it has been tested systematically to at least 100 m grid sampling. Cu and Zn geochemistry are very instructive in terms of establishing the size and relationship of the hydrothermal system. A complex Cu anomaly, ranging from 1000 to >4000 ppm blankets, the Endeavour 31 complex (Fig. 6.3). Individual highs can be related to the porphyry centres defined above. Zn geochemistry defines an annular pattern around the Endeavour 31 stock (Fig. 6.4). Breaks in this annular pattern occur where porphyry centres are located. This is consistent with these centres emerging around the margin of the 'parent' Endeavour 31 stock and overprinting the earlier zinc halo.

6.3 INTRUSIVE ROCKS AT ENDEAVOUR 26 NORTH

6.3.1 Introduction

Outcrop in the area of Endeavour 26 North area is very limited, so geological data are primarily obtained from diamond-drillcore and rock-chips from RAB and percussion drilling. Drilling density between 10 250 RL (surface) and 10 000 RL is sufficient to provide good geological control, and a plan of the area at 10 000 RL is given in Figure6.5 and a geological section in Figure 6.6. The intrusions at Endeavour 26 North were emplaced into trachytic lavas, pyroclastics and breccias of the Wombin Volcanics. They can be conveniently considered in three categories: pre-mineralised, mineralised and post-mineralised intrusions. The reader is referred to Plans 4 to 8 in Part 2 of the thesis for detailed geology.

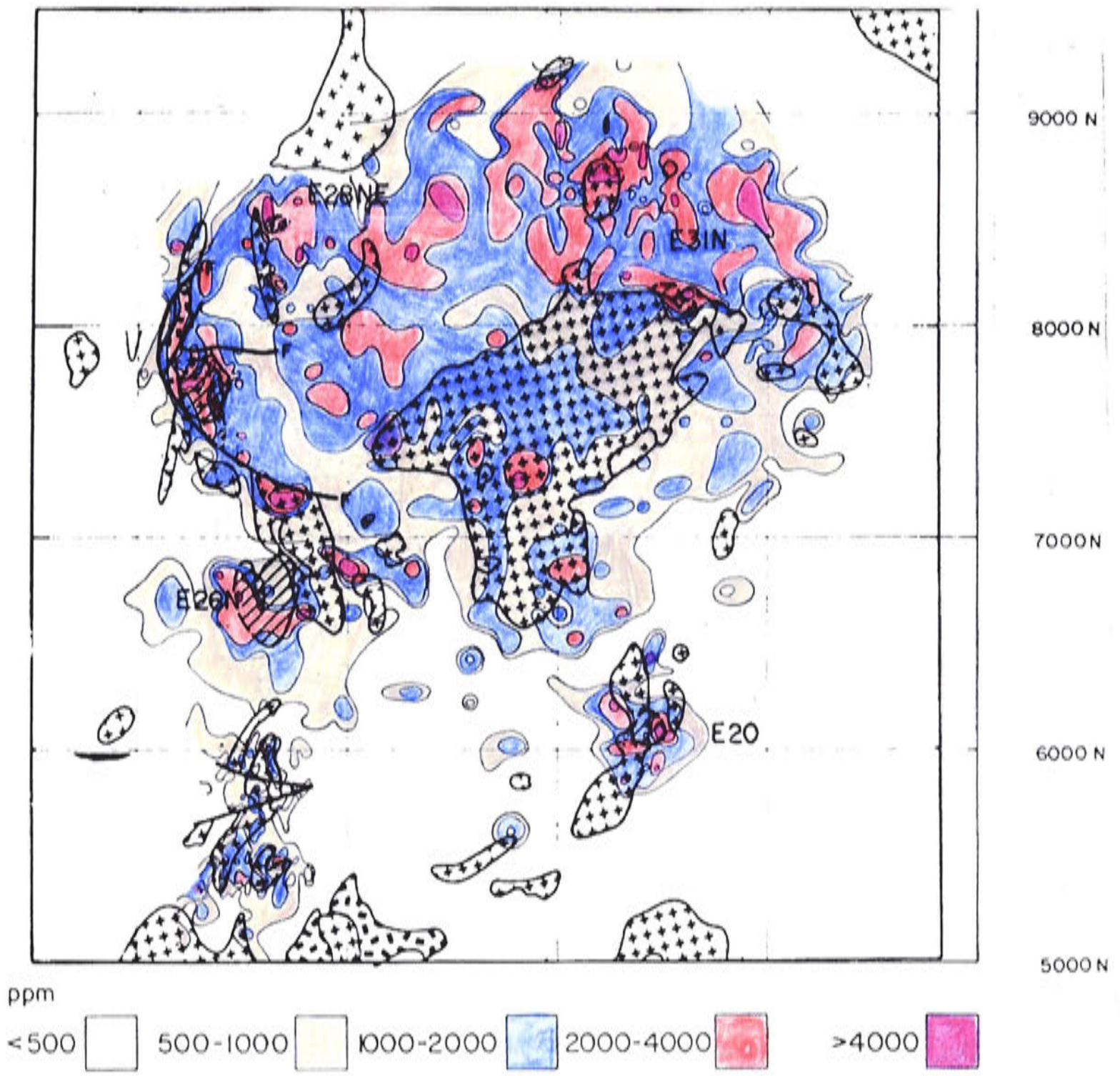

Figure 6.3 Cu geochemistry around the Endeavour 31 complex.

6.3.2 Pre-mineralisation intrusions

The earliest intrusion is poorly defined. Deep drilling encountered a 100 m thick monzodiorite sill, which is crosscut by all other intrusions and associated mineralisation (Fig. 6.6). In detail, this holocrystalline medium-grained rock consists of euhedral and zoned andesine (50–60%), hornblende (5–10%) and clinopyroxene (5–10%) with interstitial perthitic K-feldspar (15%). Biotite poikilitically encloses earlier formed plagioclase, hornblende and clinopyroxene. Magnetite and apatite are common accessories.

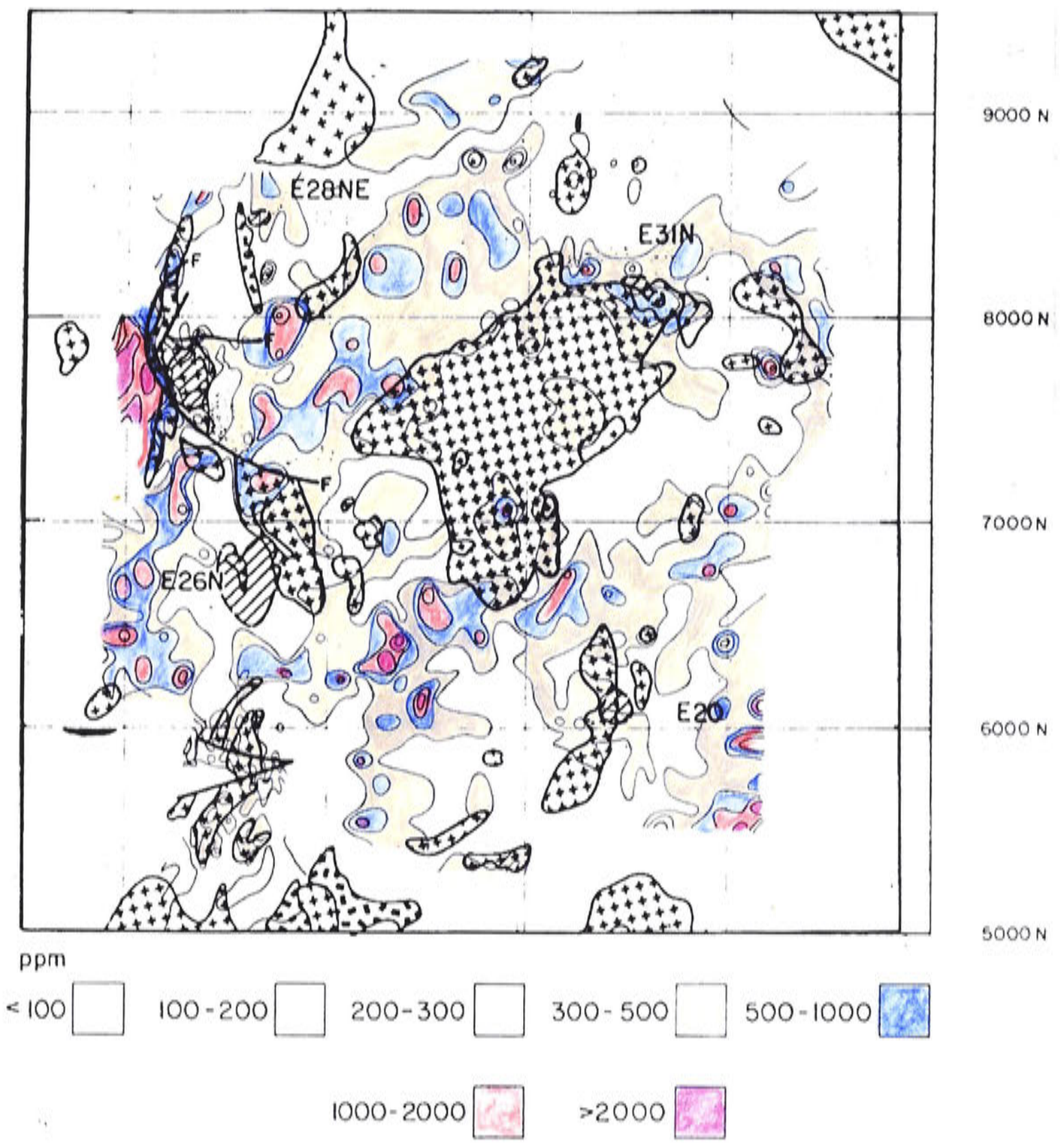

Figure 6.4 Zn geochemistry around the Endeavour 31 complex.

6.3.3 Mineralised intrusive rocks

As discussed above, the Endeavour 31 stock is the earliest mineralised intrusive in the system, and from the documented spatial relationships it is clearly the parent stock. The low-grade mineralisation which occurs in this intrusion can be related to weakly mineralised veinlets of quartz and K-feldspar distributed throughout the stock. Endeavour 26 North is centred on two porphyry intrusions, QMP1 and QMP2 (Figs 6.5, 6.6; Plates 6.1, 6.2). They are known locally as the Mosaic Porphyry and the Square Porphyry

(Dunn and O'Neill, 1984, Geopeko unpublished report) and are texturally and compositionally very similar. The timing relationships between them and the Endeavour 31 stock is complex. The Endeavour 31 stock forms the base and eastern wall to the deposit. Limited deep drilling through the stock has intersected several weakly mineralised felsic monzonite porphyries. Some of these intersections show sharp contacts with thin chilled margins, whilst others are gradational. These intercepts are some 600 m vertically away from well-controlled geology, hence, correlation with either QMP1 or QMP2 is speculative. It appears possible, however, that some of these intrusions are cutting a previously crystallised phase of the stock, whilst others may be closely related in time to the crystallisation of the Endeavour 31 stock.

Establishing the timing relationships between QMP1 and QMP2 has been difficult because of their similarity in composition and texture, and because of the masking effects of the hydrothermal alteration. Further complications arise as both intrusions can resemble the porphyritic volcanics they intrude, particularly near the top of the deposit. The following observations apply some constraints to timing relationships.

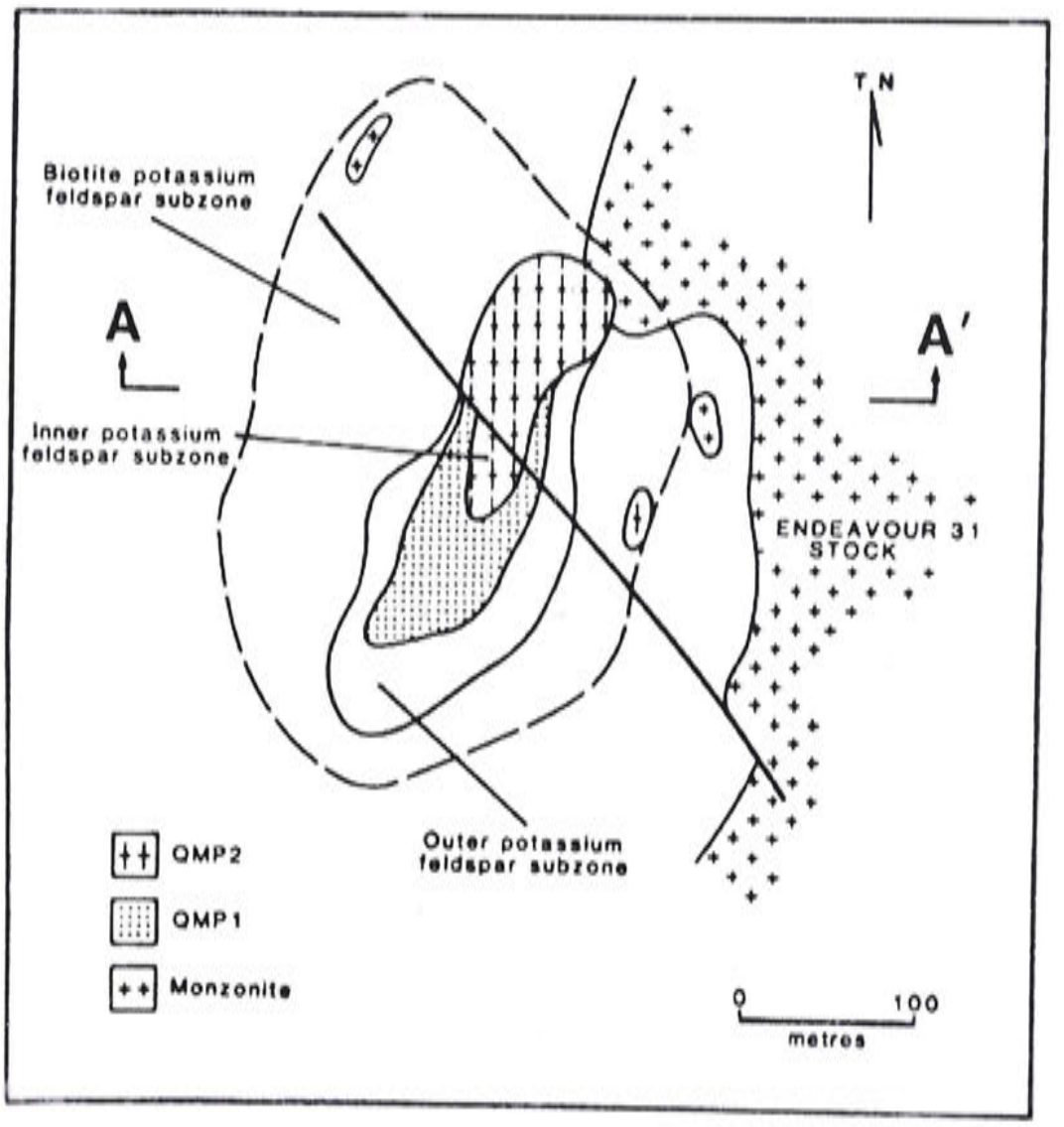

Figure 6.5 A geological plan for the Endeavour 26 North area at 10 000 RL.

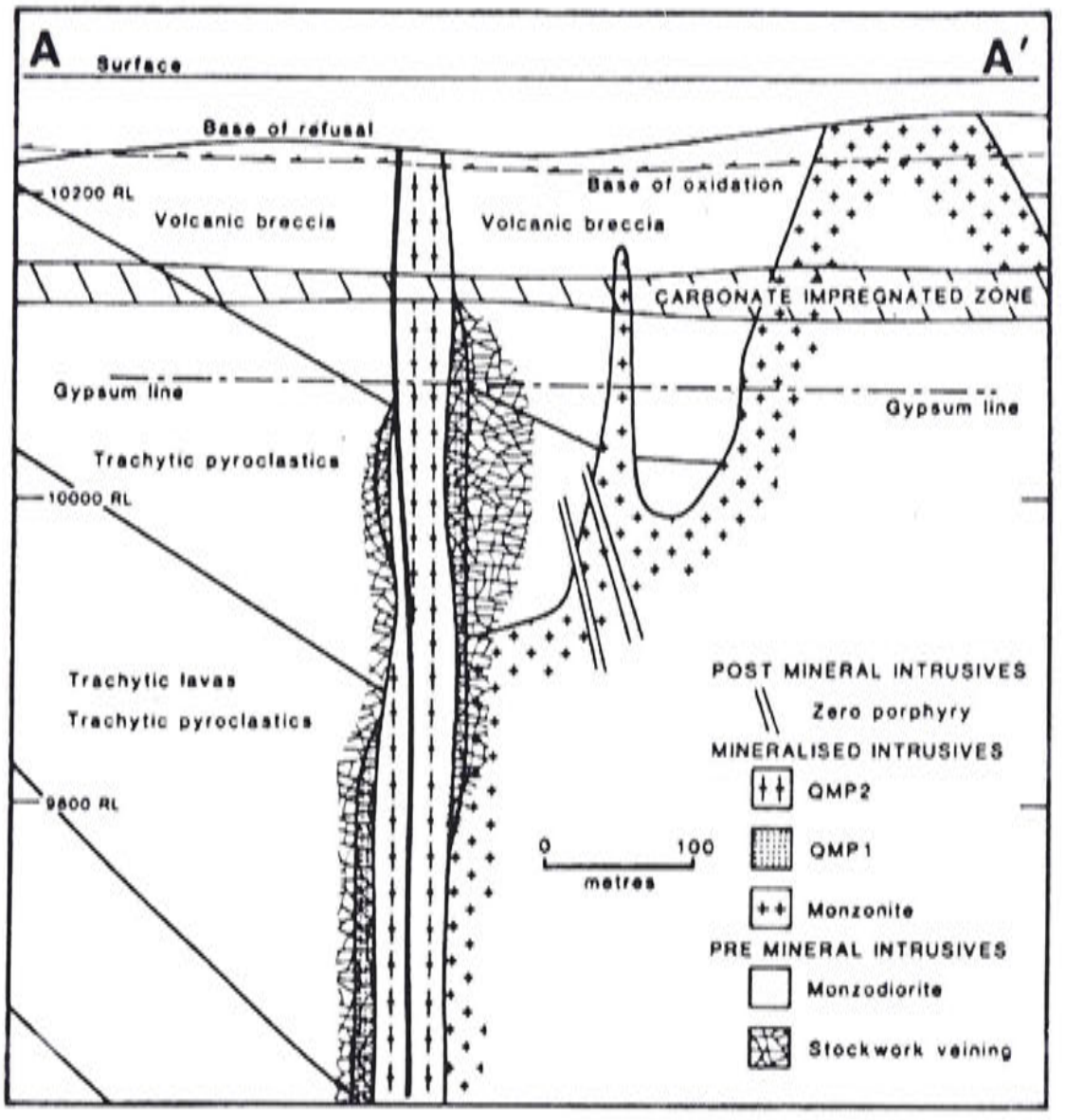

Figure 6.6 A geological cross-section for the Endeavour 26 North area at 53450N. Line of section is located in Figure 6.5.

QMP1 is always highly altered and mineralised and, commonly, the contact between QMP2 and QMP1 is marked by an abrupt change from high-grade to very low-grades of Cu. QMP2 is itself moderately altered and mineralised. However, intense veining and mineralisation are observed in QMP2 and in volcanic clasts near its margins. Fragments of mineralised vein quartz (Plate 6.3) and blobs of copper sulphides are commonly included in this intrusion near its contacts with QMP1. Additionally, narrow dykelets of QMP2 are commonly seen to crosscut veined QMP1 and host volcanics (Plate 6.4). The spatial relationship of the two intrusions are shown in Figures 6.5, 6.6 and the block diagram in Figure 6.7a. These relationships, together with the temporal constraints, indicate that QMP2 intruded the northern margin of QMP1 and apparently replaced pre-existing mineralisation within QMP1.

QMP2 is conspicuously porphyritic, containing grey, evenly distributed albite to oligoclase lathes (20–30%) set in a pink fine-grained K-feldspar, quartz groundmass.

Altered biotite and hornblende are sparsely distributed throughout, and may make up 10% of the volume of the rock. Rare tablet-shaped megacrysts of perthitic orthoclase poikilitically enclose plagioclase crystals. The amount of interstitial quartz varies through the intrusive, reaching a maximum of 13%. Vein-like trails of coarse, euhedral quartz phenocrysts (3–6 mm) are noted near some intrusive contacts.

Plate 6.1 QMP1 (Mosaic Porphyry DDH 29, 506m). Note veined clast of QMP1 included in QMP 2

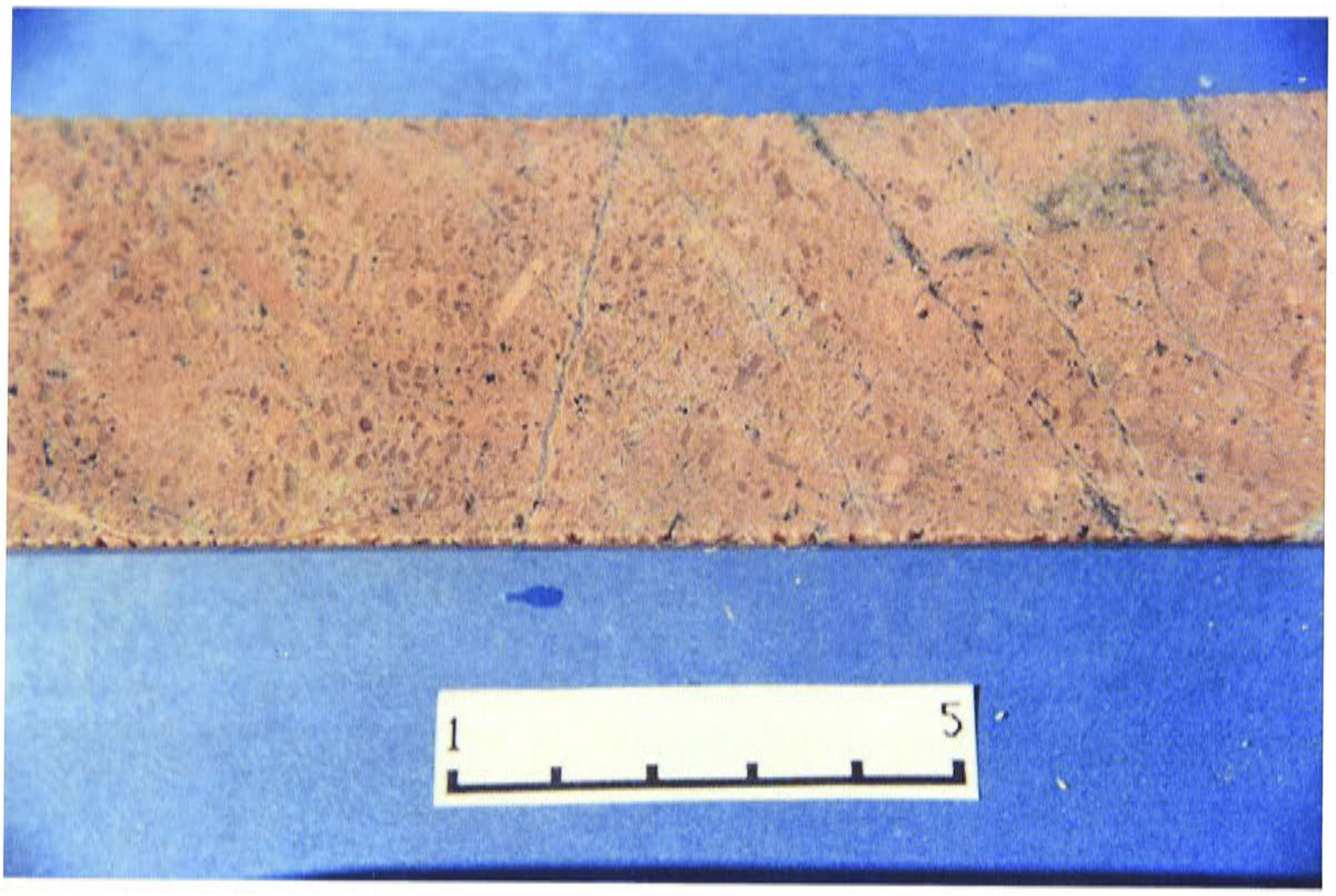

Plate 6.2 QMP2 or Square Porphyry showing plagioclase phenocrysts mantled by K Feldspar..

Plate 6.3 Fragments of mineralised vein quartz and blobs of copper sulphides near the margins of QMP1.

Plate 6.4 Narrow dykelets of QMP2 cutting veined QMP1.

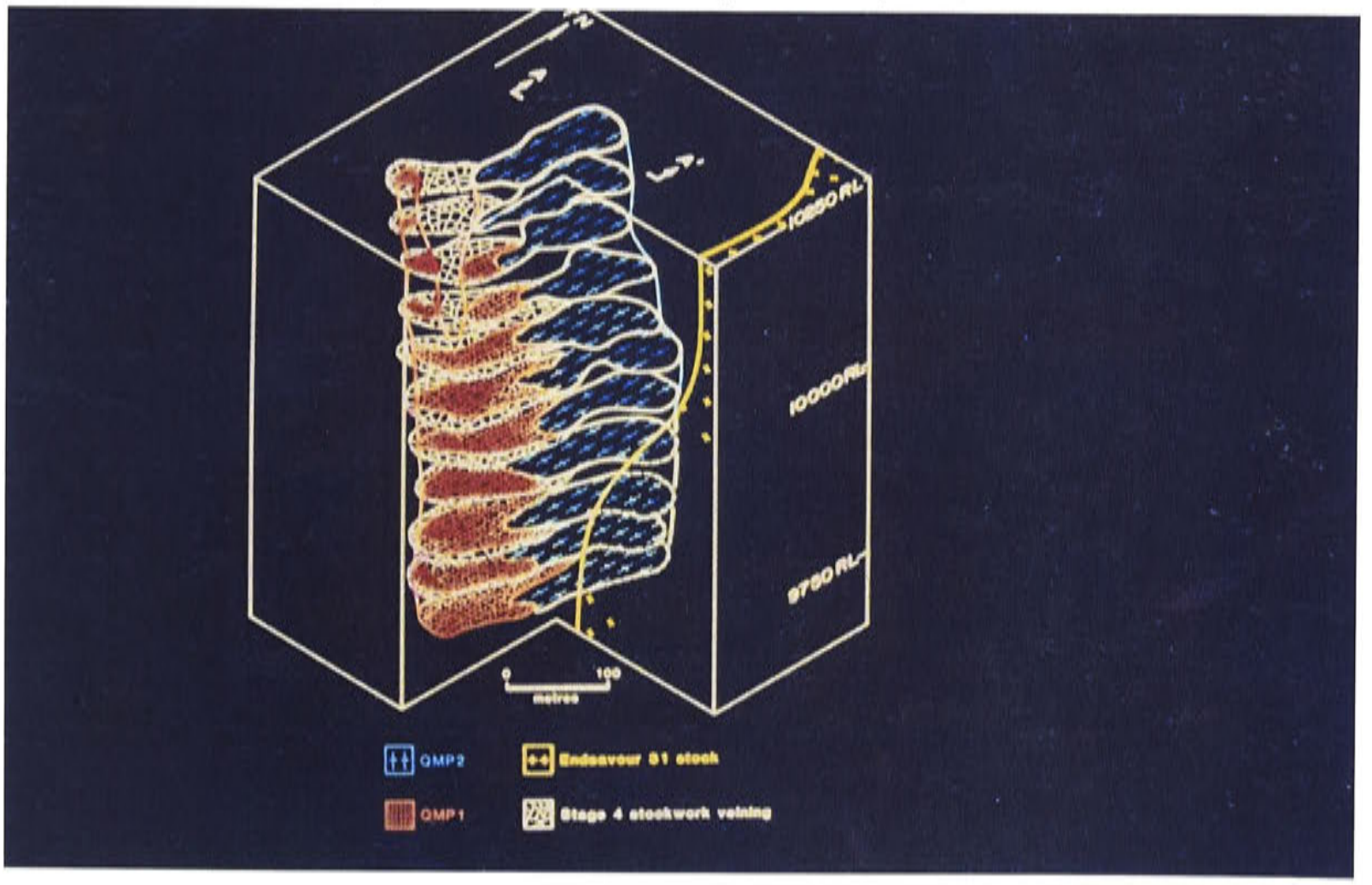

Figure 6.7a Schematic block diagram of intrusive and stockwork geometry, Endeavour 26 North.

QMP1 is usually overprinted by potassic hydrothermal alteration, and it is therefore difficult to define accurately. Recent drilling, however, has defined a zone of less-intense veining in QMP 1 at ~10 600 RL and 53350N. In this interval alteration is

still extreme with Cu grades >1%; however the porphyritic nature of the rock is clear and K-feldspar phenocrysts, similar to those in QMP2, are present.

Vein-dykes cut both QMP1 and QMP2, as well as the host volcanics. These irregular, narrow (generally of the order of a few millimetres in width) vein-like features have both the characteristics of igneous dykes and hydrothermal veins. They show a variety of textures, including veins with a crystalline quartz margin, and central vein infill of saccharoidal quartz and alkali feldspars, resembling an aplite. Some vein-dykes have graphic intergrowths of quartz and alkali feldspar, with a central selvage of hydrothermal quartz plus sulphides. Others form dykes containing complex graphic and feathery intergrowths of quartz and alkali feldspars. These dykes commonly exhibit irregular blebs of quartz, with euhedral crystals of alkali feldspar lining the margin of the bleb.

Spatially related to these vein-dykes is a breccia texture in which the breccia infill is commonly a quartz – alkali feldspar intergrowth, similar to that seen in the vein dykes with bornite and chalcopyrite. The igneous–hydrothermal breccia infill may develop spectacular graphic intergrowths of quartz and alkali feldspars. Earlier formed stockwork veins are commonly broken apart and infilled with this aplite-textured breccia infill. Taken together, the distribution of vein-dykes and igneous–hydrothermal breccia form a mappable zone around the mineralising intrusions.

6.3.4 Post-mineralisation intrusive rocks

Narrow dykes of monzonite porphyry are the last intrusive event. These conspicuously glassy porphyritic rocks are totally devoid of Cu mineralisation (<10 ppm), and commonly have well-developed chilled margins. These porphyries are known locally as Zero Porphyries. Narrow pebble dykes also occur at Endeavour 26 North.

6.3.5 Compositions of magmatic biotites

The compositions of magmatic biotites were analysed by the electron microprobe to investigate changes in composition with time, and to compare with secondary hydrothermal biotites (Fig. 6.8).

The primary biotites from the Endeavour 31 stock and the QMP1 generally form a tight cluster compared with the hydrothermal biotites. However, there is a clear

variation on the basis of Mg number between biotites from the Endeavour 31 stock and QMP2. Mg number is a common measure of oxygen fugacity, and it would appear that an oxidation shift occurs between formation of the biotites in the Endeavour 31 stock and QMP2. Mason (1978) studied the major element compositions of the biotites of Cu-bearing and barren plutons of Papua New Guinea. On the basis of the evolution of the Fe/(Fe + Mg) contents of the ferromagnesian minerals, he concluded that the barren porphyries had low-oxygen fugacities and mineralised plutons had high-oxygen fugacities that increased with crystallisation and alteration. Chivas (1981) found similar trends in the Koloula Igneous Complex. In both cases, the increase in oxygen fugacity is believed to result from separation of increasingly greater amounts of fluid with crystallisation of the magma. Figure 6.9 shows a clear separation between the hydrothermal biotites with low Ti, and magmatic biotites with high Ti. Figure 6.10 shows that most of the biotites at Goonumbla are relatively iron poor.

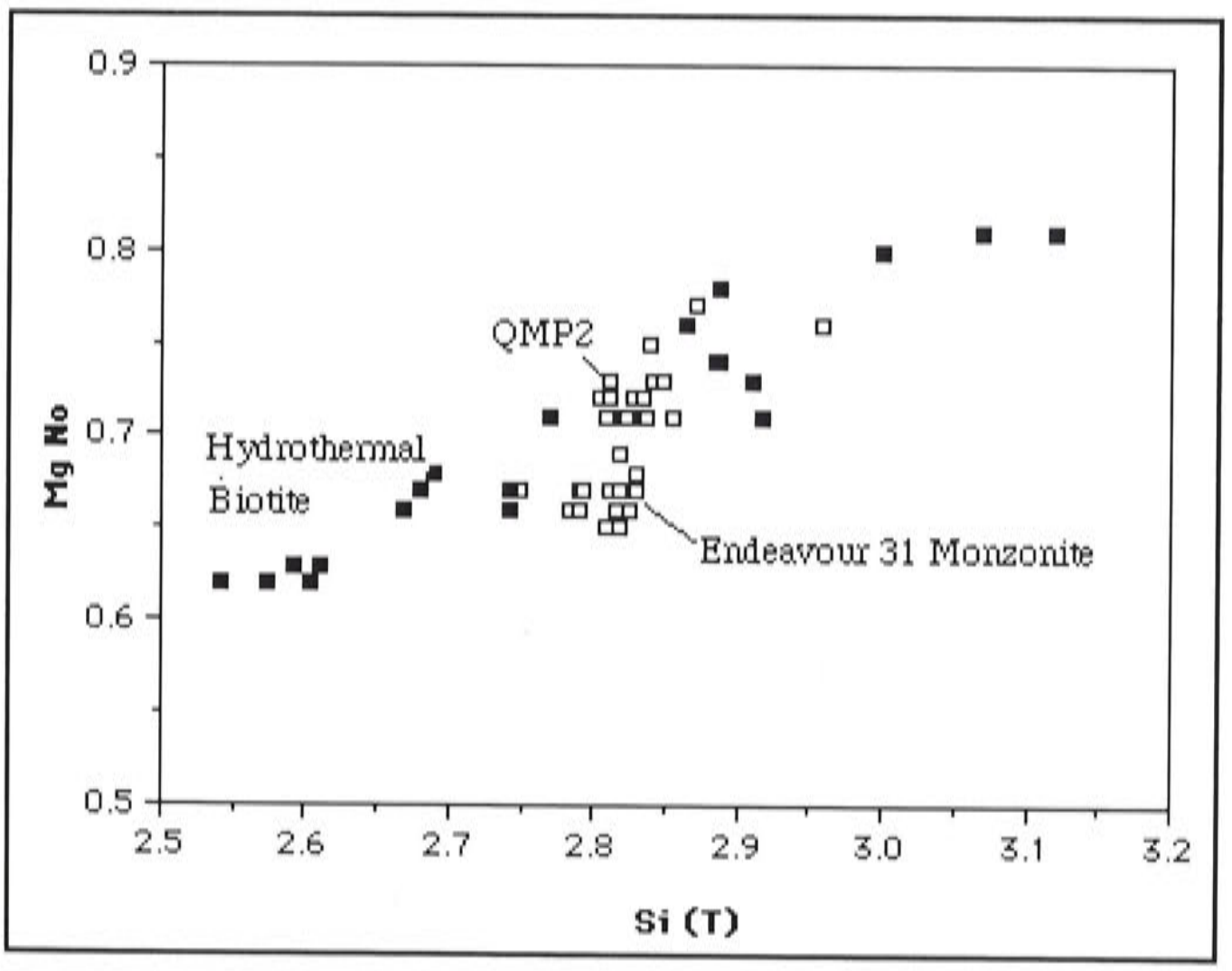

Figure 6.8 Variation in Mg number vs Si (T) for hydrothermal and primary biotites from Endeavour 26 North,

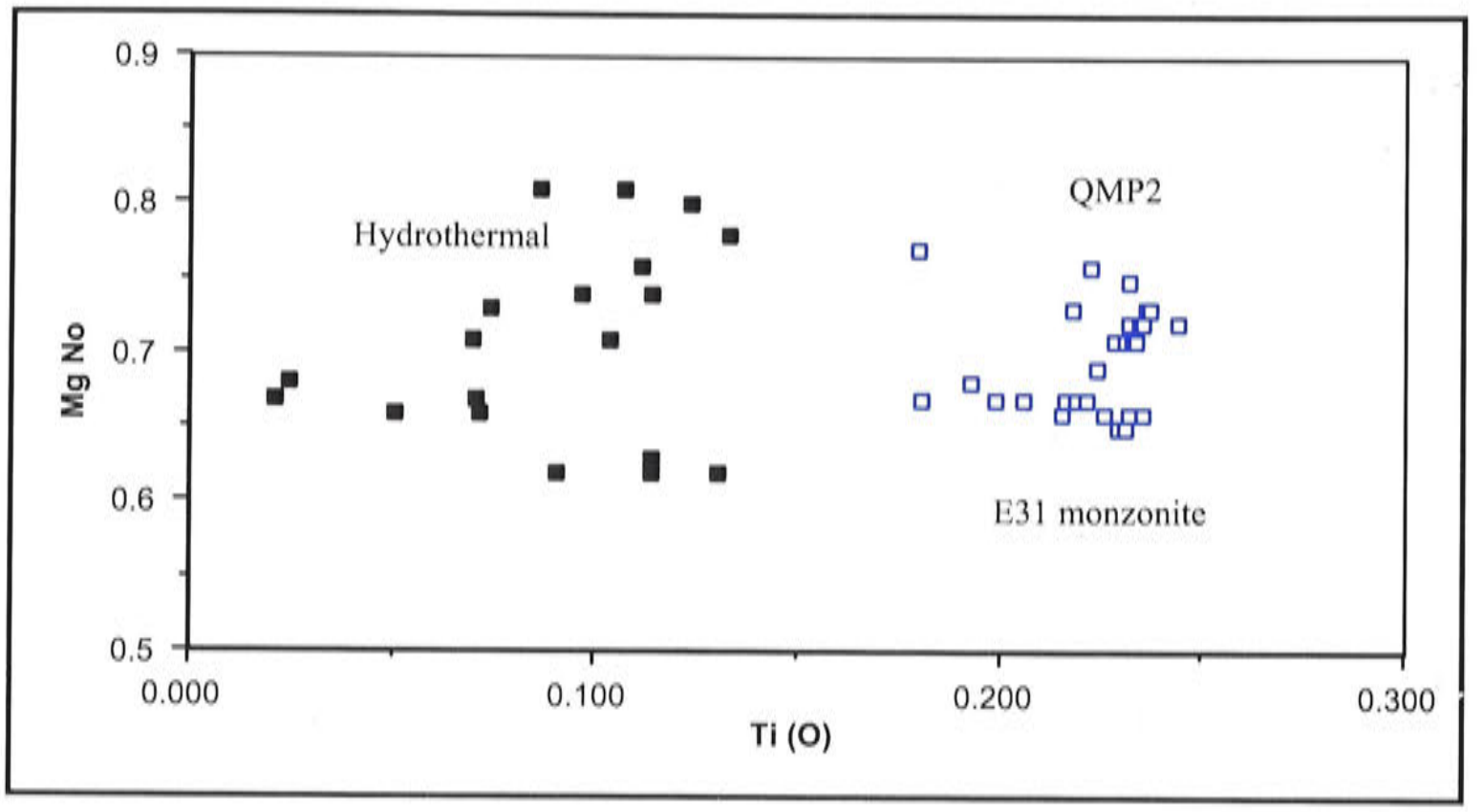

Figure 6.9 Variation in Mg number vs Ti (octahedral site) for hydrothermal and magmatic biotite, Endeavour 26 North.

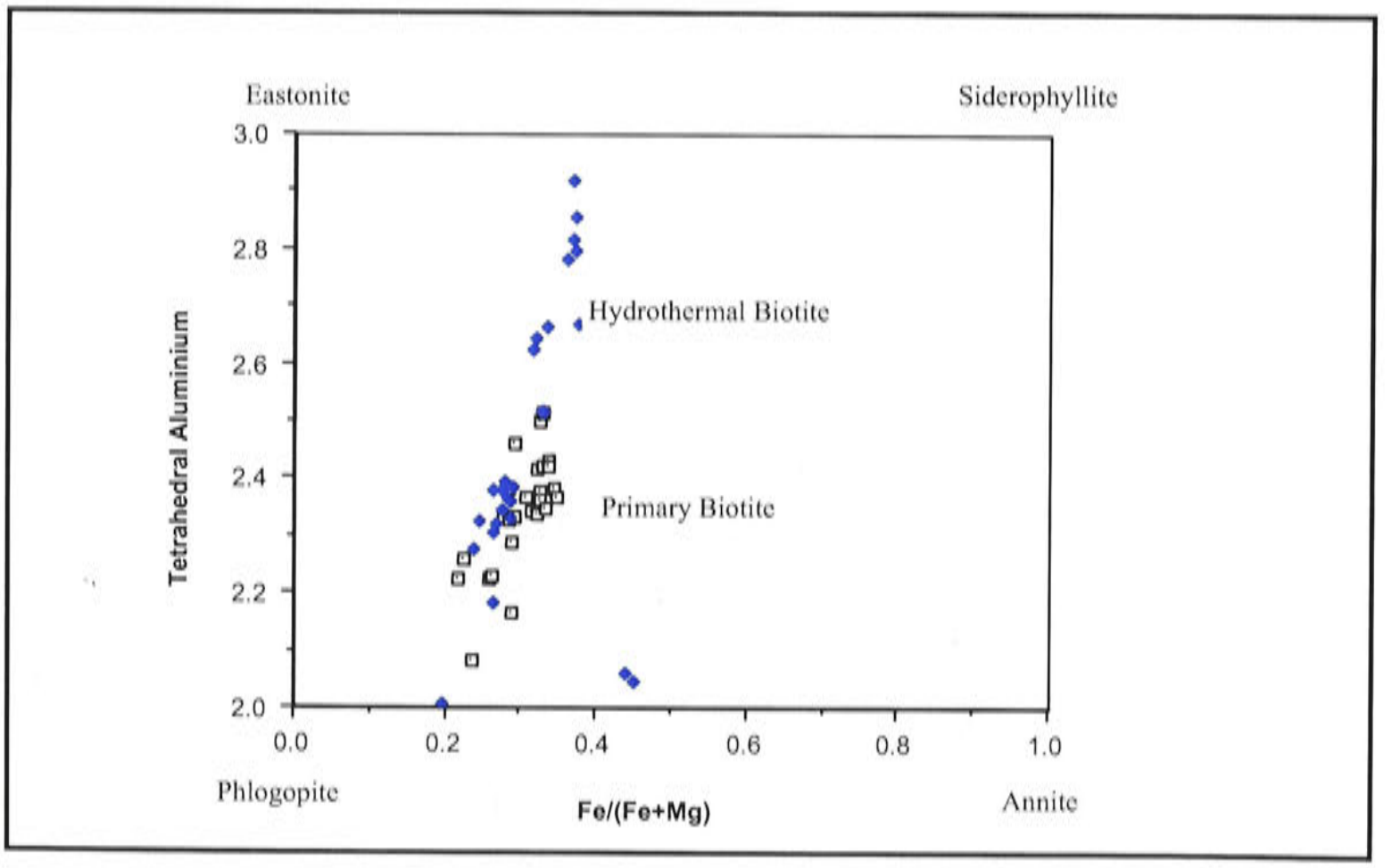

Figure 6.10 Biotites projected on to the phlogopite–annite–siderophyllite–eastonite quadrilateral,Endeavour 26 North Goonumbla region.

6.4 MINERALISATION AND ALTERATION IN THE GOONUMBLA VOLCANIC COMPLEX

This aspect is discussed in detail in Chapter 7, but the following brief comments provide an overview. All of the deposits show a close spatial relationship to quartz monzonite porphyries. The deposits are generally pipe-like and range in diameter from a few tens of metres to >300 m. Disseminated and fracture, or vein-controlled, mineralisation occurs both in the porphyry intrusions and the host volcanics. The strongest mineralisation is associated with quartz stockwork veining within a centre of pervasive potassic alteration; a characteristic of these deposits. Grade, vein intensity and fracture intensity diminish away from the centre of this zone. Generally there is an outward zonation from bornite to chalcopyrite to pyrite.

The shape of the Endeavour 26 North orebody, as defined by the 1% eCu grade contour, is clearly a vertical cylinder (Fig. 6.7b) with a vertical extent of >900 m. In plan view it has dimensions of 250 x 300 m. Comparison of Figures 6.7a and b illustrates the correlation of grade with stockworking in QMP1. The indentation in the northern part of the orebody is clearly related to the presence of QMP2, and supports the textural evidence which suggests that QMP2 intrudes QMP1. Pervasive potassic alteration has been subdivided into an outer zone of K-feldspar alteration centred on QMP1 and an inner zone centred on QMP2 (Fig. 6.5), surrounded by a K-feldspar–biotite–magnetite zone (Figs 6.5, 6.11).

At the Endeavour 22 and 27 deposits, a regular Cu/Au ratio is apparent with (% Cu):(g/t Au) close to 1:1. In other deposits Au grades are not as high, but elevated Au grades are commonly associated with strong bornite mineralisation. Fine Au grains (Plate 6.5), and Au tellurides, calaverite, hessite and altaite have been observed in fractures in coarse-grained bornite. The reason for the variance in Au grade is not understood. Minor galena and sphalerite have been identified in the propylitic zones in the volcanics, and may produce coherent soil geochemical anomalies as described around Endeavour 31. Skarn mineralisation has not been observed within the circular feature, although skarn related Pb–Zn mineralisation does occur close to its southern margin at Endeavour 6 and 7.

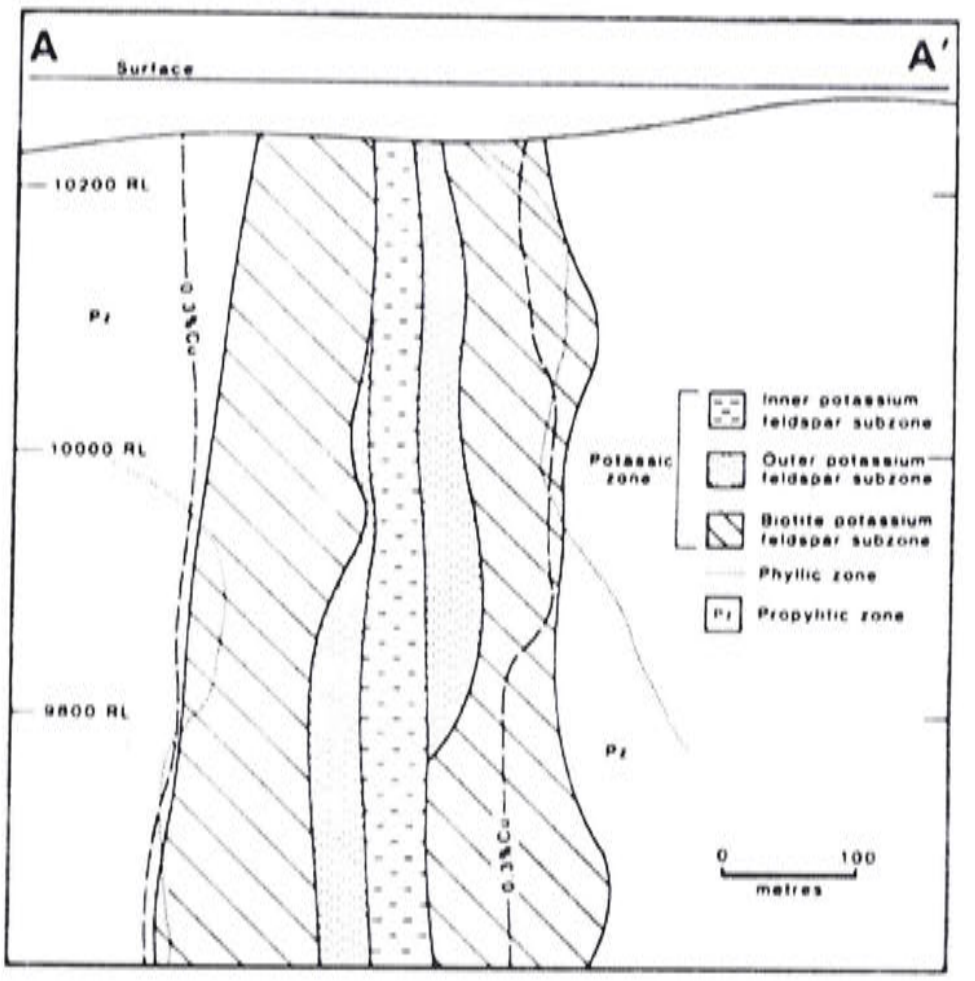

Figure 6.11 Cross-section at 53150N looking north, showing alteration zones at Endeavour 26 North.

Plate 6.5 Fine gold grains in coarse-grained bornite.

6.5 STRUCTURE

The Endeavour 26 North deposit lies within a structural corridor dominated by the Endeavour Linear which trends at 345° (Fig. 3.10). Detailed structural analysis (P.G. Dunn, Geopeko, unpublished data, 1986) indicates that the dominant orientation of quartz–bornite–chalcopyrite veins is around 035°, and parallel to the long axes of QMP1 and QMP2. This trend, which is oblique to the Endeavour Linear, suggests that the orientations of the veins and intrusions may reflect right lateral movement along the Endeavour structural corridor. Such movement could have created the space for the intrusions, as well as influencing principal orientations of veins.

6.6 SUPERGENE EFFECTS

The depth of weathering and oxidation is variable. At Endeavour 31 bornite can be chipped from outcrop, whereas elsewhere, the depth to fresh sulphide may exceed 80 m. Most of the Goonumbla area is covered by a variable thickness of clays, which are for the most part the product of in-situ weathering. In areas of stream activity, transported material has been encountered to a depth of 40 m.

At Endeavour 26 North a thin layer of supergene chalcocite is present between the upper oxidised strata and the first appearance of primary sulphides. This supergene ore zone is generally <10 m thick and extends over most of the deposit. At present it forms only a small part of the total ore resource.

Supergene leaching of sulphates has led to the development of a horizontal plane (Fig. 6.6) above which gypsum has been removed, leaving holes and open fractures. Jones (1985) suggested that the unusually planar nature of this surface, points to the presence of a chemical interface between two groundwater systems. Sillitoe and Gappe (1984) note that leaching of gypsum to quite deep levels is common in Philippine porphyry-Cu systems, and similar features are documented at the El Salvador porphyry-Cu deposit in Chile (Gustafson and Hunt, 1975) and Cerro Colorado, Panama (P.G. Dunn, Geopeko, pers. comm., 1984).

A second, poorly understood supergene feature occurs 20–30 m above the gypsum line (Fig. 6.6). It consists of an irregular zone of pervasive carbonate-impregnation leading to a hard, grey featureless rock with disseminated pyrite.

6.7 COMPARISON TO OTHER ALKALIC PORPHYRY DEPOSITS

6.7.1 Examples

British Columbia Iron Mask batholith deposits – Afton, Ajax, Mt. Polley, Cariboo Bell, Mt. Milligan, Copper Mt./Ingerbelle , Galore Creek (Barr, D.A., 1976; McMillan, W.J. 1991; McMillan and Panteleyev, A. 1988; Sutherland Brown, A. Editor, 1976.)

Papua New Guinea Ok Tedi (Sillitoe, 1990)

Philippines Marian, Didipio (Sillitoe, 1990a Sillitoe and Gappe, 1984; Sillitoe 1990b)

6.7.2 Description

In general Alkalic Porphyry systems are made up of stockworks, veinlets and disseminations of pyrite, chalcopyrite, bornite and magnetite occur in large zones of economically bulk-mineable mineralization in or adjoining porphyritic intrusions of diorite to syenite composition. The mineralization is spatially, temporally and genetically associated with hydrothermal alteration of the intrusive bodies and hostrocks. In comparison **Endeavour 26 North** is dominated by bornite associated with pencil like monzonite to quartz monzonite porphyry bodies. Magnetite is widespread throughout except where overprinted by potassic flooding. Diorites and syenites are present in the local geology but largely as host rocks. Mineralisation is mainly in the wallrocks.

6.7.3 Tectonic Setting

Alkalic porphyries in Canada appear in oceanic volcanic island arcs overlying oceanic crust. Chemically distinct magmatism with alkalic intrusions varying in composition from gabbro, diorite and monzonite to nepheline syenite intrusions and coeval shoshonitic volcanic rocks, takes place at certain times in segments of some island arcs. The magmas are introduced along the axis of the arc or in cross-arc structures that coincide with deep-seated faults. The alkalic magmas appear to form where there is slow subduction in steeply dipping, tectonically thickened lithospheric slabs, possibly when polarity reversals (or `flips') take place in the subduction zones. In British Columbia all known deposits are found in Quesnellia and Stikinia terranes. **Endeavour 26 North** occurs in a mixed volcanic and sediment dominated package of Early to Late Ordovician

age. Geology and geochemistry point to island arc affinities and isotopes point to no effective crustal contamination. However granite chemistry points to an older non-oceanic substrate. Intrusives form on cross structures (Endeavour Linear, Lachlan River Lineament).

6.7.4. Depositional Environment/ Geological Setting.

High level (epizonal) stock emplacement levels in magmatic arcs, commonly oceanic volcanic island arcs with alkalic (shoshonitic) basic flows to intermediate and felsic pyroclastic rocks. Commonly the high-level stocks and related dikes intrude their coeval and cogenetic volcanic piles. At **Endeavour 26 North**, high level epizonal intrusions intrude its own coeval pile made up of potassic volcanics.

6.7.5 Age of Mineralisation.

Deposits in the Canadian Cordillera are restricted to the Late Triassic/Early Jurassic (215-180 Ma) with seemingly two clusters around 205-200 and ~ 185 Ma. In southwest Pacific island arcs, deposits are Tertiary to Quaternary in age. In contrast **Endeavour 26 North** is considerably older with dates on mineralisation of 440 Ma (Late Ordovician). The dating principally initiated in this study shows that the 440 Ma " metallogenic punctuation mark" is well established, highlighting the extremely narrow range of the mineralising event.

6.7.6 Ore host and associated rock types.

Intrusions in Canadian alkalic porphyry systems range from fine through coarse-grained, equigranular to coarsely porphyritic and, locally, pegmatitic high-level stocks and dike complexes. Commonly there is multiple emplacements of successive intrusive phases and a wide variety of breccias. Compositions range from (alkalic) gabbro to syenite. The syenitic rocks vary from silica- undersaturated to saturated compositions. The most undersaturated nepheline normative rocks contain modal nepheline and, more commonly, pseudoleucite. Coeval volcanic rocks are basic to intermediate alkalic varieties of the high-K basalt and shoshonite series and rarely phonolites. At **Endeavour 26 North** the host rocks are potassium rich andesites and trachytes. No rock with the characteristic of

undersaturation is known. Endeavour 26 North is characterised by multiple emplacement of successive intrusive phases each more fractionated than the previous intrusion.

Chapter 7

ENDEAVOUR 26 NORTH: ALTERATION AND MINERALISATION

7.1 INTRODUCTION

The key to understanding any hydrothermal mineral deposit lies in understanding the spatial and temporal effects of the interaction of the hydrothermal fluid with the host rock. Fluids continuously modify the volume of rock surrounding fluid pathways by dissolution of pre-existing minerals and precipitation of new phases. It is rare for reactions to proceed to completion, so that the ore body and alteration system overall is a snapshot of a complicated and interrelated series of reactions which have proceeded to various stages of completion. The methodology for describing and interpreting the spatial and temporal evolution of a porphyry-Cu system has developed over the last several decades, based on the assumption that local equilibrium is attained between fluid and rock. The salient steps are:

1. Classification of alteration zones on the basis of mineral assemblages (Meyer and Hemley, 1967).
2. Description of the spatial distribution of hydrothermal alteration assemblages (Lowell and Guilbert, 1970; Rose, 1970).
3. Description of the mode of alteration (pervasive, vein, vein envelope), and documentation of the paragenetic relations (Gustafson and Hunt, 1975; Haynes and Titley, 1980; Preece and Beane, 1982).
4. Development of an alteration progress diagram to summarise the spatial and temporal evolution of the system (Titley, 1982).

The following description of the Goonumbla mineralisation in part reflects this historical development. Discussion of the nature of the alteration assemblages found in the Goonumbla Volcanic Complex is followed by a summary of the modes of alteration found in the Complex, and a discussion of notable differences with other well-documented porphyry systems. The distribution of alteration assemblages and mineral zonation within the Endeavour 26 North deposit is then considered. Finally, documentation of the paragenetic relations between veins and vein envelopes leads to an overview of the evolution of the deposit in time and space.

7.2 ALTERATION ASSEMBLAGES

Figure 7.1 compares the alteration assemblages occurring within the Goonumbla Volcanic Complex with a generalised scheme after Meyer and Hemley (1967). Potassic, propylitic and quartz–sericite (phyllic) are the dominant assemblages at Goonumbla. The potassic alteration is critically important, as the bulk of the high-grade mineralisation is associated with it.

The assemblage is defined by the abundance of secondary K-feldspar and it is e. Anhydrite occurs at Endeavour 26 North, but it is absent at Endeavour 22 and 27. Minor albitisation of plagioclase is a common phenomenon where strong to intense K-feldspar flooding has occurred in porphyritic rocks. It is preserved in plagioclase phenocrysts. Chlorite and sericite that occur in this assemblage post-date biotite and K-feldspar. Important secondary accessory minerals in this assemblage include apatite, rutile, fluorite and corundum.

The propylitic assemblages (Fig. 7.1) are widespread regionally in the Goonumbla Volcanic Complex. Epidote is characteristic but not ubiquitous and, together with, chlorite, sericite and carbonate commonly replace the phenocrysts in the volcanics. Irregular alteration 'spots' of epidote, chlorite, carbonate and pyrite may be up to several centimetres in diameter and, where intense, give the rock a strongly mottled appearance. Whilst common at Endeavours 22 and 27, this assemblage is weakly developed at Endeavour 26 North. Magnetite and pyrite associated with propylitic alteration forms a definable zone around mineralisation at Endeavour 27. Magnetite in association with propylitic assemblages appears to form a definable circular zone at Endeavour 26 South.

Sericitic assemblages (Meyer and Hemley, 1967) or quartz–sericite alteration (Rose, 1970) is common place in the Goonumbla Volcanic Complex (Fig. 3.7). Regionally these assemblages are related to major structural trends within the volcanic complex (Fig. 3.7). Only at Endeavour 26 North does the quartz–sericite alteration appear to be intimately related to Cu mineralisation. At depth in DDH46, quartz–sericite alteration is associated with anhydrite. Chalcopyrite, pyrite and minor galena and magnetite define subzones in this alteration assemblage. Whilst not listed as a sericitic assemblage by Meyer and Hemley (1967), quartz–sericite–anhydrite is documented as a phyllic alteration assemblage at the El Salvador deposit (Gustafson and Hunt, 1975).

Argillic assemblages have been noted at Nash's Hill, ~5 km to the south, in some percussion holes 2 km northeast of Endeavour 26 North and at Endeavour 29. All the minerals listed as intermediate and advanced assemblages are present in these areas. Epithermal-style veining with minor Au has been located at Endeavour 29. Nash's Hill exposes argillically altered breccias, which may be hydrothermal in origin. No Au has been found to date in this area.

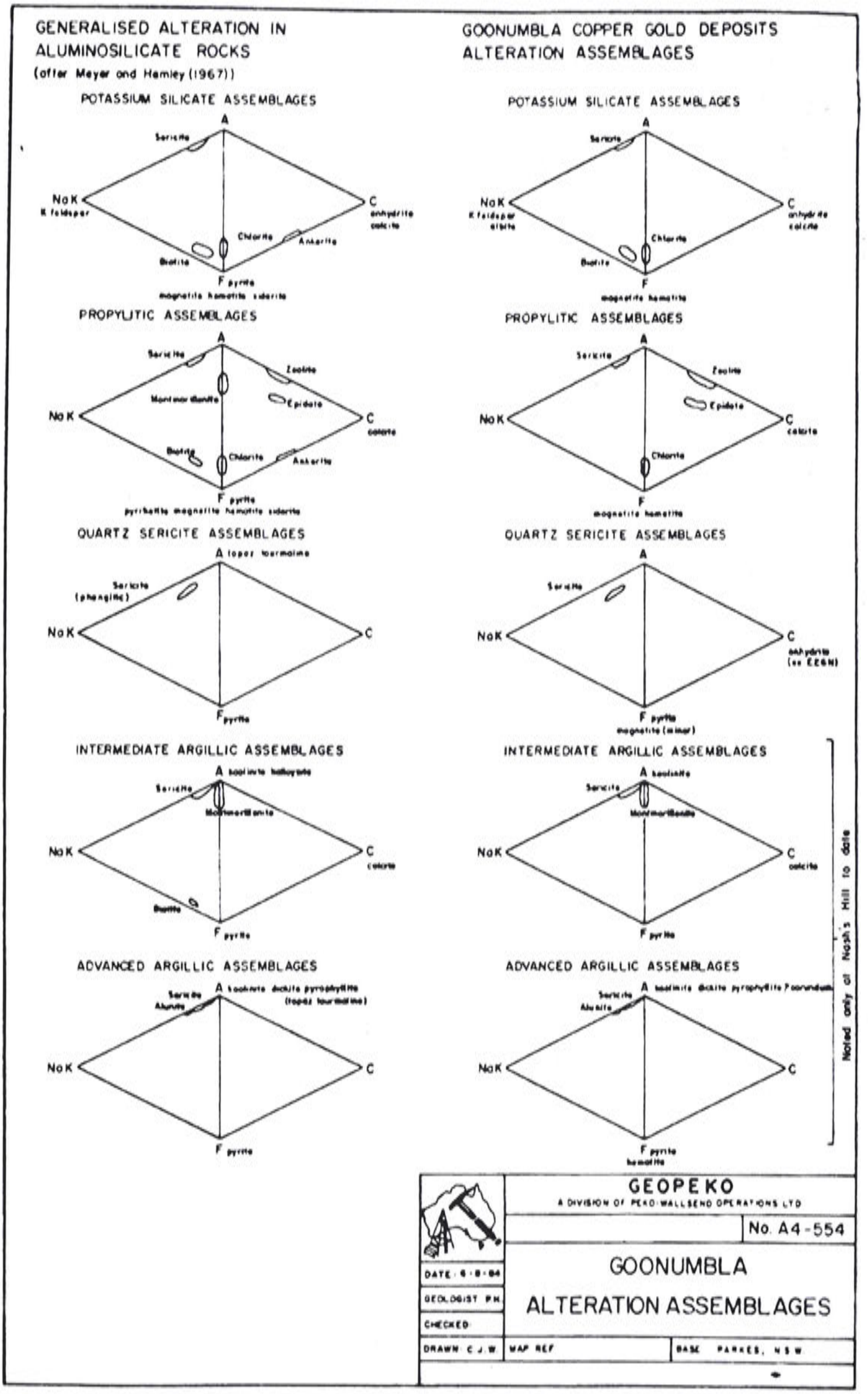

Figure 7.1 Comparison of Goonumbla alteration and generalised alteration assemblages.

7.3 ALTERATION MODES

The mode of alteration is important when considering the alteration systems of the Goonumbla Volcanic Complex. The pervasively altered zones, which are zoned laterally over hundreds of metres, and typify the southwest USA porphyry-Cu deposits (Rose and Burt, 1979), are not present in the Goonumbla alteration systems.

The modes of alteration common to the Goonumbla Volcanic Complex can be divided into three categories: selectively pervasive alteration; pervasive alteration; and veins and vein envelopes. These terms are modified after Titley (1982). The superimposition of these modes of alteration can result in pervasive, fracture-related quartz–sericite alteration juxtaposed against site selective alteration of plagioclase to sericite, carbonate and epidote; a propylitic assemblage as defined by the previous section. Similarly 'potassic' veins containing quartz, carbonate, K-feldspar and bornite may radiate through rock that has been selectively pervasively altered to an assemblage of chlorite, carbonate and magnetite, and therefore is arguably a propylitic assemblage. Clearly, the mode of alteration needs to be considered when trying to define zones of alteration. Similarly the timing of alteration is significant, and is addressed in a later section.

7.3.1 Selectively pervasive alteration

This alteration mode refers to the selective alteration of specific minerals. It occurs within both volcanics and intrusive rocks, and may be very extensive. It is commonly manifest in mafic minerals, where, for example, hornblende and biotite are converted to chlorite and sericite. Ragged remnants of biotite may remain. Plagioclase, particularly in intrusive rocks, commonly has variable amounts of sericite dusting in the crystals. Carbonate and, less commonly, epidote may selectively alter the plagioclase.

7.3.2 Pervasive alteration

Pervasive alteration refers to replacement of primary minerals by a secondary assemblage with almost total destruction of the primary texture. This type of alteration is particularly confined to:

1. quartz–sericite assemblages
2. potassic assemblages, notably pervasive secondary biotite and pervasive K-feldspar flooding
3. argillic assemblages.

1. Quartz–sericite assemblages typically form pervasive zones from centimetres to tens of metres in apparent thickness. Rarely do pervasive quartz–sericite zones obtain

thicknesses over 100 m. These zones account for ~30% of the altered volume of rock around Endeavour 26 North. They typically consist of a fine-grained aggregate of saccharoidally textured secondary quartz and sericite. This alteration commonly grades into zones where relict primary textures can be seen, with sericite as the dominant secondary mineral. Lesser chlorite and quartz may also be present. Sulphides are disseminated throughout.

2. Pervasive potassic alteration is the most complex alteration style, and commonly the hardest to identify, particularly in trachytes. In porphyritic rocks the groundmass is typically transformed into a microgranular aggregate of K-feldspar, whilst plagioclase phenocrysts are either wholly or partly replaced by an aggregate of K-feldspar and sericite. Commonly albitised and sericitised cores of plagioclase laths will remain even in zones of intense K-feldspar development. Rare corundum has been reported in these sites by Barron (1984; unpublished Geopeko report), but not confirmed by this study. Pervasive and vein-like forms of intergrown quartz and K-feldspar commonly form an 'aplitic' textured phase. Patchy development of anhydrite, quartz, apatite and accessory fluorite and rutile accompany this pervasive potassic alteration.

The texture of potassic flooding at Goonumbla is clearly different from the type example of potassic alteration from the San Manuel Deposit. In reference specimens (Southwest USA Porphyry Copper Alteration Suite-Reference Collection), K-feldspar occurs as veinlets with, or without, quartz, and replaces primary K-feldspar and plagioclase. K-feldspar replaces plagioclase crystals, however, the resulting texture is similar to the original primary texture. This is in contrast to the highly modified microgranular texture resulting from intense potassic alteration at Goonumbla.

Pervasive biotite alteration is patchily developed on the margins of, and on top of, the potassic zone at Endeavour 26 North. It is more widespread at Endeavour 22 and 27 and, in particular, it forms a broad halo around Endeavour 22. At Endeavour 27 carbonate, sericite and biotite occur pervasively. Biotite is very finely divided (0.01–0.03 mm) and difficult to detect without a microscope. For this reason secondary pervasive biotite may not have been detected at other prospects.

3. Pervasive development of argillic alteration is present at the Nash's Hill area in the form of alunite within a volcanic breccia. It is possible that the alteration zoning and sulphide–oxide species may define an ancient hot springs system. The assemblages almost totally detexture the pyroclastic host rocks and are strongly controlled by lithology. Selectively pervasive propylitic assemblages surround the argillic zone identified at Nash's Hill.

7.3.3 Veins and vein envelopes

Veins and vein envelopes are the most obvious style of 'alteration' at Endeavour 26 North, and, indeed at most porphyry-Cu deposits (Beane and Titley, 1981). Specific discussion of vein – vein envelope zoning is, however, surprisingly lacking in the literature. Study of this style of alteration is critical at Goonumbla as it is responsible for the bulk of the mineralisation. Even apparently disseminated mineralisation can be shown to follow microveinlets.

It is generally recognised (e.g. Rose and Burt, 1979) that transport of materials involved in wallrock alteration can occur by infiltration (mass movement due to fluid flow through the rock), or by diffusion (transport by diffusion of chemical species through stagnant pore fluids). Infiltration dominates in, and near, fractures through which fluid is flowing, whilst diffusion may be dominant a short distance away. At Goonumbla the overall patchy and discontinuous nature of pervasive alteration, and the juxtaposition of alteration styles and assemblages attests to the dominance of infiltration as the major means of mass transfer. Hence the examination of vein distribution is a valid way of typing alteration zoning. When combined with selectively pervasive and pervasive styles of alteration, generalised alteration zones can be defined.

Detailed logging of vein assemblages, their density and average thickness was completed on 40 diamond-drillholes through the deposit. Examples of the detailed logging are enclosed in Plans 2 and 3 (Part 2). An excellent lateral zonation of vein types can be demonstrated around the central intrusives at Endeavour 26 North, and an indication of vertical zonation can be documented.

The results of the logging of Endeavour 26 DDH 38 and 39 are included as an example of the graphical approach adopted (Plans 2, 3). The plans document lithology, selective alteration, pervasive alteration and distribution, Cu and Au grades, average vein thickness, and density and magnetic susceptibilities.

7.4 ENDEAVOUR 26 NORTH ALTERATION ZONES

7.4.1 Sulphide zonation

During the course of this study, the zoned relationship of sulphides with respect to mineralised centres was highlighted. This is shown in Figure 7.2, which shows the zonal relationship of sulphides with respect to the Endeavour 26 North mineralised centre. Information was derived from all available drillhole data, and ~25 m of core from each diamond-drillhole at Endeavour 26 North was examined in detail. The intercepts examined are generally just below the base of oxidation, and the aim of the exercise was to produce a plan of primary alteration below the base of oxidation. The patterns that emerge highlight a central bornite-dominant zone (>0.5% bornite) with lesser chalcocite and digenite, and a

chalcopyrite-dominant zone (>0.5% chalcopyrite) that appears to form an annular pattern and, in part, overlaps the bornite dominant zone. Surrounding and overlapping these zones is the pyrite-dominant zone (1–5% pyrite). On average the pyrite zone contains <3% pyrite by volume. The outer limits of this zone are somewhat arbitrary. The patterns shown must be qualified by the relatively limited data points; however the general zonal pattern is real and could be expected at other mineralised centres of significance. Noteworthy is the scale of these zones at this level. The bornite zone is ~200 m in diameter, the chalcopyrite zone ranges from 350 to 450 m in diameter, and the pyrite zone can extend from 600 m to >1 km from the deposit. This must be qualified by the probability of this zone overlapping with other barren pyritic horizons.

7.4.2 Potassic alteration zones

Secondary K-feldspar forms a coherent zone some 300–450 m across at Endeavour 26 North (Fig. 7.3). The bulk of mineralisation is contained within the potassic zone, which can be further separated into three subzones as noted in Chapter 6 (section 6.4). These are the inner K-feldspar subzone centred on QMP2, the outer K-feldspar subzone centred on QMP1, and the biotite–K-feldspar subzone. The names reflect the dominant potassic alteration minerals in each case. The outer margin of the biotite–K-feldspar subzone corresponds approximately to the 0.3% Cu grade contour. Bornite gives way to chalcopyrite as the dominant sulphide in the outer parts of this subzone. The boundary between the biotite–K-feldspar subzone and the outer K-feldspar subzone corresponds with the outer limits of the high-grade Cu mineralisation (>1.0% Cu).

The modes of the potassic alteration are summarised in Figure 7.4. The biotite–K-feldspar subzone is characterised by a distinctive fine-grained dark rock reflecting the abundance of biotite. The biotite occurs as vein envelopes with minor quartz as rare, fine veinlets. Biotite and K-feldspar replace pyroxenes and pre-existing biotite. They replace them with clusters of finely divided biotite. Pre-existing biotite will recrystallise and often form a spotted texture in the rock. The K-feldspar is perthitic and always impregnated with very fine hematite.

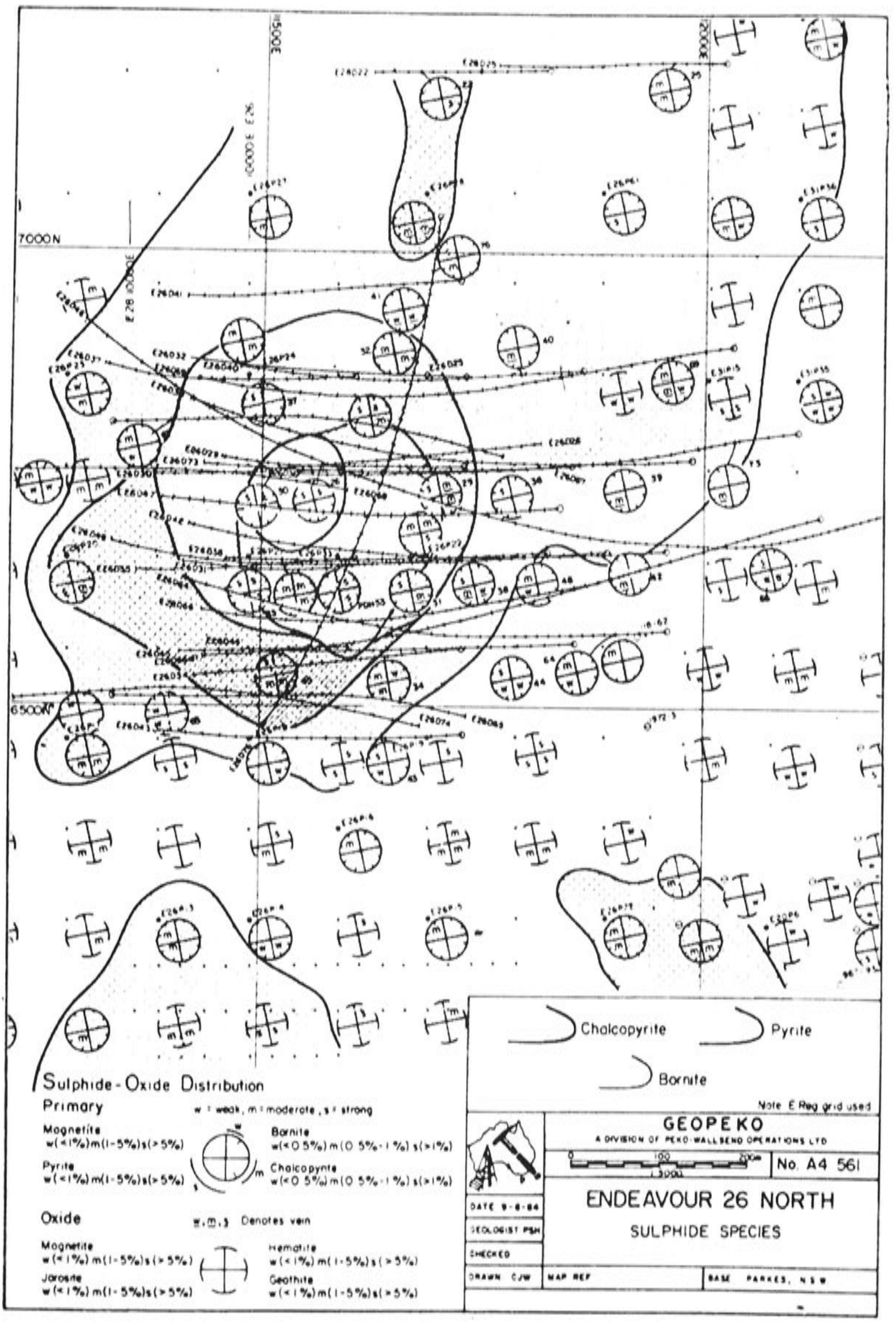

Figure 7.2 Map showing the zoning of sulphide species around the Endeavour 26 North area based on analysis of RAB chips.

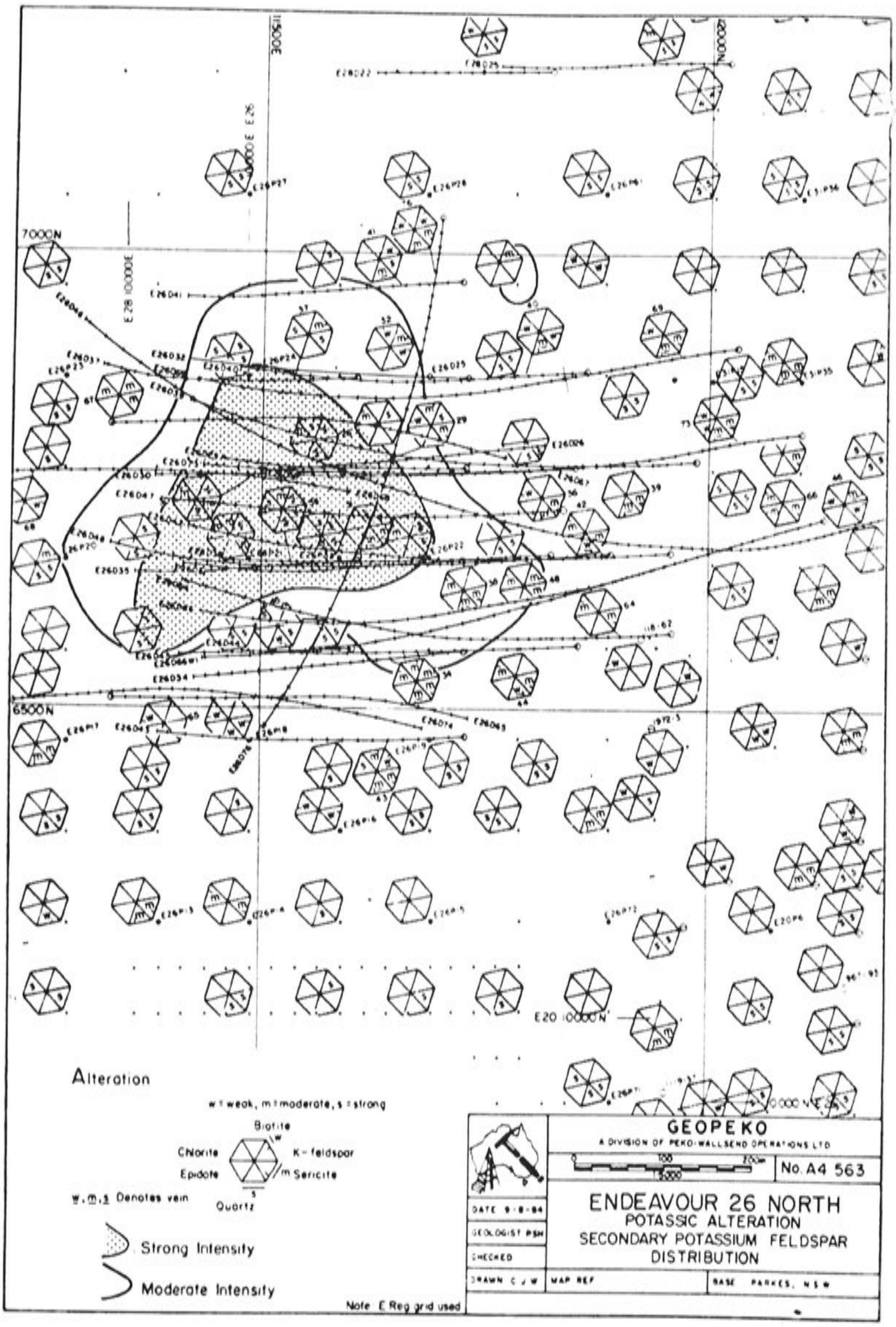

Figure 7.3 Map showing the zoning of secondary K-feldspar around the Endeavour 26 North area based on analysis of RAB chips.

Coarse fragmental heterogeneous tuff	minor control over vein walls
Trachyte	quartz K feldspar and gypsum veinlets dominant form of K alteration
Mafic volcanics	development of K feldspar selvedge with quartz bornite stockwork veins
Monzonite intrusions	minor control
Vein mineralogies	biotite , quartz, chlorite, magnetite quartz, K feldspar, gypsum, bornite, chalcopyrite quartz, bornite, chalcopyrite, (stockwork veins) gypsum, quartz, chlorite, chalcopyrite

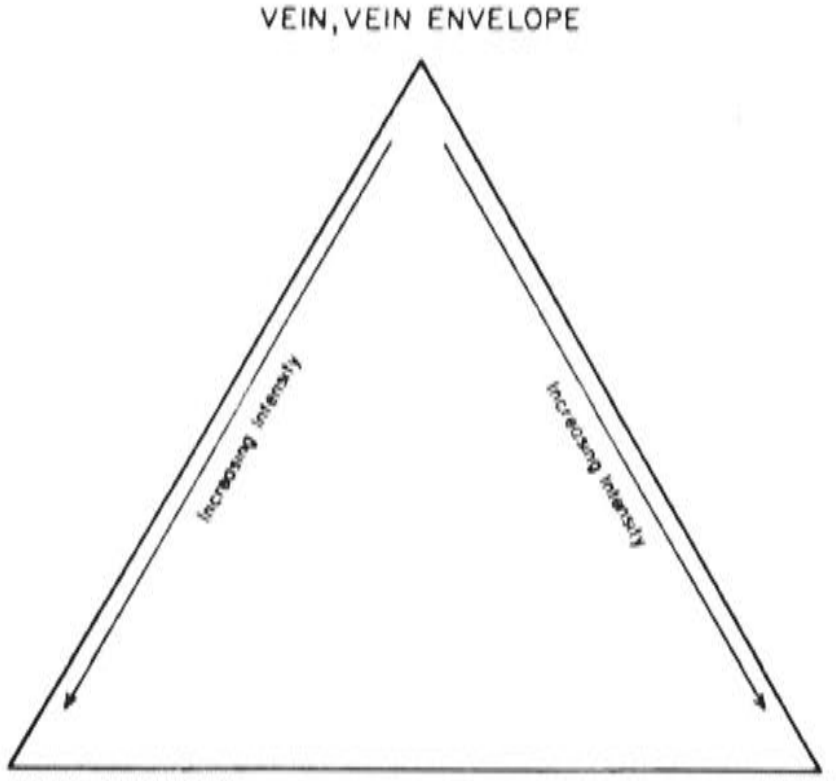

Coarse fragmental heterogeneous tuff	mantling and replacement of plagioclase phenocrysts by K feldspar	Coarse fragmental heterogeneous tuff	pervasive introduction of K feldspar with hematite dusting
	complete replacement of plagioclase by sericite, biotite		pervasive aplitic composition, introduction
	formation of fine biotite from chloritic centres		
Trachyte	mantling and replacement of plagioclase phenocrysts when crossed by K feldspar bearing veinlets	Trachyte	no pervasive alteration
	secondary quartz, anhydrite, gypsum		
Mafic volcanics	———	Mafic volcanics	pervasive secondary biotite
Monzonite intrusions	mantling and replacement of plagioclase phenocrysts	Monzonite intrusions	pervasive K feldspar introduction
	secondary biotite in chloritic centres		aplitic introduction
Diorite	secondary biotite		

GEOPEKO
A DIVISION OF PEKO-WALLSEND OPERATIONS LTD

No. A4 579

ENDEAVOUR 26 NORTH
CHARACTERISTICS OF POTASSIC ALTERATION

DATE: 8-8-84
GEOLOGIST: P.S.H
CHECKED:
DRAWN: C.J.W
MAP REF
BASE: PARKES, N.S.W.

Figure 7.4 Map showing the modes of potassic alteration at Endeavour 26 North area.

There is a narrow transition between the biotite–K-feldspar subzone and the outer K-feldspar subzone, marked by an increased reddening of the rock due to hematite dust in the secondary K-feldspar that overprints the biotite. At the hand-specimen scale, the K-feldspar is observed replacing biotite along microfractures and vein margins (Plate 7.1). In thin section the fine-grained, textureless, cloudy feldspar surrounds and initially bleaches the biotite, and then total replacement can leave a cluster of rutile needles. The outer K-feldspar subzone, which in part overprints QMP1 and the Endeavour 31 stock as well as the host volcanics, is the most intensely altered and mineralised zone in the deposit. Here quartz veining (Stage 4 below) is so dense that associated alteration of the rock amounts to a pervasive flooding by K-feldspar and quartz. The intensity of alteration is such that most primary textures and earlier alteration phases have been obliterated in what is now a pink aphanitic rock. In thin section the rocks are a turbid mass of K-feldspar, or in more extreme situations they appear aplitic, consisting entirely of saccharoidal quartz and K-feldspar. The density of quartz veining (Stages 5–7 below) in the inner K-feldspar subzone is considerably less than in the other potassic subzones. Hence the intensity of alteration and Cu grade are correspondingly low.

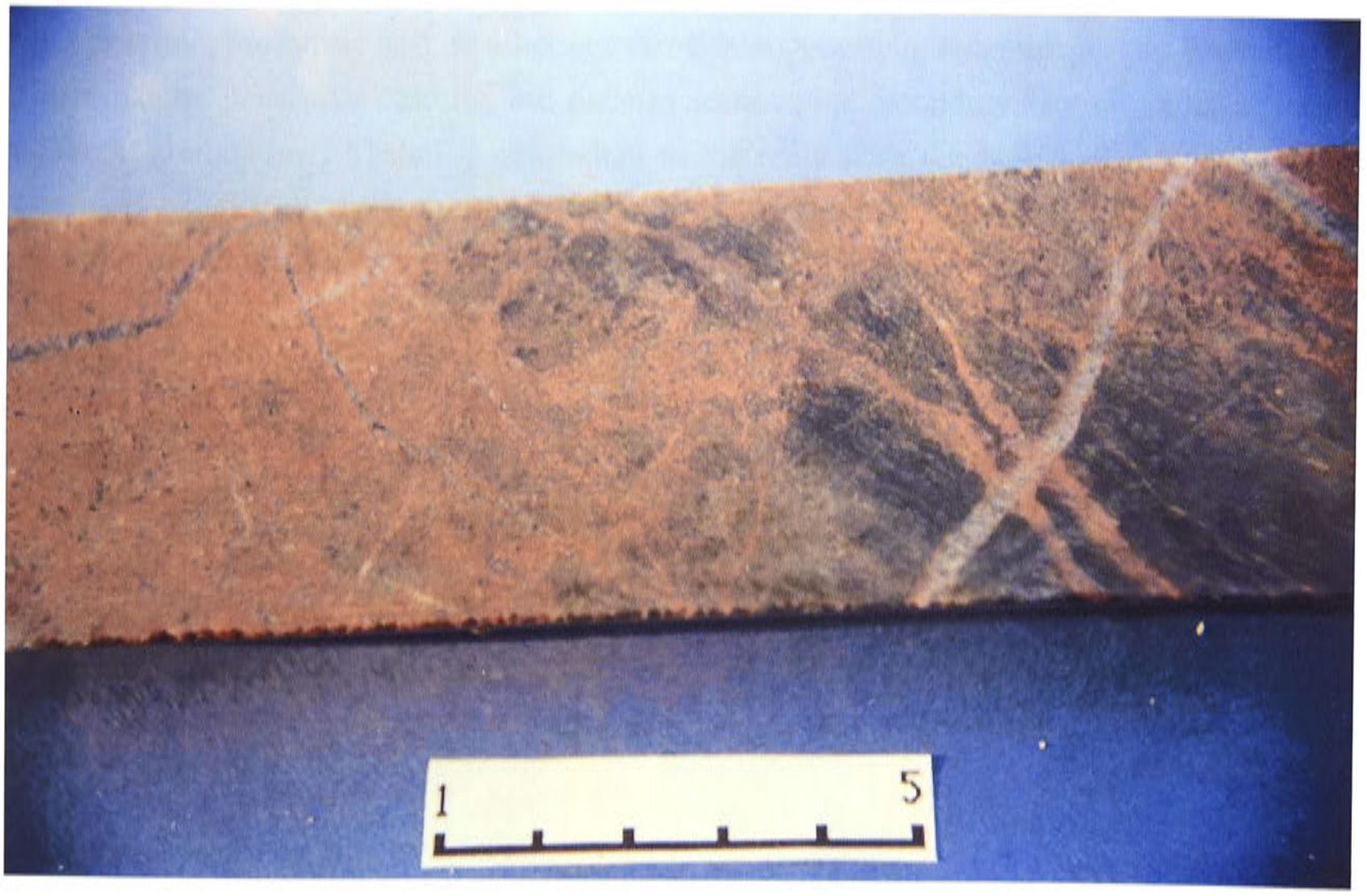

Plate 7.1 K-feldspar replacing biotite along microfractures and vein margins leading to potassic flooding on the left hand side.

7.4.3 Magnetite distribution

The distribution of secondary magnetite is complex but important for exploration in the Goonumbla Volcanic Complex. At Endeavour 26 North magnetite is a minor but significant phase in the biotite–K-feldspar subzone. Its distribution at the level of Figure 7.5 yields a coherent pattern, but at depth this is severely modified by intense potassic and quartz–sericite alteration. The abundance of magnetite in this zone is generally around 1–4 %. It occurs as fine intergrowths with biotite, as fine isolated crystals and small clusters in the groundmass. In the outer margins of the biotite subzone small biotite clusters occur rimmed by K-feldspar. Magnetite or hematite form the core of these features.

The magnetite content of the rocks decreases abruptly from the biotite–K-feldspar subzone to the outer K-feldspar zone, that is, from the margins of the system to the centre. In thin section, bornite, which coexists with hematite as distinct grains, is noted rimming magnetite.

7.4.4 Chlorite

As mentioned above, chlorite is a widespread alteration assemblage, occurring in association with potassic, propylitic and, to a lesser extent, quartz–sericite assemblages. At Endeavour 26 North patchy pervasive chlorite and sericite accompany secondary biotite. Chlorite forms a coherent zone (Fig. 7.6) that is coincident in the main with the biotite–K-feldspar subzone, but overlaps with the fringing phyllic zone. On average chlorite constitutes ~0.5–10% of the rock through this zone but it is commonly difficult to distinguish, at a hand-specimen scale, chlorite from sericite

In thin-section chlorite is clearly in part retrograde after biotite; however chlorite also occurs occasionally in veins or veinlets. The most common form for chlorite is as retrograde replacements after secondary biotite. This is particularly evident after the biotite spots mentioned above. These textures are often overprinted by K-feldspar, which suggests that peripheral propylitic alteration occurred at the same time as the early biotite alteration.

7.4.5 Quartz–sericite alteration

The quartz–sericite (phyllic) assemblage forms a broad irregular zone around Endeavour 26 North (Figs 7.7, 7.8). This zone clearly coalesces with other large quartz–sericite altered zones, and the definition of a discrete phyllic zone associated with Endeavour 26 North based solely on *silicate* assemblages is not possible. However, by combining these data with the sulphide species map, a poorly defined quartz–sericite–sulphide zone related to Endeavour 26 North is possible. The inner boundary of the quartz–sericite zone, depicted in the above figures, is somewhat arbitrary as narrow vein – vein envelope style quartz–sericite alteration zones cut through the central potassic zone (see below).

The modes of phyllic alteration are summarised in Figure 7.9. Sericitic replacement occurs in the three forms mentioned above. Selective replacement of fragmental units picks out plagioclase and mafic sites, and forms clusters around these sites. This style of alteration forms on the periphery of vein and vein envelopes. The vein and vein envelope style forms a uniform vein mineralogy unrelated, generally, to rock type. While the great bulk of the sericitic alteration occurs peripheral to, and away from, the mineralised centre, some narrow veinlets of sericite occur in the mineralised centre, often following stage 5 veins. These have yet to be tested but they are thought to be totally magmatic in origin, and may represent refluxing of condensed acid fluids.

Argillic alteration, as defined to date, has only been recognised to the northeast of Endeavour 26 North and well away from the deposit, and does not appear to form well-defined zonal patterns.

7.5 THE SPATIAL AND TEMPORAL EVOLUTION OF THE ENDEAVOUR 26 NORTH HYDROTHERMAL SYSTEM

The study of Endeavour 26 North has been facilitated by the lack of large mineral-destructive, pervasive alteration zones. The detailed examination of vein and vein envelopes in drillcore has proven to be the most successful way of characterising alteration zonation and paragenesis. Plans 2 and 3 show the detailed logging of the various vein and vein envelope phases, along with other parameters such as vein number per metre and vein thickness. The spatial and temporal position of the principal vein alteration types, and the best estimates of the more pervasive phases, are shown in Figure 7.10. This presentation is a modification of an alteration progress diagram (Titley, 1982). A schematic representation of alteration mineralogy and relative abundances forms the other half of the diagram. The general sequence of events depicted in Figure 7.10 is as follows:

Stage 1: Vein dyking and incipient fine veining representing the precursor to QMP1.

Stage 2: Pervasive and selectively pervasive albitisation of feldspars. Concomitant alteration of magmatic biotite to chlorite, quartz, calcite and fluorite.

Stage 3: Pervasive and vein envelope controlled biotite development with associated anhydrite, alkali feldspar and magnetite.

Stage 4: Veinlets containing quartz, alkali-feldspars, anhydrite, fluorite, biotite, apatite and rutile. Bornite is the main Cu ore mineral, with chalcopyrite and hematite also present. Veins of this stage range in density from ~hundreds to thousands veinlets per metre.

Stage 5: Multi-stage veins ranging in thickness from 50 to 100 mm. These stockwork-style veins consist of quartz with alkali-feldspars, anhydrite, sericite and carbonate. Bornite is the dominant ore mineral with minor chalcopyrite. Au, Au tellurides and Pb selenides associated at this stage.

Stage 6: Magmatic–hydrothermal brecciation and vein dyke development.

Stage 7: Fine veinlets of quartz, alkali-feldspar, biotite and anhydrite. Chalcopyrite is the dominant sulphide with subordinate bornite.

Stage 8: Straight-walled, milky quartz veins with minor anhydrite, fluorite, bornite and chalcopyrite. These veins are 5–10 mm thick.

Stage 9: A quartz, sericite, pyrite ± chalcopyrite overprint which is pervasive or vein – vein envelope controlled.

Stage 10: Veins of carbonate, sulphate and zeolites.

Stage 11: Anhydrite to gypsum veins.

Stage 2 albitisation tends to preferentially alter clasts in trachyandesitic and trachytic breccias. Within the Endeavour 31 stock, as well as QMP 1 and QMP2, plagioclase is selectively replaced by patchy albite and fine sericite flakes. As noted above, in the zones of intense alteration and mineralisation albitised and sericitised relicts of plagioclase laths remain.

Stage 3 biotite formation is best developed in trachyandesites. Within the Endeavour 31 stock, QMP1 and QMP2, albite phenocrysts are impregnated with very fine biotite and vein envelope control is more obvious. The biotite–K-feldspar subzone is easily mapped, as biotite and alkali feldspars from Stages 1, 2 and 3 are preserved through a weak to moderate overprint of later veins with a selvage of K-feldspar alteration. The secondary K-feldspar is cloudy with very fine iron-oxide inclusions, hence the vein margin appears bright pink-red against a darker biotitised rock. Within the outer K-feldspar subzone the intensely altered, aphanitic, pink rock contains trails of fine sulphides attesting to the presence of Stage 4 veins (Plate 7.2). Hydrothermal biotites are shown in Figure 7.11 in comparison to primary, magmatic biotites.

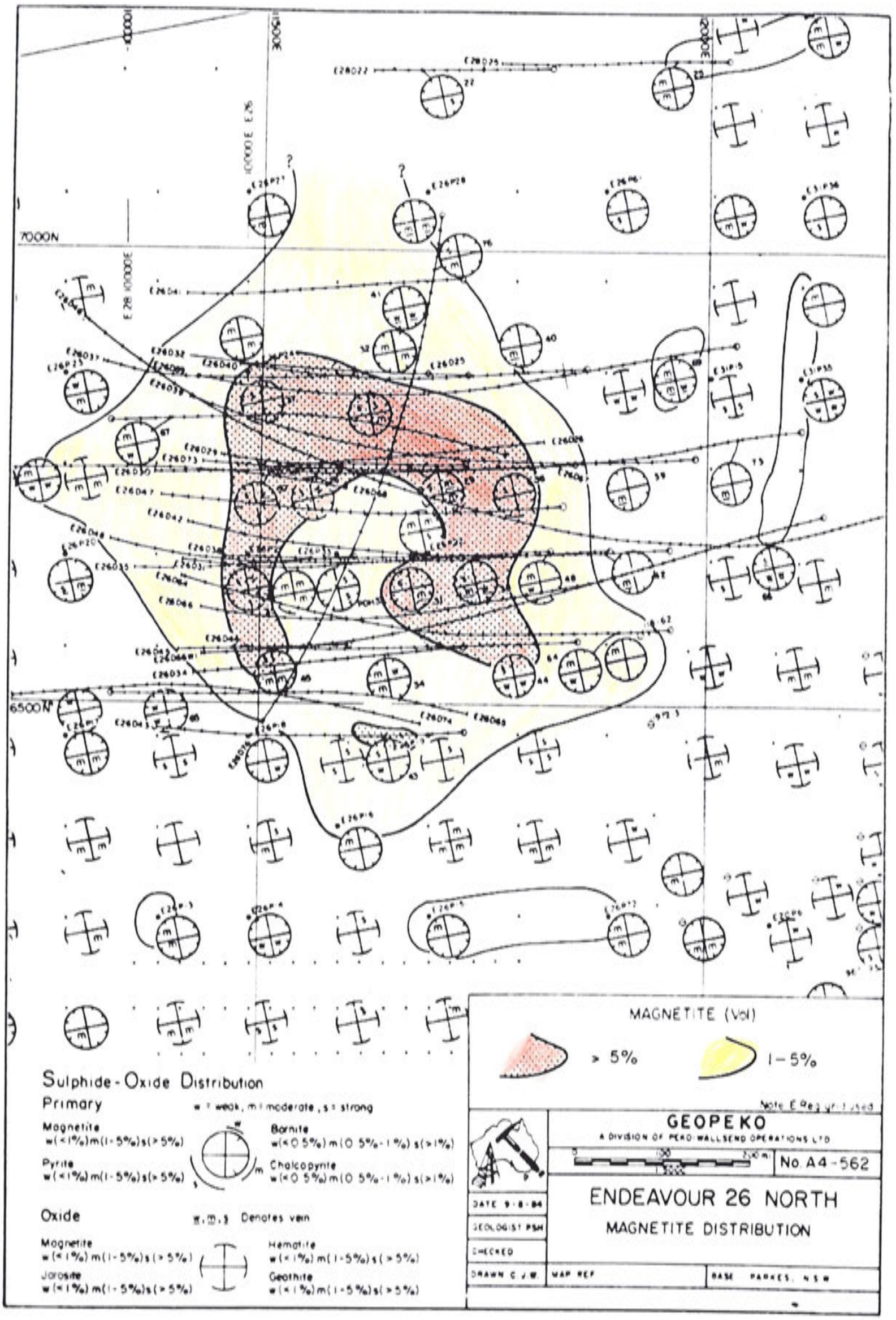

Figure 7.5 Map showing the zoning of magnetite around the Endeavour 26 North area based on analysis of RAB chips.

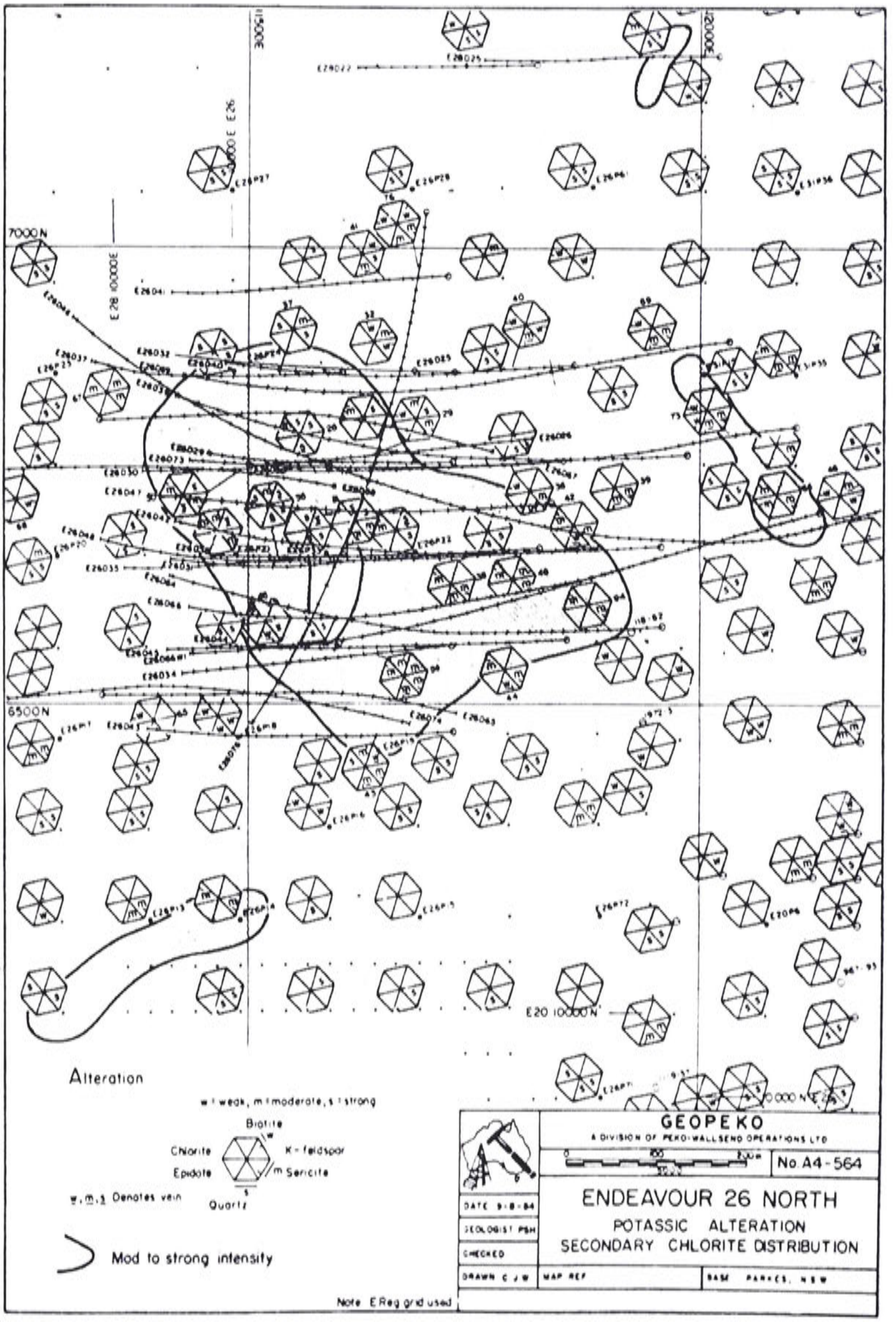

Figure 7.6 Map showing the distribution of chlorite around the Endeavour 26 North area based on analysis of RAB chips.

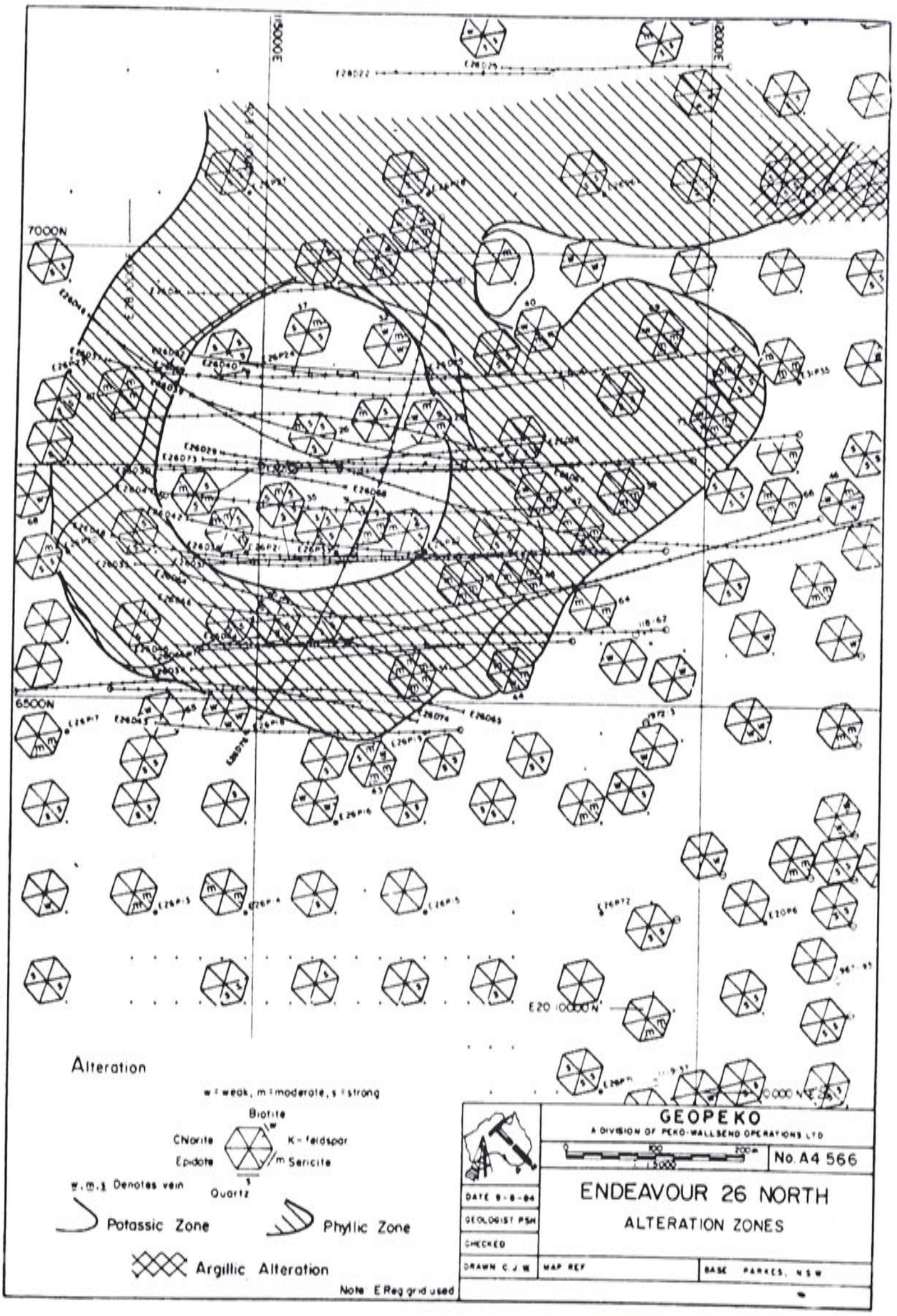

Figure 7.7 Map showing the distribution of phyllic alteration around the Endeavour 26 North area based on analysis of RAB chips.

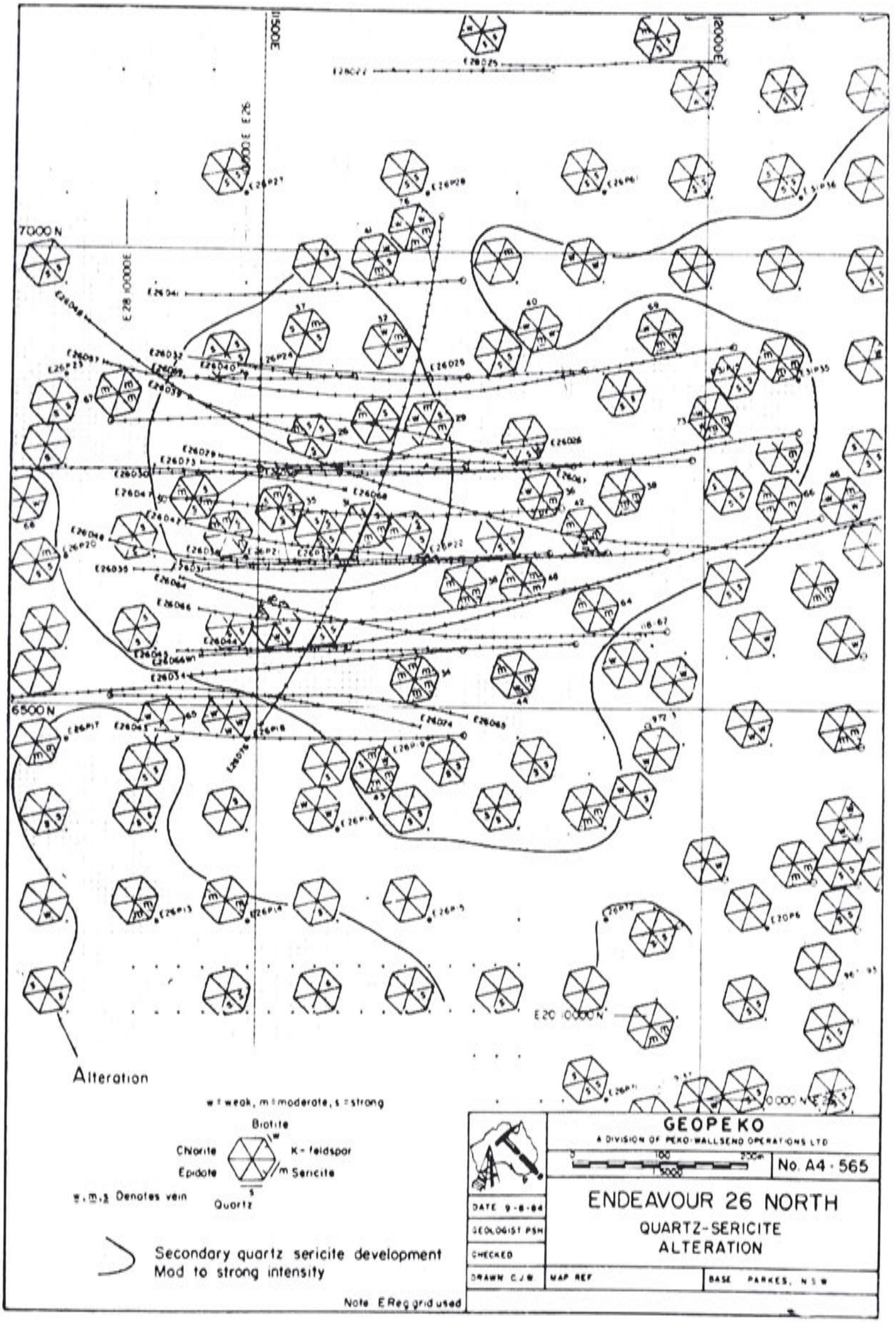

Figure 7.8 Map showing the distribution of quartz–sericite alteration around the Endeavour 26 North area based on analysis of RAB chips.

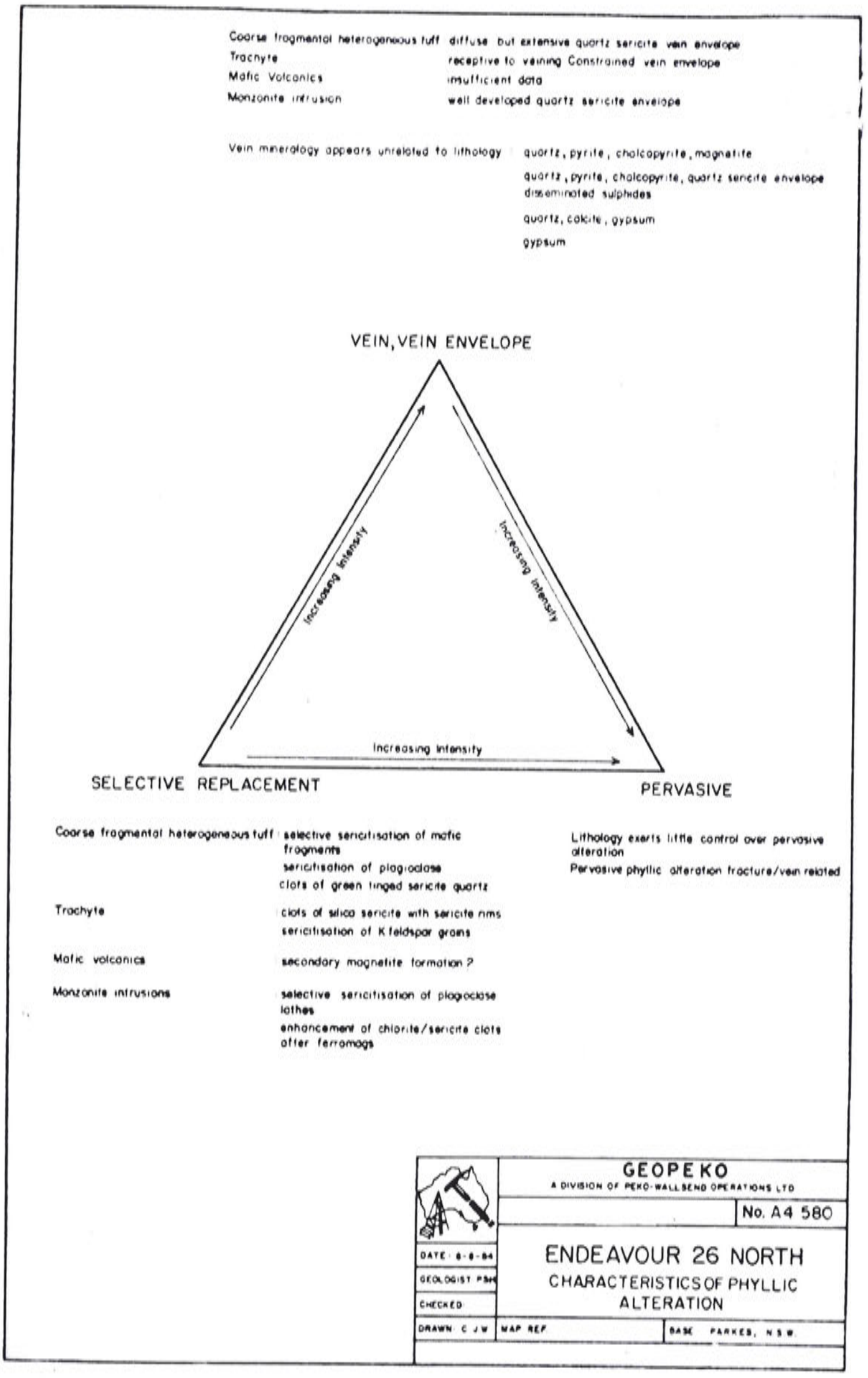

Figure 7.9 Diagram showing the modes of phyllic alteration at Endeavour 26 North area.

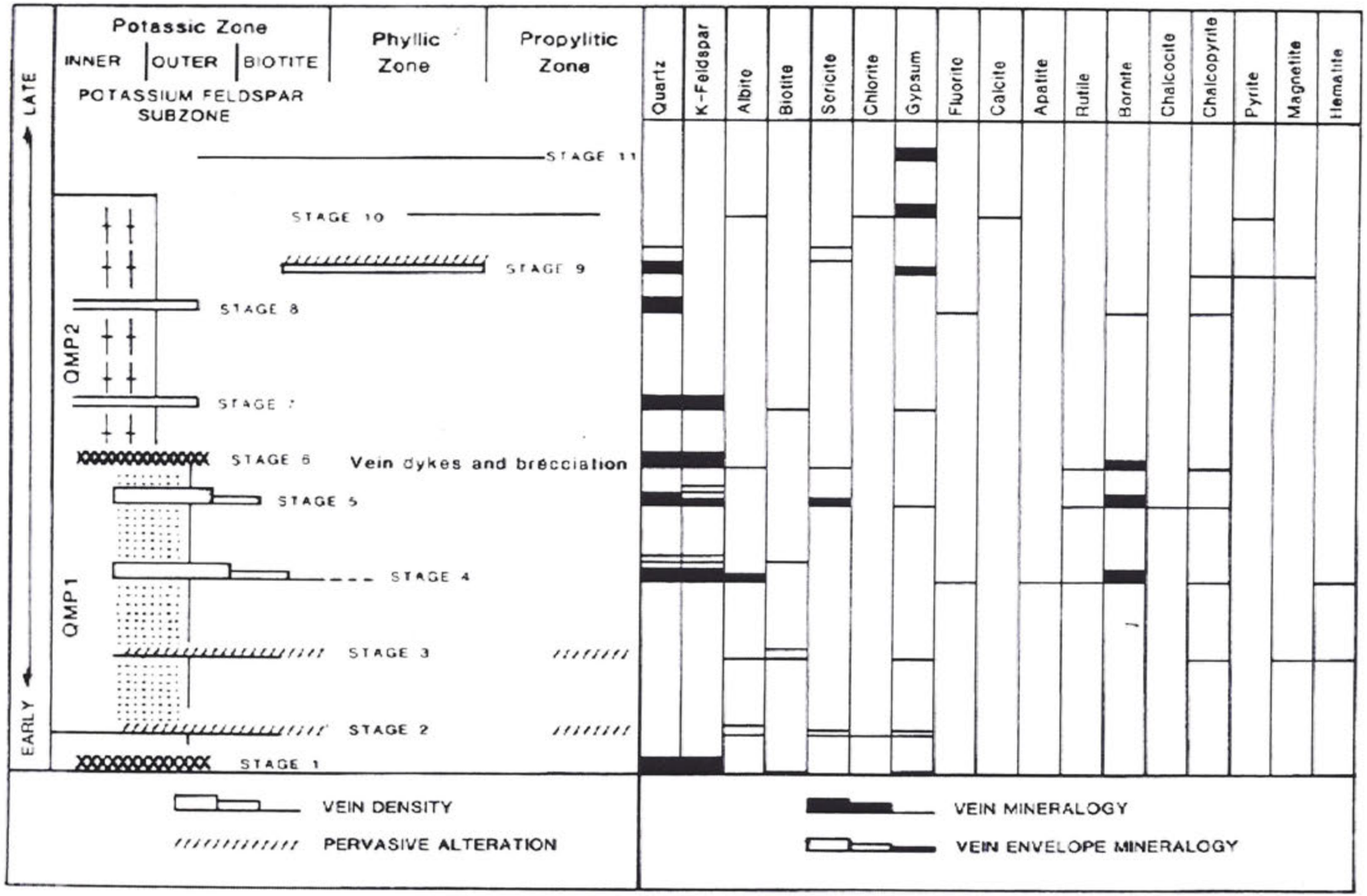

Figure 7.10 Alteration progress diagram for Endeavour 26 North.

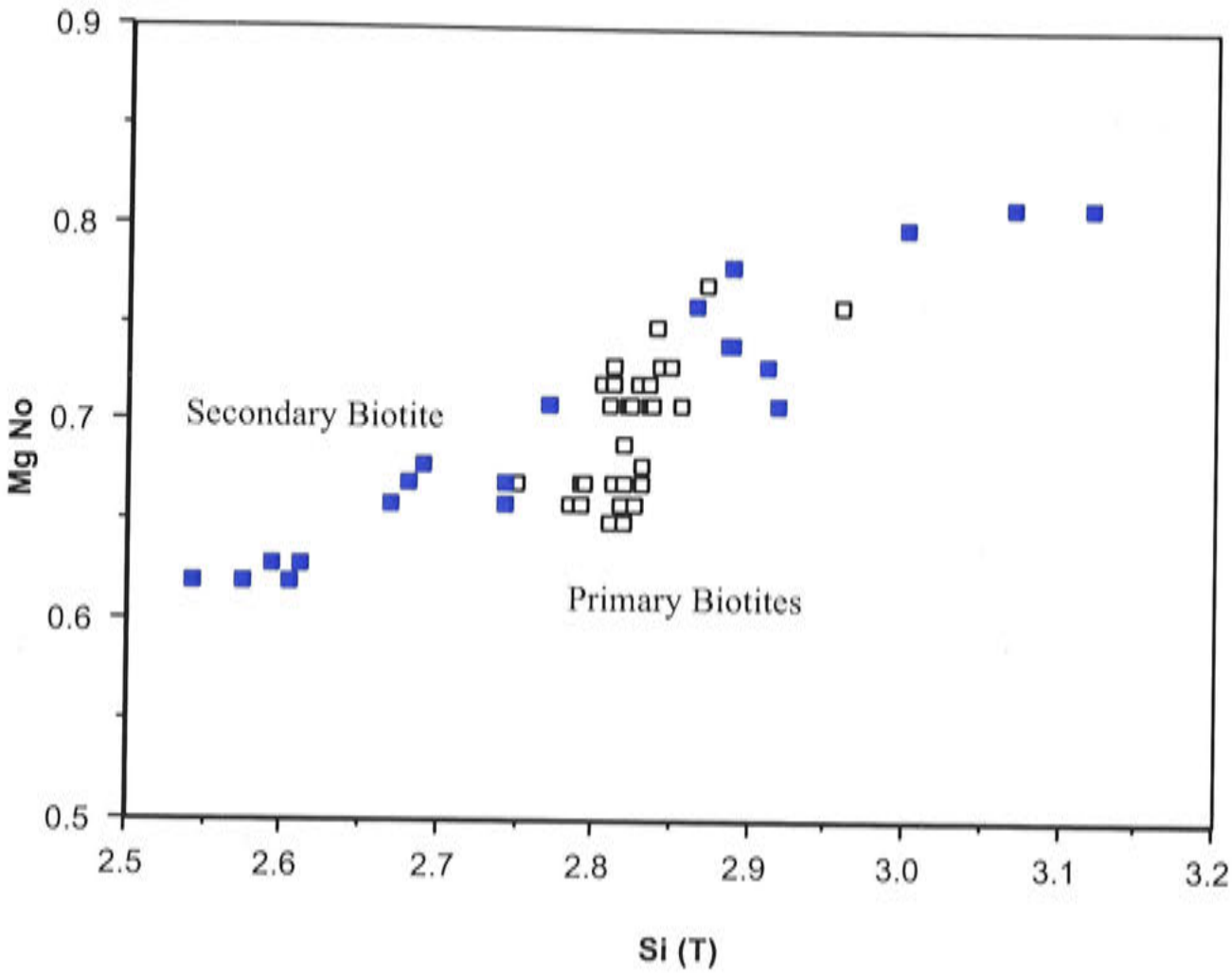

Figure 7.11 Variation in Mg number vs Si(T); hydrothermal vs primary biotites.

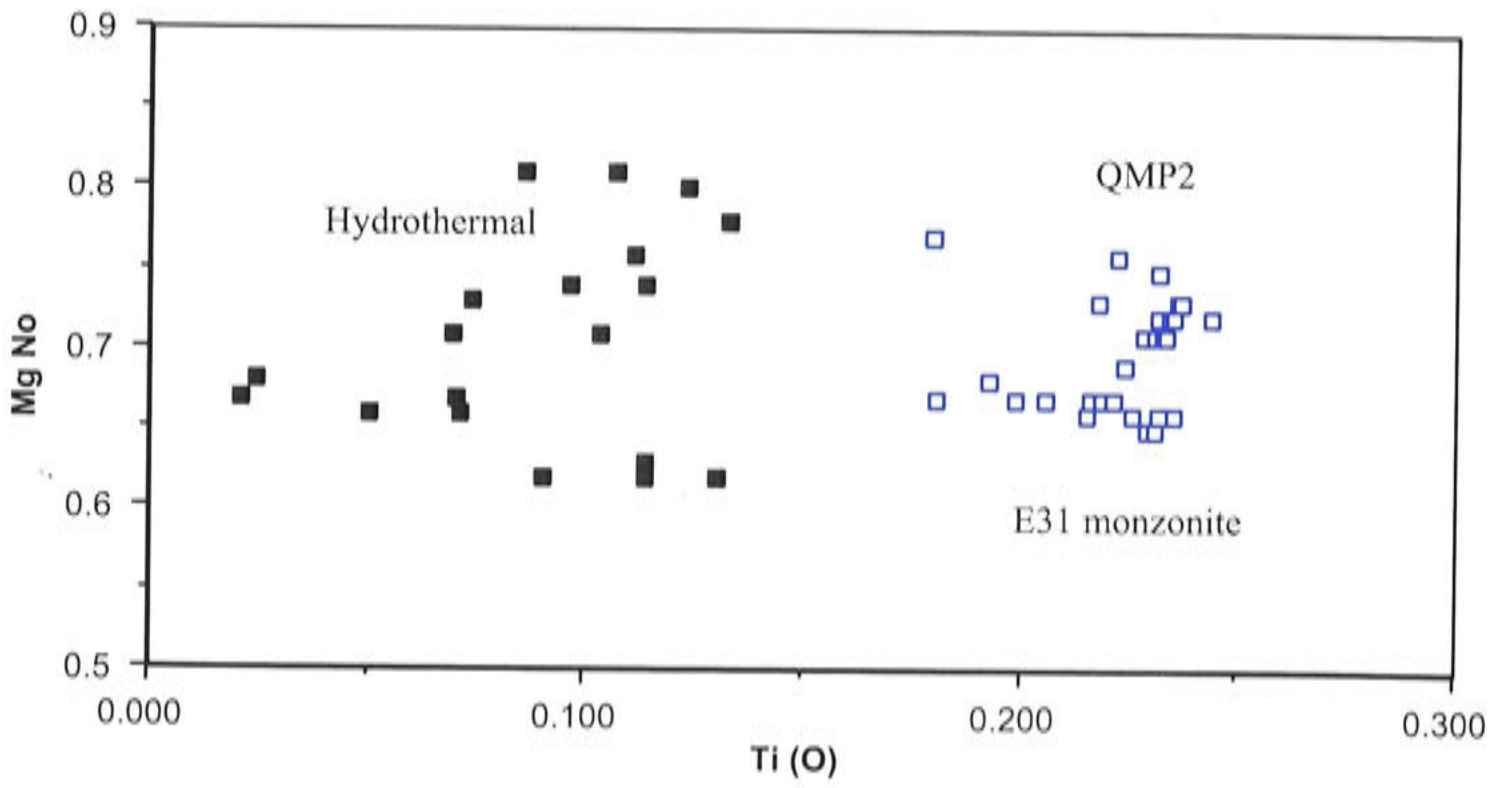

Figure 7.12 Variation in Mg number vs Ti (Octahedral Site); primary vs hydrothermal biotites

These plots show a clear separation between secondary and primary biotites based on Si (tetrahedral site) and Ti (octahedral site). The primary biotites form a tight cluster, whereas the hydrothermal varieties exhibit more of a spread — particularly with respect to Mg number, a reflection of redox state.

Plate 7.2 Sulphide trail of Stage 4 veins.

Stage 4 veinlets are commonly discontinuous, and develop irregular vein margins with euhedral quartz crystals projecting out from the vein into the vein margin. The vein margin characteristically forms an interlocking mosaic of K-feldspar rimmed with albite or quartz. Where such veins crosscut albitised plagioclase crystals, a thin selvage of quartz and K-feldspar is deposited.

This stage is the peak depositional stage for sulphides. Bornite, chalcopyrite and hematite are the stable minerals in this stage. Sulphides and sulphates are commonly intergrown. Bornite rimming magnetite and co-existing with hematite is noted in thin section. Native Au occurs as minute inclusions along microcracks in bornite grains. Au also occurs as lobate spots on the edge of, or within, bornite.

Stage 5 multi-stage veins form a stockwork system that pervades QMP1 and adjacent volcanics, but is absent in QMP2 (Fig. 7.3; Plate 7.3). They make up 10–20% of the volume of rock in places. In detail these grey, vitreous quartz veins display thin trails of sulphides, anhydrite and sericite parallel to the vein walls, suggesting repeated fracturing, fluid flow and deposition through single veins. Rarely, granular aggregates of quartz and K-feldspar form layers within these veins. Where Stage 5 veins cross more mafic-rich rocks a thin reddish K-feldspar vein margin is present.

Au is primarily and closely associated with bornite in Stage 5 veins. This is based on the observation that if Stage 5 veins are not present, then Au grades are low even though the Cu grade may be high due to Stage 4 veining. Native Au, calaverite and cuprian Au are the important phases. They occur as 5–15 μ diameter inclusions within bornite, and closely

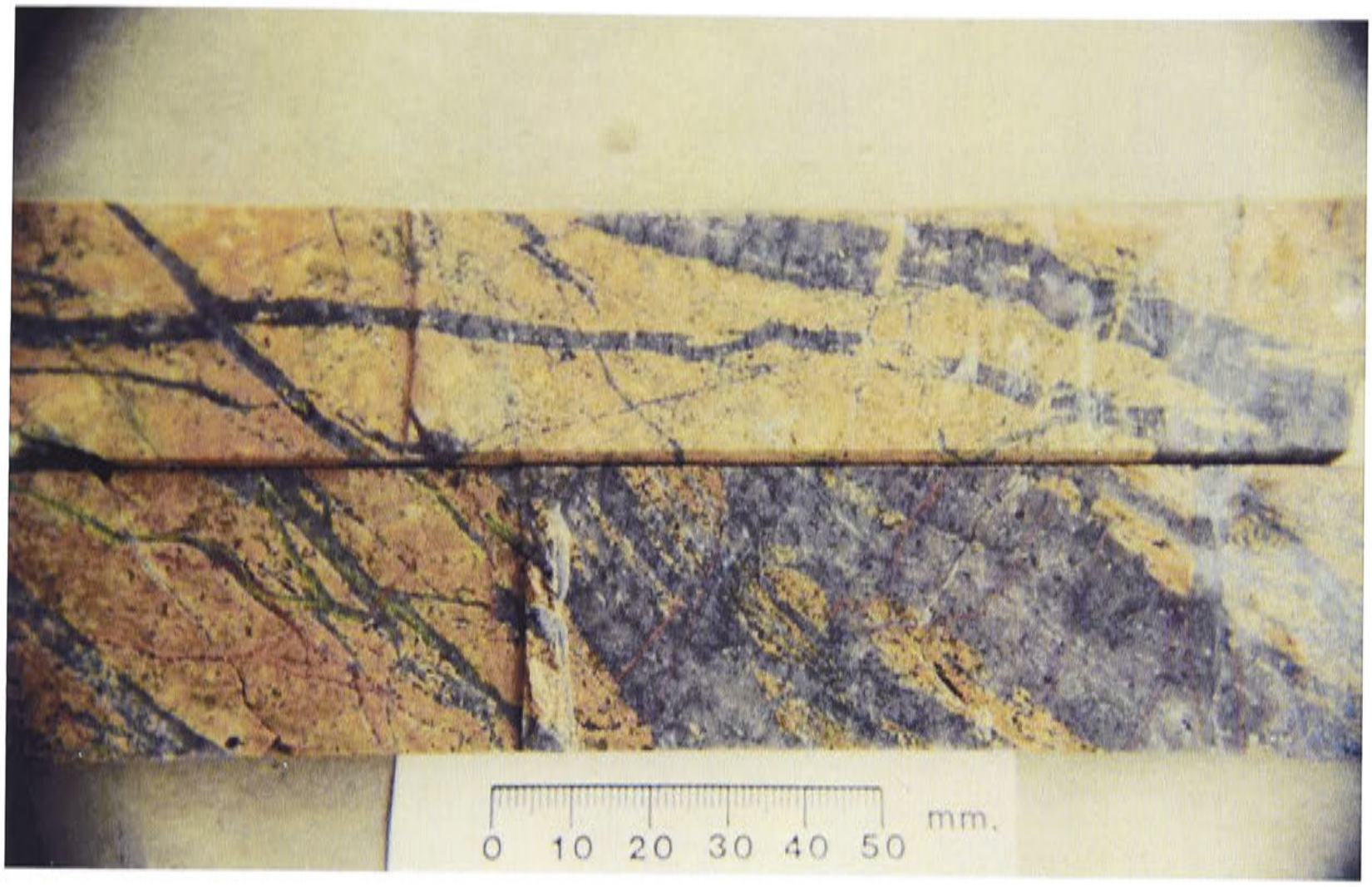

Plate 7.3 Quartz veined aplite from QMP2 crosscutting stockworked QMP1.

resemble exsolution spots. Similar relations between Au-bearing inclusions and bornite have been observed by Cuddy and Kesler (1982). They note that since bornite exhibits extensive solid solution at high temperatures (600 °C) in Cu, Fe and sulphur but limited solid-solution at low temperatures, it is likely that Au incorporated into the bornite structure at high temperatures will be forced to exsolve on cooling.

The inner K-feldspar subzone, which is confined to QMP2, contains Stages 6–8. By the end of Stage 6, the main body of mineralisation was present. Stage 6 also marks the appearance of vein dykes and hydrothermal–magmatic brecciation. The timing of these features is uncertain as they both pre-date and post-date QMP2. Vein dykes brecciate, intrude and sometimes incorporate earlier Stage 4 stockwork veins. This indicates that these features may represent late stage melt – hydrothermal fluid from QMP1, or alternatively, they may represent volatile-rich melt which had accumulated within the still molten parent magma body at depth. This modified melt preceded, or was incorporated with, the intrusive event which led to emplacement of QMP2 (Plate 7.4). Some vein dykes and breccia infills are clearly magmatic in origin, based on the observation of sparsely distributed plagioclase lathes in some dykes, whilst others develop intricate feather textured intergrowths of quartz and alkali feldspar indicating rapid undercooling of a melt. Other veins develop granular intergrowths of quartz and alkali feldspar resembling an aplite. Material of similar composition and texture fills the interstices of magmatic–hydrothermal breccias. Some vein dykes display a vein margin of graphically intergrown quartz and alkali feldspar, and vein centre consisting of hydrothermal quartz with abundant bornite. These magmatic–hydrothermal features form a narrow halo around QMP1 and QMP2.

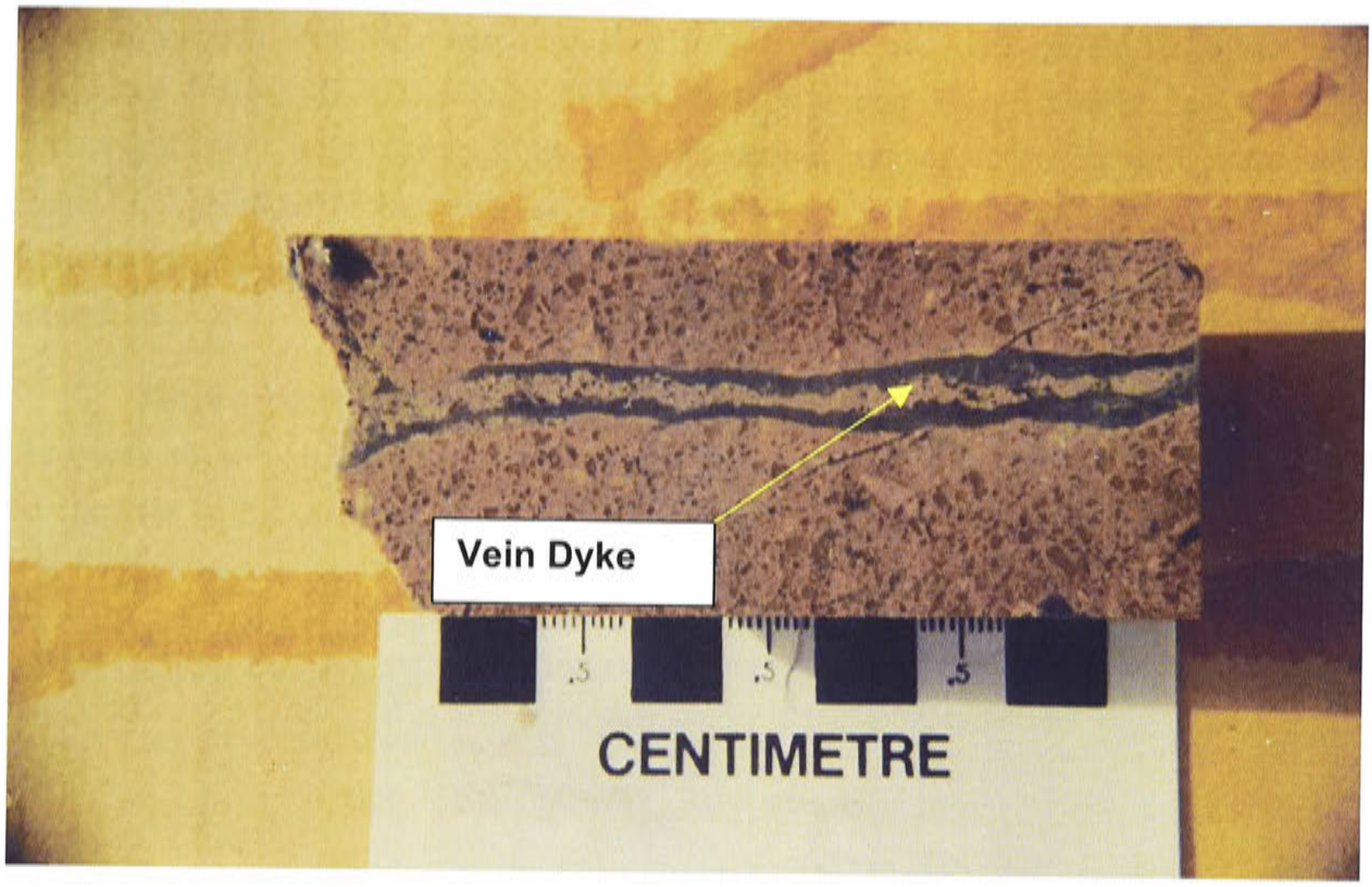

Plate 7.4 Vein-dyke within sample of QMP2.

Within QMP2 vein-like trails of subhedral quartz occur. These quartz phenocrysts can develop up to 5 mm in diameter, and appear in equilibrium with the aplitic quartz, K-feldspar groundmass of QMP2. Examples may resemble the `brain rock' texture seen in some molybdenum deposits (Plate 7.5).

Stages 7 and 8 are a repeat in QMP2, of the discontinuous fine veining of Stage 3 and stockwork style veining of Stage 5 found in QMP1. The density of these veins types is far less than the comparable Stage 4 and 5 veins. Stage 8 veins are typically straight walled and milky, containing visible traces of fluorite together with chalcopyrite and bornite.

Stage 9 vein and vein envelopes combine to form an asymmetric phyllic or quartz–sericite alteration zone to the deposit. Zones of intense quartz–sericite alteration range in thickness from a vein – vein envelope which is 50 mm across to zones up to 100 m wide. Zones of intense alteration on the scale of several metres are most common. The intervening rock may be weakly overprinted with secondary quartz and sericite, or may shown no evidence of this alteration style at all.

Quartz–sericite alteration is fracture controlled. As noted earlier it is a common alteration features in the Goonumbla region, although Endeavour 26 North is the only mineralised centre spatially related to this alteration style. Associated sulphides rarely exceed 4% by volume. Pyrite is the predominant sulphide, although chalcopyrite becomes progressively more abundant as the higher grade core is approached. Chalcopyrite is

commonly noted rimming and replacing pyrite. In some vein envelopes, sericite forms descussate plates which appear to invade sulphide grains. This indicates that fluids which have reacted with wall rock to produce quartz–sericite assemblages were undersaturated with respect to chalcopyrite and pyrite at various points in their evolution. It could be an external fluid that is upgrading its Cu content to the point of chalcopyrite saturation, but not of bornite saturation.

Stage 10 and 11 veins clearly crosscut all other stages in the deposit. Gypsum veins give way to anhydrite veins at depth, and vary in thickness from millimetres to tens of centimetres in thickness.(Plate 7.6).

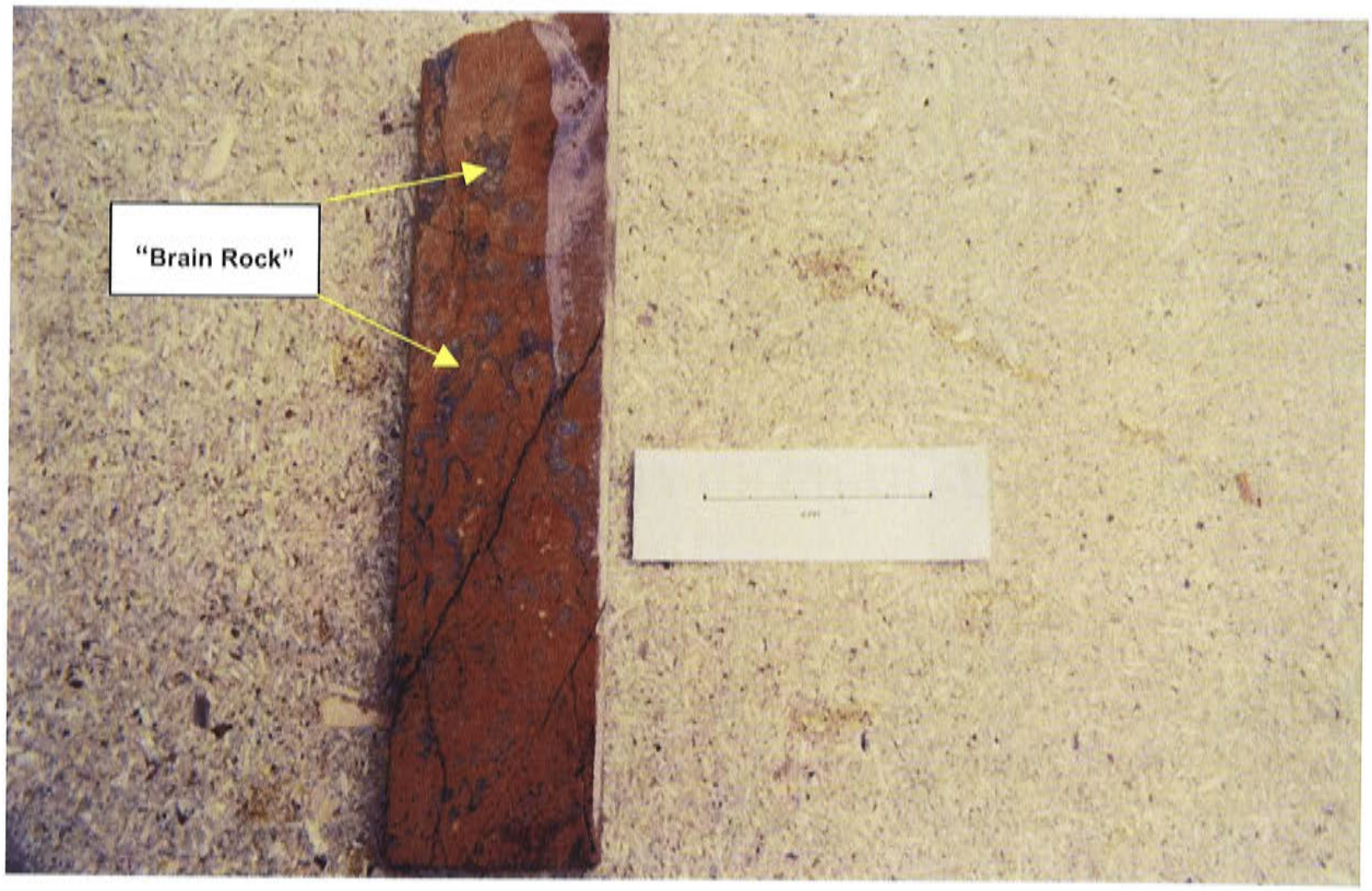

Plate 7.5 QMP 2 with 'brain rock'' textures.

Plate 7.6 Stage 10 and 11 gypsum veins crosscutting zones of sericitic alteration.

7.6 SUMMARY COMPARISON WITH OTHER ALKALIC SYSTEMS

7.6.1 EXAMPLES

British Columbia Iron Mask batholith deposits – Afton, Ajax, Mt. Polley, Cariboo Bell, Mt. Milligan, Copper Mt./Ingerbelle, Galore Creek (Barr, D.A., 1976; McMillan, W.J. 1991; McMillan and Panteleyev, A. 1988; Sutherland Brown, A. Editor, 1976.)

Papua New Guinea Ok Tedi (Sillitoe, 1990)

Philippines Marian, Didipio (Sillitoe, 1990a Sillitoe and Gappe, 1984; Sillitoe 1990b).

The following summary and comparison is drawn from these reference deposits

7.6.2 DEPOSIT FORM:

Stockworks and veinlets, minor disseminations and replacements throughout large areas of hydrothermally altered rock, commonly coincident wholly or in part with hydrothermal or intrusion breccias. Deposit boundaries are determined by economic factors that outline ore zones within larger areas of low-grade, laterally zoned mineralization. **Endeavour 26 North** also consists of overlapping and paragenetically complex veins, veinlets and rare vein dykes. The deposit form is an elongate pipe of mineralisation centred around a quartz monzonite porphyry (QMP1). Most of the ore is contained in early microveinlets that overlap and

coalesce to form "disseminated" mineralisation. Intrusion breccias are rare, very narrow and usually unmineralised.

7.6.3 TEXTURE/STRUCTURE:

Veinlets and stockworks; breccia, sulphide and magnetite grains in fractures and along fracture selvages; disseminated sulphides as interstitial or grain and lithic clast replacements. Hydrothermally altered rocks can contain coarse-grained assemblages including feldspathic and calcsilicate replacements ('porphyroid' textures) and open space filling with fine to coarse, granular and rarely pegmatitic textures. **Endeavour 26 North** contains veinlets, stockworks, breccias, sulphide and magnetite grains in fractures and along fracture selvages; and disseminated sulphides as a result of earlier discontinuous veinlets. Feldspathic and Calc silicate replacements are not evident and open space filling is rare.

7.6.4 ORE MINERALOGY

Chalcopyrite, pyrite and magnetite; bornite, chalcocite and rare galena, sphalerite, tellurides, tetrahderite, gold and silver. Pyrite is less abundant than chalcopyrite in ore zones. **Endeavour 26 North** contains the following in order of importance: bornite, magnetite, chalcopyrite,pyrite, Chalcocite, digenite, tellurides and uncommon galena, sphalerite. Gold occurs as free gold and gold tellurides in bornite grains.

7.6.5 GANGUE MINERALOGY:

Biotite, K-feldspar and sericite; garnet, clinopyroxene (diopsidic) and anhydrite. Quartz veins are absent but hydrothermal magnetite veinlets are abundant. **Endeavour 26 North** contrasts with typical alkalic porphyries in this area. Kfeldspar, biotite, sericite, albite, anhydrite and chlorite are the dominant alteration species. Quartz veining is common.

7.6.6 ALTERATION MINERALOGY:

Biotite, K-feldspar, sericite, anhydrite/gypsum, magnetite, hematite, actinolite, chlorite, epidote and carbonate. Some alkalic systems contain abundant garnet including the Ti-rich andradite variety - melanite, diopside, plagioclase, scapolite, prehnite, pseudoleucite and apatite; rare barite, fluorite, sodalite, rutile and late-stage quartz. Central and early formed potassic zones, with K-feldspar and generally abundant secondary biotite and anhydrite, commonly coincide with ore. These rocks can contain zones with relatively high-temperature calcsilicate minerals diopside and garnet. Outward there can be flanking zones in basic volcanic rocks with abundant biotite that grades into extensive, marginal propylitic zones. The older alteration assemblages can be overprinted by phyllic sericite-pyrite and, less commonly, sericite-clay-carbonate-pyrite alteration. In some deposits, generally at depth in silica-saturated types, there can be either extensive or local central zones of sodic alteration containing characteristic albite with epidote, pyrite, diopside, actinolite and rarer scapolite

and prehnite. **Endeavour 26 North** displays biotite, K- feldspar, sericite, anhydrite/gypsum, magnetite, hematite, actinolite, chlorite, apidote and carbonate. Early formed biotite and albite are overprinted by K Feldspar dominant veinlets that also contain anhydrite and closely associated with ore in common with other alkalic deposits. Outward the flanking zones contain patchy biotite grading to propylitic assemblages of chlorite, carbonate and epidote. All of these assemblages are overprinted by quartz, sericite alteration. Calc-silicate minerals are not present at Endeavour 26 North, but do occur in skarns within the district.

7.6.7 ORE CONTROLS:

Igneous contacts, both internal between intrusive phases and external with wall rocks; cupolas and the uppermost, bifurcating parts of stocks, dike swarms and volcanic vents. Breccias, mainly early formed intrusive and hydrothermal types. Zones of most intensely developed fracturing give rise to ore-grade vein stockworks. **Endeavour 26 North** ore is closely controlled by the density of overlapping veins and veinlets forming the central stockworks. The locus of mineralisation is closely controlled by the location of QMP1.

7.6.8 ASSOCIATED DEPOSIT TYPES:

Skarn copper; A-Ag and base metal bearing mantos, replacements and breccias in carbonate and non-carbonate rocks; magnetite-apatite breccias; epithermal Au-Ag : both high and low sulphidation types and alkalic, Te and F-rich epithermal deposits; auriferous and polymetallic base metal quartz and quartz-carbonate veins; placer Au. At **Endeavour 26 North** mineralisation is confined to stockwork systems. In the region, epithermal, low sulphidation veins (Endeavour 29) copper and lead zinc gold skarns (Endeavour 44) occur. Breccias are evident but not as common as in other alkalic systems.

Chapter 8

ENDEAVOUR 26 NORTH: S ISOTOPES

8.1 INTRODUCTION

A stable isotope study, when utilised in conjunction with other geochemical and mineralogical studies, can provide constraints on the following aspects of ore genesis:

1. Physical conditions (temperature, pressure and depth) of ore formation.
2. Hydrological aspects of ore forming systems.
3. Sources of ore constituents, especially S and metals.
4. Chemical compositions of ore forming fluids; specifically redox state, sulphate/sulphide ratios, metal/sulphide ratios and pH.
5. Mechanisms of metal and S transport, and ore deposition.

Few S isotope studies have been done on porphyry Cu–Au deposits. Field (1966) documented S isotope data for the Bingham district, and prepared a companion benchmark paper on the S isotopes of the El Salvador porphyry deposit in Chile (Field and Gustafson, 1976). Other deposits for which S isotopes ratios have been documented include Butte (Lange and Cheney, 1971), Valley Copper in British Columbia (Osatenko and Jones, 1976), and the Panguna and Frieda deposits in Papua New Guinea (Eastoe, 1983). Rye and Ohmoto (1979) summarised data on sulphides and sulphates from porphyry Cu deposits of the American Cordillera (Fig. 8.1). As they point out, this presentation suffers from the limitation of not showing the time–space relations, or the intensive chemical variables which play a role in determining the range and mode of these distributions. The $\delta^{34}S$ values for most sulphides range from –3 to +1‰, and sulphates from +8 to +15‰. The sulphide/sulphate isotopic temperatures recorded from the data lie between 450 and 650 °C, which accords reasonably well with mineralisation formation temperatures determined by other methods, suggesting that equilibrium has been reached between the oxidised and reduced species in the fluid and mineral assemblages. Ohmoto and Lasaga (1982) conclude that rates of sulphate reduction became geologically important at temperatures above 200 °C.

In the present study a variety of sulphides and sulphates from various stages in the paragenesis were selected to determine the temporal and spatial variation in S isotope ratios in the deposit.

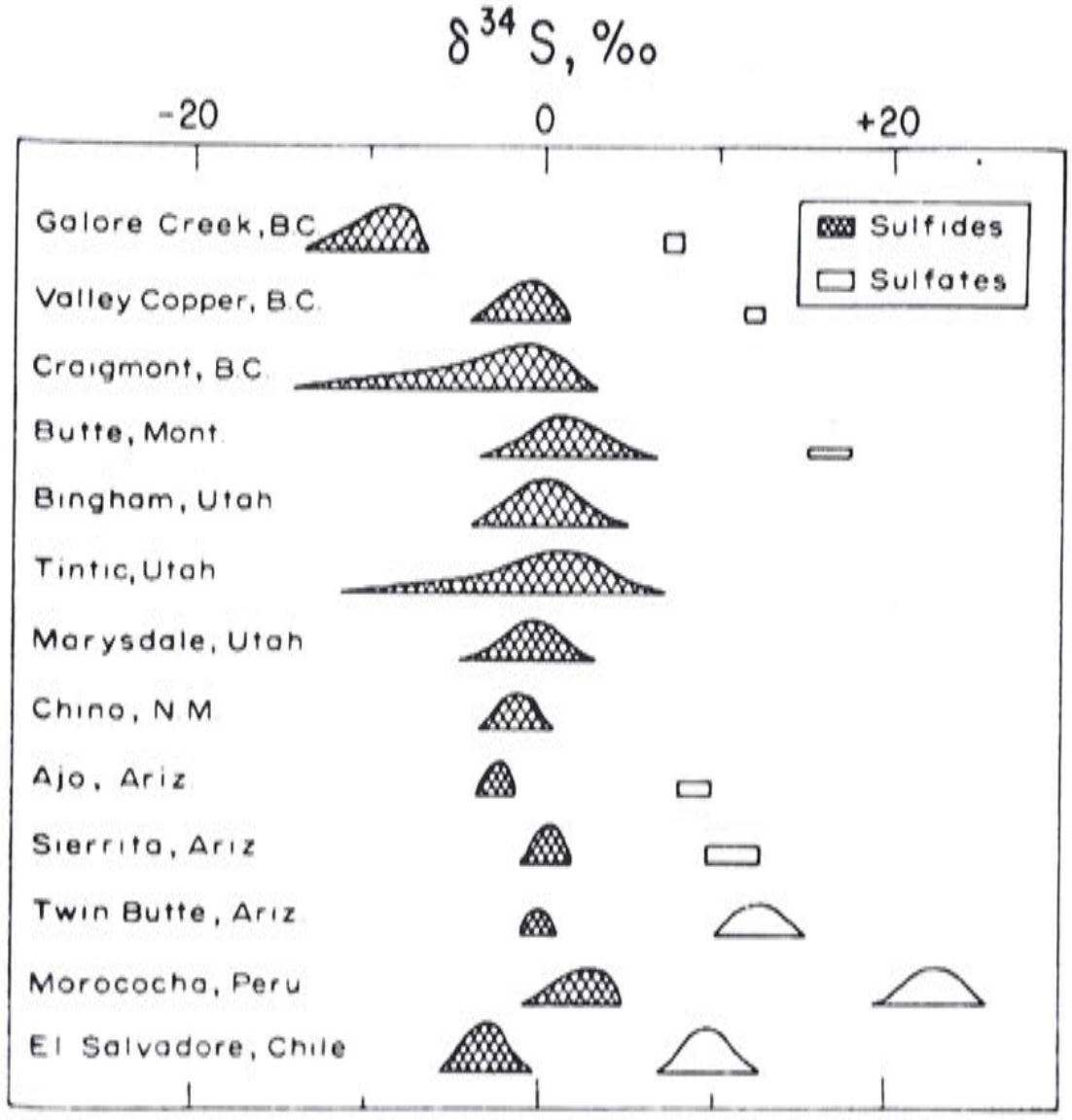

Figure 8.1 Schematic summary of S isotope data from some porphyry Cu deposits.

8.2 METHODS AND RESULTS

The S isotope analyses were done at the Central Science Laboratory, University of Tasmania, under the supervision of Mr M. Power. The minerals were hand picked from finely crushed material using a binocular microscope. They are easily separated because the sulphides and sulphates are distinctly coloured.

The isotope result is expressed as:

$$\delta^{34}S_{sample} = [(^{34}S/^{32}S_{sample} / {}^{34}S/^{32}S_{standard}) - 1] * 1000‰$$

The standard is troilite from the Cañon Diablo meteorite. The fractionation of $\delta^{34}S$ between minerals A and B is expressed as:

$$\Delta_{A-B} = \delta^{34}S_A - \delta^{34}S_B$$

Table 8.1 lists the mineral separate, paragenetic stage, vein assemblage (where sampled) and $\delta^{34}S$ value for each sample from the Endeavour 26 North deposit. The overall range of $\delta^{34}S$ values for sulphides and sulphates from the deposit are given in Figure 8.2. Values for sulphides range from –8 to –2.9‰ and values for anhydrite range from 7.3 to 16.6‰. A measurement of 21.8‰ for a sample of gypsum may be spurious as it was the last sample in the long final run for 1990. If however, the sample was not spurious could also represent a sulphate that formed at lower temperature with highly fractionated heavy sulphur. The study here is focused on the higher temperature end related to mineralisation so this datum was not followed further. Bornite shows a wide range of values from –8 to –2.9‰ (Fig. 8.3). Two samples which returned low yields, due to quartz in the sample, are included in the data set. The isotope compositions of a limited number of chalcopyrite samples (Fig. 8.4) show a similar range from –8.2 to -3.5‰. Pyrite has a restricted range between –6.8 and –7.7‰ (Fig. 8.5). Anhydrite returned values in the range from 7.3 to 16.6‰ (Fig. 8.6).

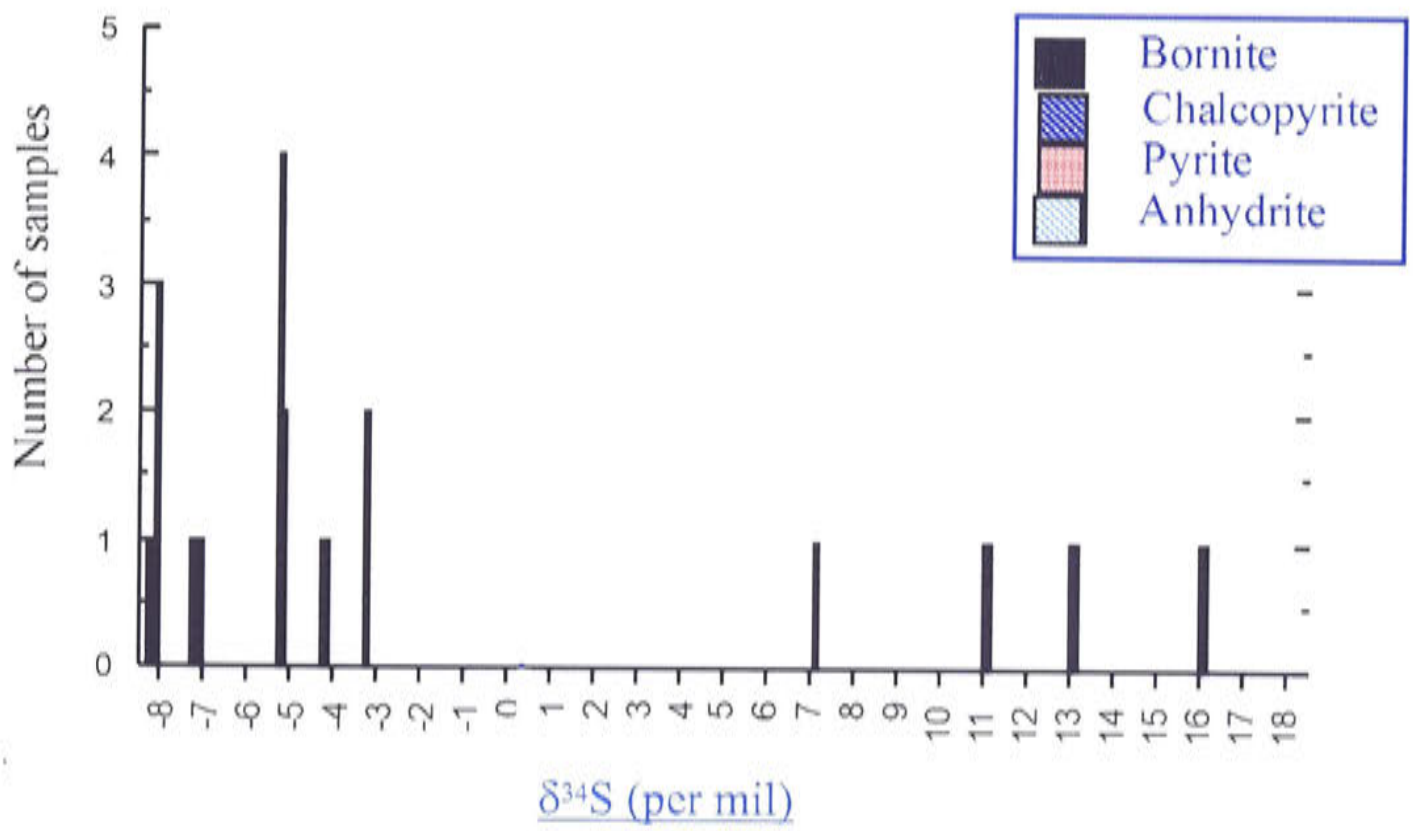

Figure 8.2 Histogram of all S isotope results, Endeavour 26 North deposit.

Table 8.1 S isotope data and sample details, Endeavour 26 North deposit.

Sample number	Mineral analysed	Stage	Vein assemblage	$d^{34}S$ (per mil)	Comment
26/135	Bornite	5	Qtz–bn–gy	–8	Vuggy quartz with bornite infill; quartz –sericite overprint.
75/173.6	Bornite	5	Qtz–bn–ser	–6.5	Silica zone; intense stockwork with selvages of bornite and sericite.
75/172.9	Chalcopyrite	5	Qtz–cpp	–7.2	Silica zone selvage of chalcopyrite.
26/214	Bornite	5	Qtz–bn	–5	Dense mass of bornite in stock vein.
PH2	Bornite	6	Qtz–bn	–4.7	Bornite clot in Square Porphyry.
38/313.3A	Bornite	5	Qtz–bn–cpp–an	–3.4	Stockwork style quartz chalcopyrite, bornite anhydrite veins.
38/313.3B	Chalcopyrite			–4.5	
38/443.3	Bornite	5	Qtz–bn, minor an	–4.4	Stockwork style veining.
42/613.5	Bornite	6	Qtz–bn	–2.9	Low yield, quartz contamination; vein dyke with aplite infill.
39/451.5A	Bornite	4		–2.9	Low yield, quartz contamination; associated with fine quartz, K-feldspar veining.
39/451.5B	Chalcopyrite			–3.5	Low yield, quartz contamination.
42/625.3	Bornite	5		–5.	Stockwork style quartz, anhydrite bornite vein.
	anhydrite			14.1	
66/1069	Chalcopyrite	5	An–cpp–qtz–bn	–4.2	Associated with stockwork style veins.
	anhydrite			7.3	
46/847.1	Pyrite	9		–7.7	Crystalline anhydrite–pyrite vein.
	anhydrite			16.6	
46/437	Anhydrite	9	An–cpp–py	11.6	Coarsely crystalline anhydrite–chalcpyrite–pyrite vein associated with intense quartz–sericite alteration.
106/340.2	Pyrite	9?	Py–qtz	–7.5	Fault breccia infilled with pyrite.
40/129	Pyrite	9	Qtz–py	–7.1	Quartz, pyrite vein associated with intense quartz–sericite alteration.
68/380	Pyrite	11	Py–gyp	–6.8	Late stage gypsum, pyrite vein.
	gypsum			21.8	

an = anhydrite; bn = bornite; cpp = chalcopyrite; gps = gypsum; py = pyrite; qtz = quartz; ser = sericite

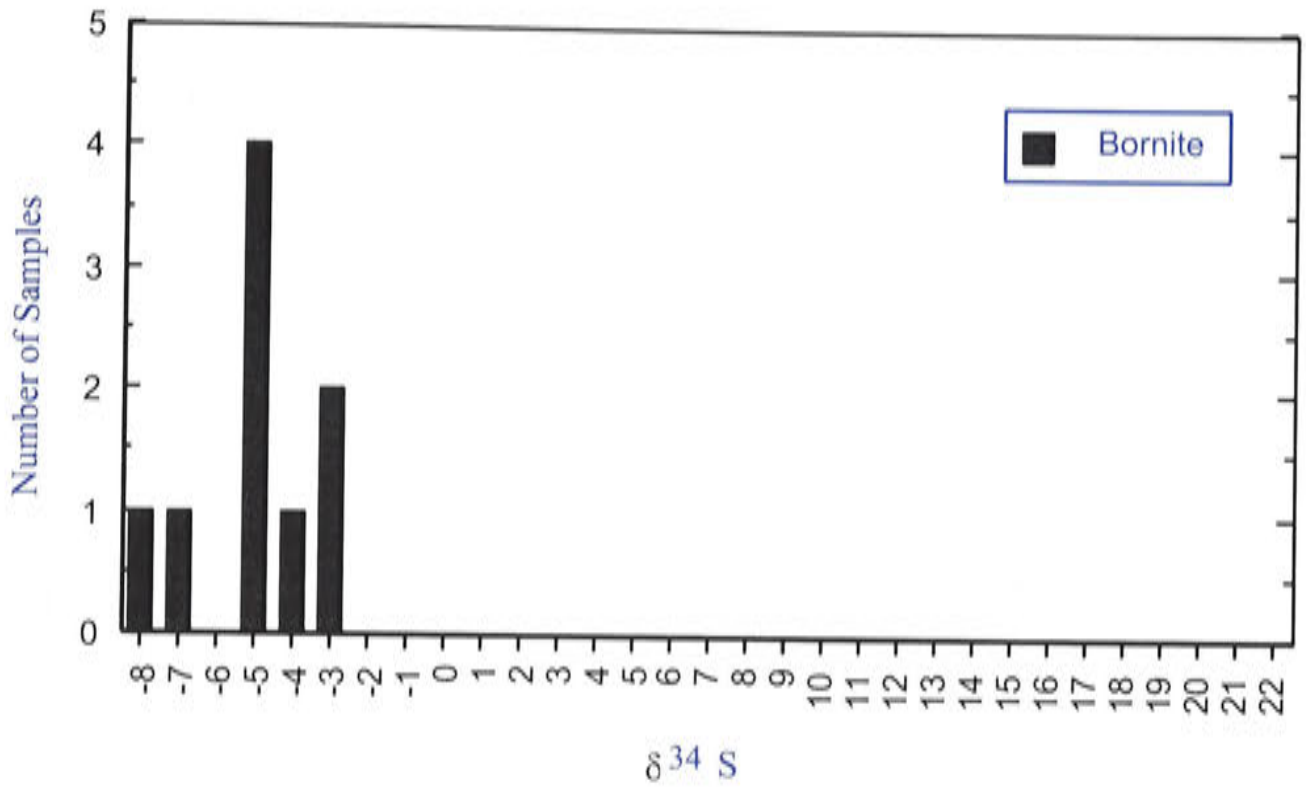

Figure 8.3 S isotope results for bornite, Endeavour 26 North deposit.

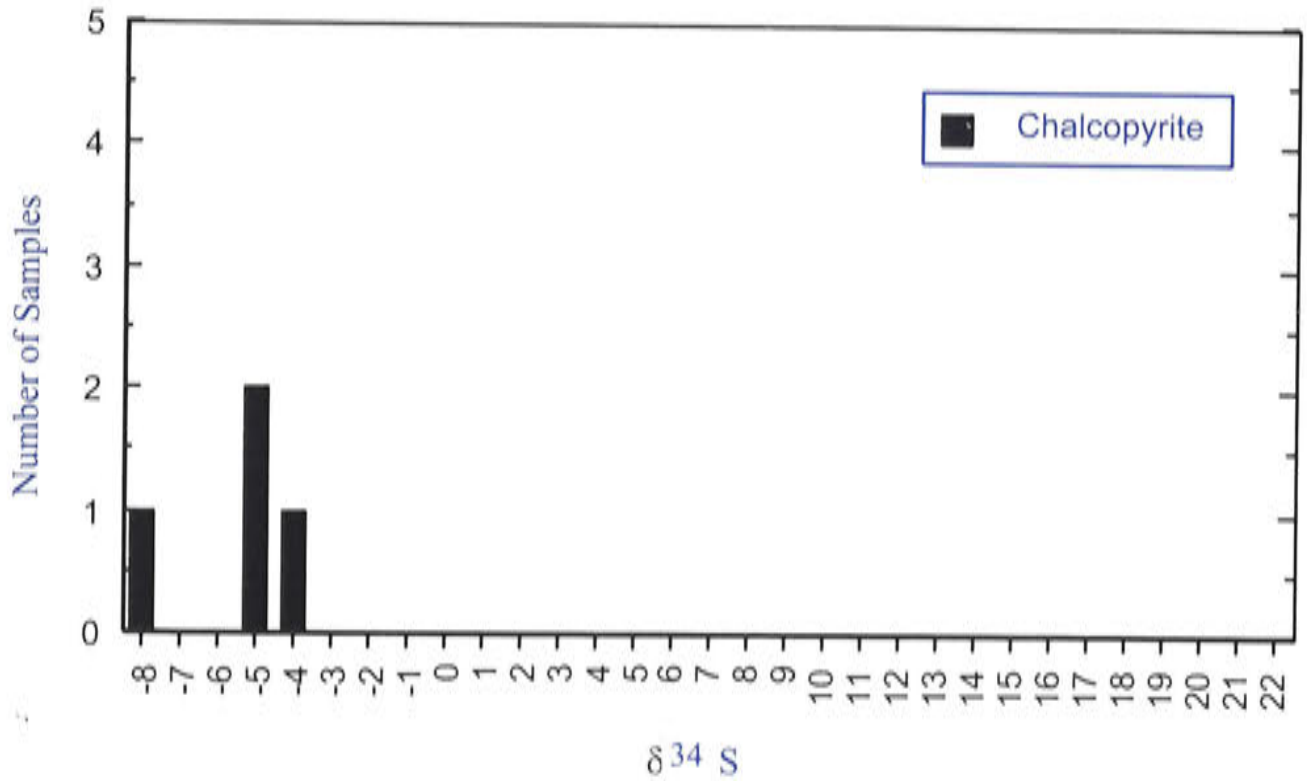

Figure 8.4 S isotope results for chalcopyrite, Endeavour 26 North deposit.

Figure 8.5 S isotope results for pyrite, Endeavour 26 North deposit.

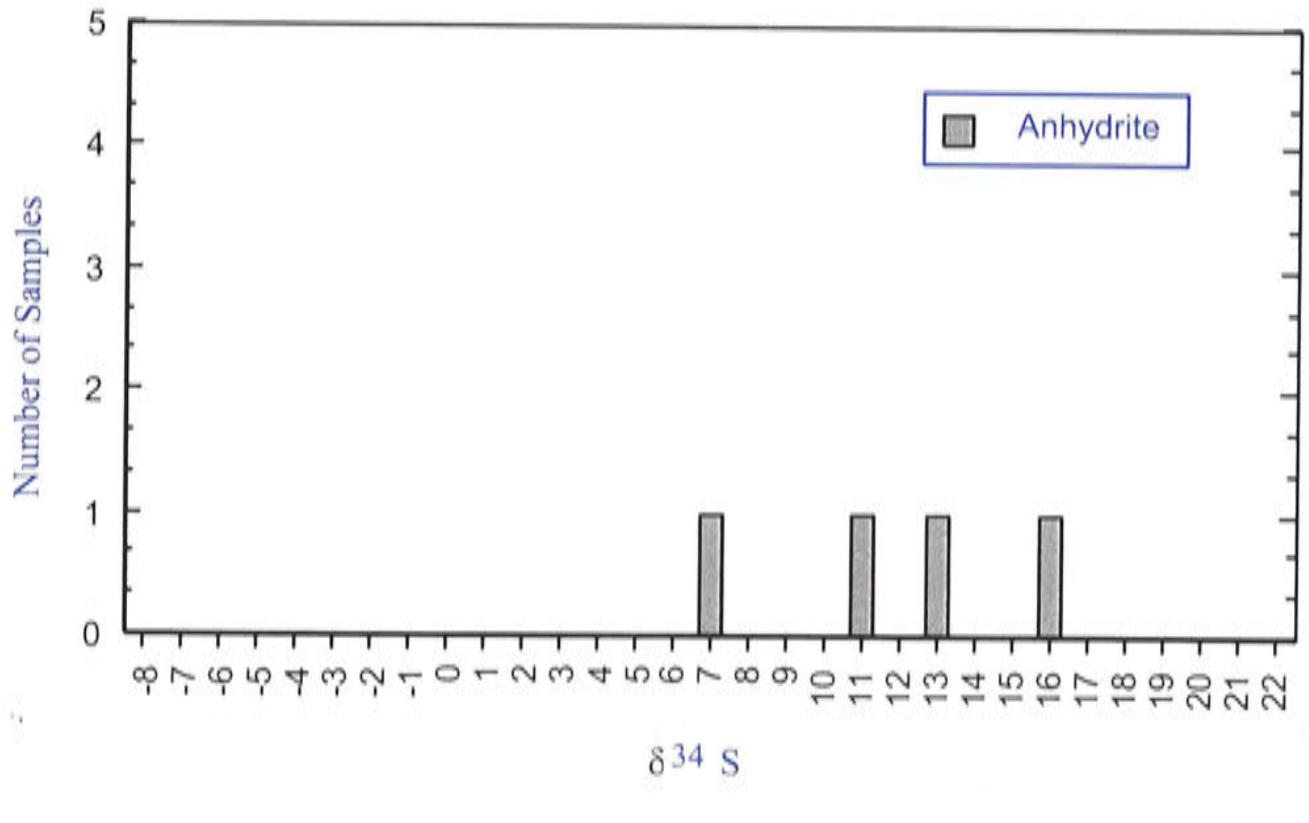

Figure 8.6 S isotope results for anhydrite, Endeavour 26 North deposit.

8.3 THERMOMETRY

The successful application of the S isotope geothermometer depends on the following conditions (Ohmoto and Rye, 1979):

1. Both mineral phases were formed in equilibrium.
2. No isotopic exchange took place between the mineral phases, or between a mineral phase and a fluid phase, after the formation of the minerals.
3. Pure mineral phases were separated for isotopic analyses.
4. The fractionation factor between a mineral pair is sensitive to temperature.

Porphyry Cu deposits commonly have sulphides which have precipitated synchronous with sulphates, chiefly anhydrite; and the studies noted above suggest an approach to isotopic equilibrium between sulphate and sulphide species is likely. Table 8.2 lists temperatures calculated for sulphide–sulphate pairs from the Endeavour 26 North deposit. The formulae for calculating temperatures are generated from isotopic fractionation factors listed in table 10.1 of Ohmoto and Rye (1979). Also listed in Table 8.2, for comparison purposes, are the temperatures of formation of six samples of bornite and chalcopyrite determined from study of fluid inclusions in the quartz-vein host. Sulphide–sulphate pairs were unobtainable from these samples. In the following discussion a comparison is made between temperatures obtained from sulphide–sulphate pairs and fluid inclusion homogenisation temperatures (T_h) obtained from coexisting quartz, stage by stage through the paragenesis.

8.3.1 Stage 4 veins

Stage 4 veins are those which give the disseminated appearance to the mineralisation. They range from a spidery network of fine quartz–sulphide veinlets with narrow K-feldspar vein envelopes, to a dense network of veinlets which impart a pervasive K-feldspar flooding to the rock. Sample 39/451 is typical of this stage. A modal temperature of 679 °C has been determined from T_h measurements .

8.3.2 Stage 5 veins

Sulphide–sulphate pairs from stockwork veins of Stage 4, samples 42/625.3 (DDH42) and 66/1069, returned calculated temperatures of 383 and 567 °C respectively. By comparison, samples 38/313.9 and 38/443 have measured modal T_h temperatures of 563 and 550 °C. Taken as a whole, these data exhibit a range of temperatures from 383 to 563 °C.

8.3.3 Stage 6 veins

Stage 6 corresponds to a prograde event associated with the second porphyry (QMP2). Veins from this stage crosscut the porphyry and earlier stockwork veins, and are regarded as

approximately synchronous with the intrusion of QMP2. They commonly take the form of vein dykes which have the characteristics of both quartz–sulphide veins and aplite dykes, and are clearly temporally and spatially related to the quartz monzonite porphyry. Sample 42/613.5 is a mineralised quartz vein with an aplitic central selvage. A bornite separate from this sample returned a S isotopic composition of –2.9‰. T_h determinations from the same sample ranged between 527 and 781 °C, with a mode of 731 °C.

Table 8.2 Temperatures calculated from sulphide–sulphate pairs, using the isotope fractionation factors of Ohmoto and Rye (1979), with fluid inclusion temperatures for comparison.

Sample	Mineral	$\delta^{34}S$	Δ (per mil)	Formula	Temp. (°C) (calc.)	T_h (°C) (mode) (range)
42/625.3	Bornite	-5	19.1	$T = \frac{2.87*103}{\sqrt{(\Delta \pm 1)}} - 273.3$	383	
	anhydrite	14.1				
66/1069	Chalcopyrite	-4.2	11.5	$T = \frac{2.85*10^3}{\sqrt{(\Delta \pm 1)}} - 273.3$	567	
	anhydrite	7.3				
46/847	Pyrite	-7.7	24.3	$T = \frac{2.16*10^3}{\sqrt{(\Delta - 6 \pm 0.5)}} - 273.3$	273	
	anhydrite	16.6				
68/380	Pyrite	-6.8	28.6	$T = \frac{2.16*10^3}{\sqrt{(\Delta - 6 \pm 0.5)}} - 273.3$	272	
	gypsum	21.8				
42/613.5	Bornite	-2.9				731 (527–781)
38/313.9	Bornite	-3.4				563 (440–796)
	chalcopyrite	-4.5				
38/443	Bornite	-2.9				550 (520–578)
39/451	Bornite	-2.9				679 (480–960)
	chalcopyrite	-3.5				

8.3.4 Stage 9 veins

Stage 9 veins are clearly associated with the quartz–sericite–pyrite phase of alteration as it occurs in this deposit. Typically they consist of a central vein of quartz ± anhydrite with pyrite ± chalcopyrite surrounded by an envelope, which may extend for centimetres or tens of centimetres away from the vein wall, of pervasive quartz–sericite–pyrite alteration. Where veins coalesce, larger intercepts of pervasive quartz–sericite altered material is encountered, commonly associated with shear zones and faults. Three samples of pyrite were taken from representatives of these veins, both deep in the system (DDH46/847.1 m) and from moderate and shallow parts of the system (DDH106/340.2 m; DDH40/129 m). S isotope ratios for all pyrites fall within a narrow range of from -6.8 to –7.7‰, including one sample of pyrite from a fault breccia. Anhydrite from these veins ranged from 11.6 to 16.6‰. Sample 46/847 consists of an anhydrite–pyrite vein central to quartz–sericite–pyrite vein envelope. The pyrite and anhydrite, which appear to be in textural equilibrium, returned values of –7.7 and 16.6‰ respectively, yielding a calculated temperature of 273 °C.

8.3.5 Stage 11 veins

Stage 11 gypsum veins grade into anhydrite veins at depth, and form a conspicuous network of white to orange-pink fibrous veins throughout the deposit. They are commonly barren but may contain coarse pyrite. A representative pyrite–gypsum pair from sample 68/380 returned S isotope values of –6.8 and 21.8‰ respectively. This implies a temperature of pyrite–sulphate equilibration of 272 °C, which is similar to that calculated for stage 8 vein sample 46/847.

8.4 VARIATION OF $\delta^{34}S$ IN TIME AND SPACE

8.4.1 Bornite

S isotope compositions of bornite samples examined in this study ranged in $\delta^{34}S$ values from –8 to –2.9‰. The results are plotted in Figure 8.7 which is a cross-sectional plane onto which all the samples are projected, and Figure 8.8 which is a plan projection of the same sample points. Although the data is limited, it is possible to systematically contour the values on these projections and suggest that vertical and lateral gradients exist. The isotopic composition of bornite changes from about –3‰ at the centre of the system to progressively more negative (or isotopically lighter) away from the centre. The vertical gradient is the clearest; the lateral gradient less so as it depends on one sample. In section the elongate shape of the contours mimic the vertically attenuated nature of the mineralisation, and in plan view (Fig. 8.8) the results can be contoured to produce a northeast-trending ellipse, which is similar to the geometry of mineralisation and the central quartz monzonite intrusions.

There are insufficient samples to be definitive about the variation of the S isotope composition of bornite through the paragenesis. From sample 39/451.5A (Table 8.1), the fine veinlets of Stage 4 have compositions closest to primitive magmatic values, with $\delta^{34}S$ values of –2.9‰. Bornite from Stage 5 stockwork veins makes up the bulk of the bornite samples, and their compositions range from –3.4 to –8‰. Fractionation within this paragenetic stage seems to largely reflect varying temperature (see below). Stage 6 veins show a progradation back to magmatic conditions, and this is reflected in the S isotope composition of sample 42/613.5 of –2.9‰.

8.4.2 Chalcopyrite

Chalcopyrite displays some spatial variation in $\delta^{34}S$ when plotted on a projected cross-section (Fig. 8.9). On the basis of this very limited data, some tentative contours can be drawn which show a similar pattern to the contours of the bornite data. Certainly a vertical zonation seems to exist, and sample 66/1069 suggests that the vertical attenuation shown in the bornite data may be reflected in the chalcopyrite data as well. There are insufficient data to comment on variation through the paragenesis.

8.4.3 Pyrite

Pyrite values are plotted on the cross-section in Figure 8.10. In contrast with bornite and chalcopyrite, pyrite appears to have uniform $\delta^{34}S$ values. There is no obvious spatial variation, and the pyrite appears uniform in composition through several paragenetic stages including semi-massive pyrite infilling fault zones.

8.4.4 Anhydrite

There is insufficient data to draw any conclusions about possible zonation in the S isotope compositions of anhydrite or gypsum.

Figure 8.7 Cross-section projection sulphur isotope results, bornite, Endeavour 26 North.

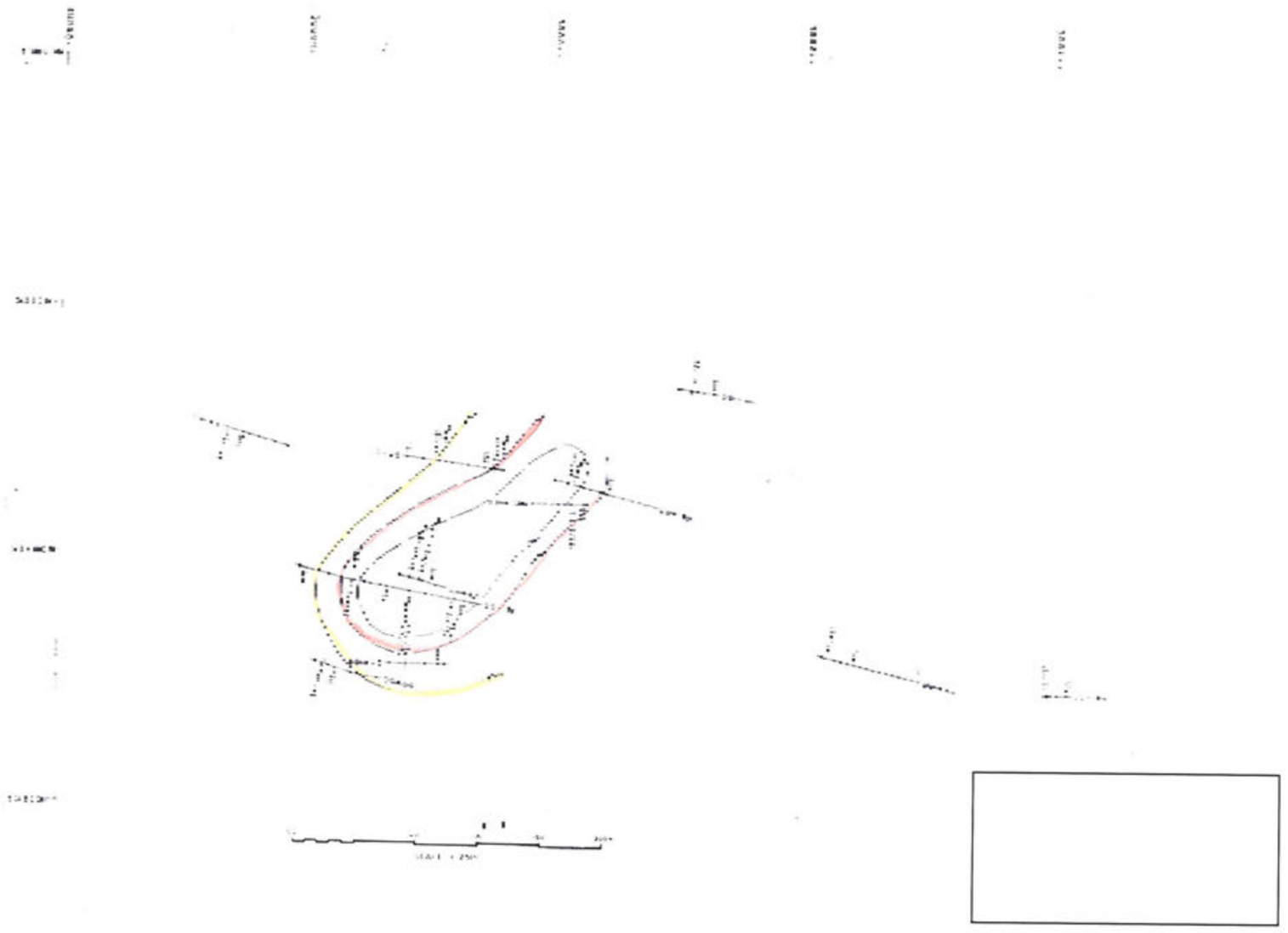

Figure 8.8 Surface projection (10 000 RL) sulphur isotope results, bornite, Endeavour 26 North.

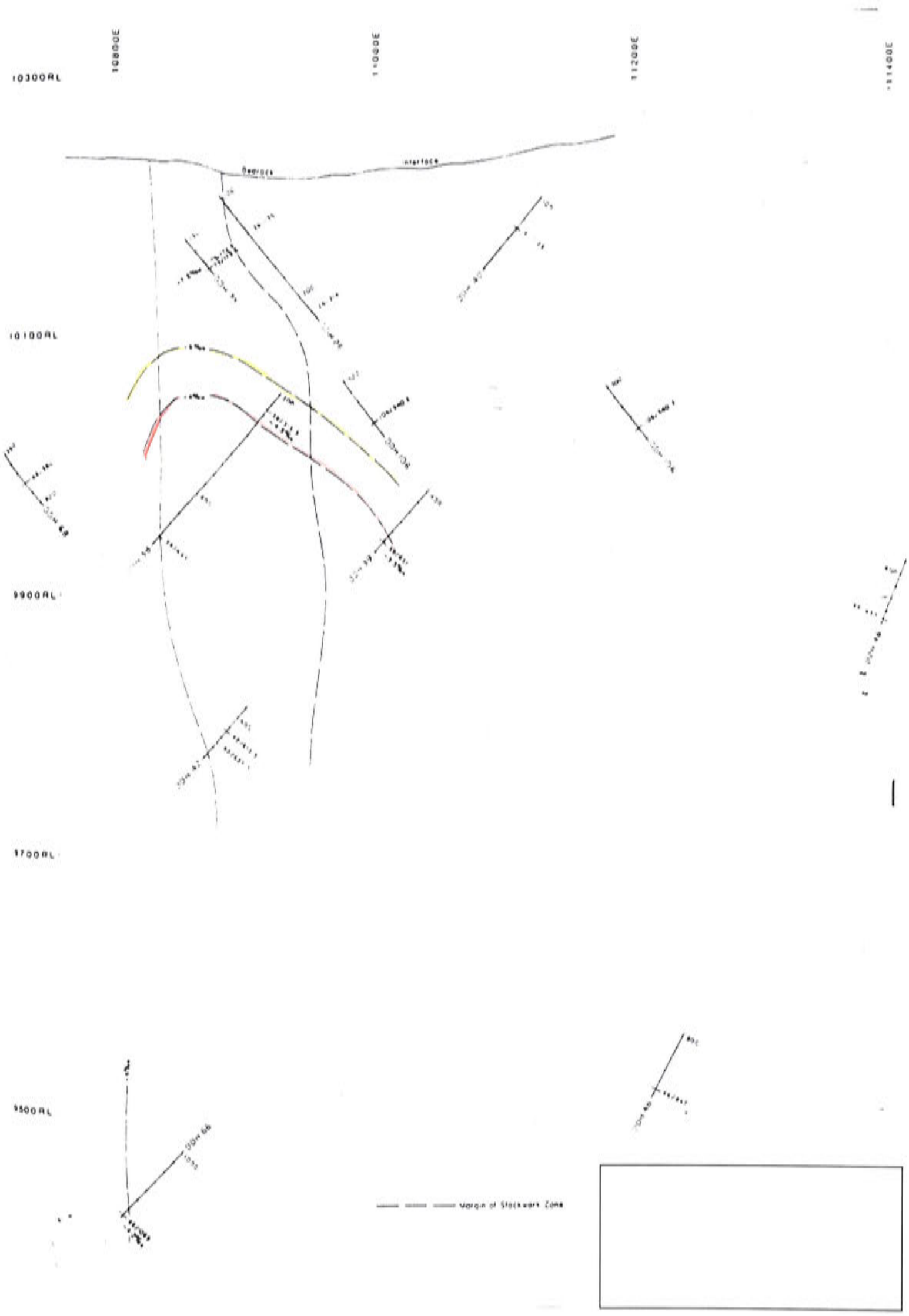

Figure 8.9 Cross-section projection sulphur isotope results, chalcopyrite, Endeavour 26 North.

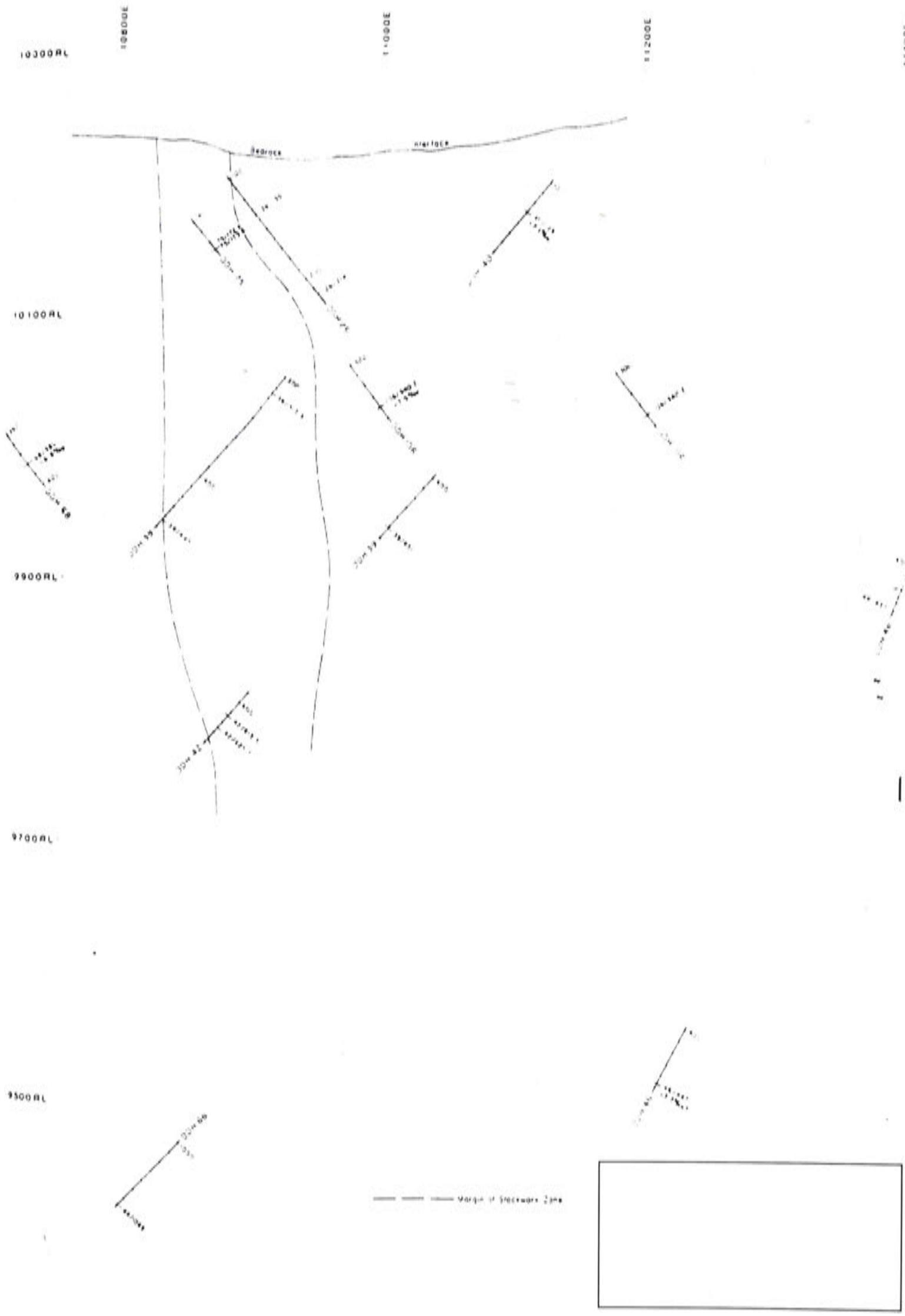

Figure 8.10 Cross-section projection sulphur isotope results, pyrite, Endeavour 26 North.

8.5 SULPHIDE–SULPHATE FRACTIONATION

Sulphide–sulphate fractionation provides information on both temperature of sulphide precipitation and the SO_2/H_2S ratio of the fluid. A number of studies have looked at this question in detail in recent years. Plots of $\delta^{34}S$ versus $\Delta_{sulphate-sulphide}$ for pairs of coexisting sulphates and sulphides from porphyry Cu deposits were prepared by Field and Gustafson (1976) for the El Salvador deposit (Chile) and by Eastoe (1983) for the Panguna and Frieda deposits (Papua New Guinea). Field and Gustafson (1976) argued that the data should plot on converging straight lines if certain conditions are met:

1. Isotopic equilibrium was maintained
2. The S reservoir was effectively infinite.
3. The $\delta^{34}S_{\sum S}$ of the S reservoir remained constant.
4. There was a consistent ratio of oxidised to reduced S species throughout the mineralising event.

It should also be noted that Ohmoto (1986) did not accept the method used by these authors and argued that analysis this way could give spurious results due the dependence of the equations involved. That possibility is acknowledged however this study also uses coexisting fluid inclusion data to constrain temperature (Figure 8.13) unlike the treatment considered by Ohmoto (1986). Field and Gustafson (1976) distinguished two trends (Fig. 8.11a) at El Salvador. The first trend was defined by pyrite–gypsum or anhydrite pairs from the Late 'D' veins, and chalcopyrite/pyrite–anhydrite pairs from the fringing zone of sericite–chlorite alteration. These data show good linearity and converge at $\Delta_{sulphate-sulphide} = 0$, with a $\delta^{34}S$ value of 6.8‰. Early anhydrite–bornite/chalcopyrite assemblages of the Early background K-silicate and 'A' vein occurrences of the deep central zone show considerably more scatter. Lines of regression converge at the $\Delta_{sulphate-sulphide} = 0$ between +1.5 and 1.7‰. Field and Gustafson (1976) state "it is tempting to interpret the two points of

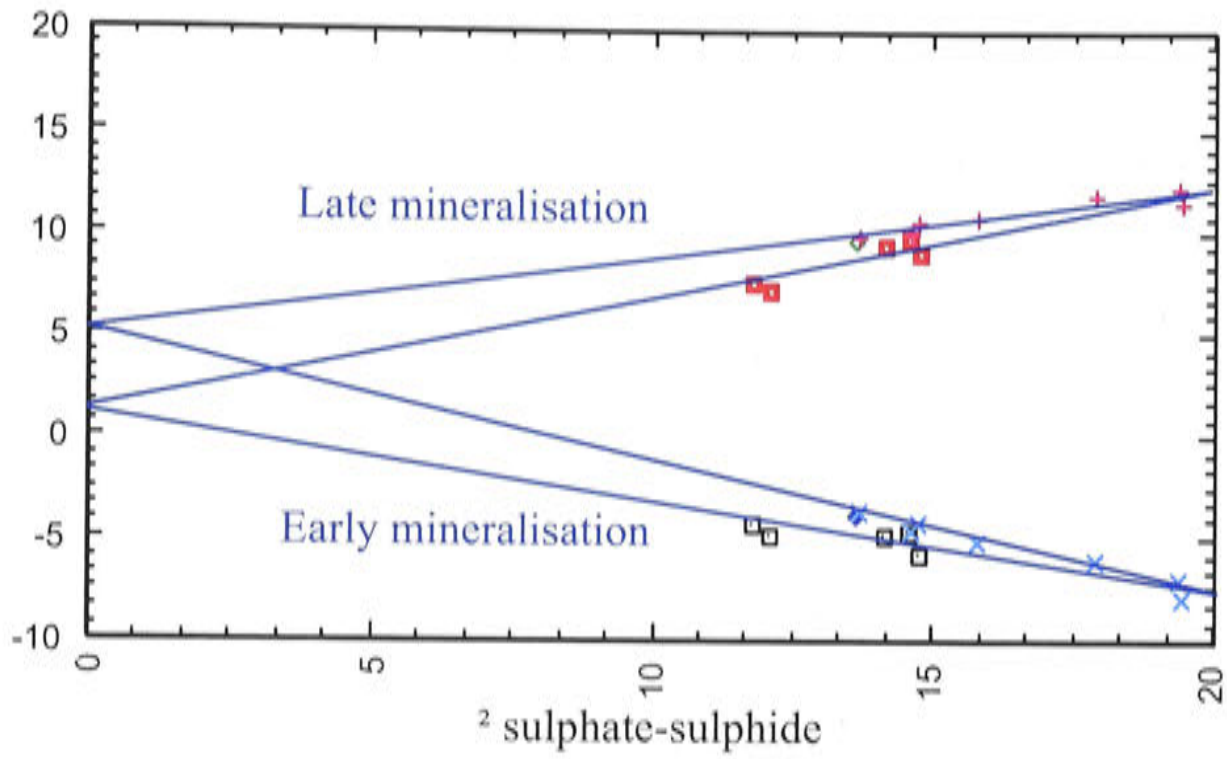

Figure 8.11a Plots of $\delta^{34}S$ vs $\Delta_{sulphate-sulphide}$ for pairs of coexisting sulphates and sulphides at El Salvador (after Field and Gustafson, 1976).

convergence as representing a real difference in the $\delta^{34}S_{\sum S}$ between the Early and Late stages of mineralisation". They conclude that the isotopic data tends to confirm the Gustafson and Hunt (1975) hypothesis, that early mineralisation was closely related to the emplacement of porphyry magmas from which the S was sourced directly. In support of this interpretation is the closeness of the interpreted bulk S value of 1.6 to 0‰, the accepted value for primitive 'magmatic' hydrothermal S.

S isotopes indicate two possible sources of S for Late mineralisation. They are as follows:

1. Magmatic S in addition to S derived from surrounding wall rocks by the late convecting meteoric hydrothermal system. A value of +6.8‰ is within the range measured for igneous rocks generally (Field and Gustafson, 1976), hence is consistent with the hypothesis.

2. Early S that was remobilised and emplaced at higher elevations during the Late hydrothermal activity.

Another model discussed by Field and Gustafson (1976) turns on reinterpreting pyrite data in the light of experimental work documented in Ohmoto and Rye (1979). They suggest that a transformation of pyrite data by subtracting –3‰ was appropriate, and that by doing so, the entire set of isotopic data "more nearly approximates a single population". However, plotting this corrected data does not provide a single population (Fig. 8.11b), and data points corresponding to late mineralisation converge

$\Delta_{sulphate-sulphide}$ t = 0 with a $\delta^{34}S$ value of 5‰. The data of Field and Gustafson (1976) are consistent with two sources of S; one wholly magmatic, the second a mixture of magmatic, remobilised S and host rock S.

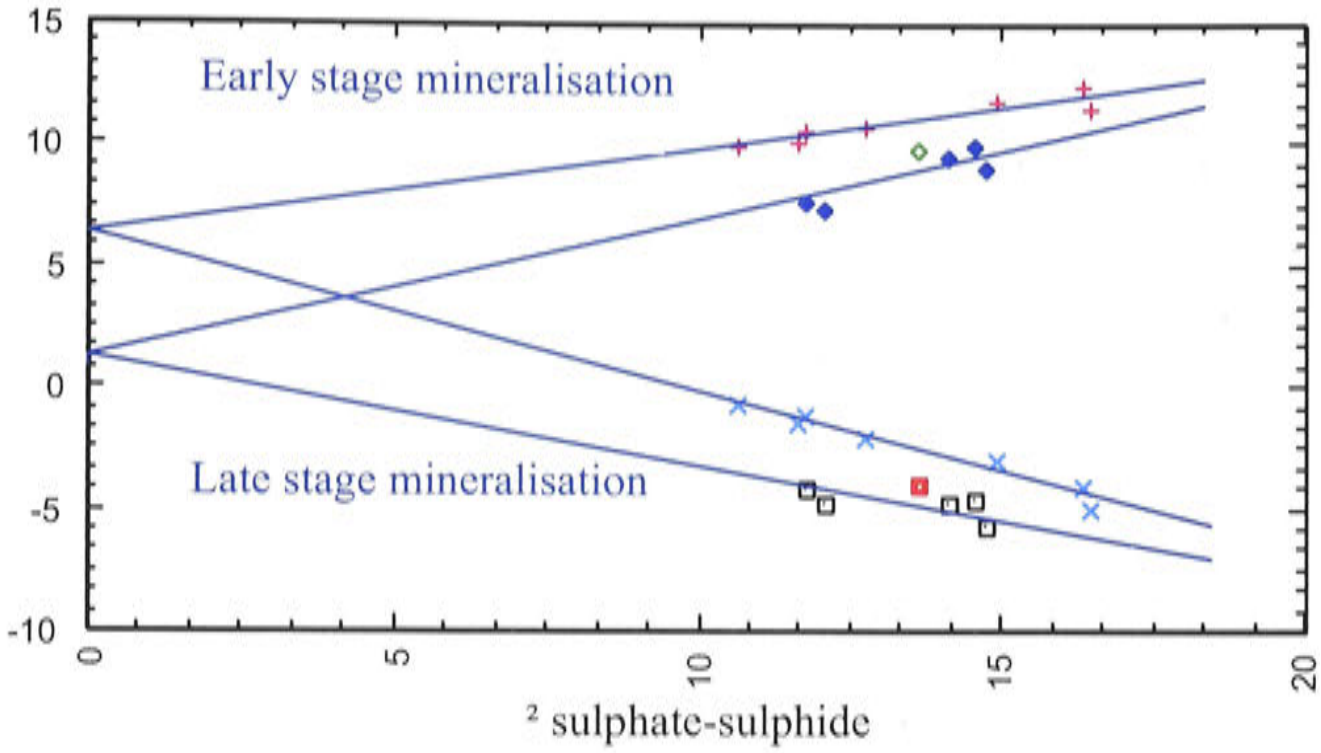

Figure 8.11b Plots of $\delta^{34}S$ vs $\Delta_{sulphate-sulphide}$ at El Salvador as in Figure 8.11a, with pyrite data transformed by subtracting 3‰.

Eastoe (1980) analysed S isotope data from the Panguna and Frieda deposits in Papua New Guinea in a similar way. For Panguna, a pair of straight lines giving an intercept near 1‰ was defined. Data from Frieda defined two populations; with data from the Koki Mineralisation converging at 2‰, in contrast to the Horse / Storm Creek mineralisation which converged at 1‰. Both populations define distinct slopes, which is a reflection of the oxidation state of the fluid (see later discussion).

Figure 8.12 is a plot of $\delta^{34}S$ versus $\Delta_{sulphate-sulphide}$ for pairs of coexisting sulphates and sulphides for Endeavour 26 North. The anhydrite–sulphide pairs converge at –2‰, which contrasts with the results from the Panguna and El Salvador deposits. In an attempt to plot other S isotope data on this diagram, samples with some temperature control from fluid inclusion determinations were added. These values together with their fluid inclusion temperatures are shown in Table 8.2. The $\Delta_{sulphate-sulphide}$ versus $\delta^{34}S$ plot is the equivalent of a temperature versus $\delta^{34}S$ plot and the results are shown in Figure 8.13. The additional S isotope data for sulphides cluster well around a line which converges at –2‰. Figures 8.12 and 8.13 suggest that the variation in S isotope ratios is best explained in terms of a variation in temperature of sulphide deposition from a fluid of constant m_{SO_2}/m_{H_2S} ratio.

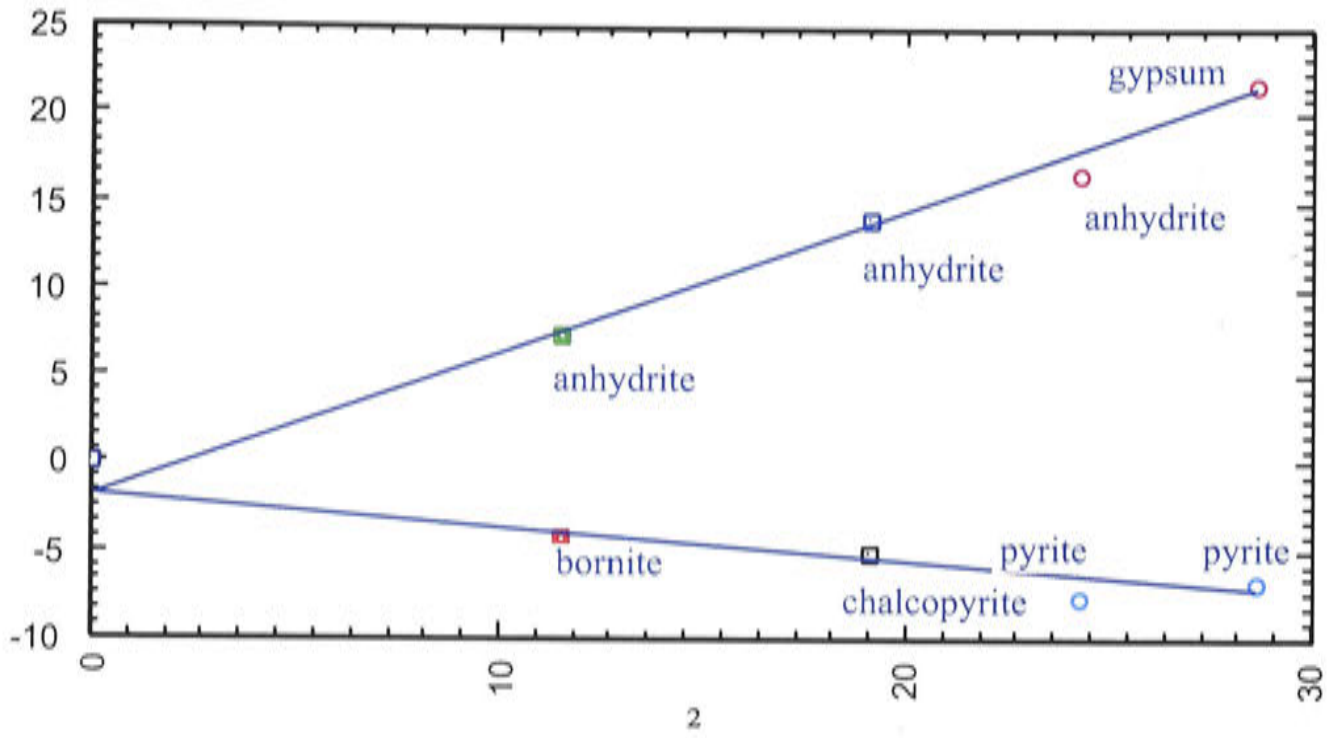

Figure 8.12 Plot of $\delta^{34}S$ vs $\Delta_{sulphate-sulphide}$ for pairs of coexisting sulphates and sulphides at Endeavour 26 North.

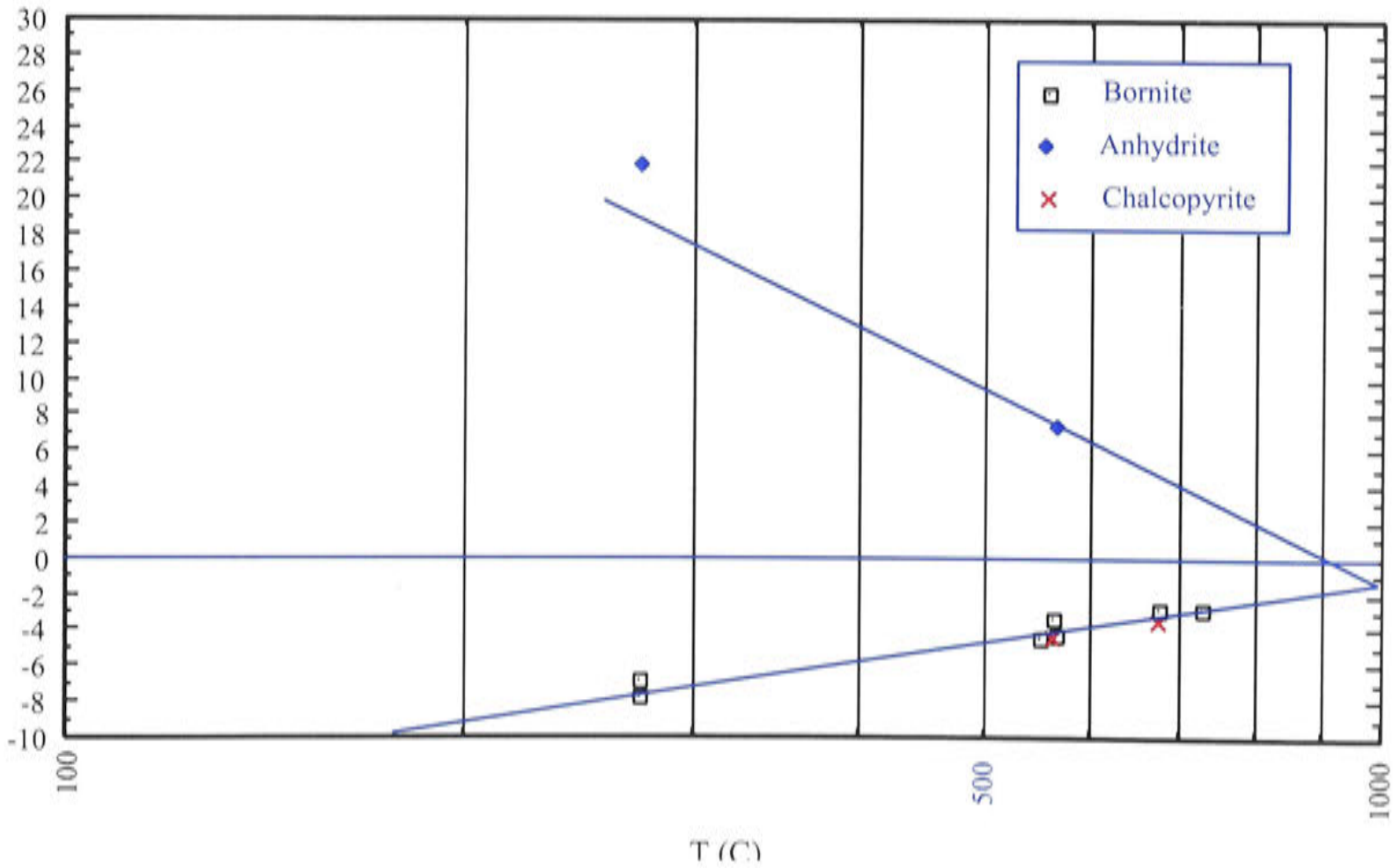

Figure 8.13 Plot of □^{34}S vs temperaturefor pairs of coexisting sulphates and sulphides at Endeavour 26 North, with $\delta^{34}S$ and temperature data for sulphides which have temperatures from fluid inclusions.

8.6 $\delta^{34}S$ AS A FUNCTION OF OXYGEN FUGACITY

The S species quantitatively important above 400 °C in hydrothermal fluids are H_2S and SO_2 (Ohmoto and Rye, 1979). The S isotopic composition of the fluid may be expressed as:

$$\delta^{34}S_{fluid} = \delta^{34}S_{H_2S} * X_{H_2S} + \delta^{34}S_{SO_2} * X_{SO_2}$$

$$= \delta^{34}S_{H_2S} + \Delta_{SO_2\text{-}H_2S} * X_{SO_2}$$

But as

$$\Delta_{SO2\text{-}H2S} = \Delta_{anhydrite\text{–}ccp} - \Delta_{anhydrite\text{–}SO_2} + \Delta_{ccp\text{–}H_2S}$$

and

$$\delta^{34}S_{H_2S} = \delta^{34}S_{ccp} - \Delta_{ccp\text{–}H_2S}$$

then

$$\delta^{34}S_{fluid} = \delta^{34}S_{ccp} + \Delta_{ccp\text{–}H2S} * (X_{SO_2} - 1) + (\Delta_{anhydrite\text{–}ccp} - \Delta_{anhydrite\text{–}SO_2}) * X_{SO_2}$$

However, since $\Delta_{ccp\text{–}H_2S}$ is small compared with $\Delta_{anhydrite\text{–}ccp} - \Delta_{anhydrite\text{–}SO_2}$, this function may be approximated to:

$$\delta^{34}S_{fluid} = \delta^{34}S_{ccp} + (\Delta_{anhydrite\text{–}ccp} - \Delta_{anhydrite\text{–}SO_2}) * X_{SO_2}$$

or

$$(1) \quad \delta^{34}S_{ccp} = -X_{SO2} * (\Delta_{anhydrite\text{–}ccp} - \Delta_{anhydrite\text{–}SO_2}) + \delta^{34}S_{fluid}$$

By substituting $\delta^{34}S_{ccp} = \delta^{34}S_{anhydrite} - \Delta_{anhydrite\text{–}ccp}$ and $X_{H_2S} = 1 - X_{SO_2}$ into equation 1 it can be seen that

$$(2) \ \delta^{34}S_{anhydrite} - \Delta_{anhydrite\text{–}SO_2} = X_{H_2S} * (\Delta_{anhydrite\text{–}ccp} - \Delta_{anhydrite\text{–}SO_2}) + \delta^{34}S_{fluid}$$

From Table 10.1 in Ohmoto and Rye (1979)

$$\Delta_{anhydrite\text{–}SO_2} = 0.41 * \Delta anhydrite\text{–}ccp - 0.5$$

for temperatures greater than 400 °C. Hence equations 1 and 2 closely approximate

$$(3) \qquad \delta^{34}S_{ccp} = -0.6 * X_{SO_2} * \Delta_{anhydrite-ccp} + \delta^{34}S_{fluid}$$

and

$$(4) \qquad \delta^{34}S_{anhydrite} = (1 - 0.6 * X_{SO_2}) * \Delta_{anhydrite-ccp} + \delta^{34}S_{fluid.}$$

Equations 3 and 4 explicitly express the slopes of the lines on a Δ versus δ diagram in terms of X_{SO_2} in the fluid, which relates to m_{SO_2}/m_{H_2S} via $X_{SO_2}/(1 - X_{SO_2})$. With increasing X_{SO_2} in the fluid, the slope to equation 3 increases as does the difference in $\delta^{34}S$ between the liquid and the sulphide. In contrast, the slope to equation 4 diminishes and the difference in $\delta^{34}S$ between the liquid and the anhydrite decreases. From Figure 8.13, the ratio of m_{H_2S}/m_{SO_2} for the Goonumbla hydrothermal fluids was around 1:1. In contrast, the ratio for the Panguna fluids has been bracketed between 9:1 and 4:1. The data from Frieda indicate values of 1:1 for the Koki deposit and 1:4 for the Horse deposit (Eastoe, 1980).

In relatively oxidised systems the decrease in $\delta^{34}S$ values with decreasing temperature should be particularly marked. This is exactly what is seen at Goonumbla in the lateral and vertical zonation of $\delta^{34}S$ values in bornite (and possibly chalcopyrite) decreasing away from the centre.

8.7 COMPARISON WITH OTHER DEPOSITS

Figure 8.1 shows S isotope data from a number of porphyry Cu deposits. There is considerable range in some sulphide analyses (e.g. Butte), and a restricted range in others such as Sierrita. Although porphyry deposits exhibit S isotope values in sulphides which range from –14 to +7‰, the median is around zero per mil.

Sulphate–sulphide pairs have been examined in relatively few deposits. The data from Field and Gustafson (1976) has been reinterpreted by Beane and Titley (1981) according to vein paragenesis. Early K-silicate veins give poorly defined slopes which project back to –1‰ if all data is used, and +6‰ if the highest pair is omitted. In later veins, sulphide–sulphide pairs project back to positive values between +8 and +11‰. Beane and Titley (1981) suggest that the change from the low to high $\delta^{34}S$ reservoir might have occurred earlier in the paragenesis than indicated by Field and

Gustafson, possibly at the onset of major deposition of sulphide with the Early 'A' veins.

Johan and Le Bel (1980) plotted sulphide–sulphate pairs from Cerro Verde – Santo Rosa (Peru), and plotted a pair of lines with a $\Delta_{sulphate-sulphide}$ =0 intercept near 6‰. Isotopic temperatures based on anhydrite–pyrite fractionation agreed with temperatures based on fluid inclusions.

The data portrayed in Figure 8.1, together with results from more recent sources, permit an approximate calculation of the redox state of the fluids. This is done by constructing a $\delta^{34}S$ versus $\Delta_{sulphate-sulphide}$ plot, using the $\Delta_{sulphate-sulphide}$ values which can be inferred from Figure 8.1, and assuming S isotopes at source were 0‰. The results of this exercise are shown in Figure 8.14. A number of deposits cluster with a m_{SO_2}/m_{H_2S} ratio around 1:6, and these include Panguna, Butte, Sierrita and Twin Butte. Another set of deposits cluster around a m_{SO_2}/m_{H_2S} ratio of 1:1, and these include Goonumbla, El Salvador and Ajo. This limited data set suggests a division of porphyry deposits based on the oxidation state of the fluid which may be H_2S dominant in Panguna, and SO_2 and H_2S in equal amounts in the case of Goonumbla. While the approach lacks precision, it does suggest an 'order of magnitude' difference in H_2S content exists between deposits such as Panguna and Goonumbla. H_2S in the fluid has a direct bearing on the amount and type of sulphide precipitated. Pyrite and chalcopyrite would be expected in the case of H_2S-rich systems, and bornite with minor pyrite in the case of more SO_2-rich systems. Goonumbla and the early stages of El Salvador and Ajo are bornite-rich systems, whereas Panguna, Sierrita , Twin Butte and other southwest USA porphyries are chalcopyrite dominant with pyrite-rich haloes. This breakup on the basis of H_2S:SO_2 values does not appear to have a bearing on Au tenor, as Goonumbla and Panguna are regarded as Cu–Au porphyries.

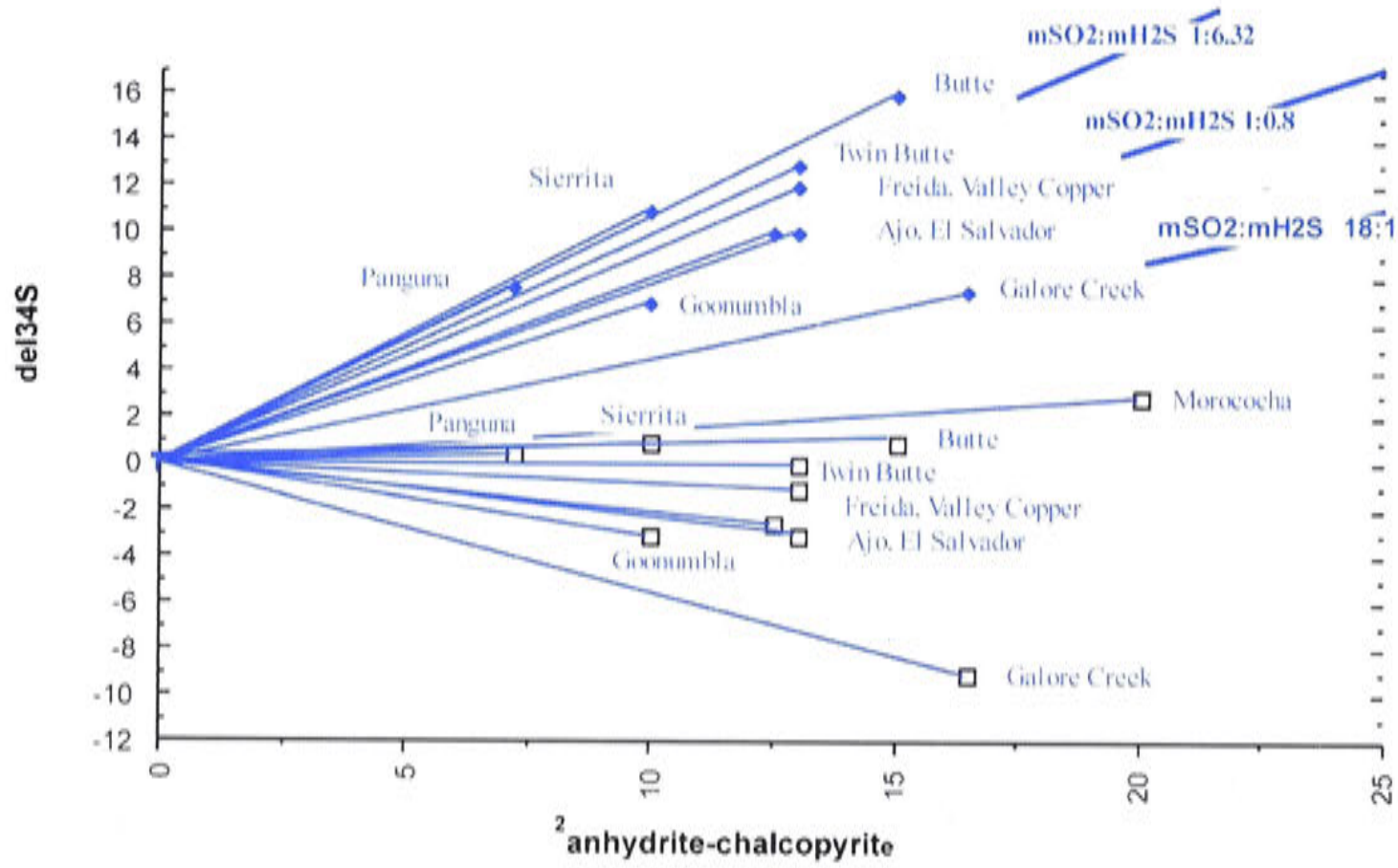

Figure 8.14 Plot of $\delta^{34}S$ vs $\Delta_{sulphate-sulphide}$ for pairs of coexisting sulphates and sulphides at a number of porphyry Cu deposits.

Chapter 9

ENDEAVOUR 26 NORTH: FLUID INCLUSIONS

9.1 INTRODUCTION

The study of fluid inclusions is well established in ore genesis research as a means of measuring some of the intensive variables of hydrothermal systems. A serious study demands accurate instrumentation and a detailed knowledge of the chemical system contained in the fluid inclusions, to allow meaningful interpretation of the measurements. Recent advances in the knowledge of the thermodynamic properties of multi-phase systems have been made, principally by the use of synthetic inclusions (Bodnar, 1985). As well, several new techniques have been developed for measuring the contents of these samples of hydrothermal fluids. These include analysis of volatiles in fluid inclusions using mass spectrometry (Norman et al., 1987), and the laser Raman microprobe (Burke et al., 1987). The proton probe is gaining acceptance as a non-destructive method of measuring the composition of fluid inclusions, particularly of elements with an atomic number greater than 11 (Horn and Traxel, 1987).

In this study interest centres on defining the evolution of the hydrothermal fluids in P–T–X space. The data of Potter (1978) on the NaCl–H_2O system has been used in determining the salinity of the low-salinity fluids via freezing-point depression measurements. For high-salinity inclusions, in which both halite and sylvite daughter salts occur and their melting points can be determined, the data of Ravich and Borovaya (1949) on the NaCl–KCl–H_2O system are used to determine fluid salinity. Commonly the KCl salt can be seen, but its melting properties cannot be determined. In such situations the fluid is treated as a pseudo-binary system, and the equivalent wt% NaCl determined from the experimental data on the NaCl–H_2O system (Sourirajan and Kennedy, 1962; Bodnar et al., 1985; Chou, 1987).

9.2 EQUIPMENT

Most of the measurements were made on a Leitz 1600 heating stage mounted on a Leitz microscope. The measurements were taken using a potentiometer linked to a platinum heating coil inside the stage. The Leitz stage was calibrated relative to the

melting points of the substances shown in Table 9.1. The calibration curve using these data is given in Figure 9.1.

Table 9.1 Measured melting points.

Substance	Melting point (°C)	Measured melting point (°C)
Lithium carbonate	618	627
Sodium chloride	800.4	810
Lithium fluoride	845	870
Sodium carbonate	851	885
Au	1064.4	1165
Potassium sulphate	1076	1170

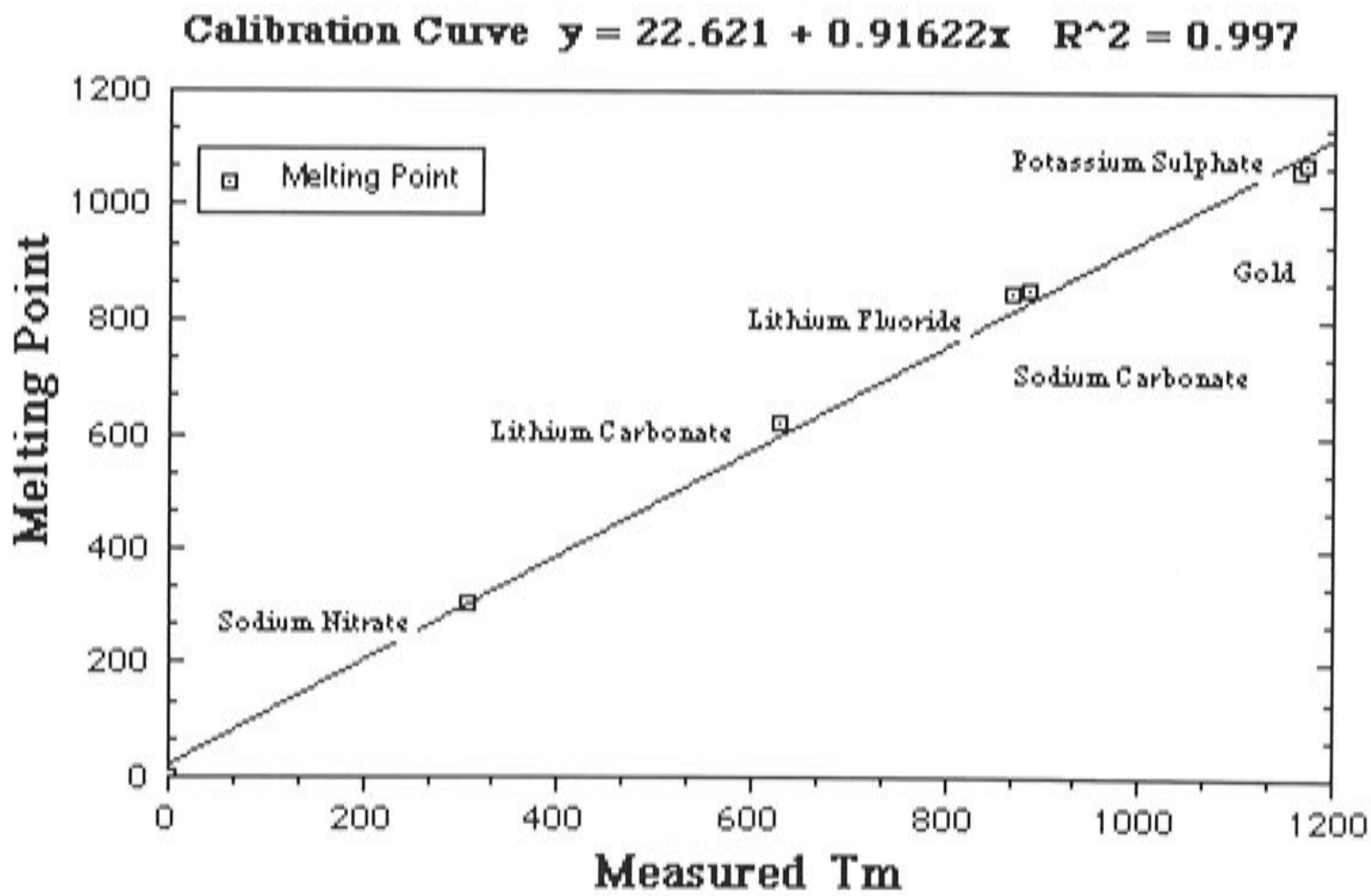

Figure 9.1 Calibration curve for the Leitz stage.

Lower temperature inclusions were measured on a Linkam TH-600 heating and freezing stage, which is designed to measure temperatures in the range between –180 and 600 °C. This stage was calibrated using organic and metal alloy cells for temperatures between –70 and 500 °C.

9.3 OBSERVATIONS

The following measurements were made on the low-salinity inclusions. Each fluid inclusion was sketched and the number of phases identified. The percentage area of each phase was calculated as a crude measure of relative abundance. The inclusion was frozen, then slowly reheated to measure the melting of ice ($T_{m,\ ice}$) and complete homogenisation of the inclusion at T_h. The formation of clathrates, which indicate the presence of CO_2, was never observed. The complete lack of any CO_2 was later confirmed by using the Laser Raman Microprobe at the Bureau of Mineral Resources, Canberra. The vapour phase of number of liquid-vapour and vapour-rich fluid inclusions was probed and only H_2O detected.

Fluid inclusions containing daughter salts were studied on the Leitz 1500. The fluid inclusion chips were first examined and, where possible, isolated fluid inclusions were selected for further study. Each inclusion was sketched and the number and relative abundances of phases were noted. The inclusion was slowly heated and phase changes noted. Where possible the following measurements were made:

1. temperature of sylvite dissolution ($T_{m\ KCL}$)
2. temperature of halite dissolution ($T_{m\ NaCl}$)
3. temperature of vapour phase homogenisation (T_h).

As measurements proceeded it became clear that a wide range of temperatures, particularly of T_h, could be determined from one fluid inclusion slide. It is salutary to briefly examine the probable causes.

1. **The presence of several generations of inclusions** is inevitable in most hydrothermal systems, but particularly so in a porphyry Cu system where vein propagation occurs, in part, due to fracturing and refracturing of the same vein structure. A range of high- to low-temperature fluid inclusions is an inevitable consequence.

2. **The trapping of solid or gaseous phases along with liquid**, the phenomenon known as heterogeneous trapping, is also an inevitable consequence of porphyry Cu formation, as two fluid phases, and possibly several solid phases, were present during most stages of the deposition of quartz at Endeavour 26 North.

3. **Necking down** of fluid inclusions is also highly likely in the high-temperature porphyry Cu environment. The annealing and re-annealing of quartz veins will allow dissolution and redeposition of quartz within a fluid inclusion to reduce the surface energy of the inclusion. Dissolution in some areas and deposition in other areas results in crystal faces forming in place of the original curving fracture surface. Eventually some of the crystal surfaces from opposite sides of

the inclusion meet, thus subdividing the original inclusion into a number of smaller inclusions with the same total volume as the original inclusion (Roedder, 1984). All stages of necking can be noted from Endeavour 26 North samples, although secondary inclusions which have proceeded to completion can be difficult to detect.

4. **Leakage** is common in the Endeavour 26 North porphyry environment, and where it occurred there was a complete loss of fluid. No loss of a small amount of fluid was observed, rather the difficulty was in recognising vapour-rich inclusions from empty ones.

A set of fluid inclusion data representing a single episode of trapping should produce a peak on a frequency distribution graph. The effects of heterogeneous trapping, necking and leakage can have the effect of skewing the distribution and increasing the variation. This will be considered when viewing the various data sets.

In selecting inclusions to study, those of irregular form were avoided because they commonly yielded dispersed data typical of the modifiers outlined above. The small size of the inclusions also proved to be a major limiting factor. Measurable inclusions varied in length from 7 to 15 μ, with the average around 10 μ. Useful measurements could be made from inclusions of 10 μ dimension, although inclusions which were sufficiently clear to allow observation of the phase changes were difficult to find. Many of the high-temperature inclusions decrepitated prior to homogenisation. Despite these difficulties it was possible to obtain representative data for the main paragenetic stages.

9.4 CLASSIFICATION AND DESCRIPTION OF INCLUSIONS

9.4.1 Solid inclusions

A variety of solid inclusions were noted in quartz associated with the fluid inclusions. These solid inclusions occur on a similar scale and distribution as the fluid inclusions. The following types of solid inclusions were recognised:

1. Colourless, rectangular crystals with high birefringence and high relief. The optical properties of this phase are consistent with anhydrite, which is commonly found in vein assemblages in association with quartz.

2. Red platelets and elongate tubes, commonly occurring in clusters. They exhibit high relief and very high birefringence, and display an almost transparent bright red colour in normal light. These observations are consistent with hematite, a common daughter mineral in the hypersaline inclusions.

3. Very thin, colourless needles occur in a few specimens, and are thought to be rutile.

4. Equant crystals of apatite varying from micron sized grains to submillimetre crystals.

9.4.2 Fluid inclusions

The fluid inclusions from the Endeavour 26 North deposit have been classified in the following way using the nomenclature of Wilson et al. (1980).

Type A Inclusions with <60 volume percent vapour and no daughter crystals (V + L).

Type B Inclusions with >60 volume percent vapour and no daughter crystals (L + V).

Type C Inclusions with <60 volume percent vapour and a halite daughter crystal (L + V + H).

Type D Inclusions with <60 volume percent vapour, and halite and sylvite daughter crystals (L+ V+ H+ S).

Type E Inclusions with < 60 volume percent vapour, and halite and sylvite daughter crystals plus unknowns.

Other phases present in Type C to E inclusions are hematite and chalcopyrite. Hematite can be identified by its characteristic red-orange translucent colour, and hexagonal platy form. Chalcopyrite exhibits a typical triangular crystal shape, and shows bright yellow reflectance in reflected light.

9.4.3 Type A inclusions

Type A inclusions are found in all veins crosscutting the Endeavour 26 North deposit. They tend to occur in two modes. The first is as clusters of irregular shaped inclusions occupying small irregular cavities. They can be equidimensional or branched in form, and consist of an aqueous liquid and a bubble occupying 5–20% of the inclusion volume (Plate 9.1). Daughter minerals or trapped solid inclusions are not seen. The second mode of occurrence is as a network of subparallel inclusions forming a fine-scale set of fractures (Plate 9.2) that are commonly normal to the vein wall. Type A inclusions are typically low temperature and are all secondary.

9.4.4 Type B inclusions

Type B inclusions occur in Stages 1 to 9 of the Endeavour 26 North deposit, that is to say, all stages associated with mineralisation. Some occur in clusters

associated with hypersaline inclusions, in otherwise inclusion-free zones near the termination of crystals. This suggests that these may be primary or at least pseudo-secondary. More commonly, however, Type B inclusions adopt equidimensional to elongate shapes, rounded shapes or negative crystal shapes. They can be distinguished from empty inclusions by the recognition of a liquid rim that is best observed in slightly cuspate inclusions. Daughter salts occur in only some of the inclusions. The presence of gas-rich inclusions with various proportions of liquid to gas is consistent with boiling, although it is not sufficient evidence in itself. Necking of inclusions can produce Type B inclusions.

9.4.5 Type C inclusions

Type C inclusions consist of liquid and vapour plus halite, and may include hematite and/or chalcopyrite. They commonly occur in association with Type B inclusions, and in some cases Type B and C inclusions occur in the same fracture. Very few Type C inclusions can be shown to be unequivocally primary, however, they can be located in relatively inclusion-free areas near crystal terminations. The shape of Type C inclusions is quite variable, ranging from irregular to equant with rounded terminations. Some adopt a negative crystal shape. They range from <5 to 15 μ, and average around 10 μ in size. The vapour bubble occupies ~10–20% of the inclusion volume, the remainder of the volume being occupied by liquid and a cubic halite crystal of varying size. Although some of these inclusions may have other daughter salts which are not visible, it is clear that there is a class of inclusions which contain halite as the only daughter mineral which dissolves upon heating. Hematite and chalcopyrite, if present, never dissolve upon heating. Hematite will turn dark brown and return to a red colour upon cooling. Salinities range from 48 to 77 wt% using the equation of Chou (1987).

9.4.6 Type D inclusions

Type D inclusions are the most common type in the Endeavour 26 North deposit. They consist of liquid, vapour and halite plus sylvite, and may include hematite and/or chalcopyrite. These inclusions commonly occur in association with Type B inclusions, and have been located with Type B inclusions on the same fracture planes. Again few are definitely primary. The inclusions are commonly crowded with daughter salts and the volume of liquid is minor. Daughter salts of hematite, chalcopyrite or opaques are abundant, but not ubiquitous. The halite commonly takes on a cubic habit, whilst sylvite presents a subrounded shape. Salinities as high as 70 wt% NaCl equivalent have been measured, particularly from the early high-temperature inclusions. The fluids truly represent saline melts rather than salt-bearing hydrothermal solutions.

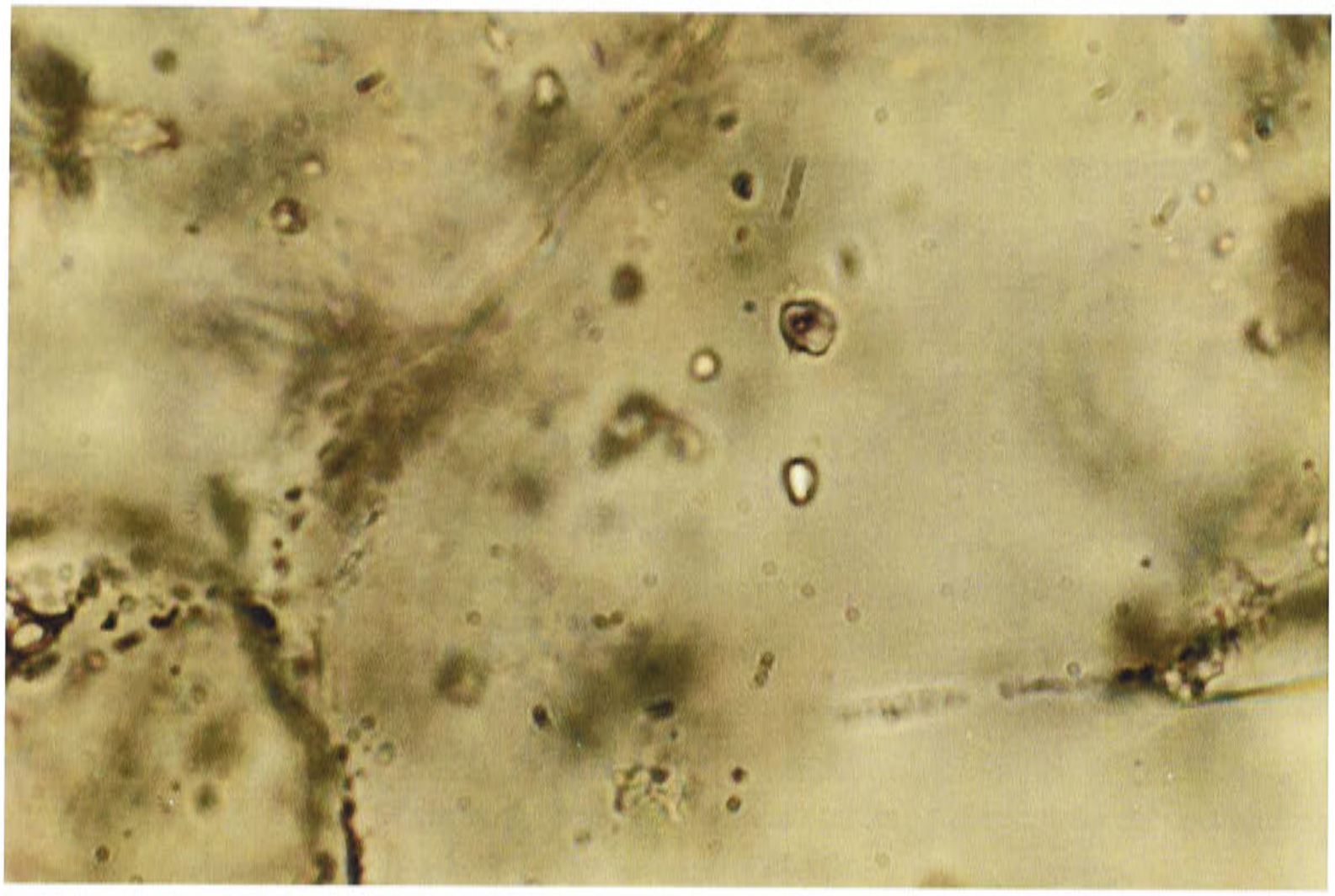

Plate 9.1 Type A inclusion showing aqueous liquid and bubble.

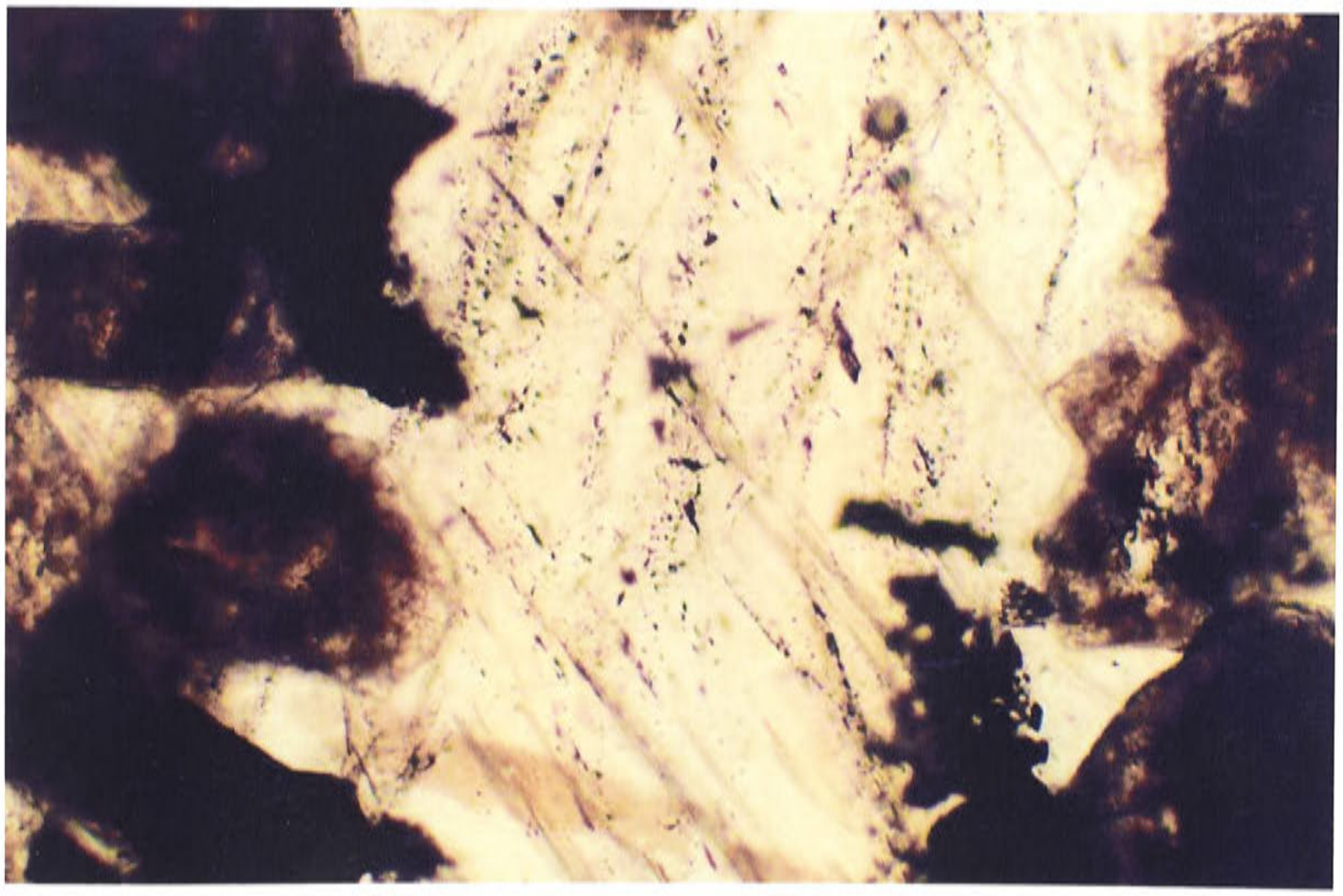

Plate 9.2 Type A inclusions forming a fine-scale set of fractures.

9.4.7 Type E inclusions

Type E inclusions consist of liquid and vapour plus halite, sylvite and unknowns, and may include hematite and/or chalcopyrite. These commonly occur in association with Type B inclusions, and have also been located on a fracture in clear association with Type B inclusions. Again few are definitely primary.

9.5 TEMPERATURE–SALINITY DATA FOR STAGE 3 VEINS

9.5.1 Morphology of vein types

The Stage 3 veins represent the earliest part of the potassic phase of alteration. The quartz veins are irregular and discontinuous within a vein envelope of mainly finely divided biotite with albite, hematite or magnetite and minor sulphides. The zone of biotite may be distinctly vein-like in form, but not have a central quartz vein. Fluid inclusions are difficult to find in these very fine veinlets. Adjacent to these veins the biotite vein envelope grades into spotty clusters of biotite grains.

9.5.2 Fluid inclusion data

The range of homogenisation temperatures spans 410 to 720 °C, a range of 300 degrees (Fig. 9.2). This is a characteristic of the early stages of veining compared with later stages. Type B to E inclusions are evident in some veins, and hypersaline and vapour-rich inclusions reside close to each other. This vein-set recorded a T_h of 662 °C for the saline inclusion, and 596 °C for the vapour-rich sample. Bodnar et al. (1985) demonstrated that vapour-rich inclusions tend to give homogenisation temperatures well below that of the coexisting saline phases. Hence, fluids that are boiling cannot be ruled out for this stage of mineralisation. $T_{m\ NaCl}$ ranges from 460 to 660 °C with a peak around 500 °C (Fig. 9.3), and $T_{m\ KCl}$ ranges between 370 to 500 °C (Fig. 9.4).

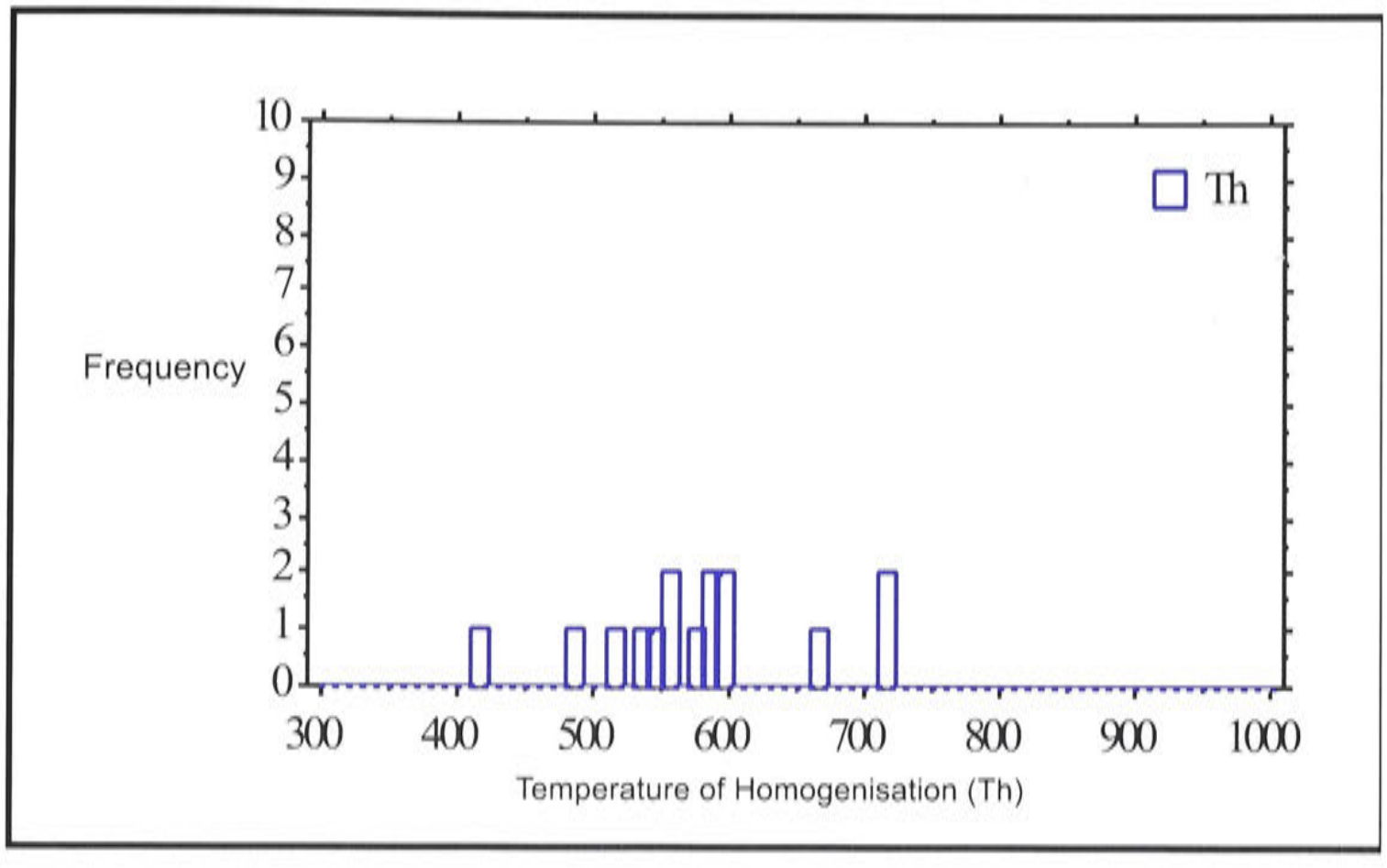

Figure 9.2 Temperature of vapour homogenisation (T_h) histogram for Stage 3.

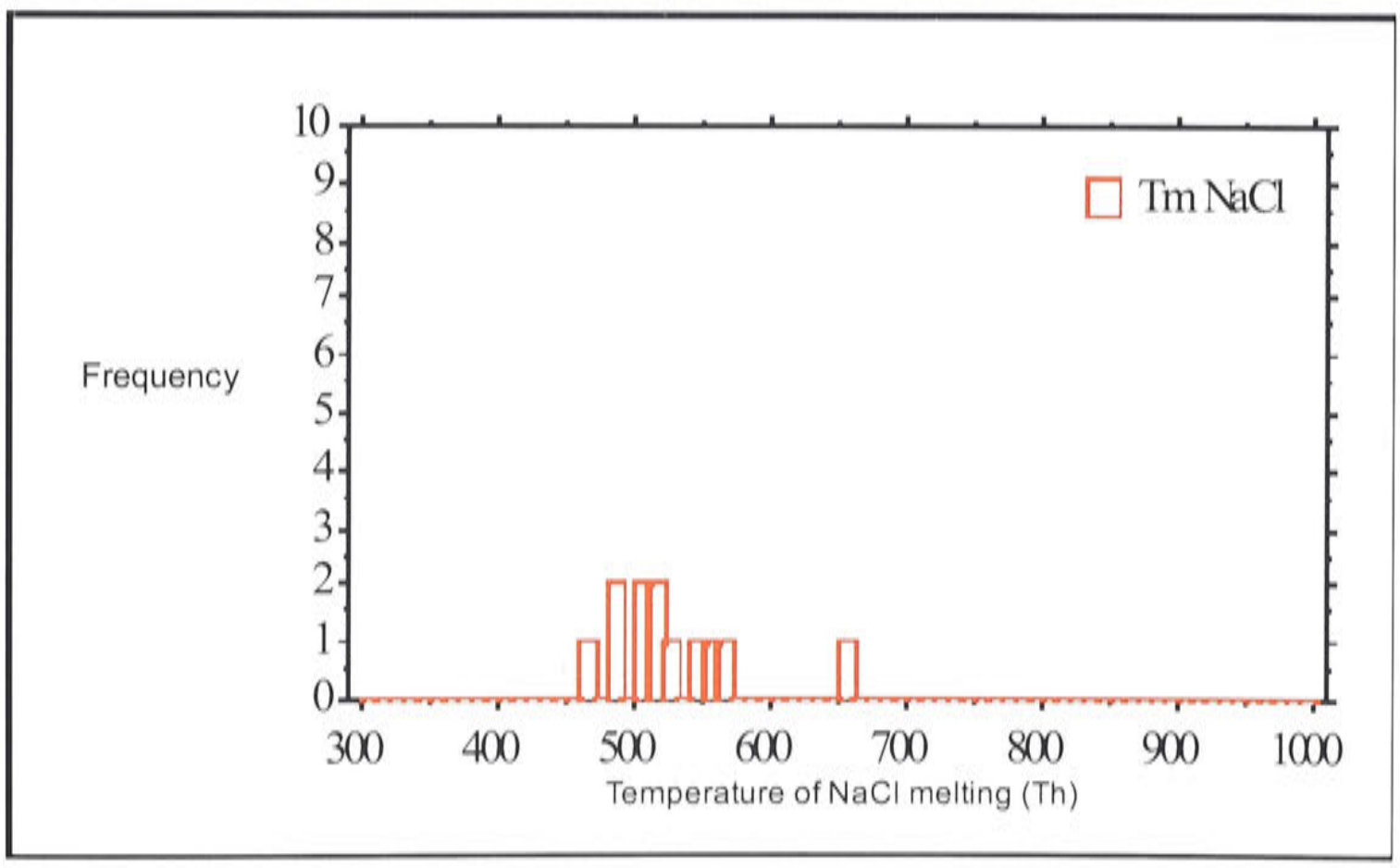

Figure 9.3 Temperature of NaCl dissolution ($T_{m\ NaCl}$) histogram for Stage 3.

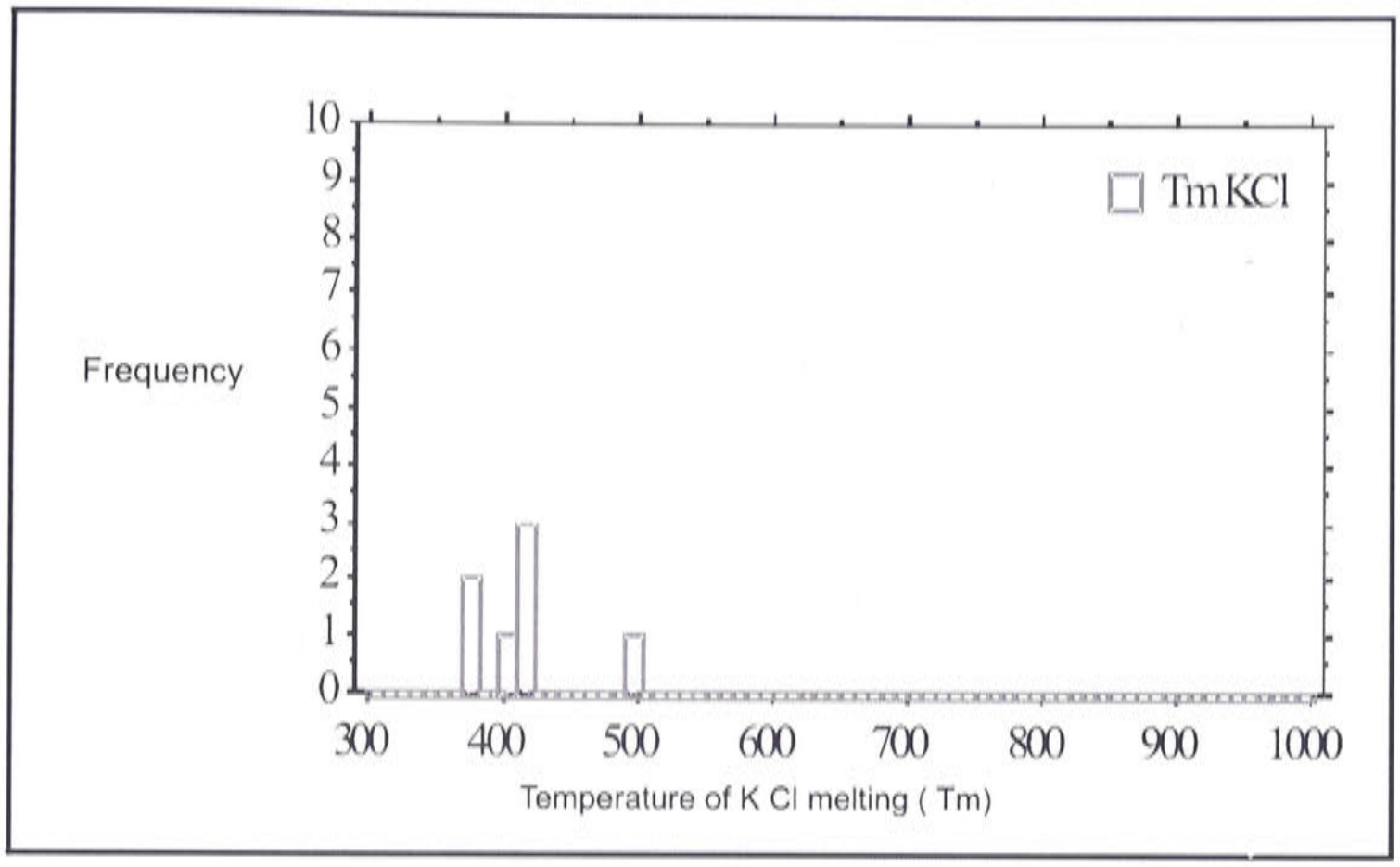

Figure 9.4 Temperature of KCl dissolution ($T_{m\ NaCl}$) histogram for Stage 3.

9.6 TEMPERATURE – SALINITY DATA FOR STAGE 4 VEINS

9.6.1 Morphology of vein types

Stage 4 veinlets are commonly discontinuous, and develop irregular vein margins with euhedral quartz crystals projecting out from the vein into the vein margin. The vein margin characteristically forms an interlocking mosaic of K-feldspar rimmed with albite or quartz. Graphic intergrowths of quartz and K-feldspar are abundant, and indicate a transition between magmatic and hydrothermal conditions. Where such veins crosscut albitised plagioclase crystals, a thin selvage of quartz and K-feldspar is deposited.

They are always less than a millimetre in width and form a fine to very dense network which gives rise to the pervasive nature of the potassic alteration. Bornite predominantly occurs with this vein type and it is an important mineralising phase. In thin section the veins are ill-defined consisting of trails of quartz intergrown with K-feldspar and anhydrite, and rare fluorite.

9.6.2 Fluid inclusion types

Fluid inclusion Types A to E are present in the Stage 4 microveinlets, and Types D and E are common. Homogenisation temperatures range from 470 to 1090 °C with peaks at 580 and 760 °C (Fig. 9.5). The range of temperatures extends well into magmatic temperatures which is consistent with the magmatic textures, such as graphic intergrowths, exhibited by this vein stage. Several T_h measurements exceeded 900 °C

with corresponding high salinities. Temperatures of melting for NaCl range from 410 to 570 °C with a peak at 580 °C, and corresponding $T_{m\,KCl}$ range from 400 to 570 °C (Figs 9.6, 9.7). Using the phase diagram for the vapour saturated NaCl–KCl–H_2O system (Roedder, 1984), the concentration of NaCl and KCl in the inclusions can be calculated. The range of salinities in Figure 9.8 shows an interesting relationship: it is clear that fluids that homogenise at high temperature have a low KCl/NaCl ratio, and that with decreasing temperature this ratio systematically increases. As can be seen from Figure 9.9, most of the inclusions homogenise by vapour disappearance (termed 'vapour homogenisation'). The remainder homogenise by dissolution of halite after the disappearance of the vapour (termed 'halite homogenisation' after Wilson et al., 1980).

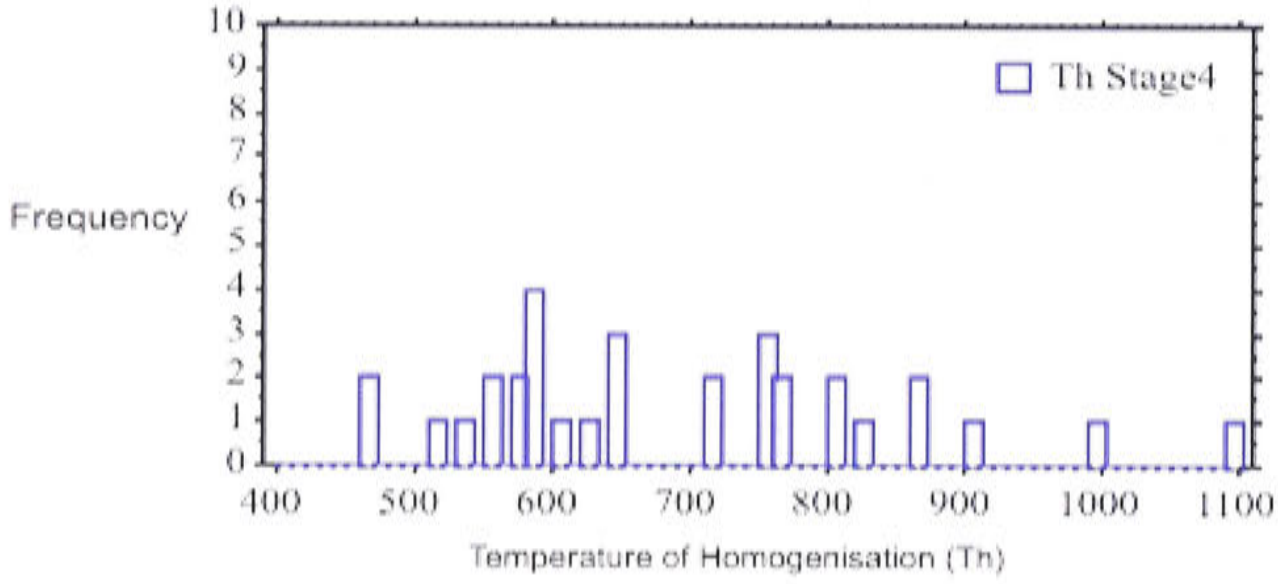

Figure 9.5 Temperature of vapour homogenisation (T_h) histogram for Stage 4.

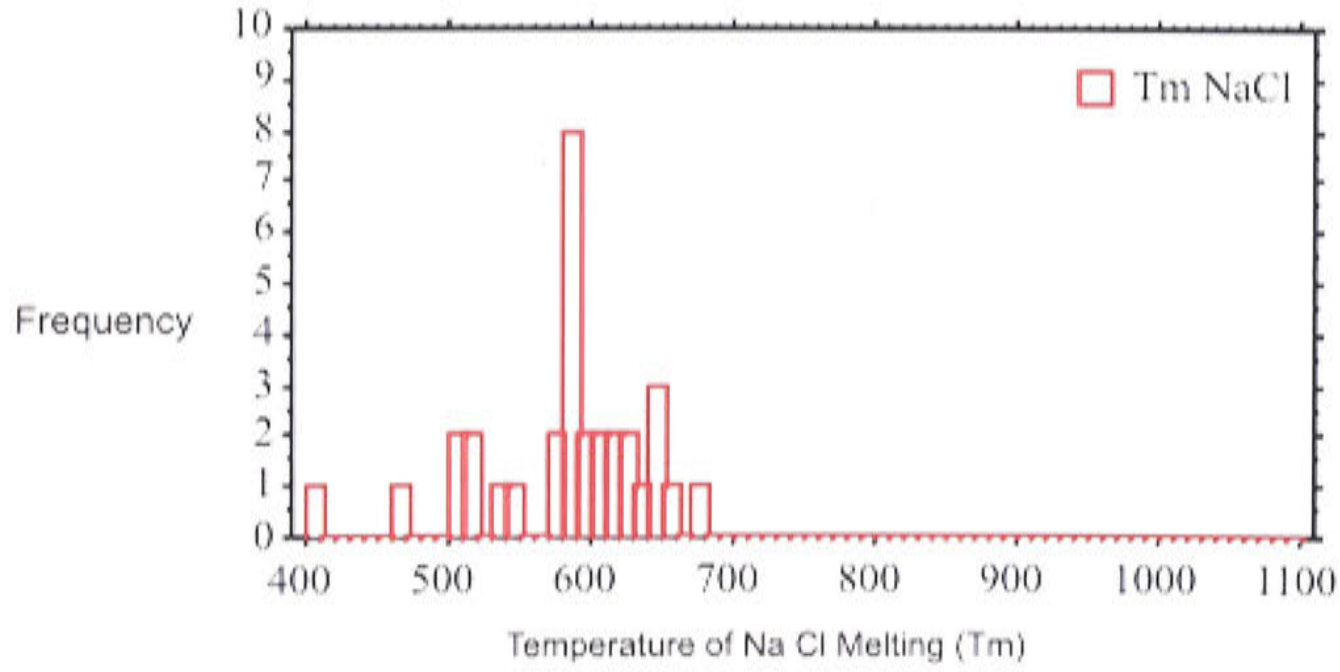

Figure 9.6 Temperature of halite dissolution ($T_{m\,NaCl}$) histogram for Stage 4.

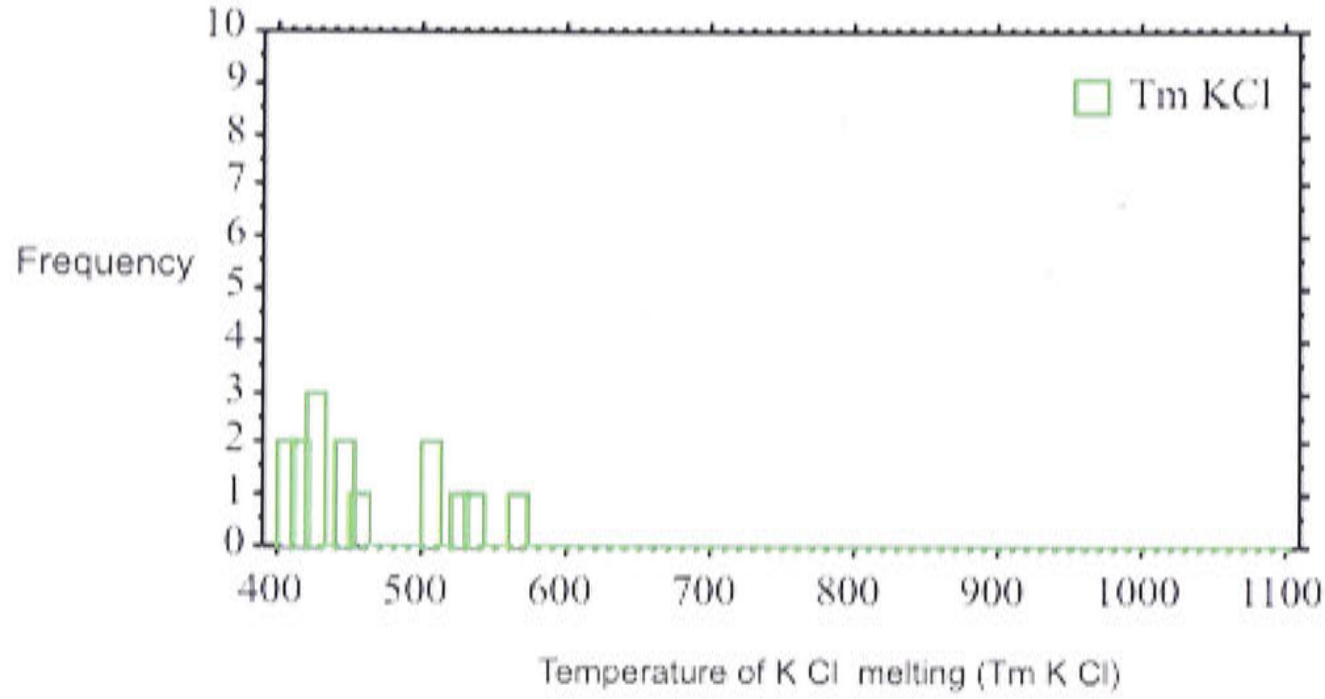

Figure 9.7 Temperature of sylvite dissolution ($T_{m\ KCl}$) histogram for Stage 4.

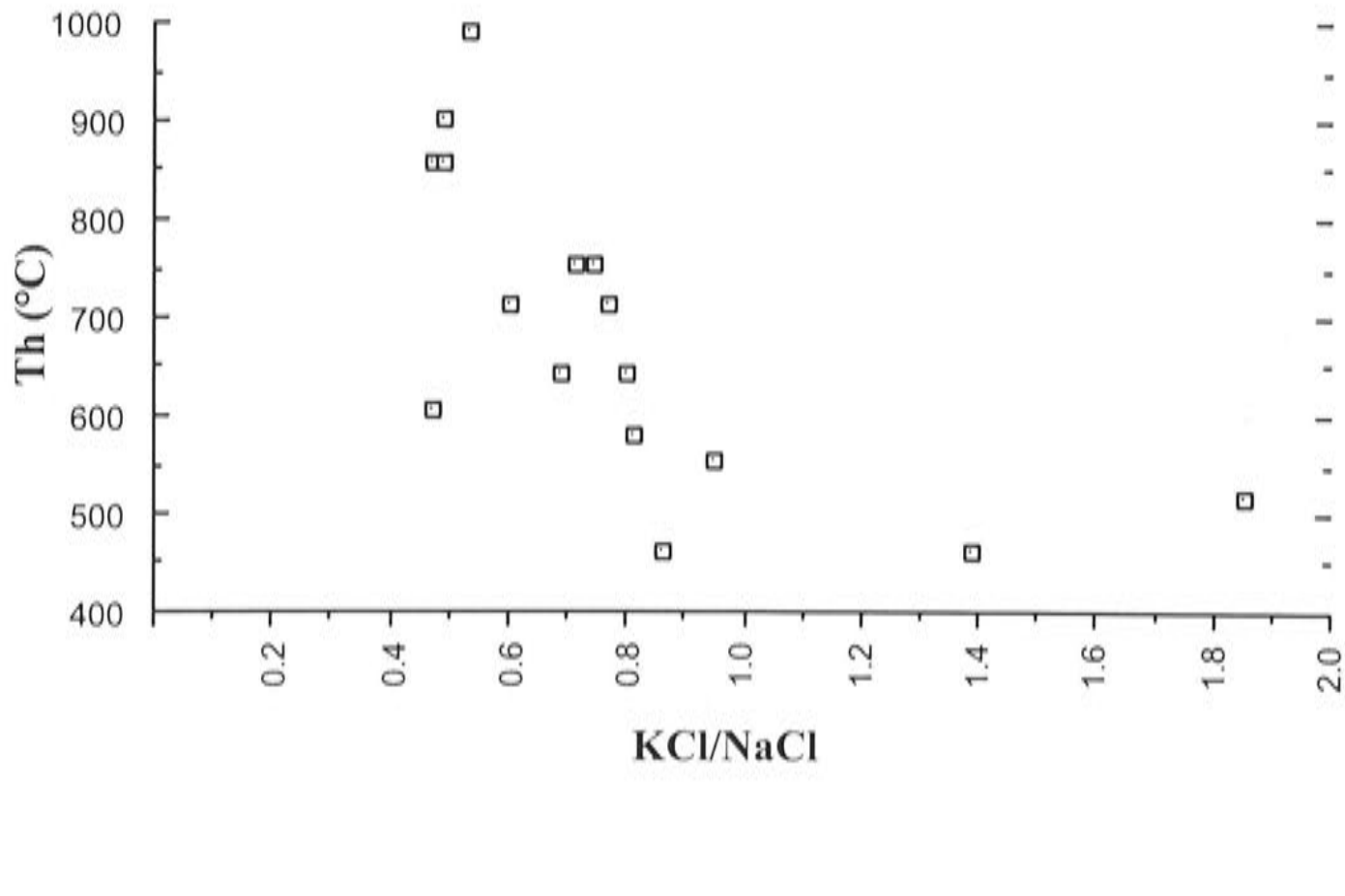

Figure 9.8 Total homogenisation temperature vs KCl/NaCl within Stage 4.

As can be seen from Figure 9.9, most of the inclusions homogenise by vapour disappearance (termed 'vapour homogenisation'). The remainder homogenise by dissolution of halite after the disappearance of the vapour (termed 'halite

homogenisation' after Wilson et al (1980).

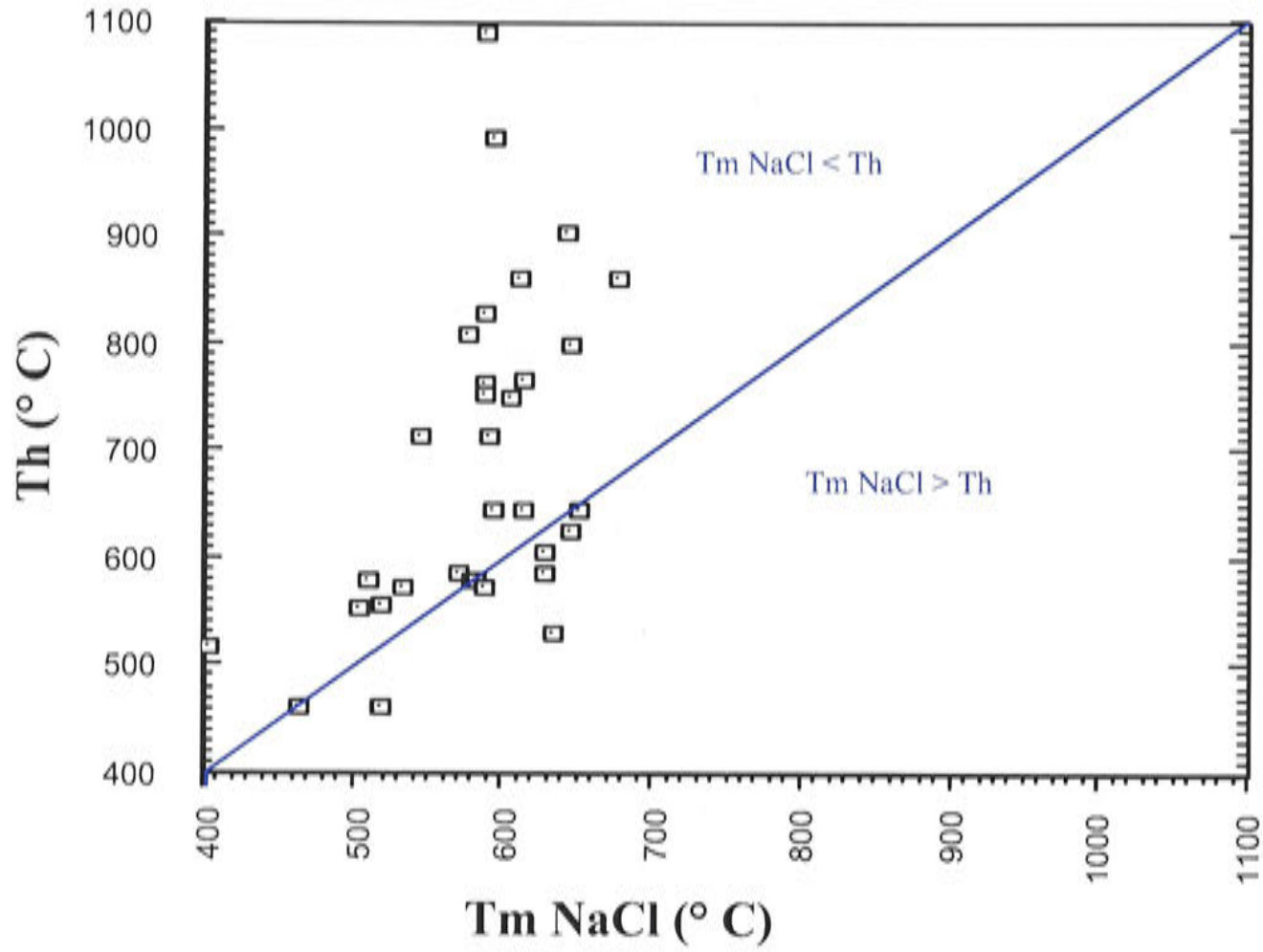

Figure 9.9 $T_{m\ NaCl}$ vs T_h plot showing vapour homogenisation vs halite homogenisation.

9.7 TEMPERATURE–SALINITY DATA FOR STAGE 5 VEINS

9.7.1 Morphology of Stage 5 veins

Stage 5 veining defines the main stockwork zone. In contrast to Stage 4, the veins in this stage range from single, sharp-walled, grey, vitreous veins through to a dense lattice of veins. In places the density of Stage 5 veins can reach a point where the rock is essentially made up of quartz. The internal vein structure varies from that of fine laminations, with fine bornite or chalcopyrite defining the lamellae, to sparry quartz with the interstices infilled with sulphides and/or sulphates. The internal structure of the Stage 5 veins is suggestive of a crack-seal style of vein formation. Vein envelope alteration is minor compared to Stage 4 veinlets.

9.7.2 Fluid inclusion types

All fluid inclusion types from A to E are present in Stage 5. Type A inclusions are clearly secondary and form arrays on fracture planes and are typically low temperature. Some exhibit quite irregular shapes with angular re-entrant angles. Vapour-rich inclusions (Type B) are common and can be identified by liquid rims,

particularly in inclusions which taper to a point. Type C to E inclusions can occur as single isolated inclusions or as small clusters. Type B inclusions commonly occur close to the hypersaline Type C to E inclusions, however, the hypersaline inclusions are more abundant than the vapour-rich variety. Large hematite plates are common in inclusion Types C to E at this vein stage. Opaques, some of which are clearly chalcopyrite, are also common in this vein stage.

T_h values span the narrow range of 430 to 610 °C with an outlier at 680 °C. Two clear peaks occur at 460 to 470 °C and at 550 to 560 °C (Fig. 9.10). These temperatures are significantly lower than those of Stage 4.

The data for dissolution of NaCl spans 460 to 650 °C, with a well-defined peak at the interval 540 to 550 °C and another single peak at 460 to 470 °C (Fig. 9.11). The T_m for KCl exhibits a range from 380 to 490 °C (Fig. 9.12). Plotting these data on the NaCl–KCl–H_2O diagram of Roedder (1984) yields NaCl concentrations which range from 28 to 66 wt%, with the main cluster between 40 and 55 wt%. KCl concentrations range between 24 to 52 wt%. The ratio of KCl to NaCl ranges from 0.3 to 1.0 but shows no correlation with temperature, in contrast with Stage 4 (compare Figs 9.13 and 9.8).

Approximately 50% of the Type C to E inclusions in Stage 5 are homogenised by vapour disappearance, and the remainder by dissolution of halite (Fig. 9.14).

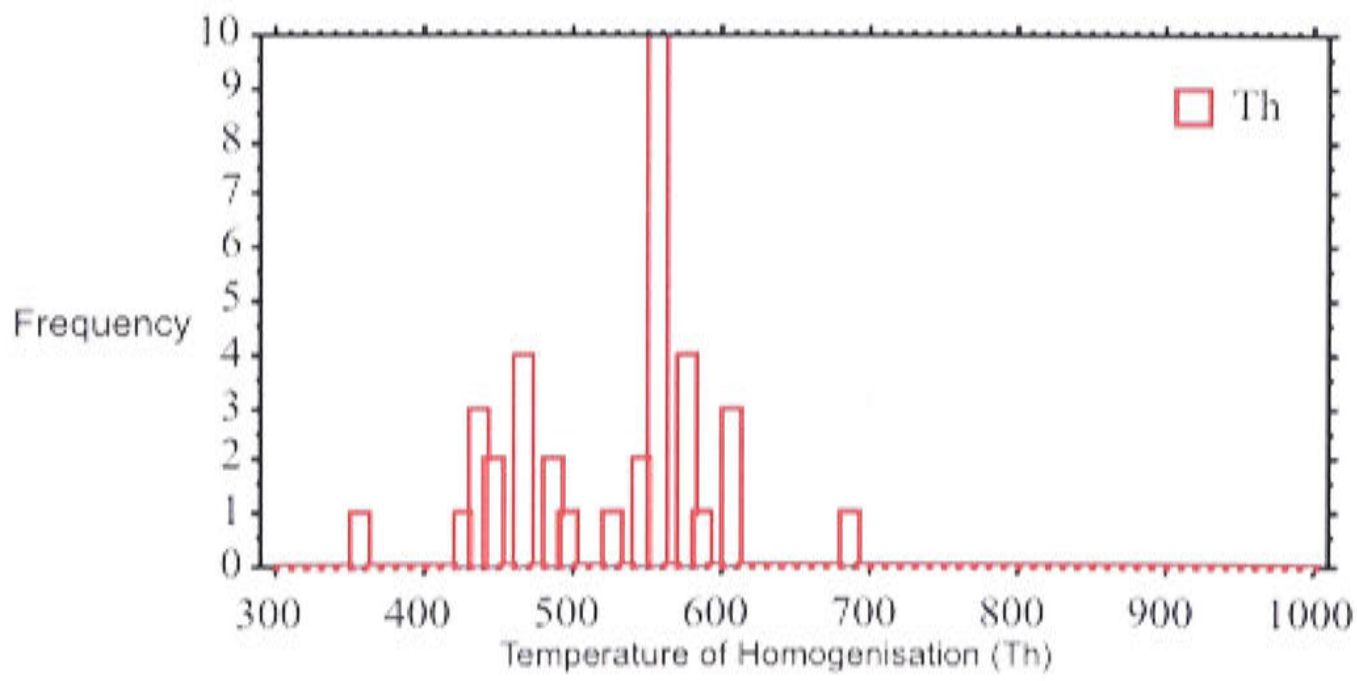

Figure 9.10 Vapour homogenisation temperature (T_h) histogram for Stage 5.

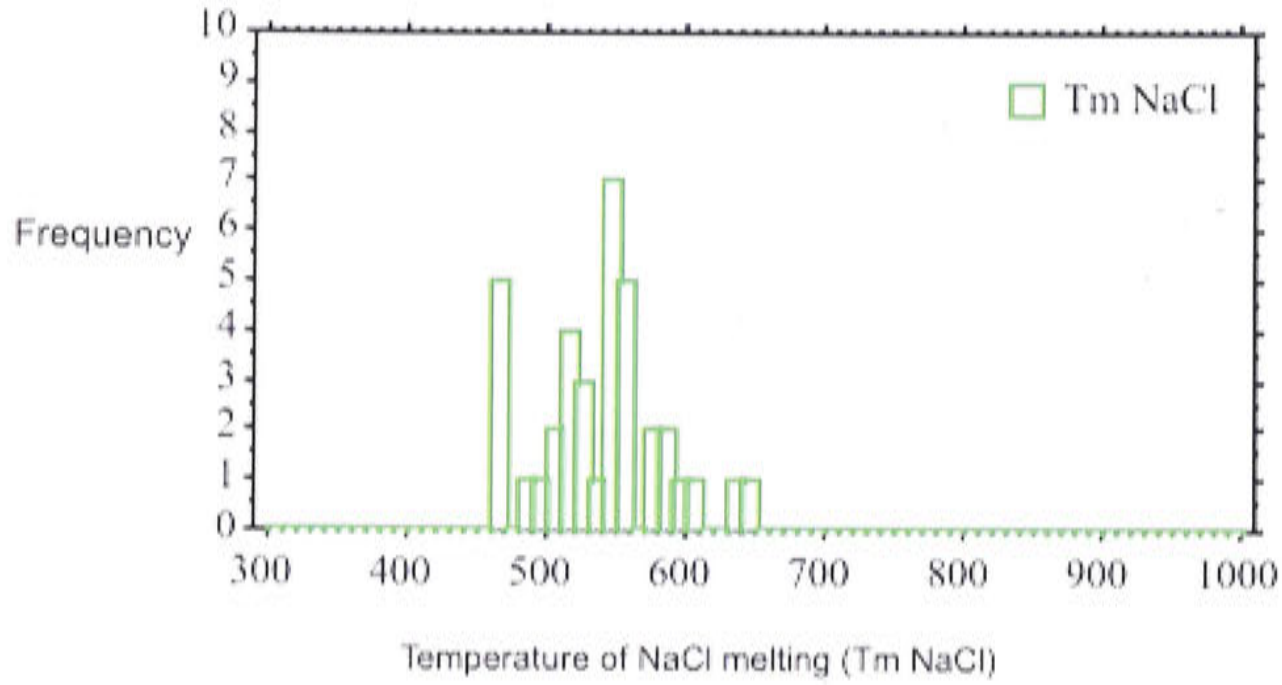

Figure 9.11 Temperature of NaCl dissolution ($T_{m\ NaCl}$) histogram for Stage 5.

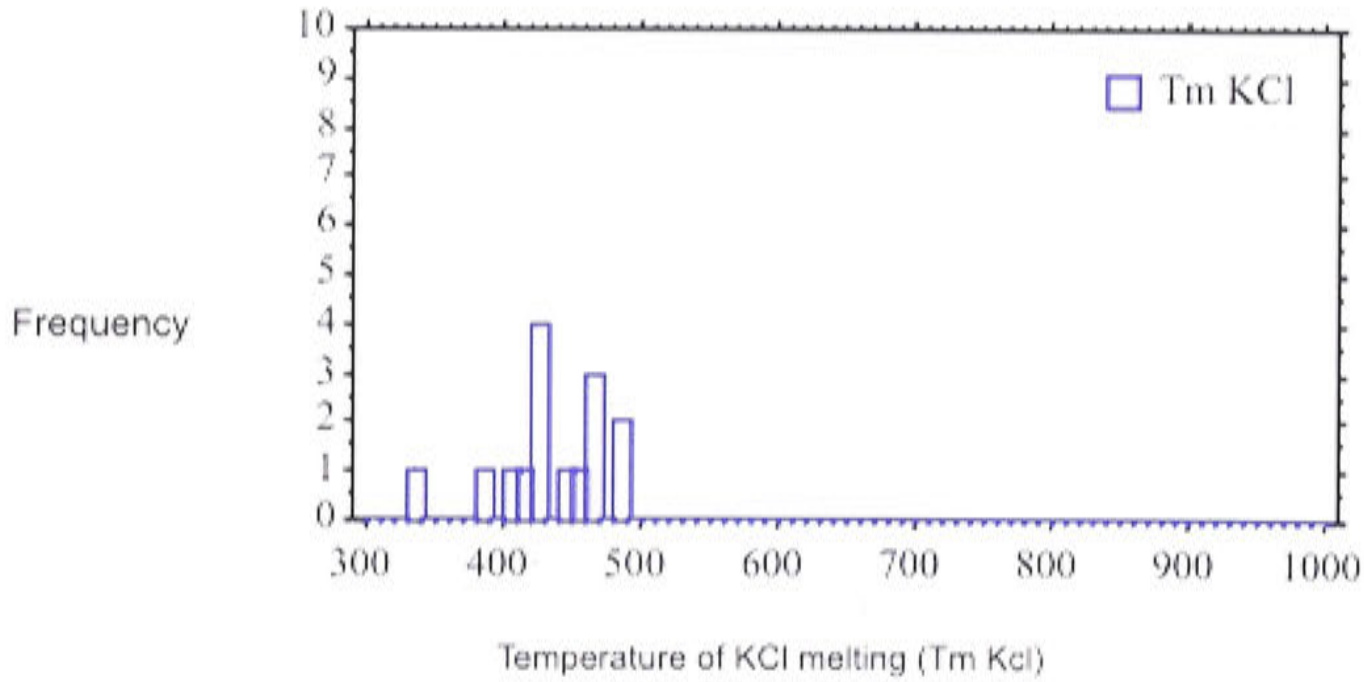

Figure 9.12 Temperature of KCl dissolution ($T_{m\ KCl}$) histogram for Stage 5.

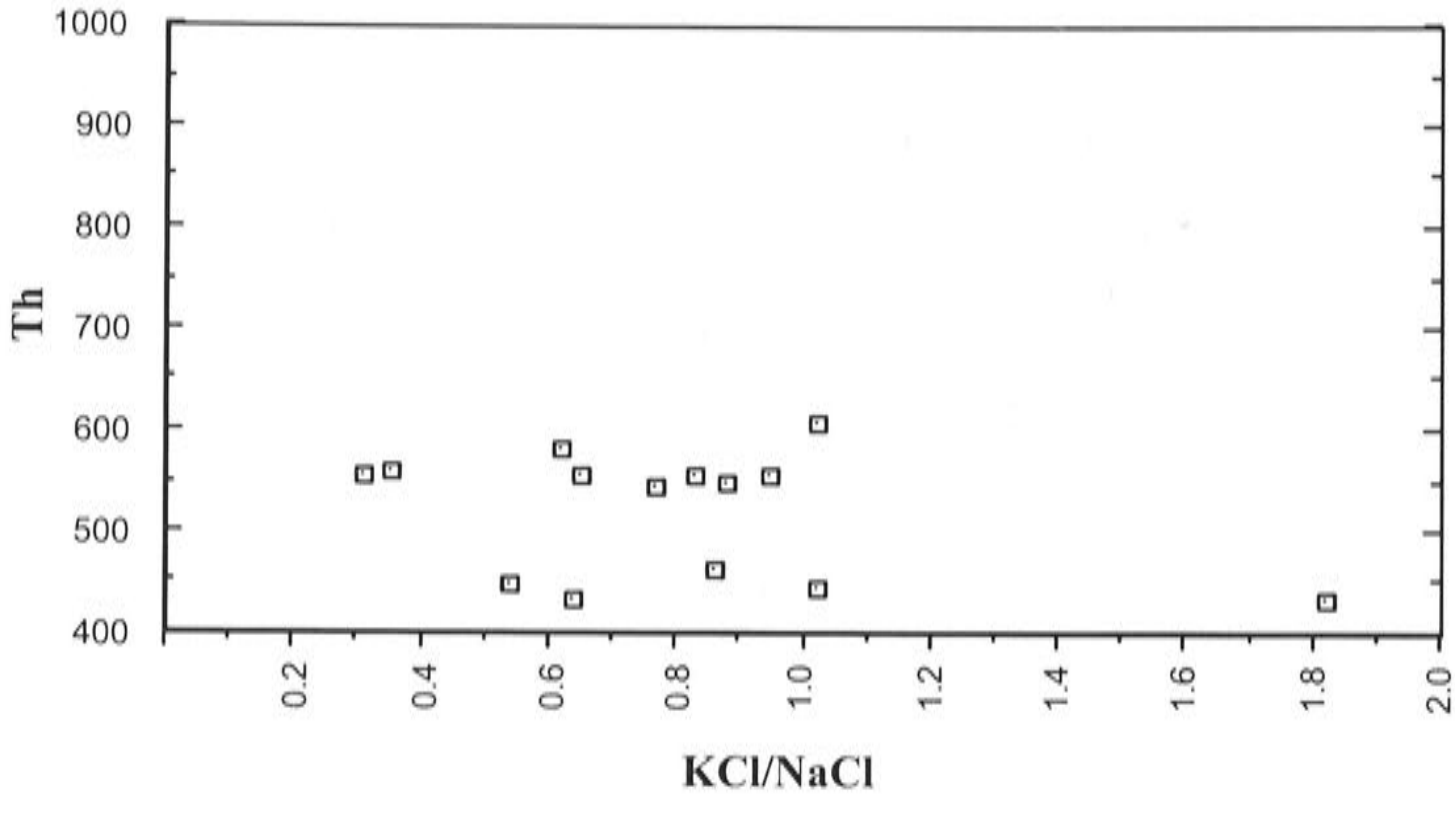

Figure 9.13 Total homogenisation temperature vs KCl/NaCl for Stage 5.

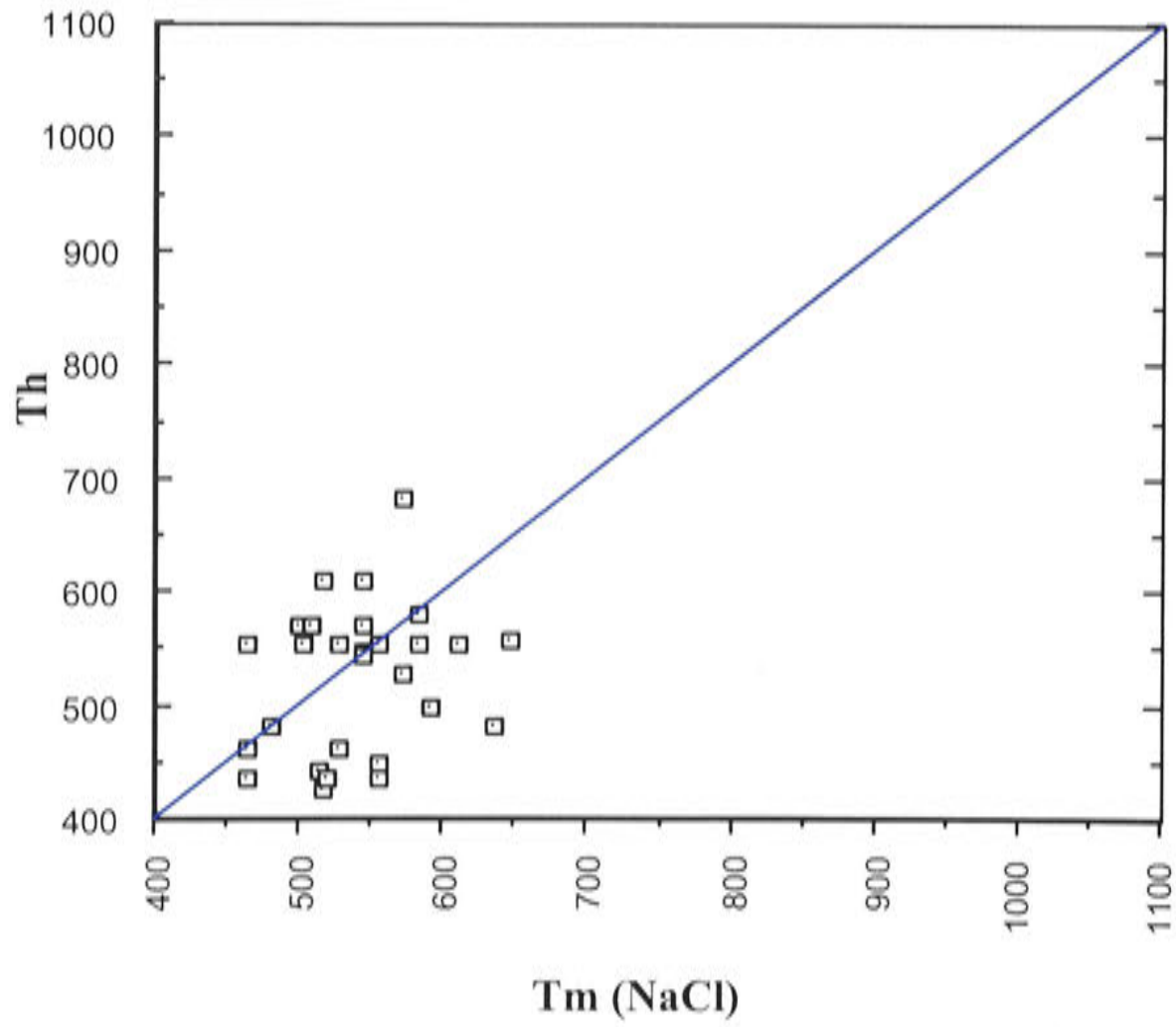

Figure 9.14 $T_{m\ NaCl}$ vs T_h plot showing vapour homogenisation vs halite homogenisation for Stage 5.

9.8 TEMPERATURE–SALINITY DATA FOR STAGE 6 VEINS

9.8.1 Morphology of Stage 6 veins and vein dykes

Stage 6 marks an important shift in the paragenetic sequence and a termination of the main stage of mineralisation. Textural evidence discussed in Chapter 7 demonstrates how this stage presents a variety of textures ranging from truly magmatic dykelets through magmatic–hydrothermal vein-dykes and to irregular veins. These features are sourced from QMP2, the second and weakly mineralised quartz monzonite porphyry. Locally, Stage 6 veins crosscut and disrupt the stockwork veining of Stage 5. The main morphological variants of Stage 6 veins are as follows:

1. Granular, aplitic, quartz and K-feldspar rich dykelets which may contain quartz inclusions or apparent vein fragments.

2. These may crosscut or grade into vein-like trails, which may have vein margins defined by graphic intergrowths of quartz and K-feldspar. Alternatively, micro-aplitic quartz and K-feldspar may be present in the centre of the vein or infilling the central part of the vein.

3. Within QMP2 itself, irregular trails of quartz occur that appear related to this stage. These range in texture from trails of discontinuous euhedral quartz with crystal terminations into the groundmass, through to rare crenulate quartz layers which have a pegmatitic appearance. Individual layers may be 2–7 mm in thickness, and are formed by euhedral crystals that sit on a base of fine-grained aplitic material and project into the porphyry groundmass. All crystals are oriented in one direction in any single layer. Individual layers are deformed into small disharmonic folds. Some of the quartz crystals are abraded and resorbed by the porphyritic groundmass; a feature which is best developed in the Endeavour 22 deposit.

This texture is reported from Climax-type molybdenum deposits (White et al. 1981) as 'crenulate quartz layers'. The authors conclude that the texture represents quartz precipitation at magmatic or near-magmatic temperatures as a result of rhythmic variations of P_{H2O} and P_{HF}. The effect of HF is to act as a flux, and to enhance the depression of the solidus of the magma (Bailey, 1977). Increases in P_{H2O} and P_{HF}, due to anhydrous crystallisation, have the effect of expanding the quartz field in the system $NaAlSi_3O_8$–$NaAlSi_3O_8$–SiO_2–H_2O. The combined effect of increasing P_{H2O} and P_{HF} causes quartz precipitation, volatile exsolution and eventual rock failure of the host. The rapid decrease in pressure shrinks the quartz field, and crystallisation of aplitic quartz and K-feldspar continues (White et al., 1981). Fluorine is a minor constituent at Endeavour 26 North, hence, if a similar process is invoked, it must be entirely due to fluctuations in P_{H2O}. Melt modifiers such as phosphorus may have a role. The textures outlined confirm the magmatic–hydrothermal transition that Stage 6 represents.

9.8.2 Fluid inclusion data

All types of fluid inclusion occur in this vein stage which is characterised by a lack of the dense network of secondary inclusions that characterise Stage 5 stockwork veins. Type A inclusions are all secondary and low temperature (<200 °C); they are clearly late stage and hence were not considered further. Type D inclusions are the most common, occurring as isolated inclusions, and also as secondary or pseudo-secondary inclusions evenly distributed along planes. Vapour-rich Type C inclusions may be present.

T_h ranges from 510 to 870 °C (Fig. 9.15). This is an increase of 100 to 200 °C from Stage 5. These temperatures and the textures are consistent with a new stage of magmatic hydrothermal activity. T_m of NaCl spans the range 470 to 580 °C, while T_m of KCl ranges between 410 and 550 °C (Figs 9.16, 9.17). Comparing these data to the T_m of Stage 4 veins ($T_{m\ NaCl}$ 500 to 680 °C, $T_{m\ KCl}$ 410 to 580 °C), it is clear that Stage 6 fluids have lower overall salinity although the temperatures are similar.

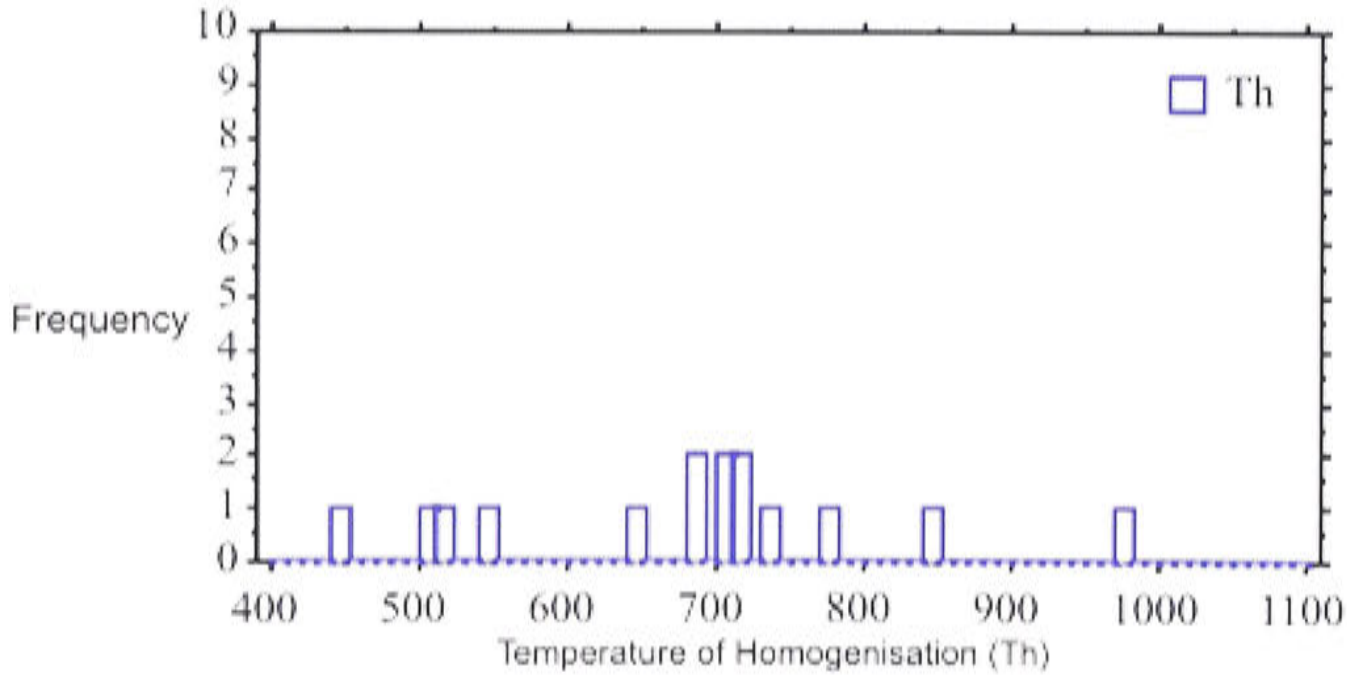

Figure 9.15 Total homogenisation temperature (T_h) histogram for Stage 6.

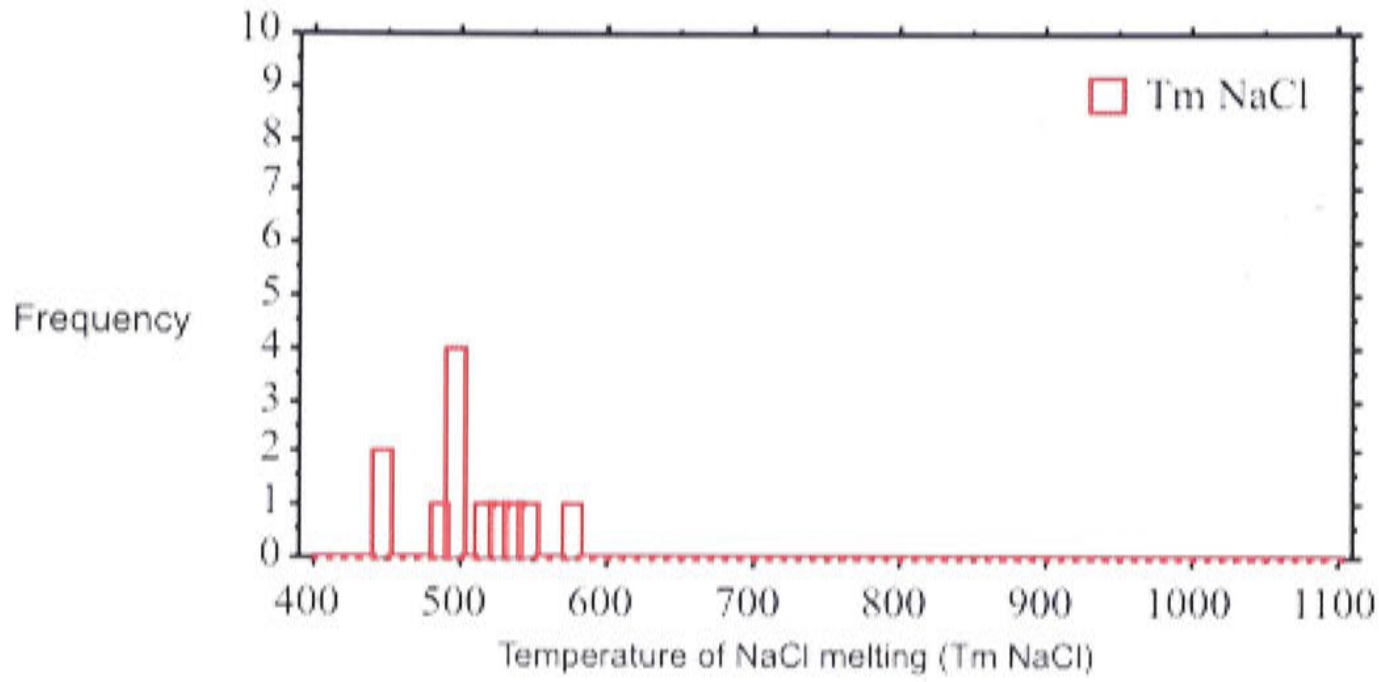

Figure 9.16 Temperature of NaCl dissolution ($T_{m\ NaCl}$) histogram for Stage 6.

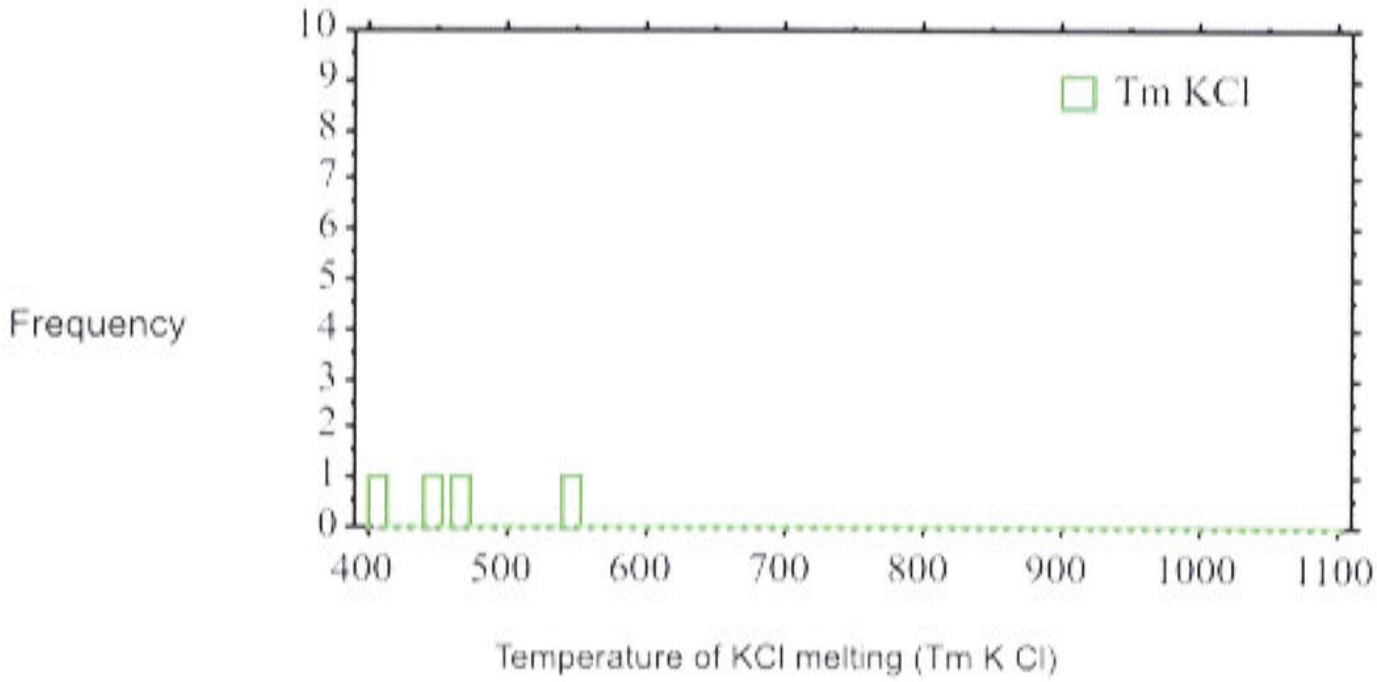

Figure 9.17 Temperature of KCl dissolution ($T_{m\ KCl}$) histogram for Stage 6.

9.9 TEMPERATURE–SALINITY DATA FOR STAGE 7 VEINS

9.9.1 Morphology of Stage 7 veins

Stage 7 veins are morphologically similar to Stage 4 veinlets, and can only be confidently identified where they crosscut the later QMP2. Typically they form very fine trails of quartz plus sulphides. They are most visible where they cross a plagioclase phenocryst, because they appear as a trail of sulphides with a narrow K-feldspar vein selvage.

9.9.2 Fluid inclusion data

Homogenisation temperatures are low, ranging from 310 to 490 °C (Fig. 9.18), which is consistent with the position late in the paragenetic sequence. $T_{m\ NaCl}$ ranges from 400 to 550 °C (Fig. 9.19) and is consistently higher than T_h (Fig. 9.20), so that total homogenisation of the fluid inclusions occurs by halite dissolution.

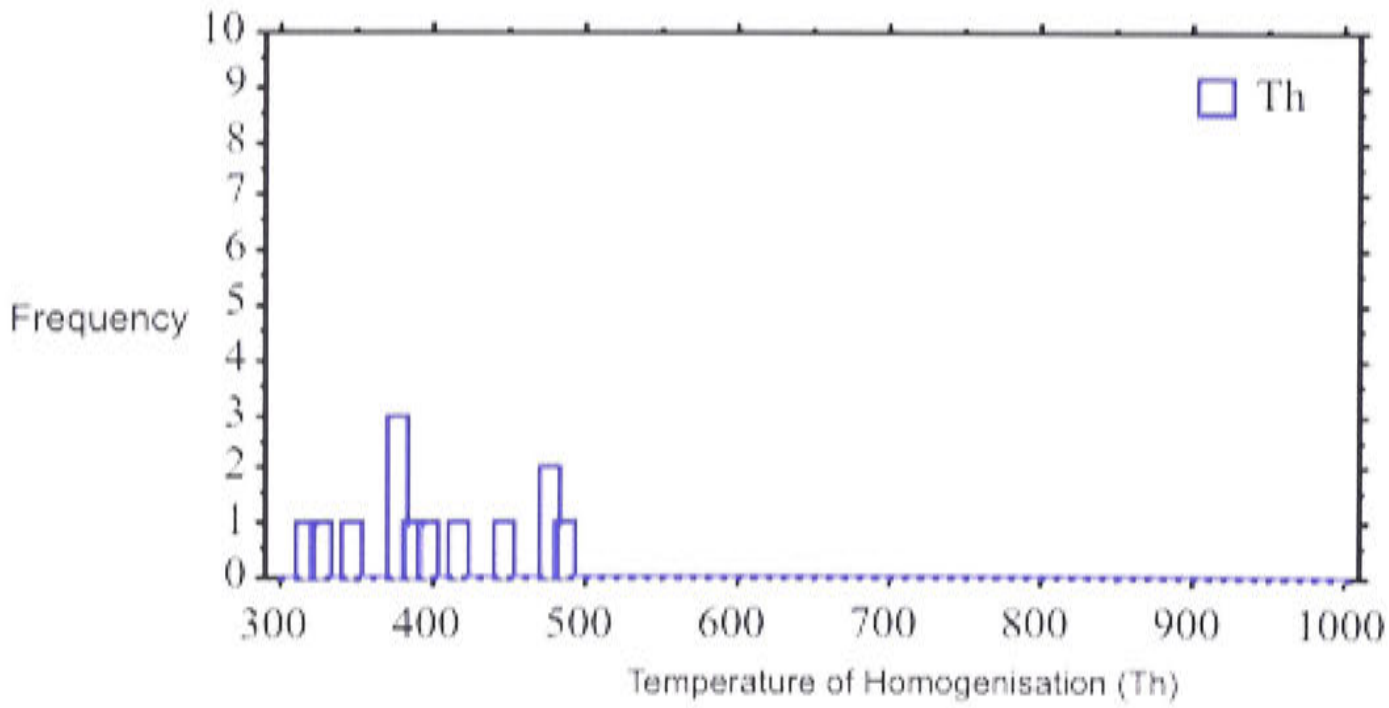

Figure 9.18 Total homogenisation temperature (T_h) histogram for Stage 7.

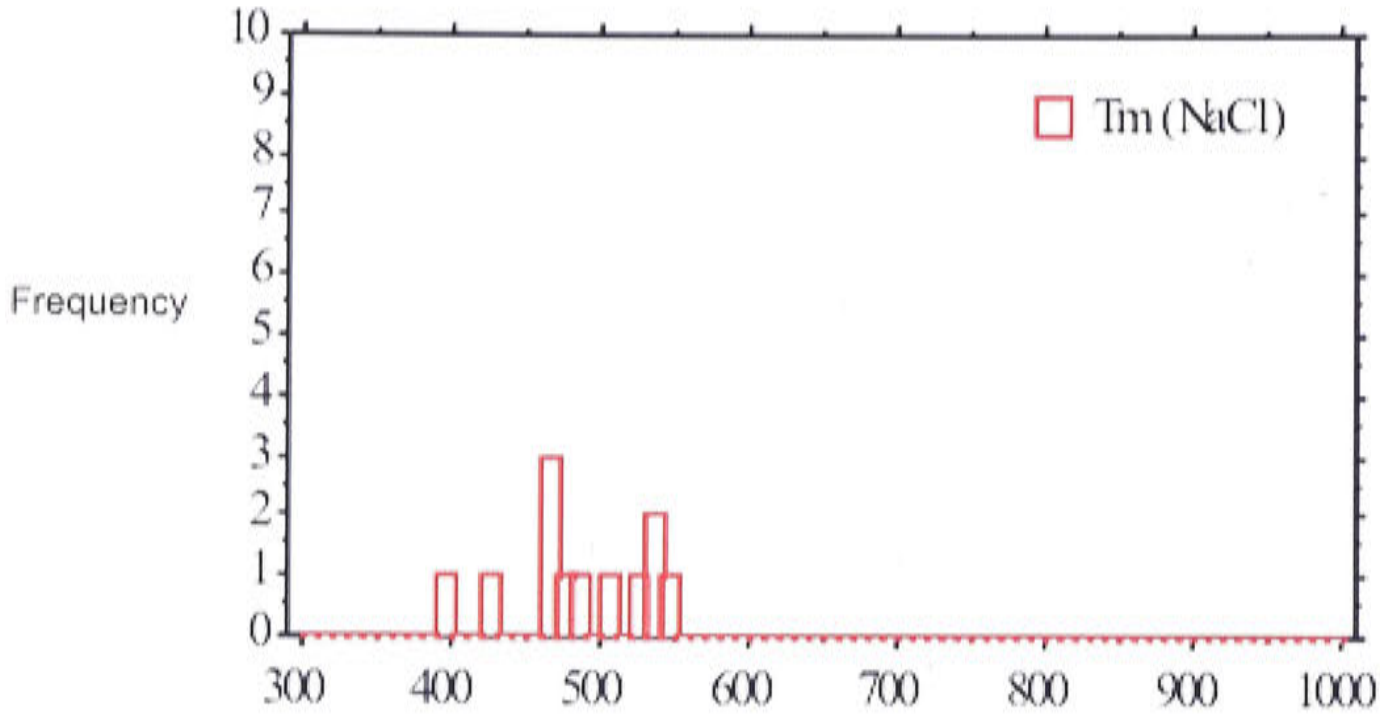

Figure 9.19 Temperature of NaCl dissolution ($T_{m\ NaCl}$) histogram for Stage 7

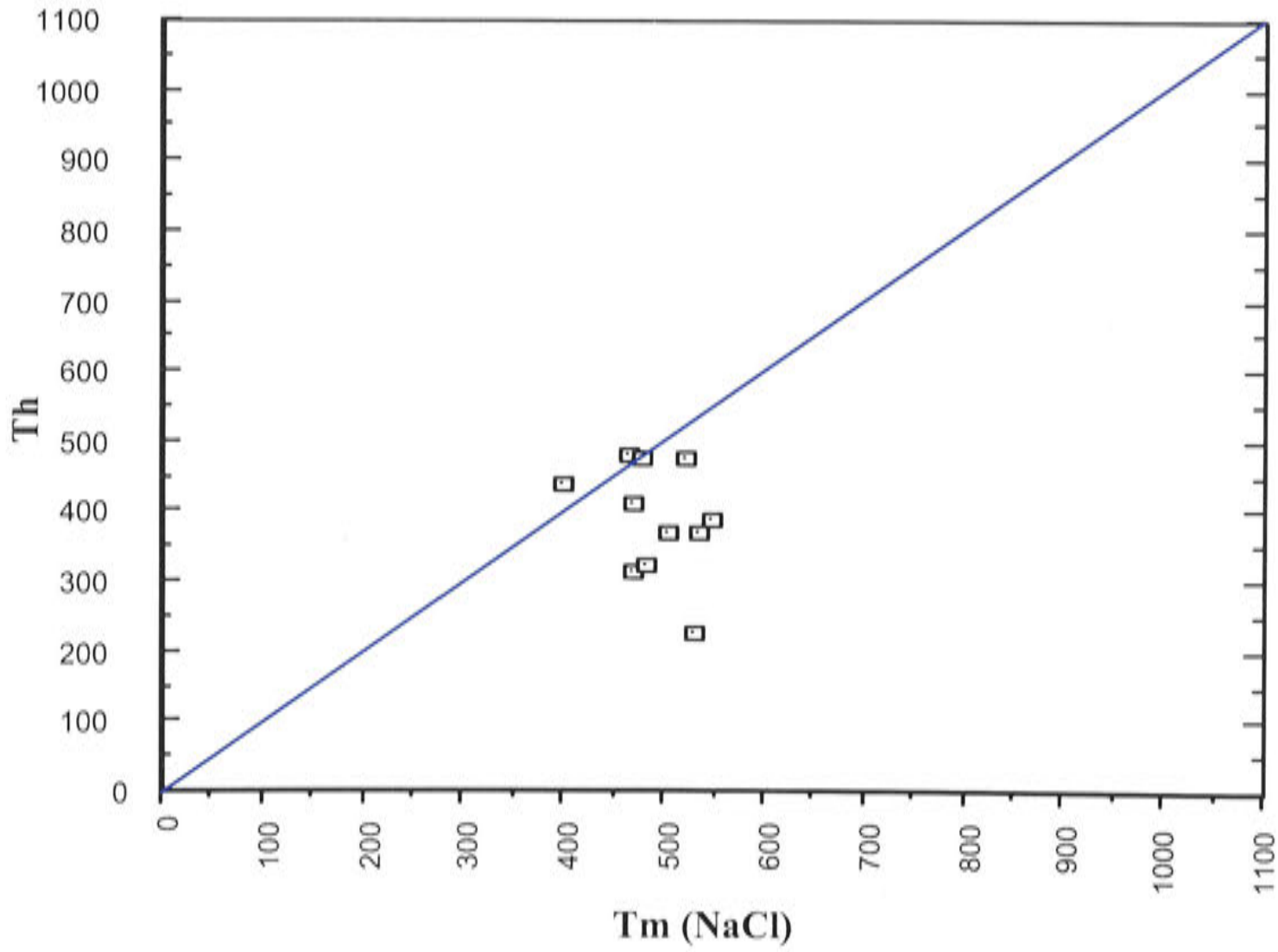

Figure 9.20 $T_{m\ NaCl}$ vs T_h plot showing vapour homogenisation vs halite homogenisation for Stage 7.

9.10 TEMPERATURE–SALINITY DATA FOR STAGE 9 VEINS

9.10.1 Morphology of Stage 9 veins

Stage 9 veining is part of the late stage sericitic overprint of the deposit. The central vein, which may not always be obvious, consists of quartz, anhydrite or gypsum and sulphides. In the upper parts of the system the main sulphide is pyrite with lesser chalcopyrite. At depth, bornite is commonly the main sulphide. The vein itself will pass imperceptibly into a quartz–sericite vein envelope. The veins can be quite irregular in shape or straight walled.

9.10.2 Fluid inclusion data

The main population of fluid inclusions have vapour homogenisation temperatures between 310 and 490 °C (Fig. 9.21). $T_{m\ NaCl}$ ranges between 400 and 550 °C (Fig. 9.22), hence a proportion of these inclusions homogenise by dissolution of NaCl.

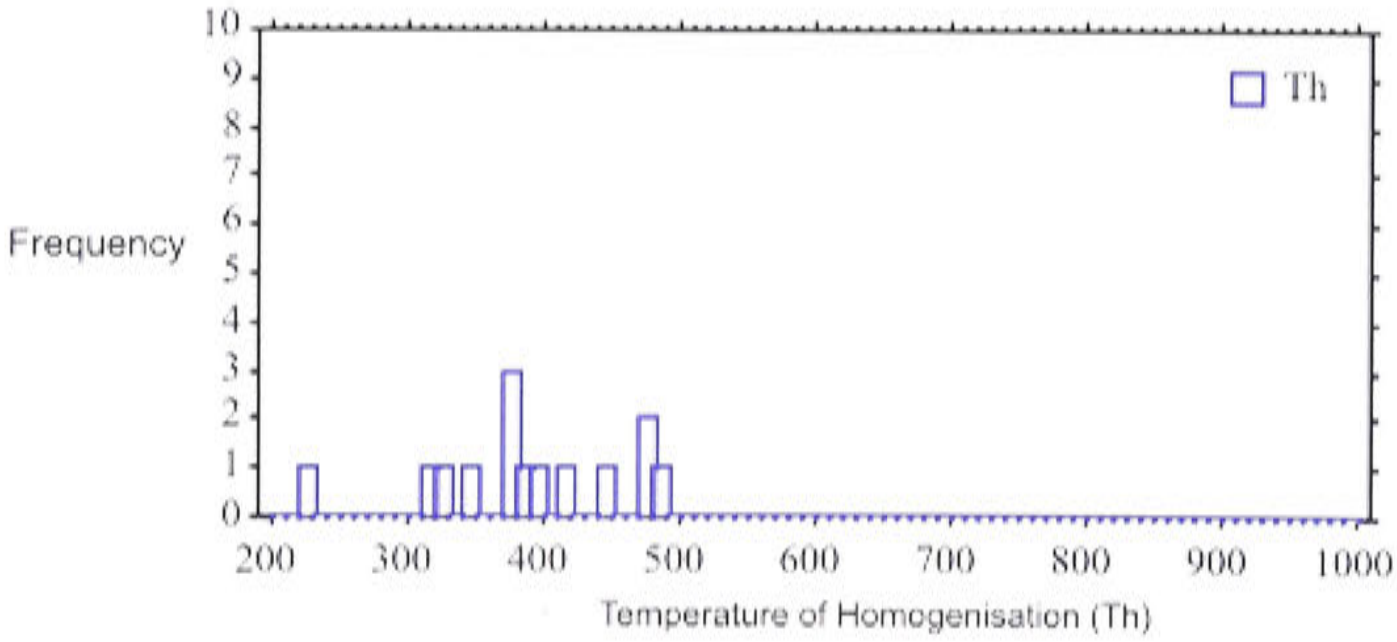

Figure 9.21 Total homogenisation temperature (T_h) histogram for Stage 9.

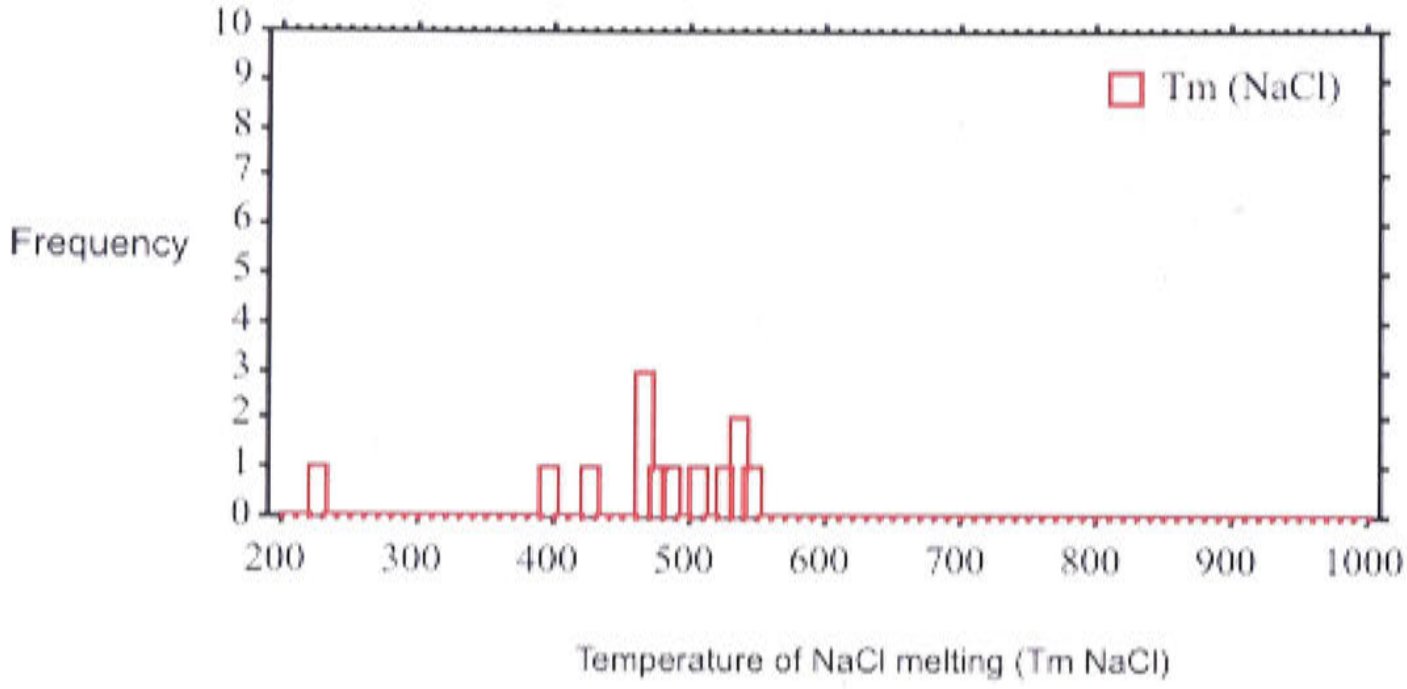

Figure 9.22 Temperature of NaCl dissolution ($T_{m\ NaCl}$) histogram for Stage 9.

9.11 HEMATITE DAUGHTER MINERALS

Hematite daughter minerals were not possible to dissolve despite heating to the limits of the stage (~1300 °C) .This non-dissolution of hematite does not result from slow kinetic effects, because two inclusions were heated to 600 °C and held at that temperature for three hours with no sign of dissolution of the margins. Roedder and Skinner (1968) suggested that hydrogen diffusion from inclusions leaves the inclusions sufficiently oxidised to leave hematite stable. Eastoe (1978) suggested, however, that solid hematite crystals are likely sites for trapping of fluids. Eastoe (1978) suggested that the relatively small number of solid hematite inclusions, and the size variation relative to the cavity volume in saline inclusions, is suggestive of trapping of salt-rich liquid about flakes of hematite already present. This present study suggests that while hematite is not present in all inclusions, the phase ratios of those present is sufficient to indicate that they are not results of accidental trapping. This feature has been noted in other fluid inclusion studies (Cloke and Kesler, 1979; Eastoe, 1978; Weisbrod, 1981).

Figure 9.23 displays the number of observations of chalcopyrite and hematite as a percentage of the total number of observations for each vein stage. While it is a crude estimate of the relative amounts of Cu and Fe in the fluid, there does appear to be an overall decrease with respect to time suggesting that random trapping of chalcopyrite and hematite is unlikely. An apparent increase in chalcopyrite daughter minerals at Stage 8 is an artefact of the limited number of samples in this stage, however, the low abundance of chalcopyrite daughter minerals in Stage 4 appears real.

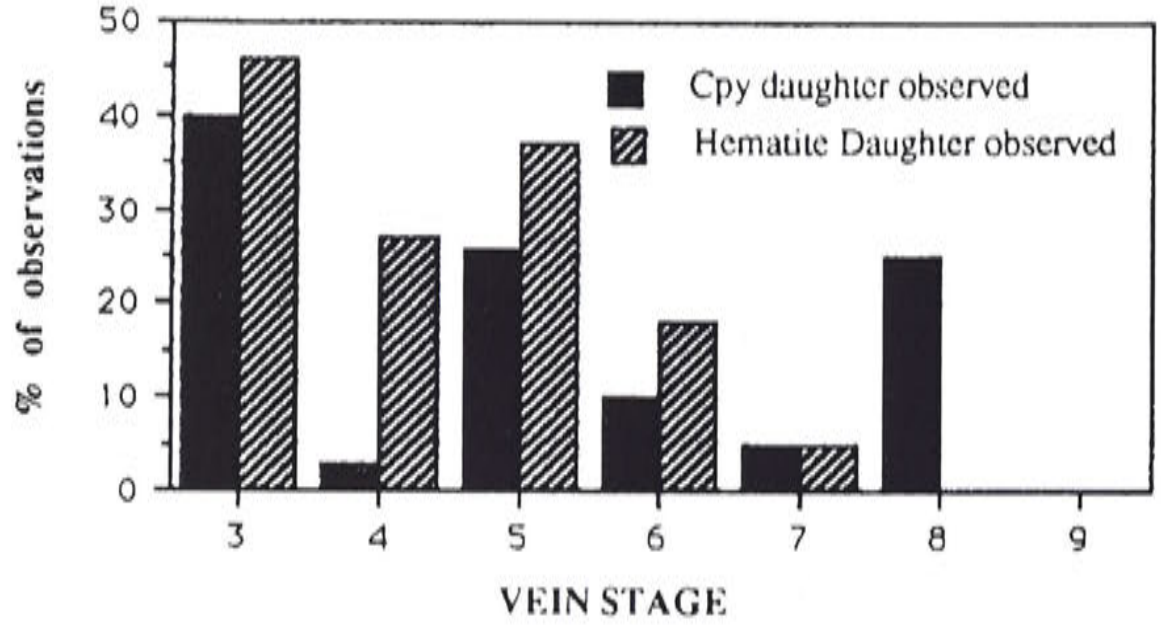

Figure 9.23 Histogram showing chalcopyrite and hematite minerals as a percentage of total observations per vein stage.

9.12 SALINITY DATA

Salinity data from the various vein stages containing NaCl and KCl can be plotted on a NaCl–KCl–H_20 ternary diagram (Fig. 9.24). A linear cluster which projects towards NaCl is clear from the Goonumbla data. This represents a version of the 'Halite Trend' first outlined by Erwood et al. (1979). Fields from Panguna, Granisle, Bell and Bingham (Wilson et al., 1980) are superimposed on the diagram, and it is clear that the Goonumbla data are different from these other data: overall KCl content is higher, and the KCl content varies with NaCl content. The significant difference in K content, between Endeavour 26 North fluids and other porphyry systems, may be a function of the high-K content of the parent monzonitic intrusion or it may point to some mechanism which has allowed increased partitioning of KCl into the magmatic fluid. It is tempting to speculate that increased partitioning of KCl into an early formed magmatic fluid may account, in part, for the relatively K-depleted 'mineralised trend' discussed in Chapter 5.

The tendency for the data to form along a restricted linear trend towards the halite apex of the diagram has been noted in several studies of porphyry systems. Cloke and Kesler (1979) examined the problem in detail and presented several scenarios that could result in a halite trend.

1. The EL (equilibrium separation of halite from liquid) path, in which halite separates from liquids under sufficient pressure to be above the liquid + vapour (L + V) surface (point 1, Fig. 9.25). Isobaric cooling will lead to halite precipitation once the liquid + halite surface appropriate for the total salinity is crossed. Continued precipitation will deplete the residual brine which, when subsequently trapped, will fall on the halite trend (points 2–3, Fig. 9.25). Fluid

inclusions trapped along this trend will homogenise upon heating by halite disappearance. If the fluid suffers a pressure drop, such as paths 1 to 5, the original solution will become saturated at 4 and crystallisation of halite will deplete the residual fluid, and trapping of various samples of this fluid will also result in a halite trend. The EL path is limited by the fact that the initial salinity must be high at pressures above the L + V curve. This brine has to be produced by means other than boiling as the liquid vapour surface is not intersected.

2. The EV trend (equilibrium separation of halite from vapour) can occur when a vapour phase crystallises halite and then separates from it and partially condenses to liquid, which in turn becomes separated and trapped in inclusions without further compositional change. This method will, however, not result in high-salinity inclusions.

3. The DL path (disequilibrium-separation of halite), in which a rapid decrease in pressure places the system into the vapour + halite field (points 6–7) causing the liquid to boil and deposit halite. Removal of heat by boiling will move the fluid towards point 8 on the solubility curve. This path is limited as the pressure required is too low to be geologically reasonable for most situations (235 b or less).

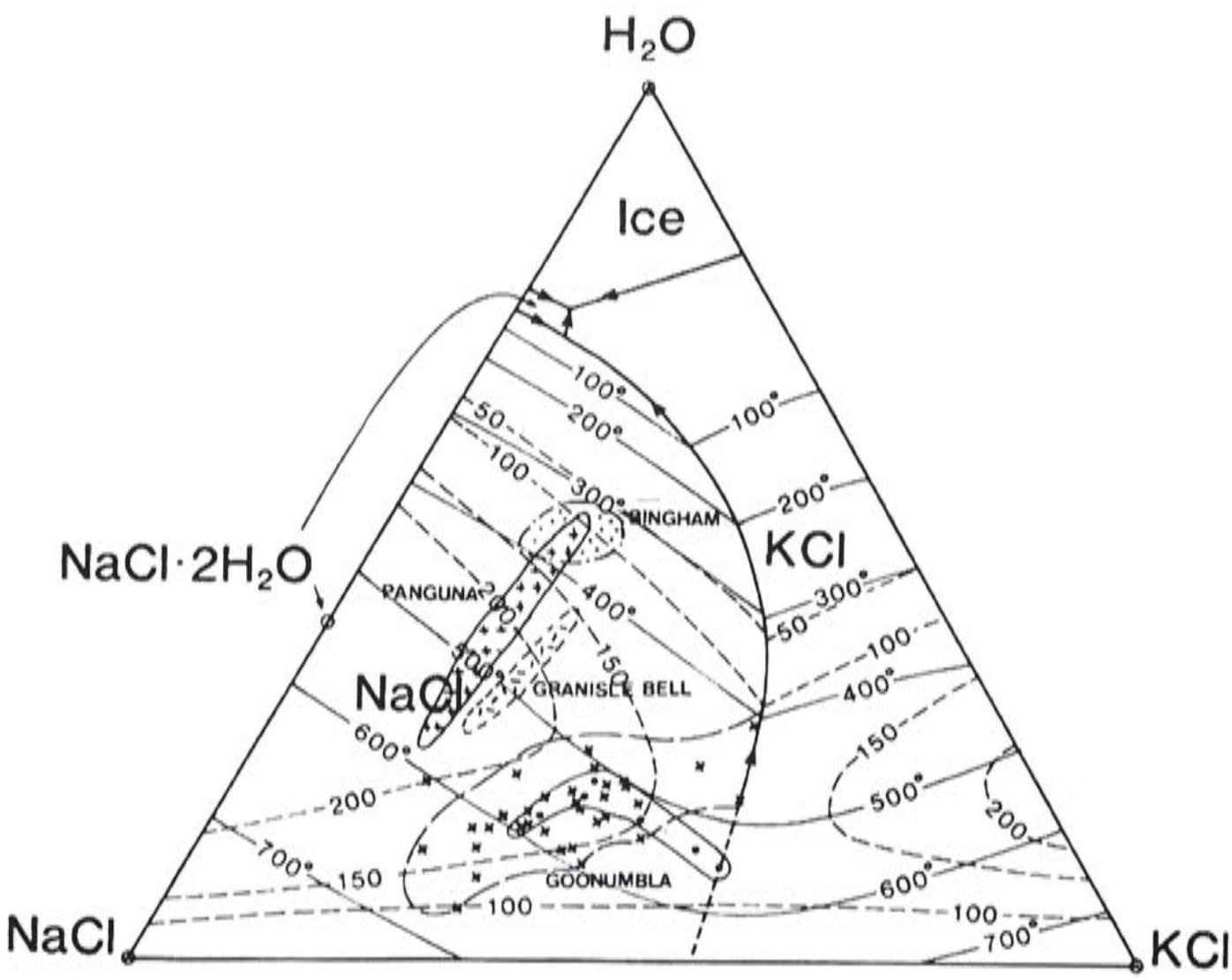

Figure 9.24 NaCl vs KCl vs H_20 diagram; results from Goonumbla (+ Stage 3.veins ▪ Stage 5 Veins) , Panguna, Bingham and Granisle Bell.

4. The SC (separation of halite along the solubility curve) path, in which liquids are trapped while on the solubility surface in the NaCl–KCl–H_20 system. Wilson et al. (1979) suggest that fluids trapped on the L + V curve would homogenise by simultaneous disappearance of vapour and halite; however this behaviour is only seen at the critical curve. Fluids trapped on the L + Y surface away from the critical curve will homogenise by vapour disappearance. Cooling away from the solubility curve, as in paths 10 to 11, will produce inclusions that homogenise by halite disappearance. This scenario is likely to happen where the coexisting vapour and brine are separated. The limitation on the SC path is the restriction that pressures not exceed those of the solubility curve. However, Bodnar et al. (1985) showed that the coexisting vapour + brine field extends well into the P–T range of most shallow magmatic regimes.

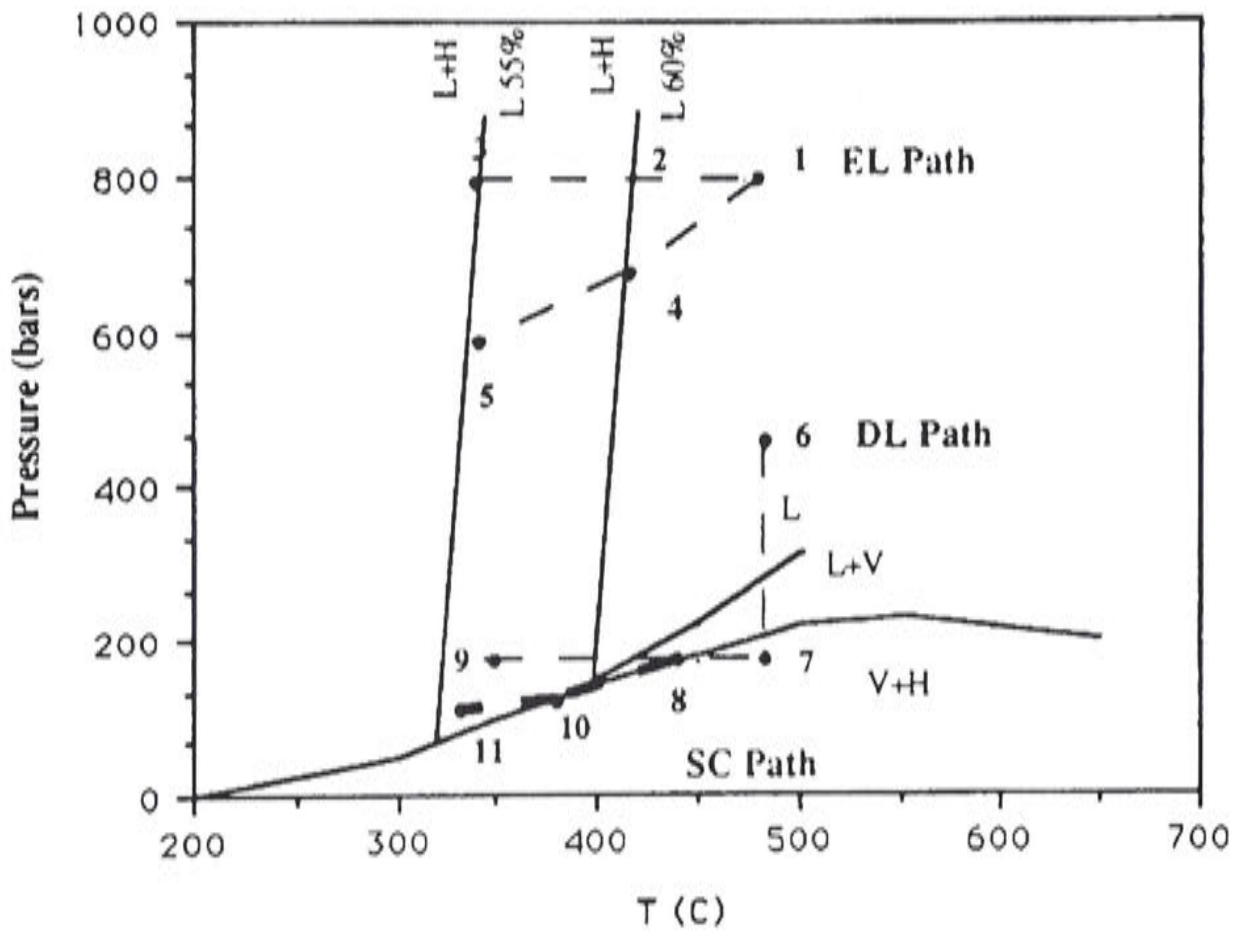

Figure 9.25 P–T projection of the H_2O–NaCl system showing reaction paths to generate a halite trend (after Cloke and Kesler 1979).

Burnham (1979) has shown that granodioritic magma emplaced at shallow levels in the earth's crust will form an aqueous phase in response to crystallisation of anhydrous phases. This work also suggested that the salinity of the initial fluid would range from a few to 20% NaCl equivalent. Bodnar et al. (1985) have shown that at the pressures and temperatures modelled by Burnham (1979), an initial low- to moderate-salinity fluid would immediately split into a high-salinity brine and a low-salinity vapour. It seems likely therefore, that the SC path is the most appropriate path for forming the Endeavour 26 North halite trend. The highly potassic nature of the parent monzonite stocks and quartz monzonite porphyries could give rise to the high KCl

content of the fluid when compared to other studied examples. Halite homogenisation appears to be best explained by brines out of equilibrium with coexisting vapour, which allows them to lift off the L + V surface and intersect the halite + liquid surface. Halite homogenisation is most pronounced in Stage 5 veins which represent the main stockwork development. It is probable that, at the point of brecciation and rebrecciation, brines may separate from the L + V curve and be ultimately trapped above it giving rise to fluid inclusions that homogenise by halite disappearance.

9.13 PRESSURE ESTIMATES

Figure 9.26 shows temperature of vapour homogenisation against wt% NaCl equivalent. Overlain on this diagram are isobars taken from Bodnar et al. (1985), and it is clear that isobaric cooling of fluids related to QM.Pl can explain the trend from high to lower salinity and high to lower temperature. These fluids bracket the 500 b isobar, and range from 300 to 750 b.

Fluids related to QMP2 stand out at a lower salinity to the QMPI fluids, and while the data scatter is large the overall salinity is restricted, suggesting isochoric cooling and pressure reduction in response to a change from lithostatic to hydrostatic conditions at this magmatic to hydrothermal brecciation stage.

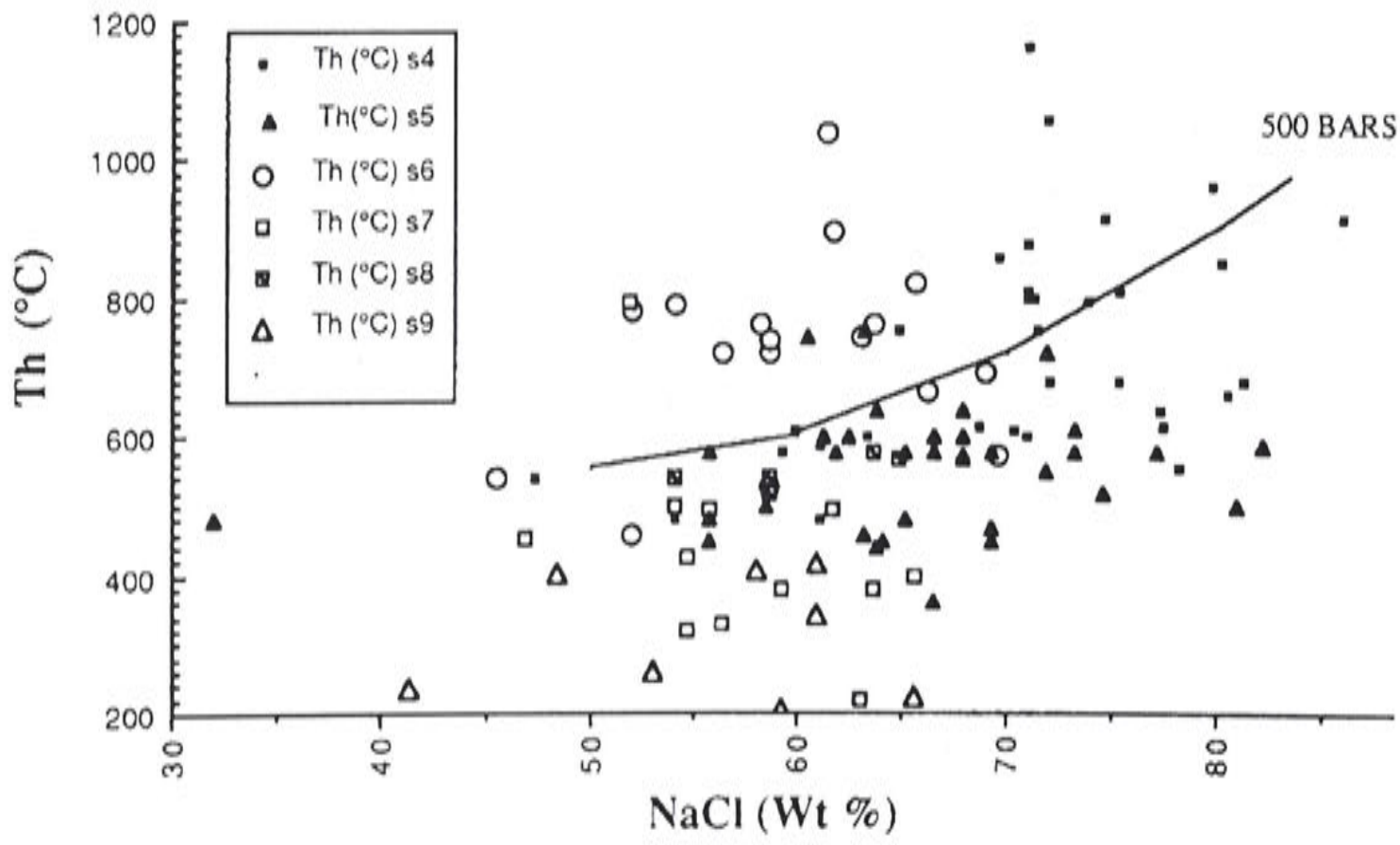

Figure 9.26 Total T_h (vapour homogenisation) vs NaCl equivalent (wt%).

9.14 DISCUSSION

This fluid inclusion study demonstrates the need to have careful paragenetic control of the mineralisation to be studied. In a complex and dynamic system, such as a porphyry Cu system, the paragenesis can help to untangle the fluid history.

Stage 1 veins and vein dykes are uncommon and no fluid inclusions were measured. Stage 2 albitisation cannot be related to any vein form, and hence no temperatures of formation were obtained. While albitisation is commonly noted through the deposit, its overall extent and intensity is impossible to ascertain. The presence of an early albitic phase in the alteration suite may be coupled with the increasing KCl/NaCl ratio noted in Stage 4 veins. Stage 3 veins are characterised by the first potassic alteration phase, biotite, which initially precedes the QMP1. This important phase is overwhelmed by hotter potassic fluids, which replace the biotite, magnetite assemblage with K-feldspar, quartz, anhydrite, hematite and sulphides. A broad spread of T_h temperatures is recorded in Stage 4 veins, ranging from 470 to 1090 °C. Magmatic textures in these irregular veins supports the extreme range of these temperatures. Vapour homogenisation temperatures of Stage 5 veins are clearly lower and more constrained in range.

This part of the paragenesis also records the most examples of homogenisation by halite disappearance. A disequilibrium decoupling of brine from its coexisting vapour appears the best explanation for this phenomena. This is not unreasonable in the context of the constant brecciation and rebrecciation of rock and pre-existing veins to form Stage 5 stockworking. Stage 6 magmatic–hydrothermal brecciation is reflected in high fluid inclusion temperatures, well above Stage 5. Abundant textural evidence representing rapid undercooling of melts attests to this event. Stage 6 heralds the emplacement of QMP2, which itself exsolves fluid. The data suggests that both T_h and salinity are diminished in this second phase of magmatic hydrothermal activity. Coexisting brine and vapour in all stages suggest that boiling has played a significant role in most stages of vein development. Figure 9.26 portrays salinity versus T_h data, and the curve of the locus of points related to QMPI is suggestive of isobaric cooling around the L + Y surface. The 500 isobar is plotted on Figure 9.26; in contrast fluids related to QMP2 ignore the isobars and cool down with loss of pressure.

However an alternative view is that the scatter and range of temperatures is reflective of pressure fluctuations between 300 to 1000 bars. This is supportive of a system that has cycled between lithostatic and hydrostatic pressures as noted in other studies such as Eastoe (1978). The range of pressures is consistent with a burial depth of about 3km. Figure 9.27 portrays the range in T_h through time and illustrates the importance of paragenesis in unravelling complex hydrothermal problems.

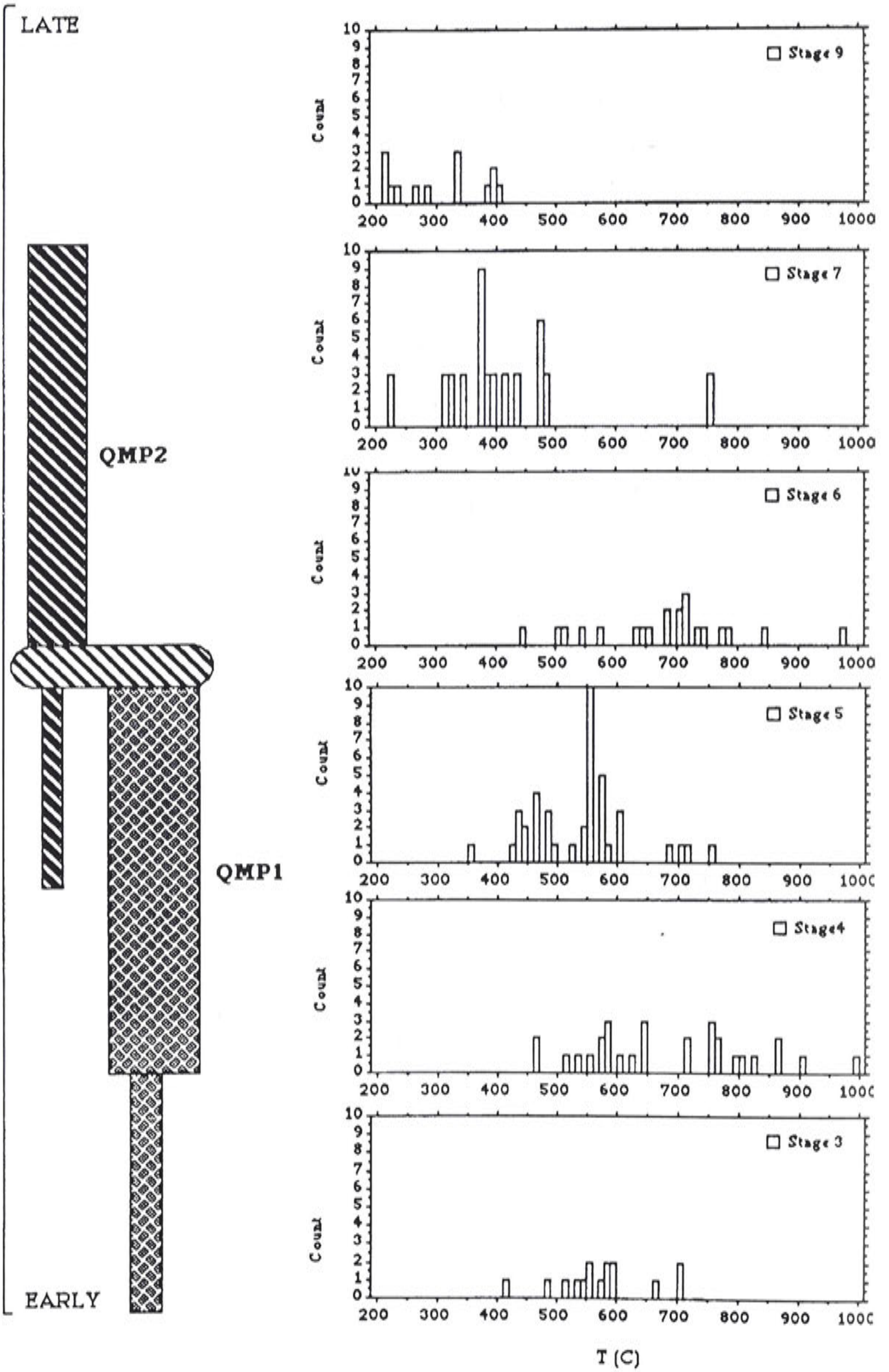

Figure 9.27 Temperature of vapour homogenisation through time.

Chapter 10

SUMMARY DISCUSSION OF THE GENESIS OF THE GOONUMBLA PORPHYRY CU–AU DEPOSITS

The geochemical character of the Goonumbla Volcanic Complex mirrors much of the character of other documented shoshonitic complexes. The initial ratios of $^{86}Sr/^{88}Sr$ and $^{143}Nd/^{144}Nd$, as well as the Pb isotope ratios, all indicate primitive source rocks for the magmas. Most importantly there is no evidence of crustal contamination, which has been recognised in the Pb isotope ratios of some base metal deposits in the Lachlan Fold Belt. Whilst these data do not uniquely resolve the question of the nature of the source rocks that produced the shoshonitic magmatism at Goonumbla, they do provide some useful constraints. The lack of a crustal signature suggests that this magmatism is unlikely to be the product of Ordovician subduction. It would be difficult, although not impossible, to avoid a sedimentary component in any material subducted in the Ordovician.

An alternative explanation is that the enriched source material reflects a subducted or buried and delaminated Cambrian volcanic arc. This proposal is attractive on two accounts. Firstly, the source material would have the characteristic HFSE array that is common to shoshonites and island arcs. Secondly, it would neatly account for the 510 Ma inheritance age in zircons from the Goonumbla Volcanic Complex. The components of Cambrian arc systems —boninites, calc-alkaline basalts and arc tholeiites — are present in Victoria along major thrust boundaries ,and they are inferred to occur extensively beneath these thrusts. A similar situation is conceivable further to the north. A Cambrian arc system could be an element of the basement terrane model proposed by Chappell et al. (1988), who envisage a number of Proterozoic to Cambrian microplates which remain unsutured until the Late Cambrian. Collision in the Late Cambrian, as envisaged by Coney et al (1990), would have closed subduction with some probable thrusting leading to fault slivers of ophiolites (e.g. the Coolac Serpentinite Belt). Relaxation, post collision, would have led to remelting of an enriched mantle wedge and the accreted Cambrian volcanics. An extensional, basin-forming stage would allow the thick accumulation of turbiditic sediments. This extensional phase may be broadly a back-arc setting or possibly a passive

margin. Ponding of magmas at the base of the thickened crust may have generated the high-pressure potassic fractionation that produced the shoshonitic magmatism in the Ordovician.

The low-pressure fractionation of the Goonumbla Volcanics and intrusions is marked by the development of two subtly different fractionation trends. One of these reflects the fractionation of olivine; the other the fractionation of plagioclase and biotite. The former trend is explained in terns of 'anhydrous' fractionation, i.e. it occurs under conditions of continual loss of volatiles. The latter, which is marked by greater enrichment of silica, is taken to reflect fractionation under conditions such that most of the volatiles are contained within the system. It is this fractionation path that leads to the development of the porphyry mineralisation. This interpretation of the low-pressure fractionation of the Goonumbla Volcanic Suite is consistent with the view that the key element in developing porphyry mineralisation is the containment of the volatiles, which are subsequently released in a controlled manner. This view is reinforced by the geometric arrangement of the mineralised porphyries (Endeavour 20, 22, 26 North, 27, 28) as satellites around the Endeavour 31 stock. The documented geological relationships in the Endeavour 26 North deposit indicate that these satellite porphyries essentially sit on the shoulders of the Endeavour 31 stock and crosscut the stock at depth. The alteration and mineralisation associated with porphyries overprints an earlier propylitic alteration and the broad geochemical anomalies geometrically related to the Endeavour 31 stock. These relationships present a picture of limited release of volatiles upon initial emplacement of the Endeavour 31 stock, and subsequent focussed release of both magma and volatiles in a few places on the shoulders of the stock (Ch. 6 documents evidence for some vapour release and brecciation along the contacts of the stock during emplacement). The positioning of these 'valves' would in part reflect greater cooling and release of volatiles on the walls of the stock at depth, and the collection of the released vapour in the shoulder regions rather than the apical regions of the stock.

The earliest alteration assemblage associated with the mineralising porphyries at Endeavour 26 North is biotite, magnetite and minor chalcopyrite (Stage 3). Fluid inclusions in rare quartz veins, that are unequivocally associated with this event, indicate temperatures of formation for this assemblage of 500 to 600 °C and fluid salinities ~70 wt%. The redox conditions of biotite formation in the presence of magnetite and K-feldspar may be determined from the Mg number of biotite at a given temperature (Wones and Eugster, 1965). The expression of Wones (1972) indicates that the redox conditions of biotite formation during Stage 3 were no more than 1 to 2 log units below the hematite–magnetite buffer (Figs 10.1, 10.2), and generally consistent with the condition of $fH_2S = fSO_2$ as

indicated by the S isotopes for Stages 4 to 11 and over the temperature interval of 300°C to 700°C as well as being around the sphene/rutile/quartz/anhydrite buffer.

Peak hydrothermal conditions were attained in Stage 4 of the paragenesis. Homogenisation temperatures for this stage range from 470 to 1090 °C, with peaks at 580 and 760 °C. Salinities range between 50 and 80 wt%, and there is a systematic increase in the K/Na ratio in the fluid with declining temperature. Bornite, anhydrite and K-feldspar (with minor chalcocite, digenite, rutile and hematite) is the stable assemblage.

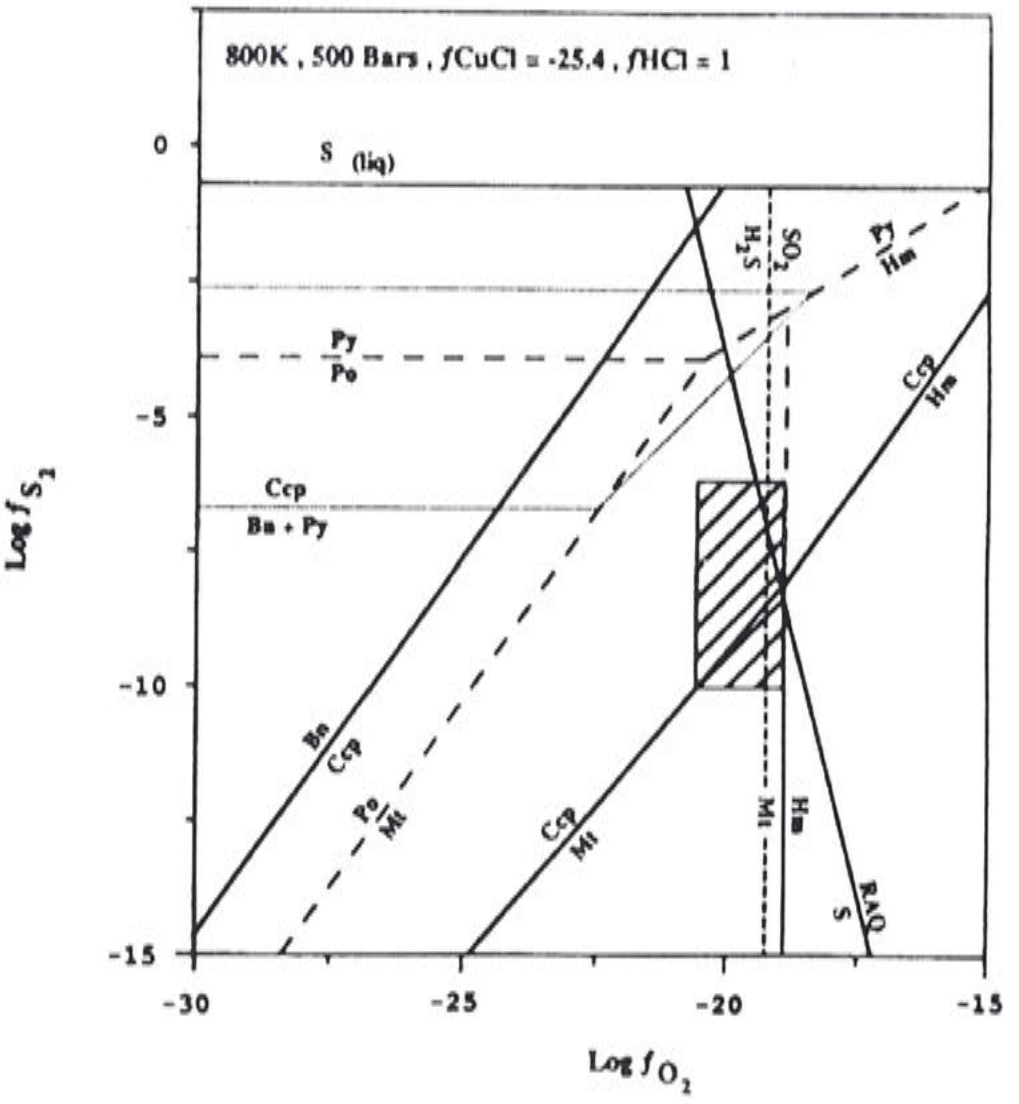

Figure 10.1 Log f_{S2} vs log f_{O2} plot. S = sphene, R=rutile, Q= quartz, A=anhydrite. Boundaries Bn/Ccp and Ccp/Mt are derived from Ccp/Hm log K at 800 °C, from Eastoe (1978).

The constraint of $f_{H2S} = f_{S02}$ is compatible with the presence of hematite in all . stages after Stage 3, provided temperatures are below about 550 °C (Fig. 10.2). At temperatures above 550 °C, magnetite not hematite is the stable iron oxide on the $S0_2/H_2S$ buffer (Fig. 10.2). This implies that neither hematite nor magnetite are stable at high temperature after Stage 3, and that the concentration of Cu and S in the fluid must always be sufficient to maintain bornite saturation. This condition is illustrated in Figure 10.3. These constraints suggest an increase in the Cu and S content of the fluids from Stage 3 to Stage 4 as the system heats

up. The increase in temperature from Stage 3 to Stage 4 is also sufficient to account for the dissolution of the secondary biotite formed in Stage 3 (Fig. 10.2).

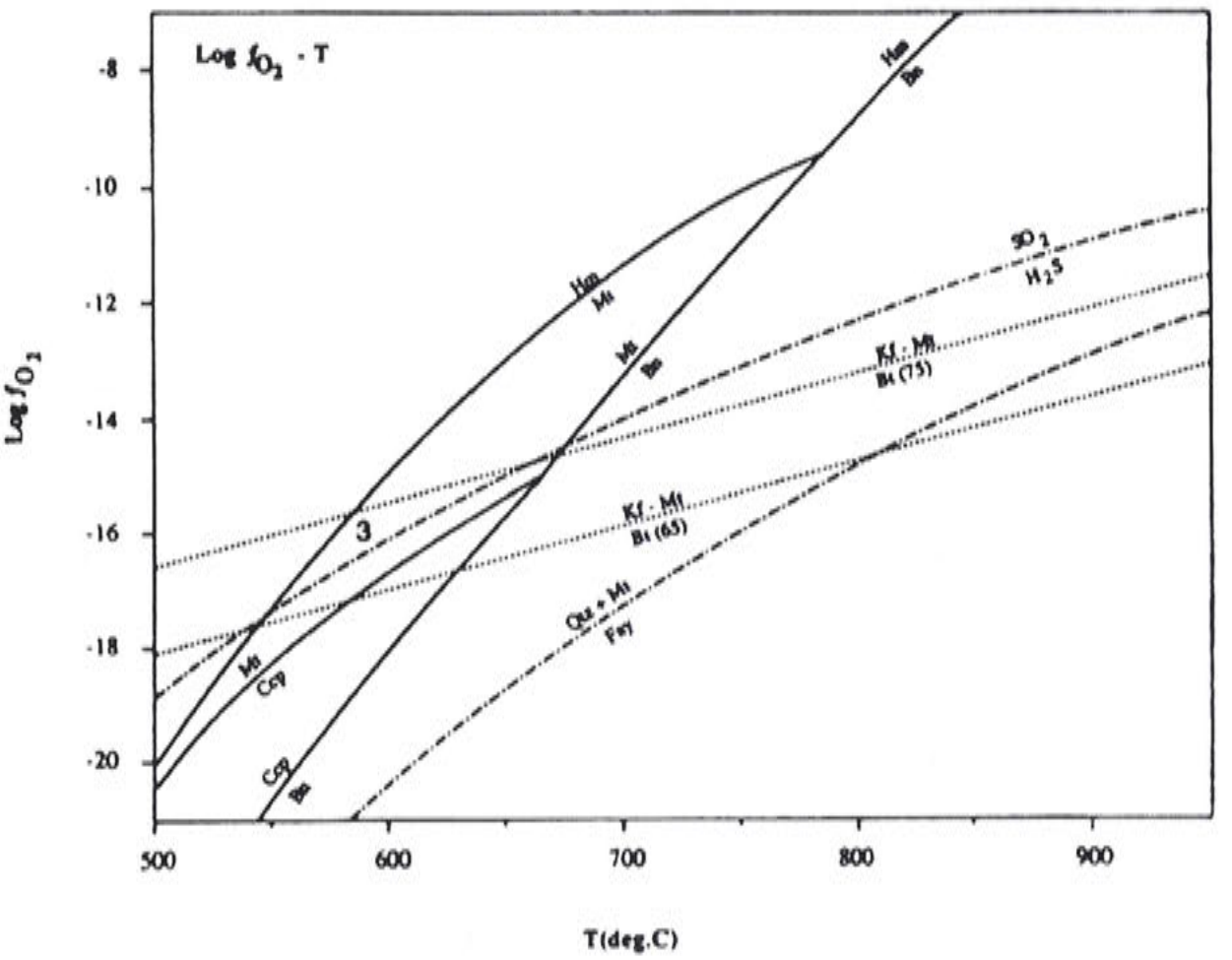

Figure 10.2 Log f_{O2} vs T plot. All sulphides and oxides assumed in equilibrium with SRAQ (defined in 10.1). f_{CuCl} varied with temperature. Values at 523 and 723°C as for Figures 10.1 and 10.3, respectively.

The available information on magmatic biotite compositions from the Endeavour 31 stock and QMP2 indicate Mg numbers around 65 to 75. Ti and Si levels in the biotite are relatively constant through this range, suggesting little change in temperature. Assuming magmatic temperatures around 900 to 1000 °C would imply redox conditions in the melts approximating QFM (Fig. 10.2).

Stage 5 represents the main mineralising event at Endeavour 26 North. The mineralogy is quartz, bornite, anhydrite and sericite, with minor chalcopyrite, digenite, hematite and rutile. Temperatures by this stage had declined to around 400 to 600 °C. The variation in K/Na ratio of the fluid in Stage 5 is not related to temperature, although overall through Stages 4 and 5 there is a decline in salinity and an increase in the K/Na ratio of the fluid with declining temperature. The former is best explained by phase separation at a constant pressure in the vicinity of 300 to 500 b. The latter is not understood.

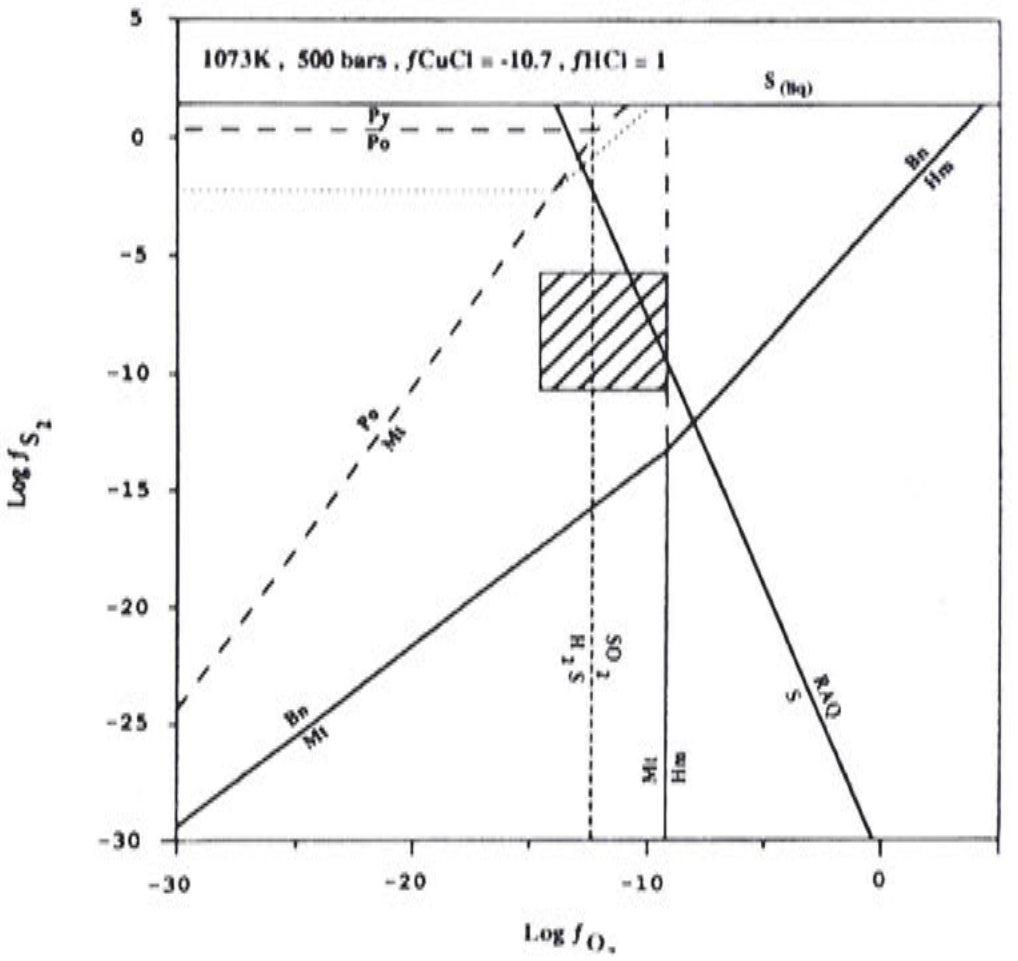

Figure 10.3 Log f_{S2} vs log f_{O2} plot. S = sphene, R = rutile, Q = quartz, A = anhydrite. Boundaries Bn/Ccp and Ccp/Mt are derived from Ccp/Hm log K at 800 °C, from Eastoe (1978).

The waning hydrothermal system was reactivated post Stage 5 by the emplacement of the second porphyry, QMP2. This intrusion partially digested the previously formed mineralisation. Clasts of vein quartz and sulphide are found in QMP2 near its margins with QMPl. The prograde event at this stage in the development of the deposit may have prevented the influx of meteoric waters and the pervasive development of quartz–sericite alteration, that is a common feature of porphyry Cu deposits. QMP2 is only weakly mineralised. A consequence of this is that features indicative of the earliest stages of fluid segregation from a silicate melt, such as vein-dykes and crenulate quartz layers or 'brain rock', are preserved in this porphyry.

Th values for Stage 6 of the paragenesis are higher by 100 to 2000 °C in comparison to Stage 5. This is consistent with renewal of the magmatic–hydrothermal system. However, the salinities of the fluids in the stages that post-date the emplacement of QMP2 are lower overall than the salinities of the fluids in the earlier part of the paragenesis, by about a factor of 2. There is no apparent difference in the K/Na ratio of the fluids that post-date the emplacement of QMP2.

Whilst the Goonumbla deposits clearly belong to the porphyry Cu clan, they are 'a variation on a theme'. The notable differences are the extreme pipe-like or pencil like geometry, the extreme focusing of the magmatic and hydrothermal activity into these 'pipes', and the satellite distribution of the deposits around the parent stock. The conventional model of porphyry Cu development involves mineralising the carapace of the parent stock by progressive inward crystallisation and vapour evolution through second boiling (e.g. Burnham, 1979). Rather than mineralising the parent stock, fluids from the Endeavour 31 stock have been focused to the margins of the body and released, together with residual magma, up vertical conduits. Successive stages of melt and fluid have been focused through these conduits.

REFERENCES

Allen, D.G. Panteleyev, A., and Armstrong, A.T., 1976, Galore Creek, in Porphyry Deposits of the Canadian Cordillera, A. Sutherland Brown , editor, C.I.M., Special Vol. 15, p. 402-414.

Bailey, J.C., 1977, Fluorine in granitic rocks and melts: a review: Chemical Geology, v.19, p. 1-42.

Ballhaus, C.G., Berry, R.F., and Green, D.H., 1990, Oxygen fugacity controls in the Earth's upper mantle: Nature (London), v. 348, no. 6300, p. 437–440.

Barr, D.A., Fox, P.E., Northcote, K.E. and Preto, V.A., 1976, The Alkaline Suite Porphyry Deposits – A Summary; in Porphyry Deposits of the Canadian Cordillera, Sutherland Brown, A., Editor, Canadian Institute of Mining and Metallurgy, Special Volume 15, p359-367.

Barron, B.J., 1976, Recognition of the original volcanic suite in altered mafic volcanic rocks at Sofala, New South Wales. American Journal of Science, v. 276, p. 604–636.

Barron, L.M., Slansky, E., Suppel, D., Johan, Z., and Ohnenstetter, M., 1990, Late- to post-magmatic PGE mineralisation in the Fifield Platinum Province and the Owendale Intrusive Complex, NSW: Geological Society of Australia Abstracts 25, p. 132.

Barron, L.M., Suppel, D.W., Slansky, E., Johan, Z., Ohnenstetter, M., and Spencer, R., 1991, The Fifield platinum province: Geological Society of Australia Abstracts 29, p. 3.

Basden, H., 1982, Preliminary report on the geology of the Tumut 1:100,000 Sheet area, southern New South Wales: New South Wales Geological Survey Quarterly Notes 46, p. 1–18.

Beane, R.E., and Titley, S.R., 1981, Porphyry copper deposits, II: Hydrothermal alteration and mineralization: Economic Geology 75th Anniversary Volume, p. 235–269.

Bloomer, S.H., Stern, R.J., Fisk, E., and Geschwind, C.H., 1989, Shoshonitic volcanism in the Northern Mariana Arc, 1, Mineralogic and major trace element characteristics: Journal of Geophysical Research, v. 94, no. B4, p. 4469–4496.

Bodnar, R.J., Burnham, C.W., and Sterner, S.M., 1985, Synthetic fluid inclusions in natural quartz, III, Determination of phase equilibrium properties in the system H_2O-NaCl to 1000 °C and 1500 bars: Geochimica et Cosmochimica Acta, v. 49, p. 1861–1873.

Bowman, H.N., Richardson, S.J., and Dolanski, J., 1982, Narromine 1:250,000 Metallogenic Map SI 55-3, Mine data sheets and metallogenic study: New South Wales Geological Survey, Sydney, 337 p.

Burnham, C.W., 1979, Magmas and hydrothermal fluids, in Barnes, H.L., ed., Geochemistry of Hydrothermal Ore Deposits, 2nd ed.: New York Wiley –Interscience, p 71 –136.

Burnham, C.W., and Ohmoto, H., 1980, Late-stage processes of felsic magmatism: Mining Geology Special Issue, v. 8, p. 1–11.

Carr, G.R., Dean J.A., Gulson, B.L., and Suppel, D.W., 1991, Lead isotope signatures of Ordovician to Permian mineralisation in the Lachlan fold belt. In Geological Society of Australia conference on Tectonics and metallogenesis of the Lachlan fold belt. Convenors C. Fergusson and R. Glen. Abstracts Geological Society of Australia v29, p 6.

Carr, P.F., 1985, Geochemistry of Late Permian Shoshonitic Lavas from the Southern Sydney Basin. Geological Society of Australia Publication, N.S.W. Division. p. 165 -183

Carroll M. R. and Rutherford, M. J., 1985. Sulphide and sulphate saturation hydrous silicate melts: Journal of Geophysical Research, v. 90, p.c601–c602.

Cas, R.A.F., 1983, A review of the facies patterns, paleogeographic development and tectonic context of the Palaeozoic Lachlan Fold Belt of southeastern Australia: Geological Society of Australia Special Publication 10, p. 104.

Cas, R.A.F., Powell, C.McA., and Crook, K.A.W., 1980, Ordovician palaeogeography of the Lachlan Fold Belt : a modern analogue and tectonic constraints: Geological Society of Australia Journal, v. 27, p. 19–32.

Chadwick, R.A., 1970, Belts of Eruptive Centers in the Absoroka – Gallatin Volcanic Province, Wyoming – Montana. Geological Society of America Bulletin, v. 81, p. 267 –274.

Chappell, B.W., and White, A.J.R., 1974, Two contrasting granite types: Pacific Geology, v. 8, p. 173–274.

Chappell, B.W., White, A.J.R., and Hine, R., 1988, Granite provinces and basement terranes in the Lachlan Fold Belt, southeastern Australia: Australian Journal of Earth Sciences, v. 35, p. 505–521.

Chivas, A.R., 1981, Geochemical evidence for magmatic fluids in porphyry mineralisation. Part 1. Mafic silicates from the Koloula Igneous Complex: Contributions to Mineralogy and Petrology, v. 78, p. 389-403.

Chou, I-Ming, 1987, Phase relations in the system NaCl-KCl-H20. III: Solubilities of halite in vapor-saturated liquids above 445 °C and redetermination of phase equilibrium properties in the system NaCl–H_20 to 1000 °C and 1500 bars: Geochimica et Cosmochimica Acta, v. 51, p. 1965–1975.

Civetta, L., Innocenti, F., Manetti, P., Peccerillo, A., and Poli, G., 1981, Geochemical characteristics of potassic volcanics from Mts. Ernici (Southern Latium, Italy). Contributions to Mineralogy and Petrology, v. 78, p. 37–47.

Clarke, I., 1987, Early Palaeozoic shoshonitic volcanism associated with gold and copper mineralization in the Parkes area, New South Wales: Pacific Rim Congress 87, Gold Coast, Australia, August 28–29, 1987, p. 77.

Clarke, I., 1990, Igneous petrology, *in* Clarke, I., and Sherwin, L., eds., Geological Setting of Gold and Copper Deposits in the Parkes Area, N.S.W.: Records of the Geological Survey of N.S.W. 23, 95 - 136.

Cloke, P.L., and Kesler, S.E., 1979, The halite trend in magmatic-hydrothermal mineralization Geological Society of America Abstract.

Compston, W., and Chappell, B.W., 1979, Sr-Isotope evolution of Granitoid source rock *in* McElhinny, M.W., ed., The Earth: its origin, structure and evolution, Academic Press, London, p. 377–426.

Coney, P.J., Edwards, A., Hine, R., Morrison, F., and Windrim, D., 1990, The regional tectonics of the Tasman orogenic system, eastern Australia: Journal of Structural Geology, v. 12, p. 519–543.

Cooper, J.A., and Richards, J.R., 1966, Lead isotopes and volcanic magma: Earth and Planetary Science Letters, v. 1, p. 259–269.

Cosgrove, M.E., 1972, The geochemistry of the potassium-rich Permian volcanic rocks of Devonshire, England: Contributions to Mineralogy and Petrology, v. 36, no. 2, p. 155–170.

Cuddy, A.S., and Kesler, S.E., 1982, Gold in the Granisle and Bell copper porphyry copper deposits, British Colombia, *in* Levinson, A.A., ed., Precious metals in the Northern Cordillera: The Association of Exploration Geochemists, Rexdale, Ontario, p. 139–155.

Crawford , M. L., 1981, Phase equilibria in aqueous fluid inclusions: Mineralogical Association, Canada, Short Course Handbook 6, p. 75–100.

Crawford, A.J., Beccaluva, L., and Serri, G., 1981.Tectono-magmantic evolution of the West Philippine – Mariana region and the origin of boninites: Earth and Planetary Science Letters, v. 54, p. 346–356.

Crawford, A.J., 1983, Tectonic development of the Lachlan Fold Belt and construction of the continental crust of eastern Australia: Geological Society of Australia Abstracts 9, p. 30–32.

Crawford, A.J., Cameron, W.E., and Keays, R.R., 1984, The association of boninite-low Ti andesite-tholeiite in the Heathcote Greenstone Belt: ensimatic setting for the early Lachlan Fold Belt: Australian Journal of Earth Sciences, v. 31, p. 161–177.

Crawford, A.J., and Cameron, W., 1985, Petrology and geochemistry of Cambrian boninites and low-Ti andesites from Heathcote Victoria: Contributions to Mineralogy and Petrology, v. 91, p. 93–104.

Crook, K.A.W., 1980, Fore-arc evolution in the Tasman Geosyncline: the origin of southeast Australian continental crust: Geological Society of Australia Journal, v. 27, p. 215–232.

Crook, K.A.W., Bein, J., Hughes, R.J., and Scott, P.A., 1973, Ordovician and Silurian history of the southeastern part of the Lachlan Geosyncline: Geological Society of Australia Journal, v. 20, p. 113–138.

Cumming, G.L., and Richards, J.R., 1975, Ore lead isotope ratios in a continuously changing Earth: Earth and Planetary Science Letters, v. 28, p. 155–171.

Dickinson, W.R., 1975, Potash – depth (K-H) relations in continental margin and intra-ocean magmatic arcs: Geology, v. 3, p. 53–56.

Doe, B. R. and Stacey, J. S., 1974, The application of lead isotopes to the problems of ore genesis and ore prospect evaluation: A review: Economic Geology, v. 63, p. 884–906.

Dostal, G., Zentilli, M., Caelles, J,C., and Clark, H., 1977, Geochemistry and origin of volcanic rocks of the Andes (26–28 S): Contributions to Mineralogy and Petrology, v. 63, p. 113–128.

Eastoe, C.J., 1978, A fluid inclusion study of the Panguna porphyry copper deposit, Bouganville, Papua New Guinea: Econ. Geol. v.73, p 721-748.

Eastoe, C.J. 1980, Chemistry of magmatic fluids in the Panguna (Bougainville) porphyry copper deposit: International Geological Congress, Abstracts Congress Geologique Internationale, Resumes 26, v. 3, p. 929.

Eastoe, C.J., 1983, Sulfur isotope data and the nature of the hydrothermal systems at the Panguna and Frieda Porphyry Copper Deposits, Papua New Guinea: Economic Geology, v. 78, p. 201–213.

Ellam, R.M., Hawkesworth, C.J., Menzies, M.A., and Rogers, N.W., 1989, The volcanism of southern Italy: role of subduction and the relationship between potassic and sodic alkaline magmatism: Journal of Geophysical Research, v. 94, no. B4, p. 4589–4601.

Erwood, R.J., Kesler, S.E., and Clarke P.L., 1979, Compositionally distinct saline hydrothermal solutions, Naica Chihuahua: Economic Geology, v. 74, p. 95–108.

Fergusson, C.L., Gray, D.R., and Cas, R.A.F., 1986, Overthrust terranes in the Lachlan Fold Belt, southeastern Australia: Geology, v. 14, p. 519–522.

Field, C.W., 1966, Sulfur isotope abundance data, Bingham district, Utah: Economic Geology, v. 61, p. 850–871.

Field, C.W., and Gustafson, L.B., 1976. Sulfur isotopes in the porphyry copper deposit at El Salvador, Chile: Economic Geology, v. 71, p. 1533–1548.

Fletcher R.C., and Hofmann A.W., 1974, Simple models of diffusion and combined diffusion–infiltration metasomatism, *in* Hofmans, A.W. et al., eds., Geochemical transport and kinetics, Washington D.C.: Carnegie Institution Washington Publication 634, p. 243-259.

Foley, S.F., and Wheller, G.E., 1990, Parallels in the origin of the geochemical signatures of island arc volcanics and continental potassic igneous rocks: The role of residual titanites: Chemical Geology, v. 85, p. 1–18.

Gest, D.E., and McBirney, A.R., 1979, Genetic relations of shoshonitic and absarokitic magmas, Absaroka Mountains, Wyoming: Journal of Volcanology and Geothermal Research, v. 6, p. 85–104.

Gill, J.B., 1981, Orogenic andesites and plate tectonics: Spring-Verlag, Berlin.

Gill, J., and Whelan, P., 1989, Early rifting of an oceanic island arc (Fiji) produced shoshonitic to tholeiitic basalts: Journal of Geophysical Research, v. 94, p. 4561–4578.

Griffiths, J.R., 1977, Geology and metallogeny of the Lachlan orogen, Australia: A time-space analysis and preliminary tectonic synthesis: CSIRO Mineral Research Laboratory Investigation Report 123.

Gustafson, L.B., and Hunt, J.P., 1975, The porphyry copper deposit at El Salvador, Chile: Economic Geology, v. 70, p. 857–912.

Hamlyn, P.R., Keays, R.R., Cameron, W.E., Crawford, A.J., and Waldron, H., 1985, Precious metals in magnesian low-Ti lavas: implications for metallogenesis and sulfur saturation in primary magmas: Geochimica et Cosmochimica Acta, v. 49, p. 1797–1811.

Hart, S.R., 1984, The DUPAL anomaly: A large scale isotopic anomaly in the southern hemisphere: Nature, v. 306, p. 753-756.

Haynes, F.M., and Titley, S.R. 1980, The evolution of fracture related permeability within the Ruby Star Granidiorite, Sierrita porphyry copper deposit, Pima County, Arizona: Economic Geology, v. 75, p. 673–683.

Heithersay, P.S., 1986, Endeavour 26 North copper-gold deposit, Goonumbla NSW – paragenesis and alteration zonation: Council of Mining and Metallurgical Institutions and Australasian Institute of Mining and Metallurgy 13th Congress, Publications 2, p. 181–189.

Heithersay, P.S., O'Neill W.J., van der Helder, P., Moore, C.R., and Harbon, P.G., 1990, Goonumbla porphyry copper district — Endeavour 26 North, Endeavour 22 and Endeavour 27 copper-gold deposits, *in* Hughes, F.E., ed., Geology of the mineral deposits of Australia and Papua New Guinea: (Ed. F.E. Hughes) , p. 1385–1398.

Hill, D., 1951, Geology, *in* Handbook of Queensland: Australasian Association of Advanced Science, Brisbane, Queensland, p. 13–24.

Hine, R., and Mason D.R., 1978, Intrusive rocks associated with porphyry copper mineralisation , New Britain, Papua New Guinea, *in* Gustafson, L.B., and Titley, S.R., eds., Porphyry copper deposits of the southwestern Pacific islands and Australia: Economic Geology and the Bulletin of the Society of Economic Geologists, v. 73, no. 5, p. 749–760.

Iddings, J.P., 1895, Absarokite-shoshonite-banakite series: Journal of Geology, v. 3, p. 935–959.

Jakes, P., and Gill, J., 1970, Rare earth elements and the island arc tholeiitic series: Earth and Planetary Science Letters, v. 9, p. 17–28.

Jakes, P., and White, A.J.R., 1972, Major and trace element abundance in volcanic rocks of orogenic areas: Geological Society of America Bulletin v. 83, p. 29–39.

Johan, Z., and Le Bel, L., 1980, Sulphur isotope geochemistry, and its contribution to understanding of porphyry copper mineralisation. In: Mineralisation associated with granitoids. Johan, Z. (editor).

Memoires du B.R.G.M. v. 99, p. 151 – 161.

Jones, G.J., 1985. The Goonumbla porphyry copper deposits, New South Wales: Economic Geology, v. 80, p. 591–613.

Joplin, G.A., 1964, A petrography of Australian igneous rocks: Angus and Robertson, Sydney.

Joplin, G.A., 1965, The problem of the potash-rich basaltic rocks: Mineralogical Magazine, v. 34, p. 266–275.

Karig, D.E., 1971, Origin and development of the marginal basins in the western Pacific: Journal of Geophysical Research, v. 76, p. 2542–2561.

Keller, J., 1974, Petrology of some volcanic rock series of the Aeolian Arc, Southern Tyrrhenian Sea: Calc-alkaline and shoshonitic associations: Contributions to Mineralogy and Petrology, v. 46, 29–47.

Krynen, J.P., Sherwin, L., and Clarke, I., 1990a, Stratigraphy and structure, *in* Clarke, I., and Sherwin, L., eds. Geological Setting of Gold and Copper in the Parkes Area: New South Wales Geological Survey Records 23(1), p. 1–76.

Krynen, J.P., Shewin, L., and Clarke, I., 1990b, Parkes Special 1:100,000 Geological Sheet (part 8431, 8432, 8531, 8532): New South Wales Geological Survey, Sydney.

Kudo, A.M., and Broxton, D.E., 1985, High-potassium intrusive rocks of the Crandall ring-dike complex, Absaroka Mountains, Wyoming: Geological Society of America Bulletin 96, p. 522–528.

Lange, I.M., and Cheney, E.S., 1971, Sulfur isotopic reconnaissance of Butte, Montana: Economic Geology, v. 66, p. 63–74.

Le Bas, M.J., Le Maitre, R.W., Streckeisen, A., and Zanettin, B., 1986, A chemical classification of volcanic rocks based on the total alkali-silica diagram: Journal of Petrology, v. 27, p. 745–750.

Leitch, E.C., and Scheibner, E., 1987, Stratotectonic terranes of the Eastern Australian Tasmanides: American Geophysical Union, Geodynamic Series, v. 19, p. 1–19.

Lorand, J.P., 1989, Abundance and distribution of Cu-Fe-Ni sulfides, sulphur, copper and platinum group elements in orogenic-type spinel lherzolite massifs of Ariege (northeastern Pyrenees, France): Earth and Planetary Science Letters, v. 93, no. 1, p. 50–64.

Lowell, J.D., and Guilbert, J.M., 1970, Lateral and vertical alteration-mineralisation zoning in porphyry ore deposits: Economic Geology, v. 65, p. 373–408.

MacKenzie, D.E., and Chappell, B.W., 1972, Shoshonitic and calc-alkaline lavas from the Highlands of Papua New Guinea: Contributions to Mineralogy and Petrology, v. 35, p. 50–62.

Mason, D.R., 1978, Compositional variations in ferromagnesian minerals from porphyry copper-generating and barren intrusions of the western Highlands, Papua New Guinea: Economic Geology, v. 73, p.878 – 890.

McCulloch, M.T., and Chappell, B.W., 1982, Nd isotopic characteristic s of S-and I-type granites: Earth and Planetary Science Letters, v. 58, p. 51–64.

McMillan, W.J., 1991, Porphyry Deposits in the Canadian Cordillera; in Ore Deposits, Tectonics and Metallogeny in the Canadian Cordillera, B.C. Ministry of Energy, Mines and Petroleum Resources, Paper 1991 – 4, p. 253 –276.

McMillan, W.J. and Panteleyev, A., 1988, Porphyry Copper Deposits; in Ore Deposit Models, Roberts, R.G. and Sheahan, P.A., Geoscience Canada, Reprint Series 3, p. 45 –58.

Meade, H.D., 1977, Petrology and Metal Occurrences of the Takla Group and Hogem and Germanson Batholiths, North Central British Columbia, unpub. Ph.D. thesis, University of Western Ontario.

Meen, J.K., 1990, Elevation of potassium content of basaltic magma by fractional crystallization: the effect of pressure: Contributions to Mineralogy and Petrology, v. 104, p. 309–331.

Meen, J.K., and Eggler, D.H., 1987, Petrology and geochemistry of the Cretaceous Independence volcanic suite, Absaroka Mountains, Montana: clues to the composition of the Archean sub-Montanan mantle: Geological Society of America Bulletin 98, p. 238–247.

Meyer, C., and Hemley, J.J. 1967, Wall rock alteration, *in* Barnes, H.L., ed., Geochemistry of hydrothermal ore deposits: New York, Holt, Rinehart and Winson, p. 166–235.

Miller, C.F., 1978, Monzonitic Plutons, California, and a model for generation of alkali-rich, near silica-saturated magmas. Contributions to Mineralogy and Petrology. v.67, p. 349-355.

Morrison, G., 1980, Characteristics and tectonic setting of the shoshonite rock association: Lithos, v. 13, p. 97–108.

Murray, C.G., Scheibner, E., and Walker, R.N., 1989, Regional geological interpretation of a digital coloured residual Bouguer gravity image of eastern Australia with wavelength cut-off of 250 km: Australian Journal of Earth Sciences, v. 36, p. 423–450.

Nicholls, J., and Carmichael, I.S.E., 1969, A commentary on the absarokite-shoshonite-banakite series of Wyoming, USA: Schweiz. Min. Pet. Mitt., v. 49, p. 47–64.

Norman, D.I., and Sawkins, F.J., 1987, Analysis of volatile in fluid inclusions by mass spectrometry: Chemical Geology, v. 61, p. 1–10.

Ohmoto, H., and Lasaga, A.C., 1982, Kinetics of reactions between aqueous sulfates and sulfides in hydrothermal systems: Geochimica et Cosmochimica Acta, v. 46, p. 1727–1745.

Ohmoto, H., and Rye, R.O., 1979, Isotopes of sulphur and carbon, *in* Barnes, H.I., ed., Geochemistry of hydrothermal ore deposits, 2nd edition: Wiley, New York.

Osatenko, M.J., and Jones, M.B., 1976, Valley Copper, *in* Sutherland-Brown, A., ed., Porphyry deposits of the Canadian Cordillera: CIM Special Volume 15, p. 130–143.

Oversby, B., 1971, Palaeozoic plate tectonics in the southern Tasman Geosyncline: Nature Physical Science, v. 234, p. 45–48.

Oversby, V.M., and Ewart, A., 1972, Lead isotopic compositions of Tonga-Kermadec volcanics and their petrogenetic significance: Contributions to Mineralogy and Petrology, v. 37, p. 181-210.

Oversby, V.M., and Gast, P.W., 1970, Isotopic composition of lead in oceanic islands: Journal of Geophysical Research. V.75, p. 2097-2114.

Owen, M., and Wyborn, D., 1979, Geology and geochemistry of the Tantangara and Brindabella 1:100,000 Sheet areas: Bureau of Mineral Resources Bulletin 204, p. 52.

Packham, G.H., ed., 1969, The geology of New South Wales: Geological Society of Australia, series 16, p. 654.

Packham, G.H., 1973, A speculative Phanerozoic history of the south-west Pacific, *in* Coleman, P.J., ed., The Western Pacific: island arcs, marginal seas, geochemistry: University of Western Australia Press, Perth, p. 369–388.

Packham, G.H., 1985, Transforming the eastern Lachlan Fold Belt: Geological Society of Australia, Abstracts 14, p. 56

Packham, G.H., 1987, The eastern Lachlan Fold Belt of Southeast Australia: A possible Late Ordovician to Early Devonian sinistral strike slip regime, *in* Leitch, E.C., and Scheibner, E., eds., Terrane accretion and orogenic belts: American Geophysical Union, Geodynamics Series 19, p. 67–82.

Parker, J.A., 1986, Metallogeny and tectonic development of the Kanmantoo Trough in South Australia: Ore Geology Reviews 1, p. 203–212.

Pearce, J.A., 1983, Role of the sub-continental lithosphere in magma genesis at active continental margins, *in* Hawkesworth, C.J., and Norry, M.J., eds., Continental basalts and mantle xenoliths: Shiva Geology Series, p. 230–272

Peccerillo, A., and Taylor, S.R., 1976, Geochemistry of Eocene calc-alkaline volcanic rocks from the Kastamonu area, Northern Turkey: Contributions to Mineralogy and Petrology, v. 58, p. 63–81.

Perkins C., McDougall I., Claoue-Long J., and Heithersay P.S., 1990, $^{40}Ar/^{39}Ar$ and U-Pb geochronology of the Goonumbla porphyry Cu-Au deposits, New South Wales: Economic Geology, v. 85, p. 1808–1824.

Pickett J.W., 1984, Late Ordovician marine fossils from the Parkes district: New South Wales Geological Survey Palaeontological Report 1984/05.

Pickett J.W., 1985, Plant fossils from Milpose, NE of Bogan Gate: New South Wales Geological Survey Palaeontological Report 1985/05.

Potter, R.W., Clynne, M.A., and Brown, D.L., 1978, Freezing point depression of aqueous sodium chloride solutions: Economic Geology, v. 73, p. 284–285.

Powell, C.McA., 1983b, Geology of NSW, South Coast: Geological Society of Australia, SGTSG Field Guide 1, p. 118.

Powell, C.McA., 1984a, Terminal fold-belt deformation: Relationship of mid-Carboniferous megakinks in the Tasman Fold Belt to coeaval thrusts in cratonic Australia: Geology, v. 12, no. 9, p. 546–549.

Powell, C.McA., 1984b, Ulura and Adelaidean Regimes : Ordovician to earliest Silurian marginal sea and island arc, *in* Veevers, J.J., ed., Phanerozoic Earth history of Australia: Oxford University Press, p. 290–303.

Preece, R.K., and Beane, R.E., 1982, Contrasting evolutions of hydrothermal alteration in quartz monzonite and quartz diorite wall rocks at the Sierrita Porphyry copper deposit, Arizona: Economic Geology, v. 77, p. 1621–1641.

Ravich, M.I. and Borovaya, F.E., 1949, Fazovyye ravnovyesiya v troynykh vodno-solyevykh sistemakh pri vysokikh tyempyeraaturakh, (Phase equilibria in ternary water–salt systems at elevated temperatures): Akad. Nauk. S.S.S.R., Izvyestiya Syektora Fiz.-Khim. Analiza, v. 19, p. 69–81.

Rock, N.M.S., and Groves, D.I., 1988a, Do lamprophyres carry gold as well as diamonds?: Nature, v. 332, p. 253–255.

Rock, N.M.S. and Groves, D.I. 1988b. Can lamprophyres resolve the genetic controversy over mesothermal gold deposits?: Geology, v. 16, p. 538–541.

Roedder, E., 1984, Fluid inclusions, *in* Ribbe, P.H., ed., Reviews in Mineralogy 12: Mineralogical Society of America, Washington D.C.

Roedder, E. and Skinner, B.J. (1968) Experimental evidence that fluid inclusions do not leak: Economic Geology, v63, p. 715 – 730.

Rose, A.W., 1970, Zonal relations of wallrock alteration and sulphide distribution at porphyry copper deposits: Economic Geology, v. 65, p. 920–936.

Rose, A.W., and Burt, D.M. 1979, Hydrothermal alteration, *in* H. L. Barnes eds., Geochemistry of hydrothermal ore deposits: John Wiley and Sons, New York, Chichester, Brisbane, Toronto.

Rutland, R.W.R., 1976, Orogenic evolution of Australia: Earth Science Reviews, v. 12, p. 161–196.

Rye, R.O. and Ohmoto, H., 1974, Sulfur and carbon isotopes and ore genesis: a review. Economic Geology v.69, p. 826 – 842.

Scheibner, E., 1972, Actualistic models in tectonic mapping: International Geological Congress, 24th Session, Reports 3, p. 405–422.

Scheibner, E., 1973, A plate tectonic model of the Palaeozoic tectonic history of New South Wales: Geological Society of Australia, Journal, 20, p. 405–426.

Scheibner, E., 1974, An outline of the tectonic development of New South Wales with special reference to mineralization, *in* Markham, N.L., and Basden, H., eds., The mineral deposits of New South Wales: New South Wales Geological Survey, p. 3–39.

Scheibner, E., 1976, Explanatory notes on the tectonic map of New South Wales: New South Wales Geological Survey, Sydney, 283 p.

Scheibner, E., 1978, ed., The Phanerozoic structure of Australia and variations in tectonic style: Tectonophysics, v. 48, p. 153–430.

Scheibner, E., 1985a, Unpublished schematic structural map of New South Wales, scale 1:1,000,000: New South Wales Geological Survey, Sydney.

Scheibner, E., 1985b, Suspect terranes in the Tasman Fold Belt System, eastern Australia, *in* Howell, D.G., ed., Tectono-stratigraphic terranes in the circum-Pacific Region: Circum-Pacific Council for Energy and Mineral Resources, Earth Science Series 1, p. 493–514.

Scheibner, E., 1987, Palaeozoic tectonic development of eastern Australia in relation to the Pacific Region, *in* Monger, J.W.H., and Francheteau, J., eds., Circum-Pacific orogenic belts and evolution of the Pacific Ocean Basin: American Geophysical Union Geodynamic Series, v. 18, p. 133–165.

Scheibner, E., 1989a, Geoscience transect Broken Hill to Sydney, New South Wales, Australia: International Geological Congress 28th Session, Abstracts 3 (expanded handouts), p. 42–43.

Scheibner, E., 1989b, The tectonics of New South Wales in the second decade of application of the plate tectonics paradigm: Royal Society of New South Wales Journal and Proceedings, v. 122, p. 35–74.

Sherwin, L., 1973, Stratigraphy of the Forbes-Bogan Gate district, New South Wales: Geological Survey Records 15, no. 1, p. 47–101.

Sherwin, L., 1974, Llandovery graptolites from the Forbes district, New South Wales, *in* Graptolite studies in honour of O.M.B. Bulman: Palaeontology Special Paper 3, p. 149–175.

Sherwin, L., 1975, Silurian graptolites from the Forbes Group, New South Wales: New South Wales Geological Survey Records 16, no. 3, p. 227–237.

Sherwin, L., 1979. Age of the Nelungaloo volcanics near Parkes: New South Wales Geological Survey Quarterly Notes 35, p. 15–18.

Sherwin, L., 1983, Late Ordovician graptolites from Forbes: New South Wales Geological Survey Palaeontological Report 1983/08.

Sillitoe, R., 1990a Gold-rich porphyry copper deposits: Vancouver '90: Geological Association of Canada, Mineralogical Association of Canada, Annual meeting, Program with abstracts, 15, p. 122.

Sillitoe, R.,1990b Gold rich porphyry copper deposits of the Circum Pacific region; an updated overview. In: Proceedings; Pacific Rim Congress 90. Ed. T. Brennan. Australasian Institute of Mining and Metallurgy. v., p 119 – 126.

Sillitoe, R., and Gappe, I.M., 1984, Philippine porphyry copper deposits; geologic setting and characteristics. UNDP Technical Support for regional Offshore Prospecting in East Asia; United Nations, Economic and Social Commission for Asia and the Pacific. Pages 89.

Sloman L.E., 1989, Triassic shoshonites from the Dolomites, northern Italy: alkaline arc rocks in a strike slip setting, *in* Special section on alkaline volcanism in island arcs: Journal of Geophysical Research, B, Solid Earth and Planets, v. 94, no. 4, p. 4655–4666.

Smith, I.E., 1972, High-potassium intrusives from southeastern Papua: Contributions to Mineralogy and Petrology, v. 34, p. 167–176.

Smith, R.E., and Smith, S.E., 1976, Comments on the use of Ti, Zr, Y, Sr, K, P and Nb in classification of basaltic magmas: Earth and Planetary Science Letters, v. 32, p. 114–120.

Solomon, M., and Griffiths, J.R., 1972, Tectonic evolution of the Tasman Orogenic Zone, eastern Australia: Nature Physical Science, v. 237, p. 3–6.

Sourirajan, S., and Kennedy, G.C., 1962, The system NaCl-H2O at elevated temperatures and pressures: American Journal of Science, v. 260, p. 115–141.

Spence, A. 1985, Shoshonites and associated rocks of British Columbia. Geological Fieldwork Report 1984, A summary of field activities. Paper1985 – 1. Ministry of Energy, Mines and Petroleum Resources.

Stacey, J.S., and Kramers, J.D., 1975, Approximation of terrestrial lead isotope evolution by a two-stage model: Earth and Planetary Science Letters, v. 26, p. 207–221.

Stern, R.J., Bloomer, S.H., Lin, P-G., Ito, E, and Morris, J., 1988, Shoshonitic magmas in nascent arcs: new evidence from submarine volcanoes in the northern Marianas: Geology, v. 16, p. 426–430.

Streckeisen, A.L., 1973, Plutonic rocks: Classification and nomenclature recommended by the IUGS subcommission on the systematics of igneous rocks: Geotimes, v. 18, no. 10, p. 26–30.

Sun, S.S., 1980, Lead isotopic study of young volcanic rocks from mid-ocean ridges, ocean islands and island arcs: Royal Society of London Philosophical Transactions, s. A, no. 297, p. 409–45.

Suppel, D.W., and Scheibner, E., 1990, Lachlan Fold Belt in New South Wales — regional geology and mineral deposits, in Geology of the Mineral Deposits of Australia and Papua New Guinea (Ed. F.E. Hughes) Australian Institute for Mining and Metallurgy : Melbourne , p.1321 - 1328.

Sutherland Brown, A., Editor, 1976, Porphyry Deposits of the Canadian Cordillera, Canadian Institute of Mining and Metallurgy, Special Volume 15, 510 pages.

Tatsumi, Y., and Koyaguchi, T., 1989, An absarokite from a phlogopite lherzolite source: Contributions to Mineralogy and Petrology, v. 102, p. 34–40.

Tenison Woods, K., 1990, Regional geophysics, *in* Clarke, I., and Sherwin, L., eds., Geological setting of gold and copper deposits in the Parkes area, New South Wales: New South Wales Geological Survey Records 23, no. 1, p. 77–94.

Tenison Woods, K., and Webster, S.S., 1985, Geophysical signature of gold and copper mineral deposits in the Lachlan Fold Belt, NSW: Exploration Geophysics, v. 16, p. 325–331.

Thompson, R.N., 1982, Magmatism of the British Tertiary Volcanic Province: Scottish Journal of Geology, v. 18, p. 49–107.

Titley, S.R., 1982, The style and progress of mineralisation and alteration in porphyry copper systems, American Southwest, *in* Titley, S.R., ed., Advances in geology of the porphyry copper deposits: Southwestern North America: University of Arizona Press, Tuscon, AZ.

Varecamp J.C., and Kalamarides R.I., 1989, Hybridisation processes in leucite tephrites from Vulsini, Italy, and the evolution of the Italian potassic suite, *in* Special section on alkaline volcanism in island arcs: Journal of Geophysical Research, s. B, Solid Earth and Planets, v. 94, no. 4, p. 4603–4618.

Washington, H.S., 1906, The Roman Comagmatic Region: Publications Carnegie Institute, v. 57, 1–199.

Webby, B.D., 1976, The Ordovician System in south-eastern Australia, *in* Bassett, M.G., ed., The Ordovician System: Palaeontological Association Symposium, Birmingham, September 1974, Proceedings, p. 417–446.

Webby, B.D., 1980, Biogeography of Ordovician stromatoporoids: Palaeogeography, Palaeoclimatology, Palaeoecology, v. 32, p. 1–19.

Weisbrod, A. 1981, Fluid inclusion in shallow intrusives, *in* Hollister, L.S, and Crawford, M.L., eds., Short course in fluid inclusions: Mineralogical Association of Canada, p. 53-84

White, A.J.R., Williams, I.S., and Chappell, B.W., 1976, The Jindabyne Thrust and its tectonic, physiographic and petrogenetic significance: Geological Society of Australia Journal, v. 23, p. 105–112.

White, W.H., Bookstrom A..A., Kamilli, R.J., Ganster. M.W., Smith, R.P., Ranta, D. E., and Steininger R.C., 1981, Economic Geology, 75th Anniversary Volume, p270 – 316.

Williams, I.S., Compston, W., and Chappell, B.W., 1983, Zircon and monazite U-Pb and histories of I-type magmas, Berridale Batholith, Australia: Journal of Petrology, v.24, p. 76-97.

Wilson, J.W.J., Kesler, S.E., Cloke, P.L., and Kelly, W.C., 1980, Fluid inclusion geochemistry of the Granisle and Bell porphyry copper deposits, British Columbia: Economic Geology, v. 75, p. 45–61.

Wilson, M., 1989, Igneous petrogenesis: a global tectonic approach: Unwin Hyman, London.

Wood, D.A., Joron J.L., and Treuil M., 1979, A re-appraisal of the use of trace elements to classify and discriminate between magmas series erupted in different tectonic settings: Earth and Planetary Science Letters, v. 45, p. 326–336.

Wones, D.R., 1972, Stability of biotite: A reply: American Mineralogist, v. 57, p. 316–319.

Wones, D.R., and Eugster, H.P., 1965, Stability of biotite: Experiment, theory and application: American Mineralogist, v. 50, p. 1228–1272.

Wyborn, D., 1988, Ordovician magmatism, gold mineralisation, and an integrated tectonic model for the Ordovician and Silurian history of the Lachlan Fold Belt, NSW: BMR Research Newsletter 8, p. 13–14.

Wyborn, L.A.I., 1977, Aspects of the geology of the Snowy Mountains region and their implications for the tectonic evolution of the Lachlan Fold Belt: Unpublished Ph.D. thesis Australian National University, Canberra.

Wyborn, L.A.I., and Chappell, B.W., 1979, Geochemical evidence for the existence of a pre-Ordovician sedimentary layer in southeastern Australia: Bureau of Mineral Resources, Geology and Geophysics, Australia, Record 1979/2.

Wyborn, D., and Cameron, W., 1990, Ordovician magmatism in the central Lachlan Fold Belt and precious metal potential: Geological Society of Australia Abstracts 25, p. 126–127.

Zindler, A., and Hart, S., 1986, Chemical Geodynamics: Earth and Planetary Science Annual Reviews, v.14, p. 493-571.

APPENDIX 1

Review of Shoshonite Terrains

Review of Shoshonite Terrains

Absaroka Mountains, Wyoming (Gest and McBirney, 1979).

VOLCANICS - MINERALOGY	VOLCANICS - PETROGRAPHY	PETROGENESIS	TECTONIC SETTING / FIELD RELATIONS
Absarokites (ph) olivine, pyroxene	Euhedral ol, augite (20-25%), plag (An70-An50)	Fractionation of absorokite to form shoshonite.	Higher in Ba, Rb, Sr and REE than ocean
(gm) pyx, calcic plag, sanidine		Distribution coeff. of REE in plag. gives T= 1250 degrees	island shoshonites.
Shoshonites (ph) calcic plag, ol, pyx	Euhedral plag, some resorption rims and inclusions of	Low oxygen fugacity.	Similar REE to Eolian Islands. Both settings
(gm) pyx, calcic plag, sanidine	sanidine	Depleted in HREE and enriched in LREE.	have continental basement.
		Sources: garnet peridotite, garnet amphibolite or eclogite	By analogy with shoshonitic lavas in central
		Pressure estimate: 45-65 kb.	and western Utah: extensional tectonics
			with normal faulting. Little evidence for
			contemporaneous subduction.

Independence Volcanic Suite, Absaroka Mountains, Montana (Meen and Eggler, 1987)

VOLCANICS - MINERALOGY	VOLCANICS - PETROGRAPHY	PETROGENESIS	TECTONIC SETTING / FIELD RELATIONS
HATS series (glomerocrysts) augite,	Glomerocrysts mantled by Ti biotite	HATS trend: basaltic andesite to shoshonite:	Some trace elements different from
hypersthene, magnetite,apatite, biotite		Fractionation phases: plag, two pyx, Ti magnetite.	orogenic volcs Ba/Th extreme, La/Th high.
High K dacite : Lower ratios pyx/plag and		HAB trend: Parental high-magnesium andesites	suggesting no subduction zone
Hyp/augite. Hornblende and K feldspar		Ni >170 ppm, Cr >500 ppm, high LILE, LREE, low HREE	Sourced from ancient granulite.
microphenocrysts.		Low 87Sr/86Sr and low 143Nd/144Nd implies mantle	
HAB series (ph) plag, augite, hypersthene		metasomatism, crustal contamination or disequilibrium.	
		Pb isotopes show linear trends due to mixing or isochrons	
		Parental HAB primitive (high Mg no.) Parental HATS	
		more evolved: Early frac of ol and pyx to deplete Ni, Cr.	

Crandall Ring-dyke, Absaroka Mountains, Wyoming (Kudo and Broxton, 1985).

VOLCANICS - MINERALOGY	VOLCANICS - PETROGRAPHY	PETROGENESIS	TECTONIC SETTING / FIELD RELATIONS
Medium-grained gabbros, diorites, and	Quartz monzonites: porphyritic, phaneritic gm.	Whole rock chemistry: Three groups corresponding to	Plot of the logarithm of the calc-alkalic ratio
quartz monzonites: plag, opx, cpx, minor	diorites:intergranular texture.	gabbro, diorite and quartz monzonite.	vs SiO2 (Brown, 1982) show similarities to
biotite, Ti magnetite	Most rocktypes: early formed euhedral plag	Pearce diagram shows similar trace element	a mature arc shoshonite suite .
	rims and stubby pyroxene crystals, poikilitically	pattern to shoshonite from New Hebrides.	Abundance of LREE and Th-U implies an
	enclosed by K-feldspar and/or quartz. Subophitic	LREE enriched, HREE depleted.	enriched source.
	intergrowth of plag and augite.	Gabbro Sr87/Sr86=0.7042	
		DioriteSr87/Sr86=0.7067	Absoroka volcanic province: 23,000 sq. km,
		Gabbro-diorite linked by accumulation and intruded as	Eocene andesites and breccias
		crystal mush. Low Mg no. argues against mantle source.	
		Variable Sr isotopes implies some contamination.	
		Shoshonite contaminated by plag, cpx. Diorite plutonic	

Absaroka-Gallatin Volcanic Province, Wyoming-Montana (Chadwick, 1970).

VOLCANICS - MINERALOGY	VOLCANICS - PETROGRAPHY	PETROGENESIS	TECTONIC SETTING / FIELD RELATIONS
Eastern Absaroka: monzogabbro,			Numerous centres, volcanics necks, breccia
monzodiorite, trachyandesite,orthoclase			pipes, caldera complexes, dyke swarms,
gabbro, monzonite porphyry, potassic			ring dyke and cone complexes. Generally
andesite, syenite, monzonite, latite and			northwest trend, two subparallel trends due
potassic basalt.			to Laramide to Cambrian fault zones.
Western Absaroka : Calc-alkalic suite.			

Monzonite Plutons, California (Miller, 1978)

VOLCANICS - MINERALOGY	VOLCANICS - PETROGRAPHY	PETROGENESIS	TECTONIC SETTING / FIELD RELATIONS
Diorites, monzodiorite, monzonite, quartz		High LILE (K, Rb, Ba, Sr) and LREE	Eclogite occurs as pockets in subcontinental
monzonite.		Near equality of K2O and Na2O.	mantle not related to subduction. Alkalic
Monzonites: K-feldspar, sodic plag, salitic		Sr86/Sr87=0.7057, 07053	near-saturated magmas may be related to
cpx, hornblende, quartz (<5%)		Moderate Sr87/Sr86 ratios higher than mantle, lower	partial melting of moderately potassic
		than continental crust. High Sr, absence of Eu anomaly	eclogite. Related to minor thermal events
		implies feldspar minor residue at source. High Na2O	prior to major thermal episodes which
		and high K2O imply alkali phases at source or small	generate abundant magmas to overwhelm
		eclogite component.	Monzonites occur in the batholithic belt of
			California. They are not comagmatic with more
			typical granitic intrusions but represent the
			tapping of a distinct source.

Andes (26°- 28°S), Northern Chile and Argentina (Dostal et al., 1977).

VOLCANICS - MINERALOGY	VOLCANICS - PETROGRAPHY	PETROGENESIS	TECTONIC SETTING / FIELD RELATIONS
			Increase in Rb, Ba, Sr and Zr away from
			trench. Increasing enrichment in LREE and
			fractionated HREE. Gradual change cannot
			be explained by low-pressure fractionation
			Upper enriched mantle above a Benioff Zone
			Cycles of volcanism along partially superimposed
			longitudinal belts. Furthermost volcanism 250 km
			from inner boundary of orogen. Most of the
			zones are calc-alkaline except the
			innermost zone which is shoshonitic.

Southern Latium, Italy (Civetta et al., 1981).

VOLCANICS - MINERALOGY	VOLCANICS - PETROGRAPHY	PETROGENESIS	TECTONIC SETTING / FIELD RELATIONS
KS rocks. Leucite-bearing alkali basalts	KS rocks: aphyric to porphyritic. Diopsidic	K series (KS): K20/Na2O approximately unity.	Quaternary volcanism related to extensional
trachybasalts. Aphyric to porphyritic	clinopyroxene to salite. Minor olivine (Fa = 10-15%)	K2O+Na2O = (5-6%).	tectonism. Subduction occurred in Tertiary
(ph) account for 0 -20 %, diopside to	HKS rocks: Weakly porphyritic to porphyritic with	High-K Series (HKS): K2O/Na2O = 3.	and has moved south and is still active under
salite, subordinate olivine, rare plagioclase	phenocrysts accounting for 15 - 20 %	K2O+Na20 = 9 -11 %.	the Aeolian Arc. This possibly provided the
(gm) zoned plag, zoned salite, ol, mag and	Pyx zoned: 1. ferrosalite core, diopside-salite rim	LILE Ba, Rb, Sr enriched. HKS enriched by	metasomatic fluid phase. Some contintental
alkali feldspar,	2. diopside core, salite rim	factor of 1.5-3.0.	crust involvement could supply radiogenic Sr
HKS rocks. Dominantly tephyritic leucites		Overall LREE enriched	and LILEs.
Silica undersaturated		Sr87/Sr86 (HKS) = 0.70962 - 0.70962.	Part of the Roman Magmatic Province.
(ph) cpx, minor ol,		(KS) = 0.70622 - 0.70705.	Twenty small edifices in corridor 20 km long.
(gm) leucite, salitic pyx and opaques.		Genetic model: Small degrees of partial melting of garnet	Dominantly pyroclastics, minor flows. Erupted
		peridotite enriched in LIL elements and radiogenic Sr.	after regional distension caused subsidence.
		Enrichment by fluid phase enriched in LIL elements and	K-rich volcanics erupted first followed by less
			K-rich suite.

Aeolian Arc, Italy (Keller, 1974).

VOLCANICS - MINERALOGY	VOLCANICS - PETROGRAPHY	PETROGENESIS	TECTONIC SETTING / FIELD RELATIONS
Trachybasalts: (ph) olivine, augite +/- plag.	Olivine present as resorbed grains in rhyolites.	Low in total iron, MgO, CaO, TiO2 compared to tholeite	Arc is in its final stages as oceanic crust
(gm) K-feldspar, plag (An 65 -50)		No iron enrichment. Calc-alkaline and shoshonitic	no longer available. Present seismicity
Biotite and hornblende uncommon.		association not linked by fractionation.	occurs at a depth of 200-350 km. Model
Rhyolites and alkali rhyolites : as above		Rb, Sr, Ba enriched.	is of a detached slab sinking into the mantle.
with quartz in groundmass.		Sr87/Sr86 = 0.703-0.7064 implies contamination by	Shoshonites involved with calc-alkaline rocks in
		radiogenic Sr ruled out.	island arc environment. Shoshonites generally the
			youngest.

Aeolian Islands, Southern Italy (Ellam et al., 1989).

VOLCANICS - MINERALOGY	VOLCANICS - PETROGRAPHY	PETROGENESIS	TECTONIC SETTING / FIELD RELATIONS
		Stromboli and Volcano lavas are low-K series (LKS).	Subduction: Benioff Zone dips northwest
		Majority of islands are high-K calc-alkaline to	beneath the Aeolian Islands. Subduction may
		calc-alkaline unlike Roman Region. LILE are	have ceased.
		enriched, high field strength elements (HFSE) are low.	Mixing of two subduction zone components,
		Sr/Nd vs Th/Ta plots suggest mixing of fluid from	derived from components derived from
		dehydrated slab with subducted sediment.	subducted basalt and sediment.
		Vulsini Sr87/Sr86 =0.7099-0.7016.	Associated with calc-alkaline, high-K
		Volcano Sr87/Sr86 = 0.7043-0.7049.	calc-alkaline rocks.
		Mantle source possibly ocean island basalt (OIB) affinity.	
		Pb isotopes show planar array indicating 3 components	
		mixing. Hybridisation of mantle, reaction of peridotite	
		partial melts of subducted sediment to produce	

		phlogopite which melts to produce potassic melts.	

Dolomites, Northern Italy (Sloman, 1989).

VOLCANICS - MINERALOGY	VOLCANICS - PETROGRAPHY	PETROGENESIS	TECTONIC SETTING / FIELD RELATIONS
Basalts: (ph) plag, (An49 - An88), cpx	Plagioclase (8-42%), clinopyroxene (0-24%)	SiO2 (47-53%), MgO (1.2-10.3%) Relatively poor	No evidence of contemporaneous subduction
(salite - high Ca augite), olivine (Fo)	Olivine (0-24%)	in Fe. Lies in calc-alkaline field of the AFM diagram	Strike-slip faulting in a transcurrent or
titanomagnetite	Groundmass microcrystalline or glassy. Felsitic laths	Base level of K2O high even at low silica levels.	transtensional regime. Arc signature due
	of plagioclase together with clinopyroxene, opaques ar	LILE enriched. HFSE similar to MORB.	to oceanic slab subducted prior to
	apatite. Plagioclase mantled by rim of alkali feldspar.	Range in MgO implies crystal fractionation. Al2O3	Hercynian Orogeny.
		incompatible behaviour means plag fractionation	Volcanics associated with a change from
		improbable. Rb and Sr are decoupled suggesting	continental, to marine conditions and the onset of
		contamination by crustal material rich in Rb, K2O, Na2O	block faulting..
		and SiO2 but poor in Sr. Plagioclase crystals partially	
		resorbed cores which are calcic. Abrupt change to	
		potassic and sodic exterior suggests contamination.	
		Sr87/Sr86 = 0.7042-0.7046	

Vulsini, Italy (Varecamp and Kalamarides, 1989).

VOLCANICS - MINERALOGY	VOLCANICS - PETROGRAPHY	PETROGENESIS	TECTONIC SETTING / FIELD RELATIONS
HK Series: mafic basanite suite	Modes vary between samples. Leucite absent as	Magma mixing indicated by mineral chemistry, whole	Post collisional. Volcanics located in
Leucitite, tephrite, phonolite suite	phenocryst. Plagioclase fretted and corroded. Olivine	rock and trace elements, glass inclusion data, and	Pliocene graben structure. Subduction
LK Series: trachybasalts, latites, trachytes	corroded and mantled by cpx.	oxygen isotope data. Shallow magma chamber with	superceded by extension.
HK series: (ph) ol, plag, Ti magnetite,	Olivine Fo (84 - 87%), cpx ranges from salite to	evolved LK magmas which assimilated gneissic material	
cpx, phlogopite.	diopside.	to reach high O and Sr isotope values. Underplated by VHK	
(gm) leucite, cpx, plag, Ti magnetite, glass		magma which itself is underplated by a primitive HK	
		magma. Phonolitic - trachytic magmas form in	
		carapaces where extensive wall rock interaction occurs	

Papua New Guinea (Mackenzie and Chappell, 1972).

VOLCANICS - MINERALOGY	VOLCANICS - PETROGRAPHY	PETROGENESIS	TECTONIC SETTING / FIELD RELATIONS
Wide spectrum from shoshonites to high-K	Olivine (Fo80), plagioclase have calcic cores with	Gradation from high-K andesite; low-silica high-K	No evidence of dipping subduction zone.
andesites.	marginal absorption. Aggregates of cpx+ol+/-plag,	andesite and high-K high-Al basalt to shoshonite and	Possible subduction zone in Pleistocene time
Shoshonites: (ph) plagioclase (andesine or	cpx+/-plag, olivine and plagioclase phenocrysts are	absarokite. Gradation occurs within the province	Mixture of shoshonitic and calc-alkaline
labradorite), augite, olivine. (gm) plag, augite	common suggesting crystal fractionation.	and in individual centres.	rocks argues against zonation in time and
Ti magnetite, apatite, K-feldspar.	Alkali feldspar (sanidine) commonly mantles plagioclas	As a group, the rocks have high, variable aluminium	space due to subduction. Volcanoes form a
Some shoshonites have amphibole with	phenocrysts.	high total alkalis and potassium and low total iron,	cluster rather than linear belts. Magma
magnetite, augite, plagioclase rims. These		magnesium and calcium, relative to calc-alkaline rocks	generation due to detached and sinking
shoshonites grade into high-K amphibole-		AFM diagram shows no iron enrichment and a trend to	eclogite accompanied by zone refining during

olivine basalts.		the MgO apex. K2O/Na2O vs SiO2 plot shows rapidly	passage of melt through the mantle.
Some shoshonites contain hypersthene as		increasing SiO2 in contrast with calcalkaline trend	Stratovolcanoes occupy a large area of PNG
well as amphibole and olivine. With the		which is flat. Total alkalis vs silica shows an increasing	highlands. Consist of lavas, agglomerate, tuff and
disappearance of olivine they grade into two		then flattening trend from some centres.	lahar deposits. Commonly composite calderas.
pyroxene basalts and andesites.		Rb, Sr, Ba are high compared to calc-alkali andesites.	Underlain by Mesozoic and Cenozoic sedimentary
		C, Ni, Cu,Y and Sc are within the normal range.	rocks and further by Palaeozoic basement
		Comparing Highlands shoshonites with calc-alkaline	granites and metamorphic rocks. Uplift,
		rocks:1. Cr, Ni, Cu, Rb and Sr are significantly higher	orogeny and major fault movement took place in
		in shoshonites.	the late Miocene and Pliocene. Eruption took
		2. V and Sc are slightly higher.	place in the middle Pleistocene. No seismic
		3. Ba and Y are similar.	evidence for a subduction zone.
		4. Nb is lower.	

Southeast Papua (Smith, 1972).

VOLCANICS - MINERALOGY	VOLCANICS - PETROGRAPHY	PETROGENESIS	TECTONIC SETTING / FIELD RELATIONS
Middle Miocene intrusives.	Gabbro: Biotite typically moulded around earlier forme	Near saturated rocks show even textures with regular	Middle Miocene was the beginning of a period
Near-saturated group:	minerals.	petrographic and chemical trends and is suggestive of	of tectonic activity. Tectonic style one of
Gabbro: Labradorite (An50-65), cpx, biotite	Monzonites: Ratio of K-feldspar to plagioclase increase	a crystal fractionation series. Undersaturated rocks	block faulting and vertical movement.
(up to 20%), olivine (up to 5%), apatite,	as the total mafic mineral content decreases and quart	show wide variation in textures. May have formed	High-K intrusives emplaced near the
interstitial K-feldspar.	increases. K-feldspar is perthitic and occurs	in small magma chambers by differentiation.	beginning of the period of Late Cainozoic
Monzonites, diorites: K-feldspar, andesine	interstitially and as plates enclosing early formed	Pyroxenites show affinities for K-rich rocks. No	uplift. Perhaps due to mantle instability
(An35-45), subordinate cpx, biotite, apatite	minerals and as rims surrounding plagioclase.	accumulate textures mitigates against cumulate origin.	prior to an orogenic episode.
sphene.		Wide chemical variation and high Sr and Ba with low	High-K rocks intrude >3km of tholeitic basalts.
Quartz monzonites contain up to10% quartz		Ni, V and Cr indicates fractionation. Possible parent	Gabbro, monzonite, diorite and syenite form small
Syenites: Minor mafics enclosed by coarse		magma composition.	stocks. Gabbro-monzonite and gabbro-diorite-
perthitic K-feldspar. Plag minor or absent.			monzonite are near saturated associations. The
Mafics are augite, hornblende. Opaques, zircon			undersaturated group form biotite gabbro,
and rare nepheline are accesssories.			porphyritic monzonite and porphyritic syenite
Undersaturated Group			together with trachybasalt and latite dykes.
Wide variety which is difficult to classify			Biotite pyroxenite associated with near-saturated
Gabbro: Biotite, cpx, plag set in a matrix of			gabbro of the Watuti River stock. Pyroxenite
large K-feldspar crystals.			found as inclusions in some of the undersaturated
			rocks.

Fiji (Gill and Whelan, 1989).

VOLCANICS - MINERALOGY	VOLCANICS - PETROGRAPHY	PETROGENESIS	TECTONIC SETTING / FIELD RELATIONS
Absorokites: (ph) ol, augite, +/- plag, mag		Three levels of potassium enrichment with respect	Vanuatu, Viti Levu and Lau segments of Fiji
Shoshonites : (ph) plag, augite, (ol), mag.		to silica, magnesia, and soda can be determined, low-	and Tonga are all parts of the same island
Banakites : (ph) plag, augite, mag, biotite.		medium-, and high-K shoshonites (LKS, MKS, HKS).	arc before it fragmented by rifting.

(gm) crystalline K-feldspar, biotite, rare		Shield volcanoes develop from initially absarokitic	Common arc had subduction zone to the east
nepheline		lavas and intrusions of essexite and monzonite sills.	during middle Miocene (14 my). Rifting in the
		Depletion of HFSE and HREE and high concentrations of	Pliocene (5.5-3my) with arc reversal.
		alkalies and alkali earths.	Vanuatu separated from Fiji due to
		Uniform Sr87/Sr86 ratios (0.7037-0.7039)	transverse rift and reversal of subduction.
		Nd and Pb isotopes show mantle array.	Two correlations between basalt
		Low Ni/Mg ratios possibly due to pyx accumulation.	compositions and tectonic location are:
		or early sulphide saturation or extensive olivine	1. shoshonitic rocks in the west adjacent
		fractionation.	to a transverse rift between Fiji and
		Trace element patterns between shoshonitic, calc-alkali	Vanuatu. 2. Presence of tholeites in the
		and tholeitic rocks are similar. Overall hydrous oxidised	east, adjacent to the Lau back arc basin.
		melts (contrast with Absoroka Mountains)	Inception of arc rifting responsible for
		Model: differentiation of medium-K basalt with crustal	shoshonites. Implies small percent partial melting to
		contamination during ponding canot be sustained.	give LILE source enrichments. Residual titanites give
		Mantle source likely.	HFS element depletion.
			Shoshonitic rocks associated with calc-alkaline
			and tholeitic rocks. Shoshonites associated with
			the early rifting stage. Centres structurally
			controlled along ENE alignment (Viti Levu
			Lineament and Vatulele-Beqa Lineament) and
			NNW alignment (Lomaiviti Lineament).
			Plag-phyric shoshonites and monzonites intruded
			primarily during the formation of the caldera.
			HKS banakites occur as domes in the caldera.
			Calc-alkaline magmas erupted at the same time
			from adjacent volcanoes. Overall shoshonitic
			and calc-alkaline rocks form a continuum with
			increasing alkali enrichment.

Northern Mariana Arc (Bloomer et al., 1989).

VOLCANICS - MINERALOGY	VOLCANICS - PETROGRAPHY	PETROGENESIS	TECTONIC SETTING / FIELD RELATIONS
(ph) plag, cpx, opx, Ti magnetite	Plagioclase: Often zoned with glass inclusions and ma	Most of the major element variation can be modelled by	Magmatic front of an intracratonic arc
cpx, opx, Ti magnetite	have clear rims over corroded cores. Plagioclase	fractionation or accumulation of plag, ol, and cpx, with	Mantle diapirism exposing deeper parts of
plag, cpx, ol, +/-Ti magnetite, =/-opx	commonly occurs in glomerocrysts with pyroxenes	lessor amounts of opx and magnetite.	the mantle which have not previously melted
plag, cpx, +/- Ti magnetite	and titanomagnetites.	Modelling reveals 5-10 kbar ol-cpx-plag, over 10kb it	If the mantle is veined by an enriched
	Olivine occurs as euhedral phenocrysts or as	is cpx-opx-plag.	component in a depleted matrix then rifting
	subrounded grains with rims of opx or cpx.	Possible change along strike due to the potassic series	may unroof deeper portions of the enriched
	Cpx second most abundant to plag. Forms glomerocry	derived from high-pressure crystallisation of a	mantle.
	with titanomagnetite and plagioclase.	low-K subalkaline basalt. However mineralogical	Other mechanisms may include oblique
	Phenocrysts and microphenocrysts of titanomagnetite	trends and elemental trends point to different parent	subduction zones, areas undergoing
	are ubiquitous in the more siliceous samples.	magma.	extension or volcanism with a deep

			subduction zone.
			Potassic volcanic province in the northern
			Mariana Arc. Further south subalkaline series.

Sydney Basin, Australia (Carr, 1985)

VOLCANICS - MINERALOGY	VOLCANICS - PETROGRAPHY	PETROGENESIS	TECTONIC SETTING / FIELD RELATIONS
Basalts, basaltic andesites and andesites	Feldspar: euhedral to anhedral, range from bytownite t	Generally high total alkalis, Rb, Sr, high ferric to	Subduction zone in the Late Permian absent.
Plag most abundant followed by cpx, ol	calcic andesine.	ferrous ratio. Low contents of TiO2, MgO, CaO	Evidence for an Early Permian subduction
Fe-Ti oxide. (gm) plag, K-feldspar, cpx	Thin rims of K-feldspar occur on some grains.	Cr and Ni. Al2O3 variable but high.	zone exists. This may have depressed the
Fe-Ti oxide, ol, apatite	Groundmass plagioclase has the compositional range	Mantle derived. 10-15% partial melting of a spinel	geotherm and enriched the mantle wedge
	andesine to sodic labradorite and is generally richer in	lherzolite enriched in light REE followed by high	with LILEs and water. Cessation
	albite. Plagioclase occurs as subhedral stumpy prisms	pressure fractionation of olivine and pyroxene.	of subduction would have led to increased
	whereas the K- feldspar occurs as subhedral grains o	LILE must be inherited in the source regions	temperature and coupled with water
	microlites scattered throughout the groundmass.	Possibly due to small partial melts leading to zone	caused partial melting.
	Clinopyroxene plots in the augite/salite fields.	refining.	Continuum of compositions in the series basalt-
	Phenocryst and groundmass pyroxene compositions		basaltic andesite-andesite implies link through
	similar.		crystal fractionation.

APPENDIX 2

Whole Rock and Trace Element Data

Sample number	PH1	PH4	PH7	PH9	PH16	PH17	PH18	PH19
Location East	596000	596000	601600	601600	603000	598400	605700	599800
Location North	6363000	6354700	6359000	635740	6353000	6350000	6344300	6356200
Drillhole/Depth/Location		ACH 967 100	ACH 119-3 57m		Goonumbla Hill	Nash's Hill	Goonumbla Quarry	E 31/DDH5
Geopeko Sample No.	5901	5904	5907	5209	5916	5917	5918	
SiO2	53.26	52.91	57.57	58.31	54.54	59.27	51.40	61.13
TiO2	0.66	0.52	0.44	0.53	0.75	0.42	0.77	0.39
Al2O3	19.92	20.99	17.35	18.25	17.30	18.00	18.18	17.76
Fe2O3	2.97	3.08	3.43	2.79	4.67	3.00	4.08	2.49
FeO	3.30	2.20	1.61	2.09	3.26	1.03	4.80	1.55
MnO	0.15	0.09	0.11	0.10	0.12	0.12	0.13	0.12
MgO	2.42	1.72	0.93	1.80	3.22	0.79	3.80	1.43
CaO	6.80	7.46	4.59	3.33	7.14	2.92	6.72	3.07
Na2O	5.10	5.28	4.68	4.81	4.93	6.61	4.10	5.21
K2O	3.57	3.60	3.86	4.96	2.87	4.34	2.78	4.02
P2O5	0.53	0.40	0.30	0.35	0.36	0.27	0.37	0.19
S	0.04	0.02	0.05	0.24	0.00	0.01	0.01	0.03
H2O Plus	1.49	0.93	1.87	1.79	1.37	0.94	2.68	2.68
H2O Minus	0.34	0.29	0.6	0.41	0	0	0	0
CO2	0.5	0.02	3	1.88	0.19	1.39	0.51	0.54
Total	101.05	99.51	100.39	101.64	100.72	99.11	100.33	100.61
Ba	905	760	1050	1010	550	780	770	1010
Rb	45	60	67	87	33	57	53	59
Sr	1560	1860	805	895	1140	535	1180	1220
Pb	9	4	18	10	3	13	7	9
Th	14	13	16	14	19	13	19	15
U	1	1.3	1.2	2	1.2	1.7	1.1	1.2
Zr	49	75	93	112	86	110	115	85
Nb	5	4	4	9	6	6	8	3
Y	2	2	2	6	8	12	6	-2
La	11.8	8.8	10.4	20.2	13.9	17	14.4	10.8
Ce	26	30	32	40	32	41	28	25
Nd	10.3	10.3	10.7	18.7	15.4	17.3	16.9	9.6
Sc	26	30	32	40	32	41	28	25
Cr	10	10	10	5	50	-5	90	5
Ni	5	5	-5	-5	20	-5	10	-5
Zn	212	60	182	104	44	25	159	214
Rock Name	Diorite	Trachyandesite	Monzonite	Monzonite Ring Dike	Goonumbla Volcanic	Trachyte	Latite	E31 Monzonite
Alteration (U,W,M,S)	U	U	W	M	U	U	U	U

Sample number	PH22	PH23	PH32	PH35	PH36	PH2	PH3	PH5
Location East	598156	598124	597765	598110	597700	598050	598000	598000
Location North	6354500	6354605	6354675	6354500	6354800	6354700	6354500	6358300
Drillhole/Depth/Location	E26/46/389	E26/46/222m	E26/29/325.7	E26/42/1112	E26/40/569	DDH46/850	DDH26	E 27/DDH9
Geopeko Sample No.						5902	5903	5905
SiO2	60.40	62.86	59.28	61.79	59.79	55.21	62.56	55.93
TiO2	0.37	0.26	0.55	0.28	0.36	0.52	0.28	0.43
Al2O3	17.22	16.68	17.70	17.40	17.21	17.65	16.87	16.65
Fe2O3	1.64	0.15	3.09	2.08	2.64	6.00	2.91	4.72
FeO	2.40	1.21	2.40	1.49	1.49	3.69	1.94	2.04
MnO	0.11	0.03	0.05	0.07	0.17	0.04	0.09	0.15
MgO	1.41	0.52	1.30	1.24	1.50	2.29	0.64	1.95
CaO	2.40	0.88	1.86	2.61	3.67	5.58	1.96	4.68
Na2O	6.63	4.48	5.28	5.56	5.04	4.18	6.33	3.62
K2O	4.39	6.34	5.69	3.90	3.67	3.27	4.67	3.41
P2O5	0.20	0.11	0.29	0.13	0.22	0.37	0.37	0.29
S	0.72	0.69	0.44	0.06	0.04	1.21	0.22	0.05
H2O Plus	0.601	0.601	1.2	1.59	1.31			
H2O Minus	0	0	0	0	0			
CO2	2.63	2.63	1.32	2.27	1.6			
Total	101.12	97.44	100.45	100.47	98.71			
Ba	850	15140	900	1000	875	845	980	1060
Rb	58	57	78	67	54	62	47	60
Sr	1060	1420	730	785	840	1530	660	560
Pb	11	9	17	11	6	7	9	23
Th	13	14	16	13	16	18	8	13
U	1.7	23	2.9	1.2	1.3			
Zr	110	1	142	65	75	62	63	97
Nb	3	1	7	2	3			
Y	-2	-2	8	2	4			
La	11.7	6.3	16.6	16.3	18.8			
Ce	34	24	34	26	32	33	23	29
Nd	11	7.5	17.5	11.6	14.6			
Sc	34	24	34	26	32	33		29
Cr	5	15	-5	-5	5			
Ni	-5	-5	-5	-5	-5			
Zn	1410	705	1530	211	6	2630	3080	73
Rock Name	Monzonite	Trachyte	Trachyte	QMP!	PH36 Zero Porphyry	Monzodiorite	QMP2 Quartz Monzonite Porphyry	
Alteration (U,W,M,S)	U	S	M	U	S	M	M	S

Sample number	PH8	PH10	PH11	PH12	PH13	PH14	PH15
Location East	598450	597600	600000	597720	596000	605850	602750
Location North	6354700	6357800	6356000	6353800	6362000	6347700	6352550
Drillhole/Depth/Location	DDH 46//669	E 22 DDH 6	Endeavour 31	Endeavour 26 S	ACH 967 -106	Goonumbla Siding	Goonumbla Hill
Geopeko Sample No.	5908	5910	5911	5912	5913	5914	5915
SiO2	59.32	67.80	61.74	62.75	58.49	51.48	54.38
TiO2	37.00	0.19	0.38	0.35	0.49	0.69	0.60
Al2O3	16.83	15.59	17.73	17.31	17.87	17.96	18.18
Fe2O3	4.46	1.13	3.75	3.89	4.77	8.33	5.75
FeO	2.20	1.09	1.54	1.66	1.37	2.95	2.11
MnO	0.11	0.04	0.07	0.16	0.08	0.21	0.17
MgO	1.64	1.44	1.44	1.25	1.60	3.18	1.83
CaO	3.34	1.44	1.81	1.62	2.55	7.34	6.04
Na2O	5.05	5.23	5.83	5.70	5.39	5.45	6.74
K2O	4.12	5.41	4.01	4.82	5.24	2.10	3.43
P2O5	0.20	0.06	0.20	0.18	0.32	0.51	0.37
S	0.76	0.19	0.08	0.06	0.01	0.02	0.02
H2O Plus							
H2O Minus							
CO2							
Total							
Ba	680	1600	1050	1050	875	730	705
Rb	72	74	55	63	77	23	50
Sr	800	468	1240	550	670	1010	895
Pb	9	10	10	19	10	3	7
Th	14	13	9	14	14	14	16
U							
Zr	112	76	82	117	117	31	94
Nb							
Y							
La							
Ce	32	20	27	34	32	15	30
Nd							
Sc	32	20	27	34	32	15	30
Cr							
Ni							
Zn	4220	1680	595	336	109	182	139
Rock Name	Mafic Monzonite	Quartz Monzonite Porphry	Monzonite	Mafic Monzonite	Mafic Monzonite	Monzonite	Monzonite porphyry
Alteration (U,W,M,S)	M	S	S	S	S	S	W

Sample number	PH30
Location East	597450
Location North	635497
Drillhole/Depth/Location	E26/39/576
Geopeko Sample No.	
SiO2	62.75
TiO2	0.27
Al2O3	17.43
Fe2O3	1.33
FeO	1.14
MnO	0.07
MgO	1.00
CaO	2.57
Na2O	5.80
K2O	4.16
P2O5	0.10
S	0.64
H2O Plus	
H2O Minus	
CO2	
Total	97.26
Ba	1110
Rb	48.5
Sr	1060
Pb	7
Th	7
U	0.7
Zr	57
Nb	1
Y	-2
La	8.6
Ce	25
Nd	7.5
Sc	25
Cr	-5
Ni	-5
Zn	1190
Rock Name	
	QMP2
Alteration (U,W,M,S)	W

APPENDIX 3

Fluid Inclusion Data

Endeavour 26 North Fluid Inclusion Data

Drillhole /Metre	Sample No	Measurement No	Corrected Th (oC)	Inclusion Type	T homogenisation Th (oC)	Tm NaCl	Tm KCl	Size microns	Vol Vapour	Volume H2O
39/322	4222	1	714.37	3	755	535		13		20
39/322	4222	2	480.73	3	500			13	20	20
39/322	4222	3	702.46	3	742	515	350	12	15	15
39/322	4222	4	751.02	3	795			7	15	15
39/322	4222	5	572.35	3	600	560	415	12	20	20
38/327	4234	1	581.52	3	610	530	380	7	15	20
38/327	4234	2	554.03	3	580	525	425	15	20	20
38/327	4234	3	709.79 C		750	590		7	15	15
38/327	4234	4	709.79 B		750			10		
38/327	4234	5	662.14 C		698	690	520	12	20	15
38/327	4234	6	590.68 B		620			10	90	10
38/327	4234	7	590.68 C		620	540		12	15	15
38/327	4234	8	544.87 C		570	570		13	15	15
38/327	4234	9	558.61 C		585	585	430	8	12	18
38/327	4234	10	517.38 C		540	540	380	13	13	15
38/327	4234	11	535.7 C		560	550	430	13	12	17
38/327	4234	12	485.31 C		505	500	420	14	16	23
38/327	4234	13	416.6 C		430	505		13	15	21
38/327	4234	14	581.52 C		610	480		12	20	25
38/325.3	4235	1	572.35	1	600			10	60	40
38/325.3	4235	2	572.35	2	600			12	70	30
38/325.3	4235	3	783.08	3	830	530		15	15	20
38/325.3	4235	4	0							
38/325.3	4235	5	0	3						
38/443.3	4240	1	552.2	3	578	560		12	20	20
38/443.3	4240	2	544.87	3	570	570		10	35	15
38/443.3	4240	3	499.06	3	520	520		13	15	50
38/443.3	4240	4	518.3	3	541	480		12	15	50
38/443.3	4240	5	517.38	3	540	520		13	10	20
39/450.8	4243	1	799.58	3	848	678		12	10	15
39/450.8	4243	2	860.96	3	915	715	560	13	25	15
39/450.8	4243	3	753.76	3	798	617	505	13	15	15
39/450.8	4243	4	764.76	3	810	645		10	15	15

Location	Sample No	Measurement No	Corrected Th (oC)	Inclusion Type	T homogenisation Th (oC)	Tm NaCl	Tm KCl	Size microns	Vol Vapour	Volume H2O
39/450.8	4243	5	585.18	3	614	660		7	20	15
39/450.8	4243	6	627.33	3	660	680		7	20	25
39/450.8	4243	7	581.52	3	610	610		10	10	15
39/450.8	4243	8	572.35	3	600	615		8	20	20
39/450.8	4243	9	0	3					20	20
39/450.8	4243	10	462.41	3	480	480	240	8	15	20
39/450.8	4243	11	714.37	3	755	618	440	8	25	15
39/450.8	4243	12	714.37	3	755	570	440	10	15	15
39/450.8	4243	13	755.6	3	800	615	505	8	15	15
39/450.8	4243	14	0	3		608	415	8	30	20
39/450.8	4243	15	0	3				6	20	15
39/450.8	4243	16	860.96	3	915	640	420	8	15	20
39/450.8	4243	17	607.17	3	638	659	453	15	12	17
39/450.8	4243	18	644.73	3	679	645	405	9	20	20
39/450.8	4243	19	644.73	3	679	622	530	15	20	20
39/450.8	4243	20	531.12	3	555	665		15	15	25
39/450.8	4243	21	762.93	3	808	615		12	12	15
39/450.8	4243	22	586.1	3	615	598		10	15	15
39/450.8	4243	23	644.73	3	679	685		12	20	20
39/450.8	4243	24	992.9	3	1059	621	400	10	15	15
39/450.8	4243	25	572.35	3	600	558		10	20	20
39/450.8	4243	26	751.02	3	795	635		13	20	20
39/450.8	4243	27	1090.02	3	1165	615		10	20	20
39/450.8	4243	28	808.74	3	858	605		12	20	20
39/450.8	4243	29	902.19	3	960	675	520	15	15	20
39/450.8	4243	30	827.06	3	878	615		7	15	15
46/273.5	4250	1	0	3		459		12	20	20
46/273.5	4250	2	219.61	1	215			12	20	80
46/273.5	4250	3	393.69	3	405	425		15	15	30
46/273.5	4250	4	397.35	3	409	515		13	20	25
46/273.5	4250	5	402.85	3	415	538		12	12	28
46/273.5	4250	6	260.84	3	260	470		7	10	30
46/273.5	4250	7	210.45	3	205	525		7	15	25
46/273.5	4250	8	237.93	3	235	350	436	10	12	28

Location	Sample No	Measurement No	Corrected Th (oC)	Inclusion Type	T homogenisation Th (oC)	Tm NaCl	Tm KCl	Size microns	Vol Vapour	Volume H2O
46/273.5	4250	9	219.61	3	215			7	20	30
46/273.5	4250	10	384.53	3	395			7		
46/273.5	4250	11	338.72	3	345			12	20	80
46/273.5	4250	12	192.12	1	185			12	20	80
46/273.5	4250	13	284.66	3	286			15	20	80
46/273.5	4250	14	334.14	1	340			15	20	80
46/273.5	4250	15	228.77	3	225	575		10	20	30
46/273.5	4250	16	338.72	3	345	538		9	10	40
42/601.15	4266	1	389.11	3	400	575		9	10	25
42/601.15	4266	2	397.35	3	409			12	20	25
42/601.15	4266	3	476.15	3	495	545		7	25	30
42/601.15	4266	4	476.15	3	495	495		11	20	20
42/601.15	4266	5	480.73	3	500	480		12	10	20
42/601.15	4266	6	370.78	3	380	560		12	20	30
42/601.15	4266	7	412.01	3	425	485		7	25	30
42/601.15	4266	8	0	3		221	245	15	10	25
42/601.15	4266	9	224.19	3	220	555		12	10	30
42/601.15	4266	10	439.5	3	455	410		10	20	30
42/601.15	4266	11	370.78	3	380	525		15	25	15
42/601.15	4266	12	324.97	3	330	500		12	20	35
42/601.15	4266	13	315.81	3	320	485		13	15	30
46/891.5	4287	1	343.3	3	350			7	15	30
46/891.5	4287	2	751.02	3	795	459		12	15	30
46/891.5	4287	3	0	3		441		7		
46/891.5	4287	4	375.37	3	385				15	85
42/610	4326	1	0	3				15	15	60
42/610	4326	2	0	3		545		10	10	15
42/610	4326	3	659.39	3	695	600	425	15	20	15
42/610	4326	4	631.91	3	665	580		10	10	20
42/610	4326	5	746.43	3	790	480		10	15	15
42/610	4326	6	718.95	3	760	560	540		10	15
42/610	4326	7	773.92	3	820	575	575	15	20	15
42/610	4326	8	0	3				13	10	30
42/610	4326	9	519.21	3	542	395		15	30	15

Location	Sample No	Measurement No	Corrected Th (oC)	Inclusion Type	T homogenisation Th (oC)	Tm NaCl	Tm KCl	Size microns	Vol Vapour	Volume H2O
42/610	4326	10	705.2	3	745	555	420	13	20	20
42/610	4326	11	737.27	3	780	460	460	7	10	10
42/610	4326	12	682.3	3	720	500		10	10	25
42/610	4326	13	444.08	3	460	460		15	15	20
42/610	4326	14	975.49	3	1040	542	405	12	25	20
42/610	4326	15	842.64	3	895	545	485	13	10	15
42/610	4326	16	503.64	3	525	520		13	20	15
42/610	4326	17	0	3				11	15	20
42/610	4326	18	718.95	3	760			7	10	10
42/610	4326	19	718.95	3	760	516		10	15	15
42/610	4326	20	682.3	3	720	520		14	15	20
42/610	4326	21	700.62	3	740	520		7	10	15
42/610	4326	22	645.65	2	680			10	90	10
42/610	4326	23	549.45	3	575	605		10	15	15
38/313.9	4354	1	434.92	3	450	580	400	17	15	15
38/313.9	4354	2	462.41	3	480	480		17	15	15
38/313.9	4354	3	462.41	3	480	480		12	10	20
38/313.9	4354	4	434.92	3	450	480	480	15	20	25
38/313.9	4354	5	554.03	3	580	480		12	20	20
38/313.9	4354	6	554.03	3	580	580		15	15	15
38/313.9	4354	7	122.49	1	109			10	20	80
38/313.9	4354	8	152.72	1	142			10	25	75
38/313.9	4354	9	132.57	1	120			14	25	75
38/313.9	4354	10	131.65	1	119			12	25	75
38/313.9	4354	11	158.31	1	148.1			10	25	75
38/313.9	4354	12	123.41	1	110			15	15	85
38/313.9	4354	13	101.97	1	86.6			7	20	80
38/313.9	4354	14	133.12	1	120.6			15	20	80
38/313.9	4354	15	148.6	1	137.5			12	2	
38/313.9	4354	16	554.03	3	580	550		17	15	20
38/313.9	4354	17	554.03	3	580	550		20	15	25
38/313.9	4354	18	554.03	3	580	580	480	15	15	20
38/313.9	4354	19	549.45	3	575	570	470	15	15	25
38/313.9	4354	20	609	3	640	570	500	14	15	30

Location	Sample No	Measurement No	Corrected Th (oC)	Inclusion Type	T homogenisation Th (oC)	Tm NaCl	Tm KCl	Size microns	Vol Vapour	Volume H2O
38/313.9	4354	21	609	3	640	570	500	14	25	20
38/313.9	4354	22	554.03	3	580	640	260	20	15	25
38/313.9	4354	23	544.87	3	570	570	440	15	15	20
38/313.9	4354	24	480.73	3	500	670		12	10	25
38/313.9	4354	25	572.35	3	600	520		6	20	25
38/313.9	4354	26	682.3	3	720	600		13	20	20
38/313.9	4354	27	462.41	3	480	280		12	20	20
38/313.9	4354	28	581.52	3	610	610	440	13	10	15
38/313.9	4354	29	572.35	3	600	570		13	13	17
38/313.9	4354	30	572.35	3	600	570		14	12	20
38/313.9	4354	31	572.35	3	600	530		13	25	25
38/313.9	4354	32	526.54	3	550	600		12	10	15
38/104.85	4360	1	558.61	3	585	540		7	20	25
38/104.85	4360	2	462.41	3	480	540	415	12	15	30
38/104.85	4360	3	517.38	3	540	415	420	12	10	20
31/234	4495	1	609	3	640	540		12	14	15
31/234	4495	2	554.03	3	580	525	425	15	15	15
31/234	4495	3	0	3		480	480	10	10	20
31/234	4495	4	462.41	3	480	550	440	13	15	10
31/234	4495	5	444.08	3	460	535	460		10	25
31/234	4495	6	558.61	3	585	680	415	13	20	15
31/234	4495	7	499.06	3	520	620		13	10	20
31/234	4495	8	0	3				13	15	25
31/234	4495	9	554.03	3	580	580		12	15	25
31/234	4495	10	434.92	3	450	542		12	15	25
31/234	4495	11	352.46	3	360	560		8	20	30
31/234	4495	12	554.03	3	580	610	440	13	12	25
31/234	4495	13	448.66	3	465	580	340	7	10	20
31/234	4495	14	425.76	3	440	540		7	12	20
31/234	4495	15	480.73	3	500	500		10	10	20

Endeavour 26 North Fluid Inclusion Data

Location	Sample No	Vol Solids	Tm Ice	NaCl Equivalent	Vein Stage	Corrected TmNaCl	Corrected Tm KCl	KCL Weight Percent	NaCl Weight Percent
39/322	4222	0	65	63.17	5	512.79	0	0	
39/322	4222	60		0	5	0	0	0	
39/322	4222	70		60.48	5	494.46	343.22	33	43
39/322	4222	70		0	5	0	0	0	
39/322	4222	60		66.52	5	535.69	402.76	34	47
38/327	4234	65		62.49	3	508.21	370.7	35	43
38/327	4234	60		61.82	3	503.63	411.92	39	41
38/327	4234	70		70.53	3	563.18	0		
38/327	4234	0		0	3	0	0		
38/327	4234	65		83.38	3	654.8	498.94	30	41
38/327	4234	0		0	3	0	0		
38/327	4234	70		63.84	3	517.37	0		
38/327	4234	70		67.86	3	544.86	0		
38/327	4234	70		69.87	3	558.6	416.5	33	50
38/327	4234	72		63.84	3	517.37	370.7	36	45
38/327	4234	71		65.18	3	526.53	416.5	36	44
38/327	4234	61		58.47	3	480.72	407.34	42	37
38/327	4234	64		59.14	3	485.3	0		
38/327	4234	55		55.81	3	462.4	0		
38/325.3	4235	0		0	3	0	0	0	
38/325.3	4235	0		0	6	0	0	0	
38/325.3	4235	65		62.49	6	508.21	0	0	
38/325.3	4235	0		0	6	0	0	0	
38/325.3	4235	0		0	6	0	0	0	
38/443.3	4240	60		66.52	5	535.69	0	0	
38/443.3	4240	50		67.86	8	544.86	0	0	
38/443.3	4240	35		61.15	8	499.04	0	0	
38/443.3	4240	35		55.81	8	462.4	0	0	
38/443.3	4240	70		61.15	8	499.04	0	0	
39/450.8	4243	75		81.9	4	643.81	0	0	
39/450.8	4243	60		86.38	4	677.71	535.58	30	64
39/450.8	4243	70		74.1	4	587.92	485.2	37	50
39/450.8	4243	70		77.73	4	613.57	0	0	

Location	Sample No	Vol Solids	Tm Ice	NaCl Equivalent	Vein Stage	Corrected TmNaCl	Corrected Tm KCl	KCL Weight Percent	NaCl Weight Percent
39/450.8	4243	65		79.65	4	627.32	0	0	
39/450.8	4243	55		82.15	4	645.64	0	0	
39/450.8	4243	75		73.18	4	581.5	0	0	
39/450.8	4243	60		73.84	4	586.09	0	0	
39/450.8	4243	60		0	4	0	0	0	
39/450.8	4243	65		55.81	4	462.4	242.46	46	33
39/450.8	4243	60		74.23	4	588.83	425.66	32	53
39/450.8	4243	70		67.86	4	544.86	425.66	36	47
39/450.8	4243	70		73.84	4	586.09	485.2	37	52
39/450.8	4243	50		72.92	4	579.67	402.76	31	52
39/450.8	4243	65		0	4	0	0	0	
39/450.8	4243	65		77.09	4	608.99	407.34	28	57
39/450.8	4243	71		79.52	4	626.4	437.57	28	60
39/450.8	4243	60		77.73	4	613.57	393.6	27	39
39/450.8	4243	60		74.75	4	592.5	508.1	40	50
39/450.8	4243	60		80.28	4	631.9	0	0	
39/450.8	4243	73		73.84	4	586.09	0	0	
39/450.8	4243	70		71.6	4	570.51	0	0	
39/450.8	4243	60		82.77	4	650.22	0	0	
39/450.8	4243	70		74.62	4	591.58	389.02	29	55
39/450.8	4243	60		66.26	4	533.86	0	0	
39/450.8	4243	60		76.45	4	604.41	0	0	
39/450.8	4243	60		73.84	4	586.09	0	0	
39/450.8	4243	60		72.52	4	576.92	0	0	
39/450.8	4243	65		81.53	4	641.06	498.94	30	61
39/450.8	4243	70		73.84	4	586.09	0	0	
46/273.5	4250	60		53.04	9	443.15	0	0	
46/273.5	4250	0		0	9	0	0	0	
46/273.5	4250	55		48.63	9	412	0	0	
46/273.5	4250	55		60.48	9	494.46	0	0	
46/273.5	4250	60		63.57	9	515.54	0	0	
46/273.5	4250	60		54.48	9	453.23	0	0	
46/273.5	4250	60		61.82	9	503.63	0	0	
46/273.5	4250	60		39.47	9	343.29	422	0	

Location	Sample No	Vol Solids	Tm Ice	NaCl Equivalent	Vein Stage	Corrected TmNaCl	Corrected Tm KCl	KCL Weight Percent	NaCl Weight Percent
46/273.5	4250	50		0	9	0	0	0	
46/273.5	4250	0		0	9	0	0	0	
46/273.5	4250	0		0	9	0	0	0	
46/273.5	4250	0		0	9	0	0	0	
46/273.5	4250	0		0	9	0	0	0	
46/273.5	4250	0		0	9	0	0	0	
46/273.5	4250	50		68.53	9	549.44	0	0	
46/273.5	4250	50		63.57	9	515.54	0	0	
42/601.15	4266	65		68.53	7	549.44	0	0	
42/601.15	4266	55		0	7	0	0	0	
42/601.15	4266	45		64.51	7	521.95	0	0	
42/601.15	4266	60		57.8	7	476.14	0	0	
42/601.15	4266	70		55.81	7	462.4	0	0	
42/601.15	4266	50		66.52	7	535.69	0	0	
42/601.15	4266	45		56.47	7	466.98	0	0	
42/601.15	4266	65		26.58	7	225.09	247.04	0	
42/601.15	4266	60		65.85	7	531.11	0	0	
42/601.15	4266	50		46.73	7	398.26	0	0	
42/601.15	4266	60		61.82	7	503.63	0	0	
42/601.15	4266	45		58.47	7	480.72	0	0	
42/601.15	4266	55		56.47	7	466.98	0	0	
46/891.5	4287	55		0	7	0	0	0	
46/891.5	4287	55		53.04	7	443.15	0	0	
46/891.5	4287	0		50.69	7	426.66	0	0	
46/891.5	4287	0		0	7	0	0	0	
42/610	4326	25		0	6	0	0	0	
42/610	4326	75		64.51	6	521.95	0	0	
42/610	4326	65		71.86	6	572.34	411.92	33	52
42/610	4326	70		69.2	6	554.02	0	0	
42/610	4326	70		55.81	6	462.4	0	0	
42/610	4326	75		66.52	6	535.69	517.26	50	38
42/610	4326	65		68.53	6	549.44	549.32	53	38
42/610	4326	60		0	6	0	0	0	
42/610	4326	55		44.86	6	384.52	0	0	

Location	Sample No	Vol Solids	Tm Ice	NaCl Equivalent	Vein Stage	Corrected TmNaCl	Corrected Tm KCl	KCL Weight Percent	NaCl Weight Percent
42/610	4326	60		65.85	6	531.11	407.34	36	46
42/610	4326	80		53.17	6	444.07	443.98	28	50.5
42/610	4326	65		58.47	6	480.72	0	0	
42/610	4326	65		53.17	6	444.07	0	0	
42/610	4326	55		64.11	6	519.2	393.6	36	44
42/610	4326	75		64.51	6	521.95	466.88	42	42
42/610	4326	65		61.15	6	499.04	0	0	
42/610	4326	65		0	6	0	0	0	
42/610	4326	80		0	6	0	0	0	
42/610	4326	70		60.61	6	495.38	0	0	
42/610	4326	65		61.15	6	499.04	0	0	
42/610	4326	75		61.15	6	499.04	0	0	
42/610	4326	0		0	6	0	0	0	
42/610	4326	70		72.52	6	576.92	0	0	
38/313.9	4354	70		69.2	5	554.02	389.02	32	50
38/313.9	4354	70		55.81	5	462.4	0	0	
38/313.9	4354	55		55.81	5	462.4	462.3	51	28
38/313.9	4354	60		55.81	5	462.4	0	0	
38/313.9	4354	70		69.2	5	554.02	0	0	
38/313.9	4354	0	-3	0	5	0	0	0	
38/313.9	4354	0	-3	0	5	0	0	0	
38/313.9	4354	0	-3	0	5	0	0	0	
38/313.9	4354	0	-2.9	0	5	0	0	0	
38/313.9	4354	0	-2.5	0	5	0	0	0	
38/313.9	4354	0	1	0	5	0	0	0	
38/313.9	4354	0	-9.4	0	5	0	0	0	
38/313.9	4354	0	3.8	0	5	0	0	0	
38/313.9	4354	98	-0.08	0	5	0	0	0	
38/313.9	4354	65		65.18	5	526.53	0	0	
38/313.9	4354	60		65.18	5	526.53	0	0	
38/313.9	4354	65		69.2	5	554.02	462.3	39	47
38/313.9	4354	60		67.86	5	544.86	453.14	39.5	45
38/313.9	4354	55		67.86	5	544.86	480.62	44	43

Location	Sample No	Vol Solids	Tm Ice	NaCl Equivalent	Vein Stage	Corrected TmNaCl	Corrected Tm KCl	KCL Weight Percent	NaCl Weight Percent
38/313.9	4354	55		67.86	5	544.86	480.62	44	43
38/313.9	4354	60		77.09	5	608.99	260.78	19	61
38/313.9	4354	65		67.86	5	544.86	425.66	36	47
38/313.9	4354	65		80.9	5	636.48	0	0	
38/313.9	4354	55		61.15	5	499.04	0	0	
38/313.9	4354	60		71.86	5	572.34	0	0	
38/313.9	4354	60		31.92	5	279.15	0	0	
38/313.9	4354	75		73.18	5	581.5	425.66	32	52
38/313.9	4354	70		67.86	5	544.86	0	0	
38/313.9	4354	68		67.86	5	544.86	0	0	
38/313.9	4354	50		62.49	5	508.21	0	0	
38/313.9	4354	75		71.86	5	572.34	0	0	
38/104.85	4360	55		63.84	4	517.37	0	0	
38/104.85	4360	55		63.84	4	517.37	402.76	37	43
38/104.85	4360	70		47.36	4	402.84	407.34	48	26
31/234	4495	71		63.84	5	517.37	0	0	
31/234	4495	70		61.82	5	503.63	411.92	39	41
31/234	4495	70		55.81	5	462.4	462.3	0	
31/234	4495	75		65.18	5	526.53	425.66	38	44
31/234	4495	65		63.17	5	512.79	443.98	42	41
31/234	4495	65		82.15	5	645.64	402.76	23	65
31/234	4495	70		74.49	5	590.67	0	0	
31/234	4495	60		0	5	0	0	0	
31/234	4495	60		69.2	5	554.02	0	0	
31/234	4495	60		64.11	5	519.2	0	0	
31/234	4495	50		66.52	5	535.69	0	0	
31/234	4495	63		73.18	5	581.5	425.66	34	52
31/234	4495	70		69.2	5	554.02	334.06	28	52
31/234	4495	68		63.84	5	517.37	0	0	
31/234	4495	70		58.47	5	480.72	0	0	

Endeavour 26 North Fluid Inclusion Data

Location	Sample No	Comments	No of daughter min	NaCl/KCl Ratio	KCl/NaCl ratio	Identification
39/322	4222		1	0	0	NaCl
39/322	4222	Necking	2	0	0	NaCl,KCl
39/322	4222		2	0	0.77	NaCl,KCl
39/322	4222		1	0	0	NaCl
39/322	4222		2	0	0.72	NaCl,KCl
38/327	4234		3	0	0.81	NaCl, KCl, Opaque
38/327	4234		3	0	0.95	NaCl, KCl, Opaque
38/327	4234	KCl possible	2		0	NaCl, Hem
38/327	4234				0	
38/327	4234		3		0.73	NaCl,KCl,Hem
38/327	4234				0	
38/327	4234		1		0	NaCl
38/327	4234		4		0	NaCl,KCl,Hem,op
38/327	4234		2		0.66	NaCl,KCl
38/327	4234		2		0.8	NaCl, KCl
38/327	4234		3		0.82	NaCl,KCl,Hem
38/327	4234		4		1.14	NaCl, KCl,Hem,op
38/327	4234		3		0	NaCl,KCl,Hem
38/327	4234		1		0	NaCl
38/325.3	4235			0	0	
38/325.3	4235			0	0	
38/325.3	4235	Unknown Tm 280		0	0	
38/325.3	4235	No Th Of bubble		0	0	Melt inclusion
38/325.3	4235	No Th Of Bubble		0	0	Melt Inclusion ?
38/443.3	4240			0	0	NaCl
38/443.3	4240	Vapour not clear	2	0	0	NaCl, Cpp
38/443.3	4240	Unclear		0	0	
38/443.3	4240		1	0	0	NaCl
38/443.3	4240		1	0	0	NaCl
39/450.8	4243	Hem	3	0	0	NaCl, KCl,
39/450.8	4243		2	0	0.47	NaCl,KCl
39/450.8	4243		2	0	0.74	NaCl, KCl
39/450.8	4243		1	0	0	NaCl

Location	Sample No	Comments	No of daughter min	NaCl/KCl Ratio	KCl/NaCl ratio	Identification
39/450.8	4243		3	0	0	NaCl, KCl, Hem
39/450.8	4243		3	0	0	NaCl, KCl,Hem
39/450.8	4243		3	0	0	NaCl, KCl,Hem
39/450.8	4243		3	0	0	NaCl, KCl, Hem
39/450.8	4243		3	0	0	NaCl, KCl,Hem, Cpy
39/450.8	4243		2	0	1.39	NaCl, KCl
39/450.8	4243		2	0	0.6	NaCl, KCl
39/450.8	4243		2	0	0.77	NaCl, KCl
39/450.8	4243		3	0	0.71	NaCl, KCl,Hem
39/450.8	4243		3	0	0.6	
39/450.8	4243		3	0	0	NaCl, KCl,Hem
39/450.8	4243		2	0	0.49	NaCl, KCl,Hem
39/450.8	4243		3	0	0.47	NaCl, KCl,Hem
39/450.8	4243		3	0	0.69	NaCl, KCl,Cpy
39/450.8	4243	Unknown Tm 505	4	0	0.8	NaCl, KCl,Hem,Unknown
39/450.8	4243		3	0	0	NaCl, KCl,Hem
39/450.8	4243		3	0	0	NaCl, KCl,Hem
39/450.8	4243		3	0	0	NaCl, KCl,Hem
39/450.8	4243		3	0	0	NaCl, KCl,Hem
39/450.8	4243	Th Checked Twice		0	0.53	
39/450.8	4243		3	0	0	NaCl, KCl,Hem
39/450.8	4243		3	0	0	NaCl, KCl,Hem
39/450.8	4243		3	0	0	NaCl, KCl,Hem
39/450.8	4243		1	0	0	NaCl
39/450.8	4243	Necking	2	0	0.49	NaCl, KCl
39/450.8	4243		1	0	0	NaCl
46/273.5	4250		1	0	0	NaCl
46/273.5	4250			0	0	
46/273.5	4250		1	0	0	NaCl
46/273.5	4250		2	0	0	NaCl,KCl
46/273.5	4250		1	0	0	NaCl
46/273.5	4250		1	0	0	NaCl
46/273.5	4250			0	0	
46/273.5	4250	leakage	2	0	0	NaCl, KCl

Location	Sample No	Comments	No of daughter min	NaCl/KCl Ratio	KCl/NaCl ratio	Identification
46/273.5	4250		1	0	0	
46/273.5	4250			0	0	
46/273.5	4250			0	0	
46/273.5	4250			0	0	
46/273.5	4250			0	0	
46/273.5	4250			0	0	
46/273.5	4250		1	0	0	NaCl
46/273.5	4250		1	0	0	NaCl
42/601.15	4266		1	0	0	NaCl
42/601.15	4266		3	0	0	NaCl, KCl, Hem
42/601.15	4266		2	0	0	NaCl,KCl
42/601.15	4266		1	0	0	NaCl
42/601.15	4266		1	0	0	NaCl
42/601.15	4266		1	0	0	NaCl
42/601.15	4266		2	0	0	NaCl, KCl
42/601.15	4266	Necking	2	0	0	NaCl, KCl
42/601.15	4266	Necking	1	0	0	NaCl
42/601.15	4266		1	0	0	NaCl
42/601.15	4266	Necking?	2	0	0	
42/601.15	4266		1	0	0	NaCl
42/601.15	4266		1	0	0	NaCl
46/891.5	4287		1	0	0	NaCl
46/891.5	4287		1	0	0	NaCl
46/891.5	4287		2	0	0	NaCl, Cpy
46/891.5	4287			0	0	
42/610	4326	No measurements	2	0	0	NaCl Hem
42/610	4326		2	0	0	NaCl, Hem
42/610	4326		2	0	0.63	NaCl, K Cl
42/610	4326		2	0	0	NaCl, KCl
42/610	4326		3	0	0	NaCl, KCl, Cpy
42/610	4326		3	0	1.32	NaCl, KCl, Hem
42/610	4326	Op no dissolution	3	0	1.39	NaCl, KCl, Op
42/610	4326		1	0	0	NaCl
42/610	4326	Tm KCl missed	3	0	0	NaCl, KCl

Location	Sample No	Comments	No of daughter min	NaCl/KCl Ratio	KCl/NaCl ratio	Identification
42/610	4326	Coexisting Type 2	2	0	0.78	NaCl, KCl
42/610	4326			0	0.55	
42/610	4326		2	0	0	NaCl,KCl
42/610	4326		1	0	0	NaCl
42/610	4326	UnKnown Tm 940	3	0	0.82	NaCl, KCl, Unknown
42/610	4326		3	0	1	NaCl,KCl,Op
42/610	4326			0	0	
42/610	4326		3	0	0	NaCl, KCl
42/610	4326	Min hidden	1	0	0	NaCl
42/610	4326		3	0	0	NaCl,KCl,Hem
42/610	4326		3	0	0	NaCl, KCl, Hem
42/610	4326		1	0	0	NaCl
42/610	4326	Coincident with 21		0	0	
42/610	4326		1	0	0	NaCl
38/313.9	4354	Th precedes Tm	4	0	0.64	NaCl, KCl, Hem, Cpy
38/313.9	4354	Th precedes Tm	2	0	0	NaCl, KCl
38/313.9	4354		3	0	0	NaCl, KCl, Hem
38/313.9	4354		3	0	1.82	NaCl, KCl, Hem
38/313.9	4354		2	0	0	NaCl, KCl
38/313.9	4354		3	0	0	NaCl, KCl,Hem
38/313.9	4354	Secondary		0	0	
38/313.9	4354	secondary		0	0	
38/313.9	4354	Secondary		0	0	
38/313.9	4354	Secondary		0	0	
38/313.9	4354	Secondary		0	0	
38/313.9	4354	Secondary		0	0	
38/313.9	4354	Secondary		0	0	
38/313.9	4354	Secondary		0	0	
38/313.9	4354	Secondary		0	0	
38/313.9	4354		3	0	0	NaCl, KCl,Hem,Cpy
38/313.9	4354	Minerals hidden	1	0	0	NaCl
38/313.9	4354		3	0	0.83	NaCl, KCl Hem
38/313.9	4354	Supercritical	4	0	0.88	NaCl, KCl, Cpy, Hem
38/313.9	4354	Supercritical	3	0	1.02	NaCl, KCl, Cpy

Location	Sample No	Comments	No of daughter min	NaCl/KCl Ratio	KCl/NaCl ratio	Identification
38/313.9	4354		2	0	1.02	NaCl, KCl, Opaque
38/313.9	4354		3	0	0.31	NaCl, KCl, Hem
38/313.9	4354		2	0	0.77	NaCl, KCl
38/313.9	4354		2	0	0	NaCl, Hem
38/313.9	4354		2	0	0	NaCl, Hem
38/313.9	4354		2	0	0	NaCl, Hem
38/313.9	4354	Unclear	3	0	0	NaCl, KCl, Hem
38/313.9	4354		3	0	0.62	NaCl,KCl,Hem
38/313.9	4354		3	0	0	NaCl,KCl,Hem
38/313.9	4354	KCl not viewed	2	0	0	NaCl,Hem
38/313.9	4354	Possible Necking	2	0	0	NaCl,Hem
38/313.9	4354		1	0	0	NaCl
38/104.85	4360	No KCl seen		0	0	
38/104.85	4360			0	0.86	
38/104.85	4360			0	1.85	
31/234	4495		3	0	0	NaCl, KCl, Opaque
31/234	4495		3	0	0.95	NaCl, KCl, Opaque
31/234	4495		1	0	0	NaCl
31/234	4495		3	0	0.86	NaCl, KCl, Opaque
31/234	4495		3	0	1.02	NaCl, KCl, Opaque
31/234	4495		3	0	0.35	NaCl, KCl, Hematite
31/234	4495		4	0	0	NaCl, KCl, Cpy, Hem
31/234	4495		3	0	0	NaCl, KCl, Opaque
31/234	4495		3	0	0	NaCl, KCl, Opaque
31/234	4495	Th precedes Tm	2	0	0	NaCl, Opaque
31/234	4495	Th precedes Tm	1	0	0	NaCl
31/234	4495	Th precedes Tm	3	0	0.65	NaCl, KCl, Hem
31/234	4495		3	0	0.54	NaCl, KCl, Hematite
31/234	4495	Tm preceded Th		0	0	
31/234	4495	No KCl seen	2	0	0	NaCl, Cpy

APPENDIX 4

Mineral Chemistry Data

Sample No.	**4330**					
Location	DDH 38/ 306 m					
Description	QMP 1 Quartz Monzonite Porphyry .					
Analysis	308589		308592		308593	
	Wt%	Atoms	Wt%	Atoms	Wt%	Atoms
SiO_2	38.58	2.835	38.62	2.8534	37.71	2.8315
TiO_2	4.23	0.2335	4.198	0.233	4.13	0.2331
Al_2O_3	13.97	1.2098	13.99	1.2181	13.6	1.2037
Cr_2O_3	<0.11		<0.11		0.11	
FeO	11.77	0.7233	11.72	0.7242	11.86	0.7444
MnO	0.19	0.012	0.16	0.0101	0.12	0.0079
MgO	16.72		16.42	1.8087	16.29	1.8234
CaO	<0.09	1.8316	<0.02		0.09	
Na_2O	0.32	0.045	0.2	0.0281	0.36	0.0529
K_2O	9.79	0.9175	9.4	0.8857	9.67	0.9261
Cl	<0.05		<0.05		0.11	0.0146
Total	95.57		94.7	7.7614	93.86	7.8376
Mg/Mg+ Fe	71.69	7.8078	71.41		71	
Description	Euhedral Biotite		Primary Biotite		Primary Biotite	

Sample No.	**4239**					
Location	DDH 38/ 339 m					
Description	QMP 1 Quartz Monzonite Porphyry Highly altered by secondary Biotite					
Analysis	313183		313185		313186	
	Wt%	Atoms	Wt%	Atoms	Wt%	Atoms
SiO_2	37	2.8267	37.41	2.8174	36.15	2.8073
TiO_2	4.05	0.2328	4.1	0.2324	4.01	0.2308
Al_2O_3	13.16	1.185	13.37	1.1865	13.46	1.2746
Cr_2O_3	<0.11		<0.11		<0.11	
FeO	11.68	0.7463	11.92	0.7506	10.73	0.7337
MnO	<0.11	0.012	<0.11	0.0101	<0.11	0.0079
MgO	16.33		16.74	1.8795	15.83	1.7982
CaO	<0.09	1.8591	0.43		<0.09	
Na_2O	0.39	0.0583	0.2	0.0626	0.8	0.0563
K_2O	9.62	0.9377	9.56	0.9186	9.52	0.9038
Cl	<0.05		<0.05		0.11	0.0146
Total	92.23	7.846	93.54	7.8476	90.51	7.8047
Mg/Mg+ Fe	71.36		71.46		72.45	
Description	Secondary		Secondary		Secondary	

Sample No.	**4239**					
Location	DDH 38/ 339 m					
Description	QMP 1 Quartz Monzonite Porphyry Highly altered by secondary Biotite					
Analysis	313187		313188		313189	
	Wt%	Atoms	Wt%	Atoms	Wt%	Atoms
SiO_2	37.17	2.8073	37.68	2.8099	37.38	2.8013
TiO_2	4.06	0.2308	4.21	0.2358	4.33	0.2443
Al_2O_3	14.32	1.2746	14.34	1.2598	0.11	1.2735
Cr_2O_3	0.11		<0.11		<0.11	
FeO	11.62	0.7337	10.8	0.6734	11.15	0.6988
MnO	0.11	0.012	<0.11		0.11	
MgO	15.97		16.77	1.8631	16.18	1.8074
CaO	0.08	1.7982	0.08		0.09	
Na_2O	0.38	0.0583	0.42	0.0608	0.54	0.0785
K_2O	9.38	0.9038	9.53	0.9064	9.48	0.9067
Cl			<0.05		0.11	
Total	92.91	7.8047	93.75	7.8086	93.48	7.8103
Mg/Mg+ Fe	71.02		73.45		72.12	
Description	Secondary		Secondary		Secondary	

Sample No.	**4353**			
Location	DDH 38/ 489 m			
Description	Hydrothermal sericite and biotite			
Analysis	309156		309157	
	Wt%	Atoms	Wt%	Atoms
SiO_2	34.34	2.5725	33.52	2.597
TiO_2	2.31	0.1299	2	0.1137
Al_2O_3	19.93	1.7591	19.32	1.77
Cr_2O_3	0.11		0.11	
FeO	15.26	0.9561	15.73	0.997
MnO	0.19	0.0123	0.2	0.0127
MgO	14.35	1.6027	14.97	1.6907
CaO	0.08	0.0027	0.02	0.0596
Na_2O	0.27	0.0397	0.41	0.0586
K_2O	7.65	0.7211	6.37	0.616
Cl	0.08	0.0105	0.09	0.1594
Total	94.31	7.8034	93.1	7.8106
Mg/Mg+ Fe	62.6		62.91	
Description	Secondary		Secondary	

Sample No.	**5192**					
Location	DDH 38/					
Description	Secondary biotite in quartz vein					
Analysis	90596		90598		90599	
	Wt%	Atoms	Wt%	Atoms	Wt%	Atoms
SiO_2	40.15	2.9964	37.77	2.86	39.57	2.9
TiO_2	2.2	0.1235	1.95	0.1112	1.33	0.09
Al_2O_3	11.52	1.01	13.63	1.2163	15.26	1.84
Cr_2O_3	0.03	0.0016	0.02		0.03	
FeO	8.87	0.5537	10.98	0.6954	11.78	0.9292
MnO	0.05	0.0033	0.05	0.003	0.08	0.0053
MgO	20.27	2.25	19.59	2.21	18.41	1.5527
CaO	0.01	0.0011	0.01	0.0027	0.06	0.0047
Na_2O	0.2	0.0293	0.19	0.278	0.16	0.0391
K_2O	8.62	0.8206	6.25	0.614	6.36	0.6781
Cl	0.09	0.0116	0.09	0.0118	0.18	0.09
Total	95.87	8.7162	92.56	8.6533	96.4	8.1604
Mg/Mg+ Fe						
Description	Secondary		Secondary		Secondary	

Sample No.	**5192**					
Location	DDH 48/ 400					
Description	Primary Biotite in Monzonite Porphyry					
Analysis	313178		313179		313181	
	Wt%	Atoms	Wt%	Atoms	Wt%	Atoms
SiO_2	37.76	2.8253	38.12	2.8378	39.3	2.8195
TiO_2	4.18	0.2352	3.89	0.2176	4.12	0.22
Al_2O_3	13.78	1.2155	13.77	1.2082	15.33	1.3305
Cr_2O_3	0.11	0.0016	0.11		0.11	
FeO	11.4	0.7132	11.21	0.6977	11.37	0.7003
MnO	0.05	0.0033	0.11	0.003	0.08	0.0053
MgO	16.9	1.8849	17.52	1.9002	15.7	1.723
CaO	0.01	0.0011	0.09	0.0027	0.09	0.0047
Na_2O	0.16	0.0226	0.4	0.0577	0.31	31
K_2O	9.35	0.8926	9.48	0.9005	9.87	0.927
Cl	0.09	0.0116	0.09	0.0118	0.18	
Total	93.54	7.7893	93.98	7.8196	95.02	7.773
Mg/Mg+ Fe	72.55					
Description	Primary Biotite		Primary		Primary	

Sample No.	4246					
Location	DDH 38/ 489 m					
Description	Porphyritic Trachyte overprinted by Secondary Biotite					
Analysis	90579		90580		90582	
	Wt%	Atoms	Wt%	Atoms	Wt%	Atoms
SiO_2	33.96	2.6089	33.38	2.5911	34.27	2.677
TiO_2	1.97	0.1139	1.94	0.1131	1.2	0.0707
Al_2O_3	19.74	1.7871	19.8	1.8111	18.77	1.7282
Cr_2O_3	0.11		<0.02		<0.02	
FeO	14.24	0.9147	14.25	0.9249	12.57	0.8211
MnO	0.07	0.0043	0.07		0.08	0.0053
MgO	14.1	1.6147	13.68	1.8631	14.83	1.727
CaO	0.05	0.0038	0.02	0.0016	0.03	0.0023
Na_2O	0.27	0.0408	0.26	0.0398	0.26	0.0387
K_2O	6.41	0.6284	6.9	0.6832	6.77	0.6748
Cl	0.06	0.0081	0.1	0.134	0.09	0.09
Total	93.02	8.2423	92.58	8.3018	91.77	8.1604
Mg/Mg+ Fe						
Description	Secondary		Secondary		Secondary	

Sample No.	4246					
Location	DDH 38/ 489 m					
Description	Porphyritic Trachyte overprinted by Secondary Biotite					
Analysis	90585		90584		90587	
	Wt%	Atoms	Wt%	Atoms	Wt%	Atoms
SiO_2	36.42	2.7404	36.61	2.7397	34.08	2.6
TiO_2	0.89	0.0505	0.37	0.0209	1.57	0.09
Al_2O_3	21.11	1.872	20.71	1.8266	20.52	1.84
Cr_2O_3	0.11		<0.02		0.02	
FeO	12.21	0.76	12.47	0.7806	14.56	0.9292
MnO	0.12	80	0	0.0117	0.08	0.0053
MgO	13.7	1.5268	14.36	1.6016	13.65	1.5527
CaO	0.03	0.0027	0.02	0.0027	0.06	0.0047
Na_2O	0.2	0.0292	0.032	0.032	0.26	0.0391
K_2O	5.85	0.5613	6.83	0.6524	6.97	0.6781
Cl	0.11	0.014	0.1	0.1594	0.1	0.09
Total	92.66	8.0603	92.56	7.8399	94.01	8.1604
Mg/Mg+ Fe						
Description	Secondary		Secondary		Secondary	

Sample No.	4246					
Location	DDH 38/ 489 m					
Description	Porphyritic Trachyte overprinted by Secondary Biotite					
Analysis	90589		90584		90587	
	Wt%	Atoms	Wt%	Atoms	Wt%	Atoms
SiO_2	36.24	2.6854	36.61	2.7397	34.08	2.6
TiO_2	0.44	0.0244	0.37	0.0209	1.57	0.09
Al_2O_3	20.6	1.7991	20.71	1.8266	20.52	1.84
Cr_2O_3	0.02		<0.02		0.02	
FeO	12.94	0.802	12.47	0.7806	14.56	0.9292
MnO	0.1	0.0061	0	0.0117	0.08	0.0053
MgO	15.57	1.7203	14.36	1.6016	13.65	1.5527
CaO	0.03	0.0027	0.02	0.0027	0.06	0.0047
Na_2O	0.2	0.04	0.032	0.032	0.26	0.0391
K_2O	6.96	0.6575	6.83	0.6524	6.97	0.6781
Cl	0.08	0.0105	0.1	0.1594	0.1	0.09
Total	98.87	8.3594	92.56	7.8399	94.01	8.1604
Mg/Mg+ Fe						
Description	Secondary		Secondary		Secondary	

Sample No.	5931		5934			
Location	DDH 68/455		DDH 68			
Description	Biotite rich rock					
Analysis	316030		90575		90576	
	Wt%	Atoms	Wt%	Atoms	Wt%	Atoms
SiO_2	36.56	2.6559	36.47	2.8354	37.36	2.864
TiO_2	0.1		3.96	0.2314	4.14	0.2373
Al_2O_3	23.43	2.0061	12.8	1.732	13.19	1.1847
Cr_2O_3	0.11	0.0016	0.11		0.11	0.7036
FeO	18.87	1.1464	9.91	0.6441	11.04	0.7003
MnO	0.32	0.02	0.11	0.0056	0.12	0.0075
MgO	12.62	1.3662	17.08	1.9796	17.11	1.9428
CaO	0.01		0.09	0.002	0.02	0.0019
Na_2O	0.14		0.48	0.0724	0.35	0.0522
K_2O	3.16	0.293	8.86	0.8783	7.69	0.7471
Cl	0.09	0.0116	0.09	0.0127	0.1	0.01
Total	93.96	7.4875	92.8	8.5789	94.33	8.5078
Mg/Mg+ Fe	54.37					
Description	Primary Biotite		Primary		Primary	

APPENDIX 5

Paper: Goonumbla Porphyry Copper District – Endeavour 26 North, Endeavour 22 And Endeavour 27 copper gold Deposits.

1990, Heithersay, P.S., O'Neill, W.J., van der Helder, P., Moore, C.R. and Harbon, P.

In Geology of the Mineral deposits of Australia and Papua New Guinea (ed F.E.Hughes) pp 1385 – 1398 (The Australian Institute of Mining and Metallurgy).

Heithersay, P.S., O'Neill, W.J., van der Helder, P., Moore, C.R. and Harbon, P.G., 1990. Goonumbla porphyry copper district — Endeavour 26 North, Endeavour 22 and Endeavour 27 copper-gold deposits, in *Geology of the Mineral Deposits of Australia and Papua New Guinea* (Ed. F.E. Hughes), pp. 1385–1398 (The Australasian Institute of Mining and Metallurgy: Melbourne).

Goonumbla Porphyry Copper District — Endeavour 26 North, Endeavour 22 and Endeavour 27 Copper-Gold Deposits

by P.S. Heithersay[1], W.J. O'Neill[1], P. van der Helder[2], C.R. Moore[3] and P.G. Harbon[4]

INTRODUCTION

Porphyry copper-gold mineralisation was discovered in 1977 near Goonumbla, 28 km NW of Parkes, New South Wales. The centre of the group of deposits is at about lat. 32°55′S, long. 148°02′E, on the Narromine (SI 55–3) 1:250 000 scale map sheet (Fig. 1).

The discovery was particularly significant because above average grades were encountered. Thus, for the first time in Australia, there was potential for sufficient porphyry copper mineralisation to support a large viable mining operation. Previous exploration within Australia had delineated low grade and/or limited tonnage porphyry copper mineralisation. Eleven centres of mineralisation have been identified to date, all located within a circular feature some 22 km in diameter which is defined by both aeromagnetic and gravity data, and is clearly reflected by the geology.

The three major deposits, Endeavour 26 North, 22 and 27, are described below. They were the subject of mining feasibility studies by Peko Wallsend Ltd. and the mineable reserves after dilution which were used for the 1986 studies are given in Table 1.

EXPLORATION HISTORY

Geopeko, the exploration arm of Peko Wallsend Operations Ltd, began exploration within the Palaeozoic volcanics of the Lachlan Fold Belt in 1971, and in 1974 the *Endeavour 7* (E7) lead-zinc skarn deposit was delineated (Fig. 2). This provided the impetus to conduct further exploration to the north in areas of very limited outcrop. Because of extensive soil cover, systematic reconnaissance drilling to bedrock was used to obtain both geological and geochemical information. The initial drill holes on 1 km spacing were sited along roads. One auger hole encountered visible copper mineralisation and strongly anomalous copper values to 2500 ppm in early 1977. Infill drilling to sample the bedrock defined a major geochemical anomaly and subsequent diamond drilling in 1977 intersected strong porphyry copper-gold mineralisation. This prospect became known as Endeavour 22 (E22). More extensive and closer spaced drilling led to the discovery of other major centres of mineralisation including the *Endeavour 20, 26, 27, 28* and *31* deposits (Fig. 3a).

Geochemical profiling of sample holes on E22 revealed significant gold mineralisation in the weathered rock profile (Jones, 1985). High quality air core samples enabled the oxidised zone gold resource to be calculated with confidence.

A grid magnetic survey over the E22 deposit showed a subtle magnetic low, and a regional ground magnetic survey was undertaken. Anomalies identified were tested by vertical auger-core drilling. The results were for the most part disap-

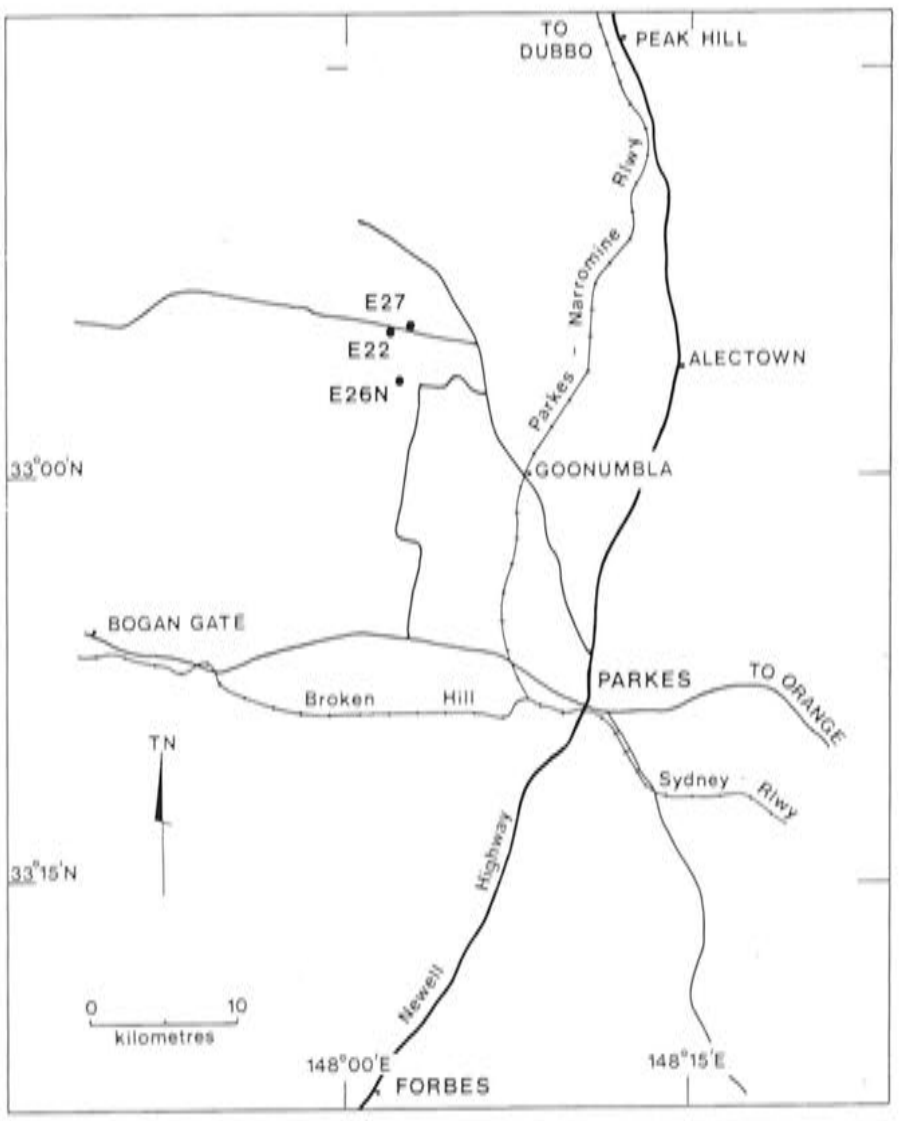

Fig. 1—Location of Goonumbla and the main porphyry copper-gold deposits.

[1] Senior Project Geologist, Geopeko, Clarke and Alluvial Streets, Parkes NSW 2870.
[2] Senior Mine Geologist, [4] Senior Geologist, Peko Wallsend Metalliferous Mining Division, Clarke and Alluvial Streets, Parkes NSW 2870.
[3] Formerly Senior Geologist, Peko Wallsend Metalliferous Mining Division, now Bond International Technical Services, PMB 90, Kalgoorlie WA 6430.

TABLE 1

Resource data, Goonumbla porphyry copper-gold deposits

1. Copper-gold resource

Deposit	Mt	% Cu	g/t Au
Open Pit:			
Endeavour 26N	9.0	1.45	0.16
Endeavour 22	13.1	0.64	0.55
Endeavour 27	7.7	0.76	0.72
Total	29.8	0.91	0.48
Underground:			
Endeavour 26N	25.2	1.52	0.63

2. Oxidised zone gold resource

	Mt	Cut off grade g/t Au	g/t Au
	1.610	0.75	2.2
	1.171	1.00	2.7

1. Resource figures from the 1987 Peko Wallsend Ltd Annual Report, after dilution.
2. Resource in the Endeavour 22 and 27 deposits, to 40 m maximum depth.

pointing, but this programme led to the discovery of the *Endeavour 34* deposit.

Bedrock geochemical sampling was a most effective exploration tool, and rotary air blast holes were drilled on 400 m centres throughout the most prospective area to discover new zones of geochemical anomalies (Fig. 3b). This programme led to the discovery of the *Endeavour 37* and *22 North* deposits.

Extensive regional IP surveys have been completed. Problems arising from conductive overburden, variable depth to bedrock and the relatively low sulphide content of the deposits have made interpretation of results particularly difficult and inconclusive.

PREVIOUS DESCRIPTIONS

Copper occurrences in the Parkes district were recorded from late last century (Carne, 1908), and these occurrences were further described by Bowman, Hobbs and Barron (1977) and Bowman, Richardson and Dolanski (1982). Detailed published descriptions of the Goonumbla porphyry deposits are restricted to those of Jones (1985), who provided a description of regional and deposit geology, and Heithersay (1986) who described the Endeavour 26 North deposit in detail.

Strong exploration activity in the Parkes district led the Geological Survey of New South Wales to undertake a detailed regional investigation known as the Parkes Project. Some results are available and include discussions on the geophysics (Tenison Woods, 1983, 1985), petrology (Clarke, 1987) and stratigraphy (Krynen, 1984; Sherwin, Clarke and Krynen, 1987).

REGIONAL SETTING

Gold and copper mineralisation in the Parkes district is hosted by a sequence of Late Ordovician to Early Silurian volcanics, intrusives and sediments that occur within the NE portion of the major structural subdivision of the Lachlan Fold Belt known as the Bogan Gate Synclinorial Zone (Scheibner, 1975).

The Late Ordovician to Early Silurian sequence forms a north trending belt which is flanked to the east and west by Late Devonian sediments, overlain to the north by Late Silurian sediments (Fig. 2) and disappears to the south beneath extensive soil cover. This belt can be subdivided into two distinct zones, the western Girilambone Anticlinorial Zone dominated by volcanics and characterised by a complex aeromagnetic signature, and the eastern Tumut Synclinorial Zone dominated by sediments. The boundary between the two zones is marked at least in part by the major Parkes Thrust fault system. The Goonumbla porphyry copper-gold deposits are located within the western zone.

The volcanics, comagmatic intrusives, volcanically derived sediments and limestones of the western zone are generally gently folded with relatively shallow dips and non-existent to very poorly developed cleavage. Metamorphism is weak to absent with occasional zeolite to lower greenschist minerals (prehnite, pumpellyite) identified.

The sediments and lesser intermediate volcanics and pyroclastics of the eastern zone are characterised by tight folding with strongly developed axial cleavage. Major faulting is common and quartz veining is widespread. Metamorphism reaches lower greenschist facies locally. The eastern zone is host to the Parkes-Forbes-Peak Hill gold belt (Clarke, 1985).

Scheibner (1976) postulated that the western zone lies above a major regional basement high known as the Parkes Terrace. Evidence of such a basement high is present in the regional gravity data (Tenison Woods, 1983). The presence of this basement block may explain the low intensity of deformation within the western zone. The inferred basement high is bounded at least in part to the east by the Parkes Thrust and to the west by the Gilmore Suture, both of which have a close spatial relation to gold mineralisation.

Several models for the geological setting of the Parkes district during the Ordovician to Early Silurian have been proposed, including a subduction-related island arc/arch model (Scheibner, 1975, 1976), a lithospheric tensional model associated with partial melting of the upper mantle and subsequent crustal melting (Wyborn, 1977) and an extensional continental rift model (Jones, 1985).

REGIONAL STRATIGRAPHY

The stratigraphic units of the Parkes district as shown on Fig. 2 are briefly described below. With minor modification, they follow closely the New South Wales Geological Survey's recent revision (Sherwin, Clarke and Krynen, 1987).

ORDOVICIAN-SILURIAN

Nelungaloo Volcanics

These are the oldest rocks in the area. Fossil evidence provides an Early Ordovician or possible Late Cambrian age (Sherwin, 1979). They are exposed in the core of the Forbes anticline and comprise andesitic flows, volcanically derived sediments, conglomerate, chert and limestone.

Goonumbla Volcanics

This dominantly volcanic sequence overlies the Nelungaloo Volcanics though the precise relation between the two is unknown. The basal sequence of the Goonumbla Volcanics includes the Billabong Creek Limestone Member and the Gunningbland Shale Member. Abundant fossil evidence provides a Late Ordovician age (Sherwin, 1973). The volcanics are potassium rich trachyandesites and consist of interlayered flows, pyroclastics and volcanomict sediments.

Similar intermediate volcanics occur within the sediments to the east of the Goonumbla volcanic complex and include the Parkes Volcanics, Nash Hill Volcanics, Back Yamma Volcanics, Daroobalgie Volcanics and Mingelo Volcanics, all regarded as time equivalents of the Goonumbla Volcanics.

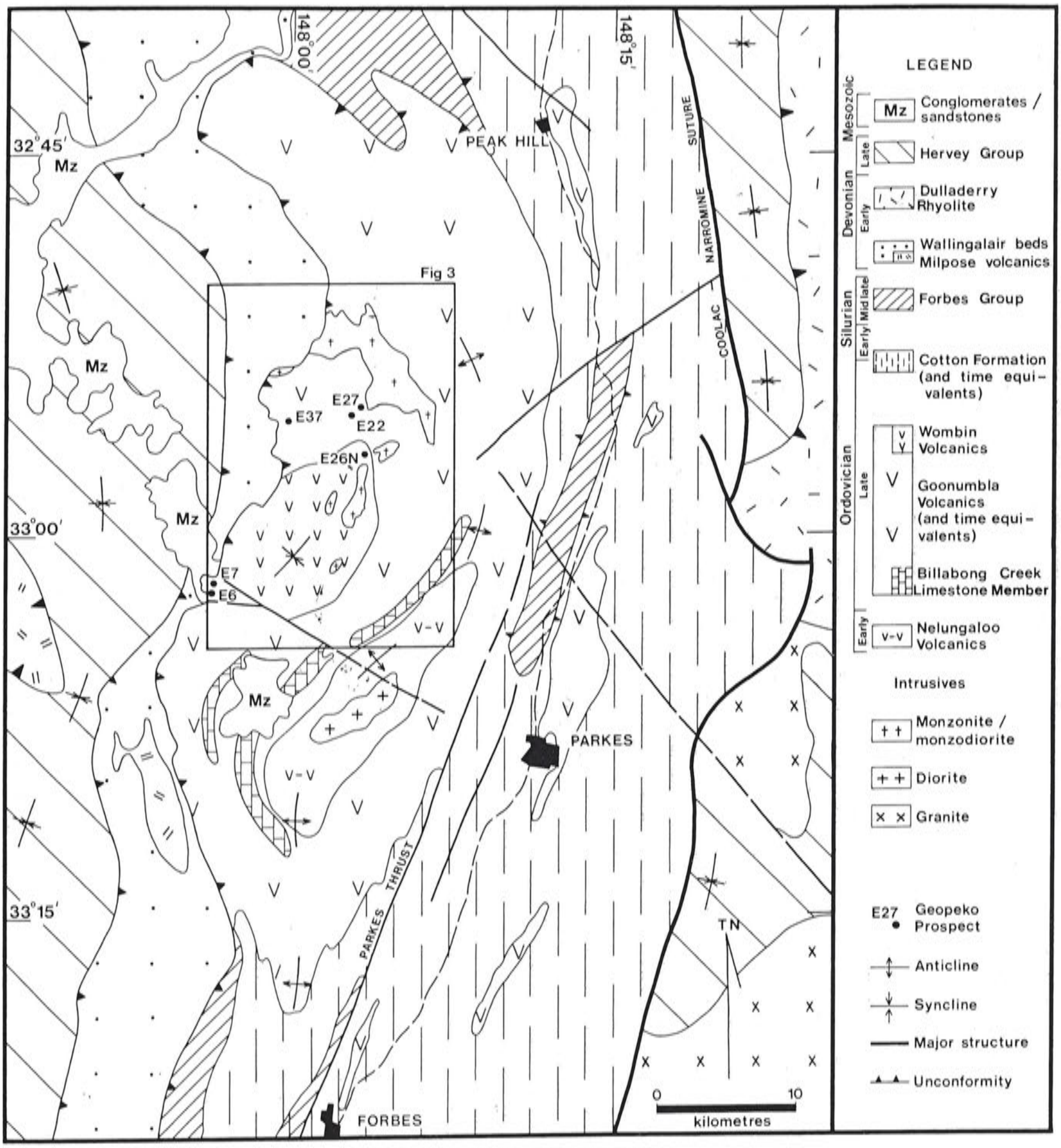

Fig. 2—Regional geology, Parkes district.

Wombin Volcanics

The relatively loose definition of the Wombin Volcanics (Bowman, Hobbs and Barron, 1977) has made it impossible to delineate this formation confidently. Jones (1985) included within his 'Wombin Group' a sequence of trachyandesites, now considered to be part of the Goonumbla Volcanics. It is preferable that the term Wombin Volcanics be restricted to a sequence of brown-red potassium rich trachytic flows, pyroclastics and associated epiclastics which immediately overlie the Goonumbla Volcanics. Recent ^{40}Ar–^{39}Ar dating of alteration assemblages cutting the trachytic volcanics returned a date of 441 ± 2 Myr (C. Perkins, unpublished data, 1988), thereby fixing the minimum age as Late Ordovician. Petrochemical evidence strongly supports the interpretation that the trachytic volcanics are late stage, more differentiated volcanics related to the waning stages of the Goonumbla volcanic event.

Cotton Formation

This formation is dominated by siltstone but includes several conglomerate and chert horizons. Fossil evidence (Sherwin, 1973) provides an age of Late Ordovician to Early Silurian. Comparable ages and field relations suggest that the unit interfingers with the Goonumbla Volcanics.

SILURIAN

The **Forbes Group** consists of the Bocobidgle Conglomerate which contains chert, quartzite and monzonite pebbles up to 10 cm diameter in a limey to lithic matrix, and the Mumbidgle Formation of silty mudstone and sandstone. Fossil evidence indicates a Middle to Late Silurian age (Sherwin, 1975). It is often difficult to distinguish between the Forbes Group and the Cotton Formation and it is possible that the Forbes Group is more extensive than currently mapped.

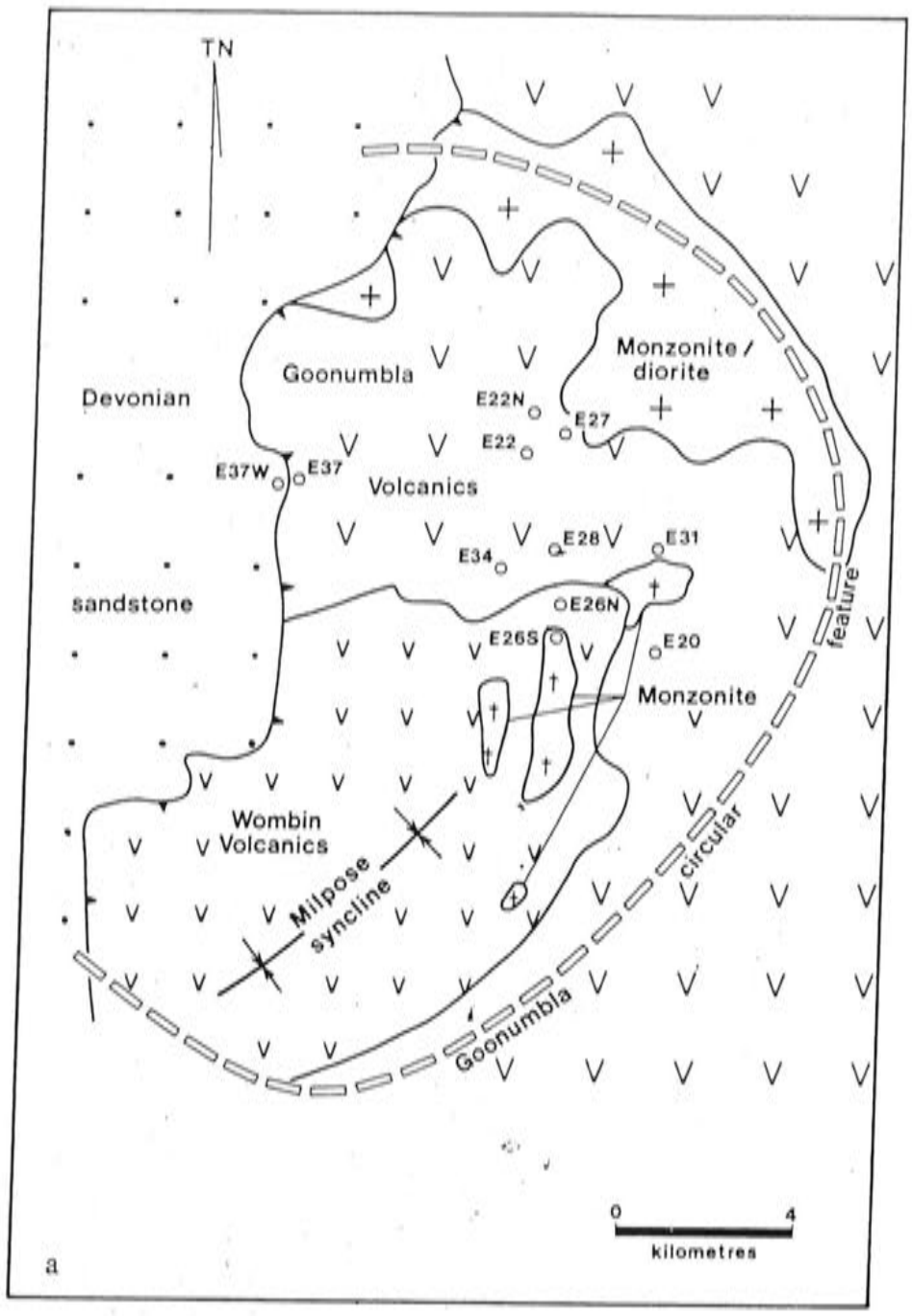

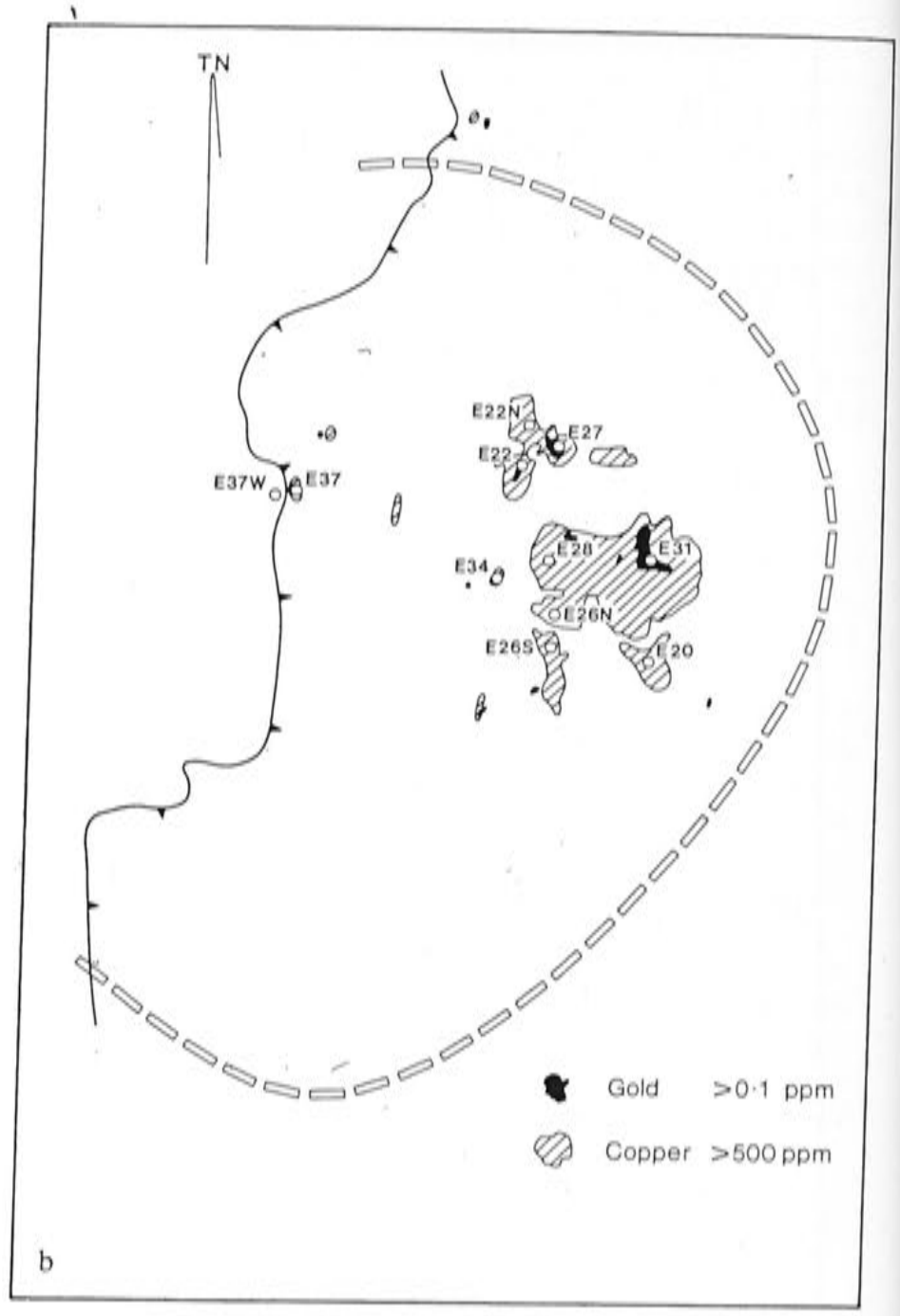

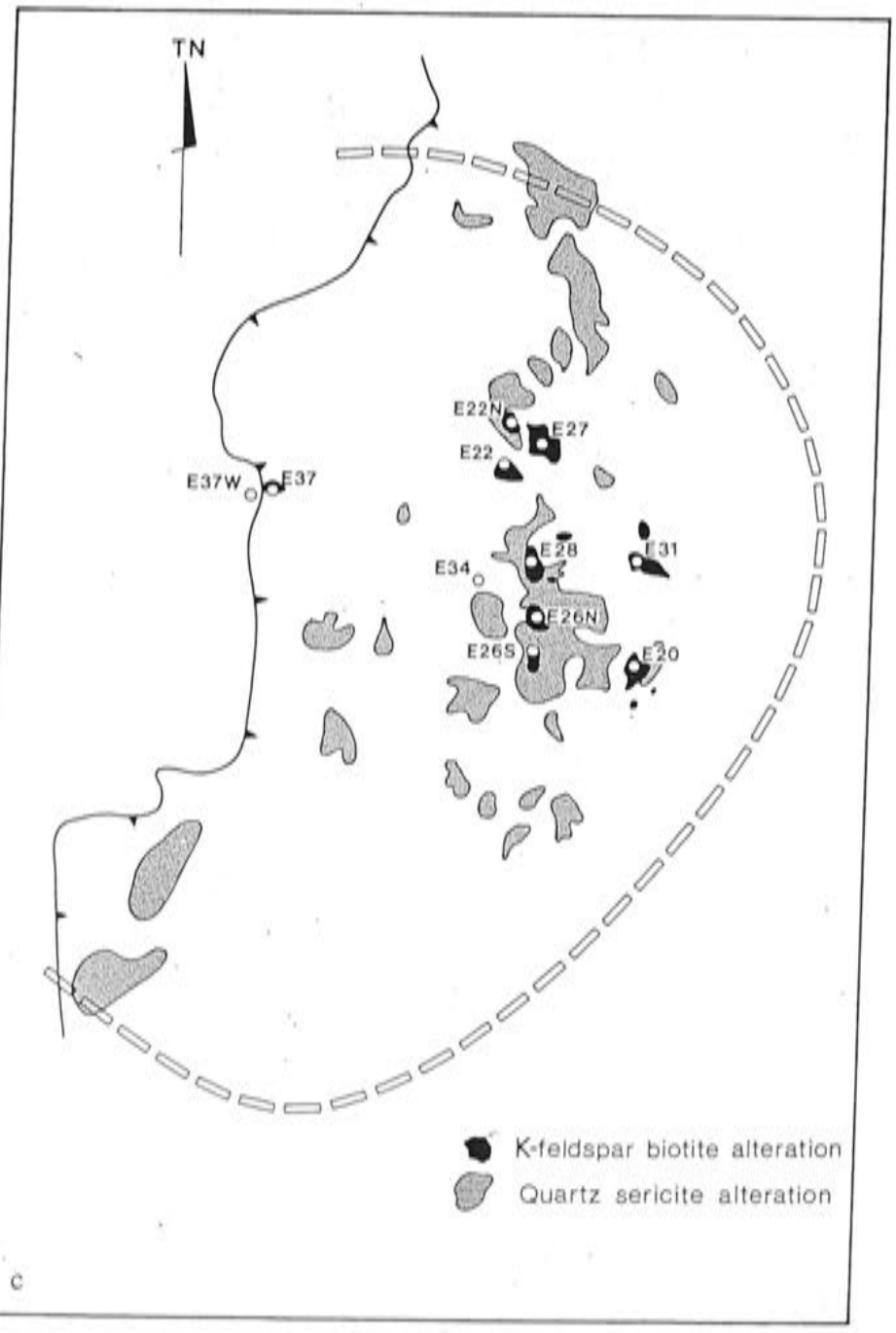

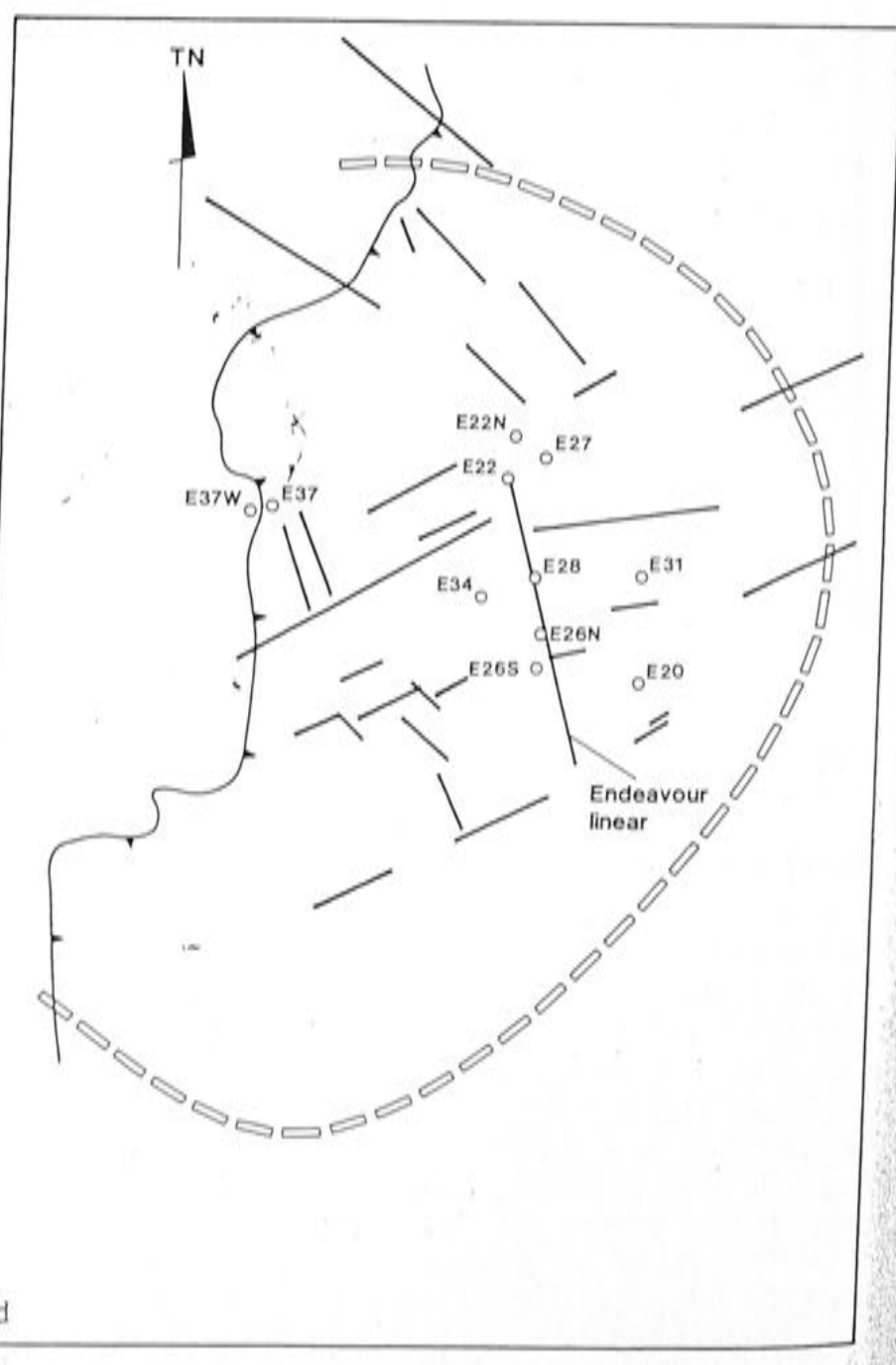

Fig. 3—Plans showing (a) geology, (b) geochemistry, (c) alteration and (d) prominent magnetic linear features, Goonumbla district.

EARLY DEVONIAN

The **Wallingalair beds** consist of quartz sandstone, conglomerate lenses, shale and impure limestone. On fossil evidence they are assigned an Early Devonian age. Included are the Calarie Sandstone and the Milpose volcanics, a sequence of flows and possible intrusions of rhyolitic to granitic composition.

LATE DEVONIAN

The **Hervey Group** is dominantly quartz sandstone and conglomerate, and unconformably overlies the Wallingalair beds.

MESOZOIC

Remnants of an ancient drainage system comprising poorly cemented coarse sandstone and conglomerate occur along the west side of the area. Poorly preserved plant fossils suggest a Jurassic age (Picket, 1985), but this sequence has been locally regarded as Tertiary.

INTRUSIVES

Ordovician intrusive activity, as currently known, is restricted to the western zone. Mafic intrusives of dioritic to monzodioritic composition intrude the Nelungaloo Volcanics and a suite of intrusives ranging in composition from diorite to quartz syenite intrudes the Goonumbla and Wombin volcanics. Quartz monzonite porphyries are intimately associated with porphyry copper-gold mineralisation.

GOONUMBLA PORPHYRY COPPER DISTRICT

Jones (1985) interpreted the circular feature within the volcanics of the western zone to be a collapsed caldera. He postulated that the discrete circular Bouguer gravity low resulted from the presence of a large and less dense intrusive body at relatively shallow depths within the caldera. A complex intrusive of monzonitic to dioritic composition which forms an arcuate dyke along the northern and northeastern perimeter of the circular feature is regarded as a ring dyke. All porphyry copper-gold mineralisation discovered to date is located within the circular feature.

STRATIGRAPHY

Outcrop within the circular feature is poor, however on the basis of limited field evidence and relatively sparse drill hole data, a broad open syncline (the Milpose syncline) plunging gently to the SW can be discerned (Fig. 3a). The district is characterised by extensive soil cover, structural complexity, sudden facies variations and monotonous rock types. Irregularities associated with a rapidly developing volcanic pile and a complex intrusive history complicate attempts at correlation.

In the northern half of the caldera, the oldest unit exposed is a sequence of high potassium trachyandesitic volcanics (shoshonites) of the Goonumbla Volcanics. These are flows of varying thickness, and pyroclastics ranging from coarse agglomerate to fine ash tuff. Minor interbedded volcanically derived fine grained sediments indicate local shallow water (possibly lacustrine) deposition. The volcanics are typically dark grey to greenish grey and are commonly porphyritic, containing 20 to 30% plagioclase phenocrysts from 2 to 6 mm long. Subordinate hornblende and augite are present. The matrix consists of fine plagioclase laths and interstitial anhedral potassium feldspar. Limestones occur outside the caldera rim, however they have not been identified within the caldera.

The Wombin Volcanics overlie and are probably conformable with the Goonumbla Volcanics. They are preserved toward the centre of the synclinal feature in the southern half of the caldera and appear to be truncated in the south by a major east trending structure. They are brownish red, potassium rich trachytes dominated by pyroclastics of variable grain size with lesser flows which may be banded to weakly porphyritic. The trachytes contain scattered euhedral plagioclase laths up to 2 mm within a sanidine rich trachytic textured groundmass. Features attributable to a rapidly developing volcanic pile are observed within the sequence, including large mass flow and slump type deposits which contain trachytic boulders up to 1 m in diameter. The thickness of the Wombin Volcanics is uncertain.

INTRUSIVES

The intrusive history within the caldera is complex. Including the northern ring dyke, approximately 20% of the rocks exposed within the caldera are of intrusive origin. Detailed work on the porphyry deposits has identified multistage intrusive activity and complex overprinting hydrothermal alteration patterns. A subvolcanic environment is envisaged.

At the E26 North deposit, Heithersay (1986) determined that the oldest intrusives are of dioritic to monzonitic composition. These are composed of euhedral zoned andesine (50 to 60%), hornblende (5 to 10%), clinopyroxene (5 to 10%) and interstitial cloudy perthitic potassium feldspar (15%). Biotite encloses plagioclase, hornblende and pyroxene, and magnetite and apatite are common accessories.

The volumetrically dominant intrusive is a medium grained monzonite to monzonite porphyry. It is commonly brick red coloured, resulting from fine hematite dusting of feldspar. It is a holocrystalline rock consisting of subhedral oligoclase to andesine crystals (20 to 35%) set in a hypidiomorphic granular groundmass of stumpy potassium feldspar crystals. Biotite (5 to 10%) and hornblende (5 to 10%) are the common mafic phases, and interstitial quartz ranges from 3 to 10%. Accessory minerals include apatite, sphene and magnetite.

The porphyry copper-gold mineralisation is invariably associated with relatively small, subvertical, pipe-like intrusive bodies of quartz monzonite porphyry (Figs 4, 5, 6, 10). Their diameters seldom exceed 100 m but they may have vertical continuity of over 900 m. A typical mineralised quartz monzonite porphyry has a strong pink to pinkish orange colour, and is often coarsely porphyritic containing 20 to 40% plagioclase feldspar phenocrysts which commonly reach 4 mm in maximum dimension. Quartz phenocrysts, seldom exceeding 1 mm, may comprise 10 to 20% of the rock and the matrix is of fine grained potassium feldspar and quartz. Biotite and hornblende are minor phases, and magnetite, sphene and apatite are accessories only.

Multistage intrusive activity of quartz monzonite porphyries is quite common, but contacts between phases are often poorly defined, suggesting that timing of the intrusive events may be very close and possibly overlapping. Individual phases are identifiable by slight textural and compositional variations.

Post-mineralisation intrusives are common and include porphyritic dykes of monzonitic to syenitic composition which contain only 10 ppm copper. They are known locally as 'Zero Porphyries' and are thought to represent the volatile-depleted phases produced during the waning stages of the magmatic event.

Thin basic dykes, 1 to 2 m wide, and andesitic to basaltic dykes occur, but are not common. These are considered to be unrelated to the mineralising event. Small pebble dykes have also been observed at several locations.

PETROCHEMISTRY

Volcanic and intrusive rocks away from the main mineralised centres are fresh, which allows primary geochemical patterns to be studied (P.S. Heithersay, unpublished data,

1989). Compositionally the volcanics range from shoshonite to latite to potassium rich trachyte, using the nomenclature of Cox, Bell and Pankhurst (1979). Latites (potassium rich trachyandesites) dominate in the Goonumbla Volcanics and potassium rich trachytes dominate in the Wombin Volcanics.

Chemically the rocks range from 50 to 65% SiO_2 with a corresponding K_2O range of 2 to 7%; $K_2O + Na_2O$ content ranges from 5 to 10%. The suite is also characterised by high Al_2O_3:FeO ratios, and low titanium, zirconium and barium contents. These features are consistent with characteristics of the shoshonite rock association as outlined originally by Joplin (1968) and in the review by Morrison (1980).

On variation diagrams the Wombin Volcanics plot on a distinct compositional trend as the fractionated end member of the Goonumbla volcanic suite. Similarly, most of the diorite to monzonite intrusives plot on the same compositional trend, which is consistent with them being coeval. Monzodiorite to quartz monzonite porphyries related to mineralisation, however, exhibit a less potassic, more silica rich compositional trend, which is distinct from the main, highly fractionated compositional trend.

MINERALISATION

Three major and eight minor centres of mineralisation have been discovered within the Goonumbla porphyry copper district to date (Fig. 3a). All the deposits demonstrate a close spatial relation to quartz monzonite porphyry intrusives and their associated zones of hydrothermal alteration. The deposits are generally pipe-like and range in diameter from a few tens of metres to more than 300 m. The mineralisation has strong vertical continuity which at E26 North has been shown by drilling to exceed 900 m.

Disseminated and fracture or vein controlled mineralisation occurs both in the intrusives and the surrounding volcanics. The strongest mineralisation is associated with quartz stockwork veining within the central potassic alteration zones and diminishes outward, accompanied by reduced vein and/or fracture density.

The distribution of mineralisation within individual deposits is dependent on the size, shape and characteristics of the intrusive bodies and the intensity of the attendant hydrothermal alteration. In their simplest forms, the deposits have an outer poorly defined and often incomplete pyritic zone, where pyrite comprises up to 3% of the rock. The pyritic zone surrounds a chalcopyrite dominant zone which in turn envelops a high grade central zone dominated by bornite and lesser chalcocite.

Copper : gold ratios vary between deposits and the reason for this is not well understood, though wall rock composition may be important. At the E22 and 27 deposits a regular copper : gold ratio is apparent where % copper : g/t gold is close to 1:1. In other deposits gold is less abundant. Elevated gold grades are usually closely associated with strong bornite mineralisation. Occasionally fine grained free gold is observed occupying fractures within coarser grained bornite.

Minor galena and sphalerite have been identified in the outer propylitic alteration zones and can produce coherent soil geochemical anomalies. Molybdenite is rarely observed. Several telluride bearing minerals including calaverite, hessite and altaite have been identified.

Skarn mineralisation has not been identified within the circular feature, although skarn related lead-zinc mineralisation does occur close to the southern margin at the *E6* and *E7* deposits (Fig. 2).

ALTERATION

The Goonumbla deposits lack large mineral destructive, pervasive alteration zones. Potassic alteration is the dominant style associated with mineralisation (Fig. 3c). It is commonly expressed as pink-red, potassium feldspar rich fracture and vein envelopes which are readily observed in the dark grey andesitic volcanics and less obvious in the pinkish red intrusives and trachytic volcanics. Where fracturing or veining is most intense, primary textures can be destroyed by potassium feldspar flooding. Secondary biotite is also a common alteration mineral, occurring as a pervasive alteration of the groundmass and as a selective replacement of mafic minerals and plagioclase. Biotite alteration is most common within the more mafic trachyandesites, whereas potassium feldspar alteration is dominant within the trachytic rocks.

The alteration zones are centred on the mineralised quartz monzonite porphyry intrusives and the intensity of the alteration diminishes outwards. The multiphase intrusive activity and subsequent overprinting of early formed assemblages can result in complex alteration patterns.

Quartz stockwork veining commonly occurs toward the centre of the alteration system with individual veins from 0.5 to 10 cm wide. Veining may comprise 10 to 20% by volume of the rock. The veins contain varying amounts of alkali feldspar, carbonate, fluorite, anhydrite, bornite, chalcopyrite and chalcocite. At the *E26* and *E20* deposits, gypsum and anhydrite are present; however this alteration assemblage is not observed in other deposits.

A pervasive quartz-sericite-pyrite overprint occurs on a regional scale (Fig. 3c) and appears to be related to major structures and the contact zones of the intrusives. This alteration often totally obliterates original rock textures.

On a regional scale there is widespread propylitic alteration which is expressed by the development of irregular blebs of epidote, chlorite, carbonate and pyrite. These blebs may reach several centimetres in diameter, commonly have reddened haloes and, where most intense, give the rock a strongly mottled appearance. This assemblage is well developed in the vicinity of E22 and E27, but elsewhere it has no obvious relation to porphyry mineralisation.

STRUCTURE

Reliable structural data are scarce because of the lack of outcrop. Regional geological mapping has defined the Milpose syncline (Fig. 3a) plunging gently to the SW with dips on the limbs of around 20°. The fold axis trends NNE and passes to the east of the E26 North deposit. Cleavage is virtually non-existent.

A number of prominent linear features can be identified from both aeromagnetic and more detailed ground magnetic data (Fig. 3d). Major linears are observed trending 345° true and 065° true. These are interpreted as major structural features, however there is little direct evidence for faulting. A major linear feature known as the Endeavour linear, trending 345° true, has a close spatial relation with a number of mineralised centres including E26 North, *26 South, 28*, 22 and 27. Both the northern and southern extensions of the Endeavour linear are marked by strong quartz-sericite-pyrite alteration. Other linear features and the intersection of these features have little obvious relation to mineralisation, probably indicating that they are post-mineralisation.

At E28 a low angle thrust fault has been defined with a displacement in the order of 300 m. Evidence of faulting is observed in most diamond drill cores indicating a complex tectonic history within the circular feature.

WEATHERING AND OXIDATION

The depth of weathering and oxidation is variable. At E31 bornite can be chipped from outcrop, whereas elsewhere, the depth to fresh sulphides may exceed 80 m. Much of the Goonumbla area is covered by a variable thickness of clays which are for the most part a product of in situ weathering. In areas of stream activity, transported material has been encountered to a maximum depth of 40 m.

In areas of deeper weathering, both copper and gold have undergone limited supergene mobilisation and enrichment. The low sulphide content of the deposits probably restricts

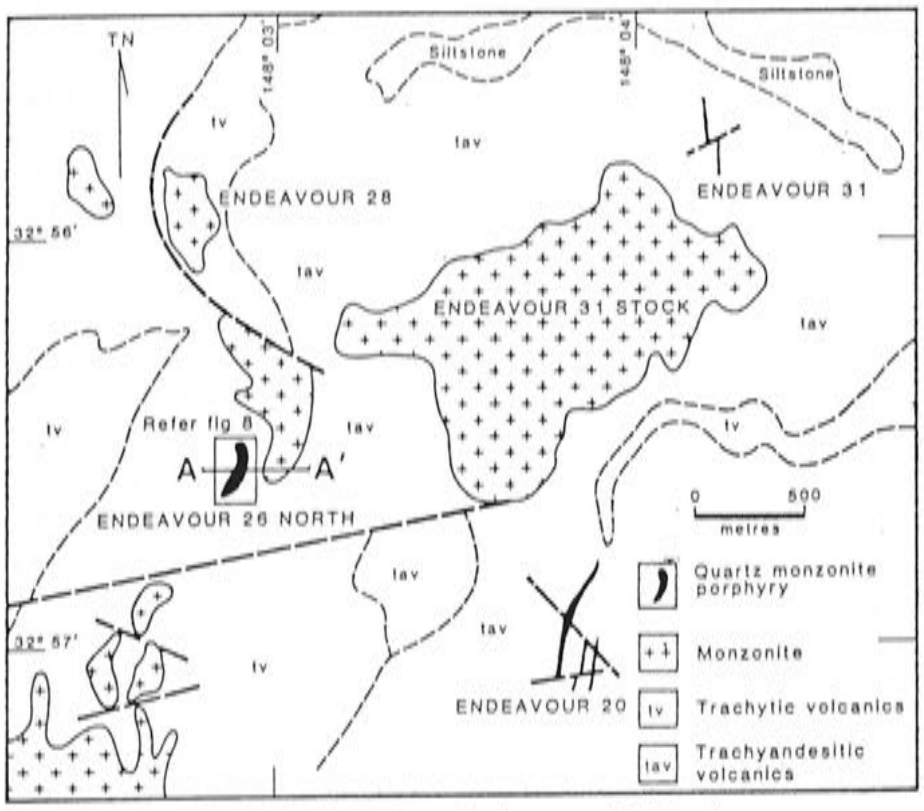

Fig. 4—Geological plan, Endeavour 26 North area.

the supergene processes, and although secondary chalcocite blankets are observed at, or immediately below, the base of oxidation, these are generally only a few metres thick and often poorly defined.

In the vicinity of the E26 and E20 deposits, sulphates (principally gypsum) and carbonates have been leached to depths of 200 m below surface leaving the rock vuggy, porous and fractured. At E26 North a carbonate impregnated zone occurs 20 to 30 m above the base of gypsum leaching. Both these features are thought to result from secondary processes related to variations in the chemistry of ground waters associated with changes in water table levels.

DATING

K-Ar dating (AMDEL, unpublished data, 1978) of biotite from a fresh intrusive mafic rock, and of a total rock sample of trachyandesitic volcanics from the Goonumbla porphyry copper district, returned dates of 427 ± 6 Myr and 423 ± 6 Myr respectively. By using more recent decay constants the dates become 435 and 431 Myr respectively. Recent ^{40}Ar–^{39}Ar dating (C. Perkins, unpublished data, 1988) on sericite separates from the E26 potassic alteration zone returned an age of 441 ± 2 Myr.

Given the above information, the preferred age for the Goonumbla porphyry copper-gold mineralisation is Late Ordovician, using the time scale of Cooper and Grindley (1982).

ENDEAVOUR 26 NORTH DEPOSIT

INTRODUCTION

The Endeavour 26 North (E26 North) deposit is 24 km NW of Parkes and 4 km south of the Endeavour 22 (E22) and Endeavour 27 (E27) deposits (Fig. 1). It was discovered in 1979 and is the largest of the 11 porphyry copper-gold deposits discovered in the Goonumbla region. Resource data are in Table 1.

The E26 North deposit has been tested by 40 deep inclined diamond drill holes totalling 25 000 m and by 23 short vertical reverse circulation percussion (RC) and diamond holes, totalling 2750 m. The open pit resource (sulphide only), extends to 210 m vertically while the underground resource is defined to 900 m depth. Sulphide mineralisation begins at the base of oxidation 30 to 50 m below surface and extends vertically beyond 900 m. In plan view, mineralisation is defined within a zone 250 m wide by 300 m long.

E26 North is a stockwork quartz-bornite pipe which is centred on small, multiphase, subvolcanic quartz monzonite porphyry intrusions. This basic pattern is repeated at E28, 31 and 20. All four deposits lie outside the margin of the Endeavour 31 monzonite stock (Fig. 4) which is itself weakly mineralised (Fig. 3b).

VOLCANIC HOST ROCKS

The host Goonumbla and Wombin volcanics, which the Endeavour 31 stock and its satellite bodies intrude, range from trachyandesitic to trachytic pyroclastics and lavas. They exhibit considerable variation in grain size and texture. Individual volcanic units are difficult to correlate; however a broad coarsening upwards sequence is evident. At the base of the sequence are porphyritic trachyte lavas with interbedded ash and lapilli tuffs (Fig. 5). The orange pink lavas are commonly flow banded and consist of sparse euhedral plagioclase phenocrysts and minor pyroxene set in an oriented decussate mat of fine sanidine laths. Further up-sequence lapilli tuffs predominate, with trachytic fragments set in a crystal rich matrix. The uppermost unit is a volcanic breccia in which heterolithic clasts up to 20 cm are set in a crystal lithic matrix.

Interbeds of finely laminated and graded sediments ranging from tens of centimetres to 100 m in thickness form useful marker beds in the sequence and possibly represent lacustrine deposits within a caldera.

INTRUSIVE ROCKS

The Endeavour 31 stock has a uniform monzonitic composition throughout, however diamond drilling has revealed at depth a 500 m thick marginal zone that varies from monzonite to diorite (Fig. 5). Crosscutting this marginal zone are several quartz monzonite porphyries which may be linked to the mineralising porphyries at E26 North. Geochemically the diorite through monzonite to quartz monzonite porphyry forms a well defined trend on variation diagrams, which is consistent with them being genetically linked. The marginal diorite is interpreted to be a cumulate phase crystallising early on the walls of the Endeavour 31 stock (P.S. Heithersay, unpublished data, 1989).

Mineralisation is centred on two quartz monzonite porphyries, the early intrusion called QMP1 and the later QMP2 (Figs 5, 6). QMP1 is largely masked by intense potassium feldspar alteration and stockwork quartz veining. Identification is made even more difficult because the por-

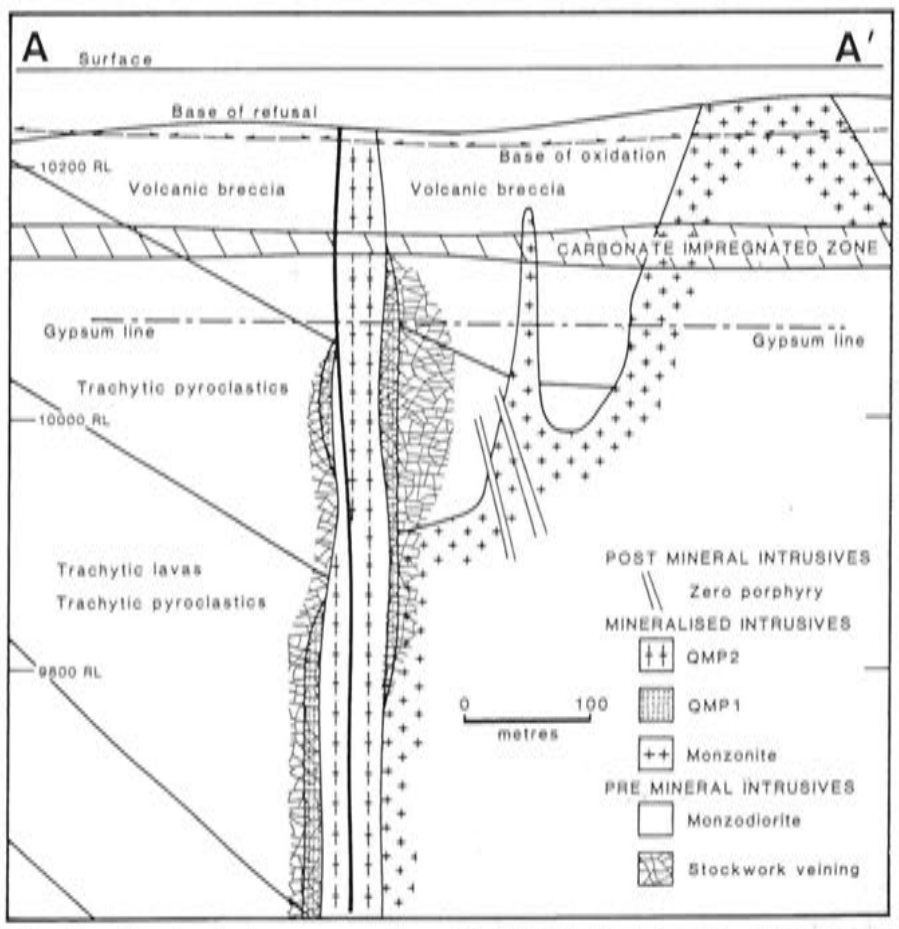

Fig. 5—Geological cross section 53 450 N, looking N, Endeavour 26 North.

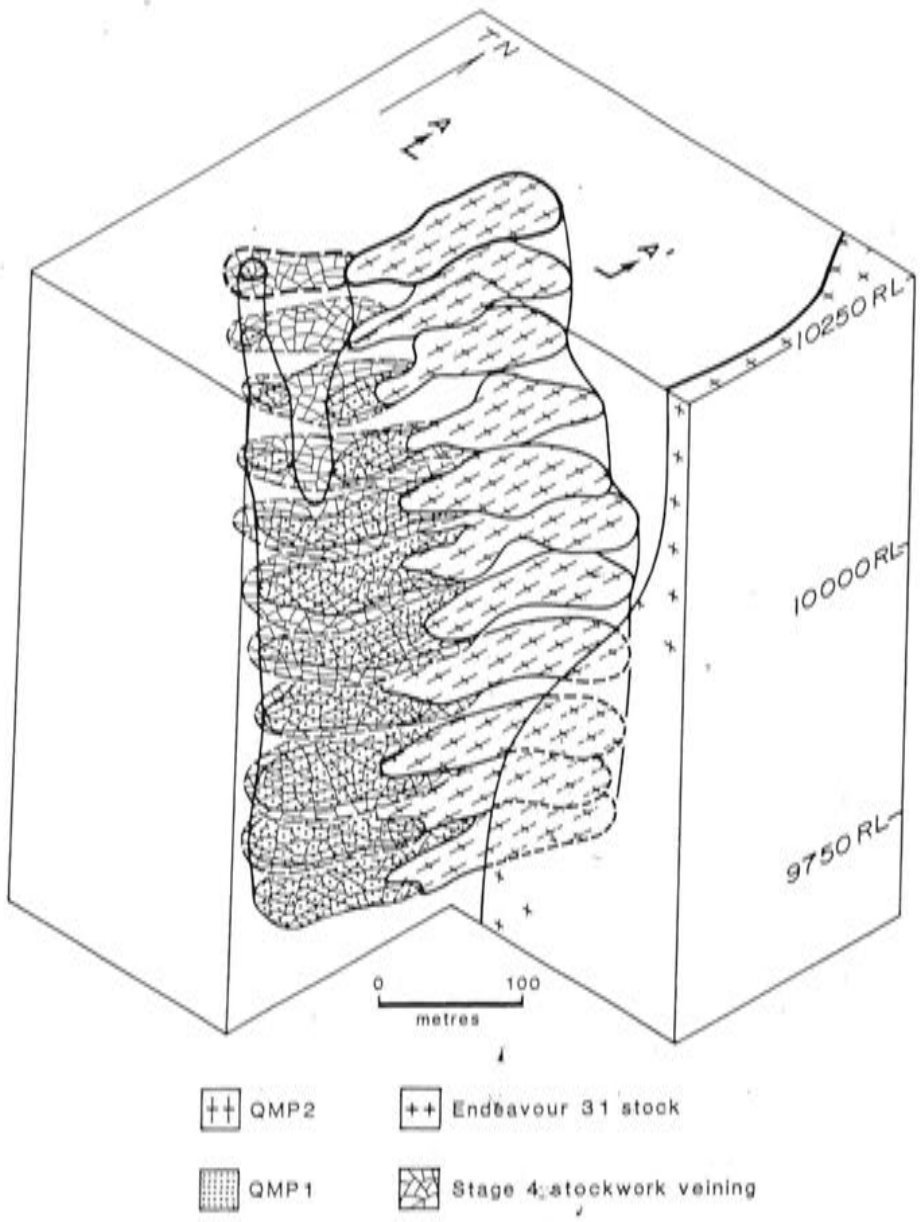

Fig. 6—Schematic block diagram of intrusive and stockwork geometry, Endeavour 26 North.

phyritic texture of the intrusion resembles the volcanics it intrudes.

QMP1 is characterised by evenly distributed albite to oligoclase phenocrysts (20%) which are uniformly mantled by potassium feldspar. The groundmass is a quartz-potassium feldspar mosaic which commonly displays a saccharoidal texture with some graphic intergrowths and imparts a pink-orange colour. Biotite is sparsely distributed throughout, but now largely altered to sericite. Irregular quartz blebs and irregular discontinuous quartz veins are common. Some of these features closely resemble the 'brain rock' described at the Henderson mine, Colorado (Wallace et al., 1978), where it is used to identify the margins of separate intrusions, and is also indicative of the earliest phase of hydrothermal fluid in equilibrium with incompletely crystallised magma.

The later QMP2 is conspicuously porphyritic, containing grey, evenly distributed albite to oligoclase laths (20 to 30%), set in a pink potassium feldspar–quartz groundmass. Altered biotite and hornblende are sparsely distributed throughout and may make up 10 vol. %. Occasional tablet shaped megacrysts of perthitic orthoclase poikilitically enclose plagioclase crystals. Interstitial quartz varies from 5 to 13%. Vein-like trails of coarse euhedral quartz crystals (3 to 6 mm) are noted near the contacts of QMP2 and are a variant of 'brain rock'.

The contacts of the two quartz monzonite porphyries are often defined by an abrupt change in intensity of mineralisation. QMP2 is moderately altered and mineralised, however clear contrasts are noted where the QMP2 contact abruptly terminates thick stockwork veins within QMP1. Fragments of these stockwork veins 'floating' within QMP2 often mark the contact between the two porphyries. This evidence suggests that QMP2 intruded the advanced hydrothermal system established by QMP1, and incorporated and remobilised the mineralisation it encountered.

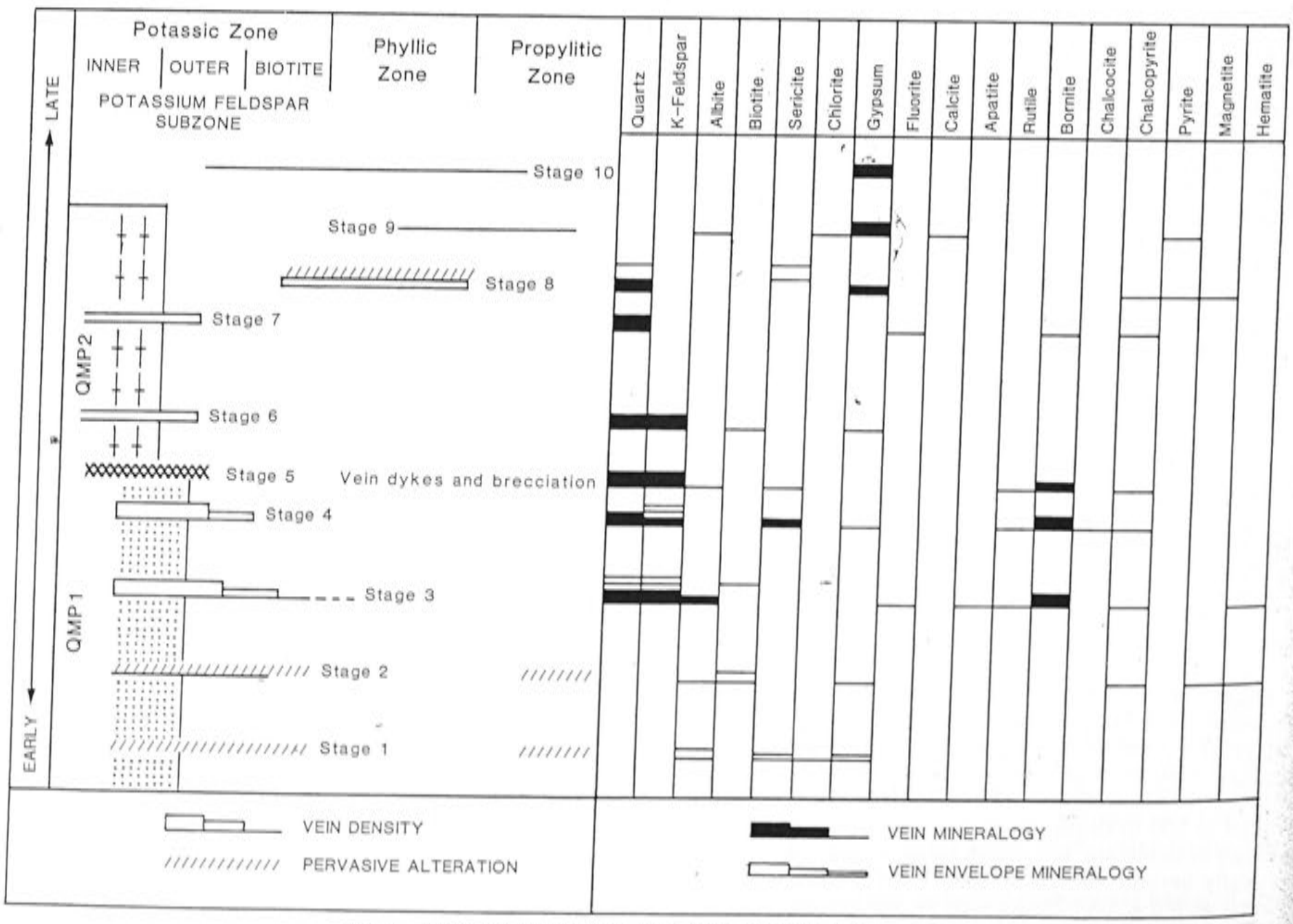

Fig. 7—Alteration progress diagram, Endeavour 26 North.

The narrow post-mineral 'Zero Porphyries' are glassy porphyritic rocks, usually with well developed chilled margins in contrast to the earlier intrusions (Fig. 5).

HYDROTHERMAL ALTERATION

The detailed paragenesis and alteration zonation of E26 North were discussed by Heithersay (1986). Figure 7 is an alteration progress diagram (Titley, 1982) which attempts to illustrate the spatial and temporal relations between the ten identified alteration stages and the early QMP1 and later QMP2. The main ore bearing events are stages 3, 4 and 5.

Stage 3 veinlets are commonly discontinuous and develop irregular vein margins with euhedral quartz crystals projecting from the vein into the vein margin. A thin margin of potassium feldspar always accompanies these veinlets, and is most obvious when they crosscut plagioclase crystals. Fine scale graphic intergrowths of quartz and potassium feldspar often define veinlet margins, suggesting some early magmatic component. The secondary potassium feldspar is cloudy with fine hematite inclusions, hence the vein margin appears bright pink-red against the darker biotite altered rock. Bornite, lesser chalcocite, digenite and chalcopyrite occur as fine crystals within these veinlets. They vary in vein intensity from tens to thousands of veins per metre. In the most intense cases, the altered volcanic or intrusive is converted to an aphanitic pink rock with most primary features totally obliterated. However trails of bornite throughout attest to the presence of healed stage 3 veinlets, although overall the texture is one of finely disseminated sulphides. Stage 3 venation is the peak depositional event for mineralisation.

Stage 4 represents a major change from the fine scale random fracturing to through going, thicker veins (0.5 to 2 cm). In detail, these grey vitreous quartz veins display thin trails of sulphides, anhydrite and sericite parallel to the vein walls, suggesting repeated fracturing and fluid flow parallel to the walls. Stage 4 veins form a stockwork system, which pervades QMP1 and adjacent volcanics, but is absent from QMP2 (Fig. 6). The distribution of gold in the deposit bears a close relation to stage 4 stockwork veining. At the northern end of the deposit, in zones of high copper grade but no stockwork development, gold grades are very low.

Stage 5 marks the appearance of vein dykes and magmatic hydrothermal breccia. Vein dykes are features which grade from normal quartz veins to aplitic dykelets. In detail vein dykes commonly develop complex graphic intergrowths of quartz and potassium feldspar and resemble micropegmatite. These features suggest rapid supercooling of a melt phase.

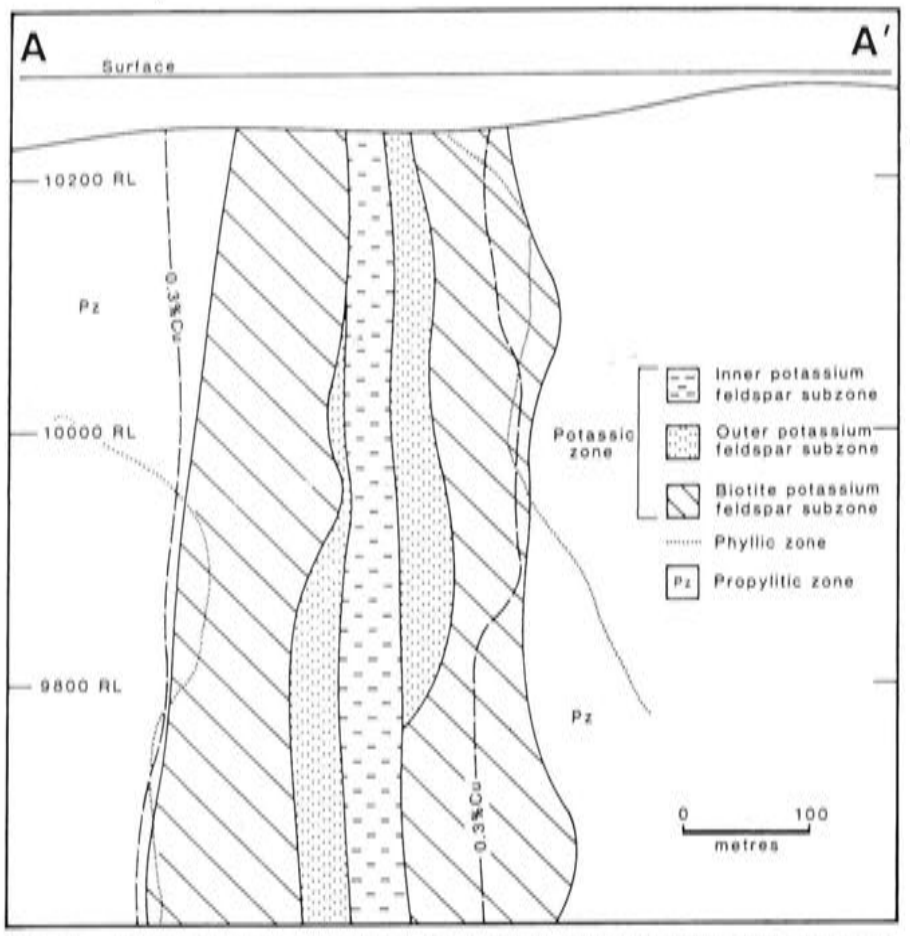

Fig. 9—Cross section 53 450 N, looking N, showing alteration zones, Endeavour 26 North.

Dykelets of QMP2 commonly crosscut and brecciate the stockwork veins of stage 4. These dykelets can be traced into vein dykes, suggesting that these magmatic hydrothermal features herald the intrusion of the QMP2 magma. The southern margin of the QMP2 together with its network of peripheral dykelets contains fragments of veined volcanics and intrusives. More commonly, fragments of stage 4 stockwork veins and irregular blobs of bornite with lesser quartz are included in the later intrusive. These unique features are interpreted as immiscible sulphides which have resulted from local saturation of the QMP2 magma, as a result of stoping of a pre-existing, mineralised stockwork zone. Stage 5 of the paragenesis has had the effect of locally remobilising sulphides and upgrading the high grade pipe which now forms the main ore zone of E26 North.

Taken together, stages 3 to 5 form the middle subzone of three within a potassic alteration halo which is broadly symmetric about QMP1 (Figs 8, 9). The potassic alteration zone is 250 m wide by 400 m long. The inner potassium feldspar subzone reflects the weak intensity quartz–potassium feldspar veining associated with, or arising from, the later QMP2 intrusive. Stages 3 to 5 make up the almost annular outer potassium feldspar subzone which is the most intensely altered and mineralised part of the potassic halo. The biotite–potassium feldspar subzone is the outermost subzone of the potassic halo.

The high grade (>1.0% copper) zone correlates with the outer potassium feldspar subzone and has a plan area of 50 to 100 m wide by 200 to 250 m long. The boundary of the low grade zone (>0.3% copper) corresponds broadly to the margin of the biotite–potassium feldspar subzone (Figs 8, 9). The boundary between these subzones is a narrow transition zone, marked by an abrupt reduction of magnetite content and subsequent increase in reddening of the rocks due to hematite dust in the overprinting secondary potassium feldspar. The passage from low to high copper grade, when seen in core, is from dark secondary biotite and magnetite rich rocks to reddish pink coloured potassium feldspar and bornite rich rocks.

Potassic alteration grades outwards into propylitic alteration. In some cores the transition appears gradational whereas in other intercepts propylitic assemblages overprint potassic alteration. Propylitic minerals, including albite, epi-

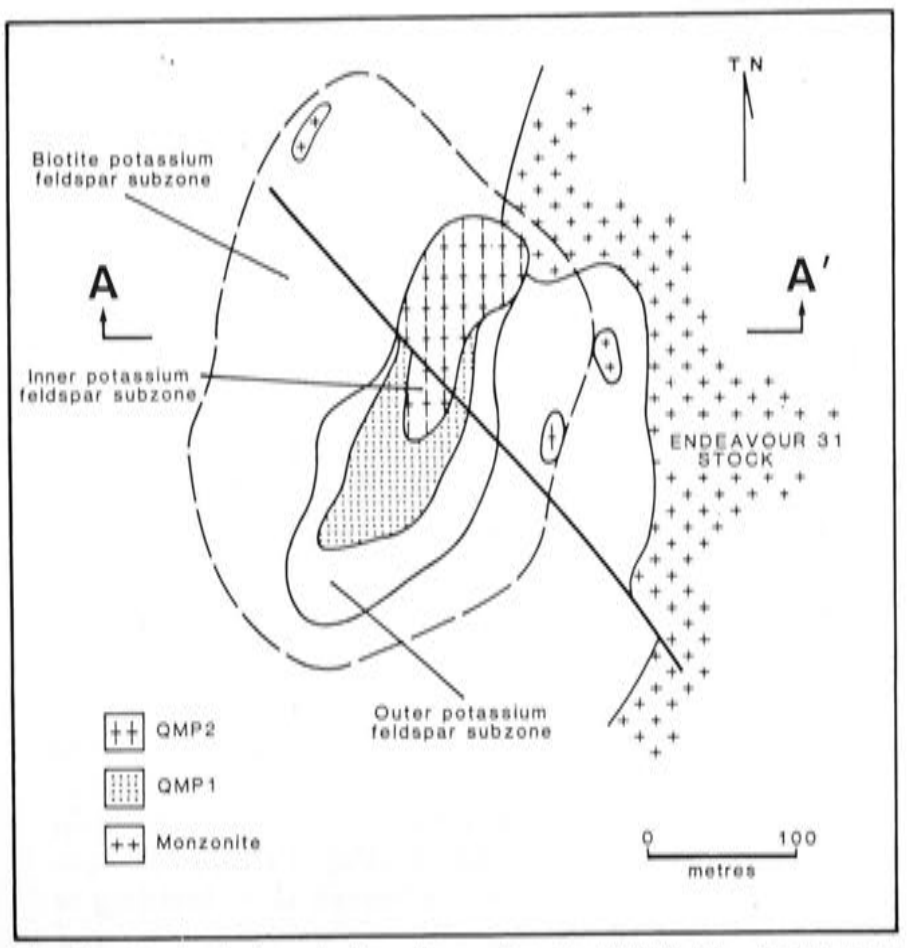

Fig. 8—Geological and alteration plan at 10 000 RL, Endeavour 26 North.

dote, chlorite and calcite, occur in a variety of textural forms ranging from site selective replacement of mafic minerals through to locally pervasive alteration due to crosscutting vein and vein envelopes. Unlike E22 and E27, this alteration style does not form a discrete halo around central porphyries, but merges into the regional background alteration.

Phyllic or quartz-sericite alteration is a common regional alteration feature which appears to follow major faults and linears and E26 North is the only deposit spatially related to this alteration style. Phyllic alteration is always fracture related and forms pervasive zones metres to tens of metres in thickness. Intense phyllic alteration totally detextures the rock and forms a pale green to white aggregate of quartz, sericite, pyrite and trace chalcopyrite. Galena and molybdenite, although uncommon, occur in the central quartz veins of these zones. The sulphides associated with this alteration style rarely exceed 4 vol. %.

MINERALISATION

A clear zonation in sulphide species follows the hydrothermal alteration pattern. Bornite with minor chalcopyrite, chalcocite and digenite occurs within the outer potassium feldspar subzone and is the main copper bearing phase. Within this subzone, gold is primarily associated with stage 4 stockwork veining. Bornite gives way to chalcopyrite in the biotite-potassium feldspar subzone. Chalcopyrite, in turn, gives way to pyrite in the surrounding propylitic and phyllic alteration zones.

Gold is closely associated with bornite. Free gold, cuprian gold and gold telluride (calaverite) are the important gold bearing phases. They always occur as 5 to 15 μm diameter inclusions within bornite grains and closely resemble exsolution spots. A similar relation between gold and bornite in British Columbia has been documented by Cuddy and Kesler (1982). They note that at high temperatures (600°C) bornite exhibits extensive solid solution of copper, iron, sulphur and probably gold. As the bornite cooled, gold was forced to exsolve because bornite exhibits no solid solution at ambient temperatures.

FLUID INCLUSIONS

At E26 North, quartz veins associated with stages 3 to 5 have fluid inclusions from 10 to 30 μm in diameter. Fluid inclusion types include liquid dominated liquid-vapour inclusions, vapour dominated liquid-vapour inclusions and salt saturated liquid-vapour-salt inclusions. Daughter salts include halite, sylvite, anhydrite, hematite, chalcopyrite and up to two unknowns.

The highly saline inclusions, which are typical of porphyry copper systems (Roedder, 1984), range in salinities from 40 to 60 wt % NaCl equivalent. Boiling is indicated in stages 3 to 5 by the presence of coeval liquid-vapour-salt inclusions and vapour dominated liquid-vapour inclusions which homogenise at approximately the same temperature (Roedder 1984).

The early fine fracturing represented by stage 3 veinlets shows discrete thermal peaks in homogenisation temperatures (T_h). The highest T_h range is between 720° and 840°C, with the next peak range between 440° and 500°C. The well mineralised stockwork veins of stage 4 gave a T_h range between 500° and 620°C for primary and pseudo-secondary inclusions. This may be the main range of ore deposition temperatures. It is clear that several thermal events are recorded by fluid inclusions associated with the two main stages of ore deposition.

Texturally stage 5 veins and vein dykes crosscut and infill brecciated stage 4 stockwork veins. Stage 5 veins are free from the dense network of low temperature secondary inclusions which characterise the stockwork veins. High homogenisation temperatures (720° to 800°C) and high salinites (50 to 60 wt % NaCl equivalent) are typical of stage 5 inclusions. These data are consistent with the magmatic hydrothermal nature of this part of the paragenesis.

STRUCTURE

The E26 North deposit lies within a corridor dominated by the Endeavour linear trending 345° true (Fig. 3d). Detailed structural analysis indicates that a dominant orientation of quartz-bornite-chalcopyrite veins is around 035° true (P.G. Dunn, unpublished data, 1986), parallel to the long axes of QMP1 and QMP2. The intrusives exhibit a sinusoidal shape in plan view. The 035° trend of intrusive and veining is oblique to the Endeavour linear, suggesting that the vein trend may be the response to a principal stress field created by lateral movement along the Endeavour linear structural corridor. Such movement would create the space for intrusive activity and strongly influence principal veining trends.

SUPERGENE EFFECTS

Gypsum has been removed by leaching, leaving holes and open fractures above a deep horizontal plane. Jones (1985) suggested that the unusually planar nature of this surface (the gypsum line; Fig. 5) points to the presence of a chemical interface between two ground water systems. A possible explanation lies in fresh ground water sourced from a caldera margin interacting with hot sulphate rich hydrothermal brines. Sillitoe and Gappe (1984) noted that leaching of gypsum to deep levels is common in Philippine porphyry copper systems and similar features are documented at El Salvador in Chile (Gustafson and Hunt, 1975).

A second poorly understood supergene feature 20 to 30 m above the gypsum line, consists of an irregular zone of pervasive carbonate impregnation forming a hard grey featureless rock containing minor pyrite.

A thin layer of supergene chalcocite is present between the upper oxidised zone and the primary sulphides. The supergene ore zone is generally less than 10 m thick, extends over the mineralised source, and forms a small percentage of the total resource.

ENDEAVOUR 22 AND ENDEAVOUR 27 DEPOSITS

INTRODUCTION

The Endeavour 22 (E22) deposit is 28 km northwest of Parkes, and Endeavour 27 (E27) is 1 km east of E22 (Fig. 1). The E22 deposit has been sampled by 23 deep inclined diamond drill holes totalling 9030 m and by 113 short vertical RC, air core and diamond holes totalling 4450 m. Twenty six deep inclined diamond holes and 214 short vertical RC, air core and diamond holes totalling 8800 m and 7560 m respectively have been drilled in the E27 area. Shallow gold and gold-copper mineralisation occurs in the oxide zone above the copper sulphide resources. Resource data are in Table 1.

In the E22 and E27 porphyry copper deposits the copper sulphide and gold mineralisation is dominantly fracture and vein controlled, and is associated with small porphyritic quartz monzonite dykes and stocks which intrude the Goonumbla Volcanics (Fig. 10). Geological interpretation is based entirely on diamond drill core. The base of oxidation is 45 to 55 m below surface, with the interval from 5 to 45 m depth strongly kaolinised.

VOLCANIC STRATIGRAPHY

Local correlation of the volcanic sequence has been made using andesitic and trachyandesitic tuffs. Tuffaceous units are generally poorly sorted, ranging from crystal and lapilli tuffs to coarse units showing agglomeratic or slumped structures. Some fine ash units occur, although their bedding is generally quite irregular. A distinctive well bedded, reworked coarse ash tuff unit has been identified at E22 (Fig. 10).

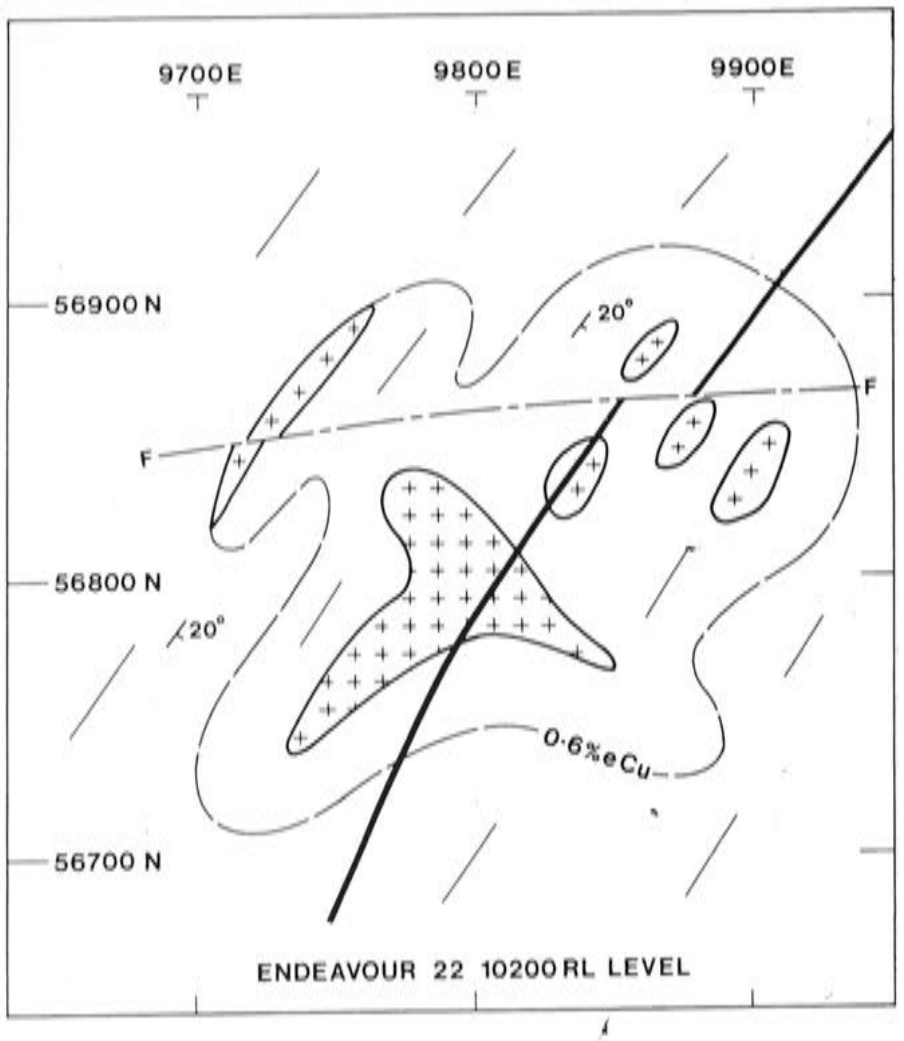

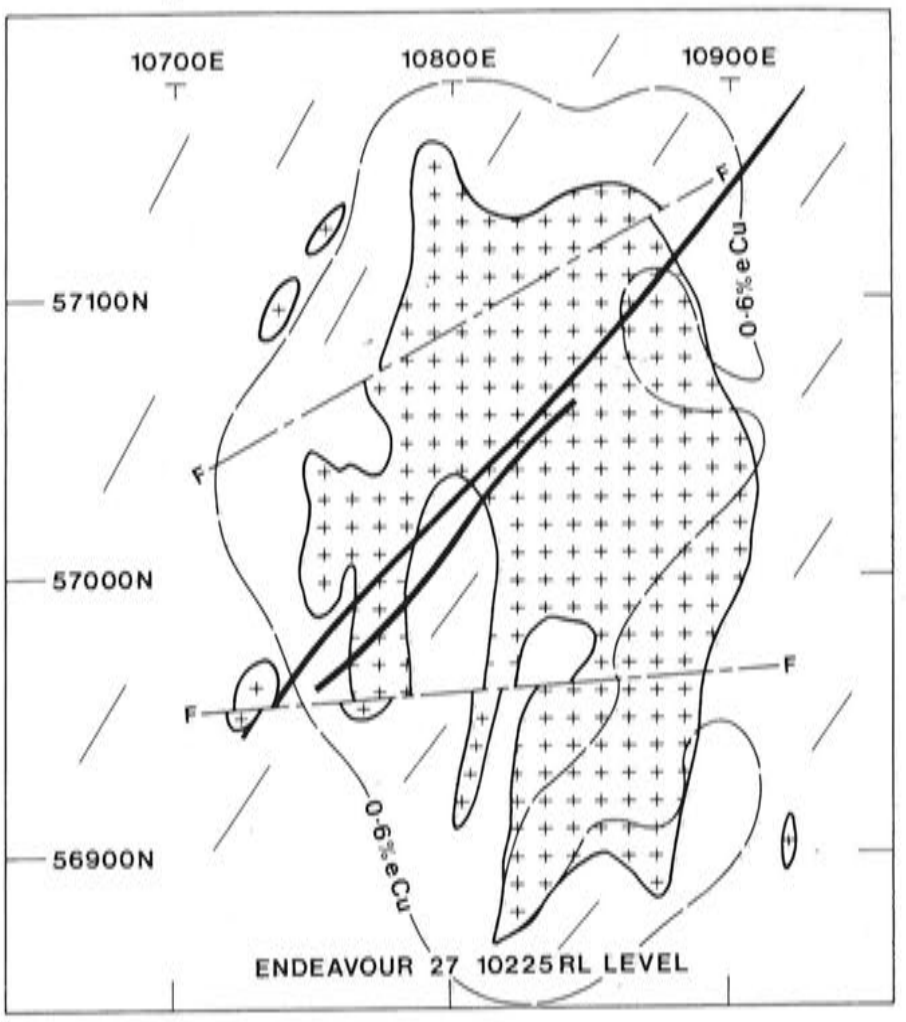

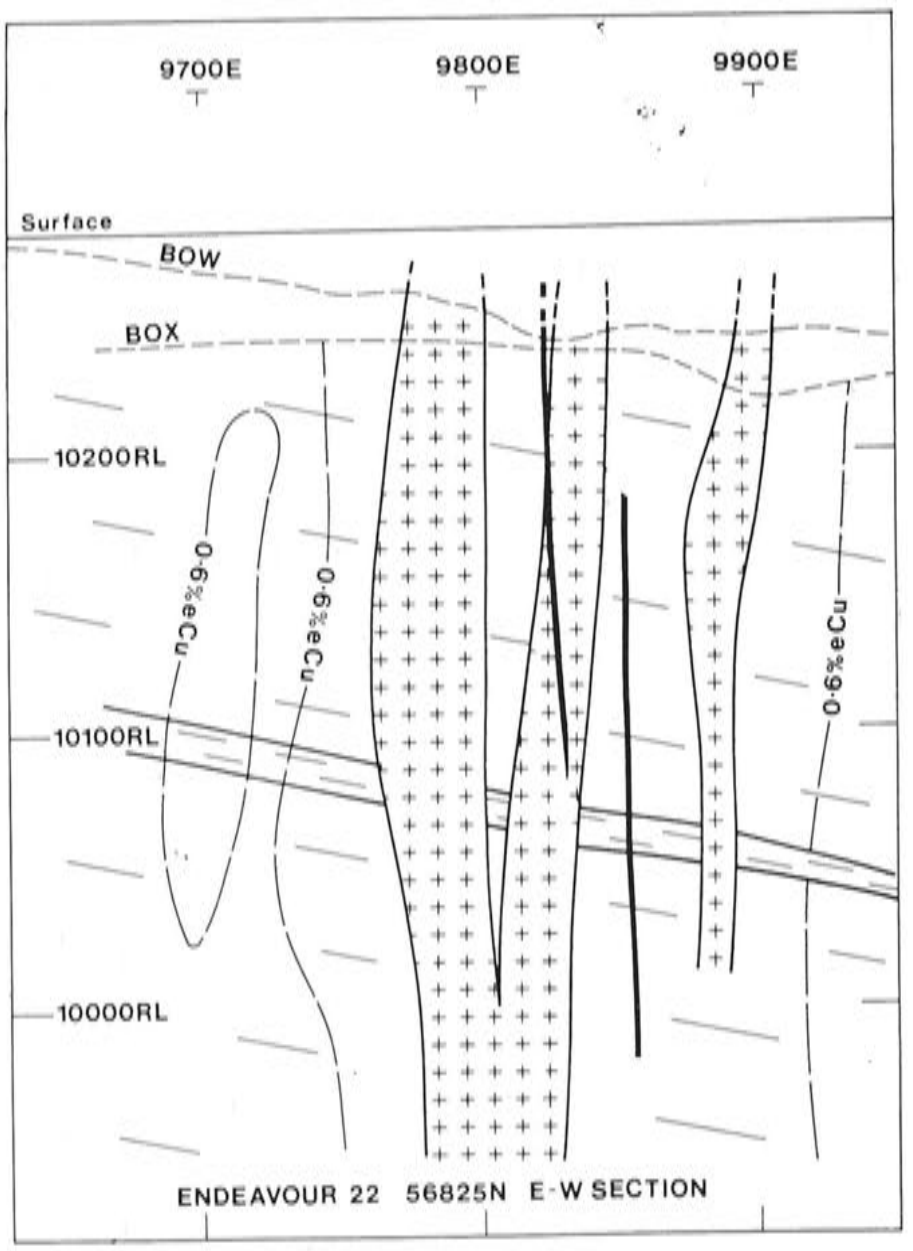

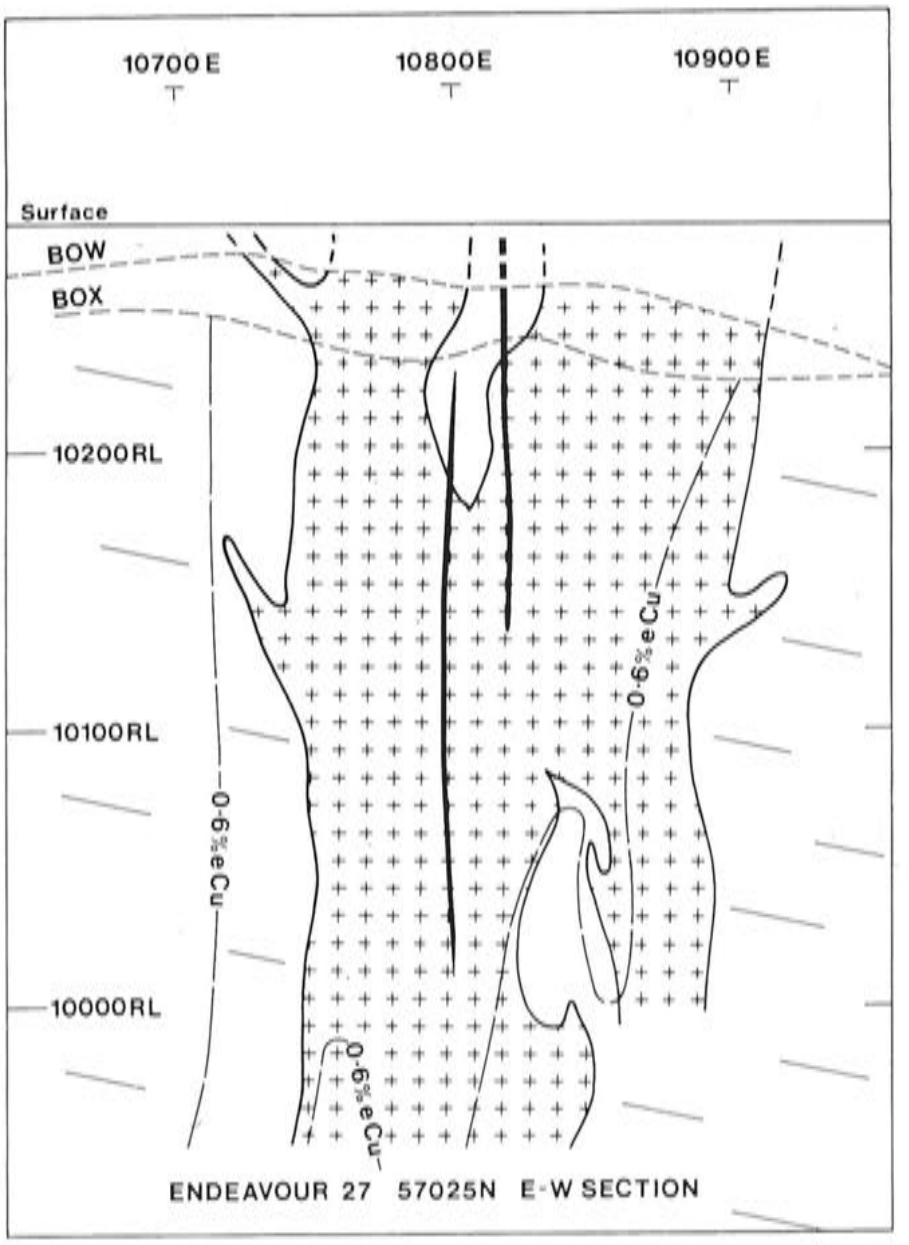

Trachyandesitic volcanics including marker horizon

Basaltic dyke

BOW Base of weathering

—0·6%eCu— Grade contour

Monzonite intrusive

F——F Inferred fault

BOX Base of oxidation

20° Strike/dip

Fig. 10—Simplified geological plans and cross sections, looking N, Endeavour 22 and Endeavour 27 deposits.

Structural measurements from oriented drill core and the correlation of this unit from hole to hole indicate that the volcanic sequence dips at approximately 25° ESE. A fine ash tuff unit at E27, 1 km to the east, has also been correlated from hole to hole indicating the sequence has a similar strike and dip here. Unless offset by major faulting, the volcanic sequence at E27 is 400 to 500 m stratigraphically above the sequence at E22.

INTRUSIVES

At each deposit the porphyritic quartz monzonite intrusives form a series of irregular subvertical stocks and dykes (Fig. 10). At E22, a swarm of at least seven small pipes and dykes with plan dimensions of less than 20 by 50 m occur within a plan area of 200 by 250 m. At E27, a larger north oriented stock having plan dimensions of 100 by 280 m is accompanied by several smaller pipes and dykes within a plan area of 200 by 300 m. At both deposits, the intrusives have been drilled to 400 m below surface and appear to coalesce at depth. The larger intrusive at E27 is thought to have been formed by several separate intrusions, although it has not yet been possible to trace each intrusive phase.

The intrusives are crowded, porphyritic monzonite to quartz monzonite, composed of 20 to 60% plagioclase, occurring as 2 to 3 mm long phenocrysts in a groundmass varying from equigranular to aphanitic. Biotite appears to have been the principal mafic component. Small quartz phenocrysts comprise up to 10% of the rock, with 1 to 2 cm diameter euhedral zoned potassium feldspar 'megacrysts' forming up to 2% of the host rock. Volcanic xenoliths are common, more rarely xenoliths of earlier intrusives and small sulphide blebs may be present. Intrusive contacts range from sharp interfaces to zones of intrusive breccia from 0.1 to 6 m wide. Chilled margins are generally only weakly developed. Both the E22 and E27 deposits are cut by several narrow, NE trending, subvertical, post-mineralisation basaltic dykes.

ALTERATION AND METAMORPHISM

Fracture controlled potassic alteration is the dominant alteration style at E22 and E27 (Fig. 3c). It is developed within the monzonite intrusives and the surrounding volcanics and occurs as potassium feldspar fracture fillings and selvages to the mineralised quartz and carbonate veins. Pervasive potassium feldspar flooding is developed only in restricted zones. Secondary biotite may accompany the feldspar as either a vein component or as a vein envelope, and is locally developed in the matrix of the more mafic volcanics. At both deposits the outer zones display a weakly developed propylitic alteration assemblage of carbonate-chlorite or epidote ± pyrite, with a prominent pink zeolite-carbonate vein assemblage.

A contact metamorphic alteration assemblage of biotite-magnetite-pyroxene is developed in the volcanics immediately surrounding the E27 intrusives. Secondary magnetite blebs up to 4 mm diameter can comprise up to 3% of the rock. A distinct annular magnetic 'high' with a central 'low' occurs over the E27 deposit. Zones of secondary magnetite are less well developed at the E22 deposit.

STRUCTURE

Volcanic rocks surrounding the intrusives are generally strongly fractured and veined by quartz, potassium feldspar and calcite. Gypsum veining, which is common at the E26 deposit (Heithersay, 1986), is very rare at E22 and E27.

Several post-mineralisation faults occur at each deposit. Many faults are partially healed by quartz-carbonate veins which carry up to 5% combined galena, sphalerite, chalcopyrite and pyrite, and are accompanied by zones of strong sericite alteration. At E22 a major 070° trending subvertical fault or fault system bisects the deposit. An apparent 20 m vertical movement, south block down, is indicated by the displacement of the volcanic marker horizon. Displacements on other faults appear to be small.

The faulting at E27 is less well understood. Information to date suggests that there are two subvertical faults similar in trend to the major fault at E22, one at the southern end of the deposit and another at the northern end. Displacements along these and other minor faults are interpreted to be relatively small.

MINERALISATION

Sulphide

Copper-gold mineralisation is disseminated and fracture controlled. The 0.6% copper equivalent contour has plan dimensions of 180 by 200 m at E22, and 150 by 300 m at E27 (Fig. 10). Both deposits are sulphur poor systems, with sulphides rarely exceeding 4%. Bornite is the dominant copper sulphide, with primary chalcocite occurring as blebs and intergrowths within the bornite in the higher grade zones. Chalcopyrite is dominant in the marginal and lower grade peripheral zones. Pyrite occurs in the outer zones, but rarely exceeds 1% of the rock.

Gold occurs within and rimming bornite, usually as fine blebs less than 5 μm in diameter. Fine gold has been recorded within pyrite and associated with silicates, and rarely within carbonate-zeolite veins. Where bornite is the dominant copper sulphide, the copper to gold ratio is approximately 1% copper to 1 g/t gold. Gold grades decrease significantly in the outer chalcopyrite zones. The copper : gold ratio does not appear to alter with depth within the known vertical extent of the deposits.

At E22 mineralisation is dominantly fracture controlled, occurring as small sulphide grains in veins and fine fractures or as fine disseminated grains in alteration envelopes surrounding the veins. Pure sulphide veins are rare. The highest grades occur in the volcanics adjacent to the intrusive contacts, with grades decreasing into the centres of the larger monzonite intrusives and decreasing out into the surrounding volcanics. Small disseminated blebs of chalcopyrite and bornite occur within the monzonite intrusives, but the grade of this style of mineralisation rarely exceeds 0.5% copper. A small breccia pipe within a monzonite intrusive at E22 is characterised by strong sericite alteration and chalcopyrite mineralisation. Numerous small pebble dykes, up to 1 m wide and carrying bornite and chalcopyrite mineralisation, have been observed in drill core.

At E27 a greater proportion of the disseminated and fracture controlled copper-gold mineralisation is hosted by the intrusives than at E22. At E27 a breccia pipe with plan dimensions of 25 by 50 m is known for a vertical extent of 140 m, occurring within the larger monzonite intrusive. The partially rotated, angular, monzonite fragments are healed by quartz, dolomite-calcite-magnesite, coarsely crystalline muscovite, biotite, potassium feldspar, barite, sericite, coarse bornite, chalcocite and chalcopyrite. Copper grades can exceed 5% within this pipe. A second smaller breccia pipe occurs on the western contact of the E27 monzonite.

Other minerals identified in trace amounts as inclusions within bornite-are tennantite, galena, covellite, gersdorffite (in the E27 breccia pipe), several tellurides and selenides. Galena and sphalerite also occur in late quartz-carbonate veins associated with faulting.

Oxide

Within the kaolinised weathering zone, which is 5 to 45 m thick, the copper sulphides have been oxidised, with most copper being leached to lower levels. Some residual copper occurs within iron and manganese oxide minerals (goethite, hematite, limonite, jarosite and pyrolusite) and within a nontronite clay. The gold has been partially mobilised to lower levels within the kaolinised zone, and occurs in a residual zone with grades two or three times higher than the underly-

ing primary sulphide zones. The plan dimensions of the oxide gold mineralisation are also larger than the dimensions of the primary sulphide mineralisation, possibly due to dispersal during weathering.

Secondary copper mineralisation occurs above the primary sulphide mineralisation, in fractured rock between the base of the kaolinised zone and the base of oxidation. The principal oxide copper mineral is malachite, with azurite and atacamite also present. Gold also occurs in this zone. Copper and gold grades are only slightly greater in this zone than in the underlying primary sulphide zone.

A 1 to 3 m thick zone of secondary copper enrichment occurs at or just below the base of oxidation, with secondary chalcocite occurring as fine blebs and fracture fillings or as rims on remnant primary bornite and chalcopyrite. Tenorite, cuprite and native copper are occasionally present.

ORE GENESIS

E22, E26N and E27 are concentrically zoned, pipe-like bodies of stockwork copper-gold mineralisation. They are centred on multiphase quartz monzonite porphyry intrusives which are themselves satellites to the larger zoned monzonitic to dioritic stock known as the Endeavour 31 stock.

Textural and spatial evidence suggests that the volcanics in the region of the deposits were initially stressed by a combination of boiling fluids emanating from fractures through the side of the Endeavour 31 stock and the stress regime imposed by the Endeavour linear structure. This initial overpressuring led to brittle failure of the rock with the resultant massive network of fine fractures through which vapour and very saline brines permeated.

The early NaCl and KCl rich fluids reacted extensively with the wallrock, due to the massive surface area exposed by the fracturing, to form the potassic alteration halo. The iron rich mafic trachyandesites that host E22 and E27 buffered the hydrothermal fluids to force biotite to be the dominant potassic mineral. In contrast, potassium feldspar is the main part of the potassic halo at E26N due, in part, to the buffering capacity of the potassium rich trachytes.

At E26N, fluid inclusions record at least three thermal events beginning with magmatic temperatures. Bornite deposition is clearly linked with magnetite destruction. Anhydrite deposition at this stage also removed oxidised sulphur species from the ore fluid promoting sulphide deposition. Total failure of the host rocks allowed through-going stockwork veining to develop as well as intrusion of the first quartz monzonite porphyry. Propagation of stockwork through the inward crystallisation and carapace brecciation of the QMP1 intrusive is favoured (Burnham, 1979), but massive fluid flux from deeper magma sources must have proceeded also, as the QMP1 intrusive mass is insufficient, by an order of magnitude, to generate enough silica and copper to form an ore deposit (P.S. Heithersay, unpublished data, 1989). Wall rock reaction was markedly less at this stage due to rapid silica deposition armouring the walls of the veins. This means that mineral deposition at this stage was primarily fluid controlled, hence the evidence of boiling may be important as a controlling factor in the deposition of the gold rich bornite.

Vein dyke formation and magmatic/hydrothermal brecciation preceded the intrusion of a second quartz monzonite porphyry (QMP2). The effective stoping of a mineralised stockwork system is reflected in some unusual features, such as massive sulphide clasts in the QMP2. This remobilisation of mineralisation contributed to the upgrading of the E26 high grade pipe and has significantly altered the geometry of the ore zone.

The later QMP2 developed a significant but weaker mineralisation and alteration system compared to QMP1, strongly suggesting that the main mass of volatiles had been removed from the parent melt by this stage.

E22 and E27 share a similar genetic parentage to E26N, with differences largely explained by dissimilar host rocks. One difference that has yet to be resolved is the high gold : copper ratio of E22 and E27 as compared to E26N.

Phyllic alteration zones are developed peripheral to E26N, but are absent from E22 and E27. This alteration style always overprints the mineralised potassic assemblages. These zones are not symmetrically disposed with respect to the deposits and appear to be controlled by later regional features.

ACKNOWLEDGEMENTS

The authors would like to acknowledge the invaluable contributions made by the many geoscientists and other Geopeko staff who have worked on and contributed to the understanding of the Goonumbla porphyry deposits. The authors are particularly indebted to P.G. Dunn, M.C. Love, G.J. Jones and G.O. Arnold, and to J.L. Walshe of The Australian National University. Permission to publish by Peko Wallsend Limited is gratefully acknowledged.

REFERENCES

Bowman, H.N., Hobbs, J.J. and Barron, L.M., 1977. The Goonumbla copper district north west of Parkes, central western New South Wales, *Geol. Surv. N.S.W. Rep.* GS1977/095 (unpublished).

Bowman, H.N., Richardson, S.J. and Dolanski, J., 1982. Narromine, New South Wales — 1:250 000 metallogenic map SI 55–3. Mine data sheets and metallogenic study, *Geol. Surv. N.S.W.*

Burnham, C.W., 1979. Magmas and hydrothermal fluids, in *Geochemistry of Hydrothermal Ore Deposits*, 2nd Ed. (Ed. H.L. Barnes), pp. 71–136 (John Wiley and Sons: New York).

Carne, J.E., 1908. The copper mining industry and the distribution of copper ores in New South Wales, *Geol. Surv. N.S.W. Miner. Resour.*, 6: 280–281.

Clarke, I., 1985. Primary mineralisation in the Forbes-Parkes-Peak Hill-Tomingley gold belt, *Geol. Surv. N.S.W. Rep.* GS1985/123 (unpublished).

Clarke, I., 1987. Petrology of igneous rocks associated with gold and copper mineralization in the Parkes area, *Geol. Surv. N.S.W. Rep.* GS1985/121 (unpublished).

Cooper, R.A. and Grindley, G.W., (Eds), 1982. *Late Proterozoic to Devonian Sequences of Southeastern Australia, Antarctica and New Zealand and Their Correlation, Geol. Soc. Aust. Spec. Publ.* 9.

Cox, K.G., Bell, J.D. and Pankhurst, R.J., 1979. *The Interpretation of Igneous Rocks* (George Allen and Unwin: London).

Cuddy, A.S. and Kesler, S.E., 1982. Gold in the Granisle and Bell Copper porphyry copper deposits, British Columbia, in *Precious Metals in the Northern Cordillera* (Ed. A.A. Levinson), pp. 139–155 (The Association of Exploration Geochemists: Rexdale, Ontario).

Gustafson, L.B. and Hunt, J.P., 1975. The porphyry copper deposit at El Salvador, Chile, *Econ. Geol.*, 70: 857–912.

Heithersay, P.S., 1986. Endeavour 26 North copper-gold deposit, Goonumbla, N.S.W. — paragenesis and alteration zonation, in *Publications of the 13th CMMI Congress, Vol. 2, Geology and Exploration* (Ed. D.A. Berkman), pp. 181–189 (The 13th Congress of the Council of Mining and Metallurgical Institutions: Melbourne; and The Australasian Institute of Mining and Metallurgy: Melbourne).

Jones, G.J., 1985. The Goonumbla porphyry copper deposits, New South Wales, *Econ. Geol.*, 80: 591–613.

Joplin, G.A., 1968. The shoshonite association: a review, *J. Geol. Soc. Aust.*, 15: 275–294.

Krynen, J.P., 1984. Geological setting of mineralisation in the Parkes area, *Geol. Surv. N.S.W. Rep.* GS1984/031 (unpublished).

Morrison, G.W., 1980. Characteristics and tectonic setting of the shoshonite rock association, *Lithos*, 13: 97–108.

Peko Wallsend Limited, 1987. *Annual Report for 1987* (Peko Wallsend Limited: Sydney).

Picket, J.W., 1985. Plant fossils from Milpose, NE of Bogan Gate, *Geol. Surv. N.S.W. Palaeontolog. Rep.* 1985/05, GS1985/124 (unpublished).

Roedder, E., 1984. *Fluid Inclusions, Reviews in Mineralogy Vol. 12* (Ed. P.H. Ribbe) (Mineralogical Society of America: Washington, D.C.).

Scheibner, E., 1975. Definition and review of structural elements, in *The Mineral Deposits of New South Wales* (Eds N.L. Markham and H. Basden), pp. 108–113 (Geological Survey of New South Wales: Sydney).

Scheibner, E., 1976. *Explanatory Notes on the Tectonic Map of New South Wales, Scale 1:1 000 000* (Geological Survey of New South Wales: Sydney).

Sherwin, L., 1973. Stratigraphy of the Forbes-Bogan Gate district, *Geol. Surv. N.S.W. Rec.*, 15(1): 47–101.

Sherwin, L., 1975. Silurian graptolites from the Forbes Group, New South Wales, *Geol. Surv. N.S.W. Rec.*, 16(3): 227–237.

Sherwin, L., 1979. Age of the Nelungaloo Volcanics, near Parkes, *Geol. Surv. N.S.W. Q. Notes*, 35: 15–18.

Sherwin, L., Clarke, I. and Krynen, J.P., 1987. Revision of stratigraphic units in the Forbes-Parkes-Tomingley district, *Geol. Surv. N.S.W. Q. Notes*, 67: 1–23.

Sillitoe, R.H. and Gappe, I.M., Jr., 1984. Philippine porphyry copper deposits: Geological setting and characteristics, UNDP, Technical Support for Regional Off-shore Prospecting in East Asia (RAS/81/120), *CCOP Tech. Publ.* 14.

Tenison Woods, K., 1983. Interpretation of regional aeromagnetic and gravity data for the Forbes and Narromine 1:250 000 sheets, *Geol. Surv. N.S.W. Rep.* GS1983/200 (unpublished).

Tenison Woods, K., 1985. Qualitative interpretation of detailed aeromagnetic and gravity data within the Forbes-Parkes-Tomingley area, N.S.W., *Geol. Surv. N.S.W. Rep.* GS1984/308 (unpublished).

Titley, S.R., 1982. The style and progress of mineralisation and alteration in porphyry copper systems; American Southwest, in *Advances in Geology of the Porphyry Copper Deposits; Southwestern North America* (Ed. S.R. Titley), pp. 93–116 (University of Arizona Press: Tucson, AZ).

Wallace, S.R., MacKenzie, W.B., Blair, R.G. and Muncaster, N.K., 1978. Geology of the Urad and Henderson molybdenite deposits, Clear Creek County, Colorado, with a section on a comparison of these deposits with those at Climax, Colorado, *Econ. Geol.*, 73: 325–368.

Wyborn, D., 1977. Discussion: the Jindabyne thrust and its tectonic, physiographic and petrogenetic significance, *J. Geol. Soc. Aust.*, 24: 233–236.

APPENDIX 6

Paper: 40 Ar/39Ar and U-Pb Geochronology of the Goonumbla Cu-Au Deposits, New South Wales.

1990, Perkins, C., McDougall, I., Claoue – Long, J.C. and Heithersay, P.S.

Economic Geology V. 85, p 1808 – 1824.

Economic Geology
Vol. 85, 1990, pp. 1808–1824

$^{40}Ar/^{39}Ar$ and U-Pb Geochronology of the Goonumbla Porphyry Cu-Au Deposits, New South Wales, Australia

CAROLINE PERKINS,

Department of Geology and Research School of Earth Sciences, Australian National University, G.P.O. Box 4, Canberra, A.C.T. 2601, Australia

IAN MCDOUGALL, JONATHAN CLAOUÉ-LONG,

Research School of Earth Sciences, Australian National University, G.P.O. Box 4, Canberra, A.C.T. 2601, Australia

AND PAUL S. HEITHERSAY

Geopeko, Alluvial and Clarke Streets, Parkes, New South Wales 2870, Australia

Abstract

The $^{40}Ar/^{39}Ar$ technique of K-Ar dating has been used to determine the age of hydrothermal sericite associated with mineralization in the Goonumbla porphyry copper-gold deposits, Lachlan fold belt, New South Wales, Australia. The $^{40}Ar/^{39}Ar$ age spectra from Goonumbla hydrothermal sericite indicate that vein and groundmass (potassic and phyllic) alteration were broadly contemporaneous at 439.2 ± 1.2 Ma (1σ). The $^{40}Ar/^{39}Ar$ dates obtained from hydrothermal alkali feldspar are considerably younger than those from coeval hydrothermal sericite. U-Pb dating of magmatic zircons by ion microprobe yields an age of 438.5 ± 3.6 Ma (1σ) for the Nelungaloo Volcanics which underlie the mineralized Goonumbla sequence, providing a maximum age for mineralization and suggesting that the two successions are largely coeval.

The $^{40}Ar/^{39}Ar$ age spectra obtained in this investigation from fine-grained sericite illustrate the amenability of this hydrothermal phase to dating by the $^{40}Ar/^{39}Ar$ technique and suggest that there is considerable potential for application of this dating method to Phanerozoic ore deposits. The close agreement in ages between the $^{40}Ar/^{39}Ar$ and U-Pb results gives confidence in the application of both dating techniques to altered Paleozoic rocks.

Introduction

HIGH precision dating of alteration minerals and host rocks to mineral deposits provides information important for the understanding of ore genesis. Problems may be encountered, however, when determining the age of hydrothermal alteration and host rocks in regions overprinted by later thermal events; for example, K-Ar dates obtained on samples in areas which have undergone repeated deformation and magmatism may be of questionable value, reflecting ages between the time of formation and subsequent events. A recent investigation by Snee et al. (1988) has shown that the $^{40}Ar/^{39}Ar$ variant of the K-Ar dating method has considerable potential in determining the age of hydrothermal minerals. The advantages of the $^{40}Ar/^{39}Ar$ technique over conventional K-Ar dating include greater precision, making possible the resolution of closely spaced events, and the possibility of determining the timing of a reheating episode. In addition, if a mineral has undergone only partial loss of its radiogenic argon ($^{40}Ar^{*}$) during a postcrystallization thermal event, an estimate of the original formation age may be obtained by the $^{40}Ar/^{39}Ar$ step heating method in favorable cases.

Propylitic alteration of igneous potassium-bearing phases commonly is widespread in mineralized districts, making it difficult to obtain an emplacement age for the host succession by dating these phases using the K-Ar or $^{40}Ar/^{39}Ar$ methods. In altered rocks proximal to an ore deposit ion microprobe U-Pb analysis offers advantages over conventional dissolution analysis of zircons similar to those of $^{40}Ar/^{39}Ar$ over conventional K-Ar dating. Where some zircons have undergone postmagmatic alteration, multiple intrazircon analyses allow the crystallization age to be distinguished from zircon domains that have lost radiogenic Pb.

Recently, mineral exploration in the Lachlan fold belt, of New South Wales, Australia, has been directed toward volcanic- and intrusive-related gold (and base metal) deposits such as epithermal, porphyry, and skarn systems, but, because little isotopic dating has been undertaken in the vicinity of these deposits, the age of mineralization and of the host rocks has been a matter of speculation. The Goonumbla porphyry copper-gold deposits near Parkes, New South Wales, were selected for study because a detailed investigation of the systems, including description of the paragenesis of hydrothermal phases, had been un-

0361-0128/90/1155/1808-17$3.00

dertaken (Heithersay, 1986, and unpub. data; Heithersay et al., 1990) and because the deposits are relatively undeformed. The aims of this investigation are to use the $^{40}Ar/^{39}Ar$ step heating method to date hydrothermal sericite associated with mineralization, to utilize U-Pb dating by ion microprobe on magmatic zircons to determine the age of volcanic rocks which underlie the deposit, and to combine both types of isotopic dating to establish the timing of mineralization relative to the host volcanic rocks.

Geologic Setting

The Goonumbla deposits are located 25 km northwest of Parkes (Fig. 1) in the northeast portion of the Bogan Gate synclinorial zone, one of the north-south-trending tectonic subdivisions of the Lachlan fold belt (cf. Scheibner, 1972). The host rocks to Goonumbla comprise part of an Early Ordovician to Late Ordovician-Early Silurian mafic to intermediate volcanic and intrusive sequence which crops out in central New South Wales (Webby, 1976). In part it is shoshonitic (Owen and Wyborn, 1979; Clarke, 1987; Heithersay et al., 1990) and forms a gold (and copper) province (Wyborn, 1988; Wyborn and Cameron, 1990). Mineralization in this succession other than Goonumbla includes the Browns Creek and Sheahan-Grants gold skarn deposits, the Glendale monzonite-hosted gold deposit (Perkins et al., in prep.), and the Gidginbung epithermal gold deposit (Thompson et al., 1986).

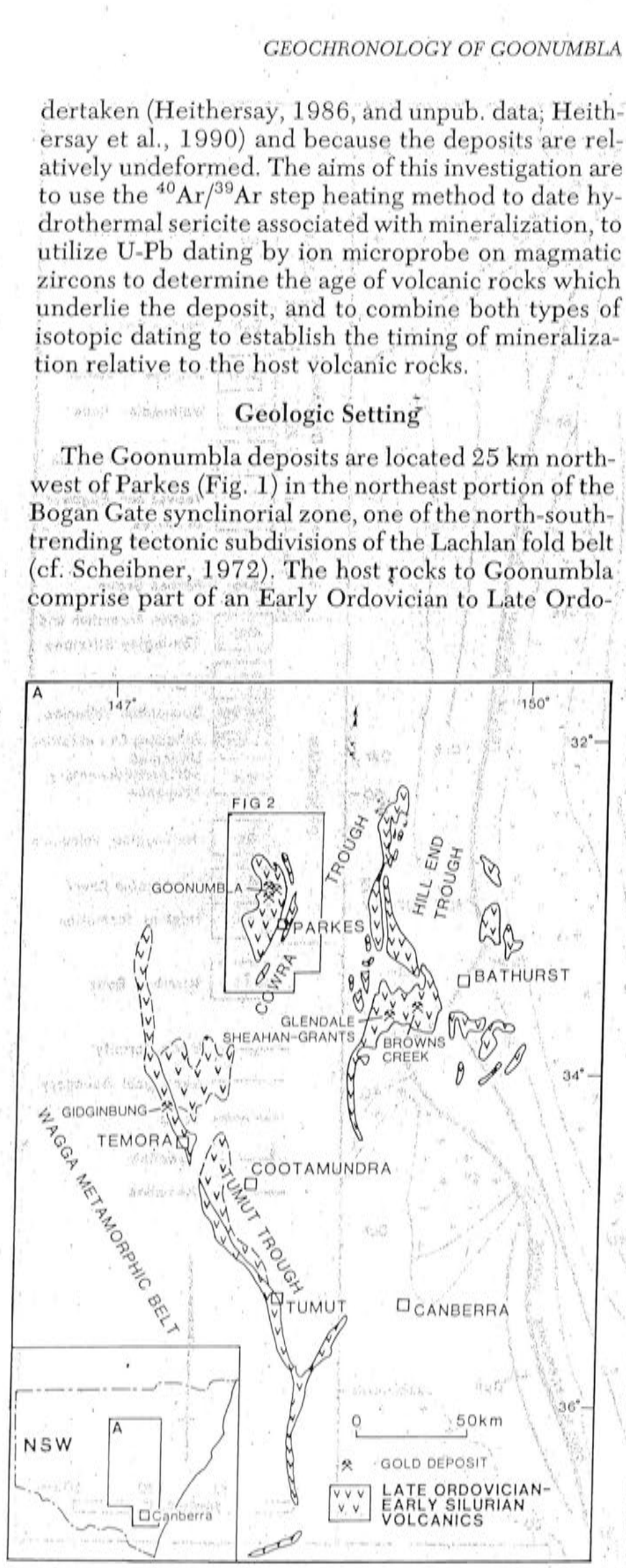

FIG. 1. Distribution of Ordovician-Early Silurian volcanics in the Lachlan fold belt, New South Wales, and location of the Goonumbla, Sheahan-Grants, Browns Creek, Gidginbung, and Glendale deposits.

In the vicinity of Parkes, the Ordovician succession is overlain to the north by Late Silurian sediments, overlain to the west by Devonian sediments and volcanics, and flanked to the east by Devonian granites and sediments (Fig. 2; Heithersay et al., 1990). The oldest rocks in the region are the Nelungaloo Volcanics, composed of high K calc-alkaline andesite (latite) lavas and shoshonites (after data presented by Clarke, 1987), fine- to coarse-grained volcaniclastic rocks, cherts, and limestones (Sherwin, 1973, 1979; Sherwin et al., 1987). Diorite to monzonite intrusions up to 5 km long and 2 km wide are emplaced into the layered succession (Heithersay et al., 1990). The base of the Nelungaloo Volcanics is not exposed, and the precise relationship between this sequence and the overlying Goonumbla Volcanics is not known (Heithersay et al., 1990).

The Goonumbla Volcanics largely comprise potassium-rich trachyandesites (latites) and minor shoshonites (Heithersay et al., 1990) and consist of interlayered flows and pyroclastic and epiclastic rocks which overlie a basal limestone and fine- to coarse-grained volcaniclastic rock sequence (Sherwin et al., 1987). The volcanic succession is intruded by bodies ranging in composition from diorite through to monzonite and quartz syenite; these exhibit similar compositional trends as the host volcanic rocks and are interpreted to be related to and coeval with the latter (Heithersay et al., 1990). The Wombin Volcanics, now considered to be part of the Goonumbla Volcanics (cf. Bowman et al., 1977; Jones, 1985), directly overlie the trachyandesite sequence and are largely composed of trachyte flows and pyroclastic and epiclastic rocks (Heithersay et al., 1990). Diorite to quartz monzonite intrusions are emplaced in the Wombin succession.

The overall sequence is largely undeformed but is folded in the broad, southwest-plunging Milpose syncline in the vicinity of the Goonumbla deposits. Bedding dips of 20° occur on the limbs of the structure, and cleavage is virtually nonexistent. Regional metamorphic grade is zeolite to lower greenschist facies, with prehnite, pumpellyite, chlorite, and epidote present in the succession.

dertaken (Heithersay, 1986, and unpub. data; Heithersay et al., 1990) and because the deposits are relatively undeformed. The aims of this investigation are to use the $^{40}Ar/^{39}Ar$ step heating method to date hydrothermal sericite associated with mineralization, to utilize U-Pb dating by ion microprobe on magmatic zircons to determine the age of volcanic rocks which underlie the deposit, and to combine both types of isotopic dating to establish the timing of mineralization relative to the host volcanic rocks.

Geologic Setting

The Goonumbla deposits are located 25 km northwest of Parkes (Fig. 1) in the northeast portion of the Bogan Gate synclinorial zone, one of the north-south-trending tectonic subdivisions of the Lachlan fold belt (cf. Scheibner, 1972). The host rocks to Goonumbla comprise part of an Early Ordovician to Late Ordovician-Early Silurian mafic to intermediate volcanic and intrusive sequence which crops out in central New South Wales (Webby, 1976). In part it is shoshonitic (Owen and Wyborn, 1979; Clarke, 1987; Heithersay et al., 1990) and forms a gold (and copper) province (Wyborn, 1988; Wyborn and Cameron, 1990). Mineralization in this succession other than Goonumbla includes the Browns Creek and Sheahan-Grants gold skarn deposits, the Glendale monzonite-hosted gold deposit (Perkins et al., in prep.), and the Gidginbung epithermal gold deposit (Thompson et al., 1986).

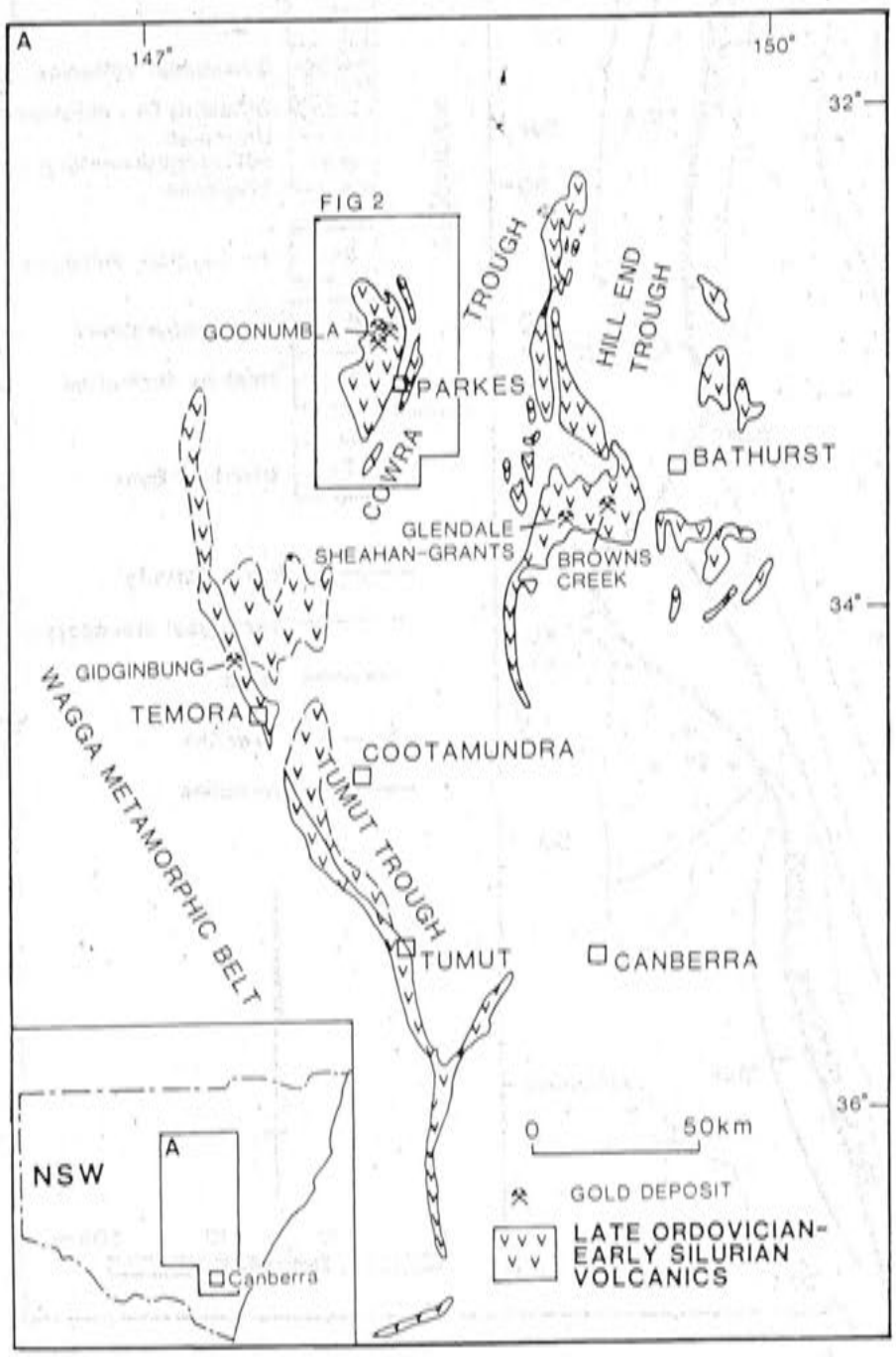

FIG. 1. Distribution of Ordovician-Early Silurian volcanics in the Lachlan fold belt, New South Wales, and location of the Goonumbla, Sheahan-Grants, Browns Creek, Gidginbung, and Glendale deposits.

In the vicinity of Parkes, the Ordovician succession is overlain to the north by Late Silurian sediments, overlain to the west by Devonian sediments and volcanics, and flanked to the east by Devonian granites and sediments (Fig. 2; Heithersay et al., 1990). The oldest rocks in the region are the Nelungaloo Volcanics, composed of high K calc-alkaline andesite (latite) lavas and shoshonites (after data presented by Clarke, 1987), fine- to coarse-grained volcaniclastic rocks, cherts, and limestones (Sherwin, 1973, 1979; Sherwin et al., 1987). Diorite to monzonite intrusions up to 5 km long and 2 km wide are emplaced into the layered succession (Heithersay et al., 1990). The base of the Nelungaloo Volcanics is not exposed, and the precise relationship between this sequence and the overlying Goonumbla Volcanics is not known (Heithersay et al., 1990).

The Goonumbla Volcanics largely comprise potassium-rich trachyandesites (latites) and minor shoshonites (Heithersay et al., 1990) and consist of interlayered flows and pyroclastic and epiclastic rocks which overlie a basal limestone and fine- to coarse-grained volcaniclastic rock sequence (Sherwin et al., 1987). The volcanic succession is intruded by bodies ranging in composition from diorite through to monzonite and quartz syenite; these exhibit similar compositional trends as the host volcanic rocks and are interpreted to be related to and coeval with the latter (Heithersay et al., 1990). The Wombin Volcanics, now considered to be part of the Goonumbla Volcanics (cf. Bowman et al., 1977; Jones, 1985), directly overlie the trachyandesite sequence and are largely composed of trachyte flows and pyroclastic and epiclastic rocks (Heithersay et al., 1990). Diorite to quartz monzonite intrusions are emplaced in the Wombin succession.

The overall sequence is largely undeformed but is folded in the broad, southwest-plunging Milpose syncline in the vicinity of the Goonumbla deposits. Bedding dips of 20° occur on the limbs of the structure, and cleavage is virtually nonexistent. Regional metamorphic grade is zeolite to lower greenschist facies, with prehnite, pumpellyite, chlorite, and epidote present in the succession.

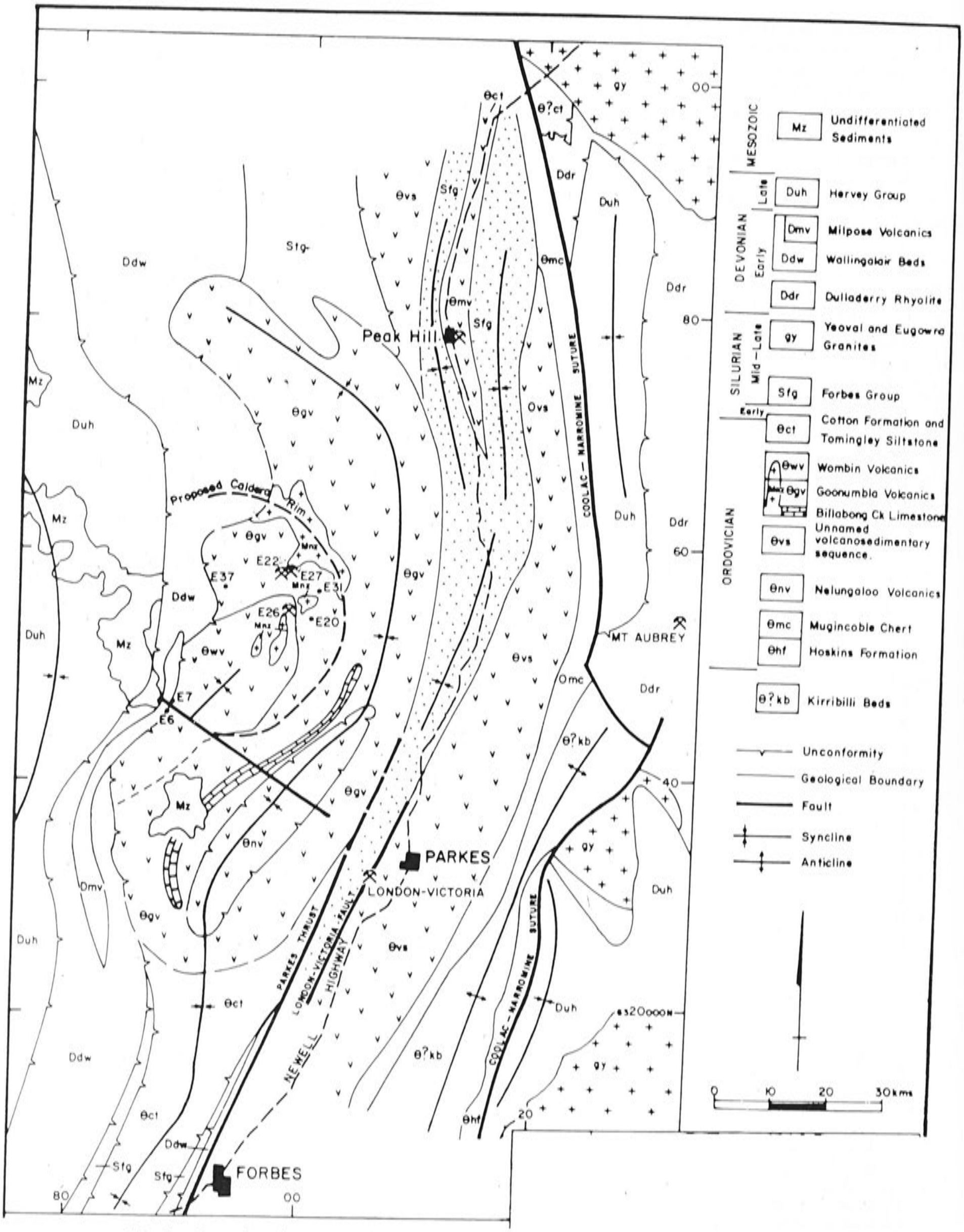

FIG. 2. General geologic map of the Parkes area, showing the distribution of the Nelungaloo, Goonumbla, and Wombin Volcanics (from Heithersay et al., 1990). E22, 26, 27, and 37 refer to the Goonumbla Endeavour deposits.

Goonumbla porphyry copper-gold deposits

Three major porphyry copper-gold deposits (Endeavour 22, 26, and 27) and eight minor centers of mineralization are located within the Goonumbla-Wombin volcanic sequence (Fig. 2). All known mineralization occurs within a circular feature, interpreted by Jones (1985) as a collapsed caldera, bounded in part by a ring dike of diorite to monzonite composition. Detailed descriptions of mineralization, alteration, and host rocks are presented by Jones (1985), Heithersay (1986), and Heithersay et al. (1990).

The porphyry copper-gold mineralization is ubiquitously associated with relatively small, subvertical, pipelike intrusive bodies of quartz monzonite porphyry, which have diameters as great as 100 m, and may have a vertical extent of as much as 900 m. These intrusions, typically pink in color, are coarsely porphyritic with phenocrysts of plagioclase and quartz in a fine-grained potassium feldspar and quartz groundmass. Biotite, hornblende, sphene, and apatite are minor phases too altered to date (cf. Heithersay et al., 1990).

Disseminated and fracture- or vein-controlled mineralization occurs in the intrusive bodies and surrounding volcanic rocks and is associated with quartz stockwork veining (Fig. 3A). Commonly, a zonation exists from an outer pyrite zone, through a chalcopyrite-dominant zone, to a central high-grade bornite-chalcocite zone (Heithersay et al., 1990). Potassic alteration is closely associated with bornite mineralization (Jones, 1985; Heithersay, 1986; Heithersay et al., 1990, and in prep.; Fig. 3B) and the paragenetic sequence for alteration and mineralization is given in Figure 4. Early potassic alteration is biotite, followed by pink alkali feldspar (orthoclase) veining (stages 3, 4, 5, and 6), or where fracturing and veining of the host rock is more intense, alkali feldspar flooding of the groundmass (potassic zone, stage 4). Sericite is present in veins (Fig. 5A) texturally associated with alkali feldspar, quartz, sulfides, and gold (stage 4) and also occurs as part of a pervasive quartz-sericite-pyrite groundmass alteration (phyllic zone) assemblage (stage 8; Fig. 5B) which is present on a regional scale. The latter alteration overprints the vein assemblage and is related to major structures and the contact zones of intrusions (Heithersay et al., 1990). There is regional propylitic alteration of the volcanics.

Isotopic Dating

For consistency, all uncertainties in isotopic dates are discussed at the 1σ level and all ages are related to the decay constants recommended by Steiger and Jäger (1977).

Jones (1985) reported conventional K-Ar dates on igneous biotite from a relatively unaltered mafic intrusion, and a whole-rock trachyandesite sample from the vicinity of the Endeavour 22 deposit as 423 ± 6 and 427 ± 6 Ma, respectively (1σ). Using the more recent decay constants of Steiger and Jäger (1977), ages of 435 ± 6 and 431 ± 6 Ma are obtained from the same data (AMDEL dates obtained for Geopeko, reported by Clarke, 1987; Heithersay et al., 1990). These latter dates establish the minimum emplacement time of the Goonumbla Volcanics and associated intrusions as Late Ordovician to Early Silurian using the time scale of Harland et al. (1989). Prior to the present study, no dating of alteration minerals had been attempted.

K-Ar and $^{40}Ar/^{39}Ar$ dating

The K-Ar isotope dating method is based upon the accumulation of radiogenic argon ($^{40}Ar^{*}$) produced from the decay of the naturally occurring radioactive isotope of potassium, ^{40}K, which has a half life of 1,250 Ma; details of the technique are given by Dalrymple and Lanphere (1969). The $^{40}Ar/^{39}Ar$ dating method (Merrihue and Turner, 1966), a variant of the conventional K-Ar technique, is described by McDougall and Harrison (1988).

Analytical methods: The most intense sericite alteration at Goonumbla occurs in the Endeavour 26 deposit, and the coarsest grained and most pervasive examples of vein (stage 4) and groundmass (stage 8) sericite from quartz monzonite porphyry were selected from this system for analysis. Samples which exhibited no mutual intergrowth between different sericite generations were chosen, and separates of a 180- to 75-μm aggregate grain size and about 60 percent or greater purity were obtained by conventional heavy liquid and magnetic separation techniques. Contaminating phases are largely quartz and plagioclase. Quartz monzonite porphyry intrusions were sampled for alkali feldspar, and separates of the groundmass alteration from Endeavour 26 (stage 3) and 22, and vein orthoclase from Endeavour 27, 26 (stage 3), and 22 were also selected for analysis. Separates of 80 percent or greater purity of the 180- to 75-μm grain size containing some contaminating quartz and plagioclase were obtained by conventional techniques. Hydrothermal biotite was sampled but proved too fine grained for adequate separation.

Scanning electron microscope analysis of sericite separates shows that this alteration phase replaces primary igneous minerals such as plagioclase (Fig. 5C). Though some fine-grained (approximately 10 μm) material is present, the separate is largely a massive intergrowth of the secondary mineral with individual grain boundaries difficult to distinguish. Sericite is largely muscovite rather than illite as shown by X-ray diffraction (cf. Brindley and Brown, 1984); the 10 Å peak has a line breadth of about 0.2° 2θ in all samples except one groundmass sericite (122), which has a 10 Å peak line breadth of 0.4° 2θ, and

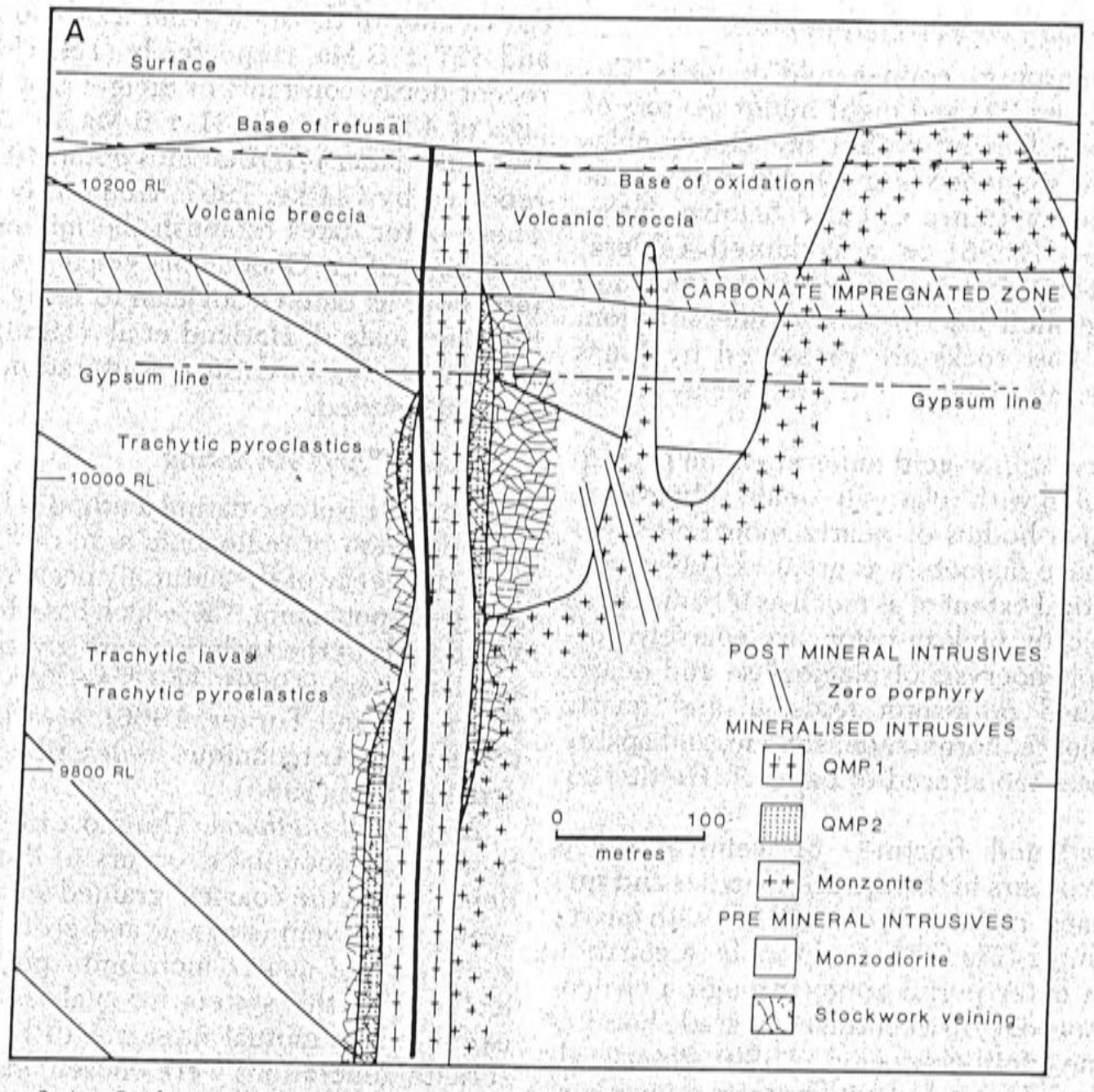

FIG. 3. A: Geologic cross section, Endeavour 26 deposit (from Heithersay et al., 1990). QMP refers to quartz monzonite porphyry intrusions.

may contain a mixture of muscovite and illite. Electron microprobe analysis reveals vein and groundmass phases to be of relatively uniform muscovite composition (Table 1). Turbid, pink, hematite-stained alkali feldspar is orthoclase (as determined by X-ray diffraction) and contains microscopic to submicroscopic albitic perthites. Electron microprobe analysis did not reveal the presence of a phase other than albite in the alkali feldspar.

Conventional K-Ar dating was undertaken on the sericite and alkali feldspar separates prior to $^{40}Ar/^{39}Ar$ dating (Table 2). Potassium was determined by flame photometry on duplicate samples of 0.05 g using an Na-Li buffer: results agreed to better than 2 percent, and commonly to better than 1 percent. Approximately 0.05 g of sample was used for each argon extraction. The sample was baked for approximately 15 hrs at about 100°C in the vacuum system prior to the extraction, then fused for 40 mins at approximately 1,400°C by means of radio frequency induction. Radiogenic argon was measured by isotope dilution, with a ^{38}Ar tracer in a mass spectrometer. Ratios were corrected for memory effects and for mass discrimination by assuming 295.5 for atmospheric $^{40}Ar/^{36}Ar$ (Nier, 1950). Precision for argon measurements is commonly about 0.5 percent (1σ), controlled mainly by uncertainties in calibration of the ^{38}Ar tracer.

Approximately 0.2 to 0.25 g of each mineral separate of sericite and alkali feldspar was packed into its own machined aluminum container for $^{40}Ar/^{39}Ar$ dating, together with a smaller, centrally located container which was packed with approximately 0.03 g Australian National University laboratory standard GA 1550 biotite (K-Ar age 97.9 Ma; McDougall and Roksandic, 1974) as flux monitor. Sample containers and corresponding flux monitors were then loaded inside a 0.2-mm-thick Cd liner to reduce the thermal neutron flux (Tetley et al., 1980), and all items were placed inside an aluminum irradiation canister. Samples were irradiated in the ×34 facility adjacent to the core of the ANSTO HIFAR reactor Lucas Heights, New South Wales, in a fast neutron flux of approximately 1×10^{-14} n/cm^2/s. The samples were irradi-

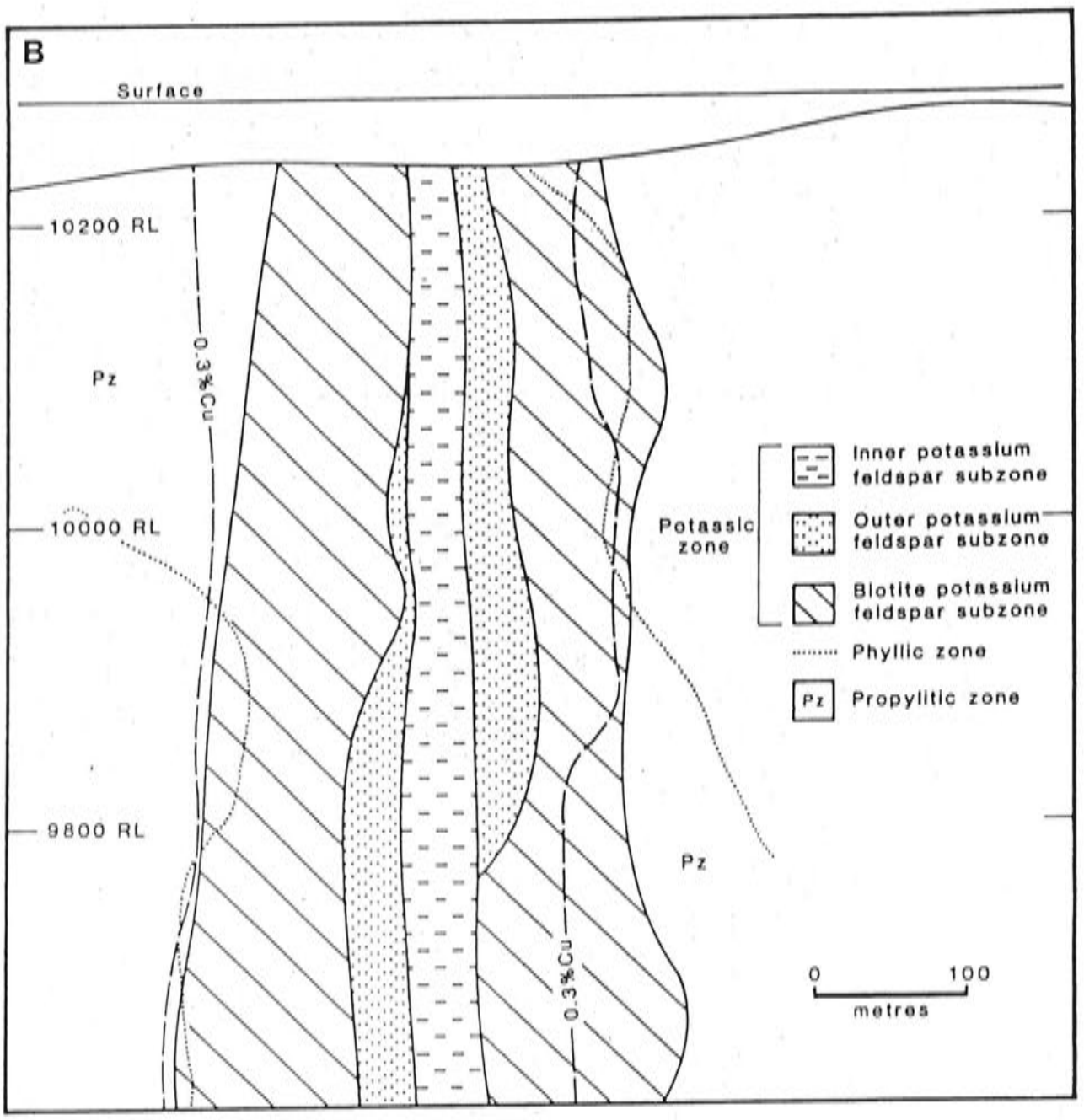

FIG. 3. B. Distribution of alteration zones, Endeavour 26 deposit (from Heithersay et al., 1990).

ated for 192 hrs, and the sample canister was inverted halfway through the irradiation to reduce the neutron fluence gradient, which was later measured to be less than 2 percent along the canister. Approximately 0.025 g of each sample was used for a total fusion experiment, and between 0.05 to 0.1 g of each sample was utilized for step heating work. Samples were consecutively placed into a resistively heated furnace, and during step heating experiments, argon was extracted at successively higher temperatures for 10 mins heating time at each designated temperature. Uncertainties in the $^{40}Ar/^{39}Ar$ ages are derived by quadratically combining precision estimates for mass spectrometer isotopic measurements and neutron fluence measurements. Data given in Table 3 are corrected for instrumental mass discrimination and for ^{37}Ar and ^{39}Ar decay during and after irradiation. Corrections for interfering reactions need to be made in calculating apparent ages. Correction factors used are $(^{36}Ar/^{37}Ar)_{Ca} = 3.20\ (\pm 0.02) \times 10^{-4}$; $(^{39}Ar/^{37}Ar)_{Ca} = 7.9\ (\pm 0.5) \times 10^{-4}$; and $(^{40}Ar/^{39}Ar)_K = 0.027$ (Tetley et al., 1980; McDougall and Harrison, 1988). Apparent K/Ca ratios were calculated using the relationship K/Ca = $2.13 \times {}^{39}Ar/{}^{37}Ar$ mole/mole determined for Australian National University laboratory standard hornblende 77–600, which has K/Ca = 0.037.

K-Ar results: The K-Ar measurements on hydrothermal groundmass and vein sericite from Goonumbla yield ages ranging from 429 ± 5 to 442 ± 6 Ma, but results for all samples cluster around 435 Ma (Table 2). The relatively poor reproducibility of the measured ages for groundmass sericite 122 may be because of sample inhomogeneity due to a mixture of plagioclase and muscovite as indicated by the poor replication of the potassium and argon measurements. The average K-Ar ages for both vein and groundmass sericite are statistically indistinguishable from each other and from the K-Ar dates reported (Clarke, 1987; Heithersay et al., 1990) on relatively unaltered lithologies adjacent to the Endeavour 22 deposit.

The alkali feldspar K-Ar ages are considerably younger than those obtained from coeval hydrothermal sericite (Table 2). The dates for hydrothermal groundmass alkali feldspar range from 374 ± 4 to 400 ± 4 Ma and the ages for vein alkali feldspar range from 392 ± 6 to 414 ± 5 Ma. Vein alkali feldspar

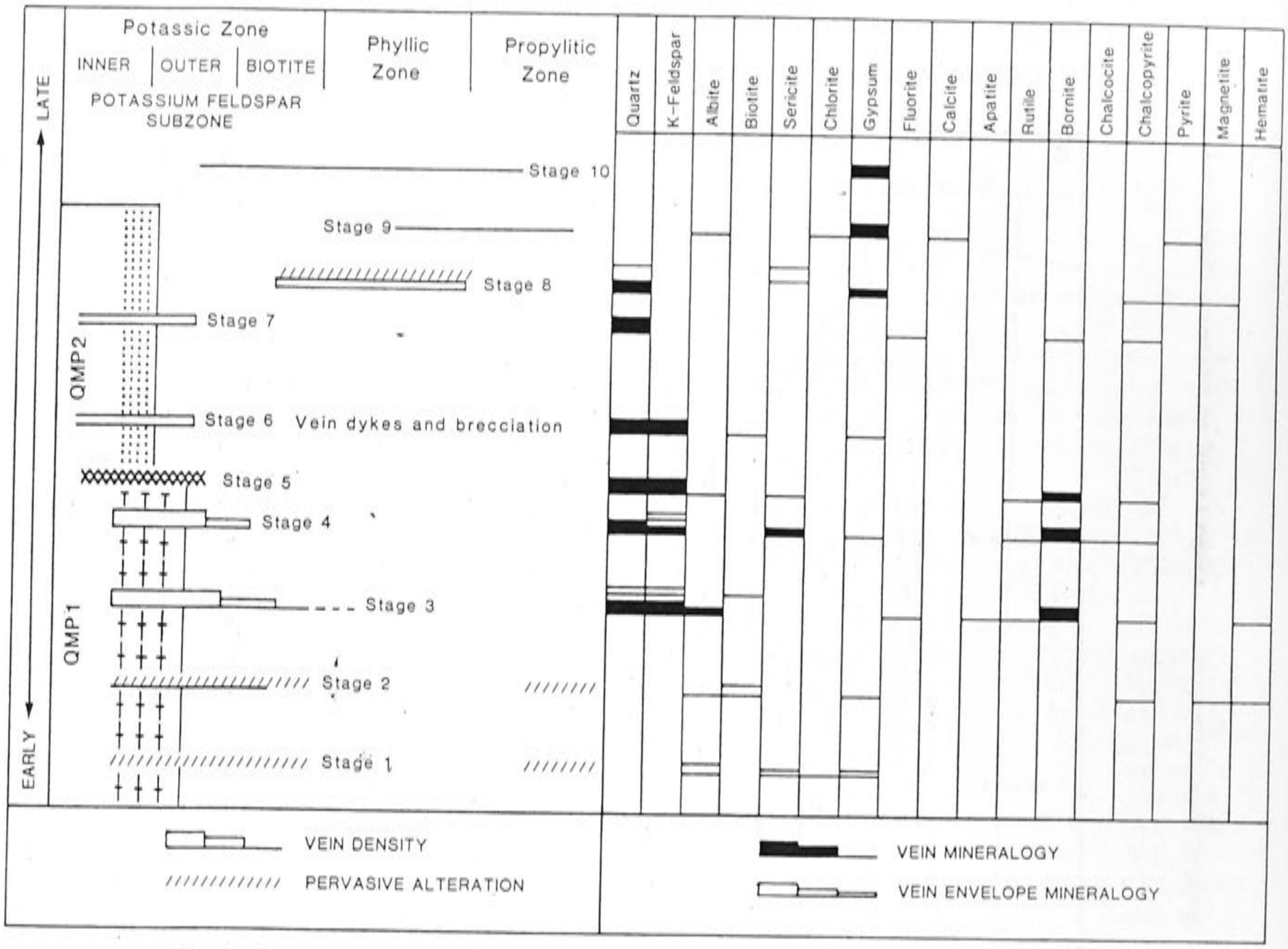

FIG. 4. Paragenetic sequence of alteration and mineralization, Endeavour 26 deposit (from Heithersay et al., 1990). Dated vein and groundmass sericite are from stages 4 and 8 alteration, respectively. Dated vein and groundmass alkali feldspar are from stage 3 alteration.

7983, Endeavour 26, has an apparent age of 392 ± 6 Ma, compared with coexisting groundmass alkali feldspar 32, which yields a date of 374 ± 4 Ma. Sample 20, groundmass alkali feldspar from Endeavour 22, has an age of 400 ± 4 Ma, and vein alkali feldspar 17 from the same deposit yields an age of 414 ± 5 Ma.

$^{40}Ar/^{39}Ar$ results: The $^{40}Ar/^{39}Ar$ step heating and total fusion data for vein and groundmass hydrothermal sericite are presented in Table 3 and Figure 6A and B.

The $^{40}Ar/^{39}Ar$ age spectrum for vein (potassic zone alteration, stage 4) sericite 120 displays an initial apparent age of approximately 424 Ma, and then rises to a flat, relatively undisturbed part of age 439.1 ± 1.1 Ma. The total fusion age of 435.9 ± 0.6 Ma is in agreement with the mathematically summed age from the step heating experiment of 435.7 Ma and statistically encompasses the average K-Ar date of 432 ± 5 Ma. Vein sericite 121 has an initial apparent age of approximately 449 Ma, decreases to an apparent age of approximately 432 Ma in the second step, and then rises monotonically to a maximum age of 438.7 ± 0.6 Ma. The total fusion date of 435.5 ± 0.5 Ma agrees with the integrated age of 434.9 Ma and the average K-Ar date of 435 ± 5 Ma.

The step heating experiment on groundmass (phyllic zone alteration, stage 8) sericite 122 yields an initial apparent age of about 420 Ma, then a spectrum which rises monotonically to a flat portion of 437.9 ± 1.1 Ma age, the last few steps showing slightly lower ages. The total fusion date of 436.5 ± 0.6 Ma agrees with the integrated age of 435.2 Ma and the average K-Ar date of 435 ± 11 Ma. Groundmass sericite 123 has an initial apparent age of approximately 370 Ma, and the spectrum then rises monotonically to an age of 441.0 ± 0.5 Ma. The total fusion date of 434.9 ± 0.7 Ma statistically encompasses the mathematically summed age of 435.2 Ma and the K-Ar date of 436 ± 5 Ma.

The high age portions of the spectra correspond to regions of low Ca/K (Fig. 6A and B), consistent with the degassing of sericite. In the case of sample

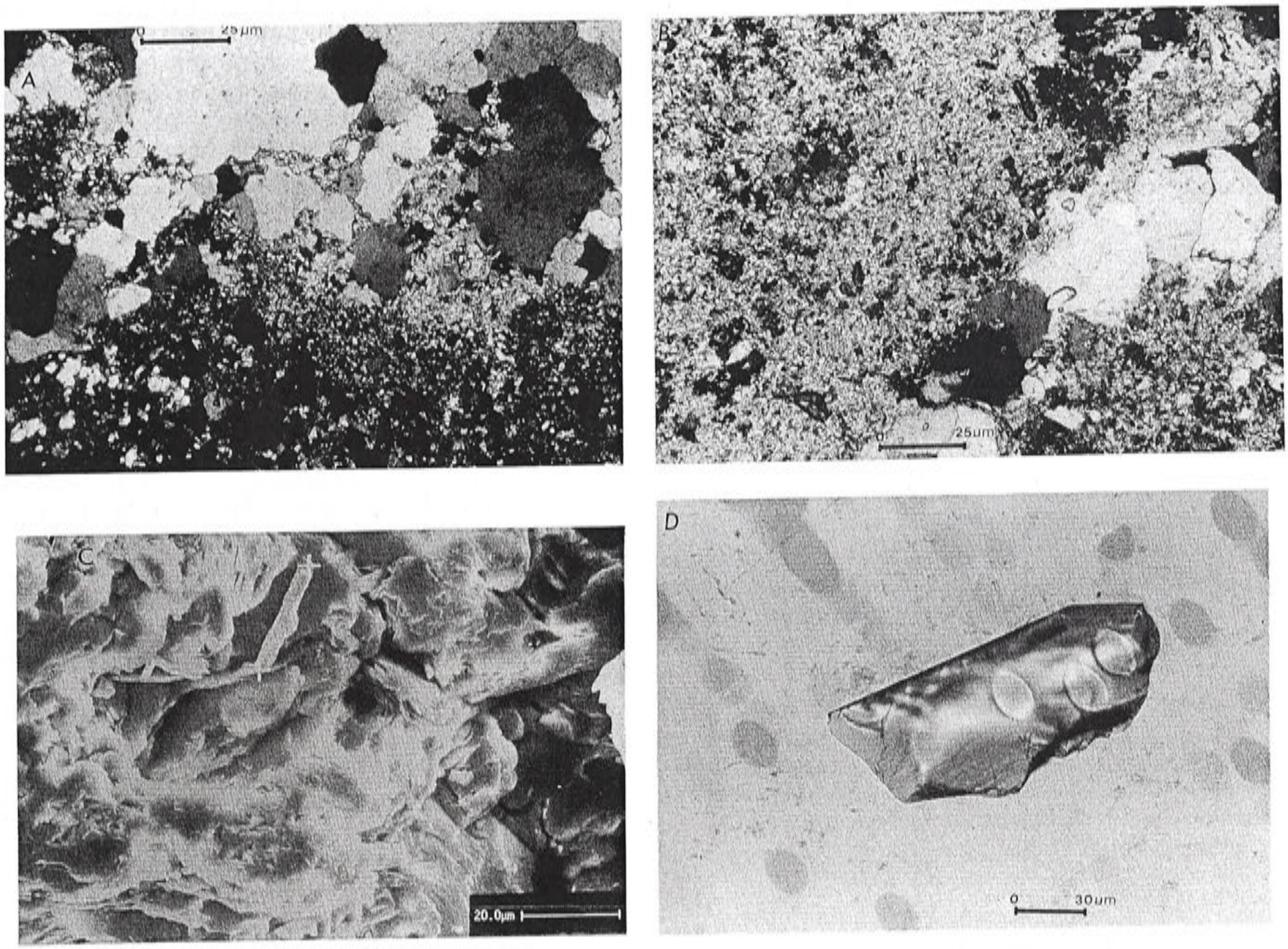

FIG. 5. Microphotographs illustrating Goonumbla hydrothermal alteration minerals. A. Vein sericite intergrown with quartz and bornite. B. Groundmass sericite overprinting a quartz bornite vein. C. Scanning electron microscope image of vein sericite. D. Magmatic zircon from the Nelungaloo Volcanics. Pits are zones analyzed by the SHRIMP ion microprobe.

122, a decrease in age in the final step is accompanied by a corresponding increase in the Ca/K ratio, suggesting that considerable plagioclase impurity in the separate may be contributing to the argon released in this portion of the spectrum. The initially high Ca/K ratios displayed by samples 122 and 120 in particular are due to some contribution of argon from partly altered igneous plagioclase.

The occurrence of a collapsed caldera structure and ring dike in the Goonumbla Volcanics suggests a subvolcanic environment of formation for the deposit and hence probable rapid cooling of the sericite to temperatures below the closure temperature for argon diffusion in muscovite (about 300°C; Harrison and McDougall, 1980). Ages derived from the higher temperature argon release are therefore taken to approximate sericite crystallization and indicate that vein alteration was broadly contemporaneous with groundmass alteration. The 441.0 ± 0.5 Ma age for sample 123, recorded from the last step in the experiment, is not statistically different from the other sericites at the 2σ confidence level. Because the spectra do show some variation from the ideal model for argon loss (e.g., the absence of a flat portion in sample 123 and the decrease in age in the last step of sample 122), it is probably not valid to compare maximum ages to establish an age difference between the samples. Therefore an average age of 439.2 ± 1.2 Ma calculated from the argon derived from the relatively undisturbed portion or highest temperature step for each sericite sample may be interpreted as an approximation of the time of alteration and mineralization at Goonumbla.

Though the first few steps in the sericite spectra generally correspond to a region where plagioclase is contributing to the released argon, in the case of sample 123 the gas in the first step indicates a rather low Ca/K; the contribution of plagioclase to the argon yielded in the next few steps is minor, and is negligible in the high-temperature steps. Monotonically rising ages are characteristic of the entire 123-age spectrum, and it is therefore concluded that this pattern is not

TABLE 1. Chemical Composition of Goonumbla Sericites

Specimen no.	Vein sericite		Groundmass sericite	
wt %	120	121	122	123
SiO_2	46.61	45.72	44.95	47.97
TiO_2	<0.09	0.30	0.33	0.18
Al_2O_3	34.12	32.87	31.98	31.51
Cr_2O_3	<0.10	<0.10	<0.10	<0.10
FeO	0.93	2.19	2.75	1.35
MnO	<0.10	<0.10	<0.10	<0.10
MgO	0.32	1.02	0.88	1.17
CaO	<0.08	<0.08	<0.08	<0.08
Na_2O	<0.17	<0.17	<0.17	<0.17
K_2O	10.12	10.56	10.48	10.06
Total	92.11	92.66	91.37	92.24
Structural formula on the basis of 22 (0)				
Si	6.359	6.283	6.290	6.546
Al	1.641	1.717	1.710	1.454
Al	3.845	3.607	3.546	3.614
Ti	0.000	0.031	0.034	0.019
Fe	0.106	0.252	0.322	0.154
Cr	0.000	0.000	0.000	0.000
Mn	0.000	0.000	0.000	0.000
Mg	0.066	0.210	0.184	0.238
Ca	0.000	0.000	0.000	0.000
Na	0.000	0.000	0.000	0.000
K	1.762	1.850	1.870	1.751
Total	13.779	13.949	13.974	13.776

All analyses made by Cameca electron microprobe, Research School of Earth Sciences, Australian National University
Total Fe calculated as Fe^{+2}

due to mixed ages caused by early degassing of a less retentive calcic contaminant but may be explained in terms of either slow cooling or partial argon loss caused by a reheating event subsequent to initial closure to argon diffusion. The subvolcanic environment of the deposit makes slow cooling unlikely, so that partial argon loss is favored. Since all the sericites are from the same deposit, it is likely that they all experienced a similar thermal history. The widespread emplacement of granitoids in the Lachlan fold belt from about 420 to 360 Ma involved a massive introduction of heat into the crust (Chappell and Stephens, 1988) and caused widespread regional metamorphism. Monzonite intrusions into Devonian sediments occur about 10 km from Goonumbla; unfortunately, the minerals proved too altered for dating work. Isotopic dating on similar composition intrusions about 50 km to the east of Goonumbla, yielded Rb-Sr whole rock-biotite isochron ages of about 400 to 360 Ma (recalculated by the authors using the decay constants of Steiger and Jäger, 1977, from data presented by Gulson and Bofinger, 1972), and the bodies nearer Goonumbla may have a similar age. The emplacement of Devonian granitoids in the Parkes area and in the Lachlan fold belt in general broadly coincides with the first step in the sericite age spectra (420–370 Ma with the exception of sample 121 which has an initially high age, possible due to excess argon), and argon loss may be attributed to the thermal event caused by the regional granitoid emplacement. When compared with the theoretical argon loss curves of Turner (1968) for aggregates of uniform spheres, most Goonumbla profiles show a small amount of loss (≤5%) during the Devonian overprinting.

The K-Ar and $^{40}Ar/^{39}Ar$ dates obtained from vein and groundmass hydrothermal alkali feldspar are considerably younger (by 20–70 Ma) than those obtained from coeval hydrothermal vein sericite. The

TABLE 2. K-Ar Dates for Goonumbla Sericite and K Feldspar

Sample no.	Alteration type, deposit[1]	K%[2]	$^{40}Ar^*$ $\times 10^{-8}$ mole/g	$100 \times \frac{^{40}Ar^*}{\Sigma Ar}$	Calc. age (Ma) ± 1 σ	Avg. age (Ma) ± 1 σ
Sericite						
120 (1)	Vein, E 26	7.973, 7.980	0.6705	99.2	429 ± 5	
120 (2)			0.6786	98.4	434 ± 5	432 ± 5
121 (1)	Vein, E 26	8.112, 8.056	0.6896	96.2	435 ± 5	
121 (2)			0.6904	98.3	435 ± 5	435 ± 5
122 (1)	Gm, E 26	5.684, 5.584	0.4894	99.0	442 ± 6	
122 (2)			0.4705	98.8	427 ± 6	435 ± 11
123 (1)	Gm, E 26	7.525, 7.434	0.6394	99.5	436 ± 5	436 ± 5
K feldspar						
32	Gm, E 26	8,094, 8.034	0.5810	90.0	374 ± 4	
20	Gm, E 22	9.940, 9.972	0.7725	96.4	400 ± 4	
7987	Vein, E 27	10.753, 10.799	0.8556	94.9	408 ± 4	
7983	Vein, E 26	8.330, 8.467	0.6392	93.2	392 ± 6	
17	Vein, E 22	9.627, 9.751	0.7821	98.3	414 ± 5	

[1] Gm denotes groundmass alteration; E 26, 27, 22 refer to the Endeavour 26, 27 and 22 deposits, respectively
[2] Determined by flame photometry

age spectra are complex, depart from the ideal Turner (1968) diffusion models, and are consequently difficult to interpret. The significantly much younger ages of the alkali feldspar relative to sericite probably reflect the low closure temperature for argon in the former mineral, so that the regional greenschist metamorphism caused considerable argon loss. Low-temperature alkali feldspar is therefore considered unsuitable for determining the age of alteration events as the mineral apparently retains little or no record of its original crystallization.

SHRIMP zircon dating

Sampling rationale: The Nelungaloo Volcanics, which underlie the host rocks to the Endeavour deposits, were selected for isotopic dating to establish whether this sequence is significantly older than the Goonumbla Volcanics. The age of the Nelungaloo Volcanics is important since they would be considered more prospective if found to be broadly contemporaneous with the Goonumbla Volcanics, which are temporally associated with mineralization. In addition, a date on the Nelungaloo Volcanics would provide a maximum age for mineralization in the stratigraphically younger Goonumbla Volcanics. The Nelungaloo Volcanics had been interpreted as Early Ordovician (Bendigonian to Lancefieldian, approximately 480–500 Ma) on the basis of graptolites found in quartzose siltstones of the Yarrimbah Chert Member, considered to be interbedded with the Nelungaloo sequence (Sherwin, 1979). An andesite lava which overlies and is about 6 km distant from the graptolite-bearing beds was chosen for isotopic dating. It is aphyric with sparse phenocrysts of plagioclase, pyroxene, and hornblende in an alkali feldspar and/or plagioclase groundmass and has undergone minor propylitic alteration to chlorite, epidote, and pyrite. Of the phases suited to isotopic dating, hornblende is present but in insufficient quantity for K-Ar or $^{40}Ar/^{39}Ar$ dating. Magmatic zircons are present in insufficient abundance for conventional zircon analysis, however, but in an adequate quantity for U-Pb dating by ion microprobe.

Analytical methods: Zircons were separated using standard heavy liquid and magnetic separation techniques and individual crystals were handpicked and mounted on the surface of an epoxy plug, to be sectioned in half by polishing to reveal grain interiors. Eighteen zircons were recovered from 500 g of rock. The grains fall into two morphological groups: one comprising rounded, equant grains which exhibit faceting on some crystal faces, and the other, composed of subhedral, elongate commonly broken grains (Fig. 5D). All zircons are internally structurally homogeneous and relatively inclusion free.

The U-Pb dating of the zircons was performed using the SHRIMP ion microprobe. The method involves firing a beam of negatively charged O_2 ions at the sectioned zircons to excavate a crater approximately 30 μm in diameter and 1 to 2 μm deep. Material sputtered from the crater is passed into a very high resolution and very high sensitivity mass spectrometer for analysis. By use of the finely focused probe, cracks and inclusions in the zircon crystals were avoided and individual growth zones targeted separately. Each analysis is the mean of seven cycles through the mass stations, and data were reduced in the manner described elsewhere (Compston et al., 1984; Williams and Claesson, 1987).

Ratios of Pb/U in each analysis are referenced to a value of 0.0928 for $^{206}Pb/^{238}U$ (equivalent to an age of 572 Ma) in our standard zircon SL13. A fragment of SL13 was cast in epoxy among the unknowns to minimize any possible bias in the conditions of analysis between the standard and the unknowns, and analyses of SL13 were alternated with analyses of the unknown. Quoted uncertainties include the uncertainties associated with calibration to the value for the standard; characteristics of the calibration upon which the age depends are described below.

Ratios of radiogenic isotopes have been corrected for initial Pb using crustal common Pb of the same age as the zircons (Cumming and Richards, 1975). The very small proportion of initial Pb in the zircons, denoted f in Table 4, may be calculated in three independent ways. The most direct calculation is by reference to the measured concentration of ^{204}Pb (the ^{204}Pb method), but counting precision on the small ^{204}Pb peak is poor. More precise calculation is possible from the difference between measured $^{208}Pb/^{206}Pb$ and that calculated from Th/U (^{208}Pb method), provided there is concordance of the ^{232}Th and ^{238}U systems. It is our experience that there are many zircon suites for which this assumption is not true, but its validity in the present case is confirmed by the fit of the analyses to a $^{208}Pb/^{206}Pb$-Th/U isochron (Fig. 7). Radiogenic isotopic ratios calculated in this way are listed in Table 4 and are used for plotting the concordia diagram (Fig. 8). The Th-U systems of three analyses are not concordant, and the ^{204}Pb correction has been substituted in these cases (see Table 4). A third method of calculating f is from the difference between measured $^{207}Pb/^{206}Pb$ and that calculated from $^{235}U/^{238}U$ (the ^{207}Pb method). This method cannot yield the $^{207}Pb/^{206}Pb$ and $^{207}Pb/^{235}U$ ratios needed to plot concordia diagrams, but given ^{235}U-^{238}U concordance, offers the advantage that precise $^{206}Pb^*/^{238}U$ ages (where $^{206}Pb^*$ is the radiogenic lead) can be calculated independent of the uncertainty and/or bias in Th/U and $^{208}Pb/^{206}Pb$ measurements. The ^{207}Pb-corrected data are also listed in Table 4 and are

TABLE 3. Ar Release Data for Goonumbla Sericites

Temperature °C	^{36}Ar $\times 10^{-19}$ moles	^{37}Ar $\times 10^{-17}$ moles	$^{39}Ar_K$ $\times 10^{-16}$ moles	Cumulative ^{39}Ar (%)	^{40}Ar $\times 10^{-14}$ moles	$^{40}Ar^*$ (%)[1]	$^{40}Ar^*/^{39}Ar_K$	Apparent age (Ma) $\pm 1\ \sigma$[2]
120 sericite, vein alteration, 0.0476 g, J = 0.00405388								
FM[3]	505 ± 282	670 ± 9	6,408 ± 6		1,032 ± 1	85.4	13.754	
TF[4]	8,763 ± 1,246	2,231 ± 50	8,805 ± 67		5,965 ± 76	99.5	67.420	435.9 ± 0.6
550	298 ± 265	49 ± 8	1,215 ± 1	2.5	882 ± 1	90.0	65.334	423.9 ± 0.6
580	3,059 ± 388	67 ± 15	661 ± 1	3.9	439 ± 1	97.9	65.117	422.6 ± 1.1
610	2,730 ± 95	368 ± 16	903 ± 1	5.8	597 ± 1	98.6	65.279	423.6 ± 0.5
640	2,752 ± 172	1,162 ± 4	1,461 ± 1	8.9	964 ± 1	99.1	65.399	424.3 ± 0.5
670	2,059 ± 300	2,390 ± 17	2,180 ± 2	13.3	1,446 ± 2	99.6	66.062	428.1 ± 0.6
700	2,547 ± 2	224 ± 1	3,213 ± 1	19.9	2,150 ± 2	99.6	66.661	431.5 ± 0.6
720	2,699 ± 163	295 ± 20	3,427 ± 31	27.0	2,305 ± 32	99.6	67.011	433.6 ± 0.6
740	2,771 ± 128	55 ± 15	3,981 ± 3	35.2	2,688 ± 3	99.7	67.281	435.1 ± 0.5
760	1,233 ± 410	25 ± 12	3,559 ± 3	42.5	2,415 ± 38	99.8	67.706	437.5 ± 0.7
780	1,861 ± 340	43 ± 19	3,623 ± 2	50.0	2,463 ± 3	99.7	67.793	438.0 ± 0.5
800	4,882 ± 444	72 ± 7	3,452 ± 2	57.2	2,347 ± 131	99.3	67.900	438.7 ± 0.5
820	636 ± 249	19 ± 6	1,254 ± 1	59.7	855 ± 1	99.7	67.984	439.1 ± 0.5
850	667 ± 341	0 ± 0	1,170 ± 9	62.2	794 ± 1	99.7	67.714	437.5 ± 0.7
900	1,951 ± 376	49 ± 28	3,509 ± 3	69.3	2,385 ± 3	99.7	67.787	438.0 ± 0.6
950	3,485 ± 336	106 ± 22	7,201 ± 6	84.2	4,910 ± 6	99.8	68.013	439.3 ± 0.6
1,000	3,221 ± 560	39 ± 7	3,782 ± 3	92.0	2,583 ± 4	99.6	68.019	439.3 ± 0.6
1,050	1,532 ± 278	13 ± 10	1,364 ± 1	94.8	934 ± 1	99.5	68.126	440.0 ± 0.6
1,300	5,614 ± 229	344 ± 1	2,498 ± 2	100.0	1,716 ± 2	99.0	68.019	439.3 ± 0.5
Total	43,797	5,320	48,453		32,873			435.7
Flat part[5]	(900–1,300°C)			27.0%				439.1 ± 1.1[6]
121 sericite, vein alteration, 0.0463 g, J = 0.00404652								
FM	442 ± 37	584 ± 14	4,679 ± 5		780 ± 1	83.1	13.846	
TF	187 ± 921	7,133 ± 36	109 ± 82		7,476 ± 89	99.2	67.828	435.5 ± 0.5
520	214 ± 232	21 ± 16	656 ± 1	1.5	524 ± 1	87.9	70.177	448.9 ± 0.8
580	2,248 ± 242	0 ± 0	828 ± 1	3.5	561 ± 1	99.8	67.144	431.6 ± 0.9
610	2,014 ± 345	0 ± 0	992 ± 1	5.8	668 ± 1	99.1	66.664	428.7 ± 0.8
640	1,396 ± 178	54 ± 28	1,390 ± 11	9.0	932 ± 1	99.5	66.757	429.4 ± 0.5
670	1,260 ± 240	35 ± 20	2,042 ± 2	13.7	1,378 ± 2	99.9	67.289	432.4 ± 0.6
700	1,015 ± 177	0 ± 0	3,124 ± 22	21.0	2,109 ± 24	99.8	67.380	433.0 ± 0.5
720	1,245 ± 398	61 ± 65	3,350 ± 22	28.8	2,262 ± 3	99.8	67.376	432.9 ± 0.5
740	1,697 ± 241	0 ± 0	3,440 ± 29	36.8	2,329 ± 3	99.7	67.509	433.7 ± 0.6
760	3,954 ± 1,165	72 ± 1	3,542 ± 1	45.1	2,393 ± 2	99.5	67.708	434.8 ± 0.6
780	825 ± 456	0 ± 0	3,318 ± 29	52.8	2,246 ± 3	99.9	67.602	434.2 ± 0.5
800	1,150 ± 251	0 ± 0	3,168 ± 2	60.1	2,148 ± 2	99.8	67.685	434.7 ± 0.5
820	1,131 ± 208	49 ± 33	2,995 ± 2	67.1	2,034 ± 2	99.8	67.764	435.2 ± 0.5
850	2,566 ± 4,946	115 ± 27	3,045 ± 2	74.2	2,071 ± 15	99.6	67.751	435.1 ± 0.5
930	2,079 ± 7	10 ± 1	5,564 ± 1	87.1	3,798 ± 3	99.8	68.132	437.3 ± 0.6
980	3,659 ± 4	20 ± 1	3,201 ± 1	94.3	2,192 ± 1	99.5	68.095	437.0 ± 0.5
1,010	3,743 ± 2	0 ± 0	1,268 ± 1	97.5	879 ± 7	98.7	68.385	438.7 ± 0.6
1,300	5,008 ± 2	66 ± 2	1,079 ± 1	100.0	750 ± 1	98.0	68.083	437.0 ± 0.6
Total	35,204	503	43,002		29,274			434.9
122 sericite, groundmass alteration, 0.0522 g, J = 0.0040136								
FM	775 ± 347	356 ± 13	5,661 ± 6		1,017 ± 2	77.3	13.891	
TF	24,050 ± 603	223 ± 50	8,295 ± 6		5,727 ± 7	98.8	68.200	436.5 ± 0.6
520	12 ± 1	220 ± 1	711 ± 1	1.9	8,118 ± 1	57.3	65.453	420.8 ± 1.5
580	2,711 ± 443	243 ± 1	488 ± 1	3.2	337 ± 1	97.6	67.302	431.4 ± 1.8
610	2,185 ± 259	385 ± 8	479 ± 1	4.4	329 ± 1	98.0	67.252	431.1 ± 1.1
640	3,952 ± 355	3,271 ± 13	1,263 ± 1	7.7	860 ± 1	98.6	67.205	430.8 ± 0.7
670	4,227 ± 212	120 ± 158	1,640 ± 2	12.1	1,120 ± 2	98.9	67.609	433.1 ± 0.9
700	3,949 ± 378	150 ± 41	2,389 ± 2	18.3	1,630 ± 2	99.3	67.810	434.3 ± 0.6
720	2,995 ± 222	126 ± 31	2,736 ± 2	25.5	1,871 ± 2	99.5	68.080	435.8 ± 0.5
740	1,840 ± 499	7,862 ± 49	3,255 ± 2	34.0	2,227 ± 3	99.7	68.241	436.7 ± 0.6
760	2,116 ± 346	2,529 ± 27	3,430 ± 3	43.0	2,356 ± 3	99.7	68.490	438.1 ± 0.6

TABLE 3. (*Cont.*)

Temperature °C	^{36}Ar $\times 10^{-19}$ moles	^{37}Ar $\times 10^{-17}$ moles	$^{39}Ar_K$ $\times 10^{-16}$ moles	Cumulative ^{39}Ar (%)	^{40}Ar $\times 10^{-14}$ moles	$^{40}Ar^*$ (%)[1]	$^{40}Ar^*/^{39}Ar_K$	Apparent age (Ma) $\pm 1\ \sigma$[2]
780	3,224 ± 257	493 ± 11	3,325 ± 3	51.8	2,289 ± 3	99.5	68.529	438.4 ± 0.6
800	2,378 ± 273	319 ± 33	3,012 ± 2	59.7	2,072 ± 2	99.6	68.518	438.3 ± 0.5
820	1,441 ± 223	299 ± 14	2,357 ± 2	65.9	1,616 ± 2	99.7	68.333	437.2 ± 0.6
850	2,365 ± 425	338 ± 19	2,474 ± 3	72.4	1,703 ± 3	99.6	68.506	438.3 ± 0.7
930	3,323 ± 381	784 ± 20	3,922 ± 4	82.7	2,689 ± 3	99.6	68.287	437.1 ± 0.6
980	2,878 ± 251	417 ± 14	2,397 ± 2	89.0	1,643 ± 2	99.4	68.136	436.1 ± 0.6
1,010	2,406 ± 258	230 ± 12	1,360 ± 1	92.6	935 ± 1	99.2	68.232	436.7 ± 0.6
1,300	9,466 ± 255	4,039 ± 14	2,827 ± 3	100.0	1,924 ± 2	98.5	67.046	430.0 ± 0.6
Total	51,468	21,825	38,065		33,719			435.2
Flat part	(760°–930°C)			48%				437.9 ± 1.1[6]
123 sericite, groundmass alteration, 0.0638 g, J = 0.00404652								
FM	544 ± 311	382 ± 12	6,766 ± 7		1,095 ± 2	85.2	13.779	
TF	28,410 ± 95	472 ± 37	9,796 ± 9		6,686 ± 9	98.7	67.365	434.9 ± 0.7
550	330 ± 342	20 ± 11	766 ± 1	1.3	533 ± 13	81.7	56.910	373.9 ± 1.1
580	4,361 ± 324	24 ± 10	387 ± 6	2.0	260 ± 1	95.0	63.976	415.3 ± 1.7
610	3,131 ± 154	24 ± 15	530 ± 1	2.9	356 ± 1	97.4	65.300	423.0 ± 0.8
640	2,661 ± 71	273 ± 15	870 ± 1	4.3	575 ± 1	98.6	65.138	422.1 ± 0.7
670	2,215 ± 107	529 ± 19	1,338 ± 1	6.6	893 ± 1	99.2	68.188	428.1 ± 0.7
700	2,241 ± 1	610 ± 13	1,908 ± 2	9.9	1,274 ± 2	99.4	66.419	429.5 ± 0.5
720	1,839 ± 31	381 ± 2	2,180 ± 2	13.6	1,460 ± 2	99.6	66.715	431.1 ± 0.6
740	1,800 ± 60	167 ± 8	2,649 ± 3	18.1	1,776 ± 2	99.7	66.799	431.6 ± 0.6
760	1,733 ± 47	84 ± 30	3,017 ± 3	23.2	2,033 ± 3	99.7	67.195	433.9 ± 0.6
780	1,515 ± 7	29 ± 9	3,329 ± 2	28.9	2,248 ± 3	99.8	67.343	434.8 ± 0.6
800	1,351 ± 3	0 ± 0	2,824 ± 21	33.7	1,916 ± 2	99.8	67.680	436.7 ± 0.6
820	4,683 ± 374	68 ± 15	4,199 ± 3	40.8	2,840 ± 4	99.5	67.279	434.4 ± 0.6
850	2,310 ± 258	41 ± 19	5,751 ± 5	50.6	3,898 ± 5	99.8	67.630	436.4 ± 0.6
870	1,847 ± 8	32 ± 22	5,314 ± 4	59.7	3,608 ± 5	99.8	67.777	437.2 ± 0.6
900	2,914 ± 4	9 ± 0	5,811 ± 4	69.6	3,956 ± 5	99.7	67.906	438.0 ± 0.5
930	2,387 ± 40	50 ± 17	5,273 ± 4	78.5	3,595 ± 4	99.8	68.012	438.6 ± 0.6
980	2,630 ± 4	18 ± 40	5,597 ± 4	88.1	3,823 ± 4	99.8	68.150	439.4 ± 0.5
1,010	2,434 ± 4	8 ± 12	2,876 ± 2	93.0	1,972 ± 2	99.6	68.285	440.2 ± 0.6
1,060	3,280 ± 677	35 ± 7	2,016 ± 1	96.4	1,386 ± 2	99.3	68.254	440.0 ± 0.5
1,300	190 ± 4	197 ± 15	2,126 ± 1	100.0	1,512 ± 2	96.3	68.456	441.0 ± 0.5
Total	45,852	2,590	58,761		39,914			435.2

[1] $^{40}Ar^*/\Sigma^{40}Ar$
[2] 1 σ uncertainty without error in J
[3] Results for GA 1550 biotite flux monitor
[4] Results for total fusion analysis for 120, sample weight = 0.025 g; for 121, sample weight = 0.0318 g; for 122, sample weight = 0.0250 g; for 123, sample weight = 0.0296 g
[5] Mean age with size of step weighting
[6] 1 σ uncertainty including error in J

used in age calculations. Uncertainties quoted include the uncertainties of common Pb correction.

U-Pb results: Analyses were collected for 28 30-μm-diameter areas of 12 zircons and the results are listed in Table 4. The most useful age information in SHRIMP analysis of Phanerozoic zircons comes from $^{206}Pb^*/^{238}U$ ratios, which have relatively good measurement precision and are insensitive to correction for initial Pb. Radiogenic ^{207}Pb ($^{207}Pb^*$) is 20 times less abundant than $^{206}Pb^*$ in zircons of this age, and consequently, suffers both from poor counting precision on the ^{207}Pb mass and from sensitivity to initial Pb correction. In the concordia diagram (Fig. 8) this is reflected in the small errors and coherent grouping of $^{206}Pb^*/^{238}U$ data and larger analytical errors and greater scatter in the $^{207}Pb^*/^{235}U$ direction. The uncertainty in $^{207}Pb^*$ measurement frustrates definitive testing for concordance of the ^{235}U and ^{238}U chronometers; incidence of Pb loss is therefore best assessed from grouping of $^{206}Pb^*/^{238}Pb$ compositions.

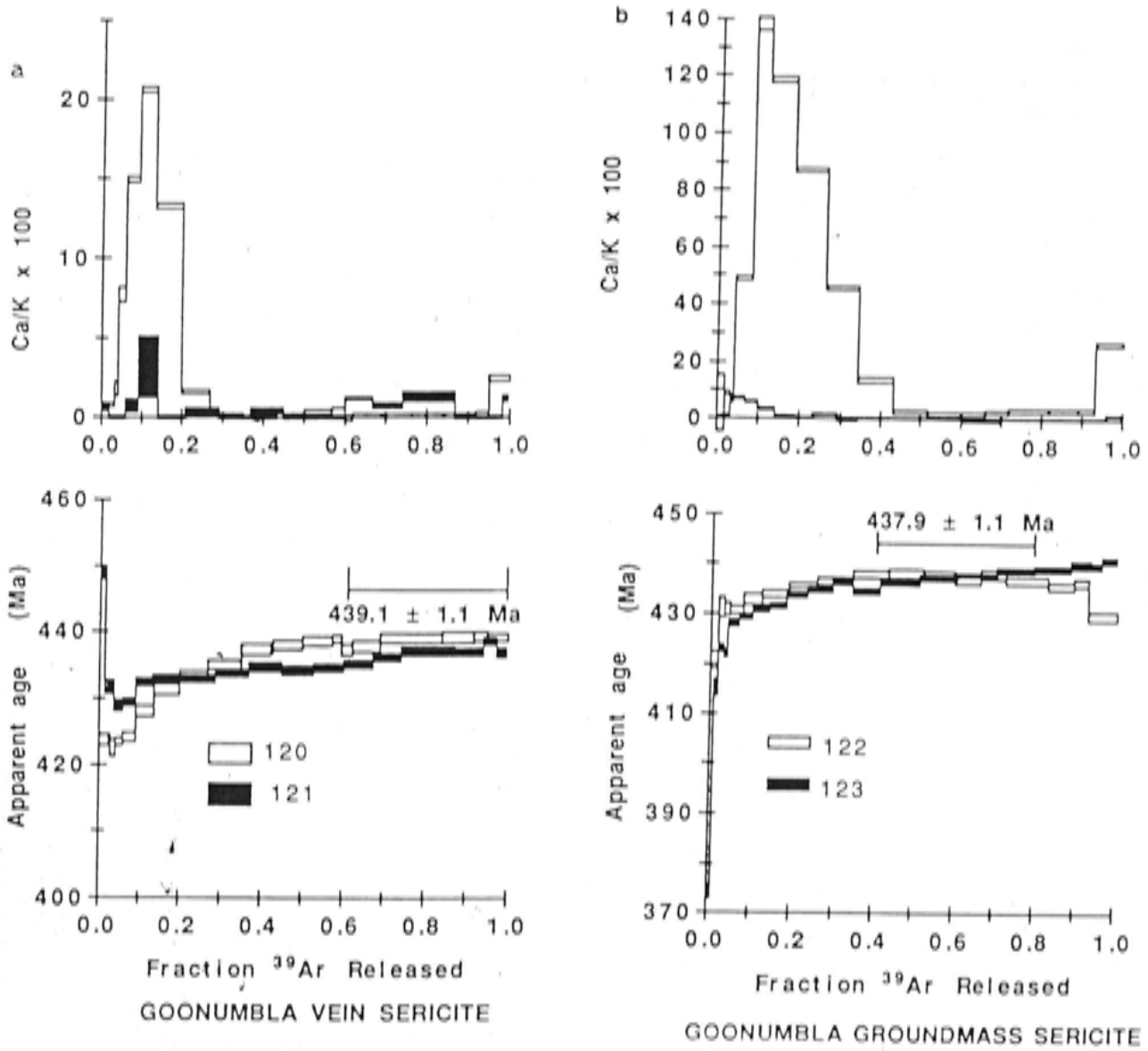

FIG. 6. $^{40}Ar/^{39}Ar$ age spectra and Ca/K ratios for Goonumbla hydrothermal alteration minerals. A. Vein sericite. B. Groundmass sericite.

Accuracy of SHRIMP $^{206}Pb/^{238}U$ ratios is mainly determined by the accuracy of machine-dependent Pb/U calibration to the known Pb/U ratio of the standard zircon, via a relationship between Pb/U and the measured UO/U (Compston et al., 1984). Over the two-day period when the Nelungaloo sample was analyzed, 14 measurements of standard zircon SL13 were alternated with those of the unknowns. The data are compared in Figure 9 with the SHRIMP calibration relationship, which is a quadratic curve of constant form but which may be displaced in x-y space (Williams and Claesson, 1987). Both sets of data adhere closely to the expected curve. The scatter of SL13 data about the curve is a direct measure of the reproducibility of a constant Pb/U target achieved during this analytical run, and the 2.51 percent (1σ) reproducibility is included in the uncertainty in Pb/U of each of the unknowns listed in Table 4. Additionally, the 0.67 percent uncertainty (1σ) in the mean position of the standard calibration curve is included in the quoted error on the mean age of the group of unknowns discussed below.

In contrast to conventional dissolution analysis of zircon (in which one or several whole grains are dissolved and their total Pb and U averaged to produce a single high-precision number), SHRIMP analysis provides a large number of lower precision analyses of minute subvolumes within single zircons. Should some or all of the analyzed subvolumes prove to have identical compositions, they may be combined as a high-precision weighted mean for the total analyzed volume. With three exceptions, the Nelungaloo zircons form a coherent group of compositions (Fig. 8), in which the degree of scatter of observed $^{206}Pb^*/^{238}U$ ratios is the same as that obtained for the homogeneous standard zircon. This indicates that the grains are all of one composition, within error, and suggests that disturbance of the isotopic systems in the zircons has not occurred. The weighted mean $^{206}Pb^*/^{238}U$ ratio of the group is 0.07039 ± 0.00061 (1σ of the mean), equivalent to an age of 438.5 ± 3.6 Ma (1σ). A dominant and coherent age grouping is the most important isotopic property expected of magmatic zircons in an erupted lava, and accordingly, the age of this population is interpreted as the age of crystallization of the andesite.

Exceptions are posed by three analyses that depart from the main population by more than can be at-

TABLE 4. Ion Microprobe U-Th-Pb Isotope Data for Zircons in the Nelungaloo Andesite

Grain area	U (ppm)	Th (ppm)	Th/U	^{208}Pb corrected concordia coordinates: ^{204}Pb (ppb)	f^{206}Pb[1] (%)	^{206}Pb/^{238}U ± 1 σ	^{207}Pb/^{235}U ± 1 σ	^{207}Pb/^{206}Pb ± 1 σ	^{207}Pb corrected data: ^{206}Pb/^{238}U ± 1 σ	Apparent age[2] (Ma) ± 1 σ
A. Analyses comprising the 438.5 ± 3.6-Ma principal population										
28.1	187	83	0.45	3	0.57	0.0693 ± 18	0.546 ± 26	0.0571 ± 22	0.0692 ± 18	431 ± 11
28.2	204	106	0.52	11	1.63	0.0695 ± 18	0.549 ± 31	0.0574 ± 27	0.0693 ± 18	432 ± 11
28.3	139	56	0.41	10	2.12	0.0693 ± 18	0.557 ± 32	0.0583 ± 28	0.0691 ± 18	431 ± 11
29.1	101	41	0.4	2	0.54	0.0707 ± 18	0.57 ± 30	0.0584 ± 26	0.0705 ± 18	439 ± 11
29.2	188	145	0.77	6	0.93	0.0706 ± 18	0.509 ± 31	0.0524 ± 27	0.0709 ± 18	441 ± 11
29.3	286	246	0.86	8	0.82	0.0748 ± 19	0.581 ± 30	0.0563 ± 24	0.0748 ± 19	465 ± 11
29.4	233	129	0.55	7	0.86	0.0722 ± 18	0.614 ± 31	0.0616 ± 25	0.0717 ± 18	446 ± 11
29.5	133	58	0.43	6	1.35	0.0687 ± 18	0.532 ± 37	0.0561 ± 34	0.0687 ± 17	428 ± 11
30.1	490	493	1.01	1	0.08	0.0707 ± 18	0.558 ± 25	0.0573 ± 20	0.0705 ± 18	439 ± 11
30.2	143	54	0.38	10	2.10	0.0716 ± 18	0.568 ± 31	0.0575 ± 26	0.0714 ± 18	445 ± 11
30.3	294	206	0.7	3	0.31	0.0725 ± 18	0.621 ± 28	0.0621 ± 21	0.0719 ± 18	448 ± 11
31.1	389	440	1.13	2	0.12	0.0708 ± 18	0.568 ± 29	0.0582 ± 24	0.0706 ± 18	440 ± 11
31.2	519	693	1.33	6	0.32	0.0717 ± 18	0.55 ± 30	0.0557 ± 25	0.0717 ± 18	446 ± 11
32.1	345	307	0.89	4	0.32	0.0661 ± 17	0.498 ± 25	0.0547 ± 22	0.0662 ± 17	413 ± 10
32.2	388	362	0.93	3	0.24	0.0707 ± 18	0.58 ± 28	0.0595 ± 23	0.0704 ± 18	439 ± 11
33.1[3]	248	112	0.45	2	0.21	0.0693 ± 18	0.547 ± 36	0.0572 ± 33	0.0692 ± 17	431 ± 11
34.2[3]	580	588	1.01	21	1.09	0.0696 ± 18	0.478 ± 27	0.0499 ± 23	0.0701 ± 18	437 ± 11
35.1	372	233	0.63	2	0.13	0.0696 ± 18	0.544 ± 22	0.0567 ± 16	0.0695 ± 18	433 ± 11
36.1	42	17	0.41	12	7.48	0.0718 ± 19	0.608 ± 68	0.0614 ± 65	0.0713 ± 19	444 ± 11
38.1	184	50	0.27	10	1.49	0.0725 ± 18	0.541 ± 25	0.0542 ± 19	0.0726 ± 18	452 ± 11
B. Analyses detectably younger than the principal population										
34.1[3]	663	1,238	1.87	107	5.81	0.0553 ± 14	0.437 ± 40	0.0573 ± 49	0.0552 ± 14	346 ± 8
C. Zircons detectably older than the principal population										
37.1	1,907	901	0.47	5	0.06	0.0833 ± 21	0.658 ± 19	0.0573 ± 6	0.0831 ± 21	515 ± 12
39.1	175	33	0.19	40	5.49	0.0825 ± 21	0.703 ± 36	0.0618 ± 26	0.0819 ± 21	507 ± 12

[1] f^{206}Pb indicates the percentage common ^{206}Pb in the total measured ^{206}Pb
[2] Apparent age is the ^{207}Pb-corrected ^{206}Pb*/^{238}U age
[3] Denotes ^{204}Pb correction substituted for the ^{208}Pb correction owing to discordant Th-U compositions

tributed to analytical uncertainty alone. One analysis of grain 34 has a young apparent age of 346 Ma, attributed to Pb loss in that area of the zircon. The analysis was obtained from a cracked portion of the grain, and a second analysis of the same zircon lies in the principal population. Two other zircons (37 and 39) targeted on morphological grounds as part of the main grouping have apparent ages of 510 to 515 Ma. Although optically similar to the other zircons, the greater age of these grains identifies them as xenocrysts in the andesite magma, possibly inherited from the source rocks of the magma.

The isotopically dated Nelungaloo andesite lavas can be considered as broadly being part of the Goonumbla magmatic episode. As a result of the dating, the relationship of the graptolite-bearing beds to the volcanics has been reassessed, and it is possible that a conglomerate bed which overlies the graptolite-bearing horizon represents a major time break within the Nelungaloo succession.

Conclusions

1. The ^{40}Ar/^{39}Ar age spectra from Goonumbla hydrothermal sericite indicate that vein and groundmass alteration in the Endeavour 26 deposit were broadly contemporaneous at 439.2 ± 1.2 Ma, despite the fact that the groundmass sericite alteration clearly overprints the vein-style sericite and is therefore later on textural grounds. This date is taken to approximate the time of gold and copper mineralization. Thermal overprinting in the Devonian has caused a small amount of partial ^{40}Ar* loss in the Goonumbla sericite. The U-Pb zircon date of 438.5 ± 3.6 Ma for the Nelungaloo Volcanics suggests that part of this sequence which underlies the Goonumbla Volcanics is essentially coeval with the latter succession and provides

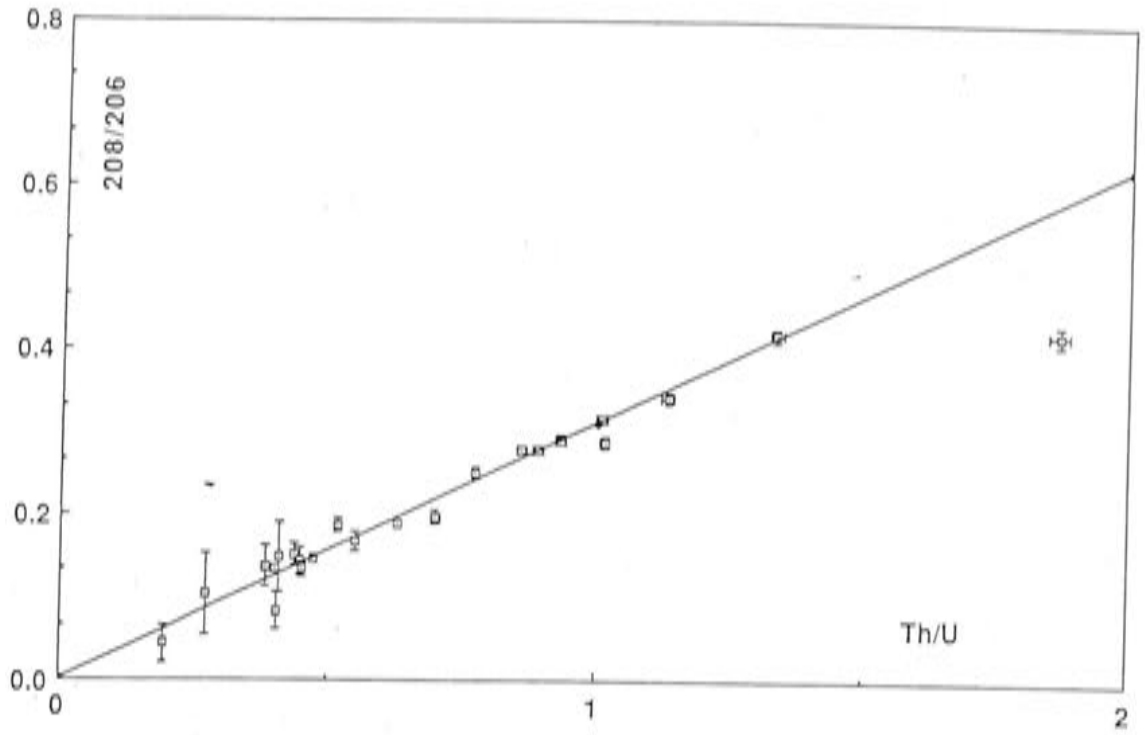

FIG. 7. $^{208}Pb/^{206}Pb$-Th/U isochron for zircon analyses obtained from the Nelungaloo Volcanics, showing the fit of all but three analyses to the theoretical isochron for 439 Ma. This plot indicates that there has been no differential movement of Th relative to U in most of the zircons and no differential movement of uranogenic and thorogenic Pb. Initial Pb corrections for the majority of the analyses can therefore be calculated accurately from the difference between the measured $^{208}Pb/^{206}Pb$ and that calculated from Th/U.

a maximum age for mineralization. A link between Late Ordovician to Early Silurian magmatism and mineralization in the Lachlan fold belt is indicated by the Goonumbla $^{40}Ar/^{39}Ar$ and U-Pb dates and is further substantiated by ages obtained by the same methods on other gold deposits elsewhere in the region (Perkins et al., 1990).

2. The K-Ar and $^{40}Ar/^{39}Ar$ dates obtained from low-temperature hydrothermal alkali feldspar are considerably younger than those from coeval hydrothermal sericite, and the former mineral is therefore considered unsuitable for dating alteration.

3. The approximately 510-Ma-age xenocryst zircons in the Nelungaloo Volcanics correspond to a group of inherited zircons of similar age described by Williams et al. (1988) from the Devonian Bega batholith about 400 km to the southeast in the Lachlan fold belt. This suggests that, at least in part, similar Cambrian source material exists for both magmas.

4. The $^{40}Ar/^{39}Ar$ age spectra obtained in this investigation from fine-grained sericite illustrates the amenability of the hydrothermal phase to this dating technique and suggests that there is considerable po-

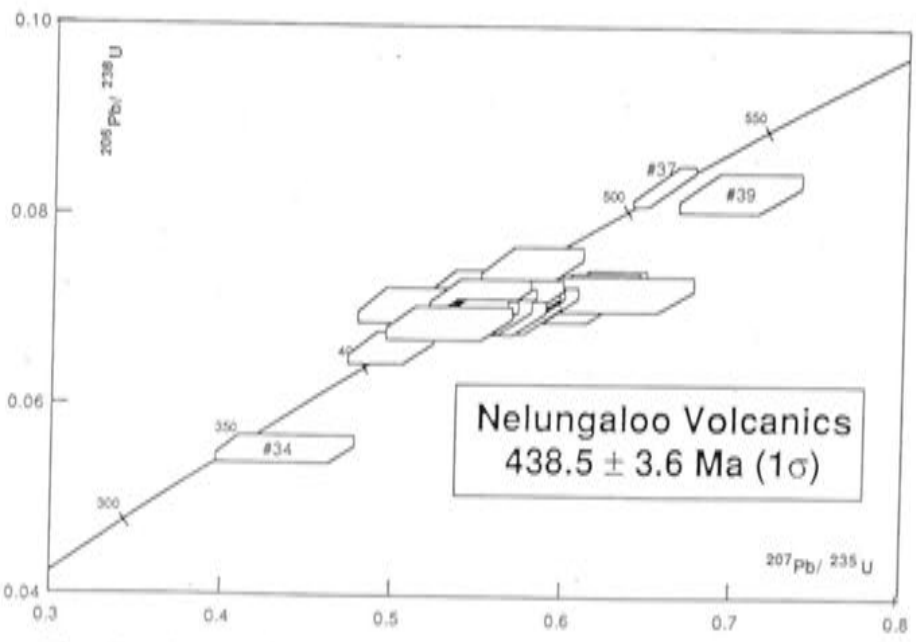

FIG. 8. Concordia diagram illustrating the range of zircon ages obtained from the Nelungaloo Volcanics.

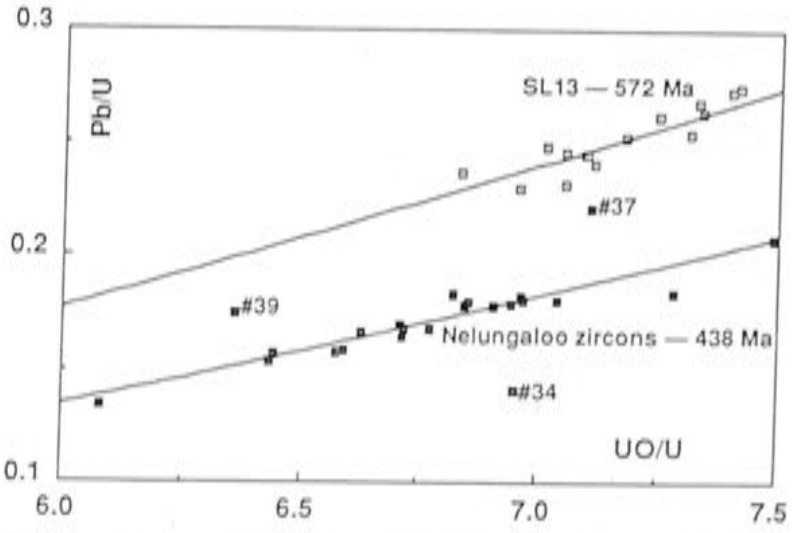

FIG. 9. Measured UO/O and Pb/U ratios for standard zircon SL13 and the Nelungaloo andesite zircons. Both sets of analyses adhere closely to the form of the SHRIMP calibration relationship indicated by the curve passing through the midpoint of each data set. Xenocrysts 37 and 39 and altered zircon 34 stand out as outliers from the main group by more than 95 percent confidence.

tential for application of the dating method to Phanerozoic deposits in general.

5. There is not a separation in hydrothermal sericite formation events on the order of several million years at Goonumbla, as reported by Snee et al. (1988) for the Panasqueira Sn-W deposit, Portugal. Further $^{40}Ar/^{39}Ar$ dating work is needed on alteration minerals from porphyry copper-gold deposits to determine whether short-lived hydrothermal activity is characteristic of these systems.

6. U-Pb dating on magmatic zircons represents an appropriate means by which the age of host magmatic rocks to deposits may be determined in zones of regional propylitic alteration where primary potassic minerals have been destroyed.

7. The close agreement in ages between the $^{40}Ar/^{39}Ar$ and U-Pb results obtained in this study gives confidence in the application of both dating techniques to altered Paleozoic rocks; the two dating methods have, however, yielded widely differing ages on samples from severely overprinted Archean gold deposits (cf. Claoué-Long et al., 1990). The Goonumbla study illustrates how a combination of these dating methods, coupled with understanding of the paragenesis of alteration phases and knowledge of the regional geology, can be successfully used to determine the geochronology of both hydrothermal phases and host rocks to mineralization.

Acknowledgments

This work was funded by a Bureau of Mineral Resources post-doctoral fellowship awarded to C. Perkins. Irradiations were undertaken with support from the Australian Institute of Nuclear Science and Engineering. The assistance of J. L. Walshe is gratefully acknowledged, and he and S. L. Baldwin and M. Honda provided helpful comments on the manuscript. Discussions with W. E. Cameron greatly helped the project, and Terry Davies, Robyn Maier, and Chris Foudoulous are thanked for their technical support. Geopeko provided invaluable assistance.

May 31, September 12, 1990

REFERENCES

Bowman, H. N., Hobbs, J. J., and Barron, L. M., 1977, The Goonumbla copper district north west of Parkes, central western New South Wales: New South Wales Geol. Survey Rept. GS1977/095, 56 p.

Brindley, G. W., and Brown, G., 1984, Crystal structures of clay minerals and their X-ray identification: London, Mineralog. Soc. London, 495 p.

Chappell, B. W., and Stephens, W. E., 1988, Origin of infracrustal (I-type) granite magmas: Royal Soc. [Edinburgh] Trans.: Earth Sciences, v. 79, p. 71–86.

Claoué-Long, J., King, R. W., and Kerrich, R., 1990, Archean hydrothermal zircon in the Abitibi greenstone belt: Constraints on the timing of gold mineralization: Earth Planet. Sci. Letters, v. 98, p. 109–128.

Clarke, I., 1987, Petrology of igneous rocks associated with gold and copper mineralization in the Parkes area: New South Wales Geol. Survey Rept. GS 1985/121, 68 p.

Compston, W., Williams, I. S., and Meyer, C., 1984, U-Pb geochronology of zircons from lunar breccia 73217 using a sensitive high-resolution ion microprobe: Jour. Geophys. Research, v. 89, p. B525–534.

Cumming, G. L., and Richards, J. R., 1975, Ore lead isotope ratios in a continuously changing earth: Earth Planet. Sci. Letters, v. 28, p. 155–171.

Dalrymple, G. B., and Lanphere, M. A., 1969, Potassium-argon dating: San Francisco, W. H. Freemam Co., 251 p.

Gulson, B. L., and Bofinger, V. M., 1972, Time differences within a calc-alkaline association: Contr. Mineralogy Petrology, v. 36, p. 19–26.

Harland, W. B., Armstrong, R. L., Cox, A. V., Craig, L. E., Smith, A. G., and Smith, D. G., 1989, A geologic time scale 1989: Cambridge, Cambridge University Press.

Harrison, T. M., and McDougall, I., 1980, Investigations of an intrusive contact, northwest Nelson New Zealand—I. Thermal, chronological and isotopic constraints: Geochim. et Cosmochim. Acta, v. 44, p. 1985–2003.

Heithersay, P. S., 1986, Endeavour 26 North copper-gold deposit, Goonumbla, NSW—paragenesis and alteration zonation, *in* Berkman, D. A., ed., Publications of the 13th CMMI Congress, vol. 2. Geology and Exploration: Melbourne, Australasian Inst. Mining Metallurgy, p. 181–189.

Heithersay, P. S., O'Neill, W. J., Van der Helder, P., Moore, C. R., and Harbon, P. G., 1990, Goonumbla porphyry copper district—Endeavour 26 North, Endeavour 22 and Endeavour 27 copper-gold deposits, *in* Geology of the mineral deposits of Australia and Papua New Guinea: Melbourne, Australasian Inst. Mining Metallurgy, v. 2, p. 1385.

Jones, G. J., 1985, The Goonumbla porphyry copper deposits, New South Wales: ECON. GEOL., v. 80, p. 591–613.

McDougall, I., and Harrison, T. M., 1988, Geochronology and thermochronology by the $^{40}Ar/^{39}Ar$ method: New York, Oxford Univ. Press, 212 p.

McDougall, I., and Roksandic, Z., 1974, Total fusion $^{40}Ar/^{39}Ar$ ages HIFAR reactor: Geol. Soc. Australia Jour., v. 21, p. 81–89.

Merrihue, C., and Turner, G., 1966, Potassium-argon dating by activation with fast neutrons: Jour. Geophys. Research, v. 71, p. 2852–2857.

Nier, A. O., 1950, A redetermination of the relative abundances of the isotopes of carbon, nitrogen, oxygen, argon, and potassium: Phys. Rev., v. 77, p. 789–793.

Owen, N., and Wyborn, D., 1979, Geology and geochemistry of the Tantangara and Brindabella 1:100,000 sheet areas: Australian Bur. Mineral Resources Bull. 204, 52 p.

Perkins, C., McDougall, I., and Claoué-Long, J., 1990, Dating ore deposits with high precision: Examples from the Lachlan fold belt, NSW, Australia: Pacrim 90 Congress, Melbourne, Proc., v. II, p. 105–112.

Scheibner, E., 1972, Tectonic concepts and tectonic mapping: New South Wales Geol. Survey Rec., v. 14, p. 37–83.

Sherwin, L., 1973, Stratigraphy of the Forbes-Bogan Gate district: New South Wales Geol. Survey Rec., v. 15 (1), p. 47–101.

—— 1979, Age of the Nelungaloo Volcanics near Parkes: New South Wales Geol. Survey Quart. Notes, v. 35, p. 15–18.

Sherwin, L., Clarke, I., and Krynen, J. P., 1987, Revision of stratigraphic units in the Forbes-Parkes-Tomingley district: New South Wales Geol. Survey Quart. Notes, v. 67, p. 1–23.

Snee, L. W., Sutter, J. F., and Kelly, W. C., 1988, Thermochronology of economic mineral deposits: Dating the stages of min-

eralization at Panasqueira, Portugal, by high-precision $^{40}Ar/^{39}Ar$ age spectrum techniques on muscovite: ECON. GEOL., v. 83, p. 335–354.

Steiger, R. H., and Jäger, E., 1977, Subcomission of geochronology: Convention on the use of decay constants in geo- and cosmochronology: Earth Planet. Sci. Letters, v. 36, p. 359–362.

Tetley, N., McDougall, I., and Heydegger, H. R., 1980, Thermal neutron interferences in the $^{40}Ar/^{39}Ar$ dating technique: Jour. Geophys. Research, v. 85, p. 7201–7205.

Thompson, J. F. H., Lessman, J., and Thompson, A. J. B., 1986, The Temora gold-silver deposit: A newly recognized style of high sulfur mineralization in the lower Paleozoic of Australia: ECON. GEOL., v. 81, p. 732–738.

Turner, G., 1968, The distribution of potassium and argon in chondrites, *in* Aherns, L. H., ed., Origin and distribution of the elements: London, Pergamon, p. 387–398.

Webby, B. D., 1976, The Ordovician system in south-eastern Australia, *in* Bassett, M. G., ed., The Ordovician system: Proceedings of a Palaeontological Association symposium: Birmingham, Univ. Wales Press, p. 417–446.

Williams, I. S., and Claesson, S., 1987, Isotopic evidence for the Precambrian provenance and Caledonian metamorphism of high grade paragneisses form the Seve nappes, Scandinavian Caledonides II. Ion microprobe zircon U-Th-Pb: Contr. Mineralogy Petrology, v. 97, p. 205–217.

Williams, I. S., Chen, Y., Chappell, B. W., and Compston, W., 1988, Dating sources of the Bega batholith granites by ion microprobe [abs.]: Geol. Soc. Australia Abstracts, v. 21, p. 424.

Wyborn, D., 1988, Ordovician magmatism, gold mineralisation, and an integrated tectonic model for the Ordovician and Silurian history of the Lachlan fold belt in NSW: Australian Bur. Mineral Resources Newsletter 8, p. 13–14.

Wyborn, D., and Cameron, W. E., 1990, Ordovician magmatism in the central Lachlan fold belt and precious metal potential [abs.]: Australian Geol. Convention, 10th, Hobart, February, 1990, Abstracts, p. 126.